NEWRAD

PROCEEDINGS OF THE
9TH INTERNATIONAL CONFERENCE
ON NEW DEVELOPMENTS AND
APPLICATIONS IN OPTICAL RADIOMETRY

17-19 OCTOBER, 2005, DAVOS, SWITZERLAND

EDITED BY
JULIAN GRÖBNER
PHYSIKALISCH-METEOROLOGISCHES OBSERVATORIUM DAVOS,
WELTSTRAHLUNGSZENTRUM

DAVOS, SWITZERLAND, SEPTEMBER 2005

Scientific Programme Committee:

Andrew Wallard, BIPM, France
Tony Bittar, IRL/CRI, New Zealand
James Butler, NASA, USA
Antonio Corrons, IFA/CSIC, Spain
Peter Foukal, Heliophysics, USA
Nigel Fox, NPL, UK
Claus Fröhlich, PMOD/WRC, Switzerland
Martin Huber, PSI, Switzerland
Erkki Ikonen, MIKES, Finland
Jürgen Metzdorf, PTB, Germany
Al Parr, NIST, USA
Maria Luisa Rastello, IEN, Italy
Gerhard Ulm, PTB, Germany

Local Organising Committee:

Physikalisch-Meteorologisches Observatorium Davos,
Weltstrahlungszentrum

Julian Gröbner
Werner Schmutz
Sonja Degli Esposti
Wolfgang Finsterle
Christoph Wehrli

ISBN-10 3-033-00570-5

ISBN-13 978-3-033-00570-9

NEWRAD 2005 Scientific Program

Day	Chair		Session	
Monday	Nigel Fox	1	Absolute Radiometry	Posters
	Erkki Ikonen/Jürgen Metzdorf	2	UV, Vis, and IR Radiometry	Posters
	Jürgen Metzdorf	3	Photolithography and UV Processing	Posters
Tuesday	Peter Foukal/Claus Fröhlich	4	Remote Sensing	Posters
	Antonio Corrons	5	Photometry and Colorimetry	Posters
	Maria Luisa Rastello	6	Novel Techniques	Posters
Wednesday	Tony Bittar	7	International Comparisons	Posters
	Tony Bittar/Martin Huber	8	Radiometric and Photometric Sources	Posters
	Gerhard Ulm	9	Realisation of Scales	Posters

Sunday, October 16, 2005

17:30 - Opening Reception in the foyer Aspen of the Conference Centre

Participant registration

Monday, October 17, 2005

8:00	Participant registration		
8:45	Welcome	Werner Schmutz, PMOD/WRC	
8:55	Information	Julian Gröbner, PMOD/WRC	

Session 1	**Chair – Nigel Fox**	**Absolute Radiometry**	
9:00	Claus Fröhlich, PMOD	1-1	**Invited Talk**, Absolute Accuracy of Total Solar Irradiance Measurements in Space (page 17)
9:30	Eric Usadi, NPL	1-2	Reflecting Cavity Blackbodies for Radiometry (page 19)
9:50	Joaquin Campos-Acosta, CSIC	1-3	Low-uncertainty absolute radiometric calibration of a CCD (page 21)
10:10	Jeanne Houston, NIST	1-4	NIST Reference Cryogenic Radiometer Designed for Versatile Performance (page 23)
10:30	Refreshment break / Poster installation		
Session 2	**Chair – Erkki Ikonen**	**UV, Vis, and IR Radiometry**	
11:10	Mario Blumthaler, UIIMP	2-1	**Invited Talk** , QA/QC of Spectral Solar UV irradiance measurements (page 59)
11:40	Gerhard Ulm, PTB	2-2	The Metrology Light Source – the new dedicated electron storage ring of PTB (page 61)
12:00	Jarle Gran, JV	2-3	Fractional self-calibration of silicon photodiodes (page 63)
12:20	Lunch Break / **Poster Session 1,2,3**		
Session 2	**Chair – Erkki Ikonen**	**UV, Vis, and IR Radiometry**	
14:30	Peter Meindl, PTB	2-4	The UV Spectral Responsivity Scale of the PTB (page 69)
14:50	Ping-shine Shaw, NIST	2-5	A method of characterizing narrow-band filtered radiometers using synchrotron radiation (page 73)

15:10	Terubumi Saito, AIST	2-6	Characterization of Photoconductive Diamond Detectors as a Candidate of FUV/VUV Transfer Standard Detectors (page 67)
15:30	Laurent Vuilleumier, SMA	2-7	Operational mode uncertainty for broadband erythemal UV radiometers (page 71)
15:50	Refreshment break		
Session 2	**Chair – Jürgen Metzdorf**	**UV, Vis, and IR Radiometry**	
16:20	George Eppeldauer, NIST	2-8	Development of a Versatile Radiometer-Photometer System (page 75)
16:40	Lasse Ylianttila, STUK	2-9	Temperature effects of PTFE diffusers (page 65)
Session 3	**Chair – Jürgen Metzdorf**	**Photolithography and UV Processing**	
17:00	Frank Scholze, PTB	3-1	Improvements in EUV reflectometry at PTB (page 139)
17:20	Rob Vest, NIST	3-2	Measuring pulse energy with solid state photodiodes (page 141)
17:40	**End of Session**		

Tuesday, October 18, 2005

Session 4	**Chair – Peter Foukal**	**Remote sensing**	
8:30	Greg Kopp, LASP	4-1	**Invited Talk**, Solar Radiometry from SORCE (page 151)
9:00	Jack Xiong, NASA/GSFC	4-2	Inter-comparison Study of Terra and Aqua MODIS Reflective Solar Bands Using On-orbit Lunar Observations (page 153)
9:20	Hugh Kieffer, CR	4-3	A Model of the Spectral Irradiance of the Moon for Calibration of Earth-orbiting Spacecraft Instruments (page 159)
9:40	Victor Sapritsky, VNIIOFI	4-4	On measuring the radiant properties of objects of observations for the Global Earth Observation System of Systems (GEOSS) (page 157)
10:00	Refreshment break		
Session 4	**Chair – Claus Fröhlich**	**Remote sensing**	
10:30	Peter Foukal, Heliophysics	4-5	**Keynote Talk**, The Solar Bolometric Imager – Recent Results and Future Plans (page 155)
11:00	Anton D. Nikolenko, INP	4-6	Procedures of absolute calibration for the Space Solar Patrol instrumentation at the Synchrotron radiation source (page 163)
11:20	Chris Gueymard, SCS	4-7	Determination of Aerosol Optical Depth and Ångström's Wavelength Exponent Using Sunphotometers and Spectroradiometers: A Preliminary Assessment (page 161)
11:40	Lunch Break / **Poster Session 4,5,6**		
Session 5	**Chair – Antonio Corrons**	**Photometry and Colorimetry**	
14:00	Georg Sauter, PTB	5-1	**Invited Talk**, Review on new developments in Photometry (page 185)
14:30	Christian Monte, BAM	5-2	Linking Fluorescence Measurements to Radiometric Units (page 187)

14:50	Hiroshi Shitomi, AIST	5-3	Photoluminescence from White Reference Materials for Spectral Diffuse Reflectance upon Exposure to the Radiation Shorter than 400 nm (page 189)
15:10	Yuqin Zong, NIST	5-4	A Simple Stray-light Correction Matrix for Array Spectrometers (page 191)
15:30	Refreshment break		
Session 6	**Chair – Maria Luisa Rastello**	**Novel Techniques**	
16:00	Petri Kärhä, TKK	6-1	Determination of luminous intensity of light-emitting diodes with modified inverse-square law (page 211)
16:20	Mike Shaw, NPL	6-2	The Measurement of Surface and Volume Fluorescence at NPL (page 215)
16:40	Antti Lamminpää, TKK	6-3	Characterization of germanium photodiodes and trap detector (page 209)
17:00	Valentina Schettini, IEN	6-4	Single-photon source heralding efficiency and detection efficiency metrology at 1550 nm using periodically poled lithium niobate (page 213)
17:20	**End of Session**		

19:00 Evening Dinner at Schatzalp

Wednesday, October 19, 2005

Session 7	**Chair – Tony Bittar**	**International Comparisons**	
8:30	Nigel Fox, NPL	7-1	**Invited Talk**,
9:00	Joachim Hussong, ATLAS	7-2	Comparison of Measurements of Spectral Irradiance (UV/VIS) by an International Round Robin Test (page 235)
9:20	Emma Woolliams, NPL	7-3	The CCPR K1-a Key Comparison of Spectral Irradiance 250 – 2500 nm: Measurements, Analysis and Results (page 233)
Session 8	**Chair – Tony Bittar**	**Radiometric and Photometric Sources**	
9:40	Joe Rice, NIST	8-1	Hyperspectral Image Projectors for Radiometric Applications (page 253)
10:00	Steven Brown, NIST	8-2	Spatial Light Modulator-based Advanced Radiometric Sources (page 259)
10:20	Refreshment break		
Session 8	**Chair – Martin Huber**	**Radiometric and Photometric Sources**	
10:40	Yoshiro Yamada, AIST	8-3	**Invited Talk**, Application of Metal (Carbide)-Carbon Eutectic Fixed Points in Radiometry (page 249)
11:10	Klaus Anhalt, PTB	8-4	Thermodynamic temperature determinations of Co-C, Pd-C, Pt-C and Ru-C eutectic fixed points cells (page 257)
11:30	David Lowe, NPL	8-5	Reproducible Metal-Carbon Eutectic Fixed-Points (page 255)
11:50	Peter Rosenkranz, BEV	8-6	On Estimation of Distribution Temperature (page 251)
12:10	Lunch Break / **Poster Session 7,8,9**		
Session 9	**Chair – Gerhard Ulm**	**Realisation of Scales**	

14:00	Howard Yoon, NIST	9-1	**Invited Talk**, The Realization and the Dissemination of Thermodynamic Temperature Scales (page 299)
14:30	Rene Monshouwer, NMI	9-2	New method for the primary realization of the spectral irradiance scale from 400 to 900 nm (page 305)
14:50	Uwe Arp, NIST	9-3	From X-rays to T-rays: Synchrotron Source-based Calibrations at SURF III (page 309)
15:10	Mathias Richter, PTB	9-4	The PTB High-Accuracy Spectral Responsivity Scale in the VUV and X-Ray Range (page 303)
15:30	Refreshment break		
Session 9	**Chair – Gerhard Ulm**	**Realisation of Scales**	
16:00	Theo Theocharous, NPL	9-5	The establishment of the NPL infrared relative spectral responsivity scale using cavity pyroelectric detectors. (page 301)
16:20	Jimmy Dubard, LNE	9-6	Infrared Radiometry at LNE: characterization of a pyroelectric detector used for relative spectral responsivity measurement (page 311)
16:40	Sergey Mekhontsev, NIST	9-7	Preliminary Realization of a Spectral Radiance Scale in the Range of 2.5 µm to 20 µm (page 315)
17:00	Pedro Corredera, CSIC	9-8	An integrated sphere radiometer as a solution for high power laser calibrations in fibre optics (page 307)
17:20	Mart Noorma, NIST	9-9	Transfer standard pyrometers for radiance temperature measurements below the freezing temperature of silver at NIST (page 313)
17:40	Chairman SC_NEWRAD	Closing words	
17:50	**End of Session/ End of Conference**		

NEWRAD 2005 Scientific Program-Posters

Day	Session
Monday	1 Absolute Radiometry
	2 UV, Vis, and IR Radiometry
	3 Photolithography and UV Processing
Tuesday	4 Remote Sensing
	5 Photometry and Colorimetry
	6 Novel Techniques
Wednesday	7 International Comparisons
	8 Radiometric and Photometric Sources
	9 Realisation of Scales

Session 1 **Absolute Radiometry**

1. **Measurement of the absorptance of a cryogenic radiometer cavity in the visible and near infrared (NIR) (page 25)**
   M. López, H. Hofer, S. Kück
2. **Grooves for Emissivity and Absorptivity Enhancement in High Performance Cavity Sources and Radiometers (page 27)**
   E. Usadi, R. Montgomery
3. **Pulsed UV spectroradiometry with the primary standard synchrotron radiation sources of high intensity (page 29)**
   S. Anevsky, V. Ivanov, O. Minaeva, V. Sapritsky, Y. Zolotarevsky
4. **New apparatus for the spectral radiant power calibration at CMS of Taiwan (page 31)**
   H.-L. Yu, S.-W. Hsu
5. **VUV and Soft X-ray metrology stations at the International Siberian Synchrotron Radiation center (page 33)**
   V.I. Buhiyarov, N.G. Gavrilov, N.A. Gentselev, B.G. Goldenberg, G.N. Kulipanov, A.A. Legkodymov, V.V. Lyakh, O.I. Meshkov, A.I. Nizovsky, A.D. Nikolenko, V.F. Pndyurin, I.V. Poletaev, E. P. Ya. V. Rakshun, Semenov, M.A. Kholopov, V.A. Chenov, M.A. Sheromov
6. **Experimental study of application of the self-calibration method to certify absolute spectral sensitivity of a scintillation counter in the soft X-ray range. (page 35)**
   A.D. Nikolenko, V.F. Pindyurin, V.A. Chernov, V.V. Lyakh
7. **The metrology line on the SOLEIL synchrotron facility (page 37)**
   M. Lièvre, M-C. Lépy, B. Rougié, J-R. Filtz, J. Bastie, M. Idir, T. Moreno, P. Mercede
8. **Cryogenic radiometer developments at NPL (page 39)**
   J. Ireland, M.G. White, N.P. Fox
9. **Energy Calorimeter for Pulsed Laser Radiometry (page 41)**
   D. Fukuda, K. Amemiya, A. Kamimura, S. Kimura
10. **Characterization of new trap detectors as transfer standards (page 43)**
    J-M Coutin, F. Chandoul, J. Bastie
11. **Measurement of Small Aperature Areas (page 45)**
    J.A. Fedchak, A.C. Carter, R. Datla
12. **Low-Background Temperature Calibration of Infrared Blackbodies (page 47)**
    A.C. Carter, R.U. Datla, T.M. Jung, A.W. Smith, J.A. Fedchak
13. **Cryogenic Radiometers and Absolute Radiometry Instrumentation (page 49)**
    S.R. Lorentz
14. **Consistency of radiometric temperature measurement with a local realization of the ITS-90 from 1700°C to 2900°C (page 51)**
    Ch.W. Park, D.-H. Lee, B.-H. Kim, S.-N. Park

15. **Project of absolute measuring instrument of power of the basis of high temperature superconducting thermometer for soft X-ray radiation (page 53)**
A.D. Nikolenko, V.F. Pindyurin, I.A. Khrebtov, V.G. Malyarov, D.A. Khokhlov, K.V. Ivanov

16. **WRR to SI Intercomparisons 1991-2005 (page 55)**
W. Finsterle, S. Möbus, C. Wehrli, I. Rüedi, and W. Schmutz

Session 2 **UV, VIS, IR Radiometry**

17. **Nonlinearity Measurement of UV Detectors using Light Emitting Diodes in an Integrating Sphere (page 77)**
D.-J. Shin, D.-H. Lee, G.-R. Jeong, Y.-J. Cho, S.-N. Park, I.-W. Lee

18. **Radiometric investigation of a compact integrating sphere based spectral radiance transfer standard (page 79)**
D.R. Taubert, J. Hollandt, A. Gugg-Helminger

19. **Accurate and independent spectral response scale based on silicon trap detectors spectrally invariant detectors (page 81)**
J. Gran, Aa. S. Sudbo

20. **Characterization of detectors for extreme UV radiation (page 83)**
F. Scholze, R. Klein, R. Müller

21. **Realization of high accuracy spectrophotometric system as national standard of regular spectral transmittance coefficient (page 85)**
V. Skerovic, P. Vukadin, V. Zarubica, Lj. Zekovic

22. **Mutual comparison of detectors spectral responsivity to prove stated measurement uncertainty (page 87)**
V. Slerovic, P. Vukadin, V. Zarubica

23. **Calibration of Space Instrumentation in the Vacuum Ultraviolet (page 89)**
M. Richter, A. Gottwald, W. Paustian, F. Scholze, R. Thornagel, G. Ulm

24. **A comparison of the performance of a photovoltaic HgCdTe detector with that of large area single pixel QWIPs for infrared radiometric applications (page 91)**
J. Ishii, E. Theocharous

25. **Stray-light correction of array spectroradiometers using tunable pulsed and cw lasers (page 93)**
A. Sperling, O. Larionov, U. Grusemann, S. Winter

26. **Characterization the performance of UV radiometers monitoring UV disinfection devices (page 95)**
W. Heering, H.-P. Daub

27. **Optical Radiation Action Spectra for Safety Regulations and Their Realization Using Integral Detector Measurement Devices (page 97)**
A. Gugg-Helminger

28. **On potential discrepancies between goniometric and sphere-based spectral diffuse reflectance (page 101)**
F. Manoocheri, S. Holopainen, S. Nevas, E. Ikonen

29. **Correcting for bandwidth effects in monochromator measurements (page 103)**
E.R. Woolliams, M.G. Cox, P.M. Harris, H.M. Pegrum

30. **Establishment of Fiber Optic Measurement Standards at KRISS (page 105)**
S.K. Kim, D.H. Lee, D.H. Lee, H.S. Moon, S.N. Park, J.C. Seo

31. **Detector-based NIST-traceable Validation and Calibration of Infrared Collimators (page 107)**
H.W. Yoon, G.P. Eppeldauer, J.P. Rice, J. Brady

32. **Long-term calibration of a New Zealand erythemal sensor network (page 109)**
J.D. Hamlin, K.M. Nield, A. Bittar

33. **Drift in the absolute responsivities of solid-state photodetectors at two NMIs (page 111)**
K.M. Nield, J.D. Hamlin, A. Bittar, P.B. Lukins

34. **Radiance source for CCD low-uncertainty absolute radiometric calibration (page 113)**
A. Ferrero, J. Campos, A. Pons

35. **Improved NIR spectral resonsivity scale of the PTB and implications for radiation thermometry (page 115)**
A.E. Klinkmüller, P. Meindl, U. Johannsen, N. Noulkhow, L. Werner

36. **Characterization of a portable, fiber-optic coupled spectroradiometer as a transfer radiometer for the calibration of the Robotic Lunar Observatory (page 117)**
B.C. Johnson, S.W. Brown, J.J. Butler, M. Hom, B. Markham, S.F. Biggar, T.C. Stone

37. **Synchrotron radiation based irradiance calibration of deuterium lamps from 200 nm to 400 nm at SURF III (page 119)**
P.-S. Shaw, U. Arp, R.D. Saunders, D.J. Shin, H.W. Yoon, Ch.E. Gibson, Z. Li, K.R. Lykke

38. **The Spectral Irradiance and Radiance responsivity Calibrations using Uniform Sources (SIRCUS) facility at NIST (page 121)**
S.W. Brown, J.P. Rice, G.P. Eppeldauer, J. Houston, J. Zhang, K.R. Lykke

39. **NIST BXR I Calibration (page 123)**
A. Smith, T. Jung, J. Fedchak, A. Carter, R. Datla

40. **NIST BXR II Infrared Transfer Radiometer (page 125)**
T. Jung, A. Smith, J. Fechak, A. Carter, R. Datla

41. **Spectral responsivity interpolation of silicon CCDs (page 129)**
A. Ferrero, J. Campos, A. Pons

42. **Monochromator Based Calibration of Radiance Mode Filter Radiometers for Thermodynamic Temperature Measurement (page 131)**
R. Gobel, M. Stock, Y. Yamada

43. **Study of the Infrared Emissivity of Fixed-Point Blackbody Cavities (page 133)**
L. Hanssen, S. Mekhontsev, V. Khromchenko, A. Prokhorov, J. Zeng

44. **Radiometric Stability of a Calibration Transfer Standard Spectroradiometer and a Spectralon Sphere Illuminated Internally or Externally (page 135)**
D.F. Heath, M.G. Kowalewski

Session 3 **Photolithography and UV Processing**

45. **Vacuum ultraviolet quantum efficiency of large-area SiC photodiodes (page 143)**
R.E. Vest, S. Aslam

46. **Spatial Anisotropy of the Exciton Resonance in CaF_2 at 112 nm and its Relation to Optical Anisotropy in the DUV (page 145)**
M. Richter, A. Gottwald, M. Letz

47. **Comparison of spectral irradiance responsivity scales of TKK and NIST in the UVA region (page 147)**
J. Envall, B.C. Johnson, P. Kärhä, T. Larason, E. Ikonen

Session 4 **Remote Sensing**

48. **Using a Blackbody to Determine the Longwave Responsivity of Shortwave Solar Radiometers for thermal offset error connection (page 165)**
I. Reda, J. Hickey, D. Myers, T. Stoffel, S. Wilcox, C. Long, E.G. Dutton, D. Nelson, J.J. Michalsky

49. **On the drifts exhibited by cryogenically cooled InSb infrared filtered detectors end their importance to the ATSR-2 and Landsat-5 earth observation mission. (page 167)**
E. Theocharous

50. **On-Orbit Characterization of Terra MODIS Solar Diffuser Bi-directional Reflectance Factor (BRF) (page 169)**
X. Xiong, V.V. Salomonson, J. Sun, J. Esposito, X. Xie, W.L. Barnes, B. Guenther

51. **Space solar patrol mission for monitoring of the extreme UV and X-ray radiation of the Sun (page 171)**
I. Afanas'ev, S. Avakyan, N. Voronin

52. **Multi-channel ground-based and airborne infrared radiometers (page 173)**
G. Brogniez, M. Legrand, B. Damiri, I. Behnert, J.-P. Buis

53. **Thermal Modelling and Digital Servo Algorithm for the next generation of Differential Absolute Radiometer (page 175)**
S. Mekaoui, S. Dewitte

54. **Calibration of Filter Radiometers for Weathering and Photostability Tests (page 177)**
A. Schönlein

55. **Radiometric Calibration of a Coastal Ocean Hyperspectral Imager Using a Blue Enhanced Integrating Sphere (page 179)**
D.R. Korwan, J.H. Bowles, W.A. Snyder, M.R. Corson, C.O. Davis

56. **A Verification of the Ozone Monitoring Instrument Calibration Using Antarctic Radiances (page 181)**
G. Jaross, J. Warner, R.P. Cebula, A. Kashlinsky

Session 5 **Photometry and Colorimetry**

57. **New robot-based gonioreflectometer for measuring spectral diffuse reflection (page 193)**
D. Hünerhoff, U. Grusemann, A. Höpe

58. **Rotational radiance invariance of diffuse reflection standards (page 195)**
A. Höpe

59. **Minimizing Uncertainty for Traceable Fluorescence Measurements – The BAM Reference Fluorometer (page 197)**
C. Monte, W. Pilz, U. Resch-Genger

60. **Development of a total luminous flux measurement facility for LEDs at the National Metrology Institute of Japan (page 199)**
K. Godo, T. Saito, H. Shitomi, T. Zama, I. Saito

61. **Determination of the diffuser reference plane for accurate photometric and radiometric measurements (page 201)**
J. Hovila, P. Manninen, L. Seppälä, P. Kärhä, L. Ylianttila, E. Ikonen

62. **Development of a luminance Standard (page 203)**
A. Corróns, J. Fontecha

63. **Measuring photon quantities in the International System of Units (page 205)**
M.L. Rastello

Session 6 **Novel Techniques**

64. **The evaluation of a pyroelectric detector with a carbon multi-walled nanotube coating in the infrared. (page 217)**
E. Theocharous, R. Deshpande, A.C. Dillon, J. Lehman

65. **UV detector calibration based on an IR reference and frequency doubling (page 219)**
J. Hald, J.C. Petersen

66. **Non selective thermal detector for low lower measurements (page 221)**
F. Durantel, D. Robbes, B. Guillet, J. Bastie

67. **Calibration of Current-to-voltage Converters for Radiometric Applications at Picoampere Level (page 223)**
P. Sipilä, R. Rajala, P. Kärhä, A. Manninen, E. Ikonen

68. **Simplified diffraction effects for laboratory and celestial thermal sources (page 225)**
E.L. Shirley

69. **Widley Tunable Twin-Beam Light Source based on Quasi-Phased-Matched Optical Parametric Generator as a Spectral Responsivity Comparator between InGaAs and Si Photodiodes (page 227)**
D.-H. Lee, S.-N. Park, S.K. Kim, J.-Y. Lee, S.-K. Choi, H.-S. Park, C.-Y. Park

70. **Measurement of quantum efficiency using the correlated photon technique (page 229)**
J.Y. Cheung, P.J. Thomas, C.J. Chunnilall, J.R. Mountford, N.P. Fox

Session 7 **International Comparisons**

71. **APMP PR-S1 comparison on irradiance responsivity of UVA detectors (page 237)**
G. Xu, X. Huang, Y. Liu

72. **Comparison Measurements of Spectral Diffuse Reflectance (page 239)**
S. Nevas, S. Holopainen, F. Manoocheri, E. Ikonen, Y. Liu, T.H. Lang, G. Xu

73. **Comparison of mid-infrared absorptance scales at NMIJ and NIST (page 241)**
J. Ishii, L.M. Hanssen

74. **Comparison of photometer calibrations at six different facilities of PTB and NIST (page 243)**
S. Winter, D. Lindner, A. Sperling, G. Sauter, S. Brown, T. Larason, Y. Zong, Y. Ohno

75. **A Comparison of Re-C, Pt-C, and Co-C fixed-point cells between NIST and NMIJ (page 245)**
N. Sasajima, F. Sakuma, Y. Yamada, H.W. Yoon, C.E. Gibson, V. Khromchenko

Session 8 **Radiometric and Photometric Sources**

76. **Novel subtractive band-pass filters based on coloured glasses. (page 261)**
E. Theocharous

77. **Analysis of the Uncertainty Propagation through Fitting Spectral Irradiance Data (page 263)**
S. Nevas, A. Lamminpää, P. Kärhä, E. Ikonen

78. **Absolute linearity measurements on a PbS detector in the infrared (page 265)**
E. Theocharous

79. **Comparison of two methods for spectral irradiance scale transfer (page 267)**
K.M. Nield, J.D. Hamlin, A. Bittar

80. **Precision Extended-Area Low Temperature Blackbody BB100-V1 for IR Calibrations in Medium Background Environment (page 269)**
S. Ogarev, M. Samoylov, V. Sapritsky, A. Panfilov, S. Koichi, T. Kawashima

81. **Flash Measurement System for the 250 – 2100 nm Wavelength Range (page 271)**
J. Blanke, G. Mathe

82. **A normal broadband irradiance (Heat Flux) calibration facility (page 273)**
M. Ballico, E. Atkinson

83. **A laser-based radiance source for calibration of radiation thermometers (page 275)**
M. Ballico, P.B. Lukins

84. **Furnace for High-Temperature Metal (Carbide)-Carbon Eutectic Fixed-Point (page 277)**
B. Khlevnoy, M. Sakharov, S. Ogarev, V. Sapritsky, Y. Yamada, K. Anhalt

85. **Investigations of Impurities in TiC-C Eutectic System as a Fixed Point (page 279)**
A. Bourdakin, M. Sakharov, B. Khlevnoy, S. Ogarev, V. Sapritsky, A. Elyutin

86. **Determining the temperature of a blackbody based on a spectral comparison with a fixed temperature blackbody (page 281)**
T. Zama, I. Saito

87. **High-temperature fixed-point radiators: The effect of the heat exchange between cavity and furnace tube on the effective emissity of the radiator (page 283)**
P. Bloembergen, Y. Yamada, B.B. Khlevnoy, P. Jimeno Largo

88. **Long-term experience in using deuterium lamp systems as secondary standards of UV spectral irradiance (page 285)**
P. Sperfeld, J. Metzdorf, S. Pape

89. **High-temperature fixed-point radiators: The effect of the heat exchange within the cavity and between cavity and furnace tube on the temperature drop across the black will of the cavity (page 287)**
P. Bloembergen, Y. Yamada, P. Jimeno Largo, B.B. Khlevnoy

90. **A Comparison of Co-C, Pd-C, Pt-C, Ru-C and Re-C eutectic fixed points independently by three different institutes (page 289)**
K. Anhalt, J. Hartmann, D. Lowe, G. Machin, M. Sadli, Y. Yamada, P. Bloembergen

91. **Irradiance measurements of Re-C, TiC-C and ZrC-C fixed point blackbodies (page 291)**
K. Anhalt, P. Sperfeld, J. Hartmann, M. Sakharov, B. Khlevnoy, S. Ogarev, V. Sapritsky

92. **Evaluation and improvement of the performance of a commercially available detector stabilized radiance sphere source (page 293)**
E.F. Zalewski, S.F. Biggar

93. **The Spectrally Tunable LED light Source – Design and Development Issue (page 295)**
I. Fryc, S.W. Brown, Y. Ohno

Session 9 **Realisation of scales**

94. **New photometric standards development at NIM-Romania (page 317)**
M. Simionescu, A. Seucan, J. Bastie, A. Stepnik

95. **Distribution temperature scale realization at NIM-Romania (page 319)**
M. Simionescu, A Seucan, B. Rougie

96. **Gloss standard calibration by spectrophotometer reflectance measurement-suggested method (page 321)**
A. Andersson

97. **Absolute cryogenic radiometry in the extreme ultraviolet at NIST (page 323)**
R.E. Vest, S. Grantham, C. Tarrio

98. **Detailed Comparison of Illuminance Scale Realizations of KRISS and TKK (page 325)**
S.-N. Park, D.-H. Lee, Y.-W. Kim, I.-W. Lee, E. Ikonen, M. Noorma, F. Manoocheri

99. **Radiometric Temperature Comparisons of Three NIST Gold Freezing-point Blackbodies (page 327)**
N. Sasajima, C.E. Gibson, V. Khromchenko, R.D. Saunders, H.W. Yoon

100. **Characterization of Thermopile for Laser Power Measurements (page 329)**
A.K. Türkoglu

101. **Detector Based Traceability Chain Established at the UME (page 331)**
F. Sametoglu, O. Bazkir, O. Celikel

102. **Comparison of the PTB Radiometric Scales for UV Source Calibration (page 333)**
R. Friedrich, J. Hollandt, W. Paustian, M. Richter, P. Sperfeld, R. Thornagel

103. **Spectral Responsivity Scale between 1 µm and 19 µm at the NIST (page 335)**
G.P. Eppeldauer, J. Zeng, L.M. Hanssen

104. **Realization of the NIST total Spectral Radiant Flux Scale (page 337)**
Y. Ohno, Y. Zong

105. **Goniometric Realisation of Reflectance Scales in the Ultra Violet to Near Infrared (page 339)**
M.J. Shaw, C.J. Chunnilall

Session 1

Absolute Radiometry

Absolute Accuracy of Total Solar Irradiance Measurements in Space

C. Fröhlich

Abstract. Accurate measurements of total solar irradiance (TSI) from space with electrically calibrated radiometers started on NIMBUS-7 launched in November 1978. Since then a set of TSI measurements is available which covers now more than 25 years. During this period results from at least two independent experiments on different spacecraft are available. Comparing the measurements made by the different radiometers, HF on NIMBUS 7, ACRIM I on SMM, ERBE on ERBS, ACRIM II on UARS, VIRGO on SOHO and ACRIM III on ACRIMSat, the differences in the absolute value decreased from more than ±0.3% to within about ±0.15% in the course of the years indicating an improvement of the scale representation and its transfer to space. This confirmed also the stated uncertainty of the individual radiometers of less than about 0.2%. With the launch of SORCE in 2003 this situation changed drastically as the radiometer TIM showed results which were more than 0.3% lower than those of the other experiments simultaneously in space, although its stated uncertainty is estimated to be of the order of a few 0.01%. This major difference initiated a workshop which was organized by NIST at Gaithersburg in July 2005 to discuss the problem in terms of absolute uncertainty estimates and how this difference could possibly be resolved. This presentation will summarize the outcome of this workshop and report on the conclusions. More specifically, the results of the detailed uncertainty analysis of all current space experiments will be discussed in some detail.

C. Fröhlich: Physikalisch-Meteorologisches Observatorium Davos, World Radiation Center, CH 7260 Davos, Switzerland
E-mail: cfrohlich@pmodwrc.ch

Reflecting Cavity Blackbodies for Radiometry

E. Usadi
National Physical Laboratory, Middlesex, UK

Abstract Nearly 20 years ago Quinn and Martin presented a novel blackbody design with an absorbing end face and highly reflecting side walls. This blackbody had the considerable advantage of being less sensitive to temperature gradients along the side walls (potentially of several degrees Celsius) compared to an all-black cavity. Recent work at NPL has developed this concept further, laying out the conceptual framework in simple terms, analyzing potential pitfalls such as diffraction, and describing a design which closely matches the theoretical best performance.

Summary

Blackbody sources with reflecting side walls are, when designed correctly, less sensitive than absorbing cavities to thermal gradients along the cavity length. This fact offers benefits for primary standard instruments, since these tend to be long and require the highest and most uniform emissivities. Furthermore, since a reflecting cavity design allows thermal engineering requirements to be relaxed, mass and size reductions for high emissivity transfer standard sources for both laboratory and space flight applications is possible.

The rationale for having a blackbody with reflecting rather than absorbing side walls was established in 1986 [Quinn]. The argument can be summarised as follows. Suppose the rear wall of the cavity is thermally uniform and has an emissivity ε_0. Here "rear wall" refers to the section of the cavity interior which can be directly viewed by a detector. Suppose further that a temperature gradient exists along the length of the cavity, i.e. along the side walls. Then as Quinn and Martin show (assuming, for simplicity, an arbitrarily small cavity aperture) the deviation from 1 of the effective emissivity of a reflecting side wall cavity is (n ε_1) times that of an absorbing side wall cavity. Here n is the number of reflections a typical ray emitted by the rear wall experiences within the cavity before impinging again on the rear wall; ε_1 is the emissivity of the reflecting side wall, equal to one minus the wall reflectivity and hence much less than one. Thus for small n, the reflecting side wall cavity has an effective emissivity closer to one than does an absorbing side wall cavity.

This argument breaks down as the thermal gradient along the cavity length approaches zero. An isothermal cavity with absorbing walls has a higher emissivity than one with partly reflecting walls. This paper will discuss, for the first time, the conditions for which a reflecting cavity is advantageous. We will answer the question: for what thermal gradients does the reflecting cavity outperform the absorbing cavity?

Since the optimal reflecting cavity reflects radiation emitted by the cavity rear plate back onto the plate after one bounce, the optimal design is a spherical reflector with a high emissivity rear plate positioned to overlap with the center of the sphere. The output aperture is a hole in the reflector, so that only the absorbing plate is directly visible to a radiometer. Radiation emitted by the plate either directly exits the aperture or returns to the plate after a single reflection from the cavity wall.

An estimate of the cavity absorptivity, and hence, by invoking the Kirchoff Law and the reciprocity theorem, the cavity emissivity, can easily be made by calculating the fractional loss of diffuse radiation from the plate through the aperture. For a fixed aperture size, increasing the distance from the plate to the aperture increases the emissivity. However, as this distance is also the radius of the spherical reflector, the size of a high emissivity blackbody can easily become unwieldy. In earlier designs, a " Christmas tree " shaped reflector was used to approximate the spherical reflector. This paper will describe our recent work, employing better ray tracing techniques than originally available, which establishes an optimum shape for a reflecting cavity which maintains practical dimensions.

An absorbing cavity absorbs and, therefore emits, radiation over a full hemisphere with an approximately lambertian distribution. This ensures that diffraction at the blackbody aperture can be neglected. For a reflecting cavity, however, the directional emissivity is sensitive to the reflector design and may be very far from lambertian. In this case diffraction cannot be neglected. Recent work on diffraction in radiometry has shown that the Fresnel and paraxial approximations used in nearly all diffraction loss calculations to date may introduce errors of several tenths of a percent [Edwards]. Therefore careful design which either creates lambertian emission over the full hemisphere or enables an accurate diffraction loss calculation is critical for reflecting cavity blackbodies. This paper will discuss the diffraction problem in some detail and include design solutions which minimise or eliminate it.

Acknowledgments The author would like to thank the Department of Trade and Industry of the UK for supporting this work.

References

Quinn, T. J., J. E. Martin, A Black-body cavity for total radiation thermometry, *Metrologia, 23*, 111-114, 1986.

Edwards, P. J., *Diffraction Theory and Radiometry*, PhD Thesis, Imperial College, 2004.

Low-uncertainty absolute radiometric calibration of a CCD

A. Ferrero, J. Campos and A. Pons
Instituto de Física Aplicada, CSIC, Madrid, Spain

Abstract. A low-uncertainty absolute radiometric calibration system for CCDs has been developed. The calibration experimental setup and procedure are shown. The calibration procedure has been carried out by direct substitution. The CCD responsivity is also shown. The uncertainty budget has been analyzed in detail. The obtained uncertainty contribution apart from the reference radiometer uncertainty (0.29%, k=1) is about 0.18%.

Introduction

In addition to their wide use as imaging systems, CCD cameras would be very interesting measurement instruments for optical radiation if the measurement uncertainty was kept low[1]. For CCD calibration, it is necessary bearing in mind, unlike a photodiode calibration, that it is a two dimensional calibration and the added charge transfer and electronic problems. The low-uncertainty calibration of a CCD requires the previous design of a stable and uniform radiance source, whose radiance could be measured with low uncertainty. The designed source was an externally dye laser illuminated integrating sphere[2]. The radiance measurement was carried out by a silicon radiometer.

In this work, the calibration procedure is explained, and the results for an absolute radiometric calibration for an interline Sony ICX414AL having 640 x 480 pixels (9.9μm x 9.9μm) are shown. It is integrated in a camera, model Imager Compact, that has got a 12 bits A/D converter.

Experimental setup and procedure

The source consists of an integrating sphere externally illuminated by a power-stabilized dye laser. It was proved that this source is uniform and lambertian[2]. A rotating diffuser is located before the sphere's entrance port in order to reducing the speckle noise of the laser radiation[3,4]. For the calibration, it is not possible to locate the CCD at the plane of the exit port plane, because it is necessary to avoid radiation from direct incidence and first reflection. The exit port-CCD distance where there is enough uniformity for the calibration was studied. For this study was considered the shadow of the CCD mount over the own CCD, the radiation from direct incidence and first reflection, the field uniformity and the variation of the responsivity at different solid angles. As the pixels have different responsivity at different solid angles, it is necessary to know the maximum solid angle that assures a responsivity variation with respect to normal incidence smaller than the wanted measurement uncertainty. For determining this solid angle, the response of every pixel was evaluated increasing the exit port-CCD distance, finding that pixels' relative response becomes constant at a given distance. This distance defines the calibration solid angle.

The calibration is carried out by direct substitution, using a 10 ms exposure time. It was proved that at this exposure time there were not linearity problems produced by the relation between the exposure time and the readout time[5]. We consider the best CCD alignment the position where the most uniform response across the whole CCD is obtained. As reference radiometer was employed a silicon photodiode of proven linearity with an aperture. This photodiode was calibrated respect to the Spectral Responsivity Scale of Instituto de Física Aplicada (IFA)[6], that has got a standard uncertainty of 0.29%.

The responsivity measurement equation is

$$R_i = \frac{(N_i - N_{o,i})R_{rad}}{C_{NL,i} t_{\exp} r_{rad}} \quad (1)$$

where N_i is the pixel i response, $N_{o,i}$ is the pixel i dark signal, t_{exp} is the exposure time, r_{rad} is the response of the radiometer, R_{rad} is the responsivity of the radiometer, and $C_{NL,i}$ is a response non linearity correction factor. We have calculated $C_{NL,i}$ by studying, at constant irradiance, the variation of $(N_i-N_{o,i})/t_{exp}$ for several exposure times. Then the relation between a relative responsivity and N_i is obtained. So, R_i is a corrected responsivity, and has to be a constant for a given wavelength.

The calibration procedure was carried out measuring R_i for several wavelengths. We did this procedure three times in order to calculate the procedure uncertainty. N_i and E_i were averaged to minimize temporal noise. The higher N_i value, the lower CCD relative uncertainty. The calibration wavelengths were chosen according to the slope and curvature of a typical R_i, bearing in mind a potential interpolation.

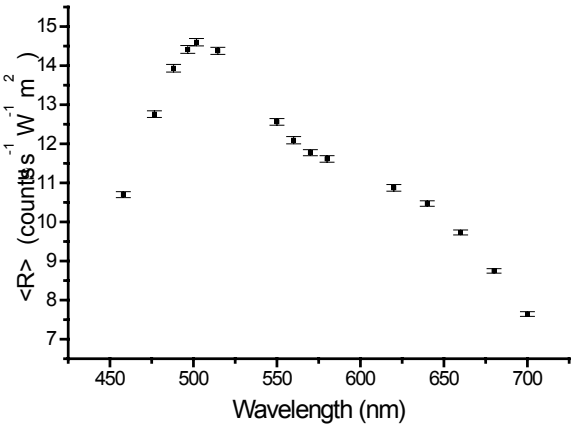

Figure 1: Average spectral responsivity of CCD Sony ICX414AL.

Results

In figure 1 the averaged spectral responsivity across the

whole CCD in the range (460 nm - 700 nm) is shown. The averaged responsivity value is very similar to the responsivity values of all the pixels. In fact, the relative standard deviation of the pixels' responsivity is between about 0.4% (at 550 nm) and about 1% (at 460 nm).

A maximum in responsivity is observed at about 500 nm, and an inflexion point at about 600 nm. All the wavelengths were obtained using only two dies (550 nm - 580 nm, 620 nm - 700 nm) and argon lines (458 nm-514.6 nm).

The total uncertainty never reaches 0.4% (k=1). It was evaluated from the field non uniformity (0.012%, calculated from a lambertian disc model for the exit port[2]), the repeatability of the calibration procedure (around 0.1%, accounting repeatability of alignment, radiometer response and CCD response), the reference radiometer uncertainty (0.29%), and the CCD uncertainty, that is estimated bearing in mind the charge transfer noise, the quantization noise and the residual non linearity noise after the correction by $C_{NL,I}$ (each of these contributions to the CCD uncertainty is shown in figure 2). The larger contribution to the CCD uncertainty is the charge transfer noise. The higher N_i, the lower the CCD relative uncertainty.

It is useful to determine a function that relates the CCD relative uncertainty to N_i in order to know it for each N_i. This uncertainty goes from 0.6% (few counts) to 0.1% (close to the count saturation level). Therefore, it is important to carry out the calibration at a high count level.

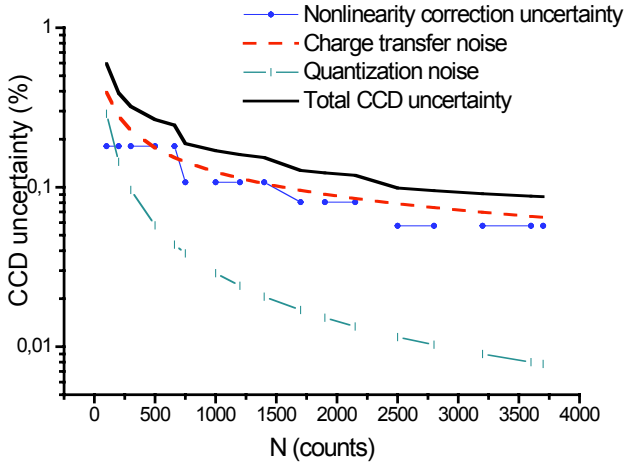

Figure 2: CCD uncertainty budget.

The total uncertainty of the absolute calibration and the quoted contributions are shown in figure 3. The obtained uncertainty contribution apart from the reference radiometer uncertainty is about 0.18%, so the calibration procedure can be considered good.

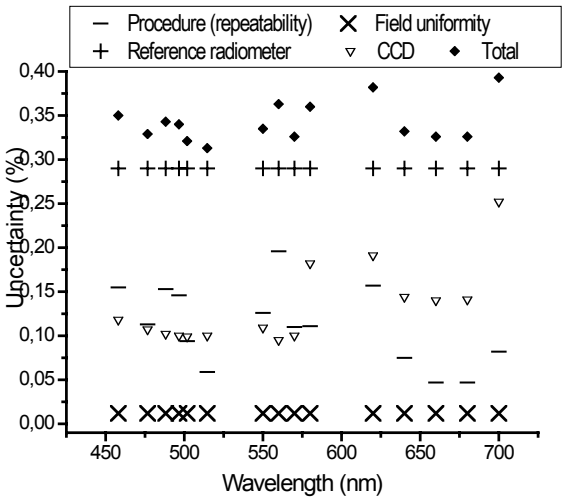

Figure 3: Calibration uncertainty budget.

Conclusions

A CCD absolute radiometric calibration system has been developed. We have analyzed in detail and quoted the uncertainty sources that contribute to the total uncertainty. The obtained uncertainty contribution apart from the reference radiometer uncertainty (0.29%, k=1) is about 0.18%.

Acknowledgments This work has been supported by the thematic network DPI2002-11636-E and the project DPI2001-1174-C02-01.

References

1. J. Campos, Radiometric calibration of charge-coupled-device video cameras, *Metrologia*, 37, 459-464, 2000.
2. A. Ferrero, J. Campos and A. Pons, Radiance source for CCD absolute radiometric calibration, *NewRad (sent)*, Davos, 2005.
3. S. Lowenthal, D. Joyeux and H. Arsenault, Relation entre le deplacement fini d'un diffuseur mobile, eclaire par un laser, et le rapport signal sur bruit dans l'eclairement observe a distance finie ou dans un plan image, *Optics Communications,* 2, No. 4, 184-188, 1970.
4. E. Schroeder, Elimination of granulation in laser beam projections by means of moving diffusers, *Optics Communications,* 3, No. 1, 68-72, 1970.
5. A. Ferrero, J. Campos and A. Pons, Violation of the radiant exposure reciprocity law in interline CCDs, *In preparation,* 2005.
6. J. Campos, A. Pons and P. Corredera, Spectral Responsivity Scale in the Visible Range based on single silicon photodiodes, *Metrologia*, 40, S181-S184, 2003.

NIST Reference Cryogenic Radiometer Designed for Versatile Performance

J. Houston, and J. Rice

National Institute of Standards and Technology, Gaithersburg, MD, USA

Abstract. We describe the unique design concept of modularity and versatility in the construction of a new cryogenic radiometer developed at NIST. We address the benefits of the modular design in the construction and development and discuss some of the device characterizations and results of a cryogenic radiometer intercomparison.

Introduction

Cryogenic electrical substitution radiometers presently provide the basis for optical measurements in most national measurement institutes. The National Institute of Standards and Technology (NIST) required a new cryogenic radiometer that would provide the lowest possible uncertainty and yet would not become quickly obsolete. The new radiometer needed to have the versatility to grow with NIST's needs, to embrace new technologies, and most especially still be able to provide laser power measurements with uncertainties of 0.01% or better over a range of power levels from μW to mW. Additionally, the radiometer needed to have an improved thermal performance and the ability to calibrate a variety of different optical detectors.

Design

The cryogenic radiometer that was designed and built at NIST is called the Primary Optical Watt Radiometer (POWR), previously known as HACR 2. POWR has replaced the previous High Accuracy Cryogenic Radiometer (HACR). While POWR measures optical power responsivity of detectors using lasers, the unique element of the NIST design is the concept of modularity. The radiometer can be divided into three main sections: the cryostat, the detector module that consists of the receiver cavity, heat sink, and thermal anchor, and finally the optics section. Each of these three components has design elements that contribute to POWR's versatility. In the cryostat itself the base of the helium reservoir is a 381 mm diameter plate, called the cold plate, that contains a series of threaded holes. The critical experimental elements mount and are thermally anchored to the cold plate and are easily removed or replaced. A series of wiring paths that support the different types of four-wire heaters and thermometry and two-wire thermometry are connectorized inside the radiometer for ease of removal. One final element in the actual cryostat design is that it can be operated at two different temperatures, at 4.2 K for most measurements and at 2 K to reduce the thermal noise in the measurement of significantly lower optical powers.

The detector module design is critical in that the goal was to achieve laser power measurements with 0.01% uncertainty at the microwatt and milliwatt levels and yet achieve the modularity to exchange receiver cavities. The detector module design is comprised of four main elements: the cold block, the thermal anchor, the heat sink, and the receiver cavity. The receiver cavity and the thermal anchor were specifically designed to provide the expected radiometric performance of POWR, the ability to measure μW to mW optical power with 0.01% uncertainties or better. The heat sink design includes a place to mount the thermal anchor and a 20 mm diameter receiver cavity combination, and a limiting entrance aperture. Heaters and thermometers on the heat sink regulate its temperature to reduce the noise and uncertainty in the receiver cavity's measurements. The receiver cavity/heat sink module then mounts into the cold block. The main purpose of the cold block is to provide a helium temperature background that surrounds the receiver cavity. The cold block is the part of the detector module that attaches to the cold plate and is thermally anchored to the liquid helium reservoir.

The front optics section includes the window section. Besides the Brewster angle window, this front optics section design provides the opportunity to measure the window transmittance in-situ. Attached between the window and the cryostat is a large, five-way cross. This cross is the location for a trap detector to be inserted to measure the transmittance of an installed window.

Construction

The cryostat is designed and tested for improved thermal and mechanical performance. The helium reservoir holds almost 100 L of liquid helium to provide a measured hold time of 14 days for normal operation. An annular reservoir of liquid nitrogen surrounds the helium reservoir for thermal insulation. The base of the helium reservoir is 304 stainless steel with helicoils for longterm mechanical performance (Figure 1). The wiring for the thermometry is phosphor bronze.

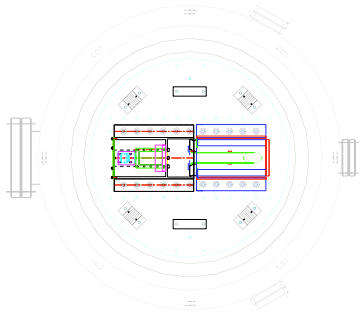

Figure 1. POWR's cold plate provides a series of threaded holes to mount all critical experimental components. The Detector Module and baffle section are mounted from right to left onto the cold plate. The laser beam enters from the left through the baffle section into the receiver cavity. Four thermal anchors for the wiring and two thermal anchors for the wire connectors are on the perimeter of the cold plate.

The detector module itself was initially built and tested with the following elements (Figure 2). The receiver cavity is an electroformed copper cylinder, 20 mm in diameter and 150 mm long. A 30-degree slant closes

off the back end of the cavity. The cavity is coated with a specular black paint. One heater is noninductively wrapped on the closed end of the cavity, with another two chip heaters attached to the back slant. The germanium resistance thermometer is located on the cylinder barrel. All wiring from the detector module ends in connectors to provide easy detachment. A Kapton thermal anchor attaches the receiver cavity to the heat sink. Both the heat sink and the cold block are made of OFHC copper that is plated first with nickel and then gold. All surfaces are highly polished and reflective to reduce any radiative effects.

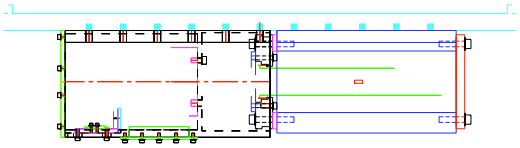

Figure 2. The Detector Module is on the right half with the receiving cavity mounted onto the heat sink and surrounded by the cold block. On the left side is the baffle section with the off axis parabolic mirror and silicon photodiode combination.

While the majority of the detector section itself remained unchanged, the receiver cavity and some thermometry evolved until POWR achieved the desired performance. The receiver cavity evolved until the performance was achieved in Detector Module 3. Additionally the wiring was changed to provide the capability for a feed-forward temperature control loop algorithm.

One element designed into the measurement is the determination of the light scatter magnitude. This was achieved by placing a baffle section attached to the cold block located directly in front of the detector module, and additional baffles along the interior optical path. The baffle section collects the scattered radiation with an off axis parabolic mirror that surrounds the laser beam and reflects the scattered radiation into a silicon photodiode for measurement.

The evolving detector module demonstrates the benefits of the modular design. While the construction and wiring of each detector module required days of work, the actual exchange of detector modules in the cryostat itself took less than one day. A connectorized detector module was easily replaced in the cryostat.

Measurements

The detector modules after being painted and built were measured outside the cryostat for reflectance (from which absorptance is inferred) at three different wavelengths. The measurements were done against NIST PTFE reflectance standards. The final cavity had absorptances of 0.999995 at 633 nm. Because the radiometer is versatile, the detector module can easily be removed and tested over time to see if the paint and absorptance is stable.

Once Detector Module 3 was installed into the cryostat two types of measurements commenced, first the characterization of the electrical to optical equivalence and second the calibration of traps. A full discussion of POWR's characterization is to be discussed in a future paper. The calibration of the traps was performed in two different configurations, one with the traps on a separate translation stage in front of the window, and a second with the traps in the optical plane of the receiver cavity on the translation stage that moves the radiometer itself. In the end the second setup was used. The same traps measured by POWR were measured by other cryogenic radiometers at NIST and the calibrations agreed within 0.01% to 0.02% which is well within the three radiometers' uncertainties (Table 1). A full discussion of this intercomparison will be published later.

Table 1. Results of a comparison of three cryogenic radiometers measuring trap detector, presented in terms of the difference from the POWR-measured responsivity of a silicon photodiode trap detector.

Cryogenic radiometer	488 nm	514 nm	633 nm
L1 ACR	-0.021%	-0.002%	-0.011%
LOCR	-0.005%	0.020%	0.001%

The radiometer Brewster-angle window was measured in-situ, but not in vacuum. The Brewster-angle window was optimized for 633 nm and maintained in that alignment for the calibrations. The transmittances at each wavelength were measured before and after the trap calibrations. For the window transmittance measurement the trap was inserted inside the five way cross and aligned to the laser beam. The trap was removed for POWR's calibration cycles. A typical window transmittance was 0.999921 with an uncertainty of .0012% at 633 nm.

Conclusion

A new NIST reference cryogenic radiometer, POWR, has been developed. The goal in the development of the POWR was to have the versatility in design so that detector modules could be exchanged while providing optical power measurements at uncertainties of 0.01% or better. Final characterization measurements on Detector Module 3 (Rice, et al.) are soon to be completed, but the exchanging of the first three detector modules and the performance of the third module shows that POWR has achieved this goal. In the future, as technology changes or there are special requests for measurements at different power levels or wavelengths, POWR will be able to meet the needs.

Acknowledgements. We would like to thank Steven Lorentz and Joe O'Connell for their contributions in the construction of POWR. Responsivity measurements from the L1 ACR were provided by Steve Brown and Keith Lykke, and for the LOCR by David Livigni. We would like to thank Albert C. Parr, Chief of the Optical Technology Division at NIST, for his continued support of this project.

Measurement of the absorptance of a cryogenic radiometer cavity in the visible and near infrared (NIR)

M. López[1,2], H. Hofer[2] and S. Kück[2]

[1] Centro Nacional de Metrología, 76241 Querétaro, México

[2] Physikalisch-Technische Bundesanstalt, Braunschweig 381116, Germany

Abstract. Results of the measurement of the absorptance of a LaseRad cavity used as an absorber in the cryogenic radiometer in the Physikalisch-Technische Bundesanstalt (PTB) are presented. The measurements were carried out at several laser wavelengths in the visible and near infrared (NIR); at 633 nm, 1280 nm - 1360 nm and 1480 nm – 1620 nm. The absorptance of 0.999885 ± 3.0 × 10^{-6} measured at 633 nm matches very well with the value of 0.999879 ± 1.0 × 10^{-5} reported by the manufacturer (Cambridge Research & Instrumentation, Inc.) . In the NIR the absorptance is approx. 1.1 × 10^{-4} ± 3 × 10^{-6} lower than at 633 nm, which is significant for high accuracy measurements. In the wavelength range from 1280 nm to 1620 nm, the absorptance varies by 19 × 10^{-6} which is almost negligible for this wavelength range.

1. Introduction

In the last decade, the demand for calibration services in the field of optical communication through optical fiber had increased substantially and consequently also the need of lower measurement uncertainties. Therefore, the PTB and also other National Metrology Institutes (NMIs) work on transfer standards (Ge and InGaAs photodiodes) calibrated directly against the Cryogenic Radiometer (CR), the primary standard for optical power measurement, in the near infrared (mainly around 1300 nm and 1550 nm) [1-4]. Thus, uncertainties below 4×10^{-4} have been obtained in these wavelength ranges. In general, two correction factors contribute to the CR measurement accuracy: the non-ideal absorption coefficient α of the cavity and the non-ideal transmittance τ of the Brewster-angle window. Usually, the absorption coefficient at 632.8 nm reported by the manufacturer is used in the PTB and other NMIs and considered to be constant for other wavelength ranges [1-4]. However, to achieve lower measurement uncertainties, it is necessary to know the exact spectral distribution of both coefficients.

In this paper, we report the absorption coefficient measurements of the LaseRad cavity carried out at several wavelengths: 632.8 nm, 1280 nm – 1360 nm and 1480 nm – 1620 nm. The cavity under measurement was purchased by the PTB from the manufacturer of our CR, Cambridge Research & Instrumentation (CRI), separately for this purpose. It has the same characteristics as the cavity contained in the CR; it is constructed from an oxygen-free high-conductivity copper (OFHC) tube and blackened with Chemglaze Z-302 black paint [5].

2. Measurement method

The absorption coefficient of the cavity is determined from the measurement of the diffuse reflection ρ by the simple formula $\alpha = 1 - \rho$. The measurement is carried out using a four-ports integrating sphere and a photodetector (see Figure 1). In the visible wavelength range, a He-Ne laser operating at 632.8 is used as radiation source. The beam irradiates a 2-mm diameter circular aperture and is imaged 1:1 by a 200 mm focal length lens - passing through the sphere - into the cavity. To reduce the fluctuation of the laser power, an external stabilizer and a monitor detector are used. An attenuator and a polarizer are used to maintain the power level and the linear polarization of the laser beam. The detector placed on the sphere for the measurement at 632.8 nm is a Si detector of 5-mm diameter (Hamamatsu S1227 66BR). In the IR, two tunable diode laser sources (Agilent 81600B) were used, whose wavelength were adjusted from 1280 nm to 1360 nm and from 1480 nm to 1620 nm, respectively. The outputs of the laser sources are fiber-optic connectors; therefore an external collimator with a fiber-optic pigtail is used to collimate the laser beam. The laser stabilizer, used during the measurement at 632.8 nm, is not needed for the measurement in the IR, instead, the collimator was placed in front of the aperture and polarizer, see also Figure 1. An InGaAs photodiode (Telcom 35PD5M) of 5-mm diameter placed on the sphere carries out the measurement of the reflected fluxes.

The reflectance measurement of the cavity is done as follows: in a first step, a laser beam illuminates the cavity attached to the sample port. The reflected flux is diffusely emitted from the cavity and is collected by the integrating sphere finally generating a signal S_c is generated by the photodetector. In this scheme the white standard is attached to the supplementary port. In a second step, the cavity and the white standard interchange their ports from where a second signal is generated S_s. A third signal S_0 is measured by taking off the white standard from the sample port. From the ratio between those signals one can get the reflection coefficient of the cavity, ρ_c:

$$\frac{S_c - S_0}{S_s - S_0} = \frac{\rho_c}{\rho_s} \cdot \delta \;\rightarrow\; \rho_c = \frac{S_c - S_0}{S_s - S_0} \cdot \frac{\rho_s}{\delta} \qquad (1)$$

where ρ_s is the reflection of the white standard and δ is the correction factor due to possible changes of the geometrical conditions of the sphere between the two measurement processes. In our case, these conditions remain unchanged, so $\delta = 1$.

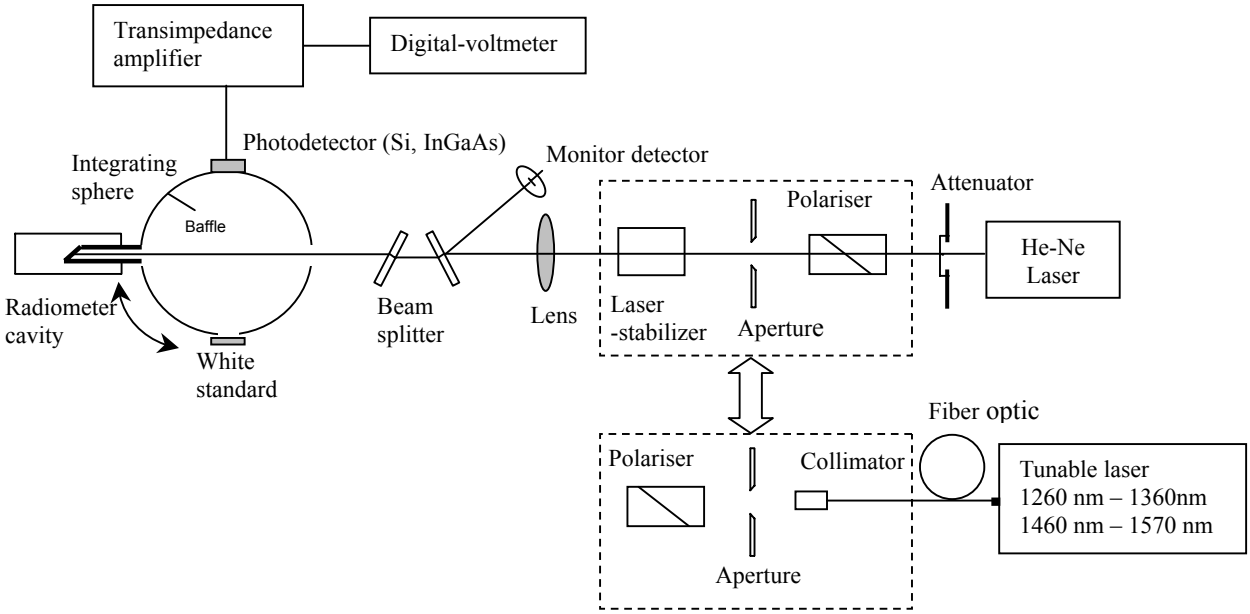

Figure1. Experimental set-up used to measure the diffuse reflectance of the radiometer cavity.

3. Measurement results

Figure 2 shows the results of the absorption coefficient measurements of the cavity. At 632.8 nm the absorption coefficient measured is 0.999885, which matches very well with the value reported by the manufacturer (0.999879). At the infrared wavelengths, the absorption coefficient varies from 0.999765 to 0.999785 between the wavelength ranges of 1280 nm – 1360 nm and 1480 nm – 1620 nm, respectively. The deviation observed for these ranges is 19×10^{-6}, which means that in this spectral range the value of the absorption coefficient is practically flat. Thus, for the whole NIR wavelength range, in principle a value of 0.999777 ± 0.000014 (k=1) can be used. Although no significant difference in the absorptance within the infrared spectral range investigated is observed, the mean value for the NIR range is about 1.1×10^{-4} lower than the value at 633 nm. This difference can be significant in the total correction factor of the CR, especially when one wish to reach uncertainties lower than 10^{-4}.

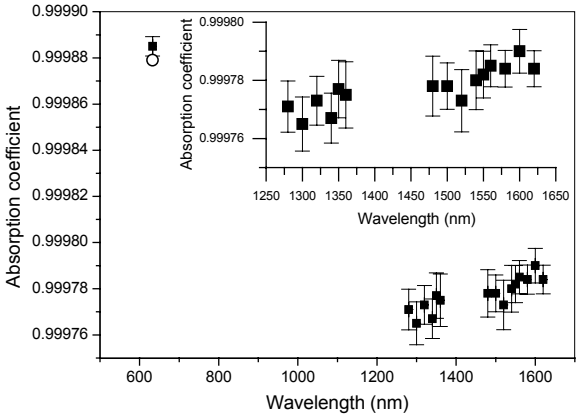

Figure 2. Absorption coefficients of the cavity measured in the visible and near infrared wavelengths. The error bars correspond to the standard uncertainty of the measurement. Open circle: manufacturer result.

4. Conclusions

The values of the absorption coefficient of a radiometer cavity in the visible and near infrared are presented. The results indicate that in the NIR, the absorption coefficient of the cavity is 1.1×10^{-4} lower than in the visible wavelength (632.8 nm).The characterization of the cavity will allow us to correct the absorption coefficient of the LaseRad cavity of the PTB cryogenic radiometer in the NIR. Thus, we expect to reach uncertainties lower than 3×10^{-4} for these wavelength ranges.

Acknowledgments The authors would like to thank the Deutscher Akademischer Austauschdienst (DAAD) for the support granted to this project through the Ph.D. scholarship A/03/18297. We also wish to thank the 4.52 Reflection measurements work group of the PTB for the white standard calibration.

References

[1] K. D. Stock and H. Hofer 1993 *Metrologia* **30** 291-296
[2] E. G. Atkinson and D. J. Butler 1998 *Metrologia* **35** 241-245
[3] L. Werner, R. Friedrich, U. Johannsen and A. Steiger 2000 *Metrologia* **37** 523-526
[4] P. Corredera, J. Campos, M. L. Hernanz, J.L. Fontecha, A. Pons and A. Corróns 1998 *Metrologia* **35** 273-277
[5] Product of Lord Corporation, Industrial Coatings Division, 2000 West Grandview Boulevard, Erie, PA 16514-0038

Grooves for Emissivity and Absorptivity Enhancement in High Performance Cavity Sources and Radiometers

E. Usadi, and R. Montgomery
National Physical Laboratory, Middlesex, UK

Abstract The emissivity of a flat emitting plate, and similarly the absorptivity of a flat absorbing plate, are well known to be enhanced by machining grooves into the flat surface. In addition to minimising retroreflection from cavities with flat end plates, grooves increase the number of absorbing surfaces a typical ray hits before exiting such a cavity. However two factors, generally overlooked in groove design, may become important for the design of ultrahigh emissivity or absorptivity cavities: (1) axial rays intersect the grooved surface off-normal, where the surface reflectivity is potentially much higher than at normal incidence, and (2) the groove angle may be difficult to define accurately, especially after the application of absorbing paint. This paper will describe ray tracing work showing that small changes in the groove angle can lead to dramatic changes in cavity emissivity or absorptivity (up to several percent) for relatively highly reflecting surface coatings. While this is not normally a problem for common black coatings and for radiation within the visible and IR spectrum below 100 microns, it may become an important correction for longer wavelengths where many common coatings become more highly reflecting and specular, especially at off-normal incidence. Since a room temperature thermal source has a significant fraction of emission at these long wavelengths, this may lead to an overall correction at the 1 – 100 ppm level when measuring the radiance of such sources.

Acknowledgments The authors would like to thank the Department of Trade and Industry of the UK for supporting this work.

PULSED UV SPECTRORADIOMETRY WITH THE PRIMARY STANDARD SYNCHROTRON RADIATION SOURCES OF HIGH INTENSITY

S. Anevsky, V. Ivanov, O. Minaeva, V. Sapritsky, Y. Zolotarevsky
All-Russian Research Institute for Optical and Physical Measurements
(VNIIOFI)
Ozernay St., 46, Moscow, 119361, Russia
Principal Contact: S. Anevsky
Phone: 007-095-437-3183
E-mail: Anevsky @ vniiofi.ru

VNIIOFI has developed table-top electron accelerators – primary synchrotron radiation sources as national standards of spectral radiance and irradiance in the range of vacuum and air UV. The creation of pulsed synchrotron radiation sources with strong magnetic field for UV spectroradiometry is based on the use of available magnetic field with induction of 10-18 T and pulse duration 3-300 μs . The small duration of synchrotron radiation pulse permit to use the strong magnetic field and to operate with low vacuum level. The value of optimal radius is about few centimeters and particles energy is about 30-100 MeV for UV spectral region. The high level of UV spectral flux makes pulsed synchrotron radiation source quite useful for calibration of the secondary standard plasma sources as capillary discharge with evaporated walls and plasma focus. The synchrotron radiation source beam diagnostics includes the measurements of orbit radius, electrons energy, particles number and radial, axial, phase dimensions of electron bunch. VNIIOFI for many years attempted to create and improve special small-size standard synchrotron radiation sources available for metrological laboratory based on technique of strong magnetic field generation: uniron low-inductive magnet system. The further development of synchrotron radiation sources is connected with optimization accelerator parameters in order to rich spectral range of EUV about 13.5 nm in regime of 1 Hz frequency.

New apparatus for the spectral radiant power calibration at CMS in Taiwan

Hsueh-Ling Yu and Shau-Wei Hsu
Center for Measurement Standards/ITRI, Hsinchu, Taiwan, R.O.C.

Abstract. A monochromator-based cryogenic radiometer (CR) facility has been established at the Center for Measurement Standards (CMS) in Taiwan, for calibrating the spectral radiant power responsivity of standard detectors. The design features of the new apparatus and uncertainty analysis are discussed. Presently the Si and Ge detectors can be calibrated in the spectral ranges 350 nm to 1100 nm and 800 nm to 1700 nm, respectively. The measured results of the Si and Ge detectors using the new apparatus were compared with the results in the NPL calibration reports to check the performance of the new apparatus. The agreement is better than 0.5 % for the Ge detector and 0.2 % for the Si detector.

1. Introduction

A new facility for the monochromator-based cryogenic radiometer [1,2] has been set up in the CMS in Taiwan. A monochromator-based cryogenic radiometer, rather than laser-based one, was established to calibrate the responsivity because of cost, convenience, and the flexibility of future applications. Instead of rotating the bellows to translate the CR and the transfer detectors as presented in Refs. 1 and 2, a linear translation stage is utilized to move the CR and the transfer detector to the focal position of the monochromatoe-source. The design of the new apparatus allows three detectors to be calibrated in a single measurement process to save time and liquid helium (LHe). The 1σ uncertainty of the Si detectors is approximately 0.2 % and that of the Ge detectors is 0.3 %.

2. Design features

Figure 1 presents the schematic overview of the new apparatus. The whole apparatus can be grouped into three categories - the CR, the detector stage, and the light source. The CR was manufactured by L-1 Standards and Technology, Inc. The hold time of LHe is well longer than 80 hours and the LN_2 for the cryostat can be refilled automatically. The relative standard uncertainty of the CR in radiant power measurement is less than 0.02 % for the monochromator-source.

The detector stage was originally designed by CMS and manufactured by L-1 Inc. The transfer detectors were placed on a holder inside a six-way reducing cross and connected to the feedthrough. It allows three detectors (depending on the size of the transfer detector) to be placed inside the cross. A thermistor was mounted on the holder to monitor the ambient temperature around the transfer detector. It showed that the ambient temperature was approximately 21.5°C during measurements. The welded bellows and linear translation stage were utilized to move the CR and the transfer detector to the focal position of the monochromator-source with an overall traveling length of around 31 cm. The X- and Z-axes of the XYZ manipulator were used to locate the center of and test the uniformity of the transfer detector. A flat fused quartz entrance window is placed in front of the welded bellows to eliminate the uncertainty form the window transmission.

A quartz- tungsten-halogen (QTH) lamp and an Xe lamp were used to cover the wavelength ranges from 400 nm to 1700 nm and below 400 nm, respectively. The F number of the monochromator is 4. After mirrors M1 to M4, the F number of the monochromator beam was about 13. Therefore, it could be absorbed totally by the CR (F/8). An aperture with a diameter of 1.9 mm was placed in front the exit port of the monochromator to make the spot diameter of the monochromator beam approximately 3 mm at its focal position.

3. Measured results and uuncertainty analysis

To verify the performance of the new apparatus, the measurements of the spectral responsivity on two NPL-calibrated Si and Ge detectors were carried out. The measured procedures involved the photocurrent measurements of the detectors, radiant power measurements with the CR, and then obtaining the spectral radiant power responsivities of the detectors. The measured results of Si and Ge detectors against the apparatus were compared with the results in their NPL calibration reports. The discrepancy is

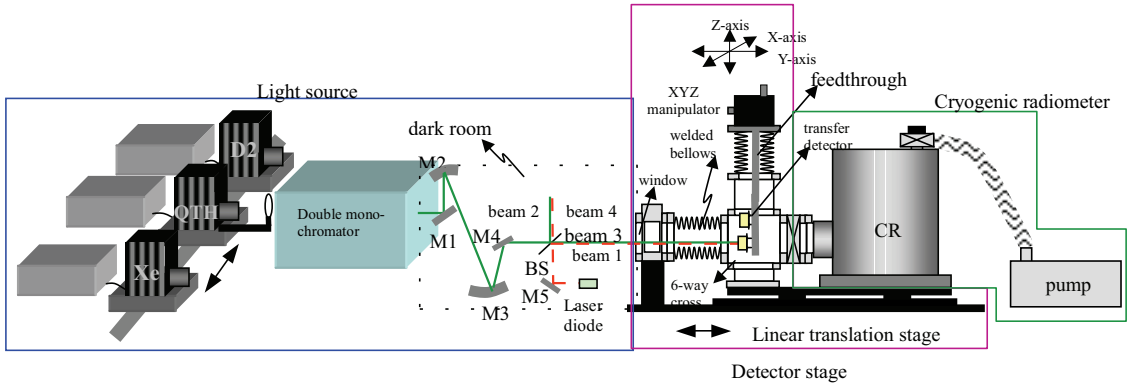

Figure 1. Schematic diagram of CMS new monochromator-based cryogenic radiometer for spectral radiant power calibration

less than 0.5 % for the Ge detector and 0.2 % for Si detector. The error sources include the bandwidth effect, wavelength accuracy, and stray light of the monochromator; the uniformity, polarization effect, and output current accuracy of the transfer detector; the measured accuracy of the radiant power of the CR. Table 1 lists the uncertainty budget and the conditions of the estimation.

Table 1. Uncertainty budget of the monochromator-based spectral radiant power responsivity calibration

Source	relative standard uncertainty	
Power measurement CR (monochromator-source)	0.02 %	
Bandwidth effect (Δ=1.5nm for Si Δ=3.5nm for Ge)	0.0001 %	(Si; 400 nm-1000 nm)
	0.01 %	(Si; other range)
	0.001 %	(Ge; 800 nm-1500 nm)
	0.04 %	(Ge; other range)
Wavelength accuracy (±0.1nm for Si ±0.2nm for Ge)	0.03 %	(Si; 400 nm-1000 nm)
	0.2 %	(Si; other range)
	0.05 %	(Ge; 800 nm-1500 nm)
	0.3 %	(Ge; other range)
Uniformity (0.3 mm deviation from the center of the diode)	0.02 %	(Si)
	0.08 %	(Ge)
Polarization (F/13, 0.2° incident angle)	0.01 %	
Current measurement	0.0005 %	
Repeatability	0.05 %	(Si; 400 nm-1100 nm)
	0.1 %	(Si; <400 nm)
	0.05 %	(Ge; 970 nm-1550 nm)
	0.1 %	(Ge; other range)
Total	0.07 %	(Si; 400 nm-1000 nm)
	0.23 %	(Si; other range)
	0.11 %	(Ge; 970 nm-1550 nm)
	0.33 %	(Ge; other range)

The error associated with the bandwidth can be calculated using the following method.

$$R_m(\lambda_o) = \int_{\lambda_o-\Delta}^{\lambda_o+\Delta} R(\lambda-\lambda_o)S(\lambda)d\lambda$$

where $R_m(\lambda)$ is the measured responsivity, $R(\lambda)$ is the real responsivity, $S(\lambda)$ is the slit function of the monochromator, and Δ is the bandwidth of the monochromator. $S(\lambda)$ is assumed to have a symmetrical tri-anglular function around λ_o, and the bandwidth error ε can thus be expressed as

$$\varepsilon = \frac{R_m(\lambda)-R(\lambda)}{R(\lambda)} \approx \frac{\Delta^2}{12R_m(\lambda)}\frac{d^2R_m(\lambda)}{d\lambda^2}$$

Conclusion and outlook

Only the spectral range from 350 nm to 1700 nm was considered. The Si and Ge detectors used in this work were not calibrated directly using the NPL primary system, so the uncertainties in the NPL reports are relatively large. Hence, a further intercomparison is required to precisely study the consistency with other relative primary standards. The future works will include extending the measurement range below 350 nm and over 1700 nm, and applying the monochromator-based CR to establish another apparatus for measuring the spectral irradiance/radiance of light sources.

References

1.L. P. Boivin and K. Gibb, Monochromator-based cryogenic radiometry at the NRC, *Metrologia*, *32*, 565-570, 1995/1996.

2.C. A. Schrama, R. Bosma, K. Gibb, H. Reijn, and P. Bloembergen, Comparison of monochromator-based and laser-based cryogenic radiometry, *Metrologia*, *35*, 431-435, 1998.

3.Peter V. Foukal, C. Hoyt, H. Kochling, and P. Miller, Cryogenic absolute radiometers as laboratory irradiance standards, remote sensing detectors, and pyroheliometers, *Applied Optics*, *29*, 988-993, 1990.

4.R. U. Datla, K. Stock, A. C. Parr, C. C. Hoyt, P. J. Miller, and P. V. Foukal, Characterization of an absolute cryogenic radiometer as a standard detector for radiant-power measurements, *Applied optics*, *31*, 7219-7225, 1992.

Acknowledgments. The authors appreciate the valuable discussions with Dr. Ping-Shine Shaw, who is a NIST fellow. The authors would also like to express their gratitude to Dr. Steven Lorentz of the L-1 Inc. and designed, built, and tested the cryogenic radiometer and the detector stage.

VUV and Soft X-ray metrology stations at the International Siberian Synchrotron Radiation centre

V. I. Buhtiyarov, N. G. Gavrilov, N. A. Gentselev, B. G. Goldenberg, G. N. Kulipanov, A. A. Legkodymov, V. V. Lyakh, O. I. Meshkov, A. I. Nizovsky, A. D. Nikolenko,[1] V. F. Pindyurin, I. V. Poletaev, E. P. Ya. V. Rakshun, Semenov, M. A. Kholopov, V. A. Chernov, M. A. Sheromov

Budker Institute of Nuclear Physics, 630090 Novosibirsk, Russian Federation

At present, there are two experimental stations under construction at the International Siberian Synchrotron Radiation centre (Novosibirsk, Russia). They are intended for metrology work in the VUV and soft X-ray spectral ranges with the application of SR from the storage rings of VEPP-3 and VEPP-4.

The soft X-ray metrology station (the spectral range is from 80 to 5000 eV) at the storage ring of VEPP-3 makes it possible to perform very different works for time and absolute spectral calibration of various X-ray detectors as well as absolute and relative certification of elements of X-ray optics (multi-layer mirrors, multi-layer lattices, absorption film filters etc). The first line of the station has been commissioned already. Certification of power of the incoming "white" SR beam is under way now. The monochromator is being prepared for commissioning. Its design allows one to use both multi-layer mirrors as wall as crystals as x-ray optical spectral elements. The first experiment is supposed to deal with experimental investigation of possibility of broadening the self-calibration method [1] in order to use it later to calibrate scintillation counters. Another task of the first experiment is a preliminary test of elements of the Space Solar Patrol (SSP, made by SOI, St. Petersburg) [2] within the framework of ISTC project #2500, which is devoted to SSP calibration.

The VUV and soft X-ray metrology station with the application of SR from the VEPP-4 storage ring is being developed at the moment. In contrast to the similar station at VEPP-3, the spectral range of this station (from 10 to 1000 eV) allows one to perform calibration measurements in the VUV range. Due to partial overlapping of the spectral ranges of these stations one can check at one station a calibration done at the other. The metrology station of VEPP-4 is to be equipped with two monochromators. Those are a lattice one (the spectral range is 10 to 100eV) and a two-mirror monochromator based on multi-layer mirrors (the spectral range is 80 to 1500 eV). Since the experimental space of the station is rather large (about 0.7x05x0.5 m^3) it will be possible to perform calibration of quite big-sized space equipment). The first series of prospective experimental works is to be devoted to absolute calibration of the equipment of the space solar patrol. The station is supposed to be commissioned in the first half of the year 2006.

The SR beamlines of both the stations have been made by a technology without windows. They are equipped with a fast closing system for the case of a vacuum damage at the station and with differential vacuum pump-down. That makes it possible to investigate unbakeable samples in the experimental spaces at an operational pressure up to 10^{-4} Pa. This report presents the optical schemes of both the stations, their main parameters and design photon flows for different operation regimes.

1. Krumrey M., Tegeler E., *Nuclear Instruments and Methods in Physics Research* A288 (1990) 114-118
2. Avakyan S., at al. *Sensors, Systems and Next Generation Satellites, Proc. SPIE,* v. 3870, pp. 451-461, 1999.

[1] A.D.Nikolenko@inp.nsk.su

Experimental study of application of the self-calibration method to certify absolute spectral sensitivity of a scintillation counter in the soft X-ray range.

A.D. Nikolenko[1], V. F. Pindyurin, V. A. Chernov, V.V. Lyakh.
Budker Institute of Nuclear Physics, 630090 Novosibirsk, Russian Federation

The self-calibration method earlier has been successfully developed by the PTB team (Berlin, Germany) for absolute certification of spectral sensitivity of semiconductor diodes [1, 2]. In these works, parameters required to determine spectral sensitivity of a detector (the dead layer on the surface of detector and sensitive area thickness) were found via measuring the spectral response of the detector at different angles of radiation incidence on the receiving surface of the detector.

In the case of absolute calibration of a scintillation counter (SC), the spectral sensitivity of the detector is described with a slightly more complicated model. Beside the dead layer thickness, the model includes the spectral efficiency of the scintillator, the efficiency of collection of visible photons on the photo-cathode, the photo-cathode efficiency and particularities of signal amplification by the dynode system of the photomultiplier. The present work describes the preliminary measurement of the spectral sensitivity of a SC based on a photomultiplier with guaranteed one-electron peak FEU-130 with a YAP scintillator. The dead layer thickness of the scintillator was determined in the same way as in [1, 2]. The efficiency of registration of X-ray photons that passed the dead layer of scintillator is found by the form of the amplitude spectrum of anode pulses of the photomultiplier.

The evident explanation of this technique briefly can be described as follows: x-ray quantum absorbed by the scintillator, is generated the light flash, which is registered by the photoelectron multiplier (PEM). In case of soft x-ray photon the number of the visible photons in each flare is not big (from units up to several tens depending on energy of x-ray photon and characteristics of scintillator) and consequently the significant part of useful pulses of PEM is situated in the one-electron peak. It means, that the average number of optical photons, be registered by the PEM from the such flash, is less then 1. Nevertheless, in a amplitude spectrum of pulse signal of PEM, we can observe not only one-electron peak, but also the effect of presence of two- and three-electron peaks. Using the relative intensity of these peaks we can to calculate the probability of registration of every x-ray photon which has penetrated through a dead layer and was registered in the scintillator.

This method does not allow one to separate the contribution of each of the SC parameters that influence its efficiency but it gives the absolute efficiency of a particular SC. The advantage of this method is that all the measurements are relative ones and can be performed on any available source of monochromatic soft X-radiation. A disadvantage of the method is its low accuracy (estimated to be not better than 10%).

The experimental checking of this method were performed at the Soft X-ray metrology station at the VEPP-3 storage ring for the few different energy of photons from 100 to 1500 eV. In the near future, as expect, the station is to be equipped with reference detectors with a calibrated spectral sensitivity, which will allow one to check correctness of calibration.

1. Krumrey M., Tegeler E., *Rev. Sci. Instrum.* 1992 **63**, 797-801
2. Krumrey M., Tegeler E., *Nuclear Instruments and Methods in Physics Research* **A288** (1990) 114-118

[1] A.D.Nikolenko@inp.nsk.su

The metrology line on the SOLEIL synchrotron facility

M. Lièvre, M-C. Lépy, B. Rougié, J-R. Filtz, J. Bastie
LNE, Paris, France

M. Idir, T. Moreno, P. Mercere
SOLEIL, Gif sur Yvette, France

Abstract. In the new SOLEIL synchrotron facility one line will be devoted to metrology, providing 3 branches for hard-X, X-UV and UV-VUV radiation applications. So metrology between about 5 eV to 14 keV (250 nm down to 0.09 nm) will benefit from this calculable radiation source. The UV-VUV branch is expected towards the end of 2006.

Introducing SOLEIL

SOLEIL (Source Optimisée de Lumière d'Energie Intermédiaire du LURE = Optimized source of mid-level energy light in LURE) is a 3rd generation 2.75 GeV synchrotron. Building began in 2000, and the first lines are to open end of 2006, followed by 14 others between 2006 and 2010 - potentially 40. It is designed and managed from the beginning to host international teams.

This synchrotron facility built in the Optics Valley addresses new or increasing needs in X to UV applications such as X lasers or deep UV lithography. It will inherit and amplify the high level-activity of the former LURE synchrotron.

The metrology line partners

There will be 3 main users of this metrology line: SOLEIL itself for its own instruments testing, the French Agency for Nuclear Energy (CEA) and the National Test and Measurement Laboratory (LNE). LNE has taken over the former BNM since beginning of 2005, including now the BNM previous members. The 3 LNE laboratories involved in the metrology line are the LNE-LNHB, the LNE-INM and the former LNE.

Radiation metrology benefits from the synchrotron radiation (SR) characteristics

Situation in France

Up to now, different laboratories (now members of LNE) have performed a metrological activity with SR. INM carried on its first SR applications in 1974, establishing an electric arc as a secondary standard by comparing both radiations. LNHB characterized and calibrated X detectors. And outside metrological laboratories, SR enabled several metrological achievements such as optical components and detectors qualification for hot plasma X diagnosis.

Situation in other countries

In Germany, PTB runs a well-known and important facility at BESSY II, providing monochromatic radiation between 3 eV and 15 keV. Due to the increasing demand for SR access, the MLS (Metrology Light Source) new facility is expected to complete BESSY II in 2008, with a spectrum ranging from infrared to deep UV.

In the US, NIST uses the SURF III facility in Gaithersburg as a calculable source in the 50 to 260 nm range, and as a UV source calibration to a cryogenic radiometer in the 125 to 320 nm range.

In Russia, the VEPP facility in Novosibirsk provides radiation between 120 and 400 nm for calibration of lamps and detectors.

Other facilities are used for radiometry in **China** and **Japan**.

One of the main issues for radiometry with SR is access to the beam: not enough available time or too scattered. And it is worse with operating requirements often incompatible with other more widespread SR applications.

Characteristics of the SOLEIL SR

The synchrotron radiation shows a broad continuous spectrum, and its characteristics (irradiance, polarization, coherence, beam profile and pulse shape) are calculable with the Schwinger theory, with an accuracy only limited by the determination accuracy of the influence parameters, which can be very good. The output power can be adjusted on a 12 orders of magnitude scale.

The SR emits pulses with a 50 ps width every 140 ns typically. Polarization can be adjusted from linear to circular.

Metrology line characteristics

SOLEIL committed the "Optics" special team to initiate and assist the users in designing the metrology line. The general requirements are a well-collimated beam, a high spectral purity (almost no harmonics), very low scattering, and a large spectral range, especially for absolute calibration of detectors, relying on the possibility to calculate the exact incident power.

The "Sources and Accelerators" special team will provide measurements and develop methods to perfectly control the key machine parameters, in agreement with the metrology users requirements.

The 8-mrad beam available at the end of the magnet will be spatially split into 3 branches, each of them devoted to a specific energy (spectral) range.

We will focus now on the VUV branch, and mention only for completeness sake the hard and soft X-ray lines.

UV-VUV branch

The design is not yet definitive. This branch is now optimized for the 7 to 70 eV (18 to 180 nm) range. The beam will pass through a monochromator yielding a simulated photon flux above $1.5.10^8$ photons/s, with a peak of 10^{11} photons/s at 50 nm, respectively above 1 nW and 300 nW. At the output focus, the beam has a rectangular shape of 45 x 600 µm. The spectral width varies between 20 and 120 pm.

X-UV branch

This branch will be operated between 30 eV and 2 keV, with a focused or collimated output beam, and a harmonic rejection rate of 0.1 %.

Hard-X branch

This branch will be operated between 0.5 and 12 keV, with a focused or collimated output beam.

Uncertainties

The main interest of SR in radiometry is the possibility to calculate the incident flux from the measurement of independent operating parameters. At BESSY, the combined uncertainty has been assessed to 0.2% at 1 eV and 0.35% at 5 keV. The dominant term belongs to the geometrical factors in the optical range, and to the electrical ring parameters in the X range.

Of course there are other contributions to the final uncertainty in a complete calibration process. In the case of the already running synchrotron calibration facilities, the final uncertainty amounts generally to a few percent. It has not yet been assessed at SOLEIL.

Expectation in UV Metrology

The SOLEIL metrology line is expected to bring a breakthrough in UV calibrations through the realization of standard references for detector sensitivity and energetic source properties (radiance, irradiance, radiant intensity). It will of course enhance comparison possibilities with other international realizations of the same quantities, and the transfer to end-users. It is true that the main demand on UV radiometric calibration is still in the less energetic range (above 200 nm), where applications such as therapy or diagnostic will bring more stringent demand on accuracy. However the emerging applications in biology, industry or scientific research (astronomy, plasma, fluorescence) and above all in photolithography are driving calibration needs toward the VUV (vacuum ultraviolet) range. In this range only will the SR prove more efficient than laser or high temperature blackbody sources.

References

Lépy, M.C., Rougié, B., Lièvre, M., Stemmler, P., Marmoret, R., Idir, M., Moreno, T., Polack, F., Ligne de métrologie sur SOLEIL, private report, September 2004

BNM, CEA, Laboratoire National Henri Becquerel, *Intérêt du rayonnement synchrotron pour la métrologie – première approche*, in French technical note LNHB/00/21 2ème version, 2000.

Bastie, J, Coutin, J-M, Rougié, B, CNAM-INM, *Contribution du BNM-INM à la préparation du projet métrologique sur SOLEIL*, in French technical note, 2001

Klein, R, Ulm, G, PTB, Abo-Bakr, M, Budz, P, Bürkmann-Gehrlein, Krämer, D, Rahn, J, Wüstefeld, G, Bessy Gmbh, *The metrology Light Source of the Physikalisch Technische Bundesanstalt in Berlin-Adlershof*, in the Proceedings of EPAC 2004, Lucerne, Switzerland, 2004

Klein, R, Thornagel, R, Ulm, G, PTB, *BESSY II operated as a primary source standard,* in the Proceedings of EPAC 2004, Lucerne, Switzerland, 2004

Wende, B, PTB, *Radiometry with synchrotron radiation*, Metrologia, 1995/1996, 32, 419-424

Furst, M.L, Graves R.M., Hamilton, A, Hughey, L.R, Madden, R.P, Vest R.E. NIST Gaithersburg, MD, Trzeciak, W.S, Bosch, R.A, Synchrotron Radiation Center, Stoughton, WI, Greenler, L, Robl, P, Wahl, D, Physical Sciences Laboratory, Stoughton, WI, *The Conversion of SURF II to SURF III*, in the proceedings of the 1999 Particle Accelerator Conference, New-York, USA, 1999

Cryogenic radiometer developments at NPL

J. Ireland, M.G. White and N.P. Fox,
National Physical Laboratory, Teddington, UK

Abstract Cryogenic radiometers are widely used as the primary standard of choice for optical radiometric measurements. This has led to increased demand for designs optimised for specific applications. NPL has pioneered the field of cryogenic radiometry, both in terms of design and application, from its first successful implementation in the 1970's through to the wide range of instruments and applications available today.

This paper will review some of these developments and how they have progressed into the designs of today. Particular emphasis will be given to a new instrument optimised for the low powers ~ 1 μW which typify the output of monochromators whilst maintaining the flexibility of mechanical cooling i.e. no liquid cryogens.

Introduction

Since the first cryogenic radiometer of Quinn and Martin, designed to measure total radiation from a black body for determining the Stefan-Boltzmann constant (1), there have been numerous designs and applications (2). NPL has been at the forefront of the technology and has been the source of many designs over the years, originally exploited by Oxford Instruments Ltd and more recently by NPL directly.

One of the trends in recent years has been the drive towards the lower cost more flexible operation of mechanical cooling engines, coupled with the desire for greater operational flexibility. This has been achieved through the use of lower power monochromator based radiation sources, eliminating the use of more expensive laser sources in wavelength regions outside of the visible spectrum.

NPL has been engaged in the parallel development and operation of a number of cryogenic radiometers;-

1/ The Absolute Radiation Detector, ARD for a new radiometric determination of the Stefan Boltzmann constant (and consequently Boltzmann constant for a potential future redefinition of the Kelvin). (3)

2/ The mechanical cooled (~15 K) cryogenic radiometer for laser based radiometry. (4)

3/ A space based cryogenic radiometer for measurements of Total Solar Irradiance and Earth reflected spectral radiance. (5)

4/ A mechanically cooled (4 K) cryogenic radiometer for lower power, monochromator based applications.

This paper will concentrate on this latter development.

Summary

The new radiometer uses a 4 K mechanical cooling engine to directly cool a "helium pot" mounted on the second stage of the cold head. This helium pot is connected to an external helium gas reservoir and the gas is cooled to the liquid phase and collected in the pot, providing a thermal buffer to which the reference block is mounted via a heat link. By pumping on the helium pot we can achieve a base temperature of around 2 K and an operating temperature of around 3.7 K.

Custom built ac resistance bridge electronics are being developed to optimise the control of temperature stability of the reference block. The three reference resistors in the bridge are mounted directly on the reference block alongside the temperature sensor, to minimise noise. The radiation cavity, also of novel design, will be operated in active mode (with a constant power). The radiometer is designed so that the cavity and heat link are modular, and can easily be changed, so that the sensitivity can be optimised for specific applications. The cavity temperature will also be monitored using an ac resistance bridge.

The cryostat is mounted on a rotating arm so that either the cavity or the detectors to be calibrated can be moved into the path of the beam. The detectors are mounted modularly to the vacuum chamber, allowing interchange of detectors when cold.

The design objectives are for a measurement of optical radiant power at the 1 μW level with uncertainties of <0.01 %.

References

1. Quinn T.J., Martin J.E., A radiometric determination of the Stefan-Boltzmann constant and thermodynamic temperatures between –40°C and +100°C, *Phil. Trans. Roy. Soc. London, 316,* 85-181, 1985
2. Fox N.P., Rice J.P., Absolute Radiometers in Optical Radiometry*, Volume 41 of Experimental methods in the Physical Sciences,* edited by A. Parr et al., pp 35-95, Elsevier inc, 2005
3. Martin J.E., Haycocks P.R., *Metrologia,* 35, 229-233 1998
4. Fox N.P., Haycocks P.R., Martin J.E., Ul-Haq I., A mechanically cooled portable cryogenic radiometer, *Metrologia*, *32, no 6*, 581-584, 1995
5. Fox N.P., Aiken J., Barnett J.J., Briottet X., Carvell R., Frohlich C., Groom S.B., Hagolle O., Haigh J.D., Kieffer H.H., Lean J., Pollock D.B., Quinn T., Sandford M.C.W., Schaepman M., Shine K.P., Schmutz W.K., Teillet P.M., Thome K.J., Verstraete K.J., Zalewski E., Traceable Radiometry Underpinning Terrestrial- and Helio- Studies (TRUTHS), *Adv. Space Res, 32*, 2253-2261 2003

Energy Calorimeter for Pulsed Laser Radiometry

Daiji Fukuda, Kuniaki Amemiya, Asuka Kamimura, and Shinji Kimura
National Metrology Institute of Japan, AIST, Tsukuba, Japan

Abstract.
We have developed an energy calorimeter that can determine absolute energy of single-shot laser pulses. The calorimeter is composed of a U-shaped absorption cavity and semiconductor-based thermocouples. The energy sensitivity is calibrated by inducing energy to an electrical heater on the cavity. To reduce a standard deviation, an optimal filtering method was used for the sensitivity calibration. As a result, we obtained that the energy sensitivity is 9.42 mV/J for 10 mJ energy with the low relative standard deviation of 0.02 %.

Introduction

The pulsed laser sources are now widely used in industry, and its precise determination of the laser energy is more important. In 2005, National Metrology Institute of Japan will start an energy sensitivity calibration service for laser energy meters as a special test. To realize this, we have developed a laser energy calorimeter. This abstract describes some characteristics of the energy calorimeter and a calibration method of the energy sensitivity.

Configuration

Figure 1 shows the absorption cavity of the laser energy calorimeter. The cavity is fabricated with free oxygen copper with a thickness of 0.2 mm. A bottom of the cavity is sloped with an angle of 60 degrees, on which a glass volume absorber of NG-1 (shott glass) with a thickness of 0.5 mm is attached. A single shot laser pulse is irradiated through an entrance, and the most of energy is absorbed in the glass volume. Some energy, which is reflected at the glass surface, is absorbed at the cavity wall by multiple reflections. The inside of the cavity is painted with velvet Nextel coating to increase the absorptance of the cavity. In this configuration, the total reflectance of the cavity for 633 nm is less than 0.02 %, which is measured by an integrating sphere.
The resulting temperature increase from the energy absorption is detected with bismuth telluride thermo-couples of seventy-two pairs at the front region of the cavity. The temperature sensitivity of the thermocouple per pair is approximately 200 μV/K, which is seven times lager than that of metal-based thermocouples.

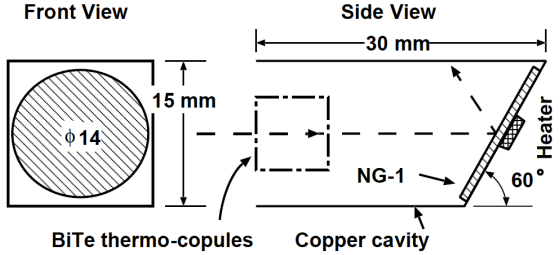

Figure 1. Schematic drawings of the absorption cavity of the energy calorimeter. Left is the front view and right is the side view. Pulsed laser enters like an arrow of broken line.

Sensitivity calibration

The sensitivity of the calorimeter is calibrated with an electrical heater on the absorption cavity. A rectangular electrical pulse of the pulse width Δt is generated with a constant voltage source and a gate switching circuit, and it is induced to the heater, as shown in fig. 2. The electrical energy E produced by Joule heating is written as

$$E = V^2 \Delta t / R,$$

where V is the voltage of the source and R is the resistance of the heater. The time-dependent temperature change of the cavity is recorded with a nanovoltmeter as the output voltage of the thermocouples.
To derive the energy sensitivity from the time-dependent output voltage signals, a theory that is based on the First Low of Thermodynamics by West is frequently used. In the theory, the output signals are divided into some regions; an initial rating period, a relaxation period, and a final rating period. The sensitivity is determined with the induced energy and a corrected voltage rise that is calculated with time integration and the voltage difference during these periods. More detail process is given by Zhang. This theory is very useful to determine the sensitivity of the calorimeter, however, intrinsically noise characteristics of the calorimeter are not considered in the theory. Thus, we tried to improve the theory by combining the optimal filtering method. In our method, a noise property of the calorimeter is considered, that would be expected to greatly reduce the standard deviation of the energy sensitivity.
In the present method, we firstly prepare a model signal waveform and a voltage noise spectrum of the calorimeter. We define these Fourier transformations as $M(f)$ and $N(f)$, respectively. Then a relative pulse height PH for measured waveform $D(t)$, which is a signal for each single energy shot, is calculated using a least square method at a frequency region as the following formula.

$$PH = \int \frac{D(f)}{M(f)} \left| \frac{M(f)}{N(f)} \right|^2 df \Big/ \int \left| \frac{M(f)}{N(f)} \right|^2 df$$

Finally, the corrected voltage rise for $D(t)$ is obtained by multiplying PH by the corrected voltage rise for the model waveform $M(t)$. More detailed methods are described by

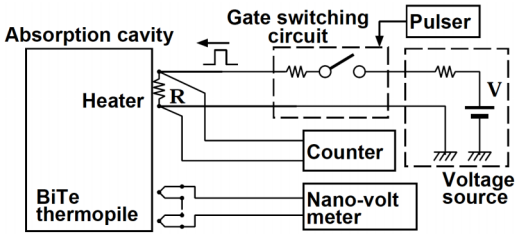

Szymkowiak and Fukuda.

Figure 2. Experimental setup for energy sensitivity determination. Rectangular-shape electrical pulses are generated, and are induced the heater. The resulting temperature rise is

measured with BiTe thermopiles.

Experimental Results

We calibrated the energy sensitivity of the calorimeter for the electrically induced energy from 1 mJ to 100 mJ using the method mentioned above. At each energy stage, we obtained five waveforms of $D(t)$ which has 1024 data points with the sampling time Δt of 0.6 s. A fall time constant of the calorimeter is 55 s, thus the calorimeter will completely return to an equilibrium state after an energy shot during the waveform measurement. As to the calculation process of the corrected voltage rise, we set the relaxation period and the final rating period to 18 s and 39 s, respectively.

The energy sensitivity obtained by our method was 9.42 mV/J, and was well agreed with the value obtained by West's method, as shown in fig. 3. For the measured energy range, the nonlinearity of the sensitivity is less than 0.1 %, which is very useful for the laser energy calibration. Figure 4 shows the relative standard deviation of the energy sensitivity for each electrical energy point obtained by both methods. In the presents method the deviation decreased by ten percents, which is very desirable for precise energy determination.

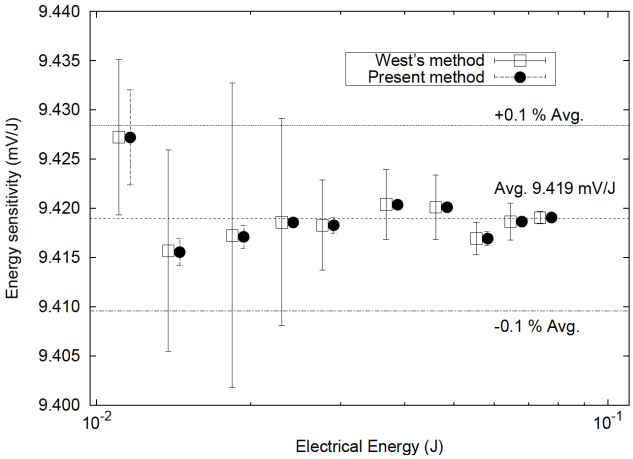

Figure 3. Measurement results for energy sensitivity of the calorimeter obtained by West's method and present method. Bars indicate the standard deviation (1σ) for five measurements.

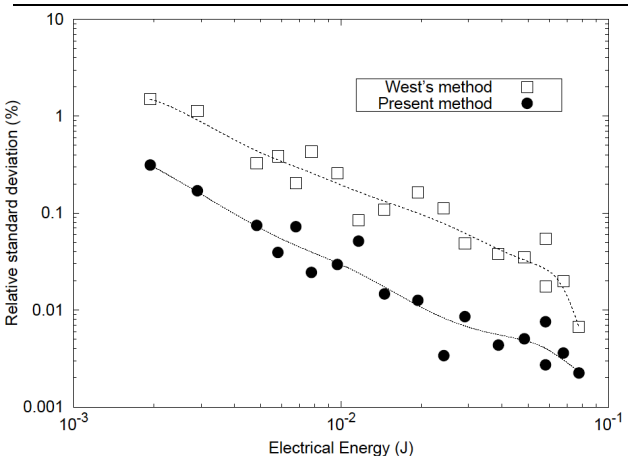

E-mail: d.fukuda@aist.go.jp

Figure 4. Relative standard deviations of the energy sensitivity. The deviations increased at lower energy, however, the deviations for the present method improved by ten percents in this energy range.

Conclusion

We developed a laser energy calorimeter that is intended as a primary standard for the calibration of the laser energy meters. The sensitivity of the calorimeter was well defined using the optimal filtering method and was found to be 9.42 mV/J. The standard deviation by our method was reduced by ten percents compared to West's method. The nonlinearity of the energy sensitivity was less than 0.1 % in the energy range from 10 mJ to 100 mJ. These performances are very desirable to calibrate laser energy meters with a low measurement calibration uncertainty.

Acknowledgments The authors would like to thank Dr. Koyanagi for encouraging this research.

References

West, E. D., A Reference Calorimeter for Laser Energy Measurements, in *J. of Res. of the National Bureau of Standards, 76A, No. 1*, pp. 13-26, 1972.

Franzen, D. L., Absolute reference calorimeter for measureing high power laser pulses, in *Appl. Optics, Vol. 15, No. 12*, pp. 3115-3122, 1976.

Zhan, Z. M., Thermal Modeling and Analysis of Laser Calorimters, in *J. of Thermo. And Heat Trans., Vol. 10, No. 2*, pp. 350-356, 1996.

Szymkowiak, A.E., Signal-processing for microcalorimters, *J. of Low Temp. Phys., vol. 93, no. 3-4*, pp. 281-285, 1993.

Fukuda, Daiji, Absolute energy reference calorimeter with BiTe thermocouples for measuring laser pulses, in preparation.

Characterization of new trap detectors as transfer standards

J-M. Coutin, F. Chandoul, and J Bastie
LNE-INM / CNAM, 292 rue Saint-Martin, 75003 Paris, France

Abstract. The French radiometric references are based on a cryogenic radiometer working at a restricted number of laser wavelengths. The traceability to the cryogenic radiometer is implemented by using transfer detectors linked in absolute spectral responsivity to the cryogenic radiometer. To improve this traceability, we have been developing new trap detectors build with new Silicon HAMAMATSU photodiodes (part number Si-S8552 and Si-S855).

Introduction

The French national standard laboratory uses an electrically calibrated cryogenic radiometer as the basis for its optical radiation measurement scales. The purpose of the work in progress is to improve the traceability to the cryogenic radiometer of the various radiometric and photometric quantities measured. This traceability is implemented by using transfer detectors linked in absolute spectral responsivity to the cryogenic radiometer.

The cryogenic radiometer allows direct calibration of detectors in absolute spectral responsivity with a relative standard uncertainty in the range of 1 part in 10^4, but only for a few laser wavelengths. In order to derive from these punctual spectral measurements all the radiometric and photometric quantities maintained by the laboratory, it is necessary to interpolate and eventually extrapolate the spectral responsivity of detectors used as transfer standards within their spectral range.

In order to facilitate and optimize the extrapolation and interpolation method, we use as transfer detectors large-area reflection silicon trap detectors. The objective is to take advantage of the main property of trap detectors : this type of detectors has an absolute spectral responsivity curve that can be modelled over the spectral range of useful wavelengths.

Description of the trap detectors

In our laboratory, we use as secondary standards trap detectors, which are the only detectors able to maintain and transfer the accuracy reached with the cryogenic radiometer. These traps are three element photodiode reflectance traps, built with three 10x10 mm^2 Silicon photodiodes having very high internal quantum efficiency [1]. But due to their geometry, they have a small area and a very limited field-of-view (FOV), so it is difficult to use them with large or not parallel beam of radiation.

In order to take advantage of the properties of trap detectors and minimize the geometrical limitation, we are studying large-area reflection silicon trap detectors, where three large-area Silicon photodiodes with an active area of 18x18 mm^2 are used. Figure 1 shows the scheme of the trap detectors we developed [2], and the arrangement of the three photodiodes inside the trap : the incident beam (arrows on figure 1) is absorbed 5 times before coming out of the trap. Due to their larger area and their wider FOV, these detectors can be used much more easily at the exit of the monochromator, in our set-up for spectral responsivity measurements.

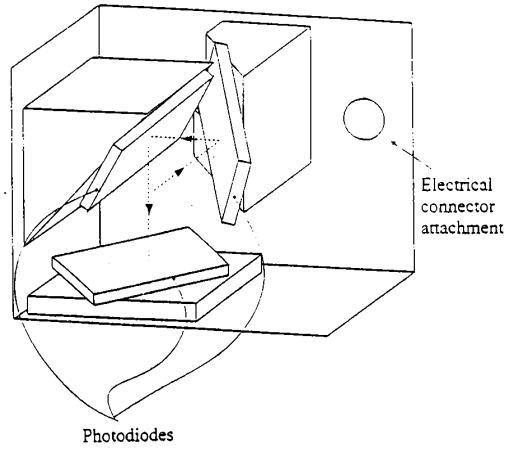

Figure 1. Scheme of principle of a large-area reflectance trap.

The first prototypes of large-area trap detectors that we studied are made with large-area windowless HAMAMATSU photodiodes (part number S3204-09) [3]. But the photodiodes mounted in these trap detectors are not suitable for the realization of trap detectors, because their reflection factor is near zero in the visible range. In addition, the measured quantum efficiency of this type of trap detector is not sufficiently close to the unity to develop easily a valuable model for the spectral responsivity.

In order to continue our study and improve the first results, we investigated the large-area Silicon windowless photodiodes proposed by HAMAMATSU. We found out new Silicon photodiodes of type S8552 that seems to be more appropriate to the problem. Furthermore, these photodiodes are designed to provide optimal performance in the VUV range and offer more stable sensitivity even after long exposure to VUV radiation, compared with conventional type. So we are now studying new trap detectors made with these photodiodes in order to make new standard detectors over the spectral range 190 nm – 1000 nm.

Characterization of the trap detectors

We are studying two types of new trap detectors. The first type is made with 10x10 mm^2 Silicon photodiodes (part number S8552) to be used as secondary standards detectors, and especially in the VUV range. In Figure 2 are shown the results of the calibration of this detector in spectral responsivity at some laser wavelengths. The measurements were made by comparison with the cryogenic radiometer, with an uncertainty of the order of 1.5 parts in 10^4 [4]. The results are very encouraging for the use of this detector as secondary standard, because the

variations of the spectral sensitivity, according to the wavelength, are relatively linear (better than 1 part in 10^3) on the whole of the measurement points. In addition, the values obtained for the spectral sensitivity are very close to the theoretical curve of trap detectors, which is obtained for quantum efficiency equal to one.

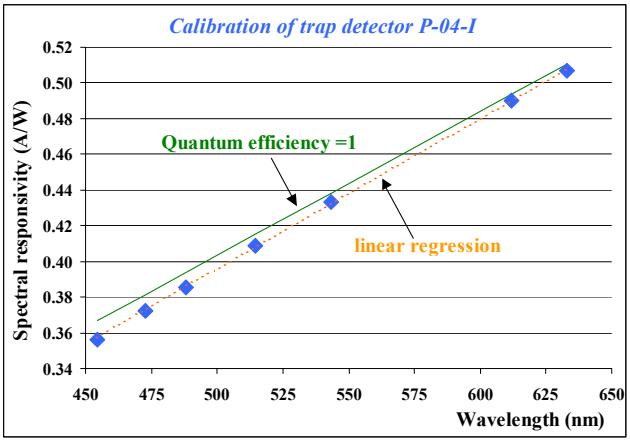

Figure 1. Results of the calibration of a small-area trap detector made with S8552 photodiodes

The second type of trap detectors we developed are made with large-area windowless HAMAMATSU photodiodes (part number S8553), to use them as transfer detectors for radiometric and photometric measurements. The absolute responsivity measurements are carried out at some laser wavelengths by comparison with the secondary standard trap detector described above, with an uncertainty of the order of 2 parts in 10^4. The results are similar to thus obtained with the small-area trap detector made with the same type of photodiodes.

To take into account the possible variations of local responsivity, and to become closer to the using conditions, which correspond to a surface of the detector much more irradiated, than during the calibration with laser beam, the spectral responsivity has been measured in various points around the centre of the active area of the detector, for two perpendicular positions of the detector. The results are shown in figure 3 : the modification of the method of calibration allowed to underline a variation of the spectral sensitivity between the two measurement positions of the detector, which is in the order of 4 parts in 10^4. But the relative uncertainty on the global value of the spectral sensitivity, for each laser wavelength, is in the order of 1 part in 10^4. The resulting global uncertainty on the calibration is then 2 to 3 parts in 10^4 that is quite acceptable.

To use the detector as standard transfer detector, it is necessary to determine the spectral responsivity of the trap detector over it using spectral range, and not only at laser wavelengths. The absolute values are then interpolated and extrapolated by comparing the trap detector to a non-selective cavity shape pyroelectric detector, on the spectral responsivity measurements set-up.

Figure 3. Local variations of the spectral responsivity obtained for the two measurement positions of the large-area trap detector

Conclusion

The determination of the absolute spectral responsivity, by using the pyroelectric detector as means of interpolation and extrapolation, can not be obtained with an uncertainty better than 1 and 2 parts in 10^{-3} that does not allow yet to improve the whole radiometric measurements notably. At present time, we are continuing the characterization of these detectors and are trying to find a mathematical model for the spectral responsivity that can permit to improve the uncertainty on the absolute values of spectral responsivity. The aim of this study is to obtain transfer detectors based on these new large-area trap detectors, to be able to maintain and transfer accurately spectral responsivity measurements with an uncertainty better than 5 parts in 10^4

References

[1] Fox N., Trap Detectors and their Properties, *Metrologia*, vol.28, 1991, p.197-201

[2] The mechanical parts of these trap detectors were bought at the AS RANTELL Company, in Estonia. The mechanical design was studied by the Metrology Research Institute of the Helsinki University of Finland in collaboration with the department of Physics of the University of Tartu in Estonia

[3] Coutin J.-M., Tayeb F., Bastie J. Development of large area trap detectors for improving spectral responsivity measurement of detectors at the BNM-INM, *Proceedings of the 25th Session of the CIE*, San Diego, USA, 25 June - 2 July; 2003, Vol.1, pages D2-50,D2-53 (CIE 152:2003 ISBN 3 901 906 21 5)

[4] Coutin J.M., Touayar O., Bastie J., The using conditions of the BNM-INM cryogenic radiometer as the basis for the French optical radiation measurement scales, *24th session of the CIE, Varsovie*, 24-30 Juin 1999, Proceedings vol. 1 part. 1, p. 729-732.

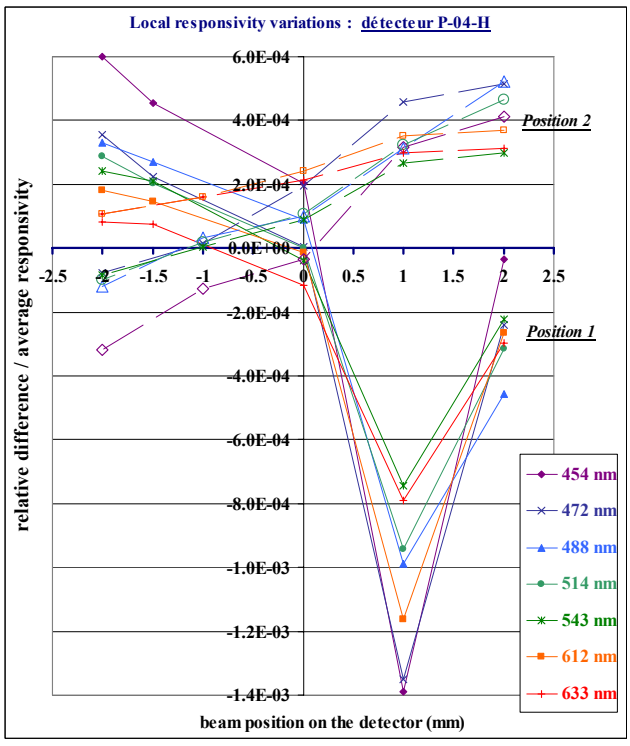

Measurement of Small Aperture Areas

J. A. Fedchak, A. C. Carter, and R. Datla
National Institute of Standards and Technology, Gaithersburg, MD, USA

1. Introduction

Precise and accurate knowledge of small aperture areas is critical to blackbody radiance temperature calibrations performed by the Low Background Infrared (LBIR) calibration facility at the National Institute of Standards and Technology (NIST). The uncertainty in the geometric size and shape of an aperture is directly related to the uncertainty of the calibration. We are presently developing a technique of measuring aperture areas with diameters as small as to 0.05 mm. We require a standard uncertainty to better than 0.1 %.

An instrument for determining the absolute geometric aperture area has been established at NIST (Fowler and Litorja 2003). The technique is based on diffraction corrected optical edge detection and utilizes a high-quality microscope, an interferometer referenced X-Y stage, and a CCD camera. Presently this instrument is limited to circular apertures of diameter greater than 0.35 mm. The measurement accuracy is better than 0.01 % for apertures greater than 3.5 mm, and is better than 0.1 % for aperture diameters larger than 0.35 mm. This instrument is highly commissioned and a single measurement can take many hours.

The LBIR facility has developed an *in situ* technique to radiometrically deduce the size of small apertures. The diffraction corrected signals due to radiation passing through small apertures is compared to those of larger apertures that have known aperture areas (Smith *et al.* 2003). This measurement is performed during a blackbody calibration and does not necessarily represent the geometric aperture area. It does, however, provide the user of the calibrated blackbody with an effective area for computing radiance.

Presently, we are developing a technique to determine the geometric area of small apertures. This is also a relative comparison technique. An integrating sphere is used as a Lambertian source. The aperture of interest is directly mounted to the integrating sphere. A detector, mounted some distance from the sphere, is used to monitor the optical flux passing through the aperture. Since the aperture is directly illuminated by a Lambertian source, diffraction corrections should be minimal. By comparing the detector signals between a large aperture with a known area to that of a smaller aperture with an unknown area, we can obtain precise and accurate measurements of the area or radius of a small aperture. In this paper we discuss the current progress and development of this aperture area measurement technique. A primary goal of this study is to understand the relationship between the effective aperture area, as seen by a detector, and the geometric aperture area. We are particularly interested in apertures with diameters between 0.350 mm and 0.050 mm, as these areas cannot be determined using the NIST absolute instrument.

2. Apparatus and Experimental Technique

In our approach we mount the aperture directly to an integrating sphere. The sphere is illuminated by a high-power LED that has a spectral output in the visible. A photodiode is also mounted to the sphere to monitor the optical intensity within the sphere. Throughout this paper, this photodiode will be referred to as the monitor detector. The aperture is the only open port on the sphere. A portion of the flux passing through the aperture is measured by a silicon photodiode aligned with the aperture and the center of the sphere. This detector, which will henceforth be referred to as the signal detector, is mounted on a 60 cm translation stage. The encoder on the translation stage has a displacement measurement accuracy of 0.1 μm. Data is collected as a function of the separation between the aperture and detector. Presently the signal detector is a 1 mm^2 photodiode. Other detector sizes or types may be used in the future.

Thus far, only green LEDs with a nominal wavelength of 530 nm have been used to illuminate the sphere. Approximately 1 W of optical power is produced by the LED. Careful baffling inside the integrating sphere insures that the light will reflect at least 3 times before exiting the aperture. Most of the optical radiation in the field of view of the signal detector will have undergone many reflections within the sphere. The electric power to the LED is electronically chopped. A lock-in amplifier technique is used to filter the signal from both the signal and monitor detectors. Reflections of the LED light from surfaces outside of the sphere may also be detected. A stationary baffle placed about 8 cm in front of the detector eliminates most of these reflections. In addition, a 3 mm aperture 50 mm in front of the signal detector limits the detector field of view to approximately 5°.

A set of circular apertures with diameters ranging from 0.05 mm to 5 mm is used to test the system as it is developed. These are photo-chemically etched metal apertures; the edge is defined by 8 μm – 13 μm thick nickel plating. The radii of the apertures with diameters larger than 0.35 mm were determined using the absolute instrument described above. These apertures are typical of those used by the users of the LBIR facility. The apertures are attached to the sphere using blackened aperture mounts. These have a 35° knife edge which faces the signal detector.

3. Data and Analysis

The optical intensity on the signal detector is related to the

aperture area by $I = \pi \cdot L \cdot F \cdot A$, where L is the radiance in the sphere illuminating the aperture, A is the aperture area, and F is the geometric configuration factor between the detector and aperture. A normalized signal is determined by dividing the signal produced by the signal detector by that of the monitor detector. The ratio I/L is proportional to the normalized signal. The configuration factor, F, is a function of the detector area, the aperture area, and the separation, d, between the signal detector and aperture. In addition, a correction should be applied which accounts for any diffraction due to the aperture or baffling. Since we will be concerned with the ratio of normalized signals between two different apertures, many of these terms, such as the detector area that appears in F, cancel or are negligible. Assuming diffraction corrections to be negligible, I/L should be proportional to $1/d^2$ for large separations.

Data is taken as a function of the separation between the detector and aperture. The absolute distance between the aperture and the detector is difficult to measure. Therefore the normalized signal is fit to a/d^2, where $d=s+b$, s is the position read from the encoder on the translation stage, and b is a fit parameter which represents the distance between the zero position of the encoder and the aperture. The amplitude of the fit, a, is proportional to aperture area. The ratio of the aperture areas between any two apertures is determined from the fit parameter a (*e.g.*, a_1/a_2). There are several advantages to this analysis technique. Random errors are minimized by taking many data points. Some systematic errors are also eliminated. For example, the distance between the zero position and aperture may depend on the aperture mount, making comparison between two different apertures difficult. However, since any offset is determined by the fit, knowledge of the absolute separation is unnecessary. In addition, deviations from a $1/d^2$ fit serves as a guide to further improvements in the apparatus. For example, stray reflections striking the signal detector may cause the signal to vary as something other than $1/d^2$, indicating that changes in baffling, or some other component of the experiment, may be necessary.

Preliminary data has been taken for the aperture set discussed in the preceding section. Aperture area ratios are determined between any two apertures by taking the ratio of the fit parameters, a, as discussed above. To facilitate a comparison to the aperture radii determined using the NIST instrument, we compare the square root of the aperture area ratio to the radii ratio calculated from the measurements of the absolute instrument. Radii ratios between apertures of similar diameter are likely to have smaller systematic uncertainty than those between large and small apertures. For example, the radii ratio between a 5 mm to 3.5 mm diameter aperture or a 0.6 mm to 0.35 mm diameter aperture may have smaller systematic uncertainties than the ratio of the 5 mm to 0.35 mm diameter aperture. We expect this because configuration factor or diffraction corrections should nearly cancel for apertures of similar diameter. In the current experimental configuration, we find aperture radii ratios typically compare to within 0.5% of those calculated from the NIST absolute instrument for apertures of similar diameter. The diameter of the largest aperture in the test set is 5 mm and the smallest aperture with a known area has approximately a 0.35 mm diameter. The measured radii ratio between these two apertures compares to within 1% of that determined with the absolute instrument.

While this is still below the ultimate goal of developing an aperture area measurement instrument capable measuring small apertures to within 0.1%, it is clear that there are many ways to improve accuracy. Structure seen in the residuals from the fitting procedure, as well as considerations derived from ray-tracing, indicates that some improvement can be achieved by adjusting the size and position of the first baffle as well as reducing the field of view of the detector. Accuracy may also be improved by using a more sophisticated configuration factor in the fit. Improvements in the optical alignment, as well as reducing stray and retro-reflections should also improve performance.

4. Conclusion

We are presently developing an instrument to measure the areas of small apertures. While the goal of 0.1% agreement has not been achieved to present date, it is believed that it will be reached in the near future based on the current results and the opportunity to resolve the perceived set of experimental deficiencies. Currently we can only test our method down the 0.35 mm diameter aperture limit of the NIST absolute instrument. Our ultimate goal is to measure apertures as small as 0.05 mm with an uncertainty of 0.1%. Systematic uncertainties will have to be well understood to measure the area of apertures with diameters as small as 0.05 mm.

In the future, we would also like to use an infrared source to illuminate an infrared integrating sphere for similar testing. Most of the radiometric calibrations performed by the LBIR facility cover a wavelength range of 2 μm to 25 μm. Configuration factors and diffraction corrections used in the calibrations are computed using the geometric area of the apertures. The geometric areas, or radii, are measured using techniques that employ optical wavelengths. The technique described in this paper will not only allow us to measure the geometric aperture area, but will also allow us to understand the difference between geometric areas and effective aperture areas at optical and infrared wavelengths.

References

Fowler, J., M. Litorja, Geometric measurements of circular apertures for radiometry at NIST, *Metrologia,* 40, S9-S12, 2003.

Smith A. W., A. C. Carter, S. R. Lorentz, T. M. Jung, R. V. Datla, Radiometrically deducing aperture sizes, *Metrologia,* 40, S13-S16, 2003.

Low-Background Temperature Calibration of Infrared Blackbodies

Adriaan C Carter, Raju U. Datla
National Institute of Standards and Technology, Gaithersburg, MD, United States

Timothy M. Jung, Allan W. Smith, James A. Fedchak
Jung Research and Development Corporation, Washington, DC, United States

Introduction

The stability of blackbody sources and their ability to be modeled accurately make them well suited for radiometric calibration activity. However, the implementation of the blackbody in industry or the laboratory may, and often does result in blackbody performance that deviates from ideal. The Low Background Infrared (LBIR) facility at the National Institute of Standards and Technology (NIST) was established in 1989 to fulfill the national need for calibrations in the infrared wavelength region in a low 20 K to 80 K background environment (Datla *et al*.). The calibration capability is based on the ability to measure infrared power absolutely using Absolute Cryogenic Radiometers (ACRs) (Foukal *et al*., Datla *et al*.). Four ACRs are maintained at the LBIR facility, two of one model, the ACR I, for measuring powers from 5 nW to 250 μW, and two of a more sensitive model, the ACR II, for measuring powers from 40 pW to 100 μW (Carter *et al*.). Power measurements of 500 pW with 4 pW standard deviation (Type A uncertainty) are now routinely achieved with the ACR II. The four ACRs are periodically compared against the NIST primary national optical power measurement standard, the High Accuracy Cryogenic Radiometer (HACR) for verification of their accuracy (Gentile *et al*.). The results of the most recent intercomparisons are presented below.

Since 2001, 8 blackbodies were calibrated against the ACRs, which demonstrated a significant spread in blackbody performance. These 8 blackbodies incorporated 5 different blackbody designs. Some blackbodies were designed with the goal of achieving near perfect blackbody performance. These blackbodies showed excellent performance and were easy to calibrate. Blackbodies that demonstrated relatively poor calibrations were typically designed with priority given to other performance requirements such as temperature ramp rate, spectral filter use between the cavity opening and the defining aperture of the system, or very low power output. This does not mean that blackbodies can not be designed to meet both industrial process requirements and high calibration quality. In most cases simple changes to those with poor calibration performance could have resolved the most significant problems without changing the desired industrial process performance. These issues are discussed to show that the quality of a delivered blackbody calibration report is a result of the combined performance of the customers blackbody and the ACR together, not just the optimal performance capabilities of the LBIR calibration facility.

Low Background Calibration Facilities

The LBIR facility performs calibration activity in a high vacuum, low temperature 20 K to 80 K background environment created in either one of two cryogenic-vacuum chambers. Both chambers are approximately 2 m in length and have cryo-shrouds that enclose a cylindrical volume that is about 1.5 m in length and about 0.5 m diameter. At test conditions the chambers are typically operated at $1.3*10^{-7}$ Pascal and the closed-cycle He refrigerators used to cool the cryo-shrouds to anywhere between 15 K and 80 K. Inside the chambers, the ACRs are mounted on liquid He cryostats which are cooled to 2 K by pumping the liquid He down to 2670 Pascal.

Absolute Cryogenic Radiometer Performance

A QED-150 trap detector was used as the transfer standard in this study in a way that was similar to previous intercomparisons (Lorentz *et al*.). This is a three Si photodiode reflectance trap detector. The optical path within the detector includes five reflections so that the total reflection at 632.8 nm should be less than 0.4%. To determine an absolute responsivity, the optical power from an intensity stabilized He-Ne laser was measured using first the NIST primary optical power measurement standard, the High Accuracy Cryogenic Radiometer (HACR) and then again later by the newer HACR II. The external responsivity of the trap was measured to be .502448 A/W by the HACR at the beginning of intercomparison effort, and 0.502457 A/W by the HACR II at the end. The uncertainty associated with the calibrated responsivity of each measurement is 0.02 %.

The light source for the intercomparison was a polarized, stabilized He-Ne laser with a maximum power output of 1.5 mW. The laser was transmitted into the cryogenic-vacuum chamber through a Brewster angle window and a 1 cm diameter hole in the cryo-shroud. The ACR under test was placed 1 m from the 1 cm hole in the cryo--shroud so that the ACR only received 20 μW to 30 μW of background radiation through the hole in the shroud. A QED-150 trap detector that was calibrated with the HACR was used to measure the laser power just in front of the Brewster angle window. The trap detector was then removed from the beam path to allow the power to be measured by the ACR inside the chamber. The effective transmission of the HeNe laser from trap detector location in front of the Brewster window to the location of the ACR 1.5 m away was measured in a separate experiment. Table 1 shows the intercomparison results as the ratio of radiometric power measured in the calibrated QED-150 trap to that measured in the ACR. In summary, the intercomparison shows that on average the LBIR ACRs agree with HACR to 0.003 %, with a standard deviation of 0.08 % (Type A). The total uncertainty of the individual intercomparisons is dominated by the Brewster window transmission measurements uncertainty. Greater detail of the intercomparison effort will be presented along with the evaluation of the non-equivalence in the ACRs.

Table 1 Ratio of radiometric power measured in the calibrated QED-150 trap to that measured in the ACR.

ACR Name	$R_{trap/ACR}$	Total Uncertainty
ACR I(a)	1.000658	.036%
ACR I(b)	1.000532	.038%
ACR II(a)	0.999753	.060%
ACR II(b)	0.998922	.040%

Blackbody Calibrations and Overall Performance

Using these ACRs, the performance of the 8 blackbodies calibrated since 2001 can be accurately assessed and compared. The blackbodies calibrated at the LBIR facility are typically cryogenic-vacuum blackbodies that operate with cavity temperatures over the range of 180 K to 800 K. All but one of the blackbodies tested used aperture wheels to vary the size of the defining aperture in front to the blackbody cavity. All of the blackbodies had space between the defining aperture and the cavity for a shutter, 1 or 2 filters wheels, or a chopper. Calibrations of the blackbodies were typically performed entirely within the cryogenic vacuum chambers at $1.3*10^{-7}$ Pascal in a 20 K to 30 K background environment.

The blackbodies were calibrated for radiance temperature using the Stefan-Boltzmann law, length measurements of the optical geometry of the calibration configuration and power measurements made by the ACRs. Expected ACR signals were computed from a simple geometric optical model that uses the radii of the blackbody and ACR defining apertures, the distance between those apertures, and the contact thermometry on the blackbody cavity. Then, all of the defining and non-limiting apertures and baffles are then used to compute diffraction corrections (Shirley *et al*.) for the power measurements actually made by the ACR. The geometrically modeled and diffraction corrected power measurements are then compared to make a radiance temperature calibration curve for that blackbody.

The results of the calibrations for the 5 different blackbody designs show an informative pattern of blackbody behavior. Blackbodies that were designed for rapid temperature ramping demonstrated the most problems. The blackbody cavity that demonstrated the largest difference between measured radiance temperature and the contact thermometry showed a temperature error that varied from 6 % at 200 K to 3 % at 600 K. It is unlikely that this was a sensor calibration error because there were two co-located sensors that measured nearly the same value and an independent experiment confirmed the radiance temperature difference. By comparison, blackbody cavities that were designed to have good thermal conductivity within the cavity showed agreement between radiance temperature and contact thermometry that varied from 0.1 % to 0.5 % at all temperatures.

Often evidence of thermal problems within a blackbody cavity is demonstrated by the temperatures sensors themselves. In one particular blackbody, the thin walls of the cavity conducted so little heat that the cavity temperature as measured by the contact thermometry dropped by 0.3 K when the shutter was opened. Furthermore, two calibrated sensors at dissimilar locations showed a temperature difference of 6 K at a cavity temperature of 400 K. The obvious and subtle causes of these and other calibration issues will be presented in more detail.

References

Datla, R. U., Croarkin, M. C., Parr, A. C., Cryogenic Blackbody Calibrations at the National Institute of Standards and Technology, *Journal of Research of the National Institute of Standards and Technology, 99*, 77-87, 1994.

Foukal, P. V., Hoyt C. C., Kochling, H., Miller, P. J., Cryogenic absolute radiometers as laboratory irradiance standards, remote sensing detectors, and pyroheliometers, *Applied Optics, 29*, 988-993, 1990.

Datla, R. U., Stock, K., Parr, A. C., Hoyt, C. C., Miller, P. J. Foukal, P. V., Characterization of an absolute cryogenic radiometer as a standard detector for radiant power measurements, *Applied Optics, 31*, 7219-7225, 1992.

Carter, A. C., Lorentz, S. R., Jung, T. M., Datla, R. U., ACR II: Improved Absolute Cryogenic Radiometer for Low Background Infrared Calibrations, *Applied Optics, 44,* 871-875, 2005.

Gentile, T. R., Houston, J. M., Cromer, C. L., Realization of a scale of absolute spectral response using the National Institute of Standards and Technology high-accuracy cryogenic radiometer, *Applied Optics, 35*, 4392-4403, 1996.

Lorentz, S. R., Datla, R. U., Intercomparison between the NIST LBIR Absolute Cryogenic Radiometer and an Optical Trap Detector, *Metrologia 30*, 341-344. 1993.

Shirley, E. L., Terraciano, M. L., Two innovations in diffraction calculations for cylindrically symmetrical systems, *Applied Optics, 40*, 4463-4472, 2001.

Cryogenic Radiometers and Absolute Radiometry Instrumentation

Steven R. Lorentz

L-1 Standards and Technology, Inc., 10097 Tyler Place, Suite 1, Ijamsville, Maryland, USA

Email: lorentz@L-1.biz

Abstract

L-1 Standards and Technology, Inc. possesses significant expertise in absolute radiometry applicable for standards laboratories, test facilities and space-based measurements. Our cryogenic radiometers are used by 16 national laboratories around the world to provide the primary standard for radiometric power measurement scales from the deep-UV to the far-IR, and can be customized to perform specific measurements such as cryogenic blackbody calibrations, detector calibrations, laser power, synchrotron radiation, and hard radiation (gamma, x-ray, and particle). L-1 delivers complete solutions to exceed customers' goals for achieving true state-of-the-art absolute radiometric standards.

L-1 Standards and Technology, Inc. acquired the cryogenic radiometer line of Cambridge Research & Instrumentation, Inc. in 2001. This product line includes the LaserRad-II, CryoRad (ACR), and the CryoRad-II primary standard electrical-substitution radiometers. CRI was a pioneer in commercializing the field of primary optical power measurements, giving laboratories around the world access to state-of-the-art instruments for use as national standards. L-1 continues to manufacture these instruments, while introducing versions with even lower noise, wider dynamic range and longer helium hold times. The CryoRad-IIC delivered recently to NIST, has a noise floor of ~0.5 nW with a natural time constant of 2 s and a liquid helium hold-time of over 80 hours. The uncertainty in the optical power measurement scale at 1 mW for this radiometer is 0.005%.

L-1 is in the process of bringing two new cryogenic radiometer products to market. One is a significant upgrade of the existing cryogenic radiometer electronics called TC-04. The new electronics will replace the TC-02 system currently in use. The communication interface is 100MBaud Ethernet. The new system increases power resolution from 10 pW to 100 fW with a proportional decrease in measurement noise. All components will be temperature controlled to better than 0.1 K. The uncertainty of the power measurement scale will be <10 ppm from 25 mW to 1 μW. The 100fW resolution meets increasingly demanding measurements in the cryogenic infrared community. The new system also includes a number of software enhancements and measurement options. One significant changes will be the incorporation of a feed-forward control algorithm to the heater servos. This significantly reduces the measurement time, allowing more measurements to be performed between re-fills of liquid helium.

The second product is a 4 K mechanically-cooled cryogenic radiometer. This new radiometer does not replace the CryoRad-II series of radiometers, but to supplements our line to further meet the needs of the community. By providing a 4 K mechanically-cooled radiometer, users located where liquid helium is prohibitively expensive or supplies are unreliable, can achieve the highest level of measurement accuracy. A 4 K cryo-cooler is used instead of the more traditional 12 K - 15 K cryo-cooler to allow performance on par with the liquid helium cooled version. The measurement uncertainty at 1 mW will be the same as the CryoRad-II series. The natural time constant and noise floor will be similar to the CryoRad-II as well. This will give the user a state-of-the-art instrument that performs exceptionally well at 1 mW, but has the added advantage of a very low noise floor. By allowing low-uncertainty measurements at 1 μW, this new instrument is suitable for measurements anyplace that lower powers are the norm, such as monochromators, synchrotrons, UV and IR detectors, etc.

Custom projects are also a specialty of L-1. The 10CC infrared collimator for the LBIR facility at NIST. The 10CC is a cryogenic infrared collimator operating at <20 K, producing a highly collimated beam of infrared radiation.

L-1 has developed or is in the process of completing a range of support items for ambient calibration work such as trap detectors, ultra-precision ultra-stable amplifiers and temperature controllers, and cryogenic items such as blackbodies, mirrors, monochromators, mechanical motion, choppers, stepper motors, electronics, and detectors. Whether you need a single radiometer or detector, or a complete calibration system, L-1 can deliver a custom, state-of-the-art system to exceed your needs.

We will present results (i.e. noise, non-equivalence, time-constant, absorptance, responsivity, etc.) from several recent cryogenic radiometers that we have developed for a variety of applications. Their responsivity ranges from 2 K/mW to 210 K/mW at operating temperatures from 2.0 K to 9 K.

Consistency of radiometric temperature measurement with a local realization of the ITS-90 from 1700 °C to 2900 °C

Chul-Woung Park, Dong-Hoon Lee, Bong-Hak Kim, and Seung-Nam Park
Division of Optical Metrology, Korea Research Institute of Standards and Science (KRISS), Korea

Abstract. We measured temperatures of a blackbody with a filter radiometer to confirm the consistency of radiometric temperature measurement with the local realization of the ITS-90 at KRISS from 1700 °C to 2900 °C. The resulting temperature differences are within a range from 1 °C to 2 °C, which is less than the measurement uncertainty as well as our calibration and measurement capability of luminous intensity that is 0.5 % (k = 2) at 2900 °C.

I. Introduction

Since high temperature blackbodies were used as the spectral radiance and irradiance sources for spectro-radiometer calibration, several NMIs compared filter radiometer measurements with the international temperature scale ITS-90 using blackbodies [1-3]. Measurement of the thermodynamic temperature of blackbodies with a filter radiometer enables us to confirm its consistency with the ITS-90 and to establish a detector-based irradiance scale [4]. Although the filter radiometry requires more advanced realization technique, it can reduce errors caused by the extrapolation of the ITS-90 above 1084.62 °C. Furthermore, if the ITS-90 and the filter radiometry are realized simultaneously within one laboratory, a high level of confidence in the radiometric scale as well as in the ITS-90 can be achieved by periodic comparison [2].

In this paper, we present the comparison results of the ITS-90 with radiometric temperature measurements at a high temperature blackbody from 1700 °C to 2900 °C. The difference between the two measurement methods is discussed considering the major uncertainty components of the radiometric temperature measurement and the ITS-90 realization in KRISS.

II. Experimental setup

The experimental setup consists of a high temperature blackbody, a filter radiometer, and the KRISS reference pyrometer, as shown Fig.1. A graphite tube with an inner diameter of 36 mm and a length of 280 mm acts as a heating element in the blackbody (Thermogage). The aperture of the graphite tube is limited by a blackbody aperture with a diameter of 6 mm. The radiometer and the pyrometer are installed on a linear translation stage. The filter radiometer is a photometer supplied by LMT with a temperature controller. An external precision aperture is installed to define the active area size of the radiometer. The size of the precision aperture is measured by the laser spot scanning method [5] with a relative uncertainty of $8 \cdot 10^{-5}$. The distance between the radiometer aperture and the blackbody aperture is fixed to 1 m. The distance of the pyrometer from the blackbody is adjusted so that the pyrometer has the same field of view as the radiometer.

The pyrometer has two spectral bands determined by interference filters with a bandwidth of 10 nm at a peak wavelength of 650 nm and 850 nm, respectively. With the 650-nm filter, an additional band suppression filter (CVI KG5) is used to reject the possible leakage light at longer wavelengths [6]. At both spectral bands, the pyrometer is scaled in reference to a copper point blackbody according to the definition of the ITS-90.

The absolute spectral responsivity of the radiometer is measured from 360 nm to 825 nm by the Spectral Responsivity Comparator (SRC) at KRISS. A trap detector (QED-200, Grasby Optronics) and a pyroelectric detector used as a transfer standard in the SRC are calibrated against the KRISS absolute cryogenic radiometer. The relative standard uncertainty of the radiometer is 0.3 % in terms of the illuminance responsivity.

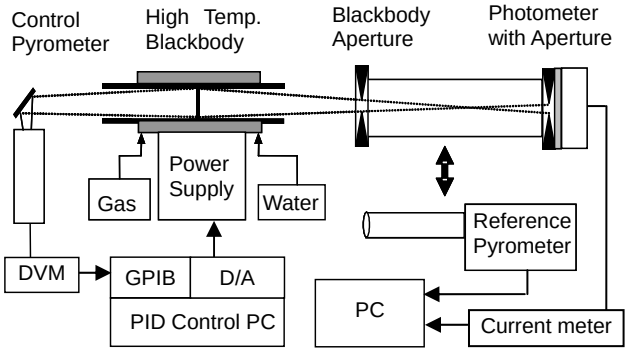

Figure 1. Schematic diagram of experimental setup for comparison between the detector-based radiometric temperature measurement and the source-based ITS-90.

III. Results

Temperature measurement is performed at each temperature setting after confirming stabilization of the blackbody with the reference pyrometer. The pyrometric temperature at each setting is determined by taking an equally weighted average of temperatures obtained with the two spectral bands.

Temperatures measured by the filter radiometer are calculated from the simplified equation [3]

$$I_D = G\,\varepsilon \int_0^\infty S(\lambda)\,L(\lambda, T)\,d\lambda$$

, where the photocurrent I_D is given by an integral of the blackbody radiance $L(\lambda,T)$ multiplied with the absolute spectral responsivity of the radiometer $S(\lambda)$. The geometric factor G is given by the aperture areas and the distance between the apertures. The blackbody emissivity ε is assumed to be unity.

Figure 2 shows the temperature difference between the local ITS-90 realized by the pyrometer and the filter radiometric measurement in a temperature range from 1700 °C to 2900 °C. The differences lie in a range from 1 °C to 2 °C. Even if the ITS-90 is smaller that the radiometric measurement, the differences are less than the comparison uncertainty (k = 2) denoted by the error bars in Fig. 2. Furthermore, the comparison shows that the relative difference of the radiometer and the ITS-90 at 2900 °C in

terms of the illuminance responsivity is less than 0.5 %, which is declared in our calibration and measurement capability (CMC) of the luminous intensity.

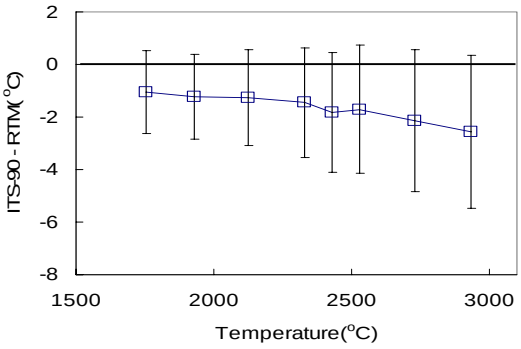

Figure 2. Temperature difference between the ITS-90 and the radiometric temperature measurement (RTM) at different temperatures.

Table 1. Uncertainty budget of comparison of the ITS-90 and the radiometric temperature measurement at 2700 °C.

Sources	Components	Uncertainty (°C; k=2)
the ITS-90	Temperature scale	0.68
Radiometric temperature measurement	Spectral responsivity	1.07
	Infrared leakage	0.17
	Distance	0.35
	Blackbody aperture	0.05
	Radiometer aperture	0.04
	Signal measurement	0.02
Comparison using blackbody	Stability	0.1
	Uniformity	0.15
Combined uncertainty (k=2)		2.1

To understand the difference and draw out ideas to improve the consistency, the comparison uncertainty at 2700 °C is evaluated as shown in Table 1, where the uncertainty from the ITS-90 realization, the radiometric temperature measurement, and the comparison process using the blackbody are considered. The uncertainty of the ITS-90 is estimated by the local realization of the ITS-90 and the measurement deviation of the two spectral bands of the pyrometer. Taking the uncertainty components such as the cooper fixed point blackbody, and the spectral characteristics, non-linearity of the pyrometer into account according to the standard method described in the reference [7], we estimated the ITS-90 realization uncertainty. The expanded uncertainty (k=1) increases from 0.1 °C at the copper fixed point to 0.7 °C at 3000 °C.

The uncertainty of the ITS-90 is smaller than that of the radiometric temperature measurement, in which the spectral responsivity uncertainty is the dominant uncertainty component. Although the temperature differences shown in Fig. 2 are within the error bars, the uncertainty evaluation seems to be somehow optimistic. A systematic error might be mainly related to our lower assignment in scaling the spectral responsivity and the illuminance responsivity, which is observed also in the key comparisons such as CCPR-K.2.b [8] and CCPR-K3.b.2 [9]. Additionally, since the silicon-based photometer can response up to 1100 nm and the spectral emission of the blackbody is more dominant in the infrared, the calibration range of the radiometer spectral responsivity needs to be extended. The uncertainty of the infrared leakage in Table 1 is estimated by assuming a uniform leakage in the order of 10^{-6} from 825 nm to 1100 nm. The infrared leakage uncertainty become more significant as the temperature deceases, resulting in 0.5 °C at 1700 °C. We expect that an improvement in the spectral responsivity measurement of the radiometer can resolve the systematic error below 2600 °C. Above 2600 °C, however, we address the pyrometer linearity as an important correction factor to be considered, which has been only measured below the irradiance level corresponding to 2600 °C.

IV. Conclusion

Consistency of radiometric temperature measurements with the local realization of the ITS-90 at KRISS is confirmed by comparing the blackbody temperatures measured with a reference pyrometer and a filter radiometer in a range from 1700 °C to 2900 °C. The differences are within 2 °C, which is less than the measurement uncertainty as well as our calibration and measurement capability of luminous intensity that is 0.5 %. More accurate calibration of the spectral responsivity of the radiometer in the IR range up to 1100 nm is expected to resolve the systematic error below 2600 °C. Above 2600 °C, it is necessary to check nonlinearity of the pyrometer.

Acknowledgement. We are grateful to Dr. Howard Yoon and Dr. Robert D. Saunders at NIST for their continuous encouragement and valuable discussions.

References

[1] Khlevnoy B. B., Harrison N. J., Rogers L. J., Pollard D. F., Fox N. P., Sperfeld P., Fischer J.,Friedrich R., Metzdorf J., Seidel J., Samoylov M. L., Stolyarevskaya R. I., Khromchenko V. B.,Ogarev S. A., and Sapritsky V. I., *Metrologia, 40*, S39-S44, 2003.

[2] Yoon H. W., Sperfeld P., Galal Yousef S., and Metzdorf J., *Metrologia, 37*, 377-380, 2000.

[3] Sperfeld, P., Raatz, K.-H., Nawo, B., Moller, W., and Metzdorf, J. *Metrologia, 32*, 435-439, 1995/6.

[4] Yoon H. W., Gibson C. E., and Barnes P. Y., *Appl. Opt., 41*, 5879-5890, 2002.

[5] Lassila, A., Toivanen, P., and Ikonen, E., *Measure. Sci. Technology, 8*, 973-977, 1997.

[6] Hahn, J. W., Park, S. N., Lee, E. S., and Rhee, C., *Temperature: Its Measurement and Control in Science and Industry 6*, 227-235, 1992.

[7] Fisher, J., Battuello, M., Sadli, M., Ballico, M., Park, S. N., Saunders, P., Zundong, Y., Carol Johnson, B., Van der Ham, E., Sakuma, F., Machin, G., Fox, N., Li, W., Ugur, S. and Matveyev, M. *Temperature: Its Measurement and Control in Science and Industry, 7*, 631-638, 2003.

[8] Goebel, R., and Stock, M., *Metrologia, 41/1A,* 2004.

[9] Ikonen, E., and Holvila, J., *Metrologia, 41/1A,* 2004.

Project of absolute measuring instrument of power on the basis of high-temperature superconducting thermometer for soft X-ray radiation.

A.D. Nikolenko[1], V. F. Pindyurin.
Budker Institute of Nuclear Physics, 630090 Novosibirsk, Russian Federation

Khrebtov I.A, Malyarov V.G., Khokhlov D.A., Ivanov K.V.
S.I.Vavilov State Optical Institute, 199034, St.Petersburg, Russian Federation

The present report considers the design and main attainable parameters of an absolute radiometer with electrical substitution of power on the base of high- temperature superconducting film bolometer cooled by the liquid nitrogen. This radiometer will be created in the framework of the ISTC project #2920 in the Vavilov State Optical Institute (St. Petersburg, Russia). As is planned, this instrument will be used as the reference detector on the "Soft X-ray metrology" station at the VEPP-3 storage ringin of the Siberian Synchrotron Radiation Center (Budker Institute of Nuclear Physics, Novosibirsk, Russia) for measurements of the soft X-ray photon flux with power circa 1mkW with an accuracy of 1%.

[1] A.D.Nikolenko@inp.nsk.su

WRR to SI intercomparisons 1991 - 2005

W. Finsterle, S. Möbus, C. Wehrli, I. Rüedi, and W. Schmutz
PMOD/WRC, Dorfstr. 33, CH-7260 Davos Dorf, Switzerland

Abstract. Since 1977 the World Radiometric Reference (WRR) has served as the primary standard for Solar Irradiance Wm^{-2} (Fröhlich et al. 1977). The WRR is realized by the World Standard Group (WSG) of pyrheliometers. In order to check the compatibility of the WRR with the SI system of units, the WSG was compared to cryogen standards in 1991, 1995, (Romero et al. 1991, 1995) and 2005 (Möbus 2005). In this poster we present an overview of these comparison. Due to a re-determination of the area of the radiometric aperture used by Romero et al. (1991, 1995) their results had to be corrected by roughly 0.1%. The corrected results still agree with the assumption WRR/SI=1. Together with the latest results of the 2005 campaign the high stability of the WRR and excellent reproducibility of the comparisons to within a few hundred ppm are shown.

Acknowledgments We thank Claus Fröhlich for helpful discussions as well as Peter Blattner of metas and Malcolm White of NPL for their support of the 2005 comparisons.

References

Fröhlich, C., et al., World Radiometric Reference, in *WMO/CIMO Abridged Final Report of the 7th session*, WMO-No. 490, 97-100, 1977

Möbus, S., Experimenteller Vergleich von Primärstandards für die optische Strahlungsmessung, *Diploma thesis*, Fachhochschle Ravensburg-Weingarten and PMOD/WRC, 2005

Romero, J., Fox, N. P., Fröhlich, C., First comparison of the Solar and an SI Radiometric Scale, *Metrologia*, 28, 125-128, 1991

Romero, J., Fox, N. P., Fröhlich, C., Improved comparison of the World Radiometric Reference and the SI radiometric scale, 1995: *Metrologia*, 32, 523-524, 1995

Session 2

UV, Vis, and IR Radiometry

QA/QC of Spectral Solar UV irradiance measurements

M. Blumthaler, and J. Schreder
Innsbruck Medical University, Austria

A. F. Bais, and S. Kazadzis
Aristotle University of Thessaloniki, Greece

J. Gröbner
Physikalisch-Meteorologisches Observatorium Davos, Switzerland

G. Seckmeyer
University of Hannover, Germany

A. R. Webb
University of Manchester, U.K.

Abstract. With a transportable spectroradiometer system routine quality assurance of spectrally resolved ultraviolet irradiance measurements were performed at 26 UV monitoring sites in Europe. 20 out of the 26 visited sites agreed to within 5% in the UVB and in the UVA range with the travelling unit. The results so far have shown the unique possibilities offered by such a travelling unit for providing on-site quality assurance of solar ultraviolet irradiance measurements.

Introduction

Solar UV irradiance is measured in Europe at more than 25 stations with spectroradiometers since several years. Most of the data are transferred to the European UV database for spectral UV irradiance, which is operated by the Finish Meteorological Institute and which was initiated within the EU-funded project EDUCE (European database for Ultraviolet radiation climatology and evaluation) from 2000 to 2003. In order to assure the quality of these data, several activities have been carried out at the measurement sites and at the data base. Routine quality control at the site is based on a careful schedule for frequent absolute calibration of the spectroradiometer by use of calibrated lamps. Furthermore, several different methods for quality control are in use by the local operators, mainly the regular comparison of weighted spectral data with collocated broadband detectors in the UVB and in the UVA wavelength range, and the comparison of measurements under clear sky conditions with results from radiative transfer model calculations. Guidelines for this quality control of UV monitoring are published by WMO (*Webb*, 2001).

A new report about the state of the art for quality assurance in monitoring solar ultraviolet radiation is published by WMO (*Webb*, 2003). Until recently, the standard method for quality assurance of spectral UV measurements was the direct intercomparison of the instruments. The spectroradiometers from different parts in Europe were gathered at one location and operated there for several days in an synchronous mode, so that the individual results could be intercompared, even when the weather conditions were changing during the scanning time (i.e. *Bais et al*., 2001).

A new approach for quality assurance at the site of the UV measurements was undertaken with a travelling spectroradiometer system, which has been developed and validated within the frame of the EU-founded project QASUME (Quality Assurance of Spectral Ultraviolet Measurements in Europe through the development of a transportable unit). The aim of the project is to establish a reliable unit which can be transported to any UV monitoring site in Europe to provide an assessment of the UV measurements performed by the local site instrument. This on-site quality assurance exercise should be viewed as an alternative to the intercomparisons performed previously. The advantages of the proposed approach are that local monitoring instruments do not need to be transported and are used in their natural environment during the intercomparison; furthermore, a site can be visited at regular intervals to check its stability over extended time periods. While this is a more realistic evaluation of a monitoring site, it places strict criteria on the performance and operation of the travelling instrument that must be proven to be stable at a level against which all other instruments will be judged.

Validation

The validation phase of the travelling unit (B5503) was scheduled for the first year of the project (2002), and consisted of an intercomparison with six qualified spectroradiometers followed by site visits to each of the home sites of these instruments. The summary of the results are shown in Figure 1. The absolute offset between five out of six instruments and the travelling unit are between –5 and

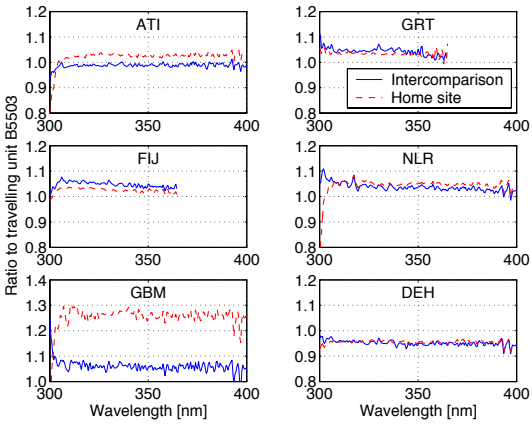

Figure 1 Mean spectral ratios between six spectroradiometers and the travelling unit B5503. The blue curves were measured during the joint intercomparison at JRC, the red (dashed) ones were obtained at the home sites of each instrument.

+5% and are in good agreement with the differences in the respective irradiance standards to which each instrument is referenced. The consistency between the intercomparison and the home site measurements is good, with four out of six site visits being within 2%. The deviations seen relative

Table 1: Summary of the quality assurance of spectral UV measurements. The ratio to the travelling unit B5503 was calculated from the mean of all simultaneously measured spectra in the wavelength range 305 to 315 nm (UVB) and above 315 nm (UVA-visible).

Site	No. of spectra / No. of days	Ratio to B5503 UVB / UVA-Vis.	Variability in % 5-95th percentile
Austria, Innsbruck	53 / 3	1.00 / 0.98	4
Austria, Wien	45 / 4	1.08 / 1.04	8
Belgium, Brussels, 1	51 / 3	1.05 / 1.03	5
Belgium, Brussels, 2	52 / 3	0.97 / 0.96	9
Belgium, Brussels, 3	52 / 3	0.95 / 0.94	7
Czech, Hradec Kralove	52 / 3	0.98 / 0.97	5
EU - JRC, Ispra	1094 / 54	1.01 / 0.99	4
Finland, Jokioinen	228 / 8	1.03 / 1.02	6
Finland, Sodankyl	67 / 3	1.05 / 1.03	4
France, Briancon	65 / 3	0.90 / 0.87	5
France, Lille	55 / 3	1.01 / 0.99	8
Germany, Hanover	13 / 3	0.96 / 0.96	8
Germany, Lindenberg	41 / 2	0.98 / 0.96	6
Germany, Neuherberg	59 / 5	1.05 / 1.01	10
Great Britain, Manchester	64 / 4	1.28 / 1.27	14
Great Britain, Reading	79 / 4	0.99 / 0.98	8
Greece, Thessaloniki	116 / 8	1.04 / 1.03	8
Italy, Lampedusa	59 / 4	1.05 / 1.04	8
Italy, Rome	53 / 3	0.98 / 0.95	5
Netherlands, Bilthoven	133 / 7	1.04 / 1.03	6
Norway, Oslo	82 / 4	0.96 / 0.95	4
Norway, Trondheim	75 / 4	0.98 / 0.99	9
Poland, Warsaw	69 / 4	0.99 / 0.97	8
Portugal, Lisbon	86 / 4	1.21 / 1.16	11
Spain, El Arenosillo	95 / 5	0.95 / 0.89	8
Sweden, Norrköping	107 / 5	1.03 / 1.03	10

to the GBM instrument are unresolved but are thought to be due to problems related with the local site instrument. Based on these measurements and on a comprehensive uncertainty estimate of all relevant parameters affecting the measurements, the conclusion is that the travelling unit is able to provide quality assurance of spectral ultraviolet measurements in the range 300 to 400 nm with an expanded uncertainty of 5%.

Results

Between May 2003 and September 2004, the travelling unit visited 19 further UV monitoring sites in Europe and performed routine quality assurance of each local site spectroradiometer. Each visit lasted between 3 and 5 days so as to gather simultaneous UV measurements between the local instrument and the travelling unit during at least two nonrainy days from morning to evening (solar zenith angle below 85°). The measurements were normalised to a common slit width of 1 nm using the publicly available SHICRivm software [*Slaper et al.,* 1995] and used successfully in previous intercomparisons. This procedure also allowed to determine the spectral wavelength shift of each local instrument.

Combined with the results from the validation round in 2002, a total of 26 UV monitoring sites were visited, of which two were visited twice. These quality assurance results are summarized in Table1. The results of each site visit are reported in individual reports which are available from the project WEB-page (http://lap.physics.auth.gr/qasume) and also as separately published documents (see *Gröbner et al.,* 2003a, b and 2004).

These results show that the majority of the instruments performed well during the intercomparison period with differences to the travelling unit of 5% or less. Even though the results from such a short intercomparison period cannot be extrapolated to the whole measurement series available at each site, it is hoped that these results are still representative for the overall performance of these site instruments.

Acknowledgments: The financial support by the European Commission through the project QASUME (EVR1-CT2001 -40011) is acknowledged. We wish to thank all institutes which participated and hosted the site intercomparisons.

References

Bais, et al., The SUSPEN intercomparison of ultraviolet spectroradiometers, *J. Geophys. Res.,* **106**, 12509-12526, 2001.

Gröbner, et al., Quality Assurance of Spectral Ultraviolet Measurements in Europe through the development of a transportable unit (QASUME); Report of visits Round 2002, EUR 20991 EN, European Commission, 2003a.

Gröbner, et al., Quality Assurance of Spectral Ultraviolet Measurements in Europe through the development of a transportable unit (QASUME); Report of visits Round 2003, EUR 20992 EN, European Commission, 2003b.

Gröbner, et al., Quality Assurance of Spectral Ultraviolet Measurements in Europe through the development of a transportable unit (QASUME); Report of visits Round 2004, EUR 21398 EN, European Commission, 2004.

Slaper, H., H. Reinen, M. Blumthaler, M. Huber, and F. Kuik, Comparing ground-level spectrally resolved UV measurements from various instruments: a technique resolving effects of wavelength shifts and slitwidths, *Geophys. Res. Lett.,* **22,** 2721-2724, 1995.

Webb, A., Guidelines for Site Quality Control of UV Monitoring, World Meteorological Organization, TD 884, GAW-report No. 126, 2001.

Webb, A., Quality Assurance in Monitoring Solar Ultraviolet Radiation: the State of the Art, World Meteorological Organization,TD 1180, GAW-report No. 146, 2003.

NEWRAD 2005

The Metrology Light Source – the new dedicated electron storage ring of PTB

R. Klein, G. Ulm
Physikalisch-Technische Bundesanstalt, Berlin, Germany

BESSY MLS Team
BESSY GmbH, Berlin, Germany

Abstract
The Physikalisch-Technische Bundesanstalt (PTB) has started the construction of a low-energy electron storage ring in the close vicinity of BESSY II where PTB operates a laboratory for X-ray radiometry. The new 600 MeV storage ring, named 'Metrology Light Source' (MLS) [1], will be mainly dedicated to metrology and technological development in the UV and VUV spectral range and thus will fill the gap in the spectral range that has opened up since the shut-down of BESSY I. Moreover, the MLS will deliver intense radiation in the IR and FIR/THz spectral range. The MLS can be operated with parameters optimized for special calibration tasks, which is rarely possible at a multi-user facility such as BESSY II. The MLS is designed in close co-operation with the BESSY GmbH, construction has started in the autumn of 2004 and user operation is scheduled to begin in 2008.

Introduction

PTB, the German National Metrology Institute, has been using synchrotron radiation for photon metrology in the spectral range from the UV to X-rays at the electron storage rings BESSY I and BESSY II for more than 20 years to fulfill its mission to realize and disseminate the legal radiometric units in this spectral range for Germany. Bending magnets which emit synchrotron radiation with well-defined properties are an ideal source for radiometry, especially when the storage ring can be operated as a primary source standard [2, 3, 4] which allows radiometry, limited so far by the utilization of black-body radiation to the infrared, visible and near UV spectral region, to be extended to higher photon energies up to the X-ray region [5]. At BESSY II, PTB operates a laboratory [4, 6], the PTB laboratory for UV and VUV radiometry [7], located at the BESSY I electron storage ring, was shut down at the end of the operation of BESSY I in 1999. Since then, PTB has lacked a dedicated source for metrology in the UV/VUV spectral region. This shortcoming will soon be overcome with the beginning of operation of the MLS.

MLS Layout

The MLS has been designed by the BESSY GmbH to meet PTB's demands for a UV/VUV source with high stability and reproducibility and to complement the spectral region covered by the BESSY II electron storage ring at the lower photon energy range. The main storage ring parameters are summarized in table 1. Injection will be from a 100 MeV microtron, the electron energy can be ramped up into the range from 200 MeV to 600 MeV, i. e. the characteristic photon energy can be tuned in the range from 11.6 eV up to 314 eV. The available spectra from the bending magnets as well as from an undulator perfectly complement the spectra available at BESSY II at the low energy side (fig. 2). The variation of the electron energy allows the high energy end of the bending magnet spectrum to be adjusted in such a way, that radiation that would lead to higher diffraction orders and stray light in a monochromator is suppressed. The electron beam current can be adjusted in a range of more than 11 orders of magnitude, i.e. from a single electron (1 pA) up to 200 mA, in order to comply with the dynamic range of a device to be calibrated. The MLS can also be operated in a special mode for the generation of coherent synchrotron radiation with greatly enhanced power in the FIR/THz spectral region.

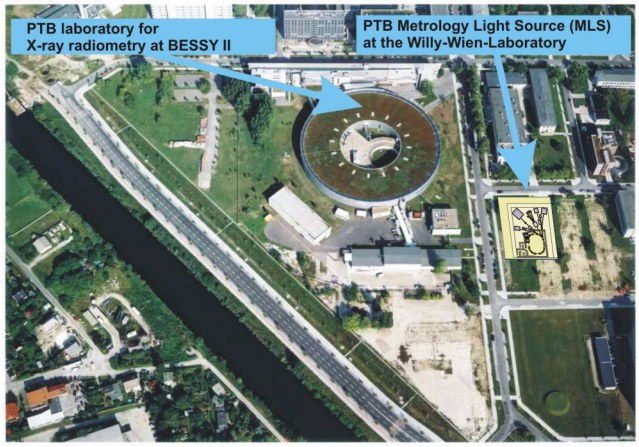

Figure 1: Aerial view of the location of the MLS in the close vicinity of BESSY II.

Table 1: Main parameters of the storage ring

parameter	value
lattice structure	DBA
circumference	48 m
electron energy	200 MeV to 600 MeV
electron beam current	1 pA to 200 mA
magn. induction of bending magnet	0.43 T to 1.3 T
char. photon energy	11.6 eV to 314 eV
nat. emittance (600 MeV)	100 nm rad
injection energy	100 MeV

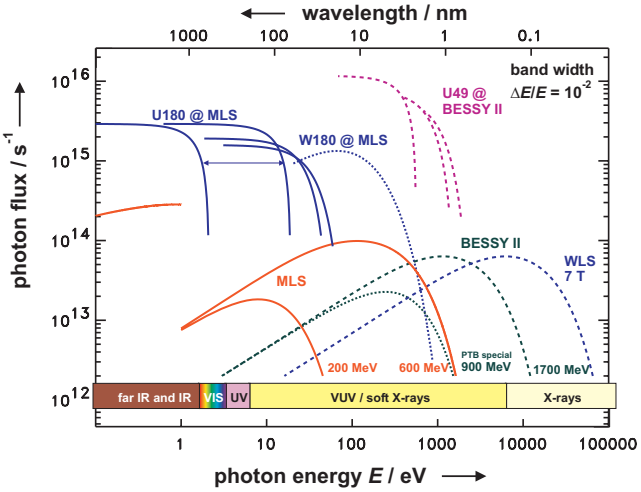

Figure 2: Spectrum of the radiation from MLS and BESSY II.

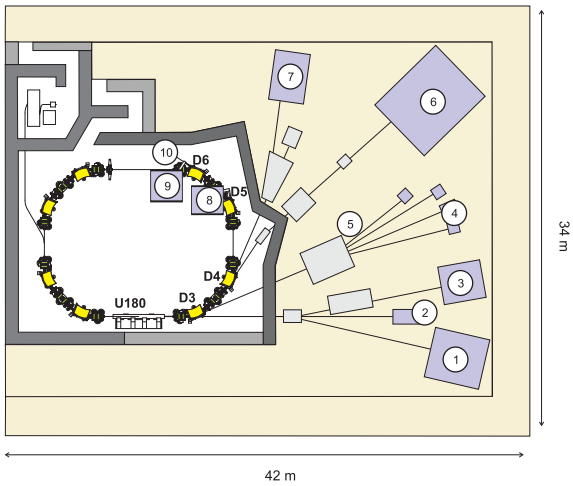

Figure 3: Planned instrumentation at the MLS.

Instrumentation and tasks

Figure 3 illustrates the planned instrumentation at the MLS, a list of the beamlines is given in table 2.

The spectral photon flux of synchrotron radiation from bending magnets can be precisely calculated from Schwinger's theory [5], given that all parameters entering the equation are known. At the MLS, PTB will install equipment for the measurement of these parameters with high accuracy. The storage ring parameters taken into account in the calculation are the electron beam current, the electron energy, the magnetic induction at the radiation source point and the vertical beam size and divergence. The electron energy will be measured by Compton backscattering of laser photons (beamline 2), the other parameters will be determined in a similar way as done at BESSY II [2, 3]. The relative uncertainty in the calculation of the spectral photon flux will be below 0.04 % for photon energies below 100 eV and will then gradually increase for increasing photon energies. For 1000 eV photons, the relative uncertainty will be 0.17 %.

PTB will use the storage ring as a primary source standard for the calibration of energy-dispersive detectors (beamline 4) and radiation sources (beamline 5). For these applications, it is essential that the electron energy and electron beam current allow adjustment as required by the current calibration task in order to achieve low relative uncertainties. In combination with a monochromator beam line as a source of monochromatic radiation of high spectral purity, the storage ring is also used for detector-based radiometry and reflectometry (beamlines 6, 7). IR (beamline 9) and FIR/THz radiation (beamline 8) will be available for radiometry, photon metrology or analytics.

Besides bending magnet radiation, highly intense undulator radiation in the spectral range from the IR to the EUV will be available for high accuracy radiometry based on a cryogenic radiometer (beamline 3) or high flux experiments (beamline 1 and 2).

Table 2: List of planned beamlines and experimental stations at the MLS

1	deflected undulator radiation
2	direct undulator radiation / IR / Compton-backscattering
3	UV/VUV monochromator for undulator radiation
4	direct bending magnet radiation
5	UV/VUV monochromator (source calibration)
6	EUV plane-grating monochromator
7	UV/VUV monochromator (detector calibration)
8	FIR/THz beamline
9	IR beamline
10	diagnostics frontend

Summary

The parameters of the MLS, especially the electron beam current and the electron energy, can be varied in a wide range in order to create measurement conditions that are tailor-made for specific calibration tasks. All storage ring parameters can be precisely measured, which enables PTB to operate the storage ring as a primary source standard. Bending magnet radiation with characteristic energies ranging from 11.6 eV up to 314 eV will be available and so will be undulator radiation from the IR up to the EUV spectral region.

The MLS complements the measurement potential available at BESSY II in the lower energy range and thus enables PTB to use synchrotron radiation from the THz up to the hard X-ray region for high-accuracy photon metrology, especially radiometry.

References

1. Klein, R. et al., Proc. of EPAC04, Lucerne, Switzerland, 2290–2292, 2004.
2. Klein, R., R. Thornagel, G. Ulm, Proc. of EPAC04, Lucerne, Switzerland, 273–275, 2004.
3. Thornagel, R., et al., Metrologia, 38, 385-389, 2001.
4. Klein, R., et al., Synchrotron Rad. News 15, no. 1, 23-29, 2002.
5. Ulm, G., Metrologia, 40, S101–S106, 2003.
6. Ulm, G., et al., Proc. SPIE, 3444, 610–621, 1998.
7. Ulm, G., et al., Rev. Sci. Instrum., 66, 2244–2247, 1995.

NEWRAD 2005

Fractional self-calibration of silicon photodiodes

J. Gran
JV, Kjeller, Norway

T. E. Hanssen
AME, Horten, Norway

A. Hallén
KTH, Kista, Sweden

J. C. Petersen
DFM, Lyngby, Denmark

Abstract. We describe the first results aiming at using specially designed silicon photodiodes as primary standards in optical radiometry. Currently the most accurate measurements of optical power are obtained using a cryogenic radiometer (CR), where the principle of operation is by electrical substitution. The CR is a rather complex and expensive device, and therefore simpler more straightforward methods are desirable. We propose to use specially designed silicon photodiodes as a primary standard, where one half of the surface will be used for calibration purposes only whereas the other half is used for measurements. By biasing the detector we eliminate the internal losses in the detector and by measuring the reflectance of the surface of the detector we estimate the two loss mechanisms separately and thus expresses the responsivity of the detector in terms of fundamental constants. The first design and initial measurements of the detectors is reported.

Introduction

The principles for the establishment of a new primary standard based on specially designed silicon photodiodes is presented. The method is a modified method of the self-calibration method established by Geist and Zalewski in 1980. The basic idea is that the responsivity, R, of an ideal photodiode can be described by fundamental constants and the wavelength of the radiation while deviations from ideal performance is described by the two loss mechanisms, reflectance from the surface and non-perfect internal quantum efficiency (IQE). The reflectance and the IQE are estimated separately in different relative experiments. Unfortunately, the initial methods turned out to change the IQE resulting in a decreased interest for using the method. The method proposed here is expected not to have the disadvantages experienced by the original self-calibration method. The initial measurements and characterizations of the detectors are presented.

Theory

The responsivity of a semiconductor photodiode can be expressed as

$$R(\lambda) = e\lambda/hc\left(1-\rho(\lambda)\right)\left(1-\delta(\lambda)\right), \qquad (1)$$

where e is the elementary charge, h is Planck's constant, c is the speed of light in vacuum, and λ is the vacuum wavelength of the radiation. These quantities form the ideal term of a quantum detector. The reflectance is given by $\rho(\lambda)$, and the internal quantum deficiency (IQD) by $\delta(\lambda)$. From (1) it is seen that by reducing the reflectance and the quantum deficiency to negligible levels the silicon photodiode would become a primary standard detector, because the spectral response $R(\lambda)$ is then expressed in terms of fundamental constants and the wavelength.

In a photodiode, one electron hole pair is created per incident photon and transported through the diode by its built in potential at the pn junction of the diode. The finite lifetime for electrons and holes makes it unlikely that all of them reach the connectors of the diode and an IQE less than one is expected and observed. In the proposed method a potential is created throughout the whole diode in order to reduce transport time of electrons and holes and thus practically eliminate the recombination probability. Since it is impossible to create fully transparent electrodes over a wide spectral range we avoided the problem by depositing a semitransparent electrode on a fraction (half) of the surface and thereby eliminated the IQD on this part. We thereby find the IQD on the uncoated surface. A picture of the detector is shown in fig.1.

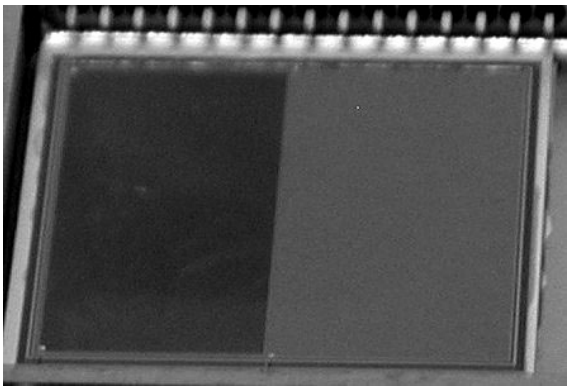

Figure 1. Picture of the Si detector. A semitransparent layer of gold is deposited on the left half of the surface. The

right half is uncoated.

Measurements

So far, only a limited number of measurements have been made. We will present the preliminary results and some preliminary conclusions. More extensive measurements are needed to make definite suggestions and conclusions.

A measurement sequence determining responsivitiy change with applied oxide bias at selected wavelengths is presented in fig. 2. The responsivity change saturates with oxide bias approaching 30 V. The saturation level is a measure of the IQD caused by recombination losses between the oxide and the pn junction of the diode.

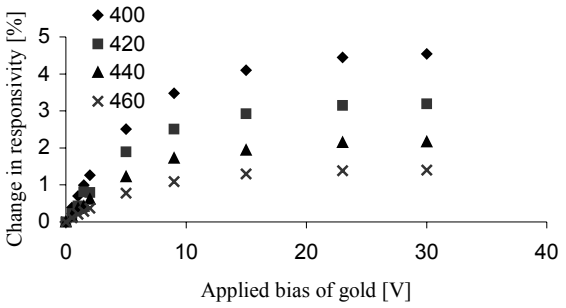

Figure 2. The responsivity change with applied oxide bias at selected wavelengths between 400 and 460 nm is presented.

The uniformity of the detector responsivity is critical in order to achieve the highest possible accuracy. The uniformity of the detector measured with a semiconductor laser at 405 nm. Simultaneously, the spatial reflectance was measured allowing decomposition of the loss mechanisms and determination of the source of the nonuniformity. In fig. 3 the measured uniformity (a) and spatial reflectance (b) is presented.

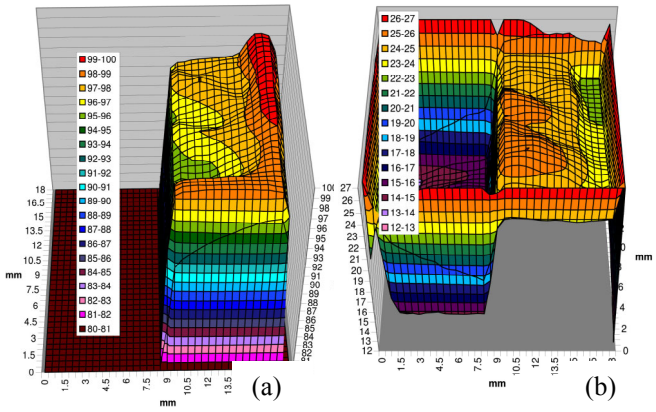

Figure 3. The detector uniformity (a) and spatial reflectance (b) is presented.

We note that the nonuniformity as shown in fig. 3 (a) is in the order of 4 %. This high nonuniformity does not make the detector suited as a standard. The uniformity measurement shows that in areas where the responsivity is high we have a dip in the reflectance and vice versa. Therefore, the reason for the nonuniformity is mainly due to the reflectance from the surface of the detector caused most likely by differences in the oxide thickness. In the next generation of these detectors a different process for the growth of the oxide layer is needed.

The detectors and the thin layer of gold have a relatively large surface. A criterion to succeed with the proposed method is that the gold bias saturates the IQE uniformly. We measured the difference in uniformity with 30 V gold bias and without bias. The results are presented in fig. 4 and shows that the change is relatively uniform taken into account that a semiconductor laser was used in the characterization.

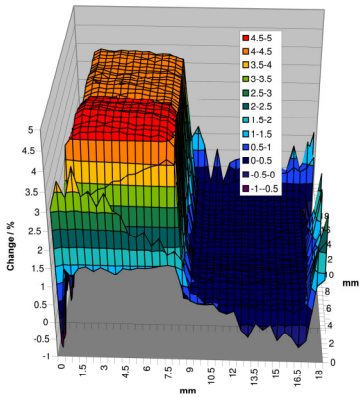

Figure 4. The uniformity change with an applied oxide bias of 30 V.

Preliminary conclusions

So far, promising results of the principles have been obtained. The responsivity changes with oxide bias have been as predicted. The uniformity of the detectors was poorer than expected, making the ones tested so far unsuited as single detector standards. However, since the reason for the nonuniformity is variations in the reflectance, mounting two detectors in a wedge trap configuration is likely to make the detectors suitable for calibration purposes as well. It is highly likely that the uniformity can be improved in the next generation of detectors. More extensive measurements and comparison to the CR will be presented at the conference. In addition, necessary corrections and caution with the method will be presented.

Acknowledgments This project is partly financed by the Nordic Innovations Center (NICe).

References

Zalewski, E. F., Geist, J., Silicon photodiode absolute spectral response self-calibration, *Appl. Optics, 19,* 1214 – 1216, 1980.

Verdebout, J., Booker R. L., Degradation of native oxide passivated silicon photodiodes by repeated oxide bias, *J. Appl. Phys., 55*, 406-412, 1984.

Gentile T. R., Houston J. M., Cromer C. L., Realization of a scale of absolute spectral response using the National Institute of Standards and Technology high-accuracy cryogenic radiometer, *Appl. Optics, 35*, 4392-4403, 1996.

Haapalinna A., Kärhä P., Ikonen E., Spectral reflectance of silicon photodiodes, *Appl. Optics, 37*, 729-732, 1998.

Temperature effects of PTFE diffusers

L. Ylianttila
STUK, Helsinki, Finland

J. Schreder
CMS, Kirchbichl, Austria

Abstract. Poly(tetrafluoroethylene) (PTFE) is the most commonly used diffuser material in ultraviolet irradiance measurements. The temperature sensitivities of five PTFE diffusers were measured over a broad temperature range. The transmittance change varied from -0.015%/°C to -0.1%/°C. At 19°C there was an unexpected abrupt change in transmittance ranging from 1% to 3%. This change is due to the change of the crystal structure of PTFE at 19°C. Temperature sensitivity decreases significantly the accuracy of high precision measurements, especially if the temperature of the diffusers is not stabilized.

Introduction

In optical radiation measurements diffusers are used for input optics in order to achieve a uniform spatial responsivity and a specific angular response, i.e. cosine response in irradiance measurements. In ultraviolet (UV) measurements the most commonly used diffuser material is poly(tetrafluoroethylene), PTFE. PTFE is better known by trade name Teflon®. PTFE has good chemical resistance, it is light- and weather-resistant and has no absorption of water. These properties make PTFE an attractive material for outdoor use.

The effect of temperature on the UV-transmittance of five PTFE diffusers and one quartz diffuser was examined [Ylianttila and Schreder, 2005].

Materials and methods

The temperature sensitivities of six different diffusers were tested. One of the diffusers was a quartz diffuser, so that the effect of the temperature change on the PTFE diffuser and on the fiber-end could be distinguished. The tested diffusers included three Schreder UV-J1002 and UV-J1003 type PTFE diffusers [Schreder et. al., 1999], a standard PTFE plane diffuser of a Bentham DM 150 spectroradiometer, a PTFE dome diffuser of an Optronic 742 spectroradiometer and a a quartz diffuser of an Optronic 742 spectroradiometer. The Schreder UV-J1002 and UV-J1003 diffusers have the same diffuser material and design. Due to the similarity they are from now on addressed as Schreder J1002 diffusers. They were also the only diffusers with a protective quartz dome. The thickness of the PTFE layer in the diffusers varied, the Optronic dome diffuser was the thinnest; 0.2 mm, the standard plane diffuser was 0.6 mm thick and the thickness of the Schreder J1002 diffuser was approx. 2.5 mm. The majority of tests were made with the Schreder J1002 diffuser (both STUK and CMS) and the other diffusers were tested to obtain additional data for comparison.

The experiment was done by controlling the temperature of the diffuser and measuring a stable reference lamp. The changes in transmittance were obtained by comparing the lamp measurements to the measurements done at reference temperature. A more detailed description of the test set-up is presented in [Ylianttila and Schreder, 2005].

Results

The transmittance change as a function of temperature from all Schreder J1002 tests is presented in figure 1. The transmittance is normalized to 1 at 26°C. The wavelength used in the measurements is 400 nm, except for the first CMS measurements, which were made at 320 nm. The transmittance of the Schreder J1002 diffuser decreased by 0.1%/°C (1%/10°C) when the temperature was increased. At 19 °C there was a sudden change of 3% in the transmittance. There was some spread (± 1 °C) in the transition temperature and there could be some hysteresis in the exact position of the transition temperature.

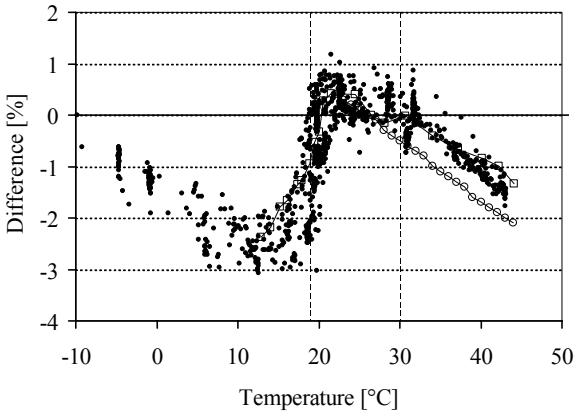

Figure 1. The change of transmittance of the Schreder J1002 PTFE diffuser as a function of temperature. The measurements done at CMS are those connected by the thin line. The transmittance is normalized to 1 at 26 °C. The phase shift temperatures of PTFE are marked as vertical dashed lines.

At CMS the measurements were made with a wider wavelength range of 280 nm - 600 nm. The transmittance change at different wavelengths is presented in figure 2. The results have been normalized at 24.5°C. The 420 nm data have also the error bars (1σ) drawn. Below 27°C only minimal wavelength dependency can be seen. Above 27°C there is a slight wavelength dependency. No wavelength dependency could be distinguished from the measurements made at STUK due to the smaller wavelength range (300 nm - 400 nm).

Figure 2. The change of transmittance of the Schreder J1002

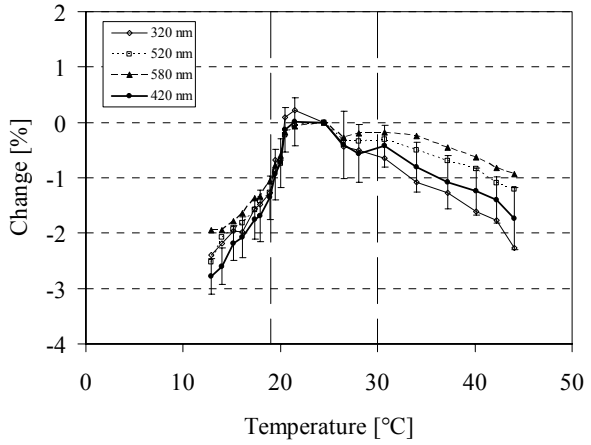

PTFE diffuser for different wavelengths. The error bars (1σ) are given for the 420 nm data. At temperatures above 27°C a clear wavelength depending difference can be seen.

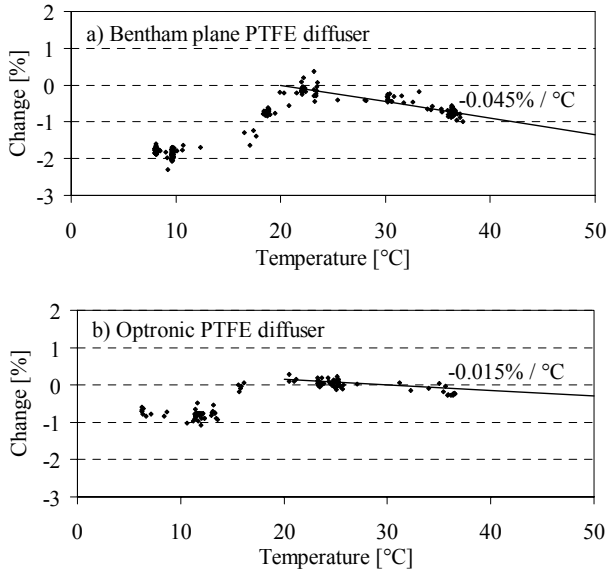

Figure 3. The transmittance change of a Bentham plane PTFE diffuser and Optronic PTFE diffuser.

The temperature response was similar with the other PTFE diffusers as can be seen in figure 3. The effects of temperature change were slightly smaller; the transmittance decreased by 0.045%/°C (1%/22°C) and the transmittance change at 19°C was 2%. The Optronic 742's PTFE diffuser had the smallest temperature sensitivity of PTFE diffusers; the transmittance decreased only by 0.015%/°C (1%/66°C) and the transmittance changed only by 1% at 19 ° C. The quartz diffuser had a different temperature response; the transmittance increased by 0.035%/°C (1%/33°C) and there were no sudden changes in transmittance in this temperature range.

Discussion

The drastic change in transmittance at 19°C is due to the properties of PTFE. The crystal structure of PTFE changes from phase II to phase IV at 19°C [Clark 1999, Briscoe et. al. 2003, Yamamoto and Hara, 1986]. This change has an influence e.g. in the density and the thermal expansion coefficient of PTFE. PTFE has another crystal structure change from phase IV to phase I at 30°C, but there was no clear change in transmittance at this temperature. The absence of the transmittance change at 19°C in the quartz diffuser measurement shows that the transmittance change is not coming from the quartz fibre.

The thickness of the PTFE layer seems to increase the temperature effects. With the thin Optronic 742 diffuser both the abrupt change at 19°C and the linear change of transmittance as a function of temperature are much smaller than with the thicker Schreder J1002 diffuser. A reason for this could be that the phase shift changes the absorbance or diffuse propagation properties of PTFE. Another reason for the difference could be the type of PTFE used in the diffusers. Different materials can be inserted into PTFE to change its properties, e.g. wear resistance. The exact type of PTFE used in the tested diffusers is not known.

These results strongly suggest that, when a PTFE diffuser's temperature is near 19 ° C, the measurement uncertainty is increased. In a temperature regulated laboratory room this is hardly a problem, as the ambient room temperature is usually kept above 20°C. In outdoor measurements, especially in the monitoring of solar UV radiation, ambient temperatures of 19°C can't be avoided. One option is to characterize the temperature effect of the diffuser and monitor the temperature of the diffuser and correct the measurement data accordingly. The possible temperature difference between the PTFE diffuser and the temperature sensor (the temperature sensor can ' t be attached directly to the optical part of the diffuser) and small temperature drifts near the transition temperature 19° C would still be problematic. The other option is to stabilize the temperature of the diffuser. By setting the stabilization temperature above ambient temperature, the condensation of water into the surface of the diffuser is also prevented.

The effect of the temperature sensitivity of PTFE diffusers have been detected in sky measurements in optimum conditions [McKenzie et. al., 2005]. Therefore the diffuser has to be temperature stabilized and the temperature has to be monitored, if the uncertainty of solar UV measurements is required to stay within the state of the art limits (± 5%).

References

Briscoe, B.J., H. Mahgerefteh, and S. Suga, The effect of gamma irradiation on the pressure dependence of the room temperature transition in PTFE, *Polymer, 44*, 783-791, 2003.

Clark E.S., The molecular conformations of polytetrafluoroethylene: forms II and IV, *Polymer, 40,* 4659-4665, 1999.

McKenzie, R., J. Badosa, M. Kotkamp, and P. Johnson, Effects of the temperature dependency in PTFE diffusers on observed UV irradiances, *Geophys. Res. Lett., 32,* L06808, 2005.

Schreder, J., M. Blumthaler and M. Huber, Design of an input opticfor solar UV-measurements, Internet Photochemistry & Photobiology, Issue: Protection against the hazards of UV, http://www.photobiology.com/UVR98/index.htm, 1999.

Yamamoto, T. and T. Hara, X-ray and Monte Carlo studies on the 19°C transition of poly(tetrafluoroethylene), *Polymer, 27*, 986-992, 1986.

Ylianttila, L. and J. Schreder, Temperature effects of PTFE diffusers, *Opt. Mater.*, in press.

Characterization of Photoconductive Diamond Detectors as a Candidate of FUV /VUV Transfer Standard Detectors

T. Saito, and I. Saito

Electromagnetic Waves Division, NMIJ, AIST, Tsukuba, Japan

K. Hayashi,

Electronics Research Laboratory, Kobe Steel, Ltd., Kobe, Japan

H. Ishihara,

Technical R & D Center, Iwasaki Electric Co., Ltd., Gyoda, Japan

Abstract. Photoconductive diamond detectors consisting of highly oriented film were characterized in temporal response, spectral responsivity and its spatial uniformity as a candidate of FUV/VUV transfer standard detectors. The results showed that the diamond detectors have a superior stability under 172 nm- irradiation but need to be improved for better carrier collection efficiency, uniformity and temporal response possibly due to photo-carrier traps.

Objectives

As a candidate for transfer standard detectors in the far ultraviolet (FUV) and vacuum ultraviolet region (VUV), we characterize photoconductive diamond detectors in temporal response, spectral response, and spatial uniformity.

Since diamonds are known to have low positive electron affinity or negative electron affinity, we investigate how much photoemission current contributes to the output signal.

Experimental

Devices under test were photoconductive detectors using highly oriented diamond (HOD) films [1-5]. The HOD films consist of azimuthally oriented (001) facets with typical area size of several μm^2 and a thickness of 10 μm. The HOD films were deposited on Si (001) substrates by microwave plasma chemical vapor deposition (CVD). A pair of interdigitated Pt electrodes were fabricated on the HOD film surface. Each electrode stripe was approximately 200-nm thick and 10-μm wide. The gap between the interdigitated electrodes was 30 μm, and the total detector area was approximately 40 mm^2.

Stability of the diamond detectors was tested by monitoring their photocurrent output under the illumination by a xenon excimer lamp whose emission is almost concentrated in the 172 nm-line and irradiance is about 37 mW/cm^2.

The spectral responsivity measurements were carried out in two wavelength regions, 10-60 nm and 190-1000 nm at the NMIJ spectral responsivity calibration facilities based on rare gas ionization chamber[6-7] and electrical substitution radiometer[8] respectively. In addition, uniformity and temporal response were characterized in the latter spectral range.

The VUV system mainly consists of the electron storage ring, TERAS as a synchrotron radiation source, pre-focusing mirror optics, a toroidal grating monochromator, post-focusing mirror optics.

The photocurrents were measured in two electrical circuits to distinguish photoemission contribution as shown in Figure 1. The first circuit is for photocurrent measurement with the switch (indicated by SW) closed (This will be referred to as the PC configuration). The second one is a circuit with the switch opened to measure the photoemission current (This will be referred to as the PE configuration). In the PC configuration, the measured current can contain both, photoemission current and photoconductive current, depending on the applied voltage.

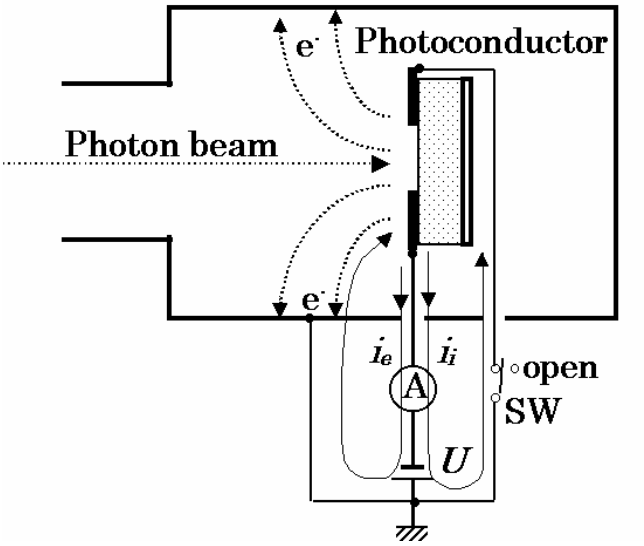

Figure 1. Schematic diagram of measurement configuration. A: electgrometer, SW: switch, *U*: applied voltage, i_i: internal photoconductive current, i_e: external photoemission current.

The longer wavelength (190-1000 nm) system mainly consists of deuterium/halogen lamps and a double grating monochromator and computer-controlled detector stage. Uniformity measurements were performed using a monochromatized beam with the beam spot size of 1 mm and the full-angle divergence of 20 mrad by controlling the lateral position of the detector stage.

Results and Summary

Successful operation of the photoconductive detectors was demonstrated in the VUV region. Detectors, which

had been accommodated to industrial use [3], did not show any degradation during 700 hour-irradiation of the intense xenon excimer lamp radiation (37 mW/cm^2 @172 nm) as shown in Figure 2.

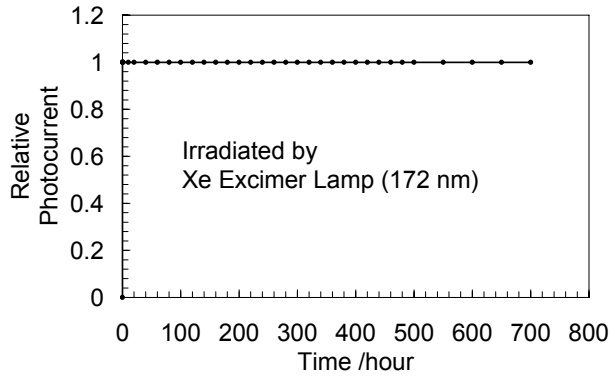

Figure 2. Stability of a diamond photoconductive detector under irradiation by xenon excimer lamp with irradiance level of about 37 mW/cm^2 at 172 nm.

Temporal measurement results for the longer wavelength region (190 – 1000 nm) showed a long time drift of the baseline that was not observed during an intense radiation, implying the presence of deep level carrier traps.

Spectral responsivities of the detectors increased with biasing voltages, but were still below those with perfect carrier collection efficiency and varied from one specimen to another even in the same batch implying the different densities of carrier traps.

All the detectors tested showed a gradual change toward a certain direction in their spatial uniformity, which was found to correlate with the facet size.

In the VUV measurements, photoemission current contribution was observed by comparison using positive and negative applied voltages, or directly (See Figure 3). Spectral responsivity including both (photoconductive and photoemission) current components becomes almost constant in the 10-40 nm wavelength range. The photoemission current contribution to the total output current can be dominant (at least 40-60 nm).

It was concluded that the successful operation throughout the FUV/VUV region and superior radiation hardness against 172 nm radiation were observed but the carrier collection efficiency, temporal response and spatial uniformity of the present detectors should be improved for the radiometric purposes. Optimizing the facet size or the device structure is expected to improve such shortcomings and might give sufficient properties required for FUV/VUV transfer standard detectors considering the proven superior radiation hardness.

Acknowledgments The authors are grateful to the AIST accelerator group, especially, Dr. S. Goko and Dr. H. Toyokawa for the operation of TERAS specialized for the measurements.

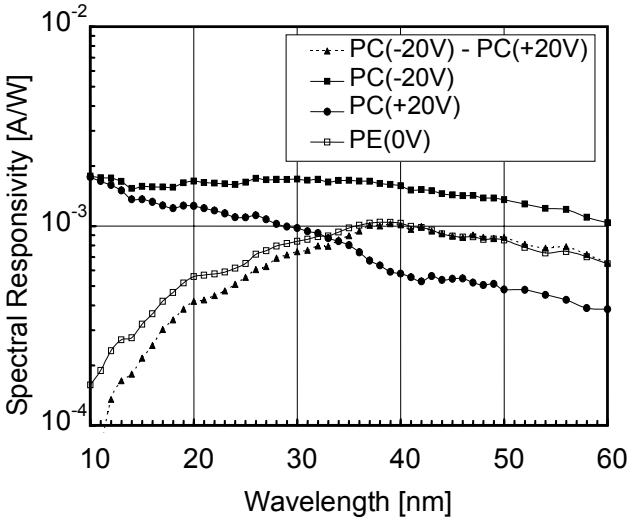

Figure 3. Spectral responsivities in the VUV obtained in the PC configuration. Applied voltages, *U*, are -20 V (filled squares) and +20 V (filled circles). The spectrum obtained in the PE configuration with *U*=0 (open squares) is also shown for comparison with the difference spectrum (filled triangles) subtracting the data for +20 V in the PC configuration from the data for -20 V in the PC configuration.

References

1 Hayashi, K., Yokota, Y., Tachibana, T., Kobashi, K., Achard, J., Gicquel, A., Olivero, C., Castex, M., Treshchalov, A., Temporal response of UV sensors made of highly oriented diamond films by 193 and 313 nm laser pulses, *Diamond and Related Materials 10* , 1794-1798, 2001.

2 Hayashi, K., Yokota, Y., Tachibana, T., Kobashi, K., Achard, J., Gicquel, A., Olivero, C., Castex, M., Treshchalov, A., Ultraviolet sensors using highly-oriented diamond films Proc. of the Seventh Applied Conference/ Third Frontier Carbon Technology Joint Conference (ADC/FCT 2003), Murakawa, M., Miyoshi, M., Koga, Y., Schafer, L., Tzeng, Y. (Editors), 130-135, 2003.

3 Uchida, K., Ishihara, H., Nippashi, K., Matsuoka, M., Hayashi, K., Measurement of vacuum ultraviolet radiation with diamond photo sensors, *J. Light & Vis. Eng. 28*, 97-100, 2004.

4 Saito, T., Hayashi K., Spectral responsivity measurements of photoconductive diamond detectors in the vacuum ultraviolet region distinguishing between internal photocurrent and photoemission current *Appl. Phys. Lett. 86,* 122113-1-3, 2005.

5 Saito, T., Hayashi K., Ishihara H., Saito, I., Characterization in temporal response, spectral responsivity and its spatial uniformity of photoconductive diamond detectors, submitted to *Proc. of ICNDST (Int. Conf. on New Diamond Science and Technology) -10*, 2005.

6 Saito, T., Onuki, H., Detector calibration in the 10-60 nm spectral range at the Electrotechnical Laboratory, *J. Optics 24*, 23-30, 1993.

7 Saito, T., Onuki, H., Detector calibration in the wavelength region 10 nm to 100 nm based on a windowless rare gas ionization chamber, *Metrologia 32*, 525-529, 1995/96.

8 Saito, T., Saito, I., Yamada, T., Zama, T., Onuki, H., UV detector calibration based on ESR using undulator radiation , *J. Electron and Spectroscopy and Related Phonomena 80*, 397-400, 1996.

The UV Spectral Responsivity Scale of the PTB

P. Meindl, A. E. Klinkmüller, L. Werner, U. Johannsen, and K. Grützmacher
Physikalisch-Technische Bundesanstalt, Institut Berlin, Abbestraße 2-12, 10587 Berlin, Germany

Abstract. A cryogenic radiometer based calibration facility utilizing monochromatized light of an argon arc plasma has been taken into operation. The rather high radiance of the plasma source allows to improve the accuracy of the UV spectral responsivity scale between 200 nm and 410 nm. A relative standard uncertainty between 0.1 % and 0.2 % was achieved. Three detectors can be calibrated simultaneously at a high degree of automation in order to make a relatively high throughput of secondary standard calibrations possible. Comparison with the PTB laser based cryogenic radiometer at five laser lines yielded excellent agreement.

Introduction

UV radiation is widely used in research and industry for lithography, non-destructive testing, water purification, environmental monitoring, atmospheric research, material curing, phototherapy and space-based astrophysical observation. The applications require the calibration of detectors with sufficient accuracy.
The PTB realisation of the spectral responsivity is based on cryogenic radiometers as primary detector standards. In the UV, it has proven a challenge to improve the accuracy of calibration because of the properties of available detectors. The spectral responsivity of Si trap detectors in the spectral range between 450 nm and 950 nm can be realized with uncertainties well below 0.1 % by calibration against a cryogenic radiometer at laser wavelengths and by interpolation of the spectral responsivity using a physical model. Due to the lack of a sufficiently accurate physical model for detectors in the ultraviolet spectral range, a calibration at laser wavelengths combined with the interpolation method does not lead to sufficiently low uncertainties. Consequently, a calibration with a light source tuneable over the whole wavelength range is mandatory. Thus a monochromator based design has been chosen for an improved UV calibration facility. A decisive property for attaining high radiant power at the detector is the spectral radiance of the light source.

Apparatus

The apparatus is a cryogenic radiometer calibration facility which contains a plasma arc as a light source combined with a monochromator for wavelength selection. The entire optical path is set up in gas- and light-tight monolithic boxes of black anodized aluminium.
The cryogenic radiometer of type CryoRad II was manufactured by Cambridge Research & Instrumentation. This radiometer has a specified wavelength range between 0.2 µm and 50 µm and a time constant of 3.5 s.
A high-current argon arc plasma is used as the light source [1]. The argon gas of the plasma is electrically heated at a pressure of $2 \cdot 10^5$ Pa within a 100 mm long bore of 4 mm diameter. The discharge is driven by a stabilized direct current of 150 A. The heating power amounts to about 40 kW. The radiation of the argon plasma shows no line structure except between 350 nm and 400 nm where a slight line structure is superimposed on an intense continuum background (ratio 1:10).
A prism-grating double monochromator is used for selecting the wavelength. The rotation angles of the prism and the grating are measured by using absolute angle encoders. By this absolute measurement, the uncertainty of the wavelength determination can be attained completely, and the wavelength calibration can be obtained easily by using laser light at one known wavelength.
UV enhanced optics are essential for sufficient radiant power throughput even at 200 nm. The mirrors used have a special UV enhanced $AlMgF_2$ coating with more than 91 % reflectivity at 200 nm. The bandwidth is 1 nm, and Fig. 1 shows the measured radiant power for this bandwidth. The available radiant power of 1.5 µW/nm at 200 nm is greater than the radiant power at synchrotron UV radiation facilities [2], and in contrast to synchrotron sources, the radiant power of the argon plasma source increases above 200 nm, up to about 7 µW/nm around 300 nm.

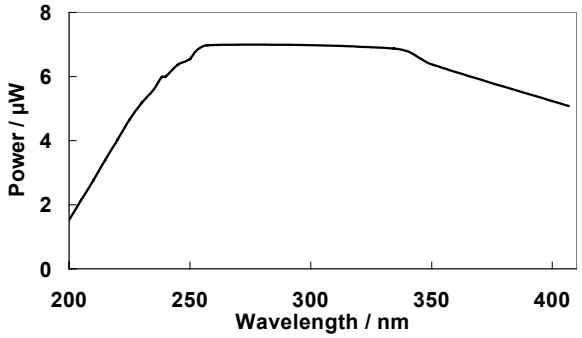

Figure 1. Measured radiant power at a bandwidth of 1 nm. The wavelength dependent power reaching the detector is shown.

Measurements and Discussion

Detectors are calibrated against the cryogenic radiometer at the same position in the beam path. Since the cryogenic radiometer measures the absolute radiant power, the responsivity of the secondary standard can be determined. A monitor detector can be used to correct for power variations between the radiometer and the detector measurement. Polarisation effects are corrected by measuring at three different angles of detector rotation. Detectors are calibrated at controlled temperature.
Si photodiodes and trap detectors have been calibrated between 235 nm and 410 nm and PtSi photodiodes and trap detectors between 200 nm and 410 nm. The relative uncertainties of the Si detector calibrations are around 0.1 % whereas the relative uncertainties of the calibration of PtSi detectors are between 0.1 % and 0.2 % except at certain wavelength regions with a high spectral gradient of the responsivity (see Fig. 2). Therefore, PtSi detectors are used as secondary standards only at wavelengths below 250 nm.

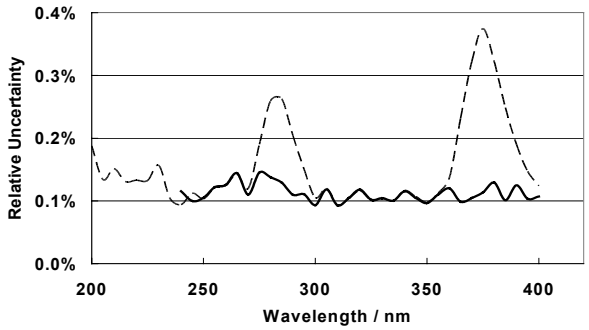

Figure 2. Relative standard uncertainties of the calibration of the spectral responsivities of trap detectors consisting of Si photodiodes (solid line) and PtSi photodiodes (dashed lines).

The calibrations were compared with measurements of the spectral responsivity at the laser based radiation thermometry cryogenic radiometer of the PTB [3] at five laser wavelengths (see Fig. 3), and good agreement was found. However, relative differences between the calibrations at both facilities are larger for PtSi detectors. This is caused by the poorer properties of these detectors.

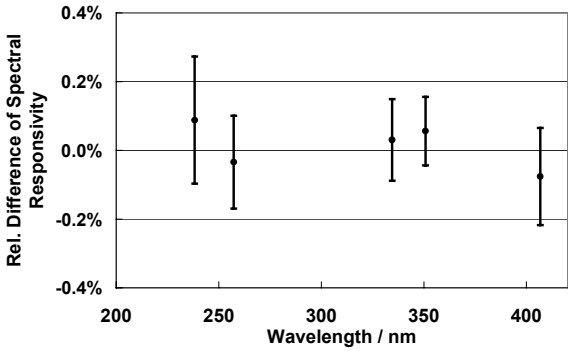

Figure 3. Relative differences of Si trap detector calibrations at the PTB radiation thermometry cryogenic radiometer at five laser wavelengths and at the new monochromator based cryogenic radiometer. The uncertainty bars indicate the standard uncertainties of the relative difference.

The new realisation of the UV spectral responsivity scale was found to agree well with the previous realisation at the PTB while being more accurate. Main contributions to the uncertainty of the calibrations are the noise and drift of the cryogenic radiometer, the fluctuations of the radiant power, stray light, and the uncertainty of the correction for the window transmittance.

The temporal drift of the cryogenic radiometer is independent of the radiant power and varies from measurement to measurement. Typical drift rates are not larger than 20 nW / 10 min presuming stable background conditions. The drift cannot be corrected completely. Being independent of the incident power, the relative significance of this contribution increases with decreasing power. This underlines the importance of having sufficient radiant power especially at short wavelengths around 200 nm.

The contribution to the relative uncertainty caused by the temporal instability of the argon plasma light source amounts to about $3 \cdot 10^{-4}$ to $7 \cdot 10^{-4}$.

The stray light was measured at different wavelengths. The largest uncertainty of $4 \cdot 10^{-4}$ was found at the shortest wavelength. The window transmittance is measured at all wavelengths before and after a calibration. Each calibration is corrected individually for the window transmittance at the assigned wavelength.

The wavelength uncertainty can become the dominant contribution to the uncertainty at certain wavelength regions with a larger spectral gradient of the spectral responsivity. This is only the case for PtSi detectors around 285 nm and 375 nm (see peaks in Fig. 2). Especially above 250 nm, Si photodiode detectors should be preferred.

Conclusion

The new calibration facility is now used to realize the PTB scale of the spectral responsivity between 200 nm and 410 nm. The accuracy of 0.1 % to 0.2 % of this facility has been proven. Since the apparatus offers a good throughput for high-accuracy calibrations it is also used to monitor the travelling detector standards during the CCPR key comparison K2.c.

References

[1] Grützmacher, K., Wall-stabilized arc-plasma source for radiometric applications in the range 200 nm to 10 μm, *Metrologia*, **37**, 465-468, 2000.

[2] Shaw, P.-S., et al., The new ultraviolet spectral responsivity scale based on cryogenic radiometry at Synchrotron Ultraviolet Radiation Facility III, *Rev. Sci. Instrum.*, Vol. 72, No. 5, 2242-2247, 2001.

[3] Werner, L., J. Fischer, U. Johannsen, and J. Hartmann, Accurate determination of the spectral responsivity of silicon trap detectors between 238 nm and 1015 nm using a laser-based cryogenic radiometer, *Metrologia*, **37**, 279-284, 2000.

Operational mode uncertainty for broadband erythemal UV radiometers

L.Vuilleumier
MeteoSwiss, Payerne, Switzerland

J. Gröbner
Physikalisch-Meteorologisches Observatorium Davos, World Radiation Centre, Davos Dorf, Switzerland

Abstract. Recommendations for measuring UV erythemal irradiance with broadband radiometers require the instruments to be calibrated by comparison to a traceable absolute spectral irradiance reference, taking into account the difference between the instrument spectral response and the theoretical CIE erythemal response [e.g., WMO, 1996]. Three instruments were calibrated according to these recommendations by two different centers and were subsequently measuring side by side in operational mode during a test period. The reproducibility of observations made according to the recommendations could then be checked, and was found to be compatible with the usually quoted uncertainty of 5-10%.

Introduction

In the framework of the Swiss Atmospheric Radiation Monitoring program (CHARM) of MeteoSwiss, UV erythemally-weighted broadband irradiance is measured using SolarLight 501A UV broadband radiometers (biometers). Three instruments (SL1903, SL1904 and SL1905) were chosen to be used as reference at MeteoSwiss based on the availability of past characterizations and stability. One instrument (SL1903) was sent for characterization to the European Reference Centre for Ultraviolet Radiation measurements (ECUV) from the Joint Research Centre at Ispra, Italy, while the two others were sent to the U.S. Central UV Calibration Facility (CUCF) at Boulder, U.S.A. After characterization at the calibration centers, the three biometers were installed in parallel at the Payerne site for measurement of global UV radiation between 31 August and 5 October 2004. The signals were sampled constantly at a 1 Hz frequency with 1-min averages recorded.

Results from the comparisons between the three biometers for 14 clear-sky days are reported here. The uncertainty of well characterized biometers is estimated to be on the order of 5-10% [Lantz et al, 1999]. The goal of the analysis reported here is to verify whether the agreement between biometers characterized at different centers and operating in standard network measurements conditions is compatible with the stated uncertainty

Spectral characterization of the biometers

The three biometers were initially characterized by the manufacturer prior to 1997 and underwent a second characterization at a Swiss facility (Novartis) between the end of 1998 and the beginning of 1999. They were characterized a third time before their calibration at CUCF or ECUV in 2004. Figure 1 shows the normalized spectral characterizations of the three biometers. The different characterizations give similar results between 290 and 330 nm, while some differences are present at wavelengths shorter than 290 nm and longer than 330 nm. Closer inspection reveals that there may also be substantial differences in the middle region. The 320-325 nm close-up part of Figure 1 shows that the responses of SL1903 and SL1905 according to the 2004 characterizations differ by about 40% in this region

Characterizations made by a given center at a given time are usually very similar, while the largest differences occur for characterizations made by different centers or at different times. The 3 original characterizations by the manufacturer yield almost identical results, except for SL1905 at wavelengths shorter than 275 nm. Similarly, the second set of characterizations by Novartis also yields strikingly similar results, although SL1905, characterized earlier than SL1903 and SL1904, seems to have a lower response in the central region. Finally, in the third set of characterizations, SL1904 and SL1905, which are characterized by CUCF, give similar results but substantially different from the previous characterizations, in the wavelength range above 330 nm, while SL1903, characterized by ECUV, is similar to the Novartis characterization in the range above 330 nm, and similar to the original characterization in the range below. Such differences may be due to instrument ageing characteristics or the influence of environmental conditions [Huber et al., 2003]. However, in light of the substantial differences that can result from small wavelength shifts and of the inconsistencies in the evolution of the biometers characteristics, it remains to be determined whether the observed differences result from

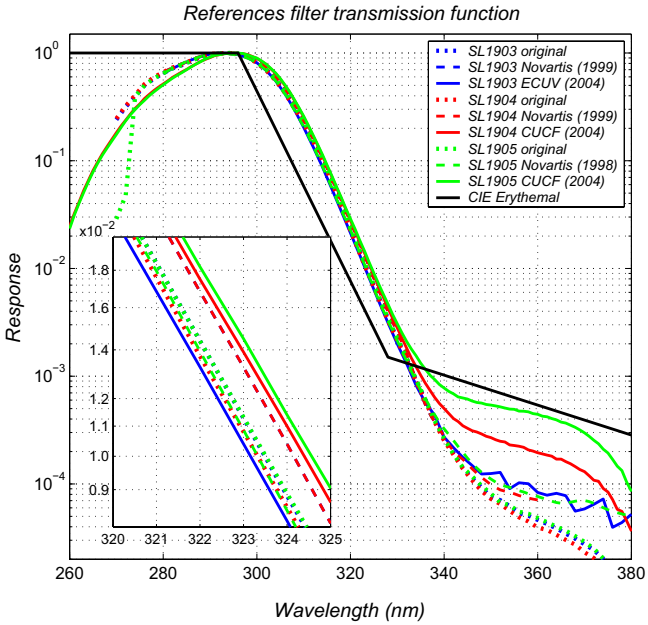

Figure 1, Comparison of filter transmission function for UV reference biometers (note: the dotted blue curve – original SL1903 – is covered by the dotted green curve – original SL1905 – and the dashed blue curve – Novartis SL1903 – is covered by the dashed red curve – Novartis SL1904).

instrument differences or from differences in the methods of the reference centers. In another study, Schreder et al. [2004] observed differences up to 20% between biometers spectral characterizations by different centers.

Comparison of biometer results

Beyond spectral and angular response, the biometers were also calibrated against traceable absolute spectral irradiance references at ECUV or CUCF. Because of the mismatch between the filter response and the theoretical erythemal function, the calibration factor is expressed as a function of total ozone column (O_3) and solar zenith angle (θ_z), and is determined using both spectral characterization and absolute calibration. UV erythemal irradiances compared below are obtained using these calibration functions.

The ratio between the pairs SL1903/SL1904, and SL1905/SL1904 are shown on Figure 2 and 3 as function of cos(θ_z) and O_3. In these figures, each black dot represents the ratio of the observations from two biometers for concurrent measurements. The semi-transparent surface is a fit of a two-dimensional polynomial function of θ_z and O_3.

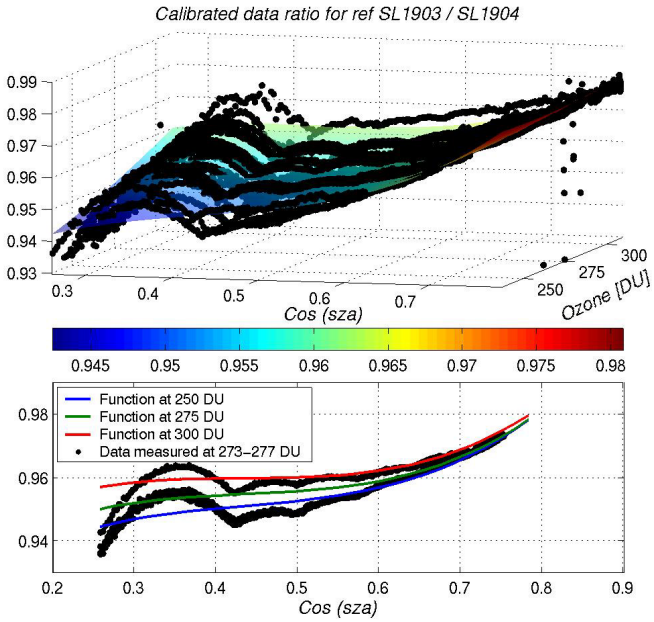

Figure 2, Ratio between calibrated measurements of biometers SL1903 and SL1904; upper panel: data and fit function vs. cos(θ_z) and O_3; lower panel: curves from fit function at O_3 = 250, 275, and 300 DU and data measured around 275 DU.

The comparison on Figure 2 and 3 show that UV erythemal irradiance measured by the three instruments are within about 7-8% at the ozone and solar angle conditions where they disagree most. The agreement between the instruments calibrated by the same center (SL1905/SL1904) is significantly better than the agreement between the instruments calibrated at different centers (SL1903/SL1904). In addition, for the latter, a hump is present in the ratio for cos(θ_z) between 0.3 an 0.4. This hump does not correspond to difference between instruments and seems to be an artifact of the calibration.

The raw data signals of the instruments before applying the calibration functions were also compared. While some difference in absolute normalization existed, the shape of the (θ_z,O_3) dependence exhibited less variability than for the calibrated data. All the raw signal data agreed within a couple percent for the SL1903/SL1904 pair and within 3 percent for the SL1903/SL1904 pair, indicating that the spectral characteristics of the three instruments should be similar. Thus, for these comparisons, the calibration process did not decrease the θ_z and O_3 dependence of the ratio.

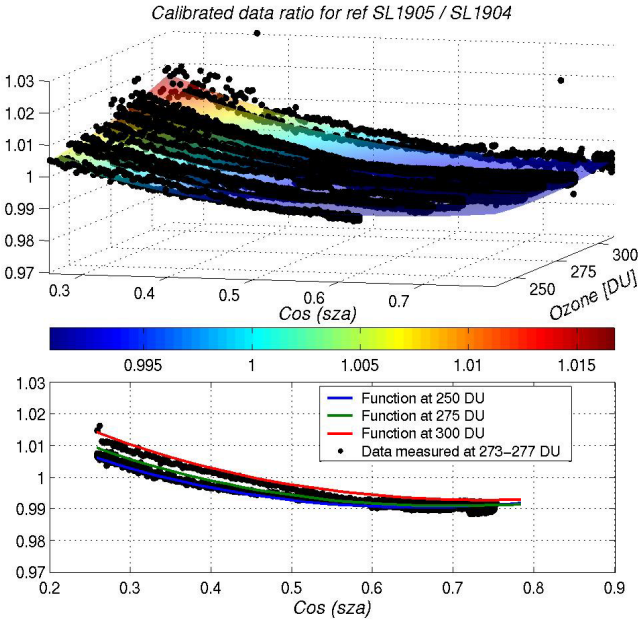

Figure 3, Same as Figure 2 for the ratio between calibrated measurements of biometers SL1905 and SL1904.

Conclusions

Comparisons of UV erythemal irradiances measured concurrently by broadband radiometers recently calibrated at two different reference centers showed an agreement that is compatible with the stated uncertainty of about 5-10%. Comparisons of the raw data signals for a range of solar zenith angle and total ozone column suggest that the three tested instruments have very similar spectral characteristics. Successive characterizations by independent centers revealed differences between the filter transmission functions, but these do not show a coherent evolution. They may originate in different ageing characteristics of the individual instruments or in differences between the methods used during the characterizations.

References

Huber, M., M. Blumthaler, and J. Schreder, Solar UV measurements with Robertson-Berger type instruments: Influence of the detector's internal humidity status, *Agric. For. Meteorol.*, **120**, 39-43, 2003, doi:10.1016/j.agrformet.2003.08.010.

Lantz K. O., P. Disterhoft, J. J. DeLuisi, E. Early, A. Thompson, D. Bigelow and J. Slusser, Methodology for deriving clear-sky erythemal calibration factors for UV broadband radiometers of the US Central UV Calibration Facility, *J. Atmospheric and Oceanic Technol.*, **16**, 1736-1752, 1999.

Schreder J., J. Gröbner, A. Los and M. Blumthaler, Intercomparison of monochromatic source facilities for the determination of the relative spectral response of erythemal broadband filter radiometers, *Opt. Lett.* **29**, 1455-1457, 2004.

WMO, WMO-UMAP Workshop on Broad-Band UV Radiometers, *WMO Global Atmosphere Watch* No. **120**, WMO TD-No. 894, 1996.

A method of characterizing narrow-band filtered radiometers using synchrotron radiation

Ping-Shine Shaw, Uwe Arp, and Keith R. Lykke
National Institute of Standards and Technology, Gaithersburg, MD, USA

Abstract. Synchrotron radiation is a primary source standard for a broad spectral range from x-rays to infrared [1,2] because synchrotron radiation can be accurately calculated by using the Schwinger equation and three parameters of the storage ring. In terms of spectral range, synchrotron radiation complements another primary standard source, black body sources, which are also calculable by using the Planck equation and temperature and emissivity. Beyond that, the two standard sources exhibit quite different characteristics. Black body source radiation is emitted in all directions uniformly with the same spectral distribution, whereas synchrotron radiation is highly concentrated in the direction parallel to the electron beam orbital plane. The angular divergence in this direction is also a strong function of the wavelength, i.e., narrower for shorter wavelength radiation and wider for longer wavelength radiation. Shown in Fig.1 is the calculated angular distribution for the storage ring of Synchrotron Ultraviolet Radiation Facility (SURF III). Typically, this phenomenon is treated as a complication and has to be dealt with carefully for radiometric applications.

Here, we propose a new technique by taking advantage of the calculable angular distribution of synchrotron radiation for the characterization of narrow-band filtered radiometers. For this technique, the narrow-band filtered radiometer under study will be used to scan the synchrotron radiation in the direction perpendicular to the orbital plane and the signal from the filtered radiometer versus the emitting angle of the synchrotron radiation is measured. Because the measured angular width depends on wavelength, one can deduce the mean wavelength of the filtered radiometer. In addition, because the incident synchrotron radiation can be accurately calculated, one can also derive the absolute integral response of the filtered radiometer. Currently, measurement of such quantities of a filtered radiometer requires very fine, and time consuming, spectral scanning of the filtered radiometer using a monochromator or, better, with a tunable laser and the transfer of the irradiance scale to the filtered radiometer. With this technique, the measurement is simple and fast. Furthermore, it can be used for any filtered radiometers in a broad spectral range from VUV to IR. We will provide detailed mathematical basis for this technique and the challenges involved in such measurements. Preliminary experimental results will be presented.

References

1. D.L. Ederer, E.B. Saloman, S.C. Ebner, and R.P. Madden, The use of synchrotron radiation as an absolute source of VUV radiation, J. Res. Natl. Bur. Stand. (U.S.) **79a**, 761 (1975).

2. M. Stock, J. Fischer, R. Friedrich, H.J. Jung, R. Thornagel, G. Ulm, and B. Wende, Present state of the comparison between radiometric scales based on three primary standards, Metrologia **30**, 439 (1993).

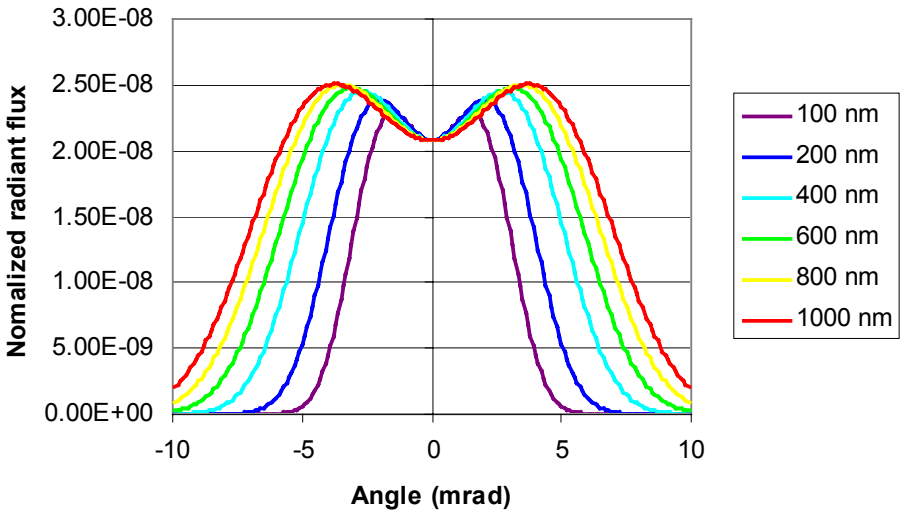

Figure 1 Calculated angular distribution of synchrotron radiation for different wavelengths using typical parameters of SURF III with 380 MeV electron energy and 84 cm of electron beam orbital radius.

Development of a Versatile Radiometer-Photometer System

George Eppeldauer[1], Richard Austin[2], and Charles Lustenberger[2]
[1]National Institute of Standards and Technology
Gaithersburg, Maryland 20899, USA
[2]Gamma Scientific, San Diego, California 92123, USA

Abstract. A new generation radiometer-photometer system has been developed in a National Institute of Standards and Technology (NIST) and Gamma Scientific (GS) cooperation to satisfy the increased requirements in the dissemination of NIST responsivity scales. The NIST responsivity scales have been extended from the silicon wavelength range to 2500 nm and in addition to the traditional spectral power responsivity calibrations, spectral irradiance and radiance responsivity calibrations are performed as well. The new generation radiometers and photometers can be utilized to maintain the NIST spectral responsivity scales and also to propagate the extended NIST scales to field applications with a minimal increase in the measurement uncertainty.

Mechanical and optical design

The new radiometer-photometer system has a versatile measuring head design. The front geometry of the heads can be simply modified to measure radiant power, irradiance, radiance, or the photometric equivalents, luminous flux, illuminance, and luminance. The different head constructions are made using the combination of apertures, diffusers, filters, filter combinations, and a variety of detectors depending on the head design for a given application. In addition to silicon photodiodes, nitride passivated silicon (for the ultraviolet), InGaAs, and extended-InGaAs photodiodes (for the near-infrared) have been applied. Detectors with large area and spatially uniform responsivity are used for power mode measurements where the detectors are underfilled with the incident radiation (beam). In addition to diffuser-input irradiance meters that can measure different source sizes [1], irradiance meters without diffusers have been developed to measure either "point sources" (where the detector is overfilled with the radiation from a small and distant source) or collimators. In these irradiance meters, the field-of-view is carefully designed and can be determined from goniometrical tests. An ultraviolet (UV) filter radiometer has been designed with interference filter and passivated silicon photodiode. It has a bandwidth of 25 nm with high ultraviolet and infrared blocking and can measure the irradiance produced by the 365 nm Hg line of UV collimators. Also, a versatile photometer has been developed where the attachable input optics can convert the illuminance measuring head into a luminance meter. The aperture plane and the outside surface of the front ring are in the same reference plane of the illuminance meter. With the luminance head attached, measurement field-of-view angles can be changed by choosing one of the six different hole-sizes in the mirror-aperture wheel. A second imaging optics is used in the input optics to produce efficient blocking for radiation outside of the target area and to maintain a constant luminance responsivity throughout the focus range of the camera lens at the front. This device can also measure radiant power, irradiance, and radiance when the photopic filter is removed.

Design of heating and cooling

For lower measurement uncertainty, both the filters and the detectors can be temperature controlled independently from each other using thermoelectric (TE) coolers/heaters. Usually, detectors are cooled to increase their shunt resistance and filters are heated to avoid condensation.

Thermistor sensors are attached to the temperature controlled components. One stage TE coolers are used for heating and 1 to 4 stage TE coolers can cool the detectors down to -85 degree C. The heat dissipation performance of the measuring heads is matched to the required cooling temperature. The thermal design of extended-InGaAs radiometers is challenging because the coldest possible detector temperature is needed with high temperature stability to produce high detector shunt resistance and low measurement uncertainty. When detectors are applied that have high shunt resistance at room temperature (such as selected silicon photodiodes), both detector and filter(s) can be temperature controlled together. The common (heated) temperature-control is frequently applied in photometers and in other filter-radiometers where the controlled temperature can be slightly higher than the ambient temperature. The spectral responsivity of the detector-filter combinations is optimized for the selected constant temperature [2].

Electronic design

Pre-amplifiers are mounted to the back of the measuring heads that are matched to the detector electrical characteristics to optimize the signal gain, loop gain, and the closed loop voltage gain at the signal frequency [3]. In DC measurements, usually the optimization is simplified for selecting (and/or cooling) the detectors for high shunt resistance. However, only the optimization of these three gain characteristics makes it possible to measure modulated (chopped) radiation with high sensitivity and low measurement uncertainty. Consequently, all three gain characteristics were optimized versus frequency for the radiometers that measure AC radiation. The selected optimum chopping frequency for AC radiation measurements is between 8 Hz and 10 Hz. This is a high enough signal frequency to get rid of the 1/f noise of the applied operational amplifiers. Also, the upper roll-off frequencies of the signal gain characteristics were tuned to 80 Hz (at 10^9 V/A signal gain selection) or higher using gain switching reed relays of low capacitance instead of the traditionally used rotary switches. For the increased roll-off

frequencies, the chopping frequency is low enough to obtain constant signal gains for all signal gain selections at the chopping frequency.

Low noise and low input current operational amplifiers with high upper roll-off frequency are used in the current measuring pre-amplifiers. The operational amplifiers and their feedback resistors have not been temperature controlled. Instead, light shutters are applied and the output (voltage) signal is measured with the shutter on and off. The temperature dependent (dark) output (offset) signal is subtracted from the sum of the output signal (to be measured) and the (dark) output signal. The feedback resistors used to have temperature coefficients of 10 ppm/degree C. The resistance uncertainties for the decade nominal values are 0.01 %. Using the low uncertainty feedback resistors and the output (dark) offset subtracting method, the photocurrent-to-voltage conversion uncertainty is 0.01 % without performing any signal gain linearity calibrations or corrections for the pre-amplifiers. The signal gain selections over eight decades can be either manual or remote controlled.

A carefully designed wiring, grounding, and shielding system for the measuring head and the control unit (that includes the power supply, the temperature controller(s), and the remote gain control circuit) minimizes noise and 60 Hz pickup.

Radiometer tests

Photodiode shunt resistances were measured to determine the three fundamental gains of photocurrent measuring detector-preamplifier circuits. A noise floor of 3 fA was measured on the prototype radiometer at 10^{10} V/A signal gain selection when a 20 Gohm shunt resistance silicon photodiode was applied. The electrical bandwidth of this DC measurement was 0.3 Hz. The 6 Mohm shunt-resistance of a 5 mm diameter InGaAs photodiode measured at room-temperature was increased to 42 Mohm when the detector was cooled to 4 degree C. This low temperature decreased the 180 fA (room temperature) noise floor to 25 fA at the 10^{10} V/A signal gain selection of the InGaAs irradiance meter.

The three fundamental gains are always optimized for the signal frequency using partial or full frequency compensations in the current measuring analog control loop of the preamplifier. In order to obtain the best results, photodiodes with the lowest junction capacitance are selected and the external feedback capacitors of the operational amplifier are changed. Because of the variation of the feedback component values (including stray capacitance as well), the 3 dB upper roll-off points of the different gain selections cannot be controlled to the same frequency. This results in significant responsivity differences at decade signal gain switching when the chopping frequency is on the slope of the signal gain versus frequency characteristics. To avoid non-decade signal gain ratios at the chopping frequency, the responsivity calibration results are usually reported at DC (zero Hz). The solution to obtain exact decade ratios for the different signal gain selections at a given signal frequency is to measure the frequency dependent gain (responsivity) curves first and then to apply correction, based on the measured data.

Operational and performance tests have been worked out for the modular radiometers/photometers to minimize errors and unacceptable performance during fabrication. First, operational DC tests are made where the detector shunt resistance and then the dark output offset voltages are measured at all gain selections. Thereafter, the dark output voltage is measured with an AC measuring digital voltmeter at all gain selections to check for oscillations. After the dark tests, the detector is exposed to different optical radiation levels and it is checked if decade changes are obtained in the output voltages when the signal gains are gradually changed from the maximum to the minimum. These photodiode and preamplifier tests are followed by the cooling tests where the biasing current is selected for the target resistance of the NTC thermistor and the voltage drops on the thermistor are measured at both the ambient and the controlled temperatures. The voltage drop on the thermistor should remain constant during operation indicating that the temperature of the monitored component is stable versus time.

References

[1] G.Eppeldauer, M. Rácz, and T. Larason, Optical characterization of diffuser-input standard irradiance meters, SPIE Proc. Vol. 3573, pp. 220-224, 1998.

[2] George P. Eppeldauer and Miklós Rácz, Design and characterization of a photometer-colorimeter standard, Applied Optics, Vol. 43, No. 13, pp. 2621-2631, 2004.

[3] George P. Eppeldauer, Editor, Optical radiation measurement with selected detectors and matched electronic circuits between 200 nm and 20 μm, NIST Technical Note 1438, April 2001, U.S. Government Printing Office, Washington, D.C.

Nonlinearity Measurement of UV Detectors using Light Emitting Diodes in an Integrating Sphere

Dong-Joo Shin, Dong-Hoon Lee, Gi-Ryong Jeong, Yong-Jae Cho,
Seung-Nam Park, and In-Won Lee

Division of Optical Metrology, Korea Research Institute of Standards and Science (KRISS),
PO Box 102, Yuseong, Daejeon 305-600, Korea

Abstract. We measured the nonlinearity of UV detectors using a linearity tester which consists of four UV light emitting diodes (LEDs) and an integrating sphere. The tester measures photocurrent ratios of a detector by flux addition for a range over 6 decades with high speed and accuracy. The nonlinearity of irradiance responsivity is determined from the measured of photocurrent ratios by interpolation. We observed a clear dependence of nonlinearity upon the size of detector aperture.

I. Introduction

In the ultraviolet (UV) radiometry, most detectors are calibrated for their spectral irradiance responsivity. Nonlinearity of a detector is the property that the responsivity does not remain constant when the signal is higher than a certain level. An established method to measure the nonlinearity of detectors is the flux addition method using lamps or lasers as light source, which requires no reference standard [1,2]. However, this method measures the nonlinearity of photocurrent ratios rather than that of detector responsivity. Another method for directly measuring the nonlinearity of responsivity is to use neutral filters with a laser [3], but this method requires a calibrated reference detector.

We present in this paper a new flux-addition type linearity tester, in which the detector under test is illuminated by LEDs inside an integrating sphere. The linearity tester using LEDs as light source is recently reported with its advantages of fast and accurate measurement in a wide range [4]. The additional use of integrating sphere eliminates the need of light shielding and flux alignment, resulting in the increased practicability and operator's safety especially in the UV radiometry. We used this linearity tester to measure the nonlinearity of a Si photodiode with different aperture sizes at a UV wavelength around 400 nm. We show how the nonlinearity of irradiance responsivity can be determined from the measured photocurrent ratios, and present also the measured effect of aperture size on the detector nonlinearity.

II. Experimental setup

Figure 1 shows schematically the experimental setup. LEDs are installed in pair on an integrating sphere and driven independently by two current sources (Keithley, Model 2400). For high irradiance level, more than one LED can be simultaneously driven by each current source, which we designate collectively as LED A or LED B. In the experiment, we used four UV LEDs (Opto Technology, Model OTLH-360-UV); two for LED A and two for LED B. Note that this scalability of irradiance level simply by changing the number of LEDs is one of the important practical advantages the LED-based linearity tester provide. The peak wavelength and the spectral bandwidth of the LEDs are measured to be 396 nm and 20 nm, respectively.

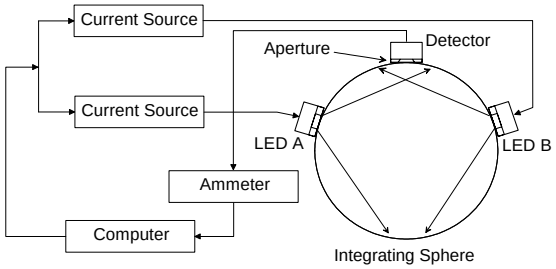

Figure 1. Schematic setup of the linearity tester using LEDs in an integrating sphere.

The integrating sphere is made of synthetic resin with a diameter of 40.0 cm, and its inside is uniformly coated with polytetrafluoro-ethylene (PTFE). Using two kinds of jig, PTFE powder is formed into the pentagonal and hexagonal shape plates, which build, similar to a football, a sphere surface with the outside diameter of 40.0 cm. The surfaces of jigs are roughened to an average roughness of (2.8 ± 0.015) μm for enhancing the diffuse reflection of the PTFE plate surface. The plates have a density of 1.2 g/cm^3 and a thickness of 1.2 cm, and are glued to the inside wall of the sphere with vacuum grease. Figure 2 shows the formed PTFE plates and the hemisphere coated with such PTFE plates.

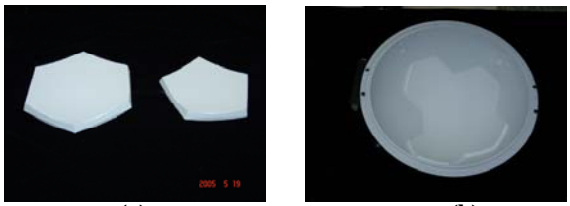

(a) **(b)**

Figure 2. Photographs of the PTFE plates formed to a pentagonal and hexagonal shape (a) and the hemisphere coated with such PTFE plates (b).

The photodiode under test (UDT Sensors Inc., Model UV-100) is positioned on a hole at the top of the integrating sphere (see Fig. 1). In order to define the active area irradiated, an aperture of known diameter is placed in front of the detector. The photocurrent of the photodiode is measured with a calibrated ammeter (Keithley, Model 6485). All instruments are interfaced with a computer.

The procedure of nonlinearity measurement in detail is described in the reference [4]. We performed the measurement for different active aperture areas with a diameter of 11.28 mm (no aperture), 8 mm, 5 mm, and 2 mm. For the apertures with diameter not smaller than 5 mm, two LEDs, i.e. one for LED A and one for LED B, were sufficient for measuring the detector nonlinearity, where the injection current for each LED is varied from 0.1 mA to 300 mA. For the 2-mm diameter aperture, however, two additional LEDs were required, i.e. two for LED A and two for LED B, so that the injection current is varied up to

600 mA for each set. In both cases, the resulting photocurrent of the photodiode spanned from 10^{-10} A to 10^{-4} A over six decades. We repeated the measurement three times for each aperture size with different initial photocurrents of $1.0\cdot10^{-10}$ A, $3.0\cdot10^{-10}$ A, and $5.0\cdot10^{-10}$ A.

III. Results

Figure 3 shows the measured photocurrent ratios $(i_{A+B})/(i_A + i_B)$ for different aperture diameters as a function of the photocurrent level i_A. Here, i_A, i_B, and i_{A+B} are the photocurrent of the photodiode irradiated by LED A, LED B, and both of them, respectively. Each symbols show the measured values, while the lines are the numerically interpolated values. From the measured photocurrent ratios in Fig. 3, the nonlinearity of the detector responsivity is determined as described below.

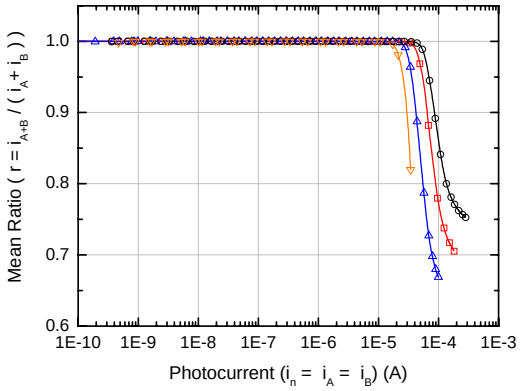

Figure 3. Plot of the measured photocurrent ratios $(i_{A+B})/(i_A + i_B)$ for different aperture diameters (○: no aperture, □: 8 mm, △: 5 mm, ▽: 2 mm) and the numerically interpolated values (lines) as a function of the single photocurrent level i_A.

According to the measurement procedure [4], the single photocurrents i_A and i_B are adjusted to be nearly the same and the combined photocurrent i_{A+B} is set as the single photocurrent level in the next step, so that the current ratio r_n in the n-th measurement step can be written as following:

$$r_n = \left.\frac{i_{A+B}}{(i_A+i_B)}\right|_n = \frac{i_{n+1}}{2\times i_n} \quad for\ i_A = i_B = i_n\ and\ i_{n+1} = i_{A+B}. \qquad (1)$$

As the initial value i_0, the lowest photocurrent can be chosen so that the repetition runs until the maximal injection currents for LEDs are achieved. Because the detector responsivity R_n in each step is defined as the ratio of the photocurrent i_n and the irradiance E_n, and the irradiance is doubled in each step, i.e. $E_{n+1} = 2E_n$, we can also write Eq. (1) as following:

$$r_n = \frac{R_{n+1}\cdot E_{n+1}}{2R_n\cdot E_n} = \frac{R_{n+1}}{R_n} \qquad (2)$$

From Eq. (2), we can calculate the relative responsivity of the detector from the photocurrent ratios r_n as

$$R_n(i_n) = r_{n-1}\cdot r_{n-2}\cdots r_0\cdot R_0(i_0)\ , \qquad (3)$$

where R_0 is the constant relative responsivity in the linear range of low photocurrent. We repeat the calculation of the relative responsivity R_n according to Eq. (3) beginning with different initial values i_0, which are photocurrent values around $1.0\cdot10^{-8}$ A in Fig. 3, such as $1.0\cdot10^{-8}$ A, $3.0\cdot10^{-8}$ A, and $5.0\cdot10^{-8}$ A. In this range, the detector can be regarded as linear ($R = R_0$). Numerically interpolating the data sets of photocurrents and relative responsivities $(i_n, R_n(i_n))$, we obtain the relative responsivity as a function of photocurrent. Finally, we obtain the nonlinearity of the detector responsivity NL as a function of photocurrent i:

$$NL(i) = \frac{R(i)}{R_0} - 1. \qquad (4)$$

Figure 4 shows the resulting nonlinearity of the irradiance responsivity for the photodiode with different aperture diameters. The result shows clearly that the photocurrent level at which the nonlinearity occurs decreases, as the aperture size decreases. The nonlinearity of the photodiode with the 2-mm diameter aperture become nonlinear to $NL = 1.0\cdot10^{-4}$ at a photocurrent of $3.0\cdot10^{-7}$ A, while the same nonlinearity occurred at $3.0\cdot10^{-5}$ A without aperture.

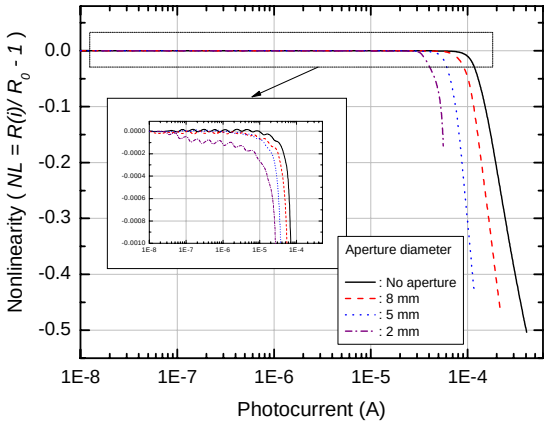

Figure 4. Nonlinearity of the irradiance responsivity for the photodiode with different aperture diameters, determined from the measured nonlinearity of the photocurrent ratios.

IV. Conclusion

We developed a linearity tester using LEDs in an PTFE coated integrating sphere. The use of integrating sphere enhanced the practicality and safety of the LED-based linearity tester in the UV radiometry. The feasibility of the tester is demonstrated by measuring the nonlinearity of a Si photodiode with different aperture sizes at a wavelength around 400 nm. We introduced a method to determine the nonlinearity of irradiance responsivity from the nonlinearity of photocurrent ratios measured by flux addition. With the presented methodology, we expect to be able to accurately calibrate a UV detector even in the nonlinear region for applications at high irradiance level.

References

[1] L. P. Boivin, Automated absolute and relative spectral linearity measurements on photovoltaic detectors, *Metrologia, 30*, 355-360, 1993.

[2] J. Fischer, L Fu, Photodiode nonlinearity measurement with an intensity stabilized laser as a radiation source, *Appl. Opt. 32*, 4187-4190, 1993.

[3] T. Kubarsepp, A. Haapalinna, P. Karha, E Ikkonen, Non-linearity measurements of silicon photodetectors, *Appl. Opt. 37*, 2716-2722, 1998.

[4] D. J. Shin, D. H. Lee, C. W. Park, S. N. Park, A novel linearity tester for optical detectors using high-brightness light emitting diodes, *Metrologia, 42*, 154-158, 2005.

Radiometric investigation of a compact integrating sphere based spectral radiance transfer standard

D.R. Taubert, J. Hollandt
Physikalisch-Technische Bundesanstalt, Abbestraße 2-12, D-10587 Berlin, Germany

A. Gugg-Helminger
Gigahertz-Optik GmbH, Puchheim, Germany

Introduction

In recent years, to fulfil the requirements of DIN EN ISO/IEC 17025, the traceability of measurements to a primary standard has become mandatory, ensuring the comparability of inter-laboratory measurements and of measurements performed over a long time period. This is also the case in the wide and ever increasing field of optical radiation measurements. To meet the demand of traceability, there is a need for highly accurate and yet simple to use robust radiometric transfer standards.

New Spectral Radiance Transfers Standards

One of the most frequently used radiometric quantity in the field of optical radiation measurements is the spectral radiance, being of importance for manufacturers of radiation sources as well as for laboratories in the calibration of their spectrometers and detection systems. The well established transfer standard for spectral radiance is the tungsten ribbon lamp. Yet of proven very high stability, this type of standard is suitable only for a small group of experienced users, i.e. national metrology institutes. For the broad community of industrial users the delicate to handle tungsten ribbon lamps are less suitable. The most promising candidates for user friendly spectral radiance transfer standards have shown to be integrating sphere based sources. In contrast to the fragile and cumbersome to align tungsten ribbon lamps, they are rather robust and offer a comparatively large and homogeneous radiating area. The emitted radiation is in good approximation lambertian and unpolarized. An important feature of this type of radiance standard is that, by adapting its design, the spectral radiance magnitude can be matched to specific calibration demands. For example, the calibration of the detection channel of a fluorometer requires a spectral radiance three to four orders of magnitudes lower than that of a tungsten ribbon lamp.

Integrating sphere radiator design

As part of the project “Development, Characterization and Dissemination of Fluorescence Standards for the Traceable Qualification of Fluorometers” the PTB and Gigahertz-Optik GmbH in close cooperation have developed and characterized a new type of integrating sphere based spectral radiance transfer standard. An image and a schematic view of the design are shown in Figure 1. The basic design consists of two hemispheres made of OP.DI.MA and separated by a nearly opaque wall with two OP.DI.MA surfaces. The 5 W, constant current driven, quartz halogen lamp integrated in the back hemisphere illuminates trough 16 holes in the wall the front hemisphere. The front hemisphere has a 20 mm diameter aperture as the radiating area.

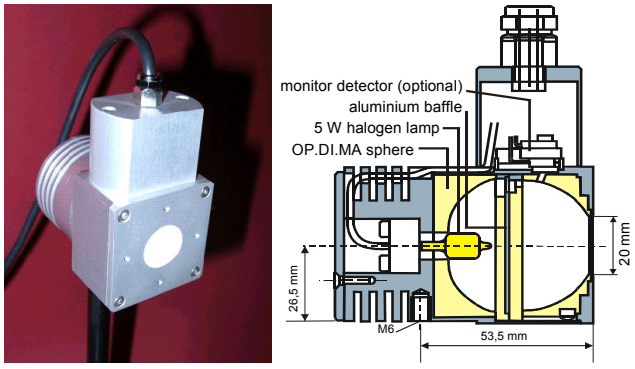

Figure 1. Compact and large radiating area integrating sphere based spectral radiance standard (left) and a schematic view of the design (right).

Radiometric Characterization

To investigate and optimize the radiometric properties of this new type of integrating sphere radiator, PTB has set up a new spectral radiance comparator facility the Spectral Radiance Comparator II. This facility is designed for low intensity measurements and traceable spectral radiance calibrations in the wavelength range from 250 nm up to 2.5 µm as they are needed i.e. for radiometric traceability in fluorometry [1,2].
The customer relevant and most important radiometric parameter investigated and optimized were:

- the distribution of the spectral radiance over the radiating area
- the angular distribution of the spectral radiance
- the mid- and long-term stability
- the influence of ambient condition changes on the spectral radiance
- the absolute spectral radiance in the UV, VIS and NIR

An optimizing process of the wall structure resulted in an excellent homogeneity of the radiating area, both in the visible and in the near infrared. Within an area of 10 mm in diameter, the relative variation of the spectral radiance is less the $5 \cdot 10^{-3}$. Measurements of the horizontal and vertical angular emission distribution proved that these sources are in very good approximation lambertian radiators: relative changes of the radiance for a ± 10° change of the observation direction to the optical axis are within $5 \cdot 10^{-3}$.

Detailed and comparative results with a tungsten ribbon lamp will be presented. Furthermore, the determination of the degree of polarization of the emitted radiation in the wavelength range from 450 nm up 1100 nm resulted in less than $4 \cdot 10^{-3}$, hence compared to tungsten ribbon lamps, these integrating spheres can be considered sources of unpolarized radiation. The temporal stability of the spectral radiance has been assessed by calibrating two integrating spheres of the same lot against a stable tungsten ribbon lamp in regular time intervals of about 100 hours. The overall time of continuous run for the integrating spheres was more than 1000 hours. The observed relative change of the spectral radiance over 100 hours of continuous operation was found to be about 1%. Within the calibration uncertainty, no change of the spectral radiance could be observed for ambient temperatures changes from 20 °C up to 30 °C.

The presented results indicate that these integrating sphere based radiators are suitable for a wide spread, easy to handle, day to day use as transfer standards for disseminating the radiometric base unit spectral radiance in the wavelength range from 350 nm up to 2 µm.

Acknowledgments This work has been funded as part of the project VI A2 -18 "Development, Characterization and Dissemination of Fluorescence Standards for the traceable Qualification of Fluorometers" by the Federal Ministry of Economics and Labour of Germany.

References

J. Hollandt, R.D. Taubert, J. Seidel, U. Resch-Genger, A. Gugg-Helminger, D. Pfeifer, C. Monte, W. Pilz, Traceability in Fluorometry—Part I: Physical Standards, *Journal of Fluorescence*, in press

U. Resch-Genger, D. Pfeifer, C. Monte, W. Pilz, A. Hoffmann, M Spieles, K. Rurack, J. Hollandt, R.D. Taubert, B. Schönenberger, P. Nording, Traceability in Fluorometry—Part II: Spectral Fluorescence Standards, *Journal of Fluorescence*, in press

Accurate and independent spectral response scale based on silicon trap detectors spectrally invariant detectors

J. Gran,
Justervesenet (JV), Kjeller, Norway

Aa. S. Sudbø
University of Oslo, University Graduate Center - UniK, Kjeller, Norway

Abstract. The established model for silicon detector responsivity is exploited to realize a very accurate independent spectral response scale with the aid of a spectrally invariant but noisy detector. Two different approaches are considered to estimate the parameters in the responsivity model, one based on a purely relative measurement between the silicon trap detector and the spectrally invariant detector, and one combining the traditional self-calibration procedure and the purely relative measurement to form a hybrid self-calibration method.

Introduction

Geist and Zalewski demonstrated in 1980 how silicon photodiodes can be used as an absolute measurements standard. Unfortunately, their earliest proposed methods turned out to change the detectors responsivity and hence made them unacceptable as a measurement standard. Since the introduction of the cryogenic radiometer in the mid eighties there has been little work of improving the self-calibration method. Large technological advances have improved the detectors and made the internal quantum efficiency more ideal. In addition, the fast technological advances of integrated circuit technology and computers have improved the availability of computational resources significantly, enabling more accurate calculations of the detectors and opened the way for improved models. In principle, it is these two improvements that are exploited in this new approach to the self-calibration procedure, which replaces the previous oxide bias method.

Theory

A silicon photodiode can be modelled as a modified ideal quantum detector, where the two loss mechanisms, reflectance from the surface and internal losses, are taken into account. The responsivity is modelled as

$$R(\lambda) = e\lambda\, hc\left(1-\rho(\lambda)\right)\left(1-\delta(\lambda)\right), \qquad (1)$$

where e is the elementary charge, h is Planck's constant, c is the speed of light in vacuum, and λ is the vacuum wavelength of the radiation. These quantities form the ideal term of a quantum detector. The spectrally dependent reflectance is given by $\rho(\lambda)$, and the quantum deficiency is given by $\delta(\lambda)$. Our approach to get a primary realisation is to estimate the reflectance and the internal quantum deficiency (IQD) separately and through that establish the link between the responsivity and fundamental constants.

Reflectance

Fresnel's equations allow us to calculate the spectral reflectance over the whole spectrum with an uncertainty of less than 1% from a single measurement, when the spectrally dependent refractive indices, polarisation, angle of incidence and oxide thickness is known. In a trap detector the geometry is fixed, and the spectral reflectance of a trap detector can be expressed by the oxide thickness only. In addition, the trap configuration reduces the reflectance by two orders of magnitude making the responsivity less sensitive to the uncertainty in the oxide thickness estimate.

Internal quantum deficiency

The IQD model $\delta(\lambda)$ is based on the assumption that the recombination probability for a generated electron hole pair (e-h) depends only upon the depth, x, into the detector where it is created. The quantum deficiency is found by integrating the product of the normalised distribution of photons and their recombination probability over the depth of the detector. The spectral dependence comes from the normalised distribution of photons given from the highly spectral dependent absorption coefficient. These values are given by the extinction coefficient of the refractive index of silicon. The recombination probability function used in our model is shown in fig. 1.

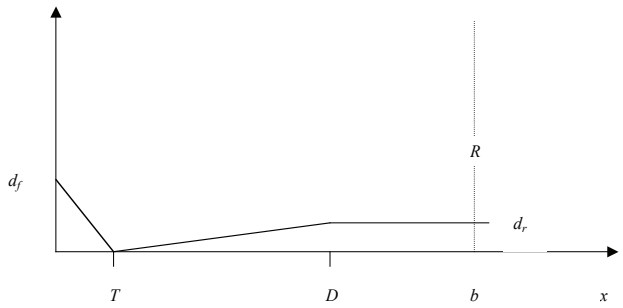

Figure 1. The recombination probability as a function of generation depth of electron – hole pairs.

The important property of the model is that the recombination probability of (e-h) pairs created at the pn junction (T) is zero. In the presented work this property is exploited by two different methods. In the purely relative method we estimated the IQD by measuring the silicon trap detector relative response to a spectrally invariant cavity pyroelectric detector (CPD) and fitted the recombination probability to the measurements. A fitted scaling constant is needed to convert the relative

measurement to an independent spectral response scale. The property of the model ensures correct scaling.

In our second method we combine the traditional self-calibration procedure and the purely relative method to a hybrid self-calibration method. The classical reverse bias experiment at 25 V was used to find the parameters d_r and D by fitting the responsivity change over the whole spectral range. The relative method was used to find the parameters that describe the losses in the front (d_f, T) and at the back of the detector (R, b) in two different but similar experiments. The uncertainty of this method is lower than the purely relative method, but it requires 3 separate experiments each determining 2 parameters in the model.

Results and uncertainty

The uncertainty in both approaches is calculated from the observed variance in the input measurement, brought through the calculations to the output covariance in the responsivity. The combined uncertainties are shown in fig. 2. The calculations are valid for random variables and are based upon the observed variance in these random variables, which requires a number of observations of those variables. Very low uncertainties are achieved by both methods.

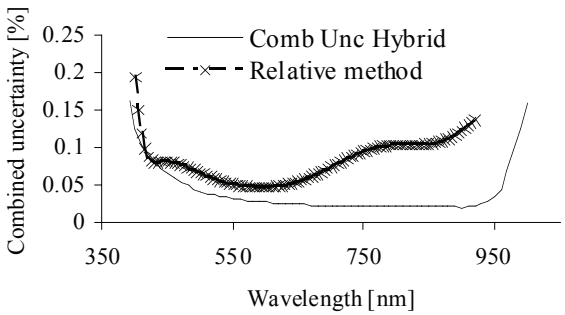

Figure 2. The calculated combined uncertainties in responsivity for the two methods are compared. The uncertainty is given with 1 σ level of confidence.

The fitting of a phododiode model to a set of responsivity measurements yields strongly correlated responsivity values. One interesting observation is the difference between the correlation coefficients of the fit function and the responsivity values in the relative method. The relation between the fit function $F(\lambda)$ and the responsivity $R(\lambda)$ is given as

$$F(\lambda) = R(\lambda)\, k\,, \qquad (2)$$

where k is a fitted scaling constant and λ is the optical wavelength. The correlation matrices for the fit function and the responsivities for a set of wavelengths are compared for the relative method in fig. 3. Whereas the correlation matrix of fit function values has a diagonal-like character, the responsivity values are strongly correlated. The responsivity values for the hybrid method have even stronger correlations than for the relative method.

Conclusions

Two different methods for using silicon photodiode trap detectors to realize spectral response scales have been investigated. In the purely relative method the uncertainty is limited by the signal noise ratio in the relative measurement, whereas in the hybrid method the uncertainty is limited by the uniformity and reflectance of

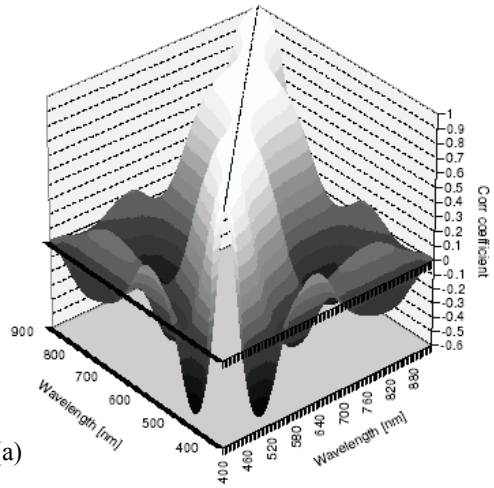

(a)

the trap detectors. The best responsivity scale is observed

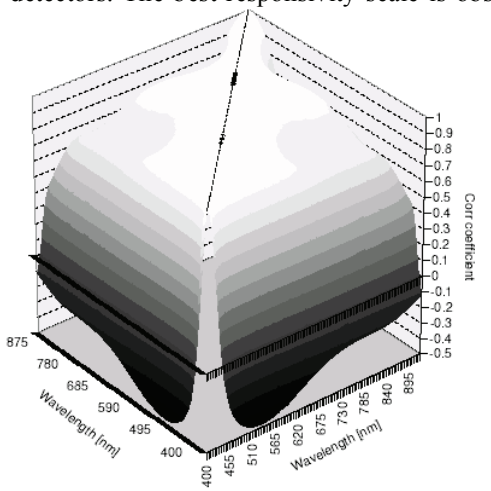

(b)

to have a combined uncertainty of less than 0.04 % between 530 and 950 nm at the 1 σ level of confidence.

Figure 3. The correlation coefficients for the fit function (a) and the responsivity (b).

References

Zalewski, E. F., Geist, J., Silicon photodiode absolute spectral response self-calibration, *Appl. Optics, 19,* 1214 – 1216, 1980.

Verdebout, J., Booker R. L., Degradation of native oxide passivated silicon photodiodes by repeated oxide bias, *J. Appl. Phys., 55*, 406-412, 1984.

Gentile T. R., Houston J. M., Cromer C. L., Realization of a scale of absolute spectral response using the National Institute of Standards and Technology high-accuracy cryogenic radiometer, *Appl. Optics, 35*, 4392-4403, 1996.

Haapalinna A., Kärhä P., Ikonen E., Spectral reflectance of silicon photodiodes, *Appl. Optics, 37*, 729-732, 1998.

Gran J., Sudbø Aa. S., Absolute calibration of silicon photodiodes by purely relative measurements, *Metrologia, 41*, 204-212, 2004.

Lira I., Curve adjustment by the least-squares method, *Metrologia, 37*, 677-681, 2000.

NEWRAD 2005:

Characterization of detectors for extreme UV radiation

F. Scholze, R. Klein, R. Müller

Physikalisch-Technische Bundesanstalt, Abbestraße 2-12, 10587 Berlin, Germany

Abstract. Photodiodes are used as easy-to-operate detectors in the extreme ultraviolet (EUV) spectral range. The Physikalisch-Technische Bundesanstalt calibrates photodiodes in the spectral range from 1 nm to 30 nm with an uncertainty of the spectral responsivity of 0.3% or better. For the dissemination of these high-accuracy calibrations, we investigated the stability and linearity of silicon n-on-p junction photodiodes under intense EUV irradiation in ultra high vacuum. We used quasi-monochromatic direct undulator radiation or focused radiation from a bending magnet to achieve high radiant power. The maximum current in linear operation (1% relative saturation) ranges from about 3 mA for 6 mm photon beam diameter to 0.2 mA for a 0.25 mm diameter spot. The corresponding irradiance increases from 30 mW/cm² for 6 mm photon beam size to about 2 W/cm² for a 0.25 mm beam. Diodes with diamond-like carbon as well as TiSiN top layer proved to be stable up to a radiant exposure of about 100 kJ/cm^2. The observed changes of the responsivity could be explained as the result of carbon contamination of the surface and changes in the electrical behaviour at the interface between top layer and sensitive silicon region. Under UHV conditions, no indication of oxidation of the surface was found.

Introduction

The Physikalisch- Technische Bundesanstalt (PTB) calibrates radiation detectors in the EUV spectral range with an uncertainty of the spectral responsivity of 0.3% or better[i]. Photodiodes are used as easy-to-operate reference detectors. The calibrations at PTB are based on the comparison of the photodiodes to a cryogenic electrical substitution radiometer radiometer (ESR) [ii] as primary detector standard using monochromatized synchrotron radiation[iii], a quasi DC- radiation with a rather low radiant power of about 1 µW. At the customer, these diodes may be used for strongly pulsed radiation and very different radiant power[iv]. We present here investigations of the stability and linearity of the diode signal.

Experimental

At present, mainly silicon n-on-p junction photodiodes of the types AXUV (nitrided siliconoxide passivation layer) and SXUV (metal silicide passivation) form International Radiation Detectors or Au/GaAsP Schottky diodes (e.g. G1127 from Hamamatsu) are used for EUV detection. PTB uses the EUV radiometry beamline with the electrical substitution radiometer SYRES I [ii] as the primary detector standard to provide calibrations of radiation detectors over a broad spectral range from 1 nm up to 30 nm with low relative uncertainty (0.3 % at 13.5 nm, k=1)[i]. Typical results are shown in Fig. 1. The Schottky diodes have the advantage of a very low dark current und thus better signal-to-noise for low power applications. They are, however, less homogeneous because of the strong absorption in the Au- top layer (dashed line in Fig. 1). The AXUV type silicon diode shows superior homogeneity and spectrally flat response. Therefore, this type seems to be suitable as a reference detector. We, however, showed that AXUV diodes degrade during storage even with no irradiation at all[v], see Fig. 2.

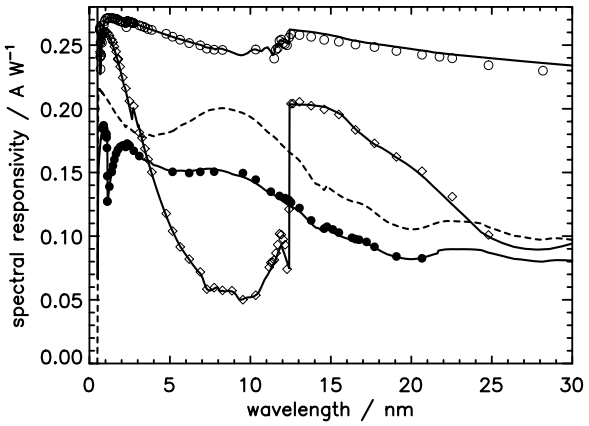

Figure 1. Spectral responsivity of three photodiodes. The upper curve (open circles) is an AXUV type diode. Data for an SXUV type diode are shown with diamonds and for a GaAsP/Au Schottky diode by solid circles. The lines represent model calculations[vi]. For the Schottky diode, the dashed line represents the responsivity that would result if the charge collection efficiency were ideal and only the Au contact layer absorption taken into account.

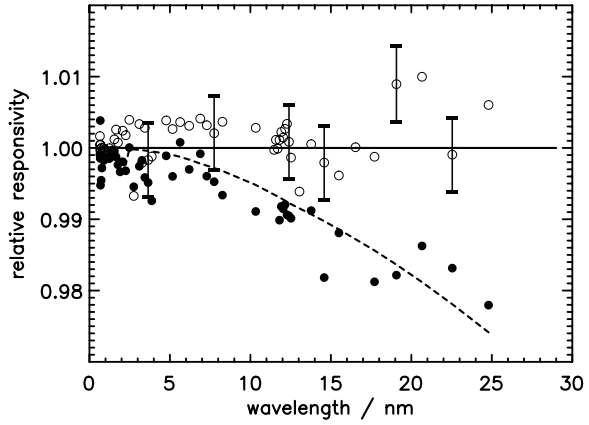

Figure 2. Ratio of spectral responsivity of an AXUV diode, six months after the initial calibration, to the responsivity measured initially (closed circles), and for an SXUV100 diode with TiSiN passivation, measured at the same times (open circles). The error bars represent the uncertainty of a single measurement with the extension factor k=2. The dashed line represents the transmittance of 0.11 µg/cm² oxygen.

The stability of silicon n-on-p junction photodiodes under intense EUV irradiation in ultra high vacuum (UHV) has also been investigated[vii]. Diodes with diamond-like carbon as well as TiSiN top layer proved to be stable up to a radiant exposure of about 100 kJ/cm^2. Although the responsivity remained unchanged within a few percent over the complete spectral range from 2 nm to 20 nm, the low uncertainty in the responsivity measurement allowed a significant spectral dependence to be revealed, see Fig. 3. Using a model for the spectral responsivity[vi], the observed changes of the responsivity could be explained as the result of carbon contamination of the surface, yielding a decrease in responsivity and changes in the electrical behaviour at the interface between top layer and sensitive silicon region. It appears that depending on the type of the top layer, part of this layer becomes either more sensitive or more non-sensitive, and also exhibits a small change in the charge collection efficiency at the interface. Under the UHV conditions of our experiment, no indication of oxidation of the surface was found.

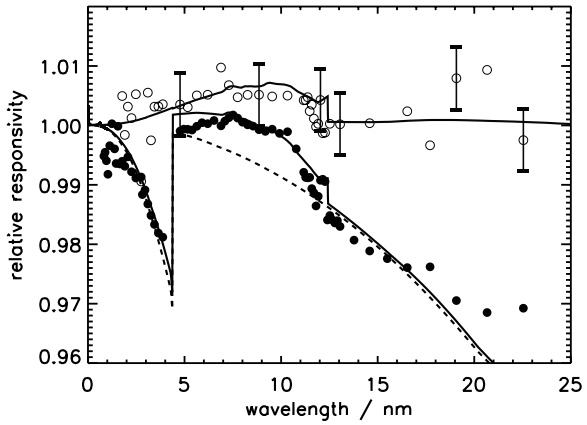

Figure 3. Ratio of responsivity after irradiation to the initial value for two SXUV type diodes. The diode coated with DLC (open circles) was exposed to 69 kJ/cm² and the diode with TiSiN (closed circles) to 143 kJ/cm². The dashed line shows absorptance of 0.57 µg/cm² carbon. The solid lines show the change in responsivity due an increase of the charge collection efficiency at the top silicon interface by 0.5 % absolutely. The error bars represent the uncertainty of a single measurement with the extension factor k=2.

The linearity of the photodiodes was tested in quasi-DC illumination using direct undulator radiation for different photon beam spot sizes[viii]. A systematic and significant variation of the maximum external photocurrent with the photon beam spot size is shown. The maximum current in linear operation (1% relative saturation) decreased from about 3 mA for 6 mm photon beam diameter to 0.2 mA for a 0.25 mm diameter. The corresponding irradiance increased from 30 mW/cm² for the 6 mm aperture to about 2 W/cm² for a 0.25 mm aperture, see Fig. 4. The behaviour is explained by a change in the effective serial resistance with photon beam size. The values derived from the saturation measurement vary between 65 Ω for a 6 mm beam and 540 Ω for 0.25 mm. This effect can be attributed to the finite conductivity of the thin front contact layer carrying the current to the electrode. For spot sizes smaller than the diode's active area, the serial resistance scales logarithmically with the spot size.

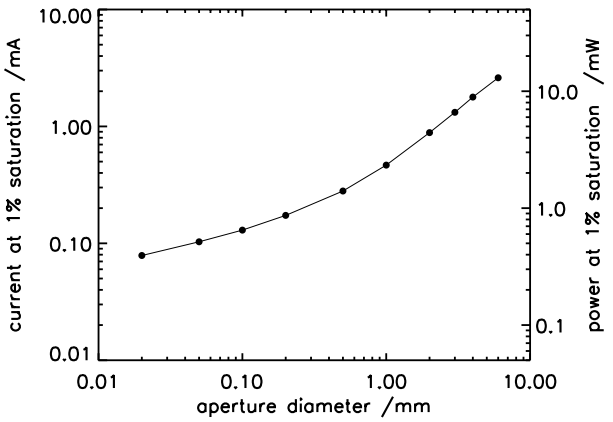

Figure 4. Relation between aperture diameter and current at 1% saturation as obtained from the relation between aperture size and serial resistance as measured down to 0.5 mm aperture size. The data for aperture sizes below 0.25 mm are calculated.

PTB at BESSY provides EUV detector calibrations with low uncertainty using an ESR and radiation of about 1µW radiant power with high spectral purity and temporal stability. Reliable information on linearity and stability for the extension of the detector calibration to higher radiant power can be obtained at hig-flux beamlines with radiant power in the mW-range.

References

[i] Scholze, F., Tümmler, J., Ulm, G., High-accuracy radiometry in the EUV range at the PTB soft X-ray radiometry beamline, *Metrologia* 40, S224-S228, 2003

[ii] Rabus H., Persch V., and Ulm G., Synchrotron-Radiation Operated Cryogenic Electrical-Substitution Radiometer as High-Accuracy Primary Detector Standard in the Ultraviolet, Vacuum Ultraviolet and Soft X-ray Spectral Ranges *Appl. Opt*., 36, 5421-5440, 1997

[iii] Scholze, F., Beckhoff, B., Brandt, G., Fliegauf, R., Klein, R., Meyer, B., Rost, D., Schmitz, D., Veldkamp, M., The new PTB-beamlines for high-accuracy EUV reflectometry at BESSY II, *Proc. SPIE* 4146, 72 – 82, 2000

[iv] Schürmann, M.C., Mißalla, T., Mann, K., Kranzusch, S., Klein, R., Scholze, F., Ulm, G., Lebert, R., Juschkin, L., Tools for EUVL-source characterization and optimization, *Proc. SPIE* 5037, 378-388, 2003

[v] Scholze, F., Brandt, G., Müller, P., Meyer, B., Scholz, F., Tümmler, J., Vogel, K., Ulm, G., High-accuracy detector calibration for EUV metrology at PTB, *Proc. SPIE* 4688, 680-689, 2002

[vi] Scholze, F., Rabus, H., Ulm, G., Mean energy required to produce an electron-hole pair in silicon for photons of energies between 50 and 1500 eV, *J. Appl. Phys*. 84**,** 2926-2939, 1998

[vii] Scholze, F., Klein, R, Bock, T., Irradiation Stability of Silicon Photodiodes for Extreme-Ultraviolet Radiation, *Appl. Opt.* 42, 5621-5626, 2003

[viii] Scholze, F., Klein, R., Müller, R., Linearity of silicon photodiodes for EUV radiation, *Proc. SPIE* 5374, 926-934, 2004

NEWRAD 2005: Preparing Final Camera-Ready

Realization of high accuracy spectrophotometric system as national standard of regular spectral transmittance coefficient

V. Skerovic, P. Vukadin, V. Zarubica
Bureau for measures and precious metals, Belgrade, Serbia and Montenegro

Lj. Zekovic
Physical faculty, University of Belgrade, Belgrade, Serbia and Montenegro

Abstract. The national standard spectrophotometric system developed in the Laboratory for photometry and radiometry of the Bureau of Measures and Precious Metals (ZMDM) is used for realization of regular spectral transmittance scale in spectral region 360 nm to 1000 nm. Evaluation of the performances of the system shows that the measurements on neutral density filters can be performed with the uncertainties in range from 0.1 % to 2 % (k = 2), depending on transmittance level and wavelength. System verification was performed according to NIST SRM reference standards. The validation of the method is expected with the results of EUROMET key comparison of regular spectral transmittance, in which, the Laboratory for photometry of ZMDM was included through the - bilateral comparison of regular spectral transmittance measurements with INM (EUROMET project No 766). Realization of the system and the method used in that bilateral comparison, together with its metrological characterization and measurement uncertainty evaluation, are presented in this paper.

Introduction

With realization of primary standard spectrophotometric system and realization by definition of the value of regular spectral transmittance coefficient [1], basic conditions for achieving measurement unity in the field of spectrophotometry are accomplished.

At the beginning of the year 2004, the bilateral comparison of spectral transmittance measurements, between Laboratory for photometry of the ZMDM and Laboratory for spectrophotometry of INM, was performed. It is officially recognized as EUROMET Project No 766. This Project is included as part of the EUROMET key comparisons of regular spectral transmittance measurements.

In this paper, measurement procedure, together with measurement results and uncertainty evaluation, regarding measurements performed in Laboratory for photometry as part of that project, are presented.

Design of the Spectrophotometric System

A single beam instrument with automated exchange of measured samples and compensation detector, based on double monochromator, is build up on the optical table, in the Laboratory for photometry (Figure 1).

The image of the halogen light source is projected on the entrance slit of the monochromator with quartz lens objective with *f*/5.5. In the plane of the exit slit of the monochromator, 3 mm in diameter, circular aperture is placed, so that, in the focal plane of the optical system, the regular circular spot may be obtained. All-mirror off-axes (off-axes angle ≤ 6°) optical system consists of one plain mirror and one spherical mirror of large diameter (152 mm, *f*/2 mirror relative aperture) projecting image of circular aperture at focal plane with 1:1.1 ratio. Beam splitter is used to divert approximately 10 % of the radiant flux on to the compensation detector. Stepp motor driven translation stage has linear resolution of 10 μm. One plane and one spherical mirror have a role to refocus the spot from the

Figure 1. The scheme of spectrophotometric system.

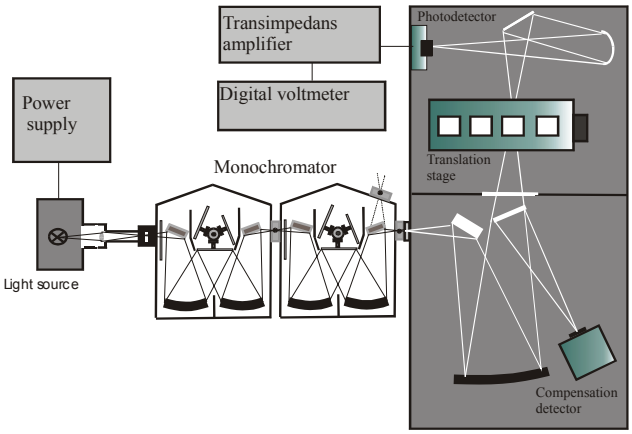

measured sample on to the detector surface with 1:1 ratio. Both detectors are silicon photodiodes Hammatsu S1337 1010BQ. Signals from photodiodes are measured through transimpendance amplifier, with scanner and digital voltmeter. The system is fully automated [2].

In the first realization of the system, refocusing optical system was achromatic objective, what results that the system was liable to interreflections [1]. The effect was larger measurement uncertainty and limited wavelength range. In order to extend the wavelength range to UV, and to reduce the measurement uncertainty, changes in refocusing optical system (Figure 1.) was made.

Description of measuring technique

Measurement procedure is automatic exchange of measured sample in the path of the light beam. Each time, signal from main and compensation detectors are measured simultaneously, ten times each detector. Average value of those readings was taken into account. At every wavelength measurements were preformed for sample and the reference (air), and before each of that, the measurement of dark current were made and correction

applied.

Reproducibility of measurements was determined up on the sample of 30 independent measurements of each sample for every wavelength. All measurements were preformed during two months.

Method of characterization of the spectrophotometer

The aim of the project of realization of the national spectrophotometric system is to develop the system that can provide realization of the unit of regular spectral transmittance coefficient at uncertainty level that can fulfill requirements for accuracy in spectrophotometric measurements. This goal can be achieved only with careful interpretation of spectrophotometric data, which means the evaluation of influential parameters and correction of systematic errors wherever it is possible.

Design of the optical system defines the light beam geometry, whose influence on measurements is manifested as beam-displacement errors, interreflection errors and obliquity errors (path-length error and Fresnel-reflectance error) [3]. Uncertainties arising from these effects are evaluated, and for pat-length error, the correction is applied. Interreflection error is evaluated by the method of transmittance measurements on tilted samples in polarized light [4].

Nonlinearity of the system is determined by double aperture method [5]. Wavelength accuracy [6], and stray light effects are discussed also. Detailed analysis of all these parameters is reported in this paper.

Uncertainty of measurement

Uncertainties given in table 1 are average values for wavelength range of 500 nm to 1000 nm, for 4 nm bandwidth measurements for the filter of nominal transmittance of 10 %. The numbers in table are relative values.

Table 1. Uncertainty budget.

Parameter	Type A	Type B	Uncertainty in spectral transmittance
Repeatability	0.000603		0.000603
Non linearity		0.0005	0.00045
Wavelength setting		0.1 nm	0.00003
Beam displacement		0.00004	0.00004
Inter-reflection		-	-
Obliquity effect		Corrected	0.00006
Polarization		-	-
Drift			0.0004
RMS total			0.000856

Specific uncertainties associated to each filter (nominal transmittances in range from 0.1 % to 90 %) on every wavelength are given with results of measurements, according to EUROMET`s “Technical protocol for key comparison of regular spectral transmittance measurements”.

In this paper, also, measurement uncertainty evaluation for the first measurement setup, with implementation of interreflection correction, is given, together with results of validation measurements made on NIST standard filters [7].

Measurement on NIST standard filters is repeated with changed (improved) system after bilateral comparison, and the results are compared with previous.

Conclusion

Validation measurements will show, that in booth cases, average difference between results obtained by measurement for NIST filters and their values from the certificate, is within the estimated measurement uncertainty, which indicate that the measurement uncertainty is well determined.

Agreement between the results from measurements made on same filters with two different measurement setups, represent real test for reproducibility of the method.

EUROMET key comparison of regular spectral transmittance measurements, when finalized, should support validation of our spectrophotometric measurements. These results will be reference for some future improvements of our spectrophotometric system.

Acknowledgments The authors wish to thank to all associates from department for metrology of the Physical faculty of Belgrade, who was engaged in the project of realization of our spectrophotometric system.

References

[1] Skerovic, V., Vukadin, P., Zarubica, V., Zekovic, Lj., Realization of primary spectrophotometric system, *Proc. Fifth General Conference of the Balkan Physical Union.*

[2] Skerovic, V., Vukadin, P., Zarubica, Application of the concept of virtual instrument in realization of primary spectrophotoradiometric system, *Proc. XLVII ETRAN Conference*.

[3] Mielenz, K. D., Physical Parameters in High-Accuracy Spectrophotometry, JOURNAL OF RESEARCH of the National Bureau of Standards – A. Physics and Chemistry, Vol. 76A, No. 5 (1972) 455-467.

[4] Mielenz, K. D., Mavrodineanu, R., Reflection Correction For High-Accuracy Transmittance Measurements on Filter Glasses, JOURNAL OF RESEARCH of the National Bureau of Standards – A. Physics and Chemistry, Vol. 77A, No. 6 (1973) 699-703.

[5] Mielenz, K. D., Eckerle, K., Spectrophotometer linearity testing usingthe double-aperture method, Applied Optics, Vol. 11, 2294 (1972).

[6] Manoochehri, F., Ikonen, E., High-accuracy spectrometer for measurement of regular spectral transmittance, Applied Optics, Vol. 34 (1995) 3686-3692.

[7] Mavrodineanu, R., Burke, R. W., Baldwin, J. R., Smith, M. V., Messman, J. D., Travis, J. C., Colbert, J. C., Glass Filters as a Standard Reference Material for Spectrophotometry - Selection, Preparation, Certification, and Use of SRM 930 and SRM 1930, NIST Special Publication 2260-166 (1994).

NEWRAD 2005: Preparing Final Camera-Ready

Mutual comparison of detectors spectral responsivity to prove stated measurement uncertainty

V. Skerovic, P. Vukadin, V. Zarubica

Bureau for measures and precious metals, Belgrade, Serbia and Montenegro

Abstract. Realization of the scale of spectral responsivity of the detectors in the Bureau of Measures and Precious Metals (ZMDM) is based on silicon detectors traceable to BNM-INM. For a laboratory, which do not has own scale realization, and establishes its traceability to other NMI, the main goal is to develop appropriate method for tracing the value of spectral responsivity. In order to provide objective information about calibration and measurement capabilities in that field, the method for proving stated measurement uncertainty based on mutual comparison of at least three detectors, is developed. In this paper, method of mutual comparison is presented, and the results with measurement uncertainty analysis are given.

Introduction

Tracing the value of the unit based on the realization of foreign Laboratory (NMI), is the case in the most of the smaller countries NMI′s. In order to evaluate measurement uncertainty of tracing the value, received measurement uncertainty must be integrated with uncertainty of the realized method of comparison. However, in such cases of tracing the value of the unit in multiple steps, stated measurement uncertainty will not always represent real truth about calibration and measurement capabilities.

Based on long tradition in realization and tracing the values of light quantities based on International Mean of the candela and lumen conserved in the BIPM [1], the method of proving measurement uncertainty by means of mutual comparisons is developed in the Laboratory for photometry and radiometry of ZMDM.

Realization of the method for comparison of spectral responsivity of silicon detectors

Measurement system [2, 3] for comparison of spectral responsivity of silicon detectors is shown in Figure 1.

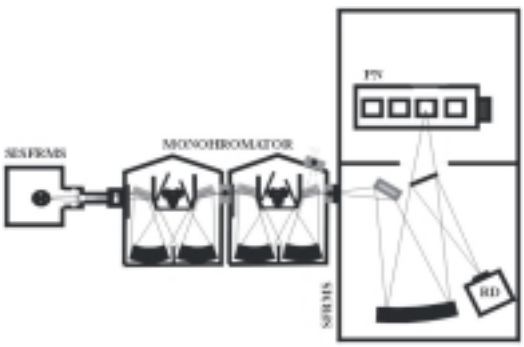

Figure 1. System of spectral comparisons. SISFRMS, light source; SFRMS, measurement station; RD, monitor detector; PN, translation stage.

System is based on double monochromator, halogen light source with 3 mW optical power at 550 nm. Beam divergence (full angle) is f/6, and spot size at focal point of the system is approximately 4 mm with bandwidth of 4 nm.

Three detectors (Hammatsu S1337 1010BQ) were calibrated at the end of year 2003 in BNM-INM. Calibrations were made in spectral range from 300 nm to 1000 nm at 23 different wavelengths. Bandwidth was 3 nm, and spot size ≈5 nm [4].

Method of comparison [5], is based on measurement equation

$$S_X(\lambda) = \frac{N_X(\lambda)}{N_0(\lambda)} \cdot \frac{G_0}{G_X} \cdot S_0(\lambda), \qquad (1)$$

where: Sx(l), S_O(l) – spectral responsivity of the test and standard detector; N_X(l), N_O(l) – ratios of the signals from test/standard and compensation detector; Gx, Go – transimedance amplifier gain for two channels (for test and standard detector signal measurements).

Detectors are automatically exchanged in the path of the light beam. Signal from main and compensation detectors are measured simultaneously, ten times each detector. Correction of dark current is applied. Signal from detector is measured with transimpendans amplifier and digital voltmeter with scanner. Transimpedance amplifier is calibrated by means of low current source calibrator and digital voltmeter. Measurement uncertainty of the method of comparison is evaluated and given in table 1.

Table 1. Uncertainty budget.

Uncertainty component	Uncertainty (Type A)	Uncertainty (Type B)
u(Nx)	2×10^{-4}	
u(No)	2×10^{-4}	
u(Gx)		$2{,}5 \times 10^{-4}$
u(Go)		$2{,}5 \times 10^{-4}$
DVM uncertainty		2×10^{-4}
beam-divergence		negligible
Nonuniformity of detectors		not analized
Nonlinearity		2×10^{-4}
Wavelength accuracy		$0{,}2 \times 10^{-4}$
Bandwith efect		negligible
Stray light		negligible
Standard uncertainty (1σ)	$2{,}8 \times 10^{-4}$	$4{,}5 \times 10^{-4}$
Combined standard uncertainty (1σ)	$5{,}3 \times 10^{-4}$	

Mutual comparison

Mutual comparison of three standard detectors (SR1, SR2, SR3) is preformed by method of comparison each by each, in both directions (measurement sequence). It means that six different comparisons are made: SR1-SR2, SR1-SR3, SR2-SR3, SR2-SR3, SR2-SR1, SR3-SR1. For each of these comparisons, five measurement cycles are made at 23 wavelengths with ten readings at every wavelength.

Results of comparison SR1-SR2, for example, is calculated as relative deviation [6] of the results of measurements for SR2 detector responsivity, using SR1 as standard, from its values given in BNM-INM certificate. Calculations are made at each point of measurement. Average value of relative deviation for every wavelength is presented. Standard deviation of all mutual comparison measurements is calculated and given as measure of reproducibility of measurements.

Preliminary results show that average deviations from certificate values for all mutual comparison measurements (all three detectors) is 0,93 % relative. Larger difference from certificate values shows detector SR3, while detectors SR1 and SR2 shows differences of about 0,7 % relative. Reproducibility of the method is tested with SR1-SR2 and SR2-SR1 measurement after complete repositioning and changed conditions in two days. The results show agreement within 0,1 %. Correction or reduction of deviations from certificate values should be made through the measurements that are still in progress. Detailed analysis of all results will be presented in the paper.

Conclusion

Differences between certificate values and values that are reproduced in the laboratory, which traces the value from other NMI, are not unusual. Dealing with that, is the one of the most complex jobs for the laboratories of that kind.

Method of mutual comparisons can be good model for smaller countries laboratories (NMI′s), to deal with that problem. Result of mutual comparison can provide basis for improvements of realized method, and can be used to prove stated measurement uncertainty. Result of mutual comparison represents real truth of uncertainty of reproducing the value of the unit that is traced from other NMI.

Acknowledgments The authors wish to thank to Prof. Lj. Zekovic and all associates from department for metrology of the Physical faculty of Belgrade, who was engaged in the project of realization of our system. Also, authors wish to thank to Dr. Z. M. Markovic who help us with his advises in writing this paper.

References

[1] Vukadin, P., Skerovic, V., Zarubica, V., *Tracing the values of light quantities in Federal bureau of measures and precious metals*, Publication CIE x020 – 2001: Proceedings of the CIE Expert Symposium 2001 on Uncertainty Evaluation Methods for Analysis of Uncertainties in Optical Radiation Measurement, January 2001, Vienna, Austria.

[2] Skerovic, V., Vukadin, P., Zarubica, V., Zekovic, Lj., Realization of primary spectrophotometric system, *Proc. Fifth General Conference of the Balkan Physical Union.*

[3] Skerovic, V., Vukadin, P., Zarubica, Application of the concept of virtual instrument in realization of primary spectrophotoradiometric system, *Proc. XLVII ETRAN Conference*.

[4] Calibration certificate N°1076-Ra-04, BNM-INM, 2003.

[5] Larason, T. C., Bruce, S. S., Parr, A. C., Spectroradiometric detector Measurements,NIST Special Publication 250-41.

[6] ISO, Guide To The Expression Of Uncertainty In Measurement, 1993.

Calibration of Space Instrumentation in the Vacuum Ultraviolet

M. Richter, A. Gottwald, W. Paustian, F. Scholze, R. Thornagel, G. Ulm
Physikalisch-Technische Bundesanstalt, Berlin, Germany

Abstract. At the Physikalisch-Technische Bundesanstalt (PTB), various radiometric techniques for the calibration of space instrumentation with synchrotron radiation in the spectral range from ultraviolet radiation to X-rays have been developed and applied. In this context, the present contribution gives an overview of PTB's measurement capabilities at the electron storage ring BESSY II. Recent examples for the calibration of space instrumentation in the vacuum ultraviolet are discussed.

Introduction

The Physikalisch-Technische Bundesanstalt (PTB) uses synchrotron radiation at the electron storage ring BESSY II for the calibration of radiation sources, detectors, and spectrometers as well as for the characterization of optical components in the spectral range from ultraviolet (UV) radiation to X-rays (*Klein et al.* 2002). Most of the measurements are based on two different primary standards, BESSY II itself as primary source standard and cryogenic radiometers as primary detector standards. They allow radiometric calibrations to be performed with relative uncertainties below 1 %. Many activities are related to the calibration of space instrumentation for extraterrestrial, solar, and astronomical missions, e.g. of the space agencies NASA and ESA (*Richter et al.* 2005).

Calibration Techniques

BESSY II is used as a primary source standard of calculable synchrotron radiation within the framework of source-based radiometry. This method is applied, e.g., for the calibration of transfer source standards, such as deuterium lamps or hollow cathode (HC) plasma sources, by comparison of the radiation with the help of a movable spectrometer. PTB had established HC sources as transfer standards in the vacuum-UV (VUV) spectral range from 13 nm to 125 nm for the calibration of space instrumentation. Outstanding examples have been the calibration of the SUMER and CDS telescopes of the Solar and Heliospheric Observatory (SOHO). Recently, the CDS calibration source has been used within a scientific cooperation at the Rutherford Appleton Laboratory (RAL) to characterize the EUV Imaging Spectrometer (EIS) for the Solar B mission and NASA's Multi-Order Solar EUV Spectrograph (MOSES, Fig. 1).

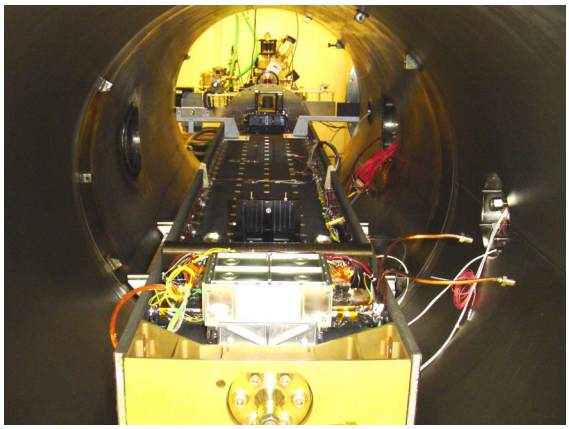

Figure 1. The MOSES instrument within the vacuum tank at the Rutherford Appleton Laboratory (RAL) during calibration by RAL and PTB with the CDS calibration source.

Within the framework of detector-based radiometry, PTB operates the cryogenic radiometers SYRES I and SYRES II to measure the radiant power of spectrally dispersed synchrotron radiation in absolute terms. It allows to calibrate transfer detector standards such as semiconductor photodiodes with low uncertainty. The corresponding beamlines in the PTB laboratory at BESSY II cover the wavelength range from 400 nm down to 0.12 nm. At the same beamlines also reflectometry is performed, i.e. the characterization of optical components by relative measurements of reflected, transmitted, or diffracted radiation with respect to the photon intensity incident on a sample. In this context, PTB characterizes detection systems and optics for various space instruments. As an example, Fig. 2 shows spectral responsivity curves of solar-blind diamond detectors which have been developed within the framework of a scientific cooperation with the Max Planck Institute for Solar System Resarch and the Solar Orbiter Detector Development Program BOLD (Blind to Optical Light Diamond). A first application of these detectors is scheduled for the Lyman-alpha Radiometer LYRA and the SWAP (Sun Watcher using APS detectors and image Processing) instrument of ESA's PROBA II mission.

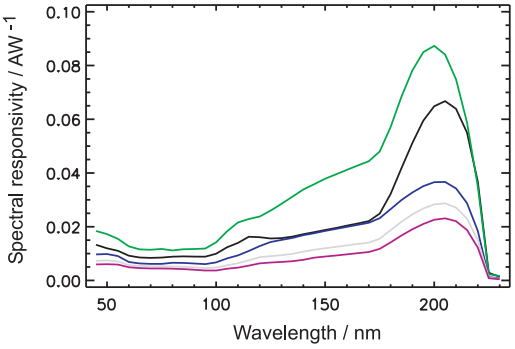

Figure 2. Spectral responsivity in the UV/VUV of different solar-blind diamond photodetectors.

References

Klein, R., Krumrey, M., Richter, M., Scholze, F., Thornagel, R., Ulm, G., *Synchrotron Radiation News*, 15, No. 1, 23-29, 2002.
Richter, M., Gottwald, A., Scholze, F., Thornagel, R., Ulm, G., *Advances in Space Research*, 2005, in press.

A comparison of the performance of a photovoltaic HgCdTe detector with that of large area single pixel QWIPs for infrared radiometric applications

J. Ishii
National Metrology Institute of Japan / AIST, Tsukuba, Japan

E. Theocharous
National Physical Laboratory, Teddington, U.K.

Abstract. Newly developed single pixel, large area Quantum Well Infrared Photodetectors (QWIPs) and a photovoltaic HgCdTe detector have been characterized using the NPL infrared detector characterization facilities. Spectral responsivity and D* values of both detector types were shown to be high enough to satisfy the requirements of a number of applications in infrared radiometery. However, neither detector type can be considered for high accuracy radiometric applications, mainly due to serious drawbacks in their spatial uniformity of response profiles.

Introduction

A previous evaluation of infrared detectors for radiometric applications has shown that the performance of commercially available detectors is far from ideal, for wavelengths longer than 5 μm [1]. For example, large area (up to 4 mm by 4 mm active area) photoconductive (PC) HgCdTe detectors exhibit very large (>20%) spatial non-uniformities in their response [1] whereas thermal detectors such as pyroelectric detectors based on non-hygroscopic crystals have relatively low specific detectivity (D*) values. Extrinsic photoconductors require cooling to well below 77 K and are not available with sufficiently large active areas [2]. Additionally, the response of PC HgCdTe devices has been shown to be non-linear at relatively low levels of incident photon irradiance [3]. If the operating temperature of the detector is restricted to 77 K or higher, then PV HgCdTe detectors offer the highest D* values in the 8 μm to 12 μm spectral region. However, PV HgCdTe detectors whose response extends to 12 μm are currently available with active areas up-to 2 mm diameter which is smaller than the active areas required for the majority of applications in infrared radiometry [1]. Quantum Well Infrared Photodetectors (QWIPs) [4] are now well established for use in state-of-the-art cooled thermal imaging systems. For fundamental optical measurement applications, for example infrared spectral responsivity standards, it is normal (and sufficient) to use a single element detector [1]. Some QWIPs are made from layers of GaAs/$Al_xGa_{1-x}As$ which can be mass grown on large substrate wafers. The fabrication of these materials is well established and promises to deliver large area, single pixel photodetectors with high spatial uniformity of response.

Results

The performance of two single pixel, large area QWIPs which were specially commissioned by NPL and manufactured by QWIP Technologies, USA, were compared with that of a commercially available 2 mm diameter photovoltaic (PV) HgCdTe detector. Parameters which were compared include the absolute spectral responsivity, Noise Equivalent Power (NEP), spatial uniformity of response, non-linearity and stability. Figure 1 illustrates the DC equivalent absolute spectral responsivity and noise equivalent power of one of the QWIP detectors in the wavelength range from 5 μm to 10 μm. Both detector types were shown to have sufficiently high spectral responsivity and D* values to satisfy a number of applications in infrared radiometry when operated at 77 K. However, the spatial non-uniformity of response of both QWIPs examined was unacceptably high. Furthermore the spatial uniformity of response of the same detectors was shown to be strongly dependent on the state of polarisation of the incident radiation as well as also exhibiting some dependency on wavelength. The spatial uniformity of response of the PV HgCdTe detector was shown to be very poor due to the very low shunt resistance of this detector. However, it exhibited no polarisation dependency and only a slight dependency on wavelength for wavelengths below 5 μm. Neither detector type could be considered for high accuracy radiometric applications in their current form.

Figure 1. Absolute spectral responsivity and NEP of the QWIP detector.

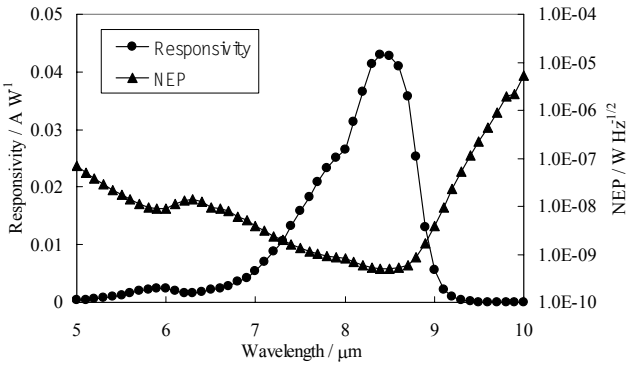

References

1. Theocharous E., Fox N. P. and Prior T. R., "A comparison of the performance of infrared detectors for radiometric applications", Optical Radiation Measurements III, SPIE Vol. **2815**, 56-68, 1996.
2. Theocharous E. and Birch J. R., "Detectors for Mid- and Far-infrared Spectroscopy: Selection and Use" Handbook of

Vibrational Spectroscopy Vol. **1**, J.M. Chalmers and P.R. Griffiths (eds), John Wiley and Sons, 2002, 349-367.
3. Theocharous E, Ishii J. and Fox N. P., "Absolute linearity measurements on HgCdTe detectors in the infrared", *Applied Optics*, 43, 4182-4188, 2004.
4. Levine, B.F., "Quantum well infrared photodetectors", *J. Appl. Phys*., **74**, R1-R81, 1993.

Stray-light correction of array spectroradiometers using tunable pulsed and cw lasers

A. Sperling, O. Larionov, U. Grusemann, and S. Winter
PTB, Braunschweig, Germany

Abstract. Array spectroradiometers are widely used in radiometry and photometry as tools for rapid measurements of the spectral distribution of lamps and other signal sources. Unfortunately, the stray-light rejection of such devices is often less than that of a scanning double or even single grating monochromator system. In addition, as array spectrometers are more or less monolithic systems, other device dependent side-effects, e. g. evoked by special order filtering in front of the diode or CCD array, by fluorescence, etc. may affect the measured spectrum.

With the availability of high power narrow bandwidth sources, tunable over the entire spectral range of a spectroradiometer from UV to IR, the possibility of correction procedures are reconceived [1,2]. A powerful new method for stray-light correction was recently presented by Y. Zong et al. [2]. He implemented a stray-light correction matrix, where the elements of the matrix have to be determined by successive measurements of the entire spectrum produced by wavelength-tunable single monochromatic laser lines.

The purpose of this contribution is to compare the results of the achievable stray-light correction based on Zongs method for different array spectrometers using the TULIP (TUnable Laser in Photometry) facility of the PTB, where a setup with tunable cw-lasers as well as a setup with pulsed lasers is used.

TULIP Facility

TULIP was build as a cw laser-based calibration setup for measurement of irradiance responsivity of large-area photometric and radiometric detectors [Figure 1]. To cover the spectral range from less than 360 nm up to 960 nm different types of cw lasers are necessary [Figure 2]. Although the spectral range of TULIP is only a small part of the range covered by SIRCUS [3], the well-proved laser facility at NIST, it is sufficient for most photometric and radiometric tasks in the visible and adjacent spectral ranges.

As cw laser-based facilities are not easy to automate for this wide spectral range and in order to overlap the spectral range between 460 nm and 560 nm with durable tunable solid state lasers, TULIP was complemented by a pulsed laser system based on optical parametric oscillators (OPOs), covering the spectral range from 410 nm to 2400 nm.

This pulsed laser system is much easier to handle than the complex cw lasers systems. In addition, the spectral range of this system is larger and tuning is very easy to automate. The disadvantage of this laser, the short pulse duration (about 4 ns only), is reduced by pulse stretching using fiber delay lines and an integrating sphere with high spectral reflectance.

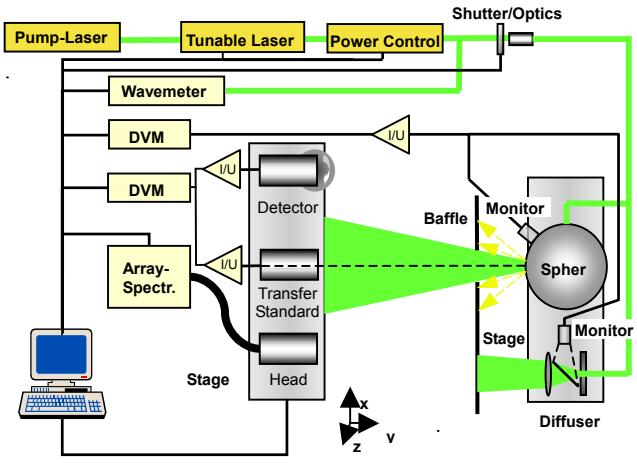

Figure 1. TULIP facility for calibration and characterization of detectors and spectroradiometers using the uniform radiation field in front of a sphere or a transparent (holographic) diffuser for higher radiation levels.

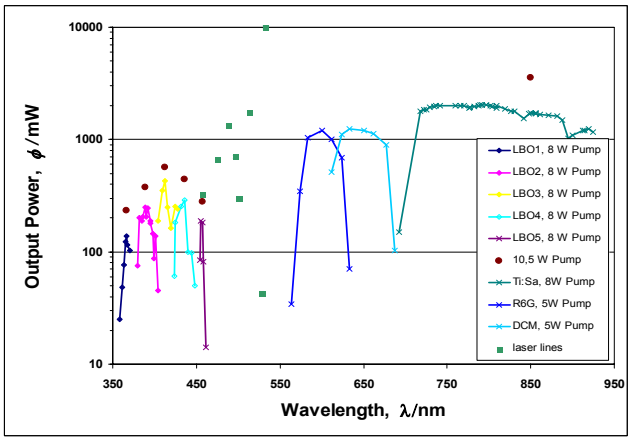

Figure 2. Output Power of the TULIP cw-laser setup. Between 358 nm and 460 nm the frequency of a Ti:Sa laser which operates between 690 nm and 960 nm is doubled. Dye laser are used in the range from 560 nm to 685 nm. Between 457 nm and 532 nm single laser lines from Argon ion and Nd:YVO_4 lasers are available.

As a result of this simple setup, the pulse length is stretched to more than 0.1 µs at a repetition rate of 22 Hz.

Comparison between Pulsed and CW Lasers

Using the setup shown in Figure 1 and provided that the correction matrix can be handled as a stable device

characteristic, both the correction of stray-light (including fluorescence) and second order images is possible. Moreover, with information about the linearity of the array spectroradiometer an absolute calibration against trap detectors can be performed.

Although it is expected that the best results for the generated correction matrix are obtained if measurements are carried out using a stable cw laser system, tuneable over the whole spectral range, the respective effort may be too large for many calibration laboratories. Therefore, we applied and tested our pulsed laser system for the measurement of the spectra [Figure 3] for different kind of array spectroradiometers. The calculated correction matrices are analysed and compared with cw laser-based measurements.

It is shown that even with CCD array spectroradiometers (CCD not gated) the results of the stray-light reduction with pulsed lasers are comparable to that, which are obtained based on calibration using a cw laser system.

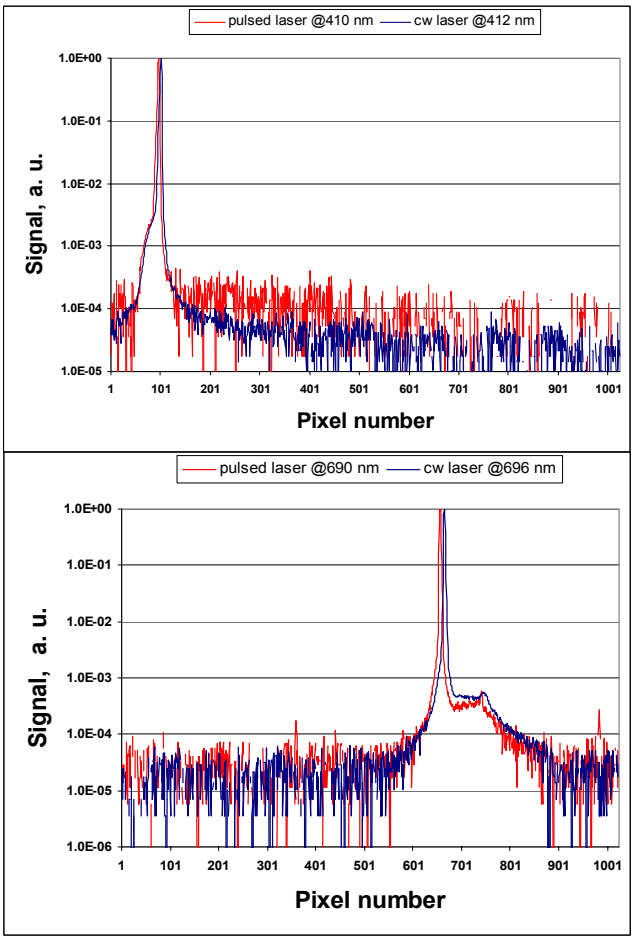

Figure 3. Measured data of pairs of slightly different (and therefore distinguishable) laser lines from a CCD array spectroradiometer (CCD not gated) a) blue: 412 nm cw, red: 410 nm pulsed; b) blue: 696 nm cw, red: 690 nm pulsed.

It is important to note that depending on the reflection path within the array spectrometer even small changes in the wavelength setting of the irradiating laser may result in big differences (peaks) within the stray-light spectrum.

Acknowledgments The authors thank Yuqin Zong from the NIST Optical Sensor Group for helpful discussions.

References

[1]Brown, S. W., B. C. Johnson, M. E. Feinholz, M. A. Yarbrough, S. J. Flora, K. R. Lykke, D. K. Clark, Stray light correction algorithm for spectrographs, *Metrologia, 40, pp* 81-83, 2003.

[2]Zong, Y., S. W. Brown, B. C. Johnson, K. R. Lykke, Y. Ohno, A Simple Stray-light Correction Method for Array Spectroradiometers, *Applied Optics, to be published.*

[3]Brown, S. W., G. P. Eppeldauer, K. R. Lykke, NIST facility for Spectral Irradiance and Radiance Responsivity Calibration with Uniform Sources, *Metrologia, 37, pp* 579-582, 2000.

Characterizing the performance of UV radiometers monitoring UV disinfection devices

W. Heering, H.-P. Daub
Lichttechnisches Institut (LTI), University of Karlsruhe, Karlsruhe, Germany

Abstract. According to the German DVGW regulations W294-3, radiometers that monitor the UV radiation of devices for disinfecting drinking water must have a prescribed geometry and angular response. They must match the spectral sensitivity of microorganisms and be absolutely calibrated at 254 nm. Testing facilities have been developed in the LTI to prove such features as well as linearity, aging and response to radiation out of the disinfecting spectral range. The uncertainties involved in such measurements will be discussed.

Introduction into W294-3

It is not acceptable to verify UV disinfection capacity continuously with seeding spores in drinking water in water works as it is done before during the biodosimetric challenge test. So the UV input into the reactor must be monitored on line by UV radiometers. This allows to maintain a reduction equivalent fluence REF of at least 400 J/m^2 of 253,7 nm radiation on each point inside of the reactor. As the spectral radiant power of lamps as well as the wavelength-dependent absorbance of the water vary, the monitoring detector must match the known actinic spectrum $s(\lambda)_{mic,rel}$ of disinfection. The degree of mismatch is described by the characteristic figure $f_{1,Z}$ where $s(\lambda)_{rel}$ is the relative responsivity of the radiometer to be characterized and normalized so that $s(254\,nm)_{rel} = s(254\,nm)_{mic,rel}$. $S_{\lambda,Z}(\lambda)$ is the standardized spectral distribution of the radiant power of the UV lamp Z used in the reactor.

$$f_{1,Z} = \frac{\int_{220}^{340} \left| s(\lambda)_{rel} - s(\lambda)_{mic,\,rel} \right| \cdot S_{\lambda,Z}(\lambda) \cdot d\lambda}{\int_{220}^{340} s(\lambda)_{mic,\,rel} \cdot S_{\lambda,Z} \cdot d\lambda}$$

Equation 1.

The requirements of W294-3 are $f_{1,Z} \leq 0{,}25$ for reference radiometers and $f_{1,Z} \leq 0{,}40$ for monitoring radiometers. In order to determine $f_{1,Z}$ the relative spectral responsivity of the radiometer has to be measured in the range from 220 nm to 340 nm. For a quick check of spectral mismatch of radiometers already in use, the relative response r_s and r_l to radiation, which has wavelengths shorter than 240 nm respectively longer than 300 nm, are appropriate figures of characterization. Definitions of r_s and r_l and measuring methods are given in W294-3.

Online measurements with UV radiometers at different monitoring positions and at different times of operations must be comparable. This is why radiometers for disinfection controlling have to be absolutely calibrated at the standardized wavelength of 253,7 nm. Reference radiometers are calibrated against a transfer standard radiometer which is traceable with an uncertainty of ± 5 % to a national or international standard. They are to check the monitoring radiometers of UV devices and especially to calibrate them. As the microbicidal irradiances on the monitoring radiometers of the reactor are up to four magnitudes higher than the irradiance level at which calibration occurs, linearity has to be tested additionally, i.e. up to 10 kW/m2 when medium pressure mercury lamps are installed.

For comparable measurements, UV radiometers for monitoring as well as those for validation must have identical angular response and entrance dimensions. In the Austrian Standard ONORM M5873-1 (2001) an acceptance (full) angel of 160° is established, in the German Standard DVGW W294 (1997) it was fixed to 40°. In each case an irradiance signal is aimed which changes nearly to the same degree as flow changes at the same REF. In the water reactor the measuring radiometer head with its entrance window made of quartz glass is separated by an 1 mm air gap and a 5 mm thick quartz window in the wall of the reactor from the water. So, because of additional refraction an incident angle on the air side of 40° respectively 160° which is really to be tested corresponds to an incident angle on the water side of only 28,8° respectively 91,4°. Furthermore a cosine response is expected within the angular range of the detector; $f_2 \leq 0{,}03$ for the 40° radiometer, $f_2 \leq 0{,}20$ for the 160° detector. Both, acceptance angle as well as cosine response, are given if the angular response is within the lower and upper curves shown for the 40° sensor in Figure 1.

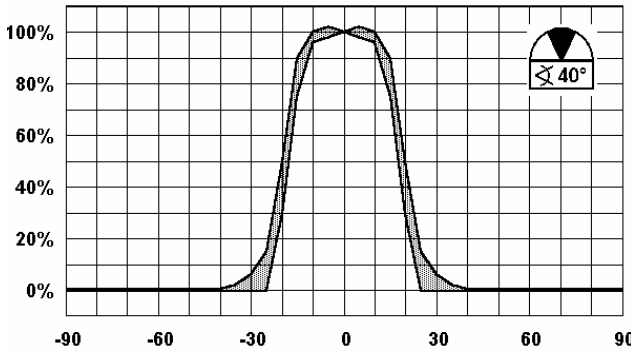

Figure 1 Angular tolerances of the 40° detector head

Testing facilities

Measuring arrangements have been developed and verified in order to determine the characteristic features of UV radiometers according to the W294-3 regulations. The key quantity used for characterization is the spectral responsivity of the UV radiometer under test. Its spectral distribution is measured in the whole air UV by comparing its photosignal produced by monochromatic irradiation at

different wavelengths with that from a standard detector at the same position. Quasi-monochromatic radiation is obtained by filtering the focused radiation from a xenon arc lamp XBO 450W/4 by a BENTHAM monochromator M300 HRA/2. The spectral half-width set at 2.0 nm is a compromise between sufficient irradiance on the detector and spectral resolution. The reference detector is a silicon photodiode HAMAMATSU S1227-1010BQ within a blackened and temperature-controlled aluminum housing and covered with an aperture stop of 7 mm diameter.

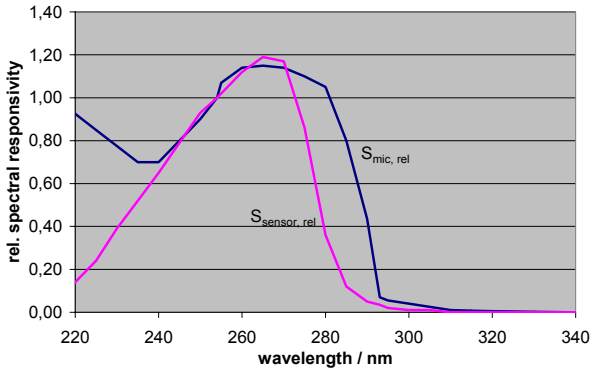

Figure 2 Measured rel. spectral radiometer responsivities $s_{sensor,rel}$ and spectrum $s_{mic,rel}$ of microbicidal action

A typical monitoring UV radiometer with responsivity curve as shown in Figure 2 fulfills $f_{1,Z} < 0.40$ if Z is for a mercury medium pressure lamp but it has too high short wave responses r_s.

Absolute spectral responsivities are obtained by calibration at 254 nm where the relative responsivity is normalized to one. The standard detector for comparison is of the same type as used for the measurement of relative spectral responsivities. At the PTB, its absolute differential spectral responsivity (DSR) has been determined for different bias currents in the range from 210 nm to 420 nm. Here, the monochromatic source is a capillary mercury low pressure lamp within a ellipsoidal reflector. The reflector opening is imaged by a Suprasil lens via an interference reflection filter with center wavelength of 254 nm and HWHM = 40 nm onto the window of the detector so that its entrance is just fully irradiated. The UV lamp is supplied by an electronic control gear and regulated by means of a monitoring SiC diode to a constant output. The extraordinary properties of this UV unit are to give a monochromatic irradiance of 6.63 W/m^2 and a uniformity of irradiance so that the irradiance within a diameter of 13 mm is only by a factor of 0.95 smaller than that within a diameter of 7 mm. Always the plane of the diffuser of the radiometer head has to be taken as the measuring plane. So take into consideration that the diffuser plane of the DVGW sensor is 20 mm behind the corresponding plane of the ONORM sensor.

Linearity tests are based on the condition that the reference detector, here a silicon photodiode HAMAMATSU S1227-1010BQ, used to compare photosignals at the same irradiance level is linear. This is true up to a short circuit current of about 5 mA corresponding to a reduction equivalent irradiance of about 1000 W/m^2. The lamp used to produce so high irradiances is a stabilized CERMAX xenon short arc lamp PE300BUVM with parabolic reflector. As the silicon photodiode is strongly responsive in the VIS and NIR where the UV radiometer is blind, the settings of different irradiance levels should be done by non-selective attenuation. We have realized this by means of metal meshes of different density.

In order to measure the angular response, the UV detector head under test is rotated around a middle axis through the outer surface of the entrance window. The CERMAX lamp described before produces behind a circular aperture stop a beam with half aperture angle of 2°. All UV radiometers which have been tested up to now according to W294-3 are within the prescribed limits of angular response and have the requested cosine response.

Other characteristic features as temperature dependence and aging of responsivity have to be proved. The respective testing facilities and measurements will be presented in the complete paper on radiometers for disinfection devices.

References

European Thematic Network for Ultraviolet Measurements – WG1, Final Report (Nov. 2000), Characterizing the performance of integral measuring UV meters, HUT, Metrology Institute, Finland.

DVGW Standard W 294-3 (2005), Ports and sensors for radiometric monitoring of UV disinfection devices – requirements, testing and calibration, Wirtschafts- und Verlagsgesellschaft Gas und Wasser, Bonn, Germany.

Hoyer, O., Heering, W., Reproducible optical monitoring of UV disinfection devices, Proceedings, 2nd Int. IUVA Congress, Vienna, July 9-11 2003.

Optical Radiation Action Spectra for Safety Regulations and Their Realization Using Integral Detector Measurement Devices

A.Gugg-Helminger
Gigahertz-Optik GmbH, Fischerstr. 4, 82178 Puchheim/Munich, Germany

Abstract. Over the years many action spectra have been created dealing with potential human health risk due to exposure to optical radiation. The main photobiological action spectra are for the eye, blue light (retina) and thermal effects within the retina and skin. Most of these spectra fall within the wavelength range from 180 to 3000 nanometers. There are many manufacturers of photobiologically weighted detectors designed to mimic these action spectra. Currently no international regulations exist on how to specify the accuracy of these measurement devices. For more reliable measurements a method to compare these devices will be proposed.
A method to reduce measurement uncertainty caused by the detector spectral mismatch will also be discussed.

BGI5006 dated October 2004 lists the following photobiological action spectra:

Wavelength (nm)	Action Spectra	Units (or J instead of W)	Health Risk
180 - 400	ICNIRP	$W/m^2.eff$	Skin
315 - 400	Radiometric	W/m^2	Eye
380 – 600	Blue Light	$W/m^2sr.eff$	Eye
380 – 600	Blue Light	$W/m^2.eff$	Eye
380 – 1400	Retinal Thermal	$W/m^2sr.eff$	Eye
780 - 3000	Radiometric	W/m^2	Eye & Skin
380 - 1000000	Radiometric	W/m^2	Skin

Table 1 List of photobiological action spectra

1. Spectral Mismatch Factor

Since calibration methods, standards and instrumentation vary from device manufacturer to manufacturer and one uniform method of calibration would not be accepted universally, another tool to provide reliable measured values is required.
One tool is the calibration correction factor using the a(Z) formula outlined below.

$$a(Z) \quad \frac{\int_0 S_{\lambda,c}\, s_{\lambda}\, _{act,rel}\, d\lambda}{\int_0 S_{\lambda,c}\, s_{\lambda}\, _{rel}\, d\lambda} \quad \frac{\int_0 S_{\lambda,Z}\, s_{\lambda}\, _{rel}\, d\lambda}{\int_0 S_{\lambda,Z}\, s_{\lambda}\, _{act,rel}\, d\lambda}$$

Formula 1 Spectral Mismatch Factor
where

$S_{\lambda,c}$ spectral distribution of the source used for calibration
$S_{\lambda,Z}$ spectral distribution of the source in a particular application
$s(\lambda)_{act,rel}$ relative spectral actinic weighting function
$s(\lambda)_{rel}$ relative spectral responsivity of the radiometer head

From this formula it can be shown that an
a(Z) >1 yields a lower real value (detector reads too high) and
a(Z) <1 a higher real value (detector reads too low)

2. Spectral distribution of 10 sources for different wavelength regions

It will be essential to have for every wavelength region a set of different sources to calculate the correction factor. The more different the sources the better is the confidence in the sensor, if all calibration correction values a(Z) are as close as possible to 1 for each source.

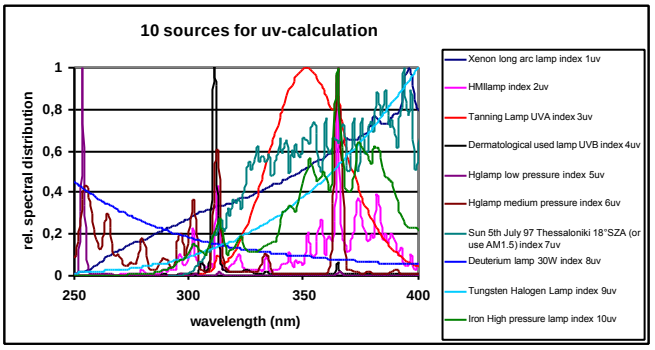

Graph 1 Relative spectral distribution of ten uv sources

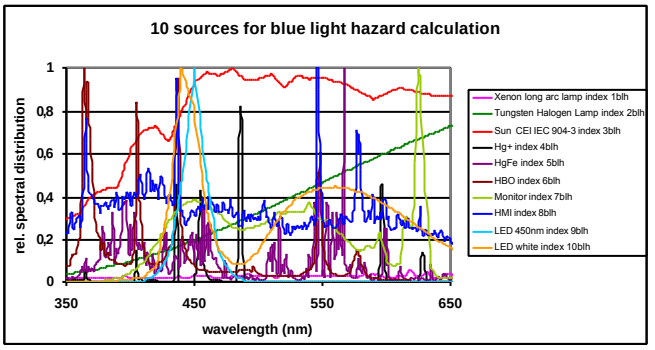

Graph 2 Relative spectral distribution of ten blue light hazard sources

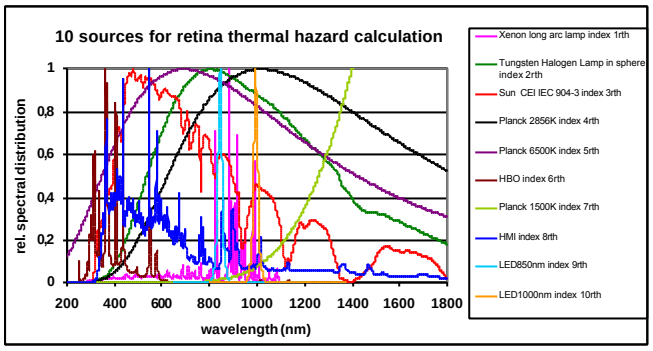

Graph 3 Relative spectral distribution of ten retina thermal hazard sources

3. Action spectra with realized detector

3.1 ICNIRP action spectra 180-400nm

To match these action spectra it is easier if the function is split into two separate ones where two different detectors can be used. Otherwise a double monochromator based spectral radiometer must be used to evaluate the entire function wavelength by wavelength.

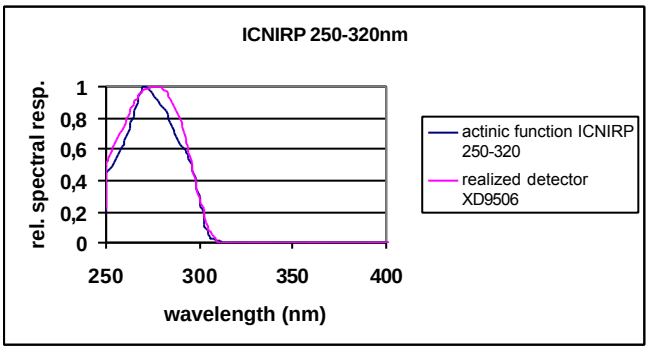

Graph 4 ICNIRP action spectra 250-320nm

Xenon long arc lamp index 1uv	a(Z)=	1,01
HMI lamp index 2uv	a(Z)=	1,00
Tanning lamp UVA index 3uv	a(Z)=	0,94
Dermatological used lamp UVB index 4uv	a(Z)=	0,88
Hg lamp low pressure index 5uv	a(Z)=	1,08
Hg lamp medium pressure index 6uv	a(Z)=	1,01
Sun 5th July 97 Thessaloniki 18°SZA (or use AM1.5) index 7uv	a(Z)=	1,10
Deuterium lamp 30W index 8uv	a(Z)=	1,00
Tungsten halogen lamp index 9uv	a(Z)=	1,01
Iron high pressure lamp index 10uv	a(Z)=	1,02

Table 2 Uncertainty of values for ICNIRP detector for wavelength range 250 to 320nm.

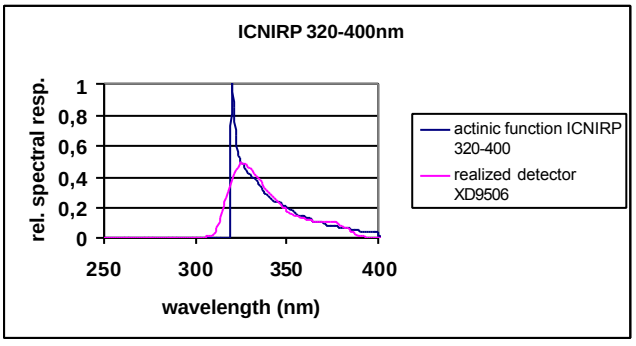

Graph 5 ICNIRP action spectra 320-400nm normalized at 320nm with a factor of 1000

Xenon long arc lamp index 1uv	a(Z)=	0,98
HMI lamp index 2uv	a(Z)=	1,00
Tanning lamp UVA index 3uv	a(Z)=	1,00
Dermatological used lamp UVB index 4uv	a(Z)=	1,85
Hg lamp low pressure index 5uv	a(Z)=	1,58
Hg lamp medium pressure index 6uv	a(Z)=	1,31
Sun 5th July 97 Thessaloniki 18°SZA (or use AM1.5) index 7uv	a(Z)=	0,98
Deuterium lamp 30W index 8uv	a(Z)=	1,04
Tungsten halogen lamp index 9uv	a(Z)=	0,95
Iron high pressure lamp index 10uv	a(Z)=	0,99

Table 3 Uncertainty of values for ICNIRP detector for wavelength range 320 to 400nm.

In table 3 we can see e.g. for Dermatological used lamp UVB index 4uv the poor a(Z) with 1.85 did not effect in case of very less weighted irradiation in this wavelength range from 320 to 400nm occur.

Any classification for UV meters should depend on the uncertainty of its spectral response, since it influences the measurement the most. To classify a meter the $f_1(Z)$ criteria can be applied again using the spectral distribution data of the light sources shown in graph 1-3.

The remaining deviation $f_1(Z)$ is given according to formula 2

$$f_1(Z) \quad a(Z) \quad 1 \quad \frac{s_Z}{s_c} \quad 1$$

Formula 2 Deviation including spectral mismatch factor

where
s_Z radiometric responsivity of the radiometer head using source Z
s_C radiometric responsivity of the radiometer head using the calibration source c
a(Z) relative responsivity correction factor according to formula 1

The groups are classified as:
$f_1(Z)$max 20% as best class (green); a(Z) between 0.8 and 1.25
$f_1(Z)$max 40% as normal class (orange); a(Z) between 0.6 and 1.66
$f_1(Z)$max 70% as worst class (red); a(Z) between 0.3 and 3.33

Radiometers with an $f_1(Z)$max 70% are not useable in general (black).
a(Z) below 0.3 an above 3.33.
But for a specific light source a generally unusable UV-radiometer could be changed into the best class within 20%.

Notice that the a(Z) value for any given lamp is typically within less than 20% of the real value.
Only those sources rich in irradiance below approximately 260nm are about 25% outside of the real value with the deuterium lamp 40% out.

A newly developed double broadband detector head device for the ICNIRP function is shown below.

Picture 1 Double Broadband Detector with Display Unit

3.2 Radiometric spectra 315-400nm (UVA)

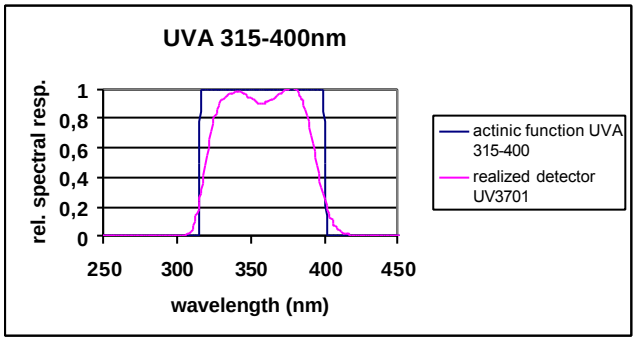

Graph 6 UVA action spectra 315-400nm

The out-of-band signal blocking capability of the measurement equipment has to be as good as possible below 315nm and above 400nm.

Xenon long arc lamp index 1uv	a(Z)=	0,93
HMIlamp index 2uv	a(Z)=	1,00
Tanning Lamp UVA index 3uv	a(Z)=	1,01
Dermatological used lamp UVB index 4uv	a(Z)=	1,27
Hglamp low pressure index 5uv	a(Z)=	1,15
Hglamp medium pressure index 6uv	a(Z)=	1,08
Sun 5th July 97 Thessaloniki 18°SZA (or use AM1.5) index 7u	a(Z)=	0,95
Deuterium lamp 30W index 8uv	a(Z)=	0,92
Tungsten Halogen Lamp index 9uv	a(Z)=	0,94
Iron High pressure lamp index 10uv	a(Z)=	0,98

Table 4 Uncertainty of values for UVA detector for wavelength range 315 to 400nm.

The groups for uva-detectors and all following detectors are classified as:

$f_1(Z)max$ 5% as best class (green); a(Z) between 0.95 and 1.05
$f_1(Z)max$ 10% as normal class (orange); a(Z) between 0.9 and 1.11
$f_1(Z)max$ 20% as worst class (red); a(Z) between 0.8 and 1.25

3.3 Blue Light hazard spectra 380-600nm

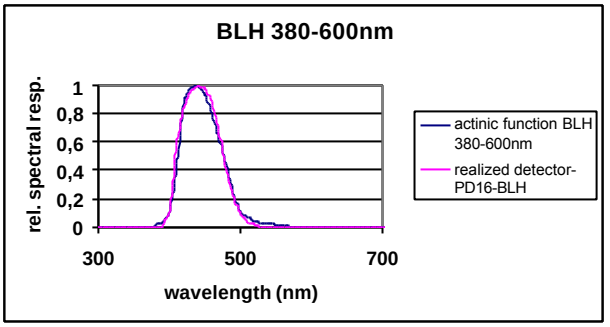

Graph 7 Blue Light Hazard action spectra 380-600nm

Xenon long arc lamp index 1blh	a(Z)=	1,01
Tungsten Halogen Lamp index 2blh	a(Z)=	0,99
Sun CEI IEC 904-3 index 3blh	a(Z)=	1,01
Hg+ index 4blh	a(Z)=	1,01
HgFe index 5blh	a(Z)=	1,03
HBO index 6blh	a(Z)=	1,03
Monitor index 7blh	a(Z)=	1,00
HMI index 8blh	a(Z)=	1,01
LED 450nm index 9blh	a(Z)=	1,03
LED white index 10blh	a(Z)=	1,00

Table 5 Uncertainty of values for BLH detector for wavelength range 380 to 600nm.

3.4 Retina Thermal hazard spectra 380-1400nm

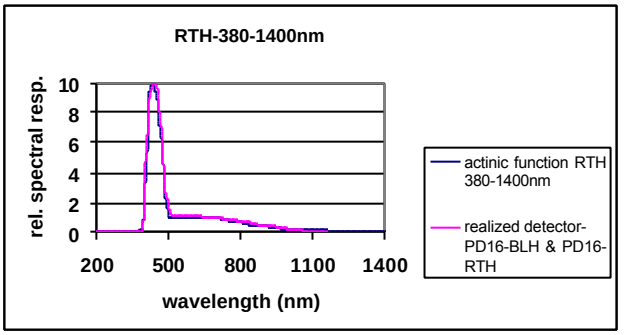

Graph 8 Retina Thermal Hazard action spectra 380-1400nm realized with two detector heads

Xenon long arc lamp index 1rth	a(Z)=	1,05
Tungsten Halogen Lamp in sphere index 2rth	a(Z)=	1,01
Sun CEI IEC 904-3 index 3rth	a(Z)=	1,03
Planck 2856K index 4rth	a(Z)=	0,98
Planck 6500K index 5rth	a(Z)=	1,02
HBO index 6rth	a(Z)=	1,02
Planck 1500K index 7rth	a(Z)=	0,52
HMI index 8rth	a(Z)=	1,02
LED850nm index 9rth	a(Z)=	1,13
LED1000nm index 10rth	a(Z)=	1,06

Table 6 Uncertainty of values for RTH detectors for wavelength range 380 to 1400nm.

As we can see from the value above for the low temperature Planck irradiation, the given value will be to low. With this knowledge however we can do an accurate measurement also from this source.

3.5 Radiometric spectra 780-3000nm

This detector is realized from 780-1700nm with two detector heads.

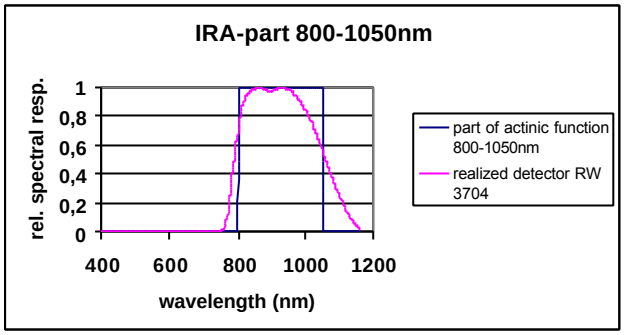

Graph 9 part of action spectra 780-3000nm

Xenon long arc lamp index 1rth	a(Z)=	0,92
Tungsten Halogen Lamp in sphere index 2rth	a(Z)=	1,00
Sun CEI IEC 904-3 index 3rth	a(Z)=	0,99
Planck 2856K index 4rth	a(Z)=	1,00
Planck 6500K index 5rth	a(Z)=	1,00
HBO index 6rth	a(Z)=	0,99
Planck 1500K index 7rth	a(Z)=	1,16
HMI index 8rth	a(Z)=	0,96
LED850nm index 9rth	a(Z)=	0,93
LED950nm index 10rth	a(Z)=	0,92

Table 7 Uncertainty of values for part of IRA detector for wavelength range 800 to 1050nm.

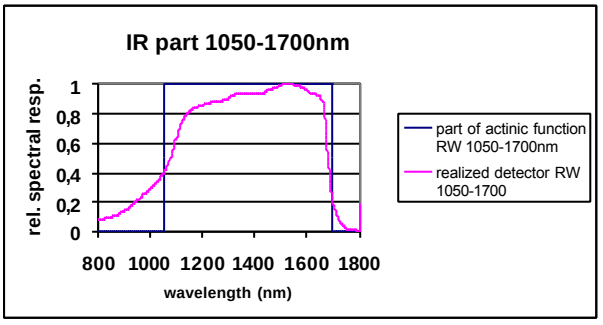

Graph 10 part of IR action spectra 780-3000nm

Tungsten Halogen Lamp in sphere index 2rth	a(Z)=	1,00
Sun CEI IEC 904-3 index 3rth	a(Z)=	1,04
Planck 2856K index 4rth	a(Z)=	0,97
Planck 6500K index 5rth	a(Z)=	0,99
HBO index 6rth	a(Z)=	1,11
Planck 1500K index 7rth	a(Z)=	0,94
HMI index 8rth	a(Z)=	1,06
LED1300nm index 9rth	a(Z)=	0,94
LED1550nm index 10rth	a(Z)=	1,02

Table 8 Uncertainty of values for part of IR detector for wavelength range 1050 to 1700nm.

3.6 Radiometric spectra 380-1000000nm

This detector is realized from 380-1700nm with three detector heads as a radiometric (flat response) unit.

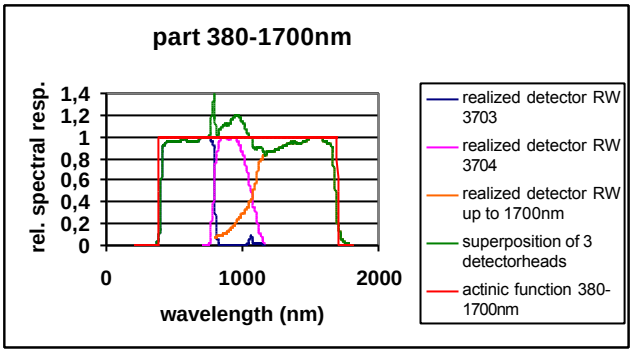

Graph 11 part of action spectra 380-1000000nm

As not having spectral irradiance values for sources up to 1mm, we calculated a Planck radiator with 2856K up to 1mm.

nm	Planck2856K
380-1700	2,31E+08
380-10000000	3,77E+08
ratio (380-1700)/(380-10000000)	0,61

Table 9 Uncertainty of values for part of IR detector for wavelength range 380 to 1000000nm.

The given value from the integral detector heads measured from 380nm up to 1700nm will be for a real Plank radiator 39% to less. The normal sources however did not irradiate up to 1mm and therefore the given value from the meter will be better.

4. Conclusion:

With state of the art broadband detectors and the relative source spectra data it is possible to measure nearly all sources within 20% total additional uncertainty.
However, knowing the broadband detectors spectral mismatch factor is a must.

References:

BG-Information; BGI 5006, Expositionsgrenzwerte für künstliche optisch Strahlung. Oktober 2004

ICNIRP Guidelines; Guidelines on limits of exposure to broadband incoherent optical radiation (0,38 to 3µm); International Commission on Non-Ionizing Radiation Protection. Health Physics Vol. 73, No. 3, p. 539-554, September 1997

European Thematic Network for Ultraviolet Measurements – UVNEWS issue 6 Nov. 2000; "Characterizing the Performance of Integral Measuring UV-Meters". Helsinki University of Technology, Metrology Institute, P.O. Box 3000, FIN-02015 HUT, Finland

European Thematic Network for Ultraviolet Measurements – UUNEWS issue 7 Nov. 2002; "Manufacturer´s view on UV meters with different action spectra ". Helsinki University of Technology, Metrology Institute, P.O. Box 3000, FIN-02015 HUT, Finland

Application & Product guide 2004/2005, Gigahertz-Optik GmbH

On potential discrepancies between goniometric and sphere-based spectral diffuse reflectance

F. Manoocheri[1], S. Holopainen[1], S. Nevas[1] and E. Ikonen[1,2]

[1] Metrology Research Institute, Helsinki University of Technology (TKK), P.O. Box 3000, FI-02015 TKK, Finland

[2] Centre for Metrology and Accreditation (MIKES), P. O. Box 239, FI-00181 Helsinki, Finland

Abstract. The potential discrepancies between the gonioreflectometer based and integrating-sphere based methods in the measurement of spectral diffuse reflectance are studied. Errors due to scattered light around the measurement beam in gonioreflectometers are a potential cause of such discrepancies. Procedures used to determine such errors and the required corrections are presented. At TKK, the corrections varied from -1,1% to -0,2% for the studied two cases. The measurement results for our diffuse reflectance reference materials with the appropriate corrections in both cases are in excellent agreement.

Introduction

Measurements of spectral diffuse reflectance are usually performed relative to a reference standard that is traceable to an absolute scale. The absolute scales of spectral diffuse reflectance are mainly based on integrating-sphere techniques [1, 2, 3]. An alternative approach to these techniques is angular integration of the gonioreflectometric measurement results [4, 5, 6]. The gonioreflectometer-based methods are becoming more popular among National Metrology Institutes for the measurements and realization of absolute scale of spectral diffuse reflectance [7, 8, 9]. However, some discrepancies between the gonioreflectometric and the integrating-sphere based methods have been reported thus raising questions about the origin of the deviations [8].

As a result of recent modifications in the light source system of our gonioreflectometer, the spatial properties of the measurement beam were improved. The most important outcome was a significant reduction in the applied correction necessary to account for the effects of light scattered about main beam. This source of error is shown to be under control in our gonioreflectometer, as proved by the good reproducibility of the test measurement results. If such effects are not properly accounted for, significant deviations may occur. The trends of such deviations are similar to those reported earlier when comparing gonioreflectometer- and integrating sphere-based measurement results of hemispherical reflectance factors [8].

Measurement setup

In the gonioreflectometer at TKK, the sample is illuminated at fixed angles and the reflected light can be measured over the polar angles in the horizontal plane. The total diffuse reflectance is determined by integrating the measured angular distribution of the reflected flux over the hemisphere.

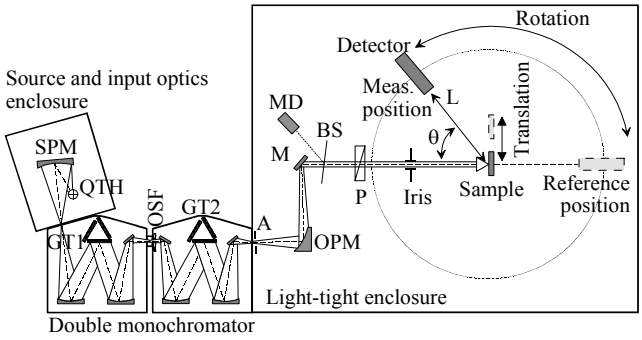

Figure 1. Schematic of the gonioreflectometer setup**:** QTH, quartz–tungsten–halogen lamp; SPM, spherical mirror; GT1, GT2, grating turrets; OSF, order-sorting filter; M, flat mirror; A, aperture; OPM, off-axis parabolic mirror; BS, beam splitter; P, prism polarizer; MD, monitor detector; L, distance between sample and detector.

The present measurement setup is shown schematically in Figure 1. The setup consists of a source system and a goniometric detection system in a light-tight enclosure. Main components of the source system are a quartz-tungsten-halogen lamp and a double monochromator. The beam is collimated and directed towards the sample by an off-axis parabolic mirror and a flat mirror. A beam splitter channels a fraction of the beam to a monitor detector for minimizing the effects of light-source instability. The rest of the beam propagates through a polarizer and an iris before irradiating the sample. The reflected light is probed by the detector over a range of polar angles selected by the detector turntable. The full intensity of the incident light is measured at the reference position of the turntable (Figure 1). During this measurement the sample is moved out of the beam path by using a linear translator. The sample is positioned on another turntable, coaxial with that rotating the detector, which allows adjusting the angle of incidence of the beam [9].

The present double monochromator makes use of toroidal mirrors. This reduces the astigmatism of the output beam to a large extent. Thus the astigmatism correction became unnecessary and some of the optical components in the light-source system became redundant. In the previous setup, a tilted spherical mirror was used for the astigmatism compensation and an extra flat mirror was also needed to guide the beam. Therefore the alignment of the source system is now less complicated than it was in the previous setup. The other important improvement is a significant reduction in the light scattered about the main beam previously referred to as isochromatic stray light [9]. Lower stray light now requires a smaller correction and introduces a lower uncertainty component.

Results

The corrections required for the scattered light were determined by measuring the beam intensity and comparing the signal readings when the detector with interchanging apertures was at the reference position and when it was near the sample plane. The simplest way to test for the existence of such scattered light is to compare the readings obtained when we use the same aperture as in the actual reflectance measurements with those obtained without aperture for the detector at the reference position.

The corrections required for the old and for the new setups are presented in Figure 2. The magnitude of the correction for the new setup has not only decreased but also has become wavelength independent.

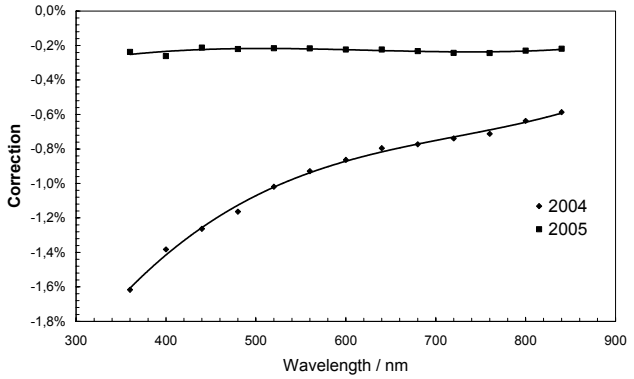

Figure 2. Correction for the scattered light in the old (2004) and the new (2005) setups.

To validate the performance of the instrument after the changes in the source system, test measurements were performed. Figure 3 presents 0/d reflectance of a Spectralon sample measured with the old and the new setups. Agreement between the measurements with the old and new setups is well within 0.1% and well below the uncertainty of the scale realization.

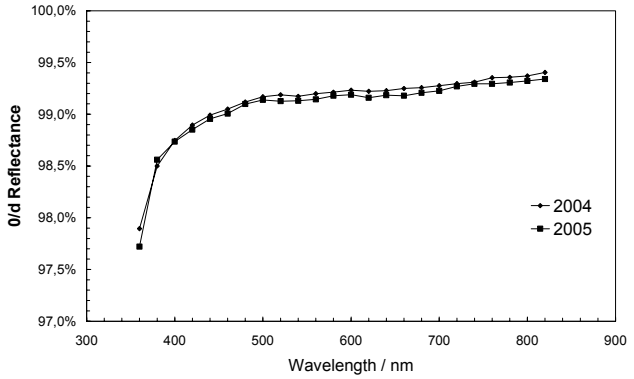

Figure 3. Spectral diffuse reflectance of a white spectralon sample measured with the old (2004) and new (2005) setups.

Conclusions

Recently some modifications were made to the gonioreflectometer at TKK leading to improvements in the spatial properties of the measurement beam. The amount of scattered light decreased significantly resulting in a drop of the correction required from about -1,1 % to -0,2 %. Since the agreement between measurements performed before and after the modifications is very good, we believe that scattering of light about the main beam has been properly accounted for. Furthermore, this effect might be one of the reasons for the discrepancies reported previously between measurements based on gonioreflectometric and integrating-sphere techniques [8]. Considering the magnitude of the correction required before the modifications, it is obvious that definite errors will occur if scattered light is not taken into account when designing and characterizing a gonioreflectometer. We will present more of our validating measurements during the NEWRAD conference and more detailed test procedures in a full paper.

Acknowledgments Silja Holopainen appreciates the support of TES and KAUTE foundations.

References

1. W Budde, and C. X. Dodd, "Absolute reflectance measurements in the d/0° geometry," Die Farbe **19**, 94-102 (1970).
2. W. Erb, "Requirements for reflection standards and the measurements of their reflection values," Applied Optics **14**, 493-499 (1975).
3. W. H. Venable, J. J. Hsia, and V. R. Weidner, "Establishing a scale of directional-hemispherical reflectance factor: The Van den Akker method," Journal of Research of the National Bureau of Standards **82**, 29-55 (1977).
4. Comission Internationale de l'Eclairage, *Absolute Methods for Reflection Measurements*, Publ. CIE 44 (CIE, Vienna, 1979).
5. L. Morren, "Mesure absolue des facteurs de luminance et de réflexion," Lux **45**, 448-453 (1967).
6. W. Erb, "Computer-controlled gonioreflectometer for the measurement of spectral reflection characteristics," Applied Optics **19**, 3789-3794 (1980).
7. J. E. Proctor and P. Y. Barnes, "NIST high accuracy reference reflectometer-spectrometer," Journal of Research of the National Institute of Standards and Technology **101**, 619-627 (1996).
8. C. J. Chunnilall, A. J. Deadman, L. Crane and E. Usadi, "NPL scales for radiance factor and total diffuse reflectance," Metrologia **40**, S192-S195 (2003).
9. S. Nevas, F. Manoocheri and E. Ikonen, "Gonioreflectometer for measuring spectral diffuse reflectance," Appl. Opt. **43**, 6391-6399 (2004).

Correcting for bandwidth effects in monochromator measurements

Emma R. Woolliams, Maurice G. Cox, Peter M. Harris, Heather M. Pegrum
National Physical Laboratory, Hampton Road, Teddington, TW11 0LW, UK

Abstract. In radiometric calibrations of detectors and sources it is common to use a monochromator-based system to compare the spectral response of an unknown detector with that of a known detector or the spectral irradiance of an unknown source with that of a known source. It is often assumed that this calibration can be considered to correspond to the central wavelength of the monochromator bandwidth. This paper considers when such an assumption is valid and how a correction can be made to convert integrated measurements into point values. It includes experimental verification of the methods described.

Introduction

The bandpass of monochromators can cause significant errors when calibrating sources or detectors that change rapidly with wavelength, particularly when the calibration is performed relative to a source or detector that has a very different spectral response [1]. Methods for correcting this for the case of a perfectly triangular slit [2,3] and for an arbitrary bandpass function [4] have been previously described.

This paper describes a method for correcting the measured data to obtain an estimate of the result that would have been obtained for an infinitely narrow bandpass. The method makes no assumptions about the shape of the bandpass function, nor does it require the measured data to be modelled. The method applies for arbitrary measurement spacings that may be greater or less than the bandwidth of the monochromator. It does however assume that the function representing the measured values is continuously differentiable with respect to wavelength to a degree appropriate to the spectral shape of interest.

The technique can be applied to any spectrally varying quantity measured using a monochromator. However, this paper considers the special case of the calibration of a deuterium lamp with respect to a blackbody source in the UV spectral region. Since the spectral irradiance of the deuterium lamp rapidly decreases with wavelength, while the blackbody's spectral irradiance rapidly increases, this represents a "worst case scenario" and as such experimental results could be obtained showing noticeable differences between a wide and narrow bandwidth. Such differences have been corrected using the method described here.

Measurement equation

The signal of a PMT detector on the exit port of a double monochromator was recorded first when a blackbody of known temperature illuminated a diffuser on the input port of the monochromator and then again when a deuterium lamp illuminated the same diffuser.

The signal obtained when using the blackbody is given by

$$\tilde{V}_{\mathrm{BB}}(\lambda_0) = \pi g \int_{\lambda_{-1}}^{\lambda_{+1}} L_{\mathrm{BB}}(\lambda, T) R(\lambda) S(\lambda)\, d\lambda \qquad (1)$$

where $\tilde{V}_{\mathrm{BB}}(\lambda_0)$ is the measured signal, g a geometric constant, $L_{\mathrm{BB}}(\lambda, T)$ the radiance of the blackbody, $R(\lambda)$ the detector responsivity and $S(\lambda)$ the bandpass function of the monochromator. Similarly, the signal obtained when measuring the lamp is given by

$$\tilde{V}_{\mathrm{lamp}}(\lambda_0) = A \int_{\lambda_{-1}}^{\lambda_{+1}} E_{\mathrm{lamp}}(\lambda) R(\lambda) S(\lambda)\, d\lambda \qquad (2)$$

where A is a geometric constant and $E_{\mathrm{lamp}}(\lambda)$ is the irradiance of the lamp.

If the bandpass function of the monochromator were infinitely narrow, the 'perfect' measured signals would be

$$V_{\mathrm{BB}}(\lambda_0) = \pi g L_{\mathrm{BB}}(\lambda_0, T) R(\lambda_0) \qquad (3)$$

and

$$V_{\mathrm{lamp}}(\lambda_0) = A E_{\mathrm{lamp}}(\lambda_0) R(\lambda_0). \qquad (4)$$

Without the integrations, the irradiance of the lamp can easily be determined by dividing the signal obtained using the lamp by that using the blackbody. It is important to understand whether the ratio for real signals is a close approximation to that for 'perfect' signals, i.e. whether, $\tilde{V}_{\mathrm{lamp}} / \tilde{V}_{\mathrm{BB}} \approx V_{\mathrm{lamp}} / V_{\mathrm{BB}}$, and the extent to which it is possible to estimate the 'perfect' signals given the real signals.

Triangular bandpass function

A solution has previously been proposed for a triangular bandpass function [3]. Given a triangular bandpass function of full width $2\Delta\lambda$ and unit area, as shown in Figure 1, and given the measured signal $\tilde{V}$, the 'perfect' signal V that would be obtained without the bandpass is given by the formula

$$V(\lambda_0) = \tilde{V}(\lambda_0) - \frac{1}{12}(\Delta\lambda)^2 \tilde{V}''(\lambda_0) + \frac{1}{240}(\Delta\lambda)^4 \tilde{V}^{\mathrm{iv}}(\lambda_0) + \cdots. \qquad (5)$$

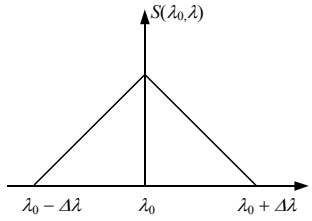

Figure 1 Defined triangular bandpass function.

This correction can be performed for any data set given enough measurements to estimate the derivatives. The measured data can be at any arbitrary step size. In practice,

the second term, containing the second derivative, can be determined as the correction and the third term, containing the fourth derivative, measures the effect of truncating the correction at the second term. If this effect is too large, the second and third terms can be used as the correction and the next term, containing the sixth derivative, used to measure the effect of truncation.

Experimental data

Measurements were made in 2.5 nm steps of a deuterium lamp and a blackbody with a monochromator set with two different slit widths. In both cases the bandpass could be realistically modelled as a triangle. With wide slits the half-width $\Delta\lambda$ was 4.05 nm and with narrow slits it was 1.49 nm. The wider bandpass is shown in Figure 2.

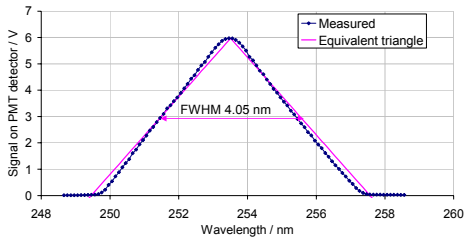

Figure 2 Monochromator bandpass with wide slits

The ratio $\tilde{V}_{\text{lamp}}/\tilde{V}_{\text{BB}}$ was compared for the wide slit and narrow slit case and there was a noticeable difference of the order of the measurement uncertainty between them (broken curve in Figure 3). Large corrections (around 15 % at the shortest wavelengths for the wide slits) were predicted by the second derivative term in Equation (5). However once these corrections were applied, the ratio $\tilde{V}_{\text{lamp}}/\tilde{V}_{\text{BB}}$ with wide slits agreed with that for the narrow slits (solid curve in Figure 3).

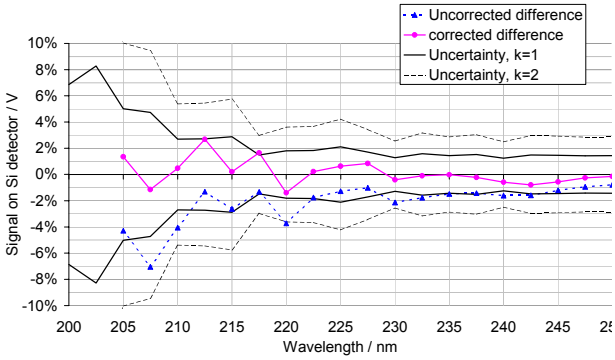

Figure 3 The effect of applying the correction on the difference between the ratio lamp to blackbody with 4.05 nm and 1.49 nm monochromator bandwidths

Generic bandpass

An approach has been developed to extend Formula (5) for an arbitrary bandpass function. The bandpass function is represented by a piecewise linear function, that is by sufficient straight-line segments to describe it. The approach provides an expression similar to Formula (5), but containing all derivatives (odd and even). The fractions in front of each term are replaced by algebraic expressions involving the terms defining the segments. For a symmetrical bandpass function, the multipliers of all odd derivates are zero.

This technique will be theoretically and experimentally investigated prior to the NEWRAD conference and will be presented along with the more straightforward case of a triangular slit function.

Acknowledgements This work was supported by the National Measurement System Policy Unit of the UK Department of Trade and Industry

References

[1] L.-P. Boivin, 'Study of bandwidth effects in monochromator-based spectral responsivity measurements'. *Applied Optics*, 2002. **41**(**10**), pp. 1929-1935.

[2] E. I. Stearns and R. E. Stearns, 'An example of a method for correcting radiance data for bandpass error'. *Color Res. Appl.*, 1988. **13**(**4**), pp. 257-259.

[3] M. G. Cox, P. M. Harris, P. D. Kenward and E. R. Woolliams. 'Spectral Characteristic Modelling'. 2003. *NPL Report CMSC 27/03*

[4] Y. Ohno. 'A flexible bandpass correction method for spectrometers'. in *10th Congress of the International Colour Association*. 2005. Grenada, Spain. pp.

Establishment of Fiber Optic Measurement Standards at KRISS

Seung Kwan Kim, Dong Hoon Lee, Duck Hee Lee, Han Seb Moon, and Seung Nam Park
Div. of Optical Metrology, KRISS, Daejeon 305-340, Republic of Korea

Jung-Chul Seo
Dept. of Nano-Optics, Korea Polytechnic University, Siheung-Si, Gyeonggi-Do 429-793, Republic of Korea

Abstract. We present our research activities on fiber optics metrology to establish fiber optic measurement standards at KRISS. Beginning from the fiber optic power responsivity for calibration of fiber optic power meters, we have developed optical fiber length, attenuation, and return loss standard as calibration references for optical time domain reflectometers. Chromatic and polarization mode dispersion measurements are discussed and finally optical fiber nonlinearity measurements are presented with newly obtained results.

I. Introduction

Research activities in photometry and radiometry are expanding toward new applications to meet the demanding requirement of the fast growing industries in fiber optics and optoelectronics. Many equipments, systems, modules, and components used in fiber optic communications and sensors are absolutely in need of calibration and test, but the realization of the measurement standards and their transfer into industry are relatively lower compared to other optics industries, such as lighting and display.

We began to establish fiber optics measurement standards at KRISS recently, mainly focused on the calibration of fiber optic power meter (FOPM) and optical time domain reflectometer (OTDR).

In this paper, we introduce our current research activities in fiber optics metrology to draw attention for the international collaborations to make better standards.

II. Fiber Optic Power Responsivity

Fiber optic power responsivity measurement at KRISS is based on the inter-comparison between the FOPM and the electrically calibrated pyroelectric radiometer (ECPR), that is traceable to the cryogenic radiometer. Our ECPR is calibrated at 633 nm using a highly stabilized He-Ne laser beam by directly comparing it to the silicon trap detector calibrated by the KRISS cryogenic radiometer. We evaluated the uncertainty of ECPR near infrared region to be 0.6 % (k=2) including the responsivity uncertainty at 633 nm and the wavelength dependence of ECPR. When we calibrate a commercial FOPM by comparing it to the ECPR, we use distributed feedback laser diodes whose wavelengths are 1310 nm and 1550 nm, respectively, collimating them in between the two fiber optic collimators so as to push in and pull out the beam chopper of the ECPR using linear translation stage. All the fiber optic connectors except for the final end to the FOPM input are FC/APCs to eliminate the unwanted Fresnel reflection. The final end is FC/PC to minimize polarization dependence. To further increase the output power stability we use fiber optic isolators in between the components having possible backscattering. The resultant output power stability is 1.0×10^{-5}. We include the uncertainty due to input polarization dependence by finding maximum and minimum value while randomizing the state of polarization using a motorized polarization controller. The overall uncertainty of the FOPM used as our working standard including connector dependence are about 0.8 % (k=2) for both wavelengths (Table 1) at the power level of 0.1 mW.

Table 1. Relative uncertainty of KRISS working standard for FOPM calibration.

Uncertainty Source	u (%)	Type
ECPR	0.3	B
Source Stability	0.001	A
Repeatability	0.058	A
Polarization Dependence	0.2	B
Fiber Optic Connector	0.08	B
Combined uncertainty (%)	0.4	
Expanded uncertainty (%), k=2	0.8	

III. Fiber Length, Attenuation, and Return Loss

Optical fiber length, attenuation, and return loss are major parameters to be measured with OTDR. In order to calibrate optical length of OTDR, we constructed a time-of-flight measurement setup (Figure 1). We use a fiber pigtailed tunable laser diode covering both 1310 nm and 1550 nm region and make it operate in pulsed mode by current modulation. The laser is divided into two ports: one is directly led into a high speed photo-detector (PD) and the other is coupled to a fiber under test (FUT) and then led to another high speed PD. If we find the modulation frequency for the two pulses to arrive at the two PDs at the same time, we can determine the delay time of the FUT by directly counting the frequency. The frequency counter is traceable to KRISS cesium atomic clock. We certificate a fiber length reference with an uncertainty of less than 0.3 m (k=2) out of 13 km delay for the temperature of 23±2 °C. Using this reference, we observed the optical length measured with a commercial OTDR has an offset of more than 2 m.

Optical fiber attenuation is measured directly using cut-back method [1]. Spectral attenuation can be correctly measured with the FOPM having nonlinearity less than 0.01 %. The nonlinearity of the FOPM is calibrated using the flux addition method. The uncertainty of 0.03 dB (k=2) has been evaluated including the repeatability of the bare fiber adaptor as well as the polarization dependence. This method can be used as a reference to calibrate not only

OTDR but also a commercial spectral attenuation measuring equipment and a simple loss meter.

Return loss of the optical fiber is measured with a fiber optic coupler having a splitting ratio of 50:50 [2]. We used the same FOPM as in the attenuation measurement. Owing to the polarization dependence of the splitting ratio and the fiber connection repeatability, the uncertainty is as much as 0.6 dB for up to 30 dB return loss. The higher return loss results in the larger uncertainty because of the bad repeatability. The uncertainty goes up to 1.2 dB for 60 dB return loss.

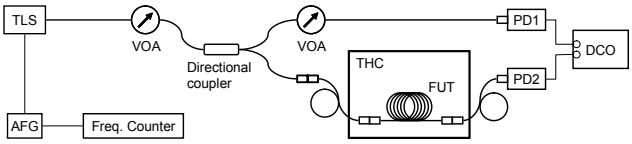

Figure 1. Schematic of time-of-flight measurement setup for optical fiber length standard. AFG, arbitrary function generator; DCO, dual channel oscilloscope; FUT, fiber under test; PD, photo-detector; THC, temperature humidity chamber; TLS, tunable laser source; VOA, variable optical attenuator.

IV. Dispersion Measurements

Chromatic dispersion (CD) and polarization mode dispersion (PMD) are essential in optical fiber specification especially for high speed and wavelength-division-multiplexing optical link.

We apply Stokes parameter evaluation technique with Jones matrix eigen-analysis as a reference method to measure PMD. Proper choice of wavelength spacing enables a repeatable measurement of PMD with an uncertainty of 3.0×10^{-4} for 1.54 ps non-polarization-mode coupled PMD. The residual PMD of our measurement setup itself was measured to be about 1 fs. In order to evaluate overall uncertainty, the uncertainty of the used fiber optic polarimeter has to be determined. With a linear polarizer having high extinction ratio (> 50 dB) and an accurate quarter-wave plate, we are going to calibrate our fiber optic polarimeter.

Regarding the CD measurement, we apply the modulation phase shift method to accurately determine zero dispersion wavelength, dispersion slope, and dispersion value as a function of wavelength. We are constructing the measurement setup at the moment and will soon be evaluating the uncertainty.

V. Fiber Nonlinearity

Nonlinear refractive index (NRI), stimulated Brillouin scattering (SBS) threshold, Brillouin and Raman gain coefficient are major parameters to be measured to characterize nonlinear effects in optical fiber.

We apply a continuous-wave dual frequency method based on self phase modulation to measure nonlinear coefficient, that is NRI divided by effective area. The major uncertainty reasons are the level accuracy of optical spectrum analyzer, CD induced error dependent on the separation of the two wavelengths, the uncertainty of FOPM to measure incident optical power, and that of OTDR to measure effective length of optical fiber under test. These uncertainty sources result in overall uncertainty of about 5 %.

Recently we modified the measurement setup to investigate the source coherence effect that possibly affect the accuracy of the nonlinear coefficient measurement [3]. As a result, we determined that the incoherence between the two optical frequencies measure 3 % less value than the coherent dual frequencies (Figure 2).

Regarding the SBS threshold measurement, we constructed an Er-doped fiber ring laser having a stable single longitudinal mode and a narrow linewidth of less than 4.3 kHz that is tunable in 1530~1570 nm region. Except for the polarization dependence of the fiber optic coupler, we can measure SBS threshold with high accuracy using this source excluding the linewidth problem of the light source.

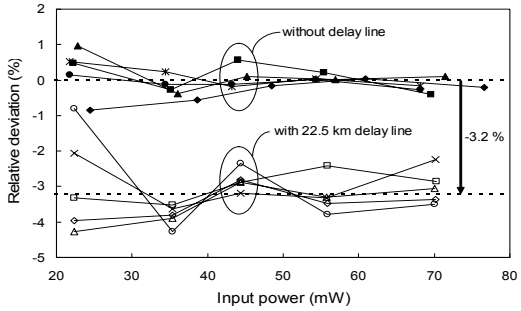

Figure 2. Relative difference of optical fiber nonlinear coefficient measured with incoherent (blank data) dual optical frequencies from that of coherent (filled data) dual optical frequencies.

VI. Conclusions

We have introduced our research activities on fiber optic metrology at KRISS. Establishment of traceability to primary standards and uncertainty evaluations enable us to provide reliable measurement and calibration services of fiber optic power meter and optical time domain reflectometer for fiber optics and optoelectronics industry. With these standards, we developed reference materials for fiber length, attenuation, and return loss as the transfer standards. We are expanding our calibration and measurement capability to chromatic and polarization mode dispersion, fiber nonlinearity, polarization dependent loss, and so forth.

References

[1] IEC 60793-1-40, Measurement methods and test procedures – Attenuation.

[2] Kapron, F. P., Thomas, E. A., and Peters, J. W., OTDR measurements of optical return loss, *NIST Special Publication, 748*, 35-38, 1988.

[3] Kim, S. K., Moon, H. S., Seo, J. C., Coherence effect of the measurement of optical fiber nonlinear coefficient, *Opt. Lett., 30*, 1120-1122, 2005.

Detector-based NIST-traceable Validation and Calibration of Infrared Collimators

H. W. Yoon, G. P. Eppeldauer, J. P. Rice
NIST, Gaithersburg, MD, USA

J. Brady
Air Force Metrology and Calibration Laboratory (AFMETCAL), Heath, OH, USA

Abstract. We describe the detector-based validation of an infrared collimator at AFMETCAL using two non-imaging InSb radiometers centered at 3.4 μm and at 4.6 μm with 400 nm to 260 nm band-pass filters, respectively. The radiometers are calibrated in irradiance mode using detector-based radiometry at the NIST IR Spectral Irradiance and Radiance Responsivity Calibrations using Uniform Sources (IR-SIRCUS) facility. The calibrated radiometers were then used to determine the irradiance at the output of the infrared collimator in an overfilled geometry, and the measured irradiances are compared to the calculated irradiances of the collimator. The differences of the calculated and the measured spectral irradiances were within the combined uncertainties of ~ 6 % (k = 2) over a range of temperatures from 450 °C to 1000 °C and various aperture sizes. The implementation of the NIST-traceable calibrations of the collimators results in total uncertainties of < 3 % (k = 2) in the infrared spectral irradiances.

Introduction

Collimators are used when sensors which radiometrically detect objects at a distance are calibrated for their irradiance responsivity. Since the optical design of the sensor is for use with collimated or low-divergence radiation, collimators are built to simulate the conditions under-use in the laboratory without requiring long object distances. Infrared collimators are critical components in the calibration procedures for many types of infrared sensors Typically, these collimators are constructed using a variable-temperature blackbody with a precision aperture and a collimating mirror.

Until now, the spectral irradiance from these infrared collimators has been determined only by using the knowledge of the individual component parameters such as the blackbody temperature and emissivity, the area of the aperture, the focal length and the spectral reflectance of the collimating mirror. The spatial uniformity of the mirror or mirrors and the atmospheric transmittance can also change the irradiance. Since the irradiance at the output of the collimator is calculated from the individual components, the total uncertainty of the irradiance depends upon measurements of the individual components and any increase in the uncertainties in the individual components could lead to increases in the final, total calculated irradiances.

An alternate approach to determining the irradiances from the collimators would be to use radiometers which do not rely upon the component characterizations. Since the radiometers are calibrated for spectral irradiance responsivity, the validation of the spectral irradiance could be performed by placing the radiometers in the collimated beam. The spectral irradiance scale for various collimators at physically different locations can be compared. We describe the development, the calibration and the use of such radiometers.

Radiometer Design and Calibrations

The InSb radiometers were constructed using a custom NIST design. The InSb detectors were constructed with precision 6.4 mm diameter apertures in front of 7 mm diameter InSb diodes. The cryogenic dewars are built with 17 ° field-of-view limiter to reduce the contribution from the room-temperature background radiation, and the spectral band-pass filters are also placed in the dewar and held at cryogenic temperatures. The InSb radiometers also constructed with the current-to-voltage converters attached to the back of the radiometer to increase the signal-to-noise ratios. The spectral irradiance responsivities of the InSb radiometers, which are shown in Fig. 1, were determined using the Electrical Substitution

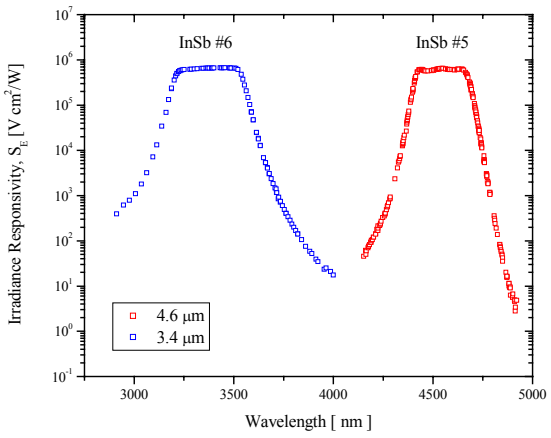

Figure. 1 The spectral irradiance responsivities of the InSb radiometers #6 (3.4 μm) and #5 (4.6 μm).

Bolometer in the IR-SIRCUS facility. The calibrations were performed with a laser-irradiated integrating sphere with a precision aperture to obtain a uniform irradiance at the plane of the entrance aperture of the InSb radiometers.

Spectral Irradiance Measurements

Due to the spectral width of the InSb radiometer spectral responsivities, the irradiance at the plane of the collimator opening can be obtained only with the knowledge of the

temperature and the spectral emissivity of the blackbody at the focus of the infrared collimator. Since the irradiance responsivity, S_E, is measured, if the spectral irradiance of the source, E_λ is known then the irradiance response, v_C, can be calculated using,

$$v_C = \int S_E \cdot E_\lambda d\lambda \,. \qquad (1)$$

If the source at the entrance of the collimator is a blackbody at a temperature, T, with emissivity, ε, then

$$v_m = \int S_E \cdot E_\lambda = \tau \cdot \Omega \int S_E \cdot \varepsilon \cdot L_\lambda(T) d\lambda \,, \qquad (2)$$

where v_m is the measured voltage and Ω is the solid angle relating the radiance to irradiance and τ is the transmittance of the source setup. The transmittance factor accounts for diffraction losses, mirror reflectance losses and imperfect imaging of the collimating mirror. The band-averaged irradiance responses needed for the determination of the throughputs are shown in Fig. 2.

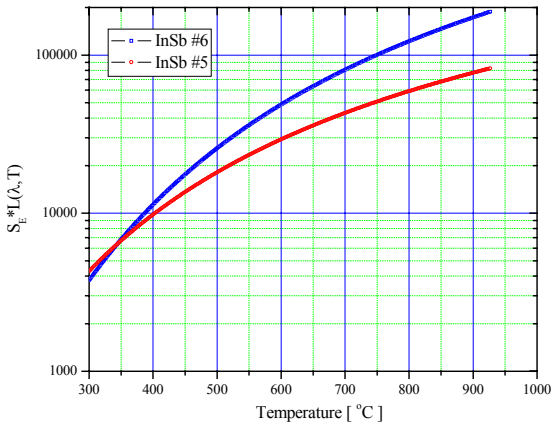

Figure 2. The calculated irradiance response using Eq. 1 for the respective InSb radiometers for a blackbody at the temperatures shown.

If the emissivity and the temperature of the blackbody at the source of the collimator is known, then the measured voltage, v_m, can be used in conjunction with the band-averaged radiance in Eq. 2 to determine the solid angle and the transmittance of the collimator. The knowledge of the transmittance, τ, and the solid angle, Ω, would specify the spectral irradiance averaged over the InSb #5 and InSb #6 wavelengths.

For a point source geometry, if the source has an area, A, then the solid angle is related to the distance from the source to the entrance aperture plane of the filter radiometer, d, by

$$\Omega = \frac{A}{d^2} \,. \qquad (3)$$

The solid angle term can be modified by additional factors such as the reflectance of mirrors if they are in the optical path from the radiance source to the irradiance measurement plane thus the solid angle in Eq. 3 is difficult to assess from the parameters of the collimator.

Comparisons with Source-based Irradiances

The InSb #5 and InSb #6 filter radiometers were used to measure the irradiances of a blackbody-based collimator at AFMETCAL. The measurements were performed with a chopper wheel placed between the opening of the blackbody and the aperture to reduce the influence of the background radiation. The signals from the radiometers were measured with a sine-wave measuring lock-in amplifier.

The comparisons reveal that under all measurements conditions, the source-based irradiance of AFMETCAL and the NIST detector-based irradiances are in agreement to < 6 % (k=2).

Further reduction in the AFMETCAL scale uncertainties can be realized by adopting the detector-based scale with the realizations as described in this work. NIST is working to improve the stability of the infrared lasers used in the IR-SIRCUS facility to reduce the total uncertainties to < 1 % (k=2).

Long-term calibration of a New Zealand erythemal sensor network

J. D. Hamlin, K. M. Nield and A. Bittar

Measurement Standards Laboratory of New Zealand (MSL), IRL, Lower Hutt, New Zealand

Abstract

New Zealand's clear skies and hence high solar ultraviolet (UV) radiation have prompted a public education and warning programme on the dangers of UV exposure. Part of this programme was the establishment since 1989 of a network consisting of six erythemal radiometers located mainly in centres of high population density and the use of measurement data in radio broadcasts of the UV index, derived from these measurements (Ryan et al 1996). The Measurement Standards Laboratory of New Zealand (MSL) has been responsible for the annual calibration of these radiometers since the network's inception and in this paper we will present the changes in spectral responsivity performance of four of these radiometers up until the present time (Bittar and Hamlin, 1991).

The six radiometers in the set are manufactured by International Light Inc. They consist of a vacuum photodiode (SED 240), a thin film filter (ACTS270) and a ground fused silica cosine diffuser (type W). The output current is measured using a current to voltage converter circuit and a data collection system.

The calibration is a two step process. Firstly, the relative spectral response shape of the radiometer is measured; this shape is then scaled to values of absolute spectral irradiance responsivity by measuring the radiometer's response to a calibrated spectral irradiance standard. Prior to 1997 the reference detector used to determine the relative spectral response shape was a Rhodamine B fluorescence quantum counter (Melhiush, 1972), since then a calibrated silicon photodiode has been used. A change in traceability also occurred in 2002 when our set of primary spectral irradiance reference lamps became traceable to the NIST detector based irradiance scale (Yoon et al, 2002). The relative expanded uncertainty in the more recent calibrations is no greater than 5 % from 310 nm to 330 nm, this being the region of significant interest for solar erythema.

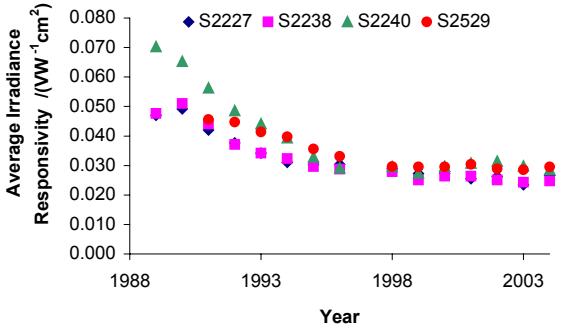

Figure 1. Average irradiance responsivity from 280 nm to 330 nm for each year of calibration for four of the six radiometers. As can be seen there is a reduction in the responsivity over this period the rate of which has recently decreased. In addition, there is agreement between the calibrations using the Rhodamine B and silicon photodiode reference sensors (1996 to 1998).

All radiometers in the set have drifted between calibrations as can be seen in Figure 1. As a performance check the transmittance of the filters in some of the radiometers has also been measured annually (Figure 2.) and the above drifts in response are mainly ascribed to changes in the transmittance of the filters. In some cases the annual changes in response are greater than the level of uncertainty in the calibration and the presence of continued drift highlights the need for regular calibration of this network of radiometers.

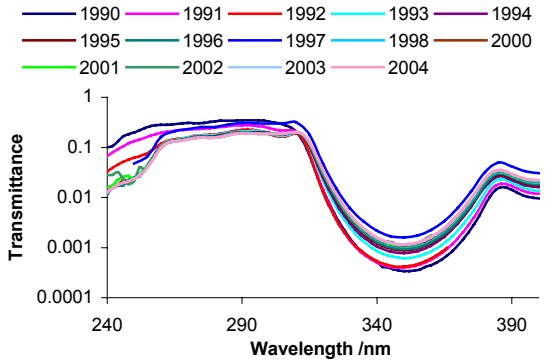

Figure 2. Spectra of filter transmittance for radiometer S2238 from 1990 to 2004. With the transmittance displayed on a logarithmic scale the change in the transmittance slope between 320 nm and 340 nm is more easily seen.

References

Ryan. K. G., Smith. G. J., Rhoades. D. A. and Coppell. R. B., Erythemal ultraviolet insolation in New Zealand at solar zenith angles of 30° and 45°, *Photochemistry and Photobiology*, 63(5), 628-632, 1996

Bittar. A. and Hamlin. J D., A perspective on solar ultraviolet calibrations and filter instrument performance, CIE 22nd Session, Volume 1, Part 1, Division 2, Melbourne 1991.

Melhuish. W. H., Accuracy in spectrophotometry and luminesence measurements, Proceedings of a conference held at NBS, Gaithersburg, Md., March 22-24, National Bureau of Standards Special Publication 378,1972

Yoon. H. W., Gibson. C. E. and Barnes. Y., Realization of the National Institutes of Standards and Technology – detector based spectral irradiance scale, *Applied Optics,* 41(28), 5879-5890, 2002.

Drift in the absolute responsivities of solid-state photodetectors at two NMIs

K. M. Nield, J. D. Hamlin and A. Bittar

Measurement Standards Laboratory of New Zealand (MSL), IRL, Lower Hutt, New Zealand

P. B. Lukins

National Measurement Institute of Australia (NMIA), Lindfield, Australia

Abstract.

The advent of cryogenic radiometers for the determination of detector responsivity at single wavelengths has reduced the uncertainties in such calibrations by an order of magnitude if not more (Fox et al 1990, Nield et al 1998). However, maintaining such uncertainties also relies upon the artifacts being stable over time to better than the uncertainty itself.

The stability of sets of radiometric quality (silicon) photodiodes has been followed for almost a decade in two different NMIs. The silicon photodiodes are invariably Hamamatsu S1337 or S6337 in both single and multi-element trap detector configurations. The trap configurations include 3-element (S1337) and 5-element (S1337) reflection traps as well as 4-element (S6337) transmission traps. In all cases, unless otherwise stated, the responsivities were measured at laser wavelengths using the cryogenic radiometers at the two NMIs.

At MSL the silicon photodiodes were initially stored with dust covers within the cryogenic radiometry laboratory. After observing the presence of NaCl contamination on the surfaces of some of the photodiodes within the trap detectors the storage and use of them was modified to holding them within a bell jar during periods when not in use. At NMIA the photodiodes have routinely been stored with dust caps within dry air purged containers, in addition the facility is both temperature and humidly controlled, unlike at MSL where only the temperature is controlled. Even with this handling visible changes in the front surface of the diodes does occur and it is the influence of this along with other possible more subtle changes in the detectors we are attempting to understand through this nascent collaboration.

For the silicon photodiodes above 600 nm, no responsivity drift was observed for any of the configurations. However, at shorter wavelengths, the responsivity decreases significantly with a drift rate that increases in magnitude as the wavelength decreases reaching almost -0.04 % per year near 476 nm (Figure 1). The drift rate appears to be least for the Hamamatsu S1337 single plane photodiodes that have received minimal exposure to radiation. For these devices, the annual drift rates at 476 nm vary between (-0.02 and -0.04) % per year depending on the particular photodiode while the average drift rate for the collection of these photodiodes was -0.03 %per year. The drift rates for the three different trap detector configurations are very similar and reach about -0.035 % per year at 476 nm.

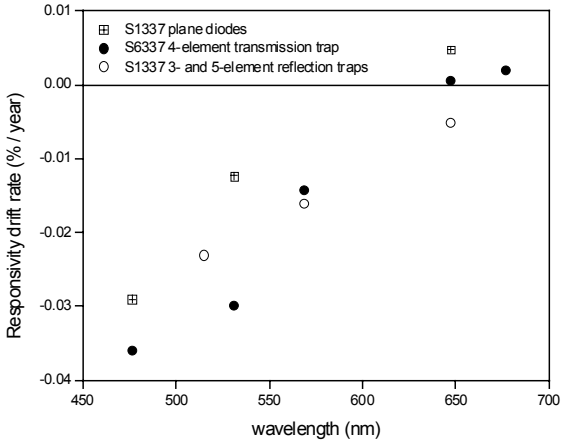

Figure 1. Responsivity drift rate, as a function of wavelength, for various silicon detectors. In the case of the NMIA detectors these have been observed over a 10 year period, the drifts at MSL have been followed for the past six years.

In each case, the trends are monotonic with similar slopes; similar drifts were observed in the detectors used in the comparison of cryogenic radiometers (Goebel et al 1999). In addition, slightly greater drift is observed for the 5-element trap detectors than the 3-element traps, this may be due to the extra exposure suffered by these devices in their use in deriving response scales in the ultraviolet and near infrared region whereas the 3-element devices have been restricted to direct calibrations in the visible region against the cryogenic radiometer.

More recent measurements at NMIA on single element diodes indicate that this behaviour extends into the near-UV region to at least around 325 nm. Indeed, at 351.1 nm calibrations of the detectors at MSL drifts over the short term of the order of -0.3% per year in reflection traps built in 1999 have been observed. However a 5-element reflectance trap detector recently fabricated from a different batch of Hamamatsu S1337 photodiodes has shown an unusually small drift of -0.005%over a one year period at this wavelength (that is within the level of measurement uncertainty) in spite of having had considerable exposure to both laser and incoherent sources.

Over a four year period, 3- and 5-element reflection traps show drifts approximately –0.02 %per year at 514.5 nm (Figure 2).

Although the optical quality, uniformity and surface characteristics of the S6337 photodiodes used in the 4-element transmission trap were not quite as good as S1337 photodiodes, their overall performance and drift behaviour are similar.

All types of silicon detector configuration appear to undergo an initial rapid decrease in responsivity over the first few years and then settle to a lower drift rate thereafter. This behaviour is not dissimilar to that reported by Werner (Werner, 1999) where Hamamatsu photodiodes were shown to drift with exposure UV laser radiation.

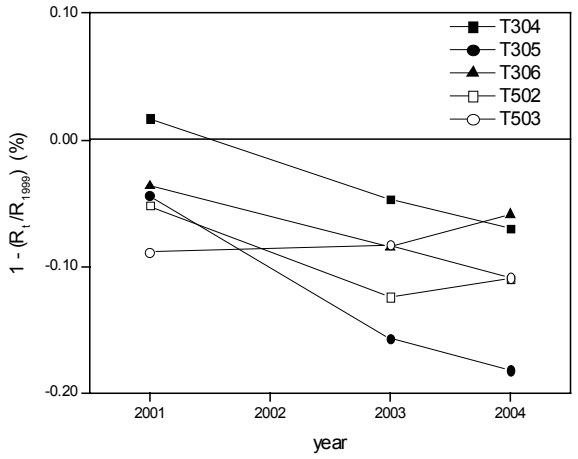

Figure 2. Short-term (5 years) responsivity drift rate at 514.5 nm for various 3- and 5-element reflection traps. Relative uncertainties for a given calibration at any year are of the order of 0.02 %.

These results can be compared with those for InGaAs photodiodes (Anadigics, 35PD10M), calibrated and monitored at NMIA, where, for example, the responsivity of a 35PD10M decreased by 0.45 % from 0.9735 A/W to 0.9692 A/W over the past seven years giving a drift rate of about 0.06 % per year. A collection of similar windowed and windowless photodiodes suffered a decrease in responsivity of about (0.2 – 0.5) % over the past seven years giving an average annual drift rate of the order of (-0.03 to -0.07) %. InGaAs photodiodes appear more prone to long-term responsivity drift compared with silicon photodiodes.

Acknowledgements

The authors would like to acknowledge the work of Dr. Duncan Butler, formerly NML, CSIRO, for the early work on the detector set at NMIA.

References

Fox, N. P., Martin, J., *Appl. Opt.* 29, 4686-4693, 1990.

Goebel. R., Stock. M. and Kohler. R., "Report on the International Comparison of Cryogenic Radiometers Based on Transfer Detectors", Bureau International des Poids et Mesures, Sevres, France, 1999.

Nield, K. M., Clare, J. F., Hamlin, J.D., Bittar, A., *Metrologia* 35, 581-586, 1998.

Werner. L., *Metrologia,* 35, 407-411, 1998.

Radiance source for CCD low-uncertainty absolute radiometric calibration

A. Ferrero, J. Campos and A. Pons
Instituto de Física Aplicada, CSIC, Madrid, Spain

Abstract. A radiant source for CCD absolute radiometric calibration based on an integrating sphere externally illuminated by a dye laser has been developed. A rotating diffuser has been used for speckle reduction. The field uniformity has been measured at several distances from the exit port, and compared to the predicted radiance of a lambertian disc.

Introduction

In addition to their wide use as imaging systems, CCD cameras would be a very interesting measurement instrument for optical radiation if the measurement uncertainty was kept low. A great part of the difficulty to do that lays in obtaining a radiant source able to produce an uniform irradiance over all the pixels (when the camera is used without its objective) and whose radiance be accurately predicted[1] (when the objective is in place) at the radiometric calibration stage. Some previous works done in our laboratory[2] have shown that an integrating sphere externally illuminated by an incandescent lamp gives very good results regarding pixel irradiance uniformity and accurate predictability of its radiance. However this source provides low power for spectral calibration which is a major disadvantage. To avoid this problem the incandescence lamp can be replaced by a dye laser, increasing the available spectral power density.

This work describes the key elements of a radiant source formed by an integrating sphere externally illuminated by a dye laser to obtain an uniform and predictable radiant source as well as the uniformity of the radiation field as a function of the distance to the sphere's exit port. Moreover, the emission of the exit port has been modelled by assuming an uniform lambertian disc. The goodness of this model has been tested by comparing the irradiance field uniformity predicted by the model to the one measured at several distances of the exit port.

The irradiance produced by a lambertian disc at a distance is given by an integral equation that has to be solved numerically. A series development of this equation has been done, and the irradiance calculated from it has been compared to that obtained from the numerical integration. The agreement between both values is very good in the distance range where the CCD calibration can be done. This result allows easily to predict the irradiance produced at any point away from the source, that is interesting in radiometric calibration.

Radiance source description

This source consists of a 50 cm diameter integrating sphere externally illuminated by a power-stabilized dye laser. A rotating diffuser is located for reducing the speckle of the laser radiation[3,4]. We have checked that the speckle noise is reduced to a negligible level by rotating the diffuser at very low frequencies. However, we had to increase the rotation frequency in order to avoid the instability due to the own rotation movement. Behind the diffuser, and before the entrance port, a 3 cm focal length lens is placed in order to focus inside the sphere the radiation diffused by the diffuser. Varying the distance from the diffuser to the lens the spot size of the radiation impinging the sphere is varied. The sphere is used without internal baffles, because the CCD will be calibrated at enough distance for avoiding radiation from direct incidence and first reflection.

Field uniformity

The field uniformity at the exit port was measured to check whether the emission could be assumed as the emission of a lambertian source. With this purpose, it was scanned by a photodiode mounted over a XY displacement system, controlled by a stepper motor. This scan was done at three different distances from the exit port (7.3 cm, 11.8 cm and 20 cm). For the three distances an irradiance distribution of concentric circles was obtained, according to the exit port geometry. The smaller the distance, the larger the non uniformity produced by this irradiance distribution. The uniformity, defined as the ratio between the standard deviation of the measurements and its mean value, inside a circle 4 mm in radius is shown in the first column of table I.

Table 1: Experimental and theoretical results on field uniformity at distance z from the sphere´s exit port.

z (cm)	Experimental uniformity (%)	Theoretical uniformity (%)
7.3	0.00657	0.00580
11.8	0.00555	0.00549
20	0.00237	0.00225

These results were obtained with the laser beam focused over the internal wall of the sphere. There are signs in the literature that point out a field uniformity dependence on the size of the spot on the sphere wall at the first incidence on the sphere[5]. The distance from the diffuser to the lens was varied for having several spot sizes. In figure 1, it is represented the relation between the irradiance over an infinitesimal surface located at a distance 'a' from the optical axis (E_a) and the irradiance over an infinitesimal surface located onto the optical axis (E_0). The error bars represent the standard deviation of all the measurements that are placed at a distance 'a' of the geometrical center of the irradiance circular distribution. For clarity, only those corresponding to the widest spot are represented in the plot. They are representative of the other cases. It can be observed that the difference due to spot size at first reflection is smaller than these error bars. So,

we have proven that field uniformity is independent on the spot size at first reflection.

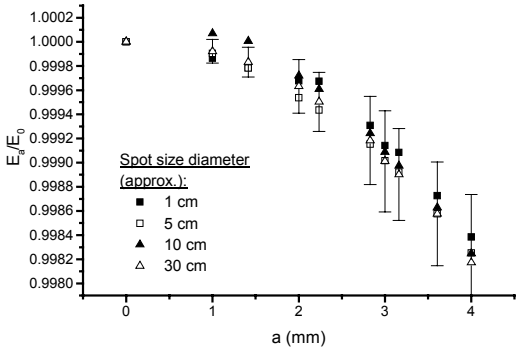

Figure 1: Uniformity experimental data for several spot sizes at first reflection in the sphere.

Lambertian disc model

As the radiance of a source depends on its geometry and it is independent on its topography[6], it can be assumed that, if the internal coating of the integrating sphere ($BaSO_4$, in this case) is perfectly lambertian, the emission of the exit port can be modeled with a lambertian disc. According to figure 2, and the relation

$$E = \int_{A_0} dE = \int_{A_0} L dA_0 \frac{\cos^4 \theta}{z^2} \quad , \qquad (1)$$

where A_0 is the exit port area and E is the irradiance in a point located at a distance 'z' to de disc, it can be written:

$$E = Lz^2 \int_0^{2\pi} d\varphi \int_0^R \frac{r dr}{(z^2 + a^2 + r^2 - 2ar\cos\varphi)^2} \qquad (2)$$

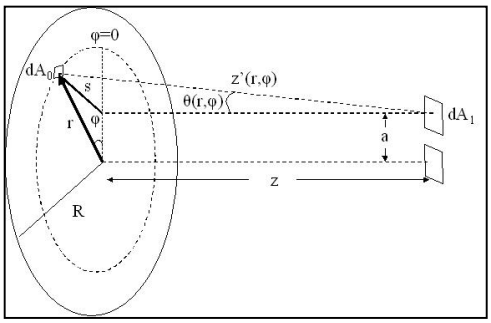

Figure 2: Irradiance produced by a lambertian disc over an infinitesimal surface.

With this equation it is possible to know the irradiance over all points. Although the integration could be numerically solved, we did an approximation based on a Taylor expansion, valid only for negligible 'a' values compared to 'z'. This approximation is written as:

$$E = \pi L \left(\frac{z^2}{z^2 + a^2} \right) \left(\frac{z^2}{R^2 + z^2 + a^2} \right) \times \times \left[1 + \left(\frac{aR}{R^2 + z^2 + a^2} \right) \left(3 + \frac{R^2}{z^2 + a^2} \right) \right] \qquad (3)$$

In figure 3 the comparison of this approximation to the exact result is shown.

After this equation the uniformity can be calculated inside an 'a' radius circle, at a distance 'z'. It was calculated for the same distances of the previous section, and the results were compared to the experimental ones. The concordance is good, as can be seen in table 1. The experimental uniformity is always higher than the theoretical one, probably due to the temporal noise. Anyway, the maximum difference between both uniformities is something less than 13%, that is produced in the 7.3 cm case.

The goodness of the comparison allows to conclude that the developed radiant source radiates as a lambertian disc, therefore, in a predictable way.

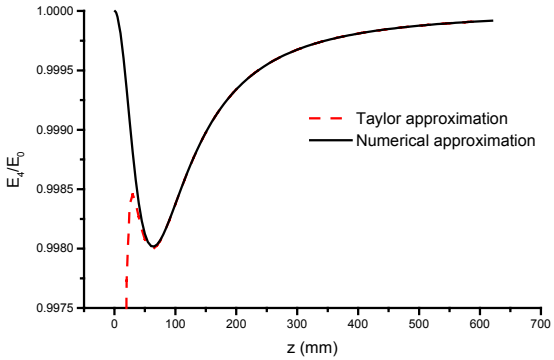

Figure 3: Comparison of Taylor approximation to the exact result.

Conclusions

A radiant source for CCD absolute radiometric calibration has been developed. This source is based on an integrating sphere externally illuminated by a dye laser. The field uniformity at the sphere exit port has been measured, at several distances from this port and several solid angles of the incident beam. It has been proven that the uniformity results can be explained assuming a lambertian disc model for the exit port. So, the emission of the exit port is predictable, resulting of great importance to do radiometric calibrations.

Acknowledgments This work has been supported by the thematic network DPI2002-11636-E and the project DPI2001-1174-C02-01.

References

1. J. Campos, Radiometric calibration of charge coupled device video cameras, *Metrologia*, 37, 459-464, 2000.
2. J. Campos, M. Rubiño and A. Pons, Spectral system for CCD video camera radiometric calibration, *Proceeding of CGIP2000*, Cépaudès-Éditions, Toulouse, France, 2000.
3. S. Lowenthal, D. Joyeux and H. Arsenault, Relation entre le deplacement fini d'un diffuseur mobile, eclaire par un laser, et le rapport signal sur bruit dans l'eclairement observe a distance finie ou dans un plan image, *Optics Communications,* 2, No. 4, 184-188, 1970.
4. E. Schroeder, Elimination of granulation in laser beam projections by means of moving diffusers, *Optics Communications,* 3, No. 1, 68-72, 1970.
5. S. W. Brown, G. P. Eppeldauer and K. R. Lykke, NIST facility for Spectral Irradiance and Radiance Responsivity Calibrations with Uniform Sources, *Metrologia*, 37, 579-582, 2000.
6. W. L. Wolfe, Radiative Transfer, in *Introduction to Radiometry,* (SPIE Optical Engineering Press, Tutorial Text in Optical Engineering, vol. TT29, 1998), pp 15-25.

Improved NIR spectral responsivity scale of the PTB and implications for radiation thermometry

A. E. Klinkmüller, P. Meindl, U. Johannsen, N. Noulkhow*, and L. Werner

Physikalisch-Technische Bundesanstalt, Institut Berlin, Abbestraße 2-12, 10587 Berlin, Germany
* Guest scientist from the National Institute of Metrology (Thailand), NIMT, Bangkok

Abstract. The NIR spectral responsivity scale has been improved using a monochromator-based cryogenic radiometer. A relative standard uncertainty of 0.1 % has been attained for the spectral responsivity between 950 nm and 1650 nm. In the limited wavelength range from 1520 nm to 1620 nm an even lower uncertainty has been demonstrated using a tuneable diode laser source. Implications to the measurement of thermodynamic temperatures with absolutely calibrated NIR filter radiometers are discussed.

Introduction

The NIR spectral responsivity scale of the PTB has been improved to meet the demanding applications of filter radiometers in radiation thermometry.
Hitherto the spectral responsivity scale between 950 nm and 1650 nm was realized by calibrating InGaAs photodiodes at four laser lines at the PTB laser-based radiation thermometry cryogenic radiometer and interpolating the spectral responsivity with thermal detectors [1]. However, the interpolation with conventional thermal detectors is very time-consuming and of limited accuracy. An interpolation of the spectral responsivity between widely separated laser-based calibrations as for Si trap detectors is not possible because of the lack of an accurate model of the responsivity for the commonly used detectors in this wavelength range. Therefore, calibrations against a cryogenic radiometer at arbitrary wavelengths have been chosen to reach a higher accuracy.

Apparatus

A calibration facility based on a cryogenic radiometer and presently optimized for UV calibrations [2] has been used for measurements in the NIR between 950 nm and 1650 nm. A halogen lamp has been chosen as light source. The facility further consists of a prism-grating double monochromator, a mirror imaging system, a cryogenic radiometer of type CryoRad II manufactured by Cambridge Research & Instrumentation, and a positioning system. A power of 1 µW to 2 µW is available with a bandwidth of 8.3 nm. The facility also allows to direct light through a fiber into the final imaging stage. A fiber coupled tunable laser has been attached to the system.

Measurements and Discussion

The detectors are calibrated by measuring their electrical signal when inserted into the beam from the monochromator at the same position where the radiant power of the beam is determined by the cryogenic radiometer. A monitor detector is used to correct for power variations between the radiometer and the detector measurement. Any polarisation dependencies are corrected by measuring at three different angles of detector rotation. The detectors are calibrated at controlled temperature.
InGaAs photodiodes are used as secondary standards for the spectral responsivity. They have been calibrated from 950 nm to 1650 nm with a relative standard uncertainty of 0.1 %. The uncertainty of this calibration is dominated by the cryogenic radiometer drift of typically 20 nW/10 min. The second largest contribution is the uncertainty of the window transmittance correction, which is measured before and after each calibration.
A comparison of these calibrations with calibrations at the laser-based radiation thermometry cryogenic radiometer at three laser wavelengths shows good agreement.
In addition, a calibration of an InGaAs photodiode between 1520 nm and 1620 nm has been performed with a tunable diode laser source. The much higher power and the narrow bandwidth allow to reduce the uncertainty to well below 0.1 %. Thus, the uncertainty of radiometric temperature measurements can also be reduced utilizing filter radiometers calibrated against InGaAs photodiodes as secondary standards. An uncertainty of 0.1 % for radiometric measurements with filter radiometers in the spectral range around 1550 nm allows to determine thermodynamic temperatures below the temperature of the Zinc fixed point (693 K) with an uncertainty of 50 mK. This is in the order of the uncertainty of the International Temperature Scale of 1990 (ITS-90).

Conclusion

The new facility allows to improve the accuracy of the NIR spectral responsivity scale at PTB to 0.1 % between 950 nm and 1650 nm. The even higher accuracy in the limited wavelength range around 1550 nm opens a perspective to extend filter radiometer measurements of thermodynamic temperatures to below the Zinc fixed point (693 K) with uncertainties comparable to those of the ITS-90.

References

[1] Werner, L., Friedrich, R., Johannsen, U., Steiger, A., Precise scale of spectral responsivity for InGaAs detectors based on a cryogenic radiometer and several laser sources, in *Metrologia, **37***, 523-526, 2000.
[2] Meindl, P., Klinkmüller, A. E., Werner, L., Johannsen, U., Grützmacher, K., The UV Spectral Responsivity Scale of the PTB, in *Proceedings of NEWRAD 2005*.

Characterization of a portable, fiber-optic coupled spectroradiometer as a transfer radiometer for the calibration of the Robotic Lunar Observatory

B. C. Johnson and S. W. Brown
NIST, Optical Technology Division, Gaithersburg, Maryland, USA

J. J. Butler, M. Hom, and B. Markham
NASA Goddard Space Flight Center, Greenbelt, Maryland, USA

S. F. Biggar
University of Arizona, Remote Sensing Group, Tucson, Arizona, USA

T. C. Stone
US Geological Survey, Flagstaff, Arizona, USA

Abstract. We report on the characterization of a portable, fiber-optic coupled spectroradiometer. The system was tested for radiometric stability and repeatability, wavelength calibration, stray light, linearity with optical flux, and sensitivity to ambient temperature. Many of the measurements were performed using the NIST laser-based facility for Spectral Irradiance and Radiance responsivity Calibrations using Uniform Sources (SIRCUS). The goal of this work was to understand the performance of the instrument as a transfer radiometer, with specific application to the *in situ* calibration of the Robotic Lunar Observatory (ROLO) in Flagstaff, Arizona. Characterization issues that apply to spectral reflectance determinations of vicarious calibration sites were also investigated.

Introduction

The Robotic Lunar Observatory (ROLO) acquires radiometric measurements of the Moon in selected spectral bands between 345 nm and 2390 nm in order to provide a stable, well-calibrated reference standard that can be observed from orbit by multiple Earth-observing satellites (Kieffer and Wildey 1996, Kieffer and Stone 2005). The radiometric calibration is based on Vega. In 2003 the National Institute of Standards and Technology (NIST), the National Aeronautics and Space Administration (NASA) Goddard Space Flight Center (GSFC), the University of Arizona (UA), and the U.S. Geological Survey (USGS) collaborated to design and execute an independent calibration using a collimated source that directly illuminated the ROLO systems. To establish the stability of the source at the focus of the collimator during the measurements, a portable, fiber-coupled spectroradiometer was used to periodically compare the output of this source to that of a stable, laboratory reference standard.

Measurement Systems

The transfer spectroradiometer was a portable, fiber-optic coupled commercial system manufactured by Analytical Spectral Devices, Inc. (ASD) of Boulder, Colorado. The Hydrospheric and Biospheric Science Laboratory at NASA/GSFC uses this ASD FieldSpec® Pro (serial number 6172) in instrument studies and occasional field exercises. The instrument consists of three separate systems that cover the spectral range from 350 nm to 2500 nm: a single grating spectrograph with a linear Si diode array and two single grating spectrometers, each with an InGaAs detector. Three optical fiber bundles, which are joined on the input side, channel light from the source to each of the three dispersing systems. In this instrument, the option of thermoelectric cooling of the Si array is installed, and we operated with the cooling on. Because of the wide spectral range and light weight, instruments in this product line are often used for *in situ* reflectance, radiance, and irradiance studies as part of vicarious calibration experiments.

At NIST, lamp illuminated integrating sphere sources, a custom five-channel filter radiometer, and the laser-based facility for Spectral Irradiance and Radiance responsivity Calibrations using Uniform Sources (SIRCUS) were the primary instruments or facilities used to characterize the ASD prior to the field measurements at ROLO.

Preliminary Results at ROLO

The repeatability and stability was tested using an Optronic Laboratories OL455 integrating sphere source in a laboratory environment. The ASD was aligned to view the exit aperture (7.6 cm diameter) normal and centered. A five-channel visible filter radiometer (Allen *et al*. 2003) was used to monitor the output of the OL455 by viewing the center of the exit aperture at an angle. Independent measurements were made on five days, with full power cycling of the ASD and the OL455 but no changes to the optical alignment. Excluding spectral regions with known atmospheric features, the within-day stability was <0.3 %. The repeatability with the ASD over the five days is shown in Fig. 1; excluding the atmospheric features, the repeatability is within +/- 0.3%. The filter radiometer, which has temperature-stabilized filters, also gave results within +/- 0.3% for the channels from 550 nm to 900 nm. Thus, the minimum uncertainty for assessing the stability of the ROLO source in the field calibration is 0.3%.

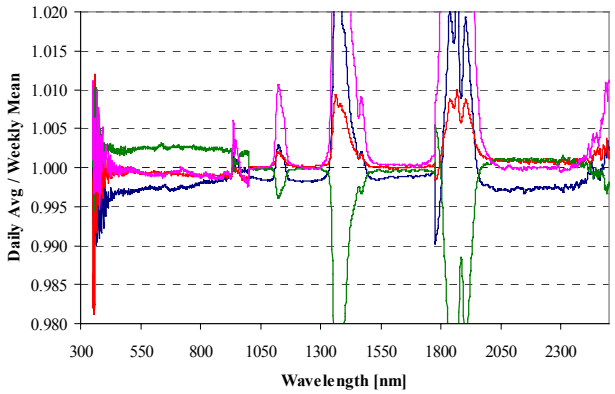

Figure 1. The repeatability of the ASD as determined at NIST using the OL455 source. Each day, data were acquired for 1 h after a determined warm-up interval.

During the field exercise at ROLO, the ASD was used to measure the radiance of the custom USGS source that was mounted at the focus of a spherical mirror. This was outdoors under varying environmental conditions. During the intervals when the ROLO telescope was observing the collimator source, the ASD was used to measure the NIST Portable Radiance (NPR) source (Brown and Johnson 2003), which was located indoors. One example of the results, for the lowest level of the ROLO source, is shown in Fig. 2. Illustrated is the ratio of the results for the two sources, normalized to the average. Based on these data, the stability of the ROLO source was <0.5% from about 450 nm to 1000 nm, <1% from 1000 nm to 1700 nm, and <3% from 1700 nm to 2450 nm.

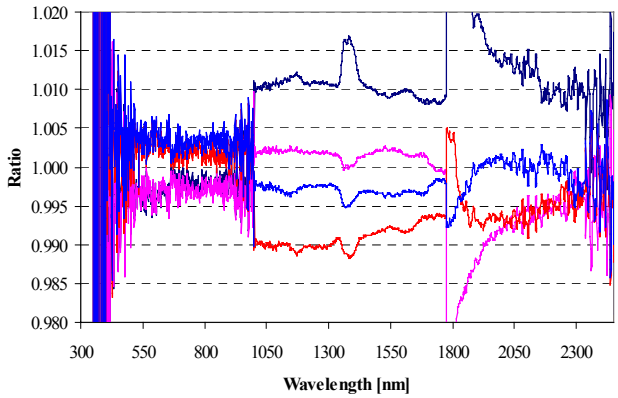

Figure 2. The results of sequential measurements of the ROLO source and the reference source during the course of one night's experiment in Flagstaff.

It is not unexpected that the repeatability of the transfer between the ROLO source and the NPR is not as satisfactory as the results obtained in the laboratory with a single source. Sensitivity to alignment, which depends on the field-of-view of the ASD systems (used in bare fiber mode), sensitivity to ambient temperature, and the dynamic range of the ASD are all factors.

Application to Land Reflectance Studies

Portable spectroradiometers such as those described here are used in spectral radiance mode to measure solar-illuminated natural targets such as the Railroad Valley Playa in Nevada at the time of a satellite overpass (Thome 2004). The instrument is calibrated during the course of the day using a white, diffuse, reflectance standard. Additional characterization issues become critical, such as linearity, spectral out-of-band response, and wavelength calibration.

The spatial imaging of monochromatic light for the visible spectrograph was determined using tunable and fixed frequency lasers on the SIRCUS facility. Sample results are shown in Fig. 3, where the normalized response along the detector array for monochromatic excitation in the red is illustrated. In order to compare the shape of the response for regions away from the image of the entrance slit, the results are referenced to the pixel with maximum response. A reasonable explanation for the broad shoulder is interreflections within the detector array.

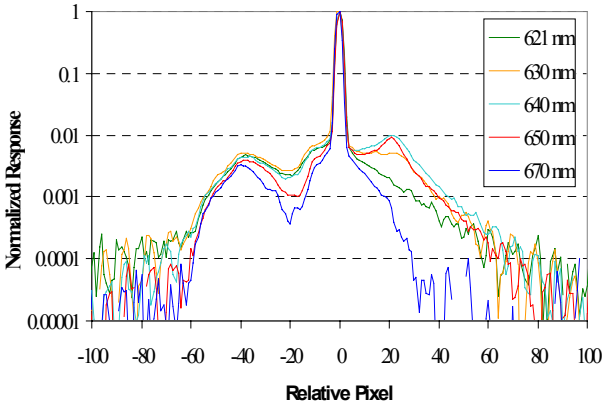

Figure 3. Normalized relative spatial scans for the visible and near infrared spectrograph in the ASD.

Summary

An ASD FieldSpec® Pro was characterized and used to establish the stability of the ROLO source during field calibrations. We will also report on additional characterization results and their significance regarding vicarious calibration experiments.

References

Certain commercial equipment, instruments or materials are identified in this paper to foster understanding. Such identification does not imply recommendation or endorsement by NIST, nor does it imply that the materials or equipment are necessarily the best suitable for the purpose.

Allen, D. W., G. P. Eppeldauer, S. W. Brown, E. A. Early, B. C. Johnson, K. R. Lykke, Calibration and characterization of trap detector filter radiometers, *Proc. SPIE*, **5151**, 471-479, 2003.

Brown, S. W., B. C. Johnson, Development of a portable integrating sphere source for the Earth Observing System's calibration validation programme, *Int. J. Remote Sensing*, **24**, 215-224, 2003.

Kieffer, H. H., T. C. Stone, The spectral irradiance of the Moon, *Astron. J.*, **129**, 2887-2901, 2005.

Kieffer, H. H., R. L. Wildey, Establishing the Moon as a spectral radiance standard, *J. Atmos. Oceanic Tech.*, 13, 360-375, 1996.

Thome, K. J., In-flight intersensor radiometric calibration using vicarious approaches, in *Post-Launch Calibration of Satellite Sensors*, edited by S. A. Morain and A. M. Budge, pp. 95-102, A. A. Balkema, Leiden, 2004.

Synchrotron radiation based irradiance calibration of deuterium lamps from 200 nm to 400 nm at SURF III

Ping-Shine Shaw[1], Uwe Arp[1], Robert D. Saunders[1], Dong-Joo Shin[2], Howard W. Yoon[1], Charles E. Gibson[1], Zhigang Li[1], and Keith R. Lykke[1]

[1]National Institute of Standards and Technology, Gaithersburg, MD, USA

[2]Korean Research Institute of Standards and Science, Daejeon, Korea

Abstract. Synchrotron radiation, with its very nature of calculability, has long been established as a primary source standard for a broad spectral range from x-rays to infrared [1,2]. In the UV and even shorter wavelength regions, synchrotron radiation stands out as the only standard source available to date since this wavelength region is out of reach to the widely used black body source standard. Transfer UV source standards, such as deuterium lamps, can be readily calibrated against synchrotron radiation. Most recently, such work was reported [3] using the Synchrotron Ultraviolet Radiation Facility (SURF II) at the National Institute of Standards and Technology (NIST) where SURF is a dedicated synchrotron source for radiometry. Since then, SURF has undergone a major upgrade to SURF III where the accuracy of all the storage ring parameters has been significantly improved [4]. A new white light beamline was constructed to direct the calculable SURF III radiation to the user station with minimum obstruction from optical components. Meanwhile, deuterium lamps with improved stability were developed as transfer standards recently [5]. Calibration of these lamps directly against SURF III will yield results with much reduced measurement uncertainty.

We report here the calibration of deuterium lamps by comparing with synchrotron radiation in the wavelength range from 200 nm to 400 nm using the new Facility for Irradiance Calibration Using Synchrotrons (FICUS). The measurements were performed using a 0.25-m monochromator with a cooled photomultiplier tube for radiation detection and an integrating sphere with a precision aperture before the entrance slit to diffuse the incident radiation. The whole assembly was mounted on an x-y translation stage and alternately measured the radiation from synchrotron and the deuterium lamp to be calibrated. Results of the calibration of three deuterium lamps are shown in Fig. 1. The estimated uncertainty is 1.2% at 2σ which is a significant improvement over current UV irradiance scale of NIST. Below we summarize the determination of parameters that could have significant contribution to the uncertainty budget:

1. Storage ring parameters: To calculate the flux of synchrotron radiation, one needs three storage parameters, namely, the electron energy, the radius of the electron beam orbit, and the electron beam current. The measurements of these parameters and the improvement in accuracy for SURF III are discussed elsewhere [5].

2. Distance of the monochromator assembly relative to the emitting point of the synchrotron radiation: The distance from the emitting point of the synchrotron radiation to the defining aperture of the monochromator assembly was measured by using both an optical technique and direct measurement. Both results agree to within 1 mm out of a distance of more than 6 meters.

3. Positioning of the monochromator assembly relative to the electron orbital plane: Synchrotron radiation is not uniform in the vertical direction or the direction perpendicular to the orbital plane. In order to find the on-orbit position accurately, the monochromator assembly used vertical scan to map the characteristic angular distribution of the synchrotron radiation and deduce the on-orbit position.

4. Window transmittance: Like previous study, the monochromator assembly measured radiation in air and a UV window is required to maintain vacuum of the beamline. The transmittance of the window has to be accounted for in irradiance calculation. Unlike the previous study where the window had to be removed to measure the transmittance, the window transmittance can be measured directly on the beamline with synchrotron radiation and the monochromator assembly to reduce the uncertainty.

5. Characterization of integrating sphere and monochromator: To characterize such quantities as the slit scattering function of the monochromator and the fluorescence from the integrating sphere, we used the UV radiation from the tunable lasers at NIST' facility of SIRCUS. An algorithm was used to correct the measured synchrotron and deuterium spectrum from both the measured monochromator slit function and fluorescence from the integrating sphere.

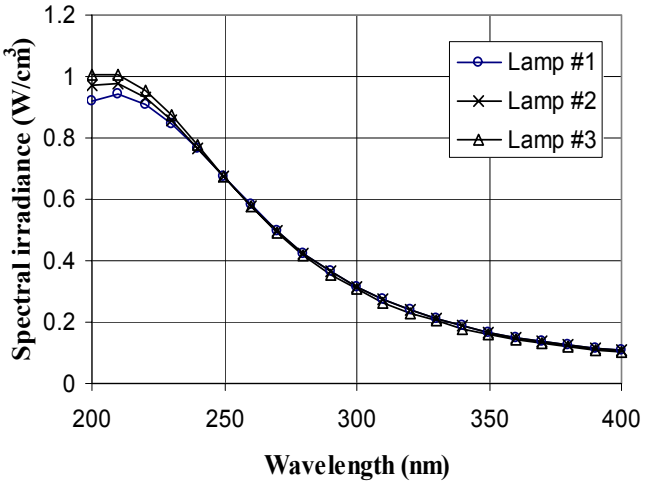

Figure 1. Measured spectral irradiance of three deuterium lamps at 30 cm based on the absolute scale of synchrotron radiation.

References

1. D.L. Ederer, E.B. Saloman, S.C. Ebner, and R.P. Madden, The use of synchrotron radiation as an absolute source of VUV radiation, *J. Res. Natl. Bur. Stand. (U.S.) 79a*, 761 (1975).

2. M. Stock, J. Fischer, R. Friedrich, H.J. Jung, R. Thornagel, G. Ulm, and B. Wende, Present state of the comparison between radiometric scales based on three primary standards, *Metrologia 30*, 439 (1993).

3. A. Thompson, E.A. Early, and T.R. O'Brian, Ultraviolet spectral irradiance scale comparison: 210 nm to 300 nm, *J. Res. Natl. Inst. Stand. Technol*. *103*, 1 (1998).

4. U. Arp, R. Friedman, M.L. Furst, S. Makar, and P.S. Shaw, SURF III - An improved storage ring for radiometry, *Metrologia, 37*, 357 (2000).

5. P. Sperfeld, K.D. Stock, K-H Raatz, B. Nawo and J. Metzdorf, Characterization and use of deuterium lamps as transfer standards of spectral irradiance, *Metrologia*, *40*, S111 (2003)

The Spectral Irradiance and Radiance responsivity Calibrations using Uniform Sources (SIRCUS) facility at NIST

S. W. Brown, J. P. Rice, G. P. Eppeldauer, J. Houston, J. Zhang, and K. R. Lykke
National Institute of Standards and Technology, Gaithersburg, MD, USA

Abstract. We describe the current status of the SIRCUS facility at the National Institute of Standards and Technology (NIST) in the U. S. Recent developments in the facility, including extension to the ultraviolet (UV) and the short-wave infrared (SWIR), are described and future directions of research are outlined.

Introduction

Detectors have historically been calibrated for spectral power responsivity at the NIST using a lamp-monochromator system to tune the wavelength of the excitation source. Silicon detectors can be calibrated in the visible spectral region with combined standard uncertainties at the 0.1 % level. However, uncertainties increase dramatically when measuring an instrument's spectral responsivity outside the silicon range, or when measuring an instrument's irradiance or radiance responsivity. The SIRCUS facility was developed to provide low uncertainties in such calibrations (Lykke, et al.). Since then the facility has been significantly improved and expanded with added capabilities and lower uncertainties.

The current SIRCUS facility combines tunable lasers with cryogenic radiometers and stable working standard detectors. Reference standard detectors are calibrated for spectral radiant power responsivity against a cryogenic radiometer directly traceable to the U.S. primary radiometric standard for spectral power responsivity, the Primary Optical Watt Radiometer (POWR) (Houston, et al.). With the development of quasi-cw lasers with extended spectral tunability in the UV and short-wave IR, the spectral radiant power responsivity can be determined in these spectral regions with uncertainties approaching those achievable in the visible, silicon range. Detectors are equipped with apertures measured on the NIST aperture area facility (Fowler and Litorja), and are used to determine the irradiance at a reference plane. Knowing the measurement geometry, the source radiance can be readily determined as well.

In SIRCUS, high-power, tunable lasers are introduced into an integrating sphere using optical fibers, producing uniform, quasi-Lambertian, high radiant flux sources. Instruments can be calibrated directly in irradiance or radiance mode at the system level, with the entrance pupil over-filled. Uncertainties approach or exceed those available for spectral power responsivity calibrations over a wide dynamic range, approaching 10 decades in some applications.

Extension of spectral coverage

The spectral coverage on SIRCUS depends on the availability of laser sources while the uncertainties achievable are based on the quality of the reference standard detectors (Eppeldauer and Lynch). Quasi-continuous-wave sources, mode-locked picosecond and femtosecond sources with repetition rates as high as 200 MHz, have been developed to extend the spectral coverage from 350 nm to 210 nm in the ultraviolet and from approximately 1 μm to 5 μm in the infrared. Tunability and power curves for the laser systems currently available in SIRCUS are shown in Fig. 1.

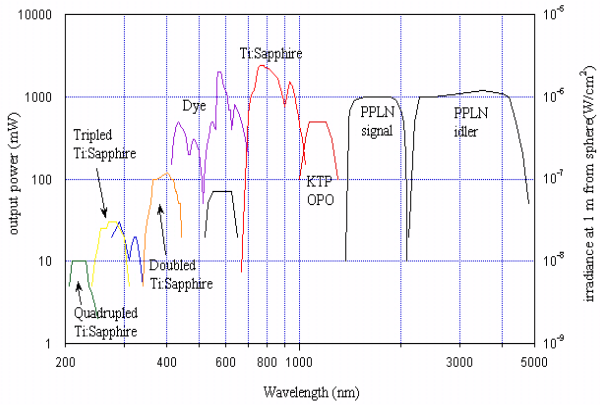

Figure 1. Lasers, output power, and spectral coverage on SIRCUS.

Reference standard detectors, UV radiation-resistant Silicon (Si) detectors for the ultraviolet and Indium Gallium Arsenide (InGaAs) detectors for the short-wave infrared, have been calibrated for radiant spectral power responsivity directly against a new cryogenic radiometer (Lorenz). The cryogenic radiometer is on a portable laboratory table, enabling the system to be readily transported to the UV, visible, or IR laser setups to calibrate reference detectors for spectral radiant power responsivity.

Applications and Future Directions

NIST primary standard radiance and irradiance detectors are transitioning from traditional calibration approaches, often source-based, to the SIRCUS facility. One example is the detector-based thermodynamic temperature scale. As discussed by Yoon et al. (2002), moving from a source-based to a detector-based spectral irradiance and radiance scale can greatly reduce the radiometric uncertainty in the measurement of higher temperature sources. Using SIRCUS to directly calibrate optical pyrometers eliminates the dependence on a blackbody and the ITS-90. Current uncertainties in radiance temperature measurements achievable by optical pyrometers calibrated on SIRCUS approach thermodynamic temperature uncertainties.

Following the re-definition of the candela in 1979,

coupling photometric and radiometric units, many national laboratories, including NIST, derive and maintain the candela and derived photometric units using calibrated standard detectors traceable to cryogenic radiometry rather than standard lamps traceable to primary standard blackbodies and international temperature scales (Ohno). The relative uncertainty for the NIST illuminance unit realized on SIRCUS is expected to be reduced approximately 40 % from the current scale. The current set of 8 NIST reference standard photometers were not calibrated in SIRCUS because large interference fringes were observed. This is a common occurrence due to the use of coherent narrow-band lasers in SIRCUS. As a first step toward the development of a SIRCUS-based photometric scale, two photometers were developed with the SIRCUS calibration in mind. They have been calibrated twice in SIRCUS, with calibrations separated by approximately 2 years. They also measured standard lamps in the photometry calibration facility. The SIRCUS calibration repeated to within 0.1 %, implying that the new photometers are stable enough to hold the photometric scale. These are the first steps toward the development of SIRCUS-derived photometric units.

Stray radiation, or scattered light, within single-grating array spectrometers is often the major source of measurement error with these instruments, limiting their use in applications requiring low measurement uncertainty. Using the tunable lasers available on SIRCUS, the scattered light within array spectrometers has been quantified and correction algorithms have been developed to greatly reduce the errors caused by scattered light in the instrument (Zong et al.). Hyperspectral imaging sensors are often based on single grating array spectrometers. We are extending the stray-light characterization work to include spatial imaging, or an instrument's point-spread function. The first characterization measurements of a hyperspectral imaging sensor, an aircraft ocean color sensor, will be presented and the image correction algorithm discussed.

Ground-based sun photometers and sky radiometers are used to characterize the radiative properties of the atmosphere. Properly characterized and calibrated, they can make key measurements of global concentrations and distributions of atmospheric constituents such as aerosols, ozone, nitrogen dioxide and water vapor. Reductions in the uncertainties using laboratory standards would allow for meaningful comparisons with results from solar-based Langley-Bouger calibration techniques, resulting in independent values of the exo-atmospheric solar irradiance at a set of measurement wavelengths. Previous laboratory comparisons with in-situ measurements showed significant differences between the two approaches (Wehrli, Schmid and Wehrli). Preliminary measurements of the irradiance responsivity of sun photometers on SIRCUS revealed significant differences from standard calibration approaches as well (Souaidia et al.). Further characterization and calibration on SIRCUS with uncertainties of 0.1 % or less approach or exceed the uncertainties in exo-atmospheric solar irradiance (Thullier, et al.).

Summary

The radiometric properties of the SIRCUS source coupled with state-of-the-art transfer standard radiometers whose responsivities are directly traceable to primary national radiometric scales, result in typical combined standard uncertainties in irradiance and radiance responsivity calibrations less than 0.1 %. Extension of the spectral coverage available on SIRCUS to 210 nm in the UV and to 5 μm in the IR will be discussed, the impact of SIRCUS on primary U.S. national radiometric, photometric, and radiance temperature scales will be mentioned; and examples of unique calibrations and future research direction in the facility will be presented.

Acknowledgments We would like to acknowledge and thank Albert C. Parr, Chief of the Optical Technology Division at NIST, and John Grangaard, U. S. Air Force (ret.), for consistent and continued support for the SIRCUS facility.

References

Eppeldauer, G. P. and D. C. Lynch, Opto-mechanical and electronic design of a tunnel-trap Si radiometer, *J. Res. Nat'l. Inst. Stands. Technol.* 105, 813-828, 2000.

Fowler, J. and M. Litorja, Geometric area measurements of circular apertures for radiometry at NIST, *Metrologia* 40, S9-S12, 2003.

Lorenz, S., L-1 Standards and Technology, Inc., Ijamsville, MD, USA.

Lykke, K. R., et al., Development of a monochromatic, uniform source facility for calibration of radiance and irradiance meters from 0.2 micrometer to 12 micrometer, *Metrologia* 35, 479-484, 1998.

Ohno, Y., Photometric Calibrations. NIST Spec. Publ. 250-37, U.S. Government Printing Office, Washington, DC, 1997.

Houston, et al., in preparation.

Schmid, B. and Ch. Wehrli, Comparison of sun photometer calibration use of the Langley technique and the standard lamp, *Appl. Opt*. 34, 4500-4512, 1995.

Souaidia, et al., A comparison of laser-based and conventional calibrations of sun photometers, *Proc. SPIE* 4481, 2003.

Thuillier, G., et al., The solar spectral irradiance from 200 to 2400 nm as measured by the SOLSPEC spectrometer from the ATLAS and EURECA missions, *Solar Physics* 214, 1-22, 2003.

Wehrli, Ch. Calibrations of filter radiometers for determination of atmospheric optical depth, *Metrologia* 37, 419-422, 2000.

Yoon, H., et al., The realization and dissemination of the detector-based Kelvin, *Proceedings of Tempmeko 04*, Dubrovnik, Croatia, 2004.

Yoon, H. W., C. E. Gibson, and P. Y. Barnes, Realization of the National Institute of Standards and Technology detector-based spectral irradiance scale, *Appl. Opt.* 41, 5879-5890, 2002.

Zong, Y., et al., A simple stray-light correction method for array spectroradiometers, submitted to *Appl. Opt.*

NIST BXR I Calibration

A. Smith, T. Jung, and J. Fedchak
Jung Research and Development Corporation, Washington, DC, United States

A. Carter, R. Datla
National Institute of Standards and Technology, Gaithersburg, MD, United States

Introduction

The Low-Background Infrared calibration facility (LBIR) at the National Institute of Standards and Technology (NIST) currently operates a portable transfer radiometer, the BXR I, that was developed to calibrate collimated infrared sources at several customer test facilities. The BXR I uses collection optics together with several narrow band-pass filters and an arsenic-doped Blocked Impurity Band (BIB) detector to scale a model of the collimated source under test. The band-pass filters cover the spectral range from 2 μm to 15 μm with pass bands of width ranging from 1-3 % of the band center wavelength. The BXR I collects collimated light passing through a 7 cm diameter entrance aperture and a spatial filter with an angular acceptance of 4 mrad (full cone). The collected light is focused onto the detector plane. The instrument noise floor is approximately 0.1 $fW/cm^2Hz^{1/2}$. Further description of the BXR I is provided by Jung (2000). In the past, a small collimating source, the 1 cm Collimator (1CC), producing a 1 cm diameter output beam was used to provide a rough calibration of the BXR I. However, over the past year we have significantly reduced our calibration uncertainty by using a larger improved collimator.

Collimator

The new collimator, the 10 cm Collimator (10CC), produces a 10 cm diameter infrared beam using a blackbody source together with several gold-plated aluminum mirrors. Light from the blackbody is collected by two identical off-axis parabolic mirrors; one has its focus at the blackbody exit and the other has its focus on a 6 position aperture wheel. In between these two mirrors there is a short section of collimated light that passes through a pair of 8 position filter wheels. Light passing through one of the limiting apertures is then collimated by a primary off-axis parabolic mirror of 1.83 m focal length and 14 cm diameter. The degree of collimation set by the limiting aperture size ranges from 30 μrad to 1 mrad (full cone).

Calibration Methodology

Calibration of the BXR I is transferred from an Absolute Cryogenic Radiometer (ACR) using the 10CC as a stable reference source. The ACR is in turn compared to the NIST primary standard radiometer, the High-Accuracy Cryogenic Radiometer (HACR). The basis of the BXR I calibration is a matching set of narrow band-pass filters, located in the BXR I and 10CC, whose transmission is known. The absolute transmission spectra of all filters were measured at NIST using a Fourier Transform Spectrometer over the approximate wavelength range from 1 μm to 100 μm. The type B uncertainty associated with the measurement is approximately 1%. Because the out-of-band transmission of the filters is not negligible a model of both the 10CC and BXR I is necessary to account for the out-of-band transmitted power. The effect is most significant when calibrating the BXR I with the ACR due to their large difference in spectral response. The latter has a flat response to all wavelengths, whereas the BXR I has a varying spectral response between 2 μm and 30 μm and is relatively insensitive to other wavelengths. Also, the out-of-band power can be significant when calibrating another collimator with the BXR I—in general the two will have differences in their relative spectral output due to differences in source temperature, diffraction effects or efficiency.

ACR measurements of the 10CC through each filter are used to scale a model of its expected broadband relative spectral irradiance. A separate calibration factor is deduced for each filter center wavelength. Variations between the calibration factors as well as the absolute value provide a check of the model. Once the broadband output of the 10CC is calibrated, it is measured with the BXR I through each of its filters. From these measurements a normalization of the modeled relative responsivity of the BXR I is deduced. Once again variations between normalization factors provide a test of the model. As a further test of the model, measurements of the 10CC output with the BXR I through each of the 10CC filters are made and compared to those made through the corresponding BXR I filters. If the model is perfect the two measurements should be identical.

The large 10 cm beam emanating from the collimator is sufficient to overfill the 7 cm diameter entrance aperture of the BXR I. While ideal for calibrating the BXR I, collecting an identical part of the large diameter beam with an ACR poses a challenge. To resolve this issue a moveable aperture wheel and parabolic mirror were positioned in front of the BXR I to redirect a 7 cm diameter section of the 10CC beam into the small 3.5 mm diameter aperture of the ACR. Pending direct measurements of the parabolic mirror reflectance, the measured reflectance of a witness sample mirror is used in the preliminary calibration.

Experimental Procedure

Both the 10CC and BXR I reside in self-contained cryogenic vacuum chambers with flanged UHV optical ports. The ACR, its parabolic collector and the aperture wheel are housed in another cryogenic vacuum chamber,

the Broadband Calibration Chamber (BCC). The 10CC and BXR I are bolted to opposite ends of the BCC in nominal alignment with one another. All three chambers are lined with a cryo-shroud to provide a low-background environment. Calibration of the BXR I is made during a single cryo-cycle of the entire system without breaking vacuum. This is possible because the off-axis ACR parabolic reflector is mounted on a two-axis stage that can move the mirror completely out of the beam path. The mirror stage is located in front of the BCC port to which the BXR I is bolted. The aperture wheel is attached to a vertical stage that is located about 30 cm away from the parabolic mirror towards the 10CC. Located between the aperture wheel and mirror stage there is a BIB detector on a two-axis stage. Raster scans with the detector are used to characterize the 10CC output beam and to aid in alignment of the ACR and BXR I apertures with respect to the 10CC optical axis.

Initially, the BCC, BXR I and 10CC are evacuated to a pressure of approximately 10^{-3} Pascal before cooling commences. The 10CC and BCC are cooled first using a closed-cycle He refrigerator. Each contains a cryo-shroud that cools rapidly compared to the optical elements. Once both cryo-shrouds are cold, cooling of the BXR I begins. First its outer shroud is cooled with liquid nitrogen and then the inner shroud and optics are cooled with a continuous flow of He gas transferred from a liquid He storage dewar. Final temperatures of the shrouds and internal optics range from 10 K to 30 K. The BXR contains a ZnSe window in front of its entrance aperture that is held at a temperature of 50 K. The window can be warmed to check for contamination when the BXR I calibrates warmer chambers.

Alignment was achieved by an iterative process involving adjustment of the 10CC pointing mirror, the BXR I optical axis and the ACR aperture wheel. Initially the 10CC beam was aligned with the ACR aperture wheel by imaging the 10CC beam edges and ACR aperture edges with raster scans of the BIB detector. Then, the BXR I pointing was adjusted until its optical axis was aligned with the 10CC beam. To ensure that both the BXR I entrance aperture and the 7 cm diameter ACR aperture sample the same portion of the 10CC beam both apertures must be aligned. This alignment was checked by monitoring the roll-off of the BXR I signal through the 7 cm ACR aperture as the aperture was moved vertically and horizontally. Because the two were slightly out of alignment, the ACR aperture wheel was moved towards the BXR I aperture center, and the entire alignment process, starting with the 10CC beam and ACR aperture, was repeated. Several iterations were required because adjustment of the BXR I pointing translates its entrance aperture slightly. Once aligned the signal measured by the BXR I only dropped by 3% as the ACR aperture wheel was changed from the largest 10 cm aperture to the 7 cm aperture (a small decrease is expected due to diffraction effects and the small geometric divergence of the 10CC beam).

Conclusion

Preliminary measurements have validated many aspects of the BXR I and 10CC models. For example, raster scans of the BIB detector across the 10CC beam revealed that its uniformity is limited primarily by diffraction effects. A scan collected through one of the 10CC narrow band filters revealed the tell-tale spatial oscillations expected from detailed diffraction calculations. One problem with the 10CC model that was revealed is that ACR and BXR I measure 10% to 20% more power than expected from the collimator. An independent calibration of the blackbody source of the 10CC has confirmed that its radiance temperature is significantly higher than that indicated by contact thermometry, which may explain the discrepancy. In spite of this issue an overall calibration uncertainty of 3% to 6% appears possible with the current filter set. However, the out-of-band transmission of the filters will significantly increase the uncertainty when calibrating a customer collimator at relatively low source temperatures and short wavelengths. Many customers are interesting in calibrations at temperatures as low as 180 K. By contrast, the BXR I calibration at NIST is performed at source temperatures ranging from 500 K to 600 K. To extend the calibration range of the BXR I to lower temperatures a new filter set having broader pass bands and better out-of-band rejection is being procured.

References

Jung, T. M., Carter, A. C., Lorentz, S. R., Datla, R. U., NIST-BMDO Transfer Radiometer (BXR), *Infrared Detectors and Focal Plane Arrays VI, Proceedings of SPIE Vol. 4028 99*, 2000.

NIST BXR II Infrared Transfer Radiometer

T. Jung, A. Smith, and J. Fedchak
Jung Research and Development Corporation, Washington, DC, United States

A. Carter, R. Datla
National Institute of Standards and Technology, Gaithersburg, MD, United States

Introduction

The Low-Background Infrared calibration facility (LBIR) at NIST is developing a transfer radiometer offering a variety of infrared source evaluation modes. The instrument is capable of measuring the absolute radiance of Lambertian sources, the absolute irradiance of collimated sources, the spectral distribution of those sources, and their polarization. The design and operation of this radiometer, named the BXR II, will be presented.

The primary mission of the LBIR facility at NIST is to maintain the infrared power measurement standard. To this end the facility operates absolute cryogenic radiometers (ACRs) which are electrical-substitution radiometers whose response is directly tied to the national standard High Accuracy Cryogenic Radiometer (HACR). The LBIR ACRs are designed to measure low optical power levels typically at the 10 nW level within a 1% standard uncertainty. Most of the effort of the LBIR facility is directed towards providing calibration support of infrared source chambers which are in turn used to calibrate space-based sensors. Whereas the LBIR facility has typically used the ACR to calibrate the blackbody sources used in the source chambers, advantages can also be realized using the ACR to calibrate portable transfer radiometers. Calibrated portable radiometers can be shipped directly to facilities maintaining source chambers to provide calibrations under conditions similar to those used to calibrate the space-based sensors. Any intervening optics between the calibrated blackbody source and the sensor can then be included in the calibration. The calibrations are based on the comparison of the measured signals from the portable radiometer and the expected signal from a source chamber model, which includes the calibrated blackbody source, the throughput of the optical components, and a correction for diffraction effects. Source calibrations using a filter-based transfer radiometer, the BXR I, have already been conducted. These calibrations have been used to compare irradiances from chambers at different facilities and different chambers within a facility. However, a growing need for greater spectral resolution and absolute power measurements has led to the development of the next generation transfer radiometer, the BXR II.

The BXR II is a liquid-helium cooled radiometer that includes a collimated blackbody source and two types of detectors, an electrical substitution radiometer and As-doped Si Blocked Impurity Band (BIB) detectors. Its collection optics include a 7 cm defining input aperture and an off-axis primary parabolic mirror with an eight-position spatial filter wheel at its focus. Apertures placed in the spatial filter wheel reduce background radiation and define the angular acceptance of the radiometer. A confocal, off-axis, secondary parabolic mirror recollimates the input beam into a smaller diameter beam into which a rotating polarizer, filters and a cryogenic Fourier transform spectrometer (FTS) can be positioned. Finally, a tertiary off-axis mirror focuses light onto any one of seven different BIB detectors mounted on a three-axis translation stage. All the radiometer optical elements are mounted on a two-axis tilt stage allowing alignment with the optical axis of a source chamber.

Although the critical components of the transfer radiometer are designed to operate at temperatures below 15 K, the BXR II is capable of providing calibrations for both ambient and low-temperature source chambers. An integral, liquid-helium cooled sliding baffle tube can be used to mate the shrouds of the radiometer with those of low-temperature source chambers. Three primary source evaluation modes are available with the instrument.

Electrical-Substitution Radiometer Mode

Absolute power measurements of both collimated and uncollimated sources can be made using the liquid-helium cooled electrical substitution radiometer, the ACR III. The ACR III is placed near the focus of the primary parabolic mirror, which along with a cold ZnSe window and the 7 cm defining aperture is the only optical element between the source being calibrated and the radiometer. The ACR III has a noise floor below 50 pW yielding an effective noise floor of 1 pW/cm^2 for BXR II irradiance measurements. This mode is particularly useful for making absolute radiance measurements of both broadband and narrow band sources using a well-defined aperture placed at the focus of the primary mirror.

Filter-Based Radiometer Mode

Four filter wheels placed in the radiometer allow source measurements over more than ten narrow bands between 4 μm and 20 μm using the BIB detectors which are operated at 11 K. This mode is capable of measuring in-band irradiances as low as 1 fW/cm^2 as well as uncollimated power. Unlike the electrical-substitution radiometer, which is absolute to better than 0.1%, the BIB detectors and all collection optics within the BXR II must be calibrated. Irradiance calibrations of the BXR II in this mode will be accomplished with an external calibrated collimated source, the LBIR 10 cm Collimator (10CC). Calibration stability in this mode will be confirmed, both after shipping the radiometer and during chamber evaluations, with the internal collimated blackbody source. A large aperture external blackbody source at the LBIR facility will be used for total radiance BXR II calibrations.

FTIR Mode

Further spectral capability of the BXR II is available by directing the beam recollimated by the secondary mirror into the cryogenic FTS. This operation is accomplished while the radiometer is cold using a translating periscope. This mode provides relative spectral measurements with 1 wavenumber resolution over the wavelength range from 2 μm to 20 μm. These relative spectra can then be fixed at the several wavelength bands in the filter-based radiometer mode. The stability of the cryogenic FTS will also be monitored using the internal collimated blackbody source. Finally, in-situ measurements of the BXR II filter transmission spectra can be collected with the FTS. A comparison of these measurements to independent absolute transmission spectra collected at NIST can be used to eliminate systematic errors due to the filters.

Conclusion

The design phase of the BXR II has been completed and many of its components have been procured. Performance testing of the ACR III has also been completed and the electrical-substitution radiometer mode of the BXR II will be fully capable by the end of 2005.

References

Jung, T. M., Carter, A. C., Lorentz, S. R., Datla, R. U., NIST-BMDO Transfer Radiometer (BXR), *Infrared Detectors and Focal Plane Arrays VI, Proceedings of SPIE Vol. 4028 99*, 2000.

Spectral responsivity interpolation of silicon CCDs

A. Ferrero, J. Campos and A. Pons
Instituto de Física Aplicada, CSIC, Madrid, Spain

Abstract. An interpolation procedure for CCD responsivity that takes into account physical considerations about the pixel is presented. The procedure has been applied to the responsivity values of a CCD and the results are shown.

Introduction

After the radiometric calibration of any detector, it may be necessary to interpolate in order to estimate responsivity values between the calibration wavelengths. A typical spectral responsivity feature of a front illuminated CCD cannot be accurately approximated by a single mathematical function because of its shape. Then a different approach must be followed to interpolate.

The spectral responsivity has to be based on the absorption and charge collection in the pixels, therefore an interpolation procedure, based on estimating the pixels' reflectance and internal quantum efficiency, is proposed in this work. Such an interpolation allows to predict responsivity changes in changing the parameters and vice versa. Its feasibility has been proved by applying it to experimental responsivity values of a CCD calibrated in our laboratory, whose results have been presented in previous works.[1,2]

Pixel responsivity

According to the international vocabulary of Illumination[3], the responsivity of a pixel (R) is the ratio between the response and the radiant exposure. So, R can be written as:

$$R(\lambda) = \frac{\eta_i(\lambda)(1-\rho(\lambda))\lambda_0 A}{Khc} \qquad (1)$$

Where h is the Planck´s constant, c is the light´s velocity, K is the conversion factor e^-/counts, λ_0 is the vacuum wavelength, ρ is the pixel reflectance, A is the pixel sense area, and η_i is the pixel internal quantum efficiency. This last quantity can be expressed for a front-illuminated CCD as[4]:

$$\eta_i = \eta_{opt}\beta\exp(-X_{PSi}\alpha)[1-\exp(-W\alpha)] \qquad (2)$$

where α is the silicon absorption coefficient, W is the depletion region depth, X_{PSi} is the width of the polisilicon layer, η_{opt} is the optical efficiency (that accounts the responsivity variation due to the incidence angle variation), and β is a factor that represents the non ideality of the charge collection and charge transfer processes, whose value is close to 1.

Interpolation procedure

The interpolation procedure consists of fitting equation 1 to the experimental spectral responsivity values, using equation 2 for the internal quantum efficiency. The variables involved in the fitting would be A, K, ρ, η_{opt}, β, X_{PSi} and W. The absorption coefficient and physical constants values can be obtained from the literature. η_{opt} can be taken as unity for the purpose of this work. In a first approach and to simplify the fitting, the discussion can be restricted to scientific CCD, then, A can be considered as a constant for all the pixels and a typical value given by the CCD manufacturer can be taken for it as well as for K. β can also be assumed to be unity for this kind of CCD and therefore the fitting variables are reduced to ρ, X_{PSi} and W. X_{PSi} and W can be assumed to be equal for all the pixels, but the reflectance may change from one to another in addition of being a function of wavelength, radiation solid angle, polarization, etc.

Since ρ is difficult to measure because the pixels are very small and difficult to predict because the CCD is a very complex system from the reflectance point of view, an iterative method can be used to obtain physically significant reflectance values:

1. From typical values for W and X_{PSi} spectral quantum efficiency values can be calculated for every pixel (eq. 2) at the wavelengths the responsivity is known.
2. From those values, spectral reflectance can be calculated from equation 1. If those values are physically significant, they are taken as the actual reflectance values, if not, new values are calculated from a different set of W and X_{PSi}.

To conclude the interpolation of the responsivity, it is necessary to interpolate the reflectance values obtained previously. Unlike the case of a single detector, the CCD responsivity interpolation has to take into account the large amount of pixels involved. So it is important for the interpolation procedure to be simple and because of that a linear interpolation of ρ is done.

The result of this interpolation procedure is a responsivity expression for each pixel, based on pixel's the physical parameters.

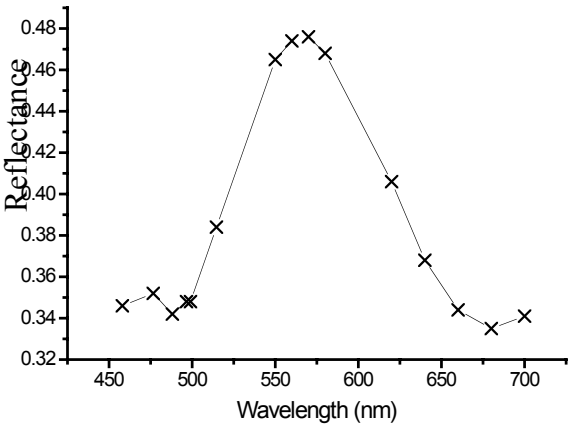

Figure 1: Calculated ρ for the average responsivity of a CCD.

Results

The procedure described before has been applied to a CCD calibrated in our laboratory. Choosing $W = 1.5$ µm and $X_{PSi} = 0.175$ µm, the resulting average ρ is shown in Figure 1. The reflectance stands between 0.34 and 0.48 (physically significant values), and has a maximum at around 570 nm. This figure also shows the linear interpolation. Notice that the maximum (the more conflictive curvature point) is well-sampled, so the linear interpolation is reliable.

The interpolation result for the average responsivity is shown in Figure 2. Notice that, although the reflectance was linearly interpolated, the responsivity presents curvatures, given by the typical shape of the internal quantum efficiency function.

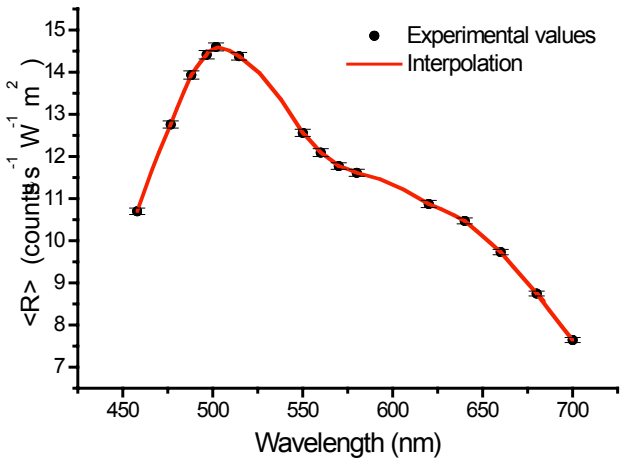

Figure 2: Average experimental responsivity of a CCD and its interpolation.

Conclusions

An interpolation procedure for the spectral responsivity of a CCD based on an estimate of the internal quantum efficiency and the reflectance of its pixels has been developed. This procedure has been applied to a CCD and the results obtained have been shown. Responsivity functions have been calculated for each pixel, being the only difference among them the pixel spectral reflectance values.

Acknowledgments This work has been supported by the thematic network DPI2002-11636-E and the project DPI2001-1174-C02-01.

References

1. A. Ferrero, J. Campos and A. Pons, Radiance source for CCD absolute radiometric calibration, *NewRad (sent)*, Davos, 2005.
2. A. Ferrero, J. Campos and A. Pons, Results on CCD absolute radiometric calibration, *NewRad (sent)*, Davos, 2005.
3. International Commission on Illumination, International Lighting Vocabulary, *Publication CIE* 17.4, Wien, Austria, 1987.
4. J. R. Janesick, QE Formulas, in "Scientific Charge-Coupled Devices", *SPIE Press, Bellingham, Washington*, USA, 2001, pp. 170-178.
5. G. C. Holst, Array Performance, in "CCD Arrays, Cameras and Displays", *SPIE Optical Engineering Press*, Bellingham, Washignton, USA, 1998, pp. 102-145.

Monochromator Based Calibration of Radiance Mode Filter Radiometers for Thermodynamic Temperature Measurement

R. Goebel, M. Stock
Bureau International des Poids et Mesures, Sèvres, France

Y. Yamada
National Metrology Institute of Japan, AIST, Tsukuba, Japan

Abstract. Filter radiometers have been calibrated for measurement of the thermodynamic temperature in radiance mode. A new spectral radiometric calibration scheme has been adopted which requires only a monochromator system and can be implemented without tuneable lasers. A lens transmittance measurement method is discussed which enables simultaneously the correction of size-of source effect to infinite source diameter.

Introduction

Determination of thermodynamic temperature of the transition temperature of metal (carbide)-carbon eutectics is a prerequisite for their application as temperature reference points. Such measurements based on absolute spectroradiometric technique is commonly made in two ways: either using filter radiometers with [1,3] or without imaging optics [2]. The latter (irradiance mode) has the advantage that it does not involve characterization of the lens transmittance and the size-of-source effect (SSE), which can sometimes complicate the procedure. However, it has the disadvantage that the blackbody source needs to be large enough compared to the geometry of the filter radiometer apertures. For metal (carbide)-carbon eutectics, current research effort on the fixed points is focussed on establishing small aperture cells, typically 3 mm in diameter, mainly due to the restriction in available high-temperature furnace dimension. Therefore, the preferable choice for the filter radiometer configuration is the former (radiance mode).

The authors have carried out a joint project to measure in radiance mode the melting temperatures of Re-C and Pt-C eutectic fixed points, with also a measurement of the Cu point performed as verification [4]. In the present paper, the calibration scheme is described. It is novel from the point of view that it is based only on existing facilities at the BIPM in contrast to the previously reported schemes in radiance mode which depend on tuneable laser based spectral characterization in combination with an integrating sphere [1,3].

Measurement Principle and Setup

The measurement setup of the thermodynamic temperature consists of a filter radiometer assembly (consisting of a photodiode, an interference filter, and a precision aperture), and a lens equipped with a lens aperture. The components are mounted on a granite linear bench of 2 m length. The lens focuses the image of the fixed point source aperture onto the filter radiometer aperture, overfilling the latter. The distance between the two apertures, which is around 1800 mm, is measured by means of a laser interferometer.

The diamond-turned apertures, made of brass and with land of 100 μm, have diameters of 5 mm for the filter radiometer apertures, and 18 mm for the lens aperture. The latter dimension was restricted by the capability of the aperture measurement system.

Two of filter radiometers were made, one with an interference filter with nominal central wavelength of 700 nm and another with 800 nm, both having a bandwidth of 20 nm. The filter radiometer housings were temperature controlled by circulating water. Initially, the detector was placed directly behind the filter. However, fluorescence from the filter was observed in the spectral responsivity measurement, described below, which showed up as an out-of-band response of the order of 10^{-4}. Increasing the detector-filter spacing to 35 mm reduced this effect to an insignificant level. No tilt was introduced in the alignment of the filter and the detector.

Following Planck's law, the voltage V measured at the output of the current-to-voltage amplifier is a function of the radiance of the source, and hence of the thermodynamic temperature T [4].

$$V = R_{ampli} \cdot \frac{A_{FR} \cdot A_L}{d^2} \cdot R_{opt} \cdot \frac{2hc^2}{n^2} \cdot \varepsilon_{BB} \cdot \int \frac{S_{FR}(\lambda)}{\lambda^5 (e^{hc/n\lambda kT} - 1)} \mathrm{d}\lambda \qquad (1)$$

where R_{ampli} is the gain of the amplifier, A_{FR} the filter radiometer aperture area, A_{L} the lens aperture area, d the distance between the two apertures, R_{opt} the term including lens transmittance, size-of-source effect, diffraction and other effects as described hereafter, h the Planck's constant, c the speed of light, k the Boltzmann constant, n the refractive index of standard air, $\varepsilon_{\mathrm{BB}}$ the emissivity of the blackbody, $S_{\mathrm{FR}}(\lambda)$ the spectral responsivity of the filter radiometer, λ the wavelength in air in the range covered by the filter radiometer.

Calibration

The calibration of the filter radiometer consists of 1) absolute spectral radiometric calibration 2) aperture area measurement and 3) lens transmittance and SSE measurement. The spectral radiometric calibration involves only the filter radiometer assembly, with the monochromator output beam collimated to be parallel and homogeneous at the filter radiometer aperture plane, simulating the situation during measurement of the blackbody radiation. The lens transmittance and SSE measurement is made with another facility in almost the same configuration as the measurement of the

blackbody, with the aim of investigating any multiple reflections, diffraction or stray light effect.

1) Absolute spectral responsivity measurement

The spectral responsivity measurement method follows what has already been described in [5], with minor but important modifications to adapt to conditions specific to the current system. The monochromator is a Czerny-Turner type double-grating system in additive configuration (manufacturer: Jobin Yvon), with focal distance of 60 cm, equipped with a grating of 1200 lines/mm. The halogen lamp source is focussed onto the entrance slit by a lens. The output monochromatic beam is collimated by a spherical mirror of focal distance 280 mm. The reference trap detector (also with a 5 mm aperture) and the filter radiometer are mounted on a computer controlled rotational stage so that they can alternately be placed in exactly the same position in the output optical path with the beam overfilling the aperture. The trap detector absolute spectral responsivity $S_{\mathrm{trap}}(\lambda)$ is calibrated at discrete laser wavelengths with a cryogenic radiometer and then interpolated.

One major source of uncertainty is related to the positioning of the apertures, combined with the inhomogeneity in the irradiance. The trap detector / filter radiometer aperture is placed at focal distance from the mirror, which is the image plane of the grating and therefore the position where the irradiance uniformity is expected to be the best. However, there was still a considerable gradient in the irradiance of 1 to 4 %/mm. To reduce this inhomogeneity, a linear gradient filter was inserted before the entrance slit. By adjusting the orientation and the distance to the slit, it was possible to reduce the nonuniformity by about a factor of 10.

The spectral responsivity of the filter radiometer $S_{\mathrm{FR}}(\lambda)$ is given by the following [6]:

$$S_{FR}(\lambda) = \frac{A_{trap}}{A_{FR}} \cdot \frac{i_{FR}(\lambda)}{i_{trap}(\lambda)} \cdot S_{trap}(\lambda) \qquad (2)$$

where $i_{\mathrm{trap}}(\lambda)$ and $i_{\mathrm{FR}}(\lambda)$ are the detected current of the filter radiometer and the trap detector, respectively. A_{trap} is the trap detector aperture area.

2) Aperture area measurement

Applying eq. (2) into eq. (1), one finds that A_{FR} is cancelled. Therefore, of the four apertures involved, precise knowledge only of A_{trap} and A_{lens} are necessary. These were measured using the laser beam superposition technique [6].

3) Lens transmittance and SSE measurement

SSE is caused by imperfection in the imaging optics, such as refraction and scattering at the lens, aperture diffraction, and multiple reflections. Multiple reflections between lens and apertures would cause an unwanted increase in the signal, and should be eliminated from the system by careful alignment and optical arrangement. All others would not have any effect to the signal if the source extended to infinite diameter. However, with finite sources, this will cause reduction in the signal and should be compensated.

Measurement of the SSE function conducted with a large aperture integrating sphere source equipped with halogen lamps indicated that it was still not saturating at the maximum measurable source diameter of 70 mm, due to the relatively large diffraction caused by the limited size of the lens aperture. Therefore it was not possible to compensate for SSE towards infinite source diameter.

To overcome this problem, a new scheme was devised [4] which combines the SSE and the lens transmittance corrections. The SSE correction is made up to 40 mm source diameter. At this diameter, correction is made from radiance mode to irradiance mode, which includes the lens transmittance compensation. The correction factor is just the ratio of the signal obtained with and without the lens with a 40 mm diameter source. Once corrected to irradiance mode, the correction to infinite source diameter can be conducted by simply taking into account diffraction effect, theoretically given in [7], since all other lens related imperfections are no longer there.

Measurement of the fixed-point temperatures

The calibration scheme has been successfully applied to fixed-point temperature measurements [4]. The freezing temperature of the primary reference copper point of the BNM-INM (currently LNE) was measured linking it to the filter radiometer through a transfer copper-point furnace. The measured thermodynamic temperature given as the average of the two filter radiometers was 0.148 K higher than the ITS-90 value, with a measurement uncertainty of 0.154 K (k=2). Although limitation in time for completion of the project restricted the measurement accuracy to be less than the highest achievable, the above result confirms the validity of the current calibration scheme and give confidence in the transition temperatures of Re-C and Pt-C eutectic fixed points measured at the BIPM with uncertainty of the order of 0.6 K and 0.3 K respectively.

The demonstrated applicability of the scheme to measurement of eutectic fixed points opens a way for laboratories without tuneable lasers to take part in the determination of their thermodynamic temperatures.

References

[1]N.P. Fox, J.E. Martin and D.H. Nettleton, *Metrologia*, 1991, **28**, 357-374.

[2]M. Stock, J. Fischer, R. Friedrich, H.J. Jung, B. Wende, *Metrologia*, 1996, **32**, 6, 441-444

[3]D.W. Allen, R.D. Saunders, B.C. Johnson, C.E. Gibson, H. Yoon, In *Temperature: Its measurement and control in science and industry*, Vol. 7 (Edited by D. Ripple), AIP Conference proceedings, Chicago, 2003, 577-582.

[4] R. Goebel, Y. Yamada, M. Stock, submitted to *Proc. TEMPMEKO 2004.*

[5] R. Friedrich, J. Fischer, M. Stock, *Metrologia*, 1996, **32**, 6, 509-513.

[6] M. Stock, R. Goebel, *Metrologia*, 2000, **37**, 5, 633-636.

[7]W.H. Steel *et al*, *Journal of Optical Society of America*, 1972, **62**, 9, 1099-1103.

Study of the Infrared Emissivity of Fixed-Point Blackbody Cavities

L. Hanssen, S. Mekhontsev, V. Khromchenko, A. Prokhorov, and J. Zeng

National Institute of Standards and Technology
Gaithersburg, Maryland 20899, USA

Abstract. We evaluate the infrared spectral emissivity of fixed-point cavities used in our infrared spectral radiance and sample emissivity measurement facilities. We compare Monte Carlo ray-trace modeling results of the cavity effective emissivity with measurement results of hemispherical reflectance. In addition, the cavity material reflectance properties are characterized for input to the model. Initial results for three cavity designs show quantitative and qualitative agreement depending on the design.

Introduction

NIST is developing facilities for the characterization of infrared spectral radiance[1] as well as the spectral emittance of materials. Both capabilities require a comparison of spectral radiance from the object to be characterized (source or sample) to that of one of a set of variable temperature blackbodies, using filter radiometers and the facility's Fourier transform spectrometer. The variable temperature blackbodies are calibrated in spectral radiance against a pair of fixed-point blackbodies with interchangeable crucibles of In, Sn, and Zn, and Al and Ag, respectively. Hence an accurate knowledge of the spectral emissivity of the fixed-point blackbodies is critical to the process. To obtain the emissivity, we combine the results of, ray-trace modeling and calculations, and measurements of directional-hemispherical reflectance (DHR), bi-directional distribution function (BRDF), and relative spectral emittance. A Monte Carlo ray-trace code is used to predict the cavity emissivity with input of the cavity shape and the emissivity and specularity of graphite, the cavity material. The reflectance measurements provide emissivity data of both the material and the cavity at room temperature. The results are used to compare with and validate the code results.

Fixed-point blackbodies

Fixed-point blackbody sources are used as reference points for temperature as defined by the ITS-90. In combination with Planck's law, these can provide a scale for absolute spectral radiance, which can, in turn, be used for the characterization of material emissivity as well as other blackbody sources. However, actual cavities employed in the fixed-point sources are never perfect blackbodies, but have spectrally dependent emissivity differing from 1 by variable amounts, in addition to possible non-isothermal temperature distributions. Generally, the emissivity of a blackbody cavitiy is determined through modeling using known values of the coating or wall material emittance. Because many materials used for blackbody cavities including graphite for fixed-point crucibles tend to have decreased emittance with increasing wavelength in the infrared spectral range, and because models always require the use of some assumptions of ideal behavior that cannot be exactly matched, we have endeavored to take a more comprehensive approach to the problem.

First, we have designed the fixed-point blackbodies to achieve the greatest degree of temperature uniformity within the restricted volume and for use up to a maximum viewing f/7 cone. The design was driven by the requirements of minimizing the size of source error while at the same time achieving high emissivity for a relatively large opening diameter of 7 mm. One implementation of the design using a Na heat pipe is shown in Figure 1.

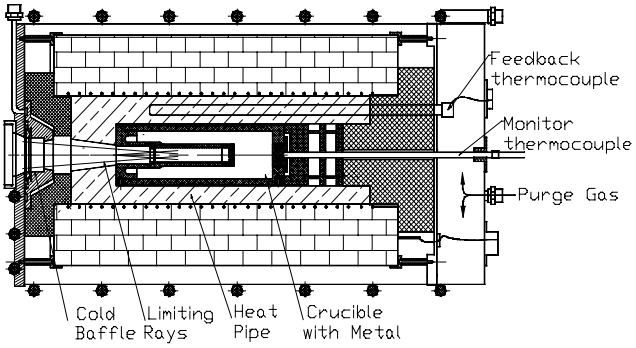

Figure 1. Fixed-point blackbody schematic for Al and Ag.

Additional details of the blackbody design can be found elsewhere.[1]

In the process of optimization, the fixed-point crucible has undergone several design changes. The most recent two designs, along with a traditional NIST design,[2] are shown in Figure 2. These three cavities are studied in this paper.

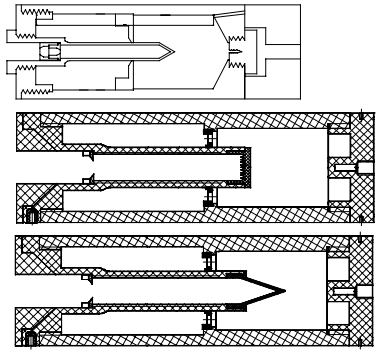

Figure 2. Three fixed-point cavities evaluated in this study.

The top design is the traditional one still in use today. The lower two are implementations of the designs described in Reference 1: the upper one with a v-grooved bottom and the lower with a cylindrical cone, although with a steeper angle than described in Reference 1.

Characterization Studies

We have measured the spectral DHR of the graphite crucible material from 2 to 18 µm. The scattering character of the reflectance was also examined. The results are shown in Figure 3, with a breakdown of reflectance into diffuse and specular components.

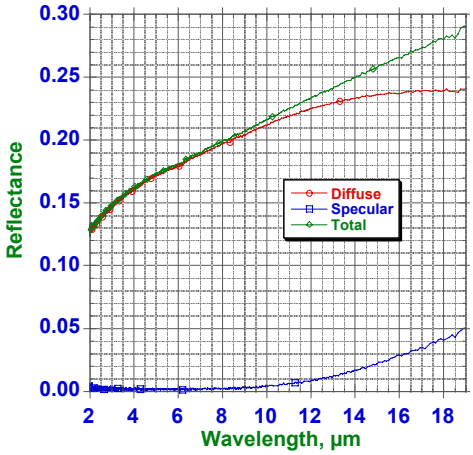

Figure 3. Reflectance of graphite used in the fixed-point crucible cavities.

The components of reflectance of the graphite have been used as one input a customized Monte Carlo ray-trace cavity modeling program to evaluate and predict the emissivity of the fixed-point cavities.[3] An analysis was made of all three designs. For the purposes of validation, a basic design of a cavity equivalent in size and shape to two in Figure 2, but with a simple flat bottom was also studied. An example result comparing the effective emissivity of three similar cavity designs, but with different bottoms is shown in Figure 4.

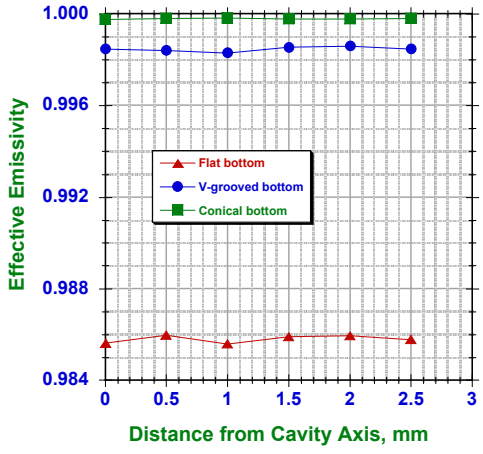

Figure 4. Model predictions of the effective emissivity of three fixed-point cavity designs.

It shows the radial variation of the emissivity for the three cases. The nominal effective emissivities are: 0.9997 for the cone bottom, 0.9984 for the v-grooved bottom, and 0.9857 for the flat bottom case.

For validation of the model results, we also performed measurements of the DHR of the cavities at 10.6 µm using a CO_2 laser and a small-entrance-aperture integrating sphere. The results of the DHR measurements were emissivities of: 0.9995 for the cone bottom, 0.996 for the v-grooved bottom, and 0.985 for the flat bottom case.

Discussion

We have reasonable agreement between the model and experimental results for the cone and flat bottom cavities, but less so for the v-grooved case. There are several factors that may account for the differences. These include the non-ideal construction of the v-grooved surface, as well as poor knowledge of the angular dependence of the graphite reflectance. We are addressing the issue of graphite data through a full characterization of the graphite BRDF at 10.6 µm, an example of which is shown in Figure 5. In addition, the Monte Carlo ray-trace program is being modified to incorporate the measured graphite BRDF results. We anticipate that these steps will lead to a better level of agreement and thus reduced uncertainties. We plan to extend our characterization efforts to the other BBs used in our spectral radiance measurement facilities.

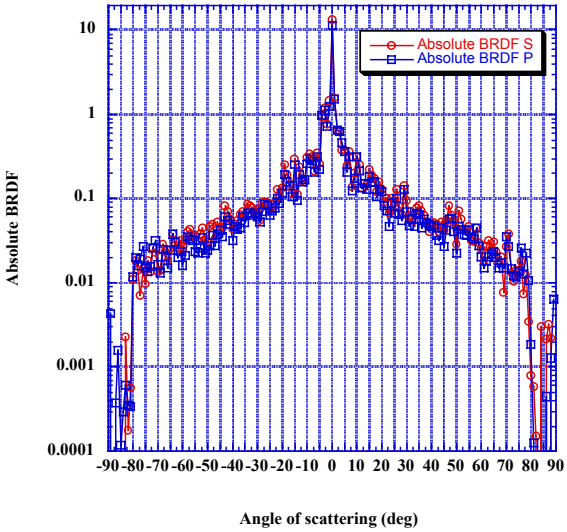

Figure 5. BRDF of a graphite sample at normal incidence.

References

1. Mekhontsev, S., Noorma, M., Hanssen, L., Preliminary realization of a spectral radiance scale in the range of 2.5 µm to 20 µm, *NEWRAD 2005*.
2. Mekhontsev, S., Khromchenko, V., Prokhorov, A., Hanssen, L., Emissivity evaluation of fixed point blackbodies, *Proc. TEMPMEKO 2004* (in print).
3. Mielenz, K.D., Saunders, R.D., and Shumaker, J., Spectro-radiometric Determination of Freezing Temperature of Gold, *J. Res. Natl. Inst. Stand. Techn. 95*, 49-67, 1990.

Radiometric Stability of a Calibration Transfer Standard Spectroradiometer and a Spectralon Sphere Illuminated Internally or Externally

D. F. Heath

Ball Aerospace and Technology Corp, Boulder, Co, USA

M. G. Kowalewski

Science Systems and Applications Inc., Lanham, MD, USA

Abstract. Results are presented on the radiometric stability of a calibration transfer standard spectroradiometer that has been calibrated repeatedly against NIST spectral irradiance standards, and it has been used in the radiometric calibrations of the Dutch Ozone Monitoring Instrument (OMI), and the Ball Aerospace & Technology Corporation (BATC) Ozone Mapping and Profiling Suite (OMPS), High Resolution Imaging Science Instrument (HiRISE), Ralph, and World View instruments. This spectroradiometer has also been used to investigate the radiometric stability of a 50.4 cm diameter Spectralon integrating sphere illuminated internally by quartz tungsten halogen (QTH) lamps or externally by xenon arc lamps.

Calibration Transfer Standard Spectroradiometer

A calibration transfer standard spectroradiometer (CTSS) was developed in the late 1990s at Research Support Instruments, Inc, (RSI). The system utilizes a series of narrow band ion-assisted-deposition filters in multiple filter wheels (23 filters) for spectral discrimination in the 250 nm-1000 nm region that is combined with either an IRD UVG-100 nitrided silicon photodiode for wavelengths < 400nm or a Hamamatsu 1337 silicon photodiode for wavelengths > 1000 nm.

The BATC/RSI transfer spectroradiometer has been calibrated for spectral irradiance against 12 different NIST standards of spectral irradiance at RSI, Technische Physiche Dienst (TPD), Goddard Space Flight Center (GSFC), and BATC with both IRD UVG-100 and Hamamatsu 1337 silicon photodiodes with the same set of narrow band hardened interference filters. The spectral radiance calibrations have been derived based on BRDF measurements of three Spectralon panel diffusers by Jim Butler's group at GSFC. One was measured in October 2000 and the other two were measured in October 2003.

A measure of the long-term radiometric stability of the CTSS is given by the standard deviation / mean if the spectral irradiance calibration constants. These data are shown in Figure 1. The measurements of the spectral irradiance calibration constants were made for NIST 1000 W FEL lamps which had been used for variable amounts of burn time.

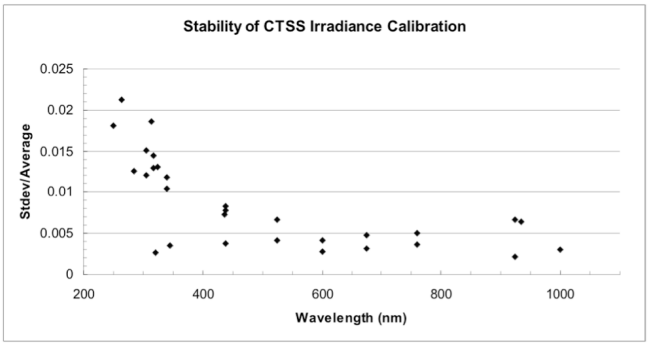

Figure 1. Standard deviation / average of the spectral irradiance calibration coefficients from 10 NIST 1000 W FEL lamps is given for the period from August 2001 to October 2004. There are multiple data points at the same wavelength due to the use of filters in two different filter wheel configurations. The uncertainty for wavelengths < 300 nm increases because of the large corrections for out-of-band contributions to the in-band signal.

Integrating Sphere Characterization

During early March 2005 as part of cooperative calibration program with GSFC, the CTSS, the BATC Labsphere 50.4 cm diameter Spectralon integrating sphere which had been modified by SphereOptics to accommodate a xenon arc for external illumination were calibrated at GSFC.

The purpose of this program was to calibrate the CTSS using GSFC NIST spectral irradiance standards and Spectralon panel diffusers with BRDF measurements from Jim Butler's group at GSFC, and to calibrate the BATC Spectralon sphere illuminated internally by QTH lamps or externally with the 150 W and 300 W Hamamatsu xenon arc sources. These cooperative calibration activities between GSFC and BATC are to be an important part of the radiometric calibration of OMPS and the subsequent participation of NIST in the OMPS calibration activities.

The results of the spectral radiance and irradiance calibrations of the CTSS are shown in Figure 2 as the ratios of the irradiance to radiance calibration constants which are invariant geometrical constants of the CTSS. The advantage of this approach is that once these ratios are determined accurately, one can then derive the spectral radiance calibration constants from the irradiance calibration coefficients and the ratios given in Figure 2. The irradiance calibration coefficients have a lower uncertainty than the radiance calibration coefficients.

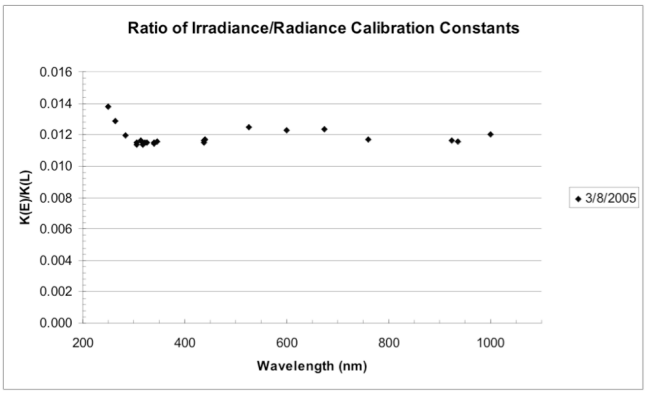

Figure 2. The ratio of the irradiance to the radiance calibration coefficients are geometrical invariants of the CTSS which to zero order is the effective solid angle of the CTSS.

After the completion of the one week of radiometric calibration activities at GSFC, all the equipment, including the integrating sphere and xenon arc sources, was shipped back to BATC for recalibration . A surprising feature of the recalibration of the BATC Spectralon sphere is shown in Figure 3.

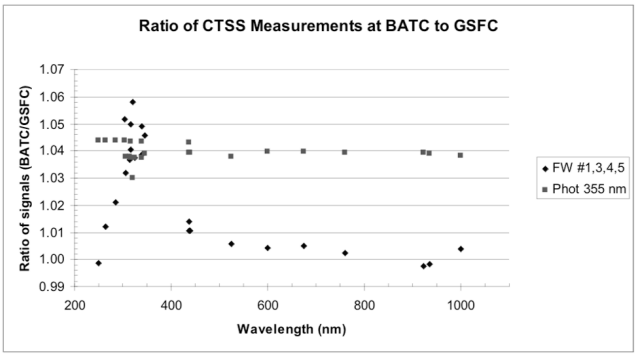

Figure 3. The ratios of the radiance calibration signals of the recalibration at BATC to the calibration signals recorded at GSFC are shown for the CTSS and a separate photometer which has a central wavelength of 355 nm. Each data point consists of 100 samples from a CTSS filter interleaved with 100 photometer samples.

These data indicate that either the sphere radiance data were abnormally low in the 300 nm to 400 nm wavelength region at GSFC or that the sphere radiance exhibited an abnormally high radiance subsequently at BATC.

Conclusions

Multiple calibrations over the course of three years has shown the CTSS to be radiometrically stable to 1.5 % or better at wavelengths greater than 300 nm. It should be noted that this uncertainty also includes any drift in the NIST 100W QTH FEL lamp standards of spectral irradiance associate with variable lamp burn times. The ratios of the irradiance to radiance calibration constants are geometrical invariants of the CTSS to within approximately 2 %.

The general conclusion is that large aperture radiance calibration source uncertainties can be reduced significantly by the combined use of National Laboratory spectral irradiance standards, derived spectral radiance standards and a calibration transfer standard spectroradiometer.

Session 3

Photolithography and UV Processing

NEWRAD 2005:

Improvements in EUV reflectometry at PTB

F. Scholze, C. Laubis, C. Buchholz, A. Fischer, S. Plöger, F. Scholz, H. Wagner, and G. Ulm
Physikalisch-Technische Bundesanstalt, Abbestraße 2-12, 10587 Berlin, Germany

Abstract. The development of EUV lithography is critically based on the availability of suitable metrological equipment. To meet the industry's requirements, the Physikalisch-Technische Bundesanstalt (PTB) operates an EUV reflectometry facility at the electron storage ring BESSY II. It is designed for at-wavelength metrology of full-sized EUVL optics with a maximum weight of 50 kg and a diameter of up to 550 mm. To meet the increasing demands of metrology for future lithography production tools, the measurement uncertainty was permanently reduced. For peak reflectance, an absolute uncertainty of 0.10 % is achieved with a reproducibility of 0.05 %. The uncertainty of 2 pm in the center wavelength is given mainly by the uncertainty for the reference wavelength of the Kr $3d_{5/2}$-5_p resonance. A long-term reproducibility of 0.8 pm has been demonstrated over a period of about 4 years. We have recently demonstrated repeatability below 0.06 pm. This good repeatability is important for the determination of the coating-thickness gradient in alpha-tool optics.

Introduction

Extreme Ultraviolet Lithography (EUVL) holds the key to the next generation of computer technology. EUVL imaging requires multilayer mirror optics being manufactured with extreme accuracy to ensure uniform illumination of the wafer plane and optimized throughput. As EUVL matures[1], the requirements for the accuracy of reflectivity and wavelength measurements become tighter. Especially the wavelength for the peak mirror reflectivity should be matched to better than 2.5 pm and the uniformity of reflectance should be better than 0.08 %[2]. In response to this demand, substantial improvements in the total measurement uncertainty and repeatability at the Physikalisch-Technische Bundesanstalt (PTB), Germany's national metrology institute, have been achieved[3]. PTB with its laboratory at the electron storage ring BESSY II, is the European centre of EUV radiometry and supports the national and European industry with high-accuracy at-wavelength measurements in the EUV spectral region, e.g. reflectance measurements as well as life-time and contamination studies[4,5]. The EUV reflectometer allows the measurement of mirrors with a diameter as large as 550 mm, a height of 230 mm, and a weight of up to 50 kg[6].

Experimental

The thickness of the Mo/Si multilayer coating of an EUV mirror can be determined from the number of layers which is known from the coating process, and the period which can be determined by reflectometry. This consideration is of practical importance because in the production process, the mirror substrate is polished to the required figure, and afterwards the multilayer coating with a total thickness of about 200 nm is deposited with a required accuracy for the final figure of 0.2 nm[1]. Therefore, we further investigated the uncertainty contributions in the wavelength measurement. The wavelength uncertainty attributed to the monochromator beamline is published elsewhere[7]. The quantity to be characterized, however, is the double-layer thickness d of the coating. This is related to the wavelength λ by the Bragg equation $\lambda = 2 \cdot n \cdot d \cdot \cos(\Theta)$, with n the (average) index of refraction, and Θ the angle of incidence with respect to the normal. Thus, thermal expansion also contributes to the measurement uncertainty in the EUV reflectometer. The temperature of the samples during measurement is between 25 °C and 30 °C. We measured the spectral reflectance of a Mo/Si multilayer for five temperatures in the range from 27 °C to 55 °C, see Fig. 1. The contribution of pure signal statistics to the uncertainty of the centre wavelength determination is only 0.06 pm (1σ). A 2σ-range is indicated by the error bars. The suspected linear relation holds within this uncertainty. The line shows a linear fit with a thermal expansion coefficient of $8.1(4)10^{-6}$ K^{-1}.

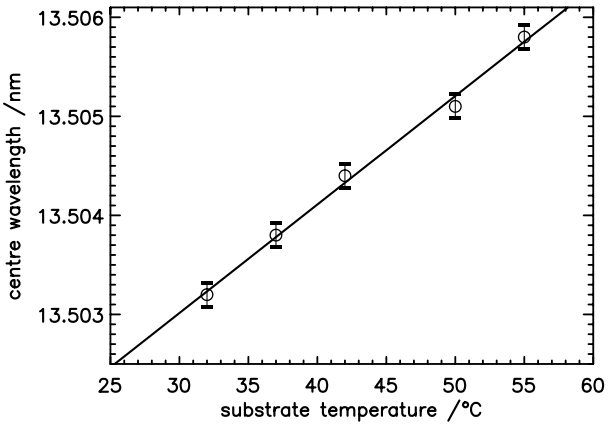

Figure 1. Measured shift of the centre wavelength of a mirror with 60(Mo/B4C/Si/C) layers as a function of substrate temperature.

Long-term stability of optical components is one of the key issues for the development of EUV lithography systems. To detect changes that are small enough to extrapolate the measurements to a system-lifetime of several thousands of hours, a high reproducibility of the measurement and a high stability of the (un-illuminated) mirrors themselves is required. Therefore, PTB regularly measures the reflectance of a set of reference mirrors to detect any drifts in the measurements. These mirrors are coated with magnetron sputtering by the Fraunhofer Institute for Material and Beam Technology in Dresden, Germany. The peak reflectance and centre wavelength of these mirrors were measured for a period of 40 months. Fig. 2 shows measurements for one of the mirrors with diffusion barriers in March 2002 and August 2004. The spectral reflectance curves are nearly identical. It was,

however, recently demonstrated that the photoelectron current from the mirror surface[8] can be used to determine the thickness of surface layers, e.g. the build-up of carbon contamination[9]. The photo yield curves obtained are also shown in Fig. 2. The phase-shift of the photocurrent curve indicates an increase in top-layer thickness[3] by about 0.2 nm. Fig. 3 shows the shift in measured peak wavelength for a set of six mirrors and a period of 40 months. Tab. 1 gives a compilation of the present status of the measurement uncertainties at PTB.

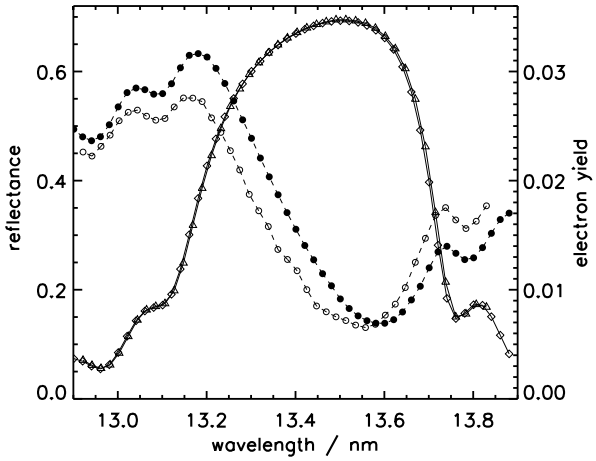

Figure 2. Reflectance of a mirror measured in March 2002 (triangels) and August 2004 (diamonds), left scale. The circles (open and closed, respectively) are the photocurrent signal, right scale. The reflectance curve is almost identical; the phase-shift of the photocurrent curve indicates an increase in top-layer thickness by about 0.2 nm.

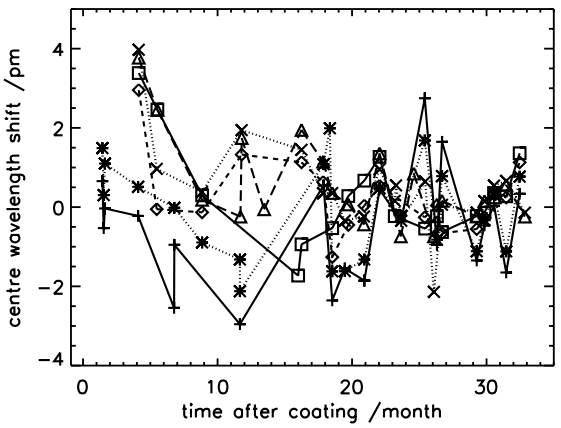

Figure 3. Measured shift of the centre wavelength of six EUV mirrors coated with diffusion barrier in December 2001. Data are normalized to the mean. For the four most homogeneous mirrors, the standard deviation of the measurements after month 18 is 0.8 pm.

Peak reflectance	**Uncertainty contribution u /%**
Stability of normalized intensity	0.02
Inhomogeneity of the detector	0.04
Higher diffraction orders	0.02
Diffuse scattered light	0.08
Total uncertainty of peak reflectance	**0.10**
Peak wavelength	**Uncertainty contribution u /pm**
Repeatability of wavelength	0.06
Reproducibility of wavelength (reference to Be K-edge)	1.1
Kr resonance wavelength	1.6
sample temperature (ΔT = 5 K)	0.6
incidence angle ($\Delta\Theta = 0.02^o$ at $\Theta = 1.5^o$)	0.1
Total uncertainty of peak wavelength	**2.0**

Table 1. Compilation of uncertainty contributions for the measurement of the peak reflectance (upper part) and peak wavelength (lower part) of Mo/Si multilayer mirrors.

References

1 Meiling, H., Banine, V., Kuerz, P., Harned, N., Progress in the ASML EUV program, *Proc. SPIE* 5374, 31 - 42, 2004

2 Gullikson, E.M., Mrowka, S., Kaufmann, B.B., Recent developments in EUV reflectometry at the Advanced Light Source, *Proc. SPIE* 4343, 363 – 373, 2001

3 Scholze, F., Laubis, C., Buchholz, C., Fischer, A., Plöger, S., Scholz, F., Wagner, H., Ulm, G., Status of EUV Reflectometry at PTB, *Proc. SPIE* 5751, 2005, in press

4 Klein, R., Gottwald, A., Scholze, F., Thornagel, R., Tümmler, J., Ulm, G., Wedowski, M., Stietz, F., Mertens, B., Koster, N., Elp, J.V., Lifetime testing of EUV optics using intense synchrotron radiation at the PTB radiometry laboratory, *Proc. SPIE* 4506, 105-112, 2001

5 Scholze, F., Beckhoff, B., Brandt, G., Fliegauf, R., Gottwald, A., Klein, R., Meyer, B., Schwarz, U., Thornagel, R., Tümmler, J., Vogel, K., Weser, J., Ulm, G., High-accuracy EUV metrology of PTB using synchrotron radiation, *Proc. SPIE* 4344, 402-413, 2001

6 Tümmler, J., Brandt, G., Eden, J., Scherr, H., Scholze, F., Ulm, G., Characterization of the PTB EUV reflectometry facility for large EUVL optical components, *Proc. SPIE* 5037, 265-273, 2003

7 Scholze, F., Tümmler, J., Ulm, G., High-accuracy radiometry in the EUV range at the PTB soft X-ray radiometry beamline, *Metrologia* 40, S224-S228, 2003

8 Scholze, F., Laubis, C., Buchholz, C., Fischer, A., Plöger, S., Scholz, F., Wagner, H., Ulm, G., High-accuracy EUV reflectometry at PTB, 3rd EUVL Symposium, Miyazaki Japan (2004)

9 van de Kruijs, R., Zoethout, E., Louis, E., Yakshin, A., Nedelcu, I., Bijkerk, F., Muellender, S., Enkisch, H., Sipos, G., Wedowski, M., Weiss, M., Mo/Si multilayers for EUVL, PXRMS 2004: 7th International Conference on the Physics of X-Ray Multilayer Structures, Sapporo 2004

Measuring pulse energy with solid state photodiodes

R. E. Vest, S. Hill, and S. Grantham
National Institute of Standards and Technology, Gaithersburg, MD, USA

Abstract. With the advent of extreme ultraviolet lithography (EUVL) the measurement of the energy contained in pulses of short-wavelength radiation is becoming increasingly important. Even low average power sources can deliver pulses of radiation with high peak power to a photodiode. For example, a 150 W EUVL production source operating at 10 kHz and 100 ns pulse length delivers a peak power of 150 kW to the detector, easily enough to drive the detector into saturation. Recently, we have reported on the non-linearity of the responsivity of Si photodiodes under pulsed illumination and developed a model that predicts the observed saturation behavior, including the dependence on reverse bias. Here we extend the characterization of solid-state photodiodes from 8 ns pulses to pulse lengths of 1 μm and examine the effect of power density (illumination area) on the saturation behavior. The model we developed has been used to validate the calibration in pulsed radiation of an EUVL source diagnostic instrument by comparison to a calibration under cw conditions at a synchrotron.

Vacuum ultraviolet quantum efficiency of large-area SiC photodiodes

R. E. Vest
National Institute of Standards and Technology, Gaithersburg, MD, USA

Sahid Aslam
GoddardSpace Flight Center, NASA, Greenbelt, MD, USA

Abstract. Wide-bandgap semiconductors show great promise for the development of solar-blind, solid-state photodetectors. The wide energy gap between the valance and conduction bands in these materials gives them an inherent cutoff in responsivity in the ultraviolet. By contrast, a traditional Si photodiode has a responsivity cutoff on the infrared part of the spectrum. Insensitivity to visible and infrared radiation is a great aide to measurements where the ultraviolet signal is much less than the visible and IR background. Such applications include solar observations and extreme ultraviolet lithography. SiC is a potentially useful material because of its wide bandgap and the similarity to Si – the processing techniques that have been developed for Si photodiode manufacture are applicable to SiC manufacture. Furthermore, SiC is expected to be resistant to radiation-induced damage. To date, SiC detectors have been available with small active areas due to the difficulty of growing high quality GaN crystals. Here, we present quantum efficiency measurements in the vacuum ultraviolet (5 nm to 254 nm) of large area SiC photodiodes with 100 mm^2 active area.

Spatial Anisotropy of the Exciton Resonance in CaF_2 at 112 nm and its Relation to Optical Anisotropy in the DUV

M. Richter, A. Gottwald
Physikalisch-Technische Bundesanstalt, Berlin, Germany

M. Letz
Schott Glas, Mainz, Germany

Abstract. Excimer lasers are widely used for industrial applications such as photolithography of semiconductor devices. The basic optical material for the excimer-laser wavelengths in the deep ultraviolet is calcium fluoride which shows an unexpected optical anisotropy at 157 nm. In this context, we have measured the spatial anisotropy of the exciton resonance at 112 nm by precision reflection measurements using dispersed synchrotron radiation on oriented samples of high purity. The results are discussed in terms of the complex dynamic dielectric function and explain the optical anisotropy by the interaction of radiation with the cubic structure of a perfect crystal.

Introduction

Fluoride crystals are strongly ionic and have the largest band gaps known for crystalline solids. As a consequence, they are transparent even in the wavelength region of deep ultraviolet (DUV) radiation and used for DUV optics. Recently, the effect of an optical anisotropy for calcium fluoride (CaF_2) has been observed at 157 nm which is of great importance for DUV lithography (*Burnett et al.* 2001). Already the measured weak birefringence of $\Delta n/n \approx 10^{-6}$ of the refractive index considerably influences the design of imaging optics.

Due to its cubic symmetry, it is generally presumed that the CaF_2 crystal shows isotropic optical properties. However, strongly ionic crystals show deep excitonic bound states. The most pronounced one in CaF_2, the Γ-exciton, is known to arise at 11.1 eV, yielding to a strong and narrow absorption structure at a wavelength of about 112 nm. Close to such a strong absorption line, an optical anisotropy can result from a slight deviation of the cubic symmetry, due to the incident radiation field even at optical wavelengths much larger than the lattice constant. The effect of optical anisotropy in the vicinity of a narrow absorption line was formulated by *Ginzburg* 1958. The effect is well established at optical wavelengths and usually called 'spatial dispersion induced birefringence'.

In this work we describe a direct measurement of the spatial anisotropy of the narrow absorption line at 112 nm (*Letz* et al. 2003). The experiments were performed at the UV and VUV beamline for detector calibration and reflectometry in the Radiometry Laboratory of the Physikalisch-Technische Bundesanstalt at the electron storage ring BESSY II on extremely pure CaF_2 samples with surface orientations in the (111) and (100) directions of the crystals. The reflectance of the samples was measured in a near-normal incidence geometry.

Results

The results of the reflection measurements are shown in Fig. 1. When comparing the data of the two different samples, a small but significant shift of about 0.2 nm becomes apparent, the resonance structure of the sample with (111) surface orientation being shifted towards smaller wavelengths. To verify the experimental significance of this small shift, the reproducibility of the wavelength was tested by simultaneously recording resonance absorption lines of Ar in a gas cell.

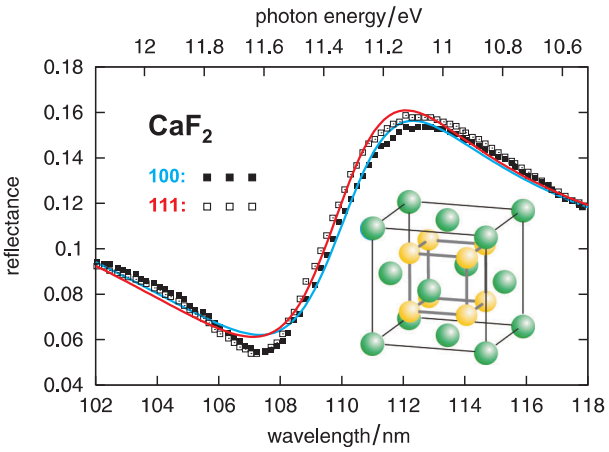

Figure 1. Experimental data (symbols) and fit (lines) of the normal-incidence reflectance around the Γ-exciton of CaF_2 for a (100) and (111) surface (*Letz* et al. 2003).

For interpreting our experimental data with regard to exciton position and lifetime, we applied a least squares fitting algorithm. The resulting fit curves are also shown in Fig. 1. For the exciton positions one obtains for the different crystal orientations:

(100): $\eta\omega_0 = 11.11(1)$ eV $\quad \lambda_0 = 111.6(7)$ nm
(111): $\eta\omega_0 = 11.13(1)$ eV $\quad \lambda_0 = 111.4(7)$ nm

Discussing the results in terms of the complex dynamic dielectric function it can be demonstrated that the direction of the shift for the exciton resonance as measured in the present work is consistent with the sign of the optical anisotropy as measured by *Burnett et al.* 2001 at 157 nm.

References

Burnett, J.H., Levine, Z.H., Shirley, E.L., Phys. Rev. B, 64, 241102R, 2001.
Ginzburg, V.L., JETP, 34, 1593, 1958.
Letz, M., Parthier, L., Gottwald, A., Richter, M., Phys. Rev. B, 67, 233101, 2003

Comparison of spectral irradiance responsivity scales of TKK and NIST in the UVA region

J. Envall[1], B.C. Johnson[2], P. Kärhä[1], T. Larason[2], and E. Ikonen[1,3]

[1]Metrology Research Institute, Helsinki University of Technology, P.O.Box 3000, FI 02015 TKK, Finland. E-mail: jouni.envall@tkk.fi

[2]Optical Technology Division, NIST, Gaithersburg, MD 20899-8441, USA.

[3]Centre for Metrology and Accreditation (MIKES), P.O.Box 239, FI-00181 Helsinki, Finland.

Abstract. This paper presents the results of a bilateral comparison of spectral irradiance responsivity scales of Helsinki University of Technology (TKK, Finland) and the National Institute of Standards and Technology (NIST, USA). The comparison was performed at UVA wavelengths by measuring the spectral irradiance responsivity of a broadband UVA detector at both laboratories. The results at the passband coincided within 1%, which is well within measurement uncertainties.

Introduction

Broadband UV detectors find use in several fields of science and technology. Calibration of such detectors is a complicated task, which requires fundamental understanding of the properties of the detector, as well as of those of the radiation source. The calibration of a broadband detector is always source dependent; it applies only to the source that was used in the calibration, or to other sources with similar spectral shape.[1] Measuring the spectral irradiance responsivity of the detector enables determination of its calibration factor for any radiation source whose spectral shape is known.[1,2]

Measurement setup at TKK

The measurement setup for the measurement of spectral irradiance responsivity at TKK consists of a 450-W xenon source (Xe900, Edinburgh Instruments Ltd) and a single grating monochromator (TMc300, Bentham Instruments Ltd). The use of an intense UV source, together with a single grating monochromator, ensures the output power to be sufficient for spectral measurements with detectors of low sensitivity. The use of a single grating monochromator, instead of a double grating monochromator, increases the level of stray light. However, studies made so far, including the comparison measurement described in this paper, indicate that the level of stray light is not significant in the UVA region. Further studies are being performed in order to characterize the effect of stray light in measurements at shorter wavelengths.

Comparison between TKK and NIST

In May 2003, TKK and NIST made a bilateral comparison of spectral irradiance responsivity scales. A broadband UVA detector, labeled FR1, was used in the comparison. The detector, property of NIST, had been measured at NIST before it was brought to TKK, where it was measured with the measurement setup described above. Figures 1 and 2 show the results.

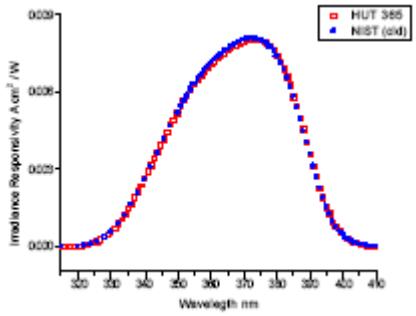

Figure 1. Measured spectral irradiance responsivity of FR1.

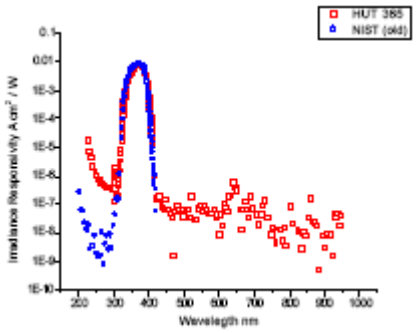

Figure 2. Measured spectral irradiance responsivity of FR1, shown on a logarithmic scale.

To compare the results between the two laboratories, integrated responses were calculated. These values differed less than 1%. The calculated effective wavelengths differed 0.04 nm.

Conclusions

The results of this comparison measurement show that the spectral irradiance responsivity scales of TKK and NIST are in agreement in the UVA region. The difference between the measured responsivities is well within measurement uncertainties, TKK uncertainty alone is 2% (k=2). The larger difference in measured responsivities at shorter wavelengths, clearly noticeable in Figure 2, is most likely due to stray light. The stray light properties of the TKK setup are to be carefully examined. The slit scattering function of the monochromator has been measured with six laser wavelengths. These data will be used in the future to estimate the magnitude of the stray light effect in the measurements, using the method described by Brown

et al.[3]

References

1. G. Xu and X. Huang, “Characterization and calibration of broadband ultraviolet radiometers,” *Metrologia* **37**, 235-242 (2000).
2. P. Kärhä, ”Calibration and intercomparison issues with broadband UV meters,” *UVNews* **7** 29-34 (2002), available on-line in http://metrology.tkk.fi/uvnet/reports.htm
3. S.W. Brown, B.C. Johnson, M.E. Feinholz, M.A. Yarbrough, S.J. Flora, K.R. Lykke, and D.K. Clark, ”Stray-light correction algorithm for spectrographs,” *Metrologia* **40**, S81-S84 (2003).

Session 4

Remote sensing

Solar Radiometry from SORCE

G. Kopp
Laboratory for Atmospheric and Space Physics, University of Colorado, Boulder, CO, USA

Abstract. The SOlar Radiation and Climate Experiment (SORCE) is a NASA mission launched in early 2003 to measure total and spectral irradiance from the Sun. Three instruments measure solar spectral irradiances from 0.1 to 2700 nm, while a fourth monitors total solar irradiance. The instruments provide daily irradiance measurements, from which solar activity and irradiance variations can be correlated on short time scales and Earth climate may be correlated on long time scales. I present an overview of the SORCE instruments and their different approaches to long-term, space-based solar radiometry.

SORCE Radiometers

The SOlar Radiation and Climate Experiment (SORCE) is a NASA mission to monitor solar irradiance inputs to the Earth's atmosphere. Launched in January 2003 into a low Earth orbit, this spacecraft monitors the Sun during the daylight portion of each 95-minute orbit. Mission operations are done from the University of Colorado's Laboratory for Atmospheric and Space Physics (LASP), and data are available via the web at both LASP (http://lasp.colorado.edu/sorce) and the NASA DAAC (http://disc.gsfc.nasa.gov/SORCE). The four solar irradiance monitoring instruments on the SORCE are described below.

TIM The Total Irradiance Monitor (TIM) is an ambient temperature, electrical substitution solar radiometer intended to achieve 100 parts per million (ppm) combined standard uncertainty in total solar irradiance (TSI). The TIM contains four electrical substitution radiometers (ESRs), providing redundancy and tracking instrument degradation due to solar exposure. Each ESR is electrically heated to maintain constant temperature while a shutter modulates sunlight through a precision aperture and into the ESR's absorptive nickel-phosphorus (NiP) cavity. The modulation in electrical heater power needed to maintain an ESR's temperature as its shutter modulates incident sunlight determines the radiative power absorbed by that ESR's cavity. Phase sensitive detection of this heater power, combined with knowledge of the aperture area over which the sunlight is collected, yields TSI in ground processing. The instrument has demonstrated extremely low noise levels due to its phase sensitive detection system and active thermal stability. This instrument continues the 26-year record of space-borne TSI measurements, and is a predecessor to the TIMs selected for flight on the future NPOESS missions.

SIM The Spectral Irradiance Monitor (SIM) is similarly an ambient temperature ESR using a NiP absorptive coating, although this instrument is designed to work at much lower power levels to measure solar spectral irradiance (SSI) over the wavelength range 200 to 2700 nm. The two SIM ESRs are mounted behind dual, redundant Fèry prism spectrometers, allowing degradation tracking. The instrument's spectral resolution varies from 0.2 to 30 nm with intended combined standard uncertainty of 300 ppm. This newly-designed instrument provides the first long-duration spectral irradiance measurements over an extended wavelength range encompassing approximately 95% of the solar irradiance.

SOLSTICE The Solar Stellar Irradiance Comparison Experiment (SOLSTICE) measures the spectral range from 120 to 300 nm with a spectral resolution of 0.1 to 0.2 nm and a combined standard uncertainty of 3-6%. This evolution of the highly successful UARS SOLSTICE consists of two fully-redundant grating spectrometers to monitor the highly-variable ultraviolet solar irradiance. SOLSTICE has the unique capability of observing bright blue stars with the same optics and detectors used for solar measurements, and uses an ensemble of these stars as a long term relative calibration standard.

XPS The X-ray Photometer System (XPS) measures the extreme ultraviolet solar irradiance from 0.1 to 31 nm with a spectral resolution of 7 to 10 nm while an additional channel monitors Lyman-α. The XPS's combined standard uncertainty is 12%, with a relative precision of 2%/yr. This instrument is of nearly identical design to the XPS on NASA's TIMED mission, and consists of a filter wheel photometer system using silicon diodes behind thin-film filters. The XPS's 12 photometers include 5 for daily XUV measurements, 1 for Lyman-α, 3 for XUV calibrations, and 3 for window calibrations. The SORCE XPS has observed over 800 solar flares to date.

Acknowledgments The author gratefully acknowledges contributions from the entire SORCE team, and particularly from mission PI Dr. Rottman and Instrument Scientists Drs. Harder, Lawrence, McClintock, and Woods. The SORCE mission is funded by NASA contract NAS5-97045.

References

Harder, J., Lawrence, G., Fontenla, J., Rottman, G., and Woods, T., "The Spectral Irradiance Monitor I: Scientific Requirements, Instrument Design, and Operation Modes," *Solar Phys.*, 2005, in press.

Kopp, G. and Lawrence, G., "The Total Irradiance Monitor (TIM): Instrument Design," *Solar Phys.*, 2005, in press.

McClintock, W., Rottman, G., and Woods, T., "Solar Stellar Irradiance Comparison Experiment II (SOLSTICE II): Instrument Concept and Design," *Solar Phys.*, 2005, in press.

Woods, T., Rottman, G., Harder, G., Lawrence, G., McClintock, B., Kopp, G., and Pankratz, C., "Overview of the EOS SORCE Mission," SPIE Vol. 4135, 2000, pp. 192-203.

Woods, T., Rottman, G., and Vest, R., "XUV Photometer System

(XPS): Overview and Calibrations," *Solar Phys.*, 2005, in press.

Inter-comparison Study of Terra and Aqua MODIS Reflective Solar Bands Using On-orbit Lunar Observations

X. Xiong

Sciences and Exploration Directorate, NASA/GSFC, Greenbelt, MD 20771, USA

J. Sun

Science Systems and Applications, Inc., 10210 Greenbelt Road, Suite 600, Lanham, MD 20706, USA

W.L. Barnes and B. Guenther

University of Maryland, Baltimore County, Catonsville, MD 21250, USA

Abstract. Long-term Earth-observing, climate, and environmental data records are often built with measurements made by different sensors, including those designed at different time and possibly with different technologies. In order to produce high quality climate data records (CDR), all the sensors must be fully calibrated and characterized, pre-launch and on-orbit, with consistent traceability to the well-established national or international standards. Ideally each sensor's mission should be overlapped for a period of time by the sensors that proceed and follow its mission. Consequently the capability and quality of inter-comparison of measurements made by different sensors are of great importance. In this paper we present an approach that could be used by most Earth-observing sensors to track their long-term data (measurements) stability and to ensure the capability of inter-comparison with other sensors through their on-orbit lunar observations and its application to the Moderate Resolution Imaging Spectroradiometer (MODIS).

The MODIS) is one of the key instruments for the NASA's Earth Observing System (EOS). It is currently operated on-board the EOS Terra and Aqua spacecraft launched in December 1999 and May 2002 respectively [1,2]. Each MODIS instrument has 36 spectral bands. Bands 1-19 and 26 are the reflective solar bands (RSB) covering wavelengths from 0.41 to 2.2 micrometers and bands 20-25 and 27-36 are the thermal emissive bands (TEB) with wavelengths from 3.7 to 14.4 micrometers. It makes observations at three nadir spatial resolutions: 0.25km (bands 1-2), 0.5km (bands 3-7), and 1km (bands 8-36) over a wide field-of-view (FOV) range. The sensor's in-flight calibration and characterization are primarily provided by a set of the on-board calibrators that include a solar diffuser (SD) panel, a solar diffuser stability monitor (SDSM), a blackbody (BB) panel, and a spectro-radiometric calibration assembly (SRCA) [3-5].

For the MODIS reflective solar bands (RSB), the specified calibration uncertainty requirements are ±2% in reflectance and ±5% in radiance. The RSB on-orbit calibration is performed regularly using the solar diffuser (SD) and solar diffuser stability monitor (SDSM) system. In addition both Terra and Aqua MODIS have been making monthly lunar observations through the space view (SV) port. The initial objective of this operation was to track the sensor's RSB radiometric stability. For this purpose, the lunar observations by each sensor have been planned to be approximately of the same lunar phase angle via spacecraft roll maneuvers. Limiting the lunar phase angle range for the long-term stability trending significantly reduces the uncertainty in the corrections to the lunar viewing geometry difference [6,7]. In addition to the viewing geometry difference, other factors, such as the spectral response function difference (center wavelength and band width) and over sampling effect must be considered.

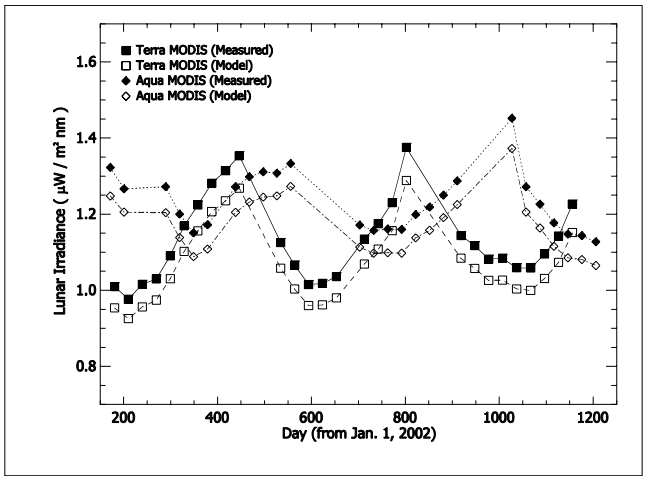

Figure 1. Measured lunar irradiance by Terra and Aqua MODIS band 3 (center wavelength of 0.47 micrometer) and corresponding modeling results under the same viewing geometry as the measurements.

This paper will focus on the methodologies developed for and the results derived from inter-comparison studies of Terra and Aqua MODIS reflective solar bands (RSB) calibration using their on-orbit lunar observations (over five years from Terra MODIS and three years form Aqua MODIS). Figure 1 shows the measured lunar irradiance by Terra and Aqua MODIS band 3 (center wavelength at 0.47 micrometer) using their lunar observations over the same period. It includes the modeling results computed under the same observation conditions. The sensor measured lunar irradiance by each spectral band or channel should be normalized to the modeling results before comparing with each other. The lunar observation results show that both Terra

and Aqua MODIS have been consistently calibrated to within 1.0% and that the overall long-term stability of each sensor is better than 0.3%. We have also applied this method to inter-compare with other sensors, such as the SeaWiFS and MISR.

Acknowledgments

The authors would like to thank Hugh Kieffer and Tom Stone (USGS) for their technical discussions and support in providing MODIS lunar modeling data.

References:

1. Barnes, W.L., V.V. Salomonson, MODIS: A global image spectroradiometer for the Earth Observing System in *Critical Reviews of Optical Science and Technology*, CR47, 285-307, 1993
2. Barnes, W.L., V. V. Salomonson, B. Guenther, X. Xiong, Development, Characterization, and Performance of the EOS MODIS Sensors in *Proceedings of SPIE – Earth Observing Systems VIII*, 5151, 337-345, 2003
3. Xiong, X., K. Chiang, J. Esposito, B. Guenther, W.L. Barnes, MODIS On-orbit Calibration and Characterization in *Metrologia* 40 89-92, 2003
4. Xiong, X., K. Chiang, B. Guenther, W.L. Barnes, MODIS Thermal Emissive Bands Calibration Algorithm and On-orbit Performance in *Proceedings of SPIE – Optical Remote Sensing of the Atmosphere and Clouds III*, 4891, 392-401, 2003
5. Xiong, X., J. Sun, J. Esposito, B. Guenther, W.L. Barnes, MODIS Reflective Solar Bands Calibration Algorithm and On-orbit Performance in *Proceedings of SPIE – Optical Remote Sensing of the Atmosphere and Clouds III*, 4891, 95-104, 2003
6. Sun J., X. Xiong, B. Guenther, W.L. Barnes, Radiometric stability monitoring of the MODIS reflective solar bands using the Moon in *Metrologia* 40, 85-88, 2003
7. Kieffer H.H., T.C. Stone, The Spectral Irradiance of the Moon in *Astronomical Journal*, 6, 129:2887-2901, 2005

The Solar Bolometric Imager – Recent Results and Future Plans

Peter Foukal
Heliophysics, Inc. Nahant, MA USA

Pietro Bernasconi, Harry Eaton, Barry Labonte and David Rust
Applied Physics Laboratory, Johns Hopkins University, Laurel, Maryland, USA.

The Solar Bolometric Imager is a novel photometric instrument developed to produce images of the Sun (or other scenes) in broad band light with non-selective spectral response. It consists of a 30-cm aperture Dall-Kirkham telescope with all - reflecting, uncoated optics enabling unfiltered imaging of the Sun. The detector is a 320 x 240 element, barium strontium titanate, un-cooled thermal array. The detector surface was coated with a thin layer of gold black to produce spectrally flat response over the wavelength range between at least 0.3 – 2.6 microns containing over 94% of the solar irradiance.

The photometric response of the chopped ferro-electric array is approximately linear at the lower end of the operating range, becoming about 10% sub-linear at higher illumination levels. This non-linearity is corrected using laboratory and in-flight calibrations.The SBI's purpose is to measure the photometric contrast of localized solar structures like sunspots, compared to their immediate surroundings, to a precision of a few percent. There is no requirement on the absolute accuracy of the SBI response. Laboratory measurements indicate that the required stability of relative response is met, at least over the limited duration of a balloon flight.

After development of a ground based prototype at CRI, Inc. (Foukal and Libonate, 2001), the SBI was modified for balloon flight at the Johns Hopkins University/Applied Physics Laboratory (Bernasconi et al., 2004), and successfully flown to an altitude of 109,000 ft on Sept 1, 2003, from the National Scientific Balloon Facility at Ft. Sumner, NM. This one-day flight produced the first broad-band photometric contrast measurement of solar magnetic faculae (Foukal et al., 2004), which make the dominant contribution to solar irradiance variation. It also produced the first measurement of photospheric limb darkening in broad-band light. These facular contrast measurements have recently been used to produce the first empirical reconstruction of solar irradiance variation with no free parameters. This reconstruction shows that spots and faculae can account for the amplitude of the radiometrically observed irradiance variation,at least on solar rotational time scales (Foukal et al., 2005).

The balloon-borne SBI being readied for its launch on Sept 1, 2003.

The SBI is presently being prepared at JHU/APL for a longer NASA balloon flight from Antarctica in late 2006. At the same time, its suitability for space flight is also being investigated. The results so far indicate that the SBI would provide an ideal complement to radiometers on a future space-borne experiment optimized to measure and also image total irradiance variations to the highest precision level achievable in next-generation pyrheliometry. Radiation testing indicates that detector response is unaffected up to an integrated dose of at least 4 krad, thus compatible with a mission lifetime of about 4 yrs on a 28 degree orbit at an altitude of 600 km, with reasonable shielding. Chopped detectors are increasingly gaining space-flight heritage thanks to NASA missions like SWAS and SST. Modeling indicates that, if necessary, a more compact SBI of smaller aperture could be used without much loss in

performance. We plan to measure the SBI spectral response to check the +/- 10% flatness over its broad wavelength range, calculated from our previous optical modeling.

References

Bernasconi, P., et al., The Solar Bolometric Imager, *Adv. Sp. Res*. 33, 1746, 2004.

Foukal,P., Libonate,S., Total – light imager with flat spectral response for solar photometric measurements, *Appl. Opt*., 40,1138,2001

Foukal, P., et al., Broad-band measurements of facular contrast using the solar bolometric imager, *Ap.J. Letts*, 611,57, 2004

Foukal,P., Bernasconi,P., Walton,S., Can changing sunspot and facular areas reproduce the amplitude of total irradiance variations? *AGU Spring Meeting New Orleans, May 2005*,abstract SH22B-02.

On measuring the radiant properties of objects of observations for the Global Earth Observation System of Systems (GEOSS)

V.N. Krutikov

Federal Agency on Technical Regulating and Metrology, Moscow, Russia

V.I. Sapritsky, B.B. Khlevnoy, B.E. Lisiansky, S.P. Morozova, S.A. Ogarev, A.S. Panfilov, M.K. Sakharov, M.L. Samoylov

All-Russian Institute for Opto- Physical Measurements (VNIIOFI), Moscow, Russia

G. Bingham, T. Humpherys, A. Thurgood

Space Dynamics Laboratory, Logan, Utah, USA

V.E. Privalsky

Vega International Inc., New York, NY, USA

Abstract. The report describes major radiometric calibration tasks arising in connection with the upcoming implementation of the GEOSS programs, including the unity of measurements and their traceability to national and international standards. The new stringent requirements for the accuracy and repeatability of radiometric observations within the GEOSS program and in other areas call for new approaches to both ground and space calibration of radiometric instruments some of which are described in this report.

The task of developing the GEOSS to support a stable development of the world community has been advanced at the beginning of this century at the highest political level by representatives of more than 50 countries and more than 30 international organizations. The GEOSS program plan defines major areas of GEOSS data application, implementation milestones and organizational structure, and involves extensive observations within the optical spectral bandwidth.

In addition to providing imagery data, planned GEOSS instruments can measure radiance, reflective properties, and radiant temperature of objects of observations. Such measurements require complete metrological support for the instruments. In general, the data supplied by various GEOSS subsystems will be used by different participants of the program under the condition of their unified standard presentation (formats, geolocation, etc.). Also, the unity of data acquired by different subsystems (traceability to national and international standards) is required for many applications such as climatology, meteorology, and environmental monitoring. This important task has not yet been adequately included into the 10-yr plan; therefore, measures need to be taken by the national metrological organizations to advance the idea and implement it at a proper international level.

The instrument designers are required to supply the program with instruments that are capable of providing high-quality data. Within the wide spectrum of the GEOSS program applications, the highest requirements for the long-term repeatability and accuracy of the optical instrumentation are imposed by climatology, which uses data accumulated over the time spans on the order of decades. According to the recently documented requirements for instrument calibrations [NISTIR 7047], the required values are, respectively:

- 0.02% per decade and 0.1% within the spectral band from 0.2 μm to 3 μm, and
- 0.01K per decade and 0.1K within the spectral band from 3 μm to 15 μm.

A necessary condition for meeting these requirements and ensuring the unity of observations is a high-level support for the methodology basis and the equipment used for both ground and space-borne radiometric calibrations. The methodology basis includes such components as unified proper terminology, common definitions of measurands and respective physical units, calibration techniques and estimation of measurement accuracy as a part of the calibration procedure.

The ground calibration tasks presented in this report include better calibration standards, techniques and means to transfer radiometric quantity dimension from standard sources to the instruments that are being calibrated, calibration installations, and international inter-comparisons of radiometric standards. These activities should result in universal, stable and highly accurate scales of radiometric quantities. The report describes the efforts that are being undertaken at

- the All-Russian Research Institute for Opto-Physical Measurements (VNIIOFI), with

the purpose of creating highly stable and highly accurate blackbodies built on the basis of phase transitions of pure metals or eutectic alloys, and

- the Space Dynamics Laboratory (SDL), with the purpose of designing high-accuracy thermo-vacuum installation for calibration of the thermal band IR sensors.

Two cryogenic vacuum chambers have been designed at SDL. The chambers are multi-functional and allow one not only to transfer the unit dimension but also to measure all the necessary output radiometric and other optical properties of the instrument that is being calibrated.

The unique reproducibility of radiometric properties of the blackbodies designed at VNIIOFI is based upon the phase transition of eutectic alloys (at 0.2 μm to 3 μm) or pure metals (at 3 μm to 15 μm); therefore, such blackbodies can be widely used to implement uniform and stable radiometric scales for GEOSS and for other programs involving radiometric observations from space.

The current and prospective techniques of in-flight radiometric calibration discussed in the report include an international radiometric standard space-borne facility as discussed earlier within the Russian/American Space Metrology Working Group. We believe that a unification of all GEOSS subsystems into a single high-quality universal data-producing system can be achieved if the problems that have been discussed in this report are solved by the joint efforts of all participants of the program.

References

NISTIR 7047. Satellite Instrument Calibration for Measuring Global Climate Change. *US Department of Commerce.* 2004.

A Model of the Spectral Irradiance of the Moon for Calibration of Earth-orbiting Spacecraft Instruments

H. Kieffer
Celestial Reasonings

T. Stone
US Geological Survey

Abstract. Observations of the Moon from an observatory designed and operated specifically for determination of absolute lunar photometry have been used to develop a spectral irradiance model of the Moon covering 340-2430 nm appropriate for calibration of Earth-orbiting spacecraft. An empirical model of irradiance has been developed that treats phase and libration explicitly, with absolute scale founded on photometry of the star Vega and the spectra of returned Apollo samples. This model has the same form at each wavelength, with 18 coefficients, 8 of which are constant across wavelength, for a total of 328 coefficients. Over 1000 lunar observations are fitted at each wavelength; the average residual is less than 1%. The irradiance model is actively being used in lunar calibration of several spacecraft instruments, and can track sensor response changes at the 0.1% level.

Introduction and Observational Data Although the brightness of the Moon varies strongly with time, the surface of the Moon has reflectance properties that are virtually invariant over time{Kieffer 1997} and the lunar irradiance is strictly a function of wavelength and geometry.

The RObotic Lunar Observatory (ROLO) project was established to accurately determine the irradiance and radiance of the Moon. Routine observations were made on every clear night during the bright half of each month for several years{Kieffer 1998, Stone 2002, Kieffer 2005}. Lunar images were acquired in 32 bandpasses covering 340-2430 nm approximately every half hour when the Moon was at least 30° above the horizon. The remainder of observing time was dedicated to stellar observations for use in determining atmospheric extinction and instrument absolute response. Stellar targets are a subset of 190 "standard" stars selected by the ROLO project specifically for their invariant properties. The same stars were imaged repeatedly through the night. The database currently contains over 85000 individual images of the Moon and several hundred thousand star images.

Model Development The ROLO irradiance model is based on 1249 observation sequences, each including all 32 ROLO bands, acquired over more than 3 years. These observations have a relatively uniform distribution over phase angle, but have some correlation with libration due to coverage of only about 1/4 of a Saros cycle. These data support modeling for phase angles from 1.5 to 90°.

It was found that no existing physically-based irradiance model supports the accuracy of the ROLO observations. Hence, we developed an empirical analytic model of the equivalent reflectance of the entire lunar disk (regardless of illuminated fraction) based on the primary geometric variables:

$$\ln A_k = \sum_{i=0,3} a_{ik} g^i + \sum_{j=1,3} b_{jk} \Phi^{2j-1} + c_1\theta + c_2\varphi + c_3\Phi\theta + c_4\Phi\varphi + d_1\exp(-g/p_1) + d_2\exp(-g/p_2) + d_{3k}\cos[(g-p_3)/p_4]$$

where A_k is the disk-equivalent reflectance, g is the absolute phase angle, θ and φ are the selenographic latitude and longitude of the observer, and Φ is the selenographic longitude of the Sun.

The first polynomial represents the basic photometric function dependence upon phase angle, disregarding any opposition effect. The second polynomial approximates the dependence upon the face of the Moon that is illuminated, primarily representing the distribution of maria and highlands. The four terms with coefficients c_n represent the face of the Moon that is seen (topocentric libration), with a consideration of how that is illuminated. The next two represent the opposition effect and the last one simply addresses a correlation seen in the irradiance residuals, possibly associated with mare/highland distribution not covered by the second polynomial.

The fitting process yields 8 values that are constant over wavelength (4 for libration and the 4 nonlinear parameters) and 10 additional values for each filter, for a total of 328 coefficients. The mean absolute residual over all observations fitted is 0.0096 in the natural logarithm of reflectance. Test runs of this model show that the extreme effects of libration (the c_x terms) could exceed 7% over a full Saros cycle.

Model Performance Uncertainty in the Vega-based radiance calibration can be no less than the absolute flux measurements on which it is based{Hayes 1985, Strecker 1979}. Hayes(1985) cites a measurement uncertainty of 1.5% for the absolute flux at 555.6 nm, the scaling point for the visible-wavelength flux spectrum. The reported experimental error for the IR measurements of Strecker(1979) is ~4% absolute. Both sets of absolute flux data rely on an assumed energy distribution for Vega.

The model based upon Vega calibration yields reflectance spectra which have modest excursions in wavelength between bands, whereas the reflectance spectrum of the Moon has only weak, broad features{McCord 1970, Lucey 1986}. An adjustment to the model absolute scale for each wavelength is based on fitting the ROLO model reflectance spectrum for g=7°, Φ=7°, θ=0, φ=0, to a composite of laboratory reflectance spectra of returned Apollo samples of soil (95%) and breccia (5%) multiplied by a linear scaling (a+bλ); this adjustment averaged 3.5%

over all bands.

ROLO Lunar Calibration Current knowledge of lunar photometry resulting from the ROLO program is adequate to support precise determination of the responsivity history of imaging instruments in orbit around the Earth. The spatially integrated radiance derived from the nominal calibration of spacecraft lunar images can be compared directly with models of the lunar irradiance to determine instrument gain factors. Descriptions of the lunar calibration technique applied to spacecraft can be found in the literature (e.g., Barnes 2001, Kieffer 1999, Kieffer 2002, Barnes 2004).

The Moon is available to all Earth-orbiting spacecraft at least once per month, and thus can be used to tie together the at-sensor radiance scales of all instruments participating in lunar calibration without requiring near-simultaneous observations. A corollary, resulting from the intrinsic stability of the lunar surface, is that any future improvements to radiometric knowledge of the Moon could be applied retroactively to instrument calibration.

Several instruments have now viewed the Moon while in orbit, and observations have been compared with the ROLO model. Typically, the spacecraft will execute a pitch maneuver while in the Earth's shadow to scan past the Moon. For instruments in a Landsat-like orbit (705 km altitude), the Moon's diameter corresponds to roughly 6.3 km on the ground, and lunar image acquisition takes only a few seconds. The lunar calibration technique can be employed for geosynchronous satellites without special attitude maneuvers, since the Moon periodically passes through the corners of the rectangular field of regard for full-disk images of the Earth.

The spacecraft instrument team supplies to ROLO the spacecraft location and time at the mid-point of the lunar observation, along with the apparent size of the Moon in the scan direction. The ROLO team then computes the relative positions of the spacecraft and the Sun in selenographic coordinates using the high-precision ephemeris of the Moon and planets{Standish 1990} and the IAU orientation of the Moon. The lunar irradiance model is computed for this geometry, and corrected for the actual Moon-Sun and Moon-spacecraft distances for comparison with the spacecraft observation.

This work has demonstrated that the lunar spectral irradiance can be modeled with a precision that enables a significant advancement in on-orbit monitoring of spacecraft instrument performance. Comparison between several spacecraft reveal substantial differences in the radiance scales of their standard imagery products. The most extensive set of spacecraft lunar observations, the six-year record of SeaWiFS, suggests that instrument response trending can be determined approaching the 0.1% level on a monthly basis over any longer time period{Barnes04}. This level of long-term stability meets the goals for radiometric calibration of decade-scale climate observations set for the upcoming National Polar-orbiting Operational Environmental Satellite System. However, this level of precision indicates that it will be useful to incorporate treatment of the variation in solar irradiance, which is at this level, to generate appropriate lunar irradiances using the lunar disk reflectance model.

Acknowledgments This work was supported by the NASA EOS Project Science Office at the Goddard Space Flight Center under contract S-41359-F.

References

Barnes, R.A., R.E. Eplee Jr., G.M. Schmidt, F.S. Patt, C.R. McClain, The calibration of SeaWiFS. Part 1: Direct Techniques, *Applied Optics, 40,* 6682-6700, 2001.

Barnes, R.A., R.E. Eplee Jr., F.S. Patt, H.H. Kieffer, T.C. Stone, G. Meister, J.J. Butler, C.R. McClain, Comparison of SeaWiFS measurements of the Moon with the US Geological Survey Lunar model, *Applied Optics, 43,* 5838-5854, 2004.

Hayes, D. S., Stellar absolute fluxes and energy distributions from 0.32 to 4.0 microns, in *Calibration of Fundamental Stellar Quantities; Proceedings of IAU Symposium No. 111*, 225-252, 1985.

Kieffer, H.H., Photometric stability of the Lunar surface, *Icarus, 130,* 323-327, 1997.

Kieffer, H.H., J.A. Anderson, Use of the Moon for spacecraft calibration over 350-2500 nm, *Proc. SPIE, 3498,* 325-335, 1998.

Kieffer,H.H., J.M. Anderson, K.J.Becker, Radiometric calibration of spacecraft using small lunar images, *Proc. SPIE, 3870,* 193-205, 1999.

Kieffer, H.H., P.Jarecke, J. Pearlman, Initial Lunar calibration observations by the EO-1 Hyperion imaging spectrometer, *Proc. SPIE, 4480,* 247-258, 2002.

Kieffer, H.H., T.C.Stone, The spectral irradiance of the Moon, *Astron. Jour., 129,* 2887-2901, 2005.

Lucey, P.G., B.R. Hawke, C.M. Pieters, J.W. Head, T.B. McCord, A compositional study of the Aristarchus region of the Moon using near-infrared spectroscopy, *Jour. Geophys. Res., 91,* D344-354, 1986

McCord, T.B., T.V. Johnson, Lunar spectral reflectivity (0.3 to 2.5 microns) and implications for remote mineralogical Analysis, *Science, 169*, 854-858, 1970

Standish, E.M., The observational basis for JPL's DE200, the planetary ephemeris of the Astronomical Almanac, *Astron. & Astroph., 233*, 252-271, 1990

Stone, T.C., H.H. Kieffer and J.M. Anderson, Status of use of Lunar irradiance for on-orbit calibration, *Proc. SPIE, 4483,* 165-175, 2002.

Strecker, D.W., E.F. Erickson and F.C. Witteborn, Airborne stellar spectrometry from 1.2 to 5.5 microns - absolute calibration and spectra of stars earlier than M3, *Astrophys. J. Supp., 41,* 501-512, 1979.

Determination of Aerosol Optical Depth and Ångström's Wavelength Exponent Using Sunphotometers and Spectroradiometers: A Preliminary Assessment

C. A. Gueymard
Solar Consulting Services, New Smyrna Beach, FL 32168, USA, Chris@SolarConsultingServices.com

Abstract. Quality measurements from sunphotometers and spectroradiometers are used here to evaluate the aerosol optical depth (AOD) and Ångström wavelength exponent (α) at various sites. Using a few examples, it is shown that, even if collocated instruments agree on AOD, they disagree on α. Knowledge of the latter's variations along the spectrum may be improved by using spectroradiometers, but only if they are high-performance instruments.

Introduction

Aerosol optical depth (AOD) is a rapidly variable characteristic of the atmosphere. Its accurate knowledge is essential for the determination of the impact of aerosols on, e.g., the radiative budget of the earth's atmosphere. For ground-based operation, which is the focus here, multi-wavelength sunphotometers (SPMs) or shadowband radiometers offer the possibility of determining AOD by discrete observations in the shortwave direct spectrum. This type of instrument is used in global networks such as AERONET and GAW. Their data is extremely valuable as ground truth for spaceborne sensors and to derive AOD climatologies over the world (e.g., Gueymard and George, 2005). SPM measurements are indirect because of their lack of absolute calibration, most generally.

Spectroradiometers (SRMs), on the other hand, are absolutely calibrated and their output spectra can therefore be directly compared to irradiance predictions from models. AOD can also be derived following a method similar to that outlined above for SPMs, albeit with considerably finer resolution. Unfortunately, SPM or SRM intercomparisons are rare events, and the two types of instrument do not usually coexist on a permanent basis.

This contribution outlines some valuable lessons learned while using and comparing the two types of data, which have been gathered for years on a relatively regular basis at the Atmospheric Radiation Measurement (ARM) Program's Cloud And Radiation Testbed (CART) site in Oklahoma, and at the National Renewable Research Laboratory (NREL) in Golden, Colorado.

Sunphotometry Issues

For proper long-term and automatic monitoring of AOD, a few important issues need to be addressed: (i) filter degradation; (ii) calibration accuracy and stability; and (iii) cloud interferences. The two first issues are such that the absolute uncertainty in individual AOD measurements is about 0.01 at best. This is a known problem, but its incidence on the derivation of the Ångström wavelength exponent, α, is more serious than is usually admitted, as discussed in the next section. Cloud-screening algorithms, such as that used to post-process AERONET data, are very efficient but still not perfect. Instances of cloud contaminated data points have been found occasionally, resulting in slightly overestimated AODs and underestimated α values in monthly-average "climatological" products.

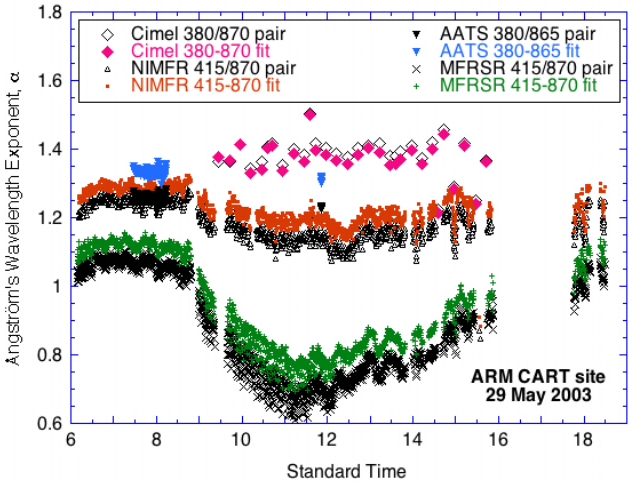

Figure 1. Ångström wavelength exponent obtained by two methods (wavelength pairs and linear fit) with four instruments.

Wavelength exponent Coefficient α can be obtained by either solving Ångström's equation for a pair of judiciously selected wavelengths for which AOD is measured (e.g., 380 and 870 nm), or by linearly fitting the observed AOD at many wavelengths to the log-log transform of Ångström's equation. The limitations and inaccuracies of the first method have been discussed long ago (Cachorro et al., 1987), but it is still being used in the AERONET and ARM datasets, for instance. Figure 1 shows that for a typical mostly-clear day, large differences in the calculated α may result— with a surprisingly large range of 0.6–1.5 near noon in this case—when the two methods are applied to data from four instruments. This considerable scatter occurs even if the measured AODs at 500 nm are relatively similar over time (Fig. 2). In Fig. 1, note also the small difference in the α values obtained by the two derivation methods with any instrument, but particularly the Cimel. This is representative of the best-case scenario only.

The linear-fitting method is potentially more accurate because it compensates (to some extent) for opposite biases in AOD due to the calibration issues mentioned earlier. The accuracy in α may also depend on the number of channels considered, and therefore vary from one SPM to the other. A more ambitious investigation—considering months of ARM data under varied atmospheric conditions—is underway to determine the uncertainty in α resulting from the combination of the instrument-dependent uncertainty in AOD and that of the derivation method.

To characterize the spectral dependency of AOD in the visible, the interval 380–870 nm, or 415–870 nm at the very least, seems the best suited, depending on instrumentation.

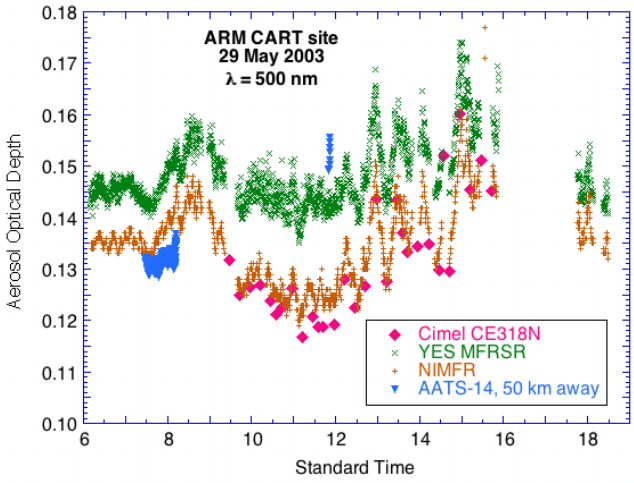

Figure 2. Example of daily course of aerosol optical depth at 500 nm: intercomparison between four instruments. Cloud passages have been filtered out.

Unless specifically designed for the UV, SPMs cover the spectral range 340–1040 nm at most. Whereas the spectral dependency of AOD (through α) is now relatively well known in the visible (to the extent that the uncertainties reported above have not blurred the picture so far), it is less known in the UV or, even more so, beyond 1100 nm. A research SPM, the AATS-14, has 14 channels, including three special channels at 1241, 1558 and 2139 nm (Schmid et al., 2005). The log-log transform of Ångström's law applied to data from these 14 channels indicate that α tends to decrease beyond 1000 nm. It is also found, however, that the behavior of α in the UV differs completely when considering the few UV channels of the AATS-14 and Cimel. More specialized equipment (UV SPM and/or SRM) will therefore rather be used for this task.

Spectroradiometry Issues

A promising application of SRMs is to use their measured irradiance to derive AOD. This is done here by comparing each measured direct spectrum to an ideal spectrum predicted by the SMARTS model (Gueymard, 2005). Inputs to the model are all known atmospheric conditions—but no aerosol. Results are smoothed to simulate the instrument's bandwidth. The spectral aerosol transmittance, $T_{a\lambda}$, is obtained at each wavelength λ by the measured/predicted irradiance ratio. The AOD is then simply $-\ln(T_{a\lambda})/m_a$, where m_a is the aerosol optical mass. (This is valid only outside of strong gaseous absorption bands.)

In theory, this method has the potential to validate Ångström's law over the whole spectral range of SRMs. In practice, however, it is found that this is not so with all SRMs. For instance, Fig. 3 shows the results of this method for different turbidity conditions, using a well-calibrated Licor LI-1800, a largely used SRM. Whereas it appears appropriate for hazy conditions, it is *not* for very clean conditions, due to some inherent spectral instability. This confirms previous findings (Carlund et al., 2003). The same conclusion is also found when the Licor-derived AODs are compared to that obtained (similarly) with a collocated higher-performance instrument, whose range extends to 2.5 µm (Fig. 4). Preliminary results with this SRM also confirm α's tendency to decrease beyond 1 µm.

Work is now underway to analyze recent SRM data at CART (using UV and VIS Rotating Shadowband Spectroradiometers) and NREL (using SRM data from various instruments) in order to validate Ångström's law in the 0.3–2.5 µm spectral range under varied conditions.

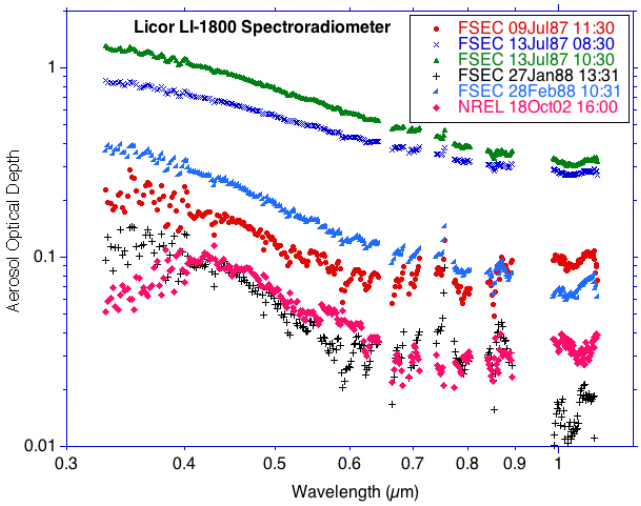

Figure 3. AOD as a function of wavelength using Licor LI-1800 spectroradiometer measurements at two locations.

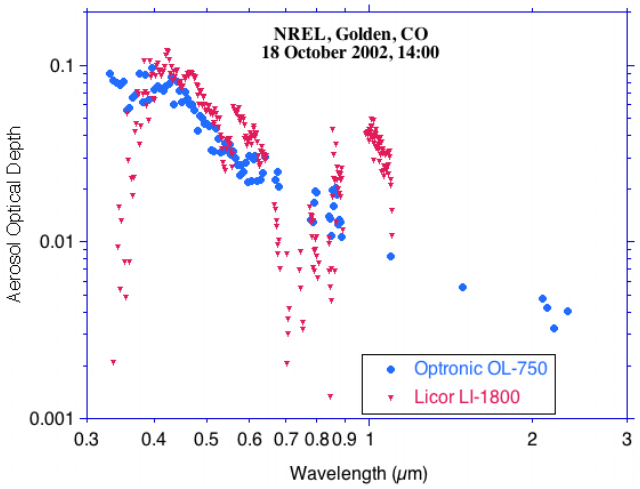

Figure 4. AOD as a function of wavelength using two spectroradiometers (Licor LI-1800 and Optronic OL-750) at NREL.

References

Cachorro V.E. et al., Determination of the Angstrom turbidity parameters, *Appl. Opt., 26*, 3069-3076, 1987.

Carlund T. et al., Comparison and uncertainty of aerosol optical depth estimates derived from spectral and broadband measurements. *J. Appl. Meteorol., 42*, 1598-1610, 2003.

Gueymard C.A., Interdisciplinary applications of a versatile spectral solar irradiance model: A review. *Energy, 30*, 1551-1576, 2005.

Gueymard C.A., George R., Gridded aerosol optical depth climatological datasets over continents for solar radiation modeling. *Solar World Congress*, International Solar Energy Soc., 2005.

Schmid B. et al., How well do state-of-the-art techniques measuring the vertical profile of tropospheric aerosol extinction compare? *J. Geophys. Res.*, 2005 (in press).

Procedures of absolute calibration for the Space Solar Patrol instrumentation at the Synchrotron radiation source

I. Afanas'ev, S. Avakyan, and N. Voronin

S.I. Vavilov State Optical Institute, St. Petersburg, Russian Federation

A. Nikolenko, V. Pindyurin

G.I. Budker Institute of Nuclear Physics, Novosibirsk, Russian Federation

Abstract. The paper describes basic and additional calibration procedures for absolute measurements of an optical-electronic instrumentation at a synchrotron radiation (SR) sources in the spectral range from 0.25 up to 122 nm (5000 - 10 eV). The procedures have been proposed to realize the absolute calibration of the Space Solar Patrol (SSP) instrumentation, which has been created to monitor the ionizing radiation from the Sun in the spectral range 0.14 – 198 nm. For this goal, the metrological stations at the SR sources of the storage rings VEPP-3 and VEPP-4 (at the Budker Institute of Nuclear Physics (INP), Novosibirsk, Russia) has been developing. The basic requirements for the absolute spectral measurements are also considered.

Introduction

The SSP instrumentation consists of a Radiometer with 20 filters and two grating spectrometers (an extreme ultraviolet (EUV) Spectrometer of normal incidence and a X-ray/EUV Spectrometer of grazing incidence) [Avakyan et al., 1998; Afanas'ev et al., 2005]. All measuring channels of the SSP have the "solar-blind" detectors – open secondary-electron multipliers (SEM), which are "blind" to near UV and visible radiation of the Sun [Avakyan et al., 1998].

The main task to perform the metrological calibration of the SSP apparatus in the wide spectral range 0.25-122 nm (5000 - 10 eV) is creation of specialized SR beamlines and experimental stations at the electron-positron storage rings VEPP-4 and VEPP-3. Calibration of the large dimension apparatus of the SSP (the radiometer and the spectrometers) is intended to execute at the SR experimental station of the VEPP-4 storage ring. But, the auxiliary measurements for small dimension devices and components of the SSP (SEMs, filters), as well as testing the reference detectors is envisaged to carry out at the VEPP-3 storage ring. Such specialized SR beamlines and experimental stations for calibration of the space-destined apparatus is creating for the first time in native practice that originates the experimental basis for further development of these works in Russia.

The calibration ranges for the SSP instrumentation:
- Radiometer with filters – from 0.25 to 122 nm;
- EUV-Spectrometer – from 56 to 122 nm;
- X-ray/EUV Spectrometer – from 1.8 to 122 nm.

Requirements to the calibration

For successful realization of the absolute spectroradiometric calibration of all SSP apparatus at a SR beam it is necessary to execute:
1) Providing the SR beam being stable in space and in time with monitoring of its intensity, lateral dimensions and position at the entrance of calibration chamber for the SSP;
2) Maintenance of the vacuum degree in an experimental calibration volume is not worse than 5×10^{-6} mm Hg;
3) Providing antijamming operation of electronics of photoreceiving tracts of the SSP apparatus in real conditions of the complex of storage rings VEPP-3 and VEPP-4;
4) Obtaining monochromatic radiation from a "white" SR beam with the help of monochromators: in range from 0.25 up to 122 nm, having not less than 60 spectral points;
5) Providing radiation intensity at the entrance of the apparatus that must not be less than the intensity of an average solar flux. Besides, the intensity of the SR beam at all wavelengths must correspond to the region of the measured counting rate from 10^3 up to 10^4 pulses/sec in the SSP channels, i.e. the middle of registering region of the SSP photoreceiving tract, that is about six orders (from 4 to 3×10^6 pulses/sec [Avakyan et al., 2001]). So, using the counting rate in this region as an index of true "one--electron" mode of input signal registration, it is possible to achieve a high accuracy calibration [Afanas'ev et al., 2004].
6) Determination of absolute SR fluxes at the entrance of calibration chamber of the SSP apparatus with the use of absolutely calibrated detectors and with the help of well-calculable "white" SR beam.
7) The required accuracy of absolute calibration of all complex of instrumentation - is not worse than 10%, thus calibration of separate devices (Radiometer, EUV-Spectrometer and X/EUV-Spectrometer) it is not worse 7%.
8) Decreasing of the high energetic particle flux (with energies more than 5 keV) in SR beams up to the reasonable level (for a given accuracy of calibration) at the entrance of the calibration chamber and providing the effective suppression of photon fluxes with energy, which is multiple of calibration energy.

The basic calibration procedure at the SR beam

In a basis of calibration of the SSP instrumentation lays the method of a reference detector according to which a radiant power of a monochromated SR beam, incoming in the SSP spectrometer or radiometer, is measured by the reference detector with known spectral sensitivity. The important element of such calibration method is the choice and verification of the reference detector. In our case, it is offered to use the silicon photodiodes AXUV-100 produced by the IRD Incorporation (USA). The spectral properties of the detector are defined by its coating (the thin metal film evaporated on the surface of the detector) and can be changed by a controllable way. This opportunity will be used for an estimation of power of parasitic background component, past through monochromator, and its contribution to the output signal of the detector. The information, given by the IRD Inc., enables to calculate spectral prop-

erties of detectors (with different coatings) with sufficient accuracy to realize the calibration. Besides, it is offered the additional calibration of the reference detectors by the method of selective absorbing filters, which has been developed and successfully applied by authors from the INP at the performance of the International Science and Technology Center (ISTC) project # 438 [Pindyurin et al., 2000].

Features of calibration of the SSP instrumentation with the method of the reference detector at the SR beam:

- Time modulation of the SR beam:

The SR beam from the storage ring VEPP-4 is the short and periodically repeated flashes (with duration less than 1 nsec and the frequency about 1 MHz). As the photodetectors of the SSP instrumentation work in an pulse registering mode [Avakyan et al., 2001], that the part of multi-electron events (i.e. more than 1 photoelectron emission from a photocathode of the detector) in the output signal grows when the loading of the detector is increased. To minimize the systematic error, which connected to this phenomenon, the loading of detectors is necessary to limit up to 10^5 pulses/sec, by decrease of intensity of the SR beam. Calculations show, that in this case the part of multi-electron events will not exceed 5.5 %. Thus maintenance of loading of the detector in a range $10^3 – 10^4$ pulses/sec gives the best accuracy of calibration measurements [Afanas'ev et al., 2004].

- Polarization of the SR beam:

In contrast to the non-polarized solar radiation, the SR beam in the median plane of the orbit is linearly polarized. To consider the possible systematic error connected to it, measurements with the spectrometers in different positions relatively to the plane of polarization are provided.

- Phase volume of a radiation source:

From the point of view of the optical circuits of the SSP spectrometers [Avakyan et al., 1998, 2002], the Sun is the removed source with the limited angular size, whereas the SR source is almost indefinitely removed point source. As the focusing optical circuits of the SSP spectrometers have been developed to register the solar radiation, then for the account of the given geometrical factor on results of calibration, it is offered to carry out additional experiments.

The additional calibration procedures

The method of the absolute calibration of SEMs, filters, gratings, as well as the apparatus as a whole, consists in a determination of a radiant power of a SR beam for a given wavelength that comes through an entrance of the element under calibration. The SR flux can be calculated theoretically or measured experimentally with calibrated detectors. The radiation of the necessary wavelength is extracted either by spectrometers or diffraction gratings, or multilayer mirrors and filters. The earliest variant of the absolute calibration method was described in Ref. [Afanas'ev et al., 2005]. Now together with the basic procedures, it is offered to apply two identical spectrometers of the SSP, located consistently [Avakyan, 2005], for the calibration goal.

The procedure consists in a performance of two stages:

1. The spectrometer #1 (we suppose to use the X-ray/EUV spectrometers) without the SEM detectors is set at a SR beam, while the completely equipped spectrometer #2 with its input slit is alternately integrated to an output slit of each channels of the spectrometer #1. After execution of measurements of a counting rate with the SEM with scanning of all ranges of the spectrum of the spectrometer #2 [Avakyan et al., 2002], the spectrometer #2 is removed, and its SEMs are replaced in corresponding channels of the spectrometer #1. Then the measurements of counting rate with scanning of all ranges of the spectrum are carried out again. The difference in results of measurements with the SEM at the spectrometers is the spectral efficiency of diffraction grating of the spectrometer #2. After that the grating from the spectrometer #2 is replaced in the spectrometer #1, and the control measurements, including measurements of absolute spectral efficiency of the SEM, and finally, a spectral throughput of the SSP spectrometer #1, are carried out. For this goal, at a final stage of theoretical and/or experimental works (with use of absolute detectors) are executed by definition of the spectral intensity of the entrance SR beam.

2. For absolute spectral calibration of the SSP radiometers (with filters) there will be used the spectrometer #1 plus a radiometer. But at the first stage the single SEM will be graduated at all four channels of this spectrometer. Then a radiation transmission of the set of filters in a disk of radiometer [Avakyan et al., 1998] in the given structure of placing of two devices is measured with the calibrated SEM. Advantage of the offered way of absolute calibration with use of the pair of the SSP devices (one of which is the spectrometer) is an opportunity of the simplified consideration of geometry of the absolute measurement experiment and, as a result, increase of accuracy of the calibration.

Conclusion

It is offered the absolute calibration procedures at the synchrotron radiation sources in the spectral range from 0.25 up to 122 nm (5000 - 10 eV) for the Space Solar Patrol (SSP) instrumentation. Thus, methods of reference detectors and selective absorbing filters are accepted as a basis. The unique methods based on use of the SSP spectrometers and radiometers are also offered as additional calibration procedures. Moreover, requirements to the metrological stations organized for the calibration have been considered.

Acknowledgments This work has been supported by the grant of International Science and Technology Center through the Project #2500 «Calibration of the Space Solar Patrol apparatus at the synchrotron source». The authors are grateful to foreign partners of the project: A. Aylward (UK), J.-P. Delaboudiniere (France), A. Hilgers (Holland), N. Pailer, G. Schmidtke, F. Scholze (Germany).

References

Afanas'ev, I. M., Mironov, A. I., Chernikov D.A. Investigation of statistic aspects of use of a synchrotron radiation beam for calibration of the "Solar Patrol" instrumentation, *Articles of the 6th Int. conf. "Applied optics", 1 (2),* 425-428, 2004.

Afanas'ev, I. M., Avakyan, S. V., et al. Achievements in creation of the Space patrol apparatus of ionizing radiation of the Sun, *Nuclear Inst. and Meth. in Phys. Res. (A), 543,* 312-316, 2005.

Avakyan, S. V., Voronin, N. A., Yefremov, A. I., et al. Methodology and equipment for space-based monitoring of ionizing solar radiation, *J. Opt. Technol., 65 (12),* 124-131, 1998.

Avakyan, S. V., Afanas'ev, I. M., Voronin, N. A., et al. Developing apparatus for permanent space patrol of the ionizing radiation of the Sun, *J. Opt. Technol. 68 (6),* 421-427, 2001.

Avakyan, S. V., Afanas'ev, I. M., Voronin, N. A., et al. Development of an x-ray spectrometer for a Space Solar Patrol, *J. Opt. Technol. 69 (11),* 818-821, 2002.

Avakyan, S. V., Space solar patrol of Absolute Measurements of Ionizing solar radiation, *Adv. in Space Res.,* 2005. In press.

Pindyurin, V. F., Subbotin, A. N., et al. Absolute calibration of X-ray semiconductor detectors against synchrotron radiation of the VEPP-3 storage ring, *Metrologia, 37, 5,* 497-500, 2000.

Using a Blackbody to Determine the Longwave Responsivity of Shortwave Solar Radiometers for thermal offset error correction

I. Reda[1], J. Hickey[2], D. Myers[1], T. Stoffel[1], S. Wilcox[1], C. Long[3], E. G. Dutton[4], D. Nelson[4], and J. J. Michalsky[4]
[1]National Renewable Energy Laboratory Golden CO [2] The Eppley Laboratory Newport RI [3]Pacific Northwest Laboratory Richland WA.
[4]National Oceanic and Atmospheric Administration, Boulder CO

Abstract : Thermopile pyranometers' thermal offsets have been recognized since the pyranometer's inception. This offset is often overlooked or ignored because its magnitude is small compared to the overall solar signal at high irradiance levels. With the demand of smaller uncertainty in measuring solar radiation, recent publications have described a renewed interest in this offset, its magnitude, and its effect on solar monitoring networks for atmospheric science and solar radiation applications. Recently, it has been suggested that the magnitude of the pyranometer thermal offset is the same if the pyranometer is shaded or unshaded. Therefore, calibrating a pyranometer using the method known as the shade/unshade method would result in accurate responsivity calculations, because the thermal offset error is canceled. Nevertheless, when the shade/unshade responsivity is used during the outdoor data collection, the resultant shortwave radiation would be underestimated if the thermal offset error is not corrected for. When using the component sum method for the calibration, the thermal offset error, which is typically negative when the sky is cloudless, does not cancel, resulting in an underestimated shortwave responsivity. Most operational pyranometers used for solar radiation monitoring networks are calibrated using the summation method since it is possible to calibrate many pyranometers simultaneously. From this arises the importance of correcting the summation method results to account for the thermal offset error. Here we describe the use of a laboratory blackbody to calculate the net-longwave responsivity of pyranometers, which is largely responsible for the offset error. This longwave responsivity is then used to correct shortwave responsivity derived from summation method calibration Procedures to accomplish the correction, and the associated uncertainties are described.
Figure 1 illustrates the NREL Blackbody calibration setup. Figure 2 shows the responses of several popular types of pyranometers to net infrared radiation measured during the laboratory calibrations.

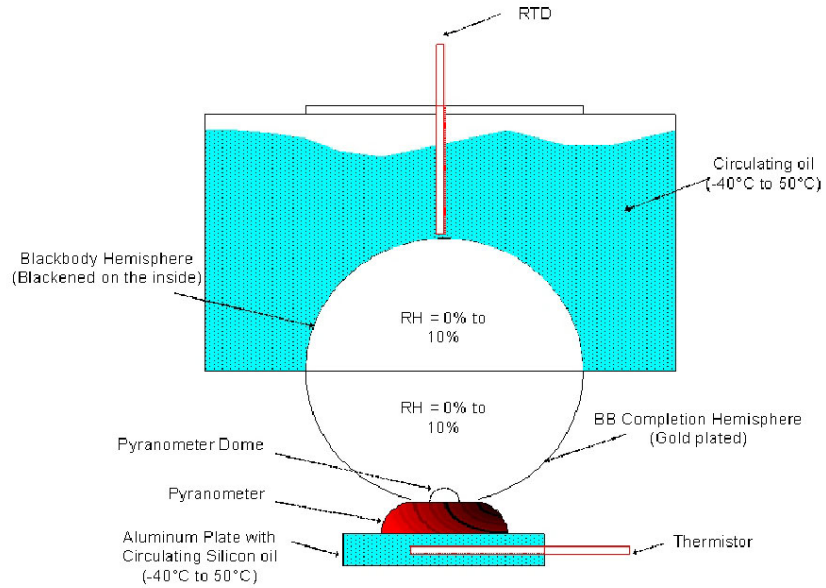

Figure 1. The Blackbody System (BBS) with a pyranometer in place.

20

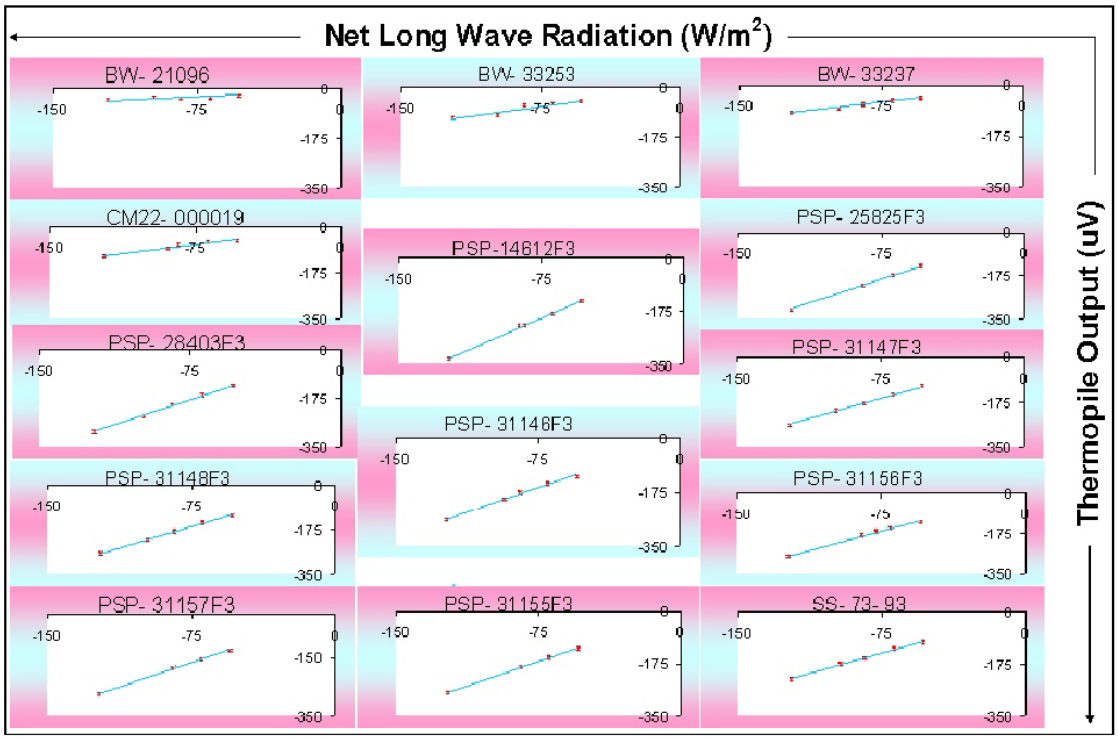

Figure 2. Thermopile voltage versus NET-IR during the Blackbody System (BBS) calibration.

On the drifts exhibited by cryogenically cooled InSb infrared filtered detectors and their importance to the ATSR-2 and Landsat-5 earth observation missions.

E. Theocharous

Optical Radiation Team, Quality of Life Division,
National Physical Laboratory, TW11 0LW, UK
Phone: +44 (0)20 8943 6977 Fax: +44 (0)20 8943 6935
e-mail: e.theo@npl.co.uk

Abstract

The spectral responsivity of commercially available InSb detectors with low-pass cold filters attached on their cold shields for optimum operation in the 1.6 μm to 2.6 μm wavelength range was observed to drift slowly with time. These drifts were shown to arise due to a thin film of water-ice depositing on the cold low-pass filters mounted on the cold shields of the detectors. The temporal characteristics of these drifts were shown to be strongly dependent on wavelength. A model is proposed for the behaviour of the water present in the dewar-vacuum which can explain and predict the temporal characteristics of the observed drifts for all wavelengths. These observations are particularly relevant to space instruments which use cryogenically-cooled infrared filter radiometers for earth observation. The temporal profile of drifts observed in missions like Landsat-5 is identical to that observed in cryogenically cooled filtered InSb detectors during laboratory measurements. This work confirms that the deposition of a thin film of a material like ice on the cold band-pass filters/windows is therefore the most likely source of the oscillatory drifts observed in the response of some of the channels of the ATSR-2, and Landsat-4 and Landsat-5 earth observation missions.

On-orbit Characterization of Terra MODIS Solar Diffuser Bi-directional Reflectance Factor (BRF)

X. Xiong and V.V. Salomonson
Sciences and Exploration Directorate, NASA/GSFC, Greenbelt, MD 20771, USA

J. Sun, J. Esposito, and X. Xie
Science Systems and Applications, Inc., 10210 Greenbelt Road, Suite 600, Lanham, MD 20706, USA

W.L. Barnes and B. Guenther
University of Maryland, Baltimore County, Catonsville, MD 21250, USA

Abstract. Remote sensing spectroradiometers often use solar diffusers (SD) as on-board calibrators for calibrating sensors' reflective solar bands (RSB), typically with wavelengths ranging from ultraviolet (UV) to short-wave infrared (SWIR), or for monitoring sensors' radiometric calibration stability [1-5]. The SD calibration accuracy and its stability monitoring capability strongly depend on the knowledge of the SD reflectance property, known as the bi-directional reflectance factor (BRF), and on the sensor's ability of tracking the on-orbit changes of the SD BRF. The Moderate Resolution Imaging Spectroradiometer (MODIS) Proto-Flight Model (PFM) is one of the five instruments on-board the NASA's Earth Observing System (EOS) Terra spacecraft launched in December 1999. Improved over its heritage sensors, the MODIS makes continuous global observations over a wide field-of-view (FOV) in 36 spectral bands covering wavelengths from 0.41 to 14.4 micrometers and at three nadir spatial resolutions: 0.25km, 0.5km, and 1km [6]. MODIS bands 1-19 and 26 are the reflective solar bands (RSB) and bands 20-25 and 27-36 are the thermal emissive bands (TEB). Figure 1 illustrates MODIS scan cavity and its on-board calibrators, including a solar diffuser (SD), a solar diffuser stability monitor (SDSM), a blackbody (BB) and a spectro-radiometric calibration assembly (SRCA) [7,8].

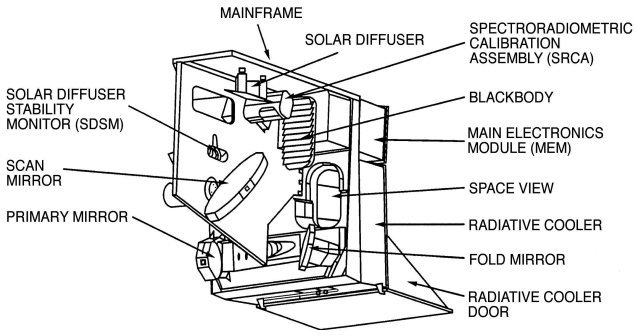

Figure 1. MODIS Scan Cavity and On-board Calibrators

The MODIS RSB calibration is reflectance based through the use of an on-board solar diffuser panel made of space-grade Spectralon materials shown in Figure 2. The MODIS SD bi-directional reflectance factor (BRF) was characterized pre-launch by the instrument vendor against reference samples traceable to NIST reflectance standards. The SD BRF measurements were made at a number of wavelengths and illumination (incident) angles (azimuth and elevation angles in the MODIS coordinates) and with the viewing angle fixed to match the sensor's on-orbit calibration configuration. The pre-launch measurements at each wavelength were fitted to a second order polynomial function of solar illumination angles. For each of the MODIS reflective solar bands, its BRF was either interpolated or extrapolated from the pre-launch characterization results. Another MODIS on-board calibrator, a solar diffuser stability monitor, was designed to track the SD on-orbit degradation. Since its launch the Terra MODIS SD and SDSM system has been effectively used on-orbit for the RSB radiometric calibration.

Figure 2. MODIS solar diffuser (SD) panel

This paper describes an approach of characterizing the sensor's SD BRF using its on-orbit SD observations made during the spacecraft yaw maneuvers. This approach has the advantage of studying the SD BRF directly using the sensor's spectral bands (or detectors) and over all possible illumination angles at the same time. For Terra MODIS, two series of yaw maneuvers have been executed for this purpose. The results derived from Terra MODIS pre-launch measurements and two sets of on-orbit characterizations (yaw maneuvers) are presented in this paper to illustrate the SD BRF uniformity and to study its on-orbit degradation characteristics. Figure 3 is an example of the BRF results derived from pre-launch measurements and that from on-orbit observations for Terra MODIS band 3 at 0.47 micrometer. The difference between on-orbit and pre-launch characterization results is less

than 0.25%. Also addressed in this paper are the impacts of the SD BRF uncertainty and its on-orbit degradation on the sensor's radiometric calibration. For Terra MODIS, the SD BRF degradation has shown a strong wavelength dependency with an annual (degradation) rate varying from 3% at 0.41 micrometer to less than 0.1% at 0.91 micrometers when it's under the nominal operational conditions.

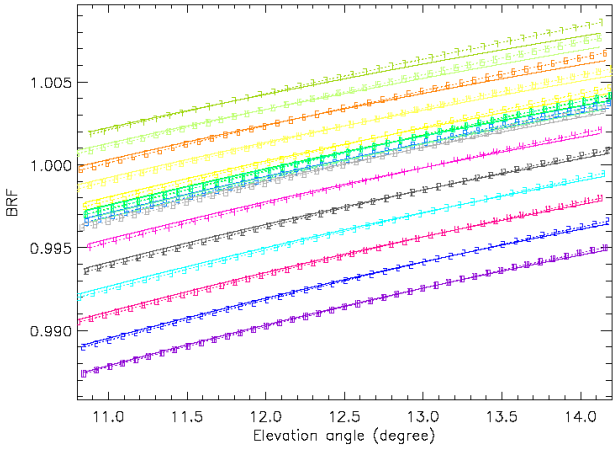

Figure 2. Comparison of pre-launch and on-orbit characterization of Terra MODIS solar diffuser (SD) BRF (band 3; solid line: pre-launch fitting; dash line: on-orbit resutls; the symbles are the spacecraft yaw numbers for differnt azimuth angles)

Acknowledgments

The authors would like to thank the many individuals of the MODIS Characterization Support Team and Raytheon Santa Barbara Remote Sensing (SBRS) MODIS Team for their support in pre-launch and on-orbit data analyses and technical discussions.

References:

1. Xiong,,X., K. Chiang, J. Esposito, B. Guenther, W.L. Barnes, MODIS On-orbit Calibration and Characterization in *Metrologia* 40 89-92, 2003
2. Bruegge, C.J., A.E. Stiegman, R.A. Rainen, A.W. Springsteen, Use of spectralon as a diffuse reflectance standard for in-flight calibration of Earth-orbiting sensors in *Opt. Eng*., 32, 804, 1993
3. Sumnich, K.H., A. Neumann, T. Walzel, G. Zimmermann, Modular optoelectronic scanner MOS in-orbit; results of the in-flight calibration in *Proceedings of SPIE*, 3118, 1977
4. Early, E.A., P.Y. Barnes, B.C. Johnson, J.J. Butler, C.J. Bruegge, S. Biggar, P.R. Spyak, M.M. Pavlov, Bidirectional reflectance round-robin in support of the Earth observing system program, in *J. Atmos. and Oceanic Tech.,* 17, No. 8, 1077, 2000
5. Anderson, N., S. Biggar, C. Burkhart, K. Thome, M. Mavko, Bi-directional Calibration Results for the Cleaning of Spectralon Reference Panels in *Proceedings of SPIE*, 4814, 2002
6. Barnes, W.L., V.V. Salomonson, MODIS: A global image spectroradiometer for the Earth Observing System in *Critical Reviews of Optical Science and Technology*, CR47, 285-307, 1993
7. Xiong, X., K. Chiang, B. Guenther, W.L. Barnes, MODIS Thermal Emissive Bands Calibration Algorithm and On-orbit Performance in *Proceedings of SPIE – Optical Remote Sensing of the Atmosphere and Clouds III*, 4891, 392-401, 2003
8. Xiong, X., J. Sun, J. Esposito, B. Guenther, W.L. Barnes, MODIS Reflective Solar Bands Calibration Algorithm and On-orbit Performance in *Proceedings of SPIE – Optical Remote Sensing of the Atmosphere and Clouds III*, 4891, 95-104, 2003

Space solar patrol mission for monitoring of the extreme UV and X-ray radiation of the Sun

I. Afanas'ev, S. Avakyan, and N. Voronin
S.I. Vavilov State Optical Institute, St. Petersburg, Russian Federation

Abstract. The paper describes our proposal to make the monitoring of the extreme UV and X-ray radiation of the Sun in the spectral range of 0.14 - 157 nm. It has been noticed that this spectral range strongly affects to solar--terrestrial relationships, especially at the periods of solar activity. But at present, solar ionizing radiation is constantly monitored only in two spectral intervals: below 0.8 nm and above 115 (119) nm. This happened because of methodological and technical difficulties, which dealt with the necessity to use detectors of windowless optics. Such "solar - blind" detectors – open secondary-electron multipliers (SEM) – has been produced by the S.I. Vavilov State Optical Institute (SOI), Russia. Nowadays, being used the SEM detectors, all Space Solar Patrol (SSP) instrumentation has been created and laboratory tested.

Introduction

In recent years there has been an increase of the interest in researches of the solar activity and its effects in phenomena on Earth. It is generally known that solar activity events cause of numerous phenomena in solar-terrestrial relations. Unfortunately, there has not been monitoring the flux in the most geoeffective region of the spectrum (0.8-119 nm) from the full disk of the Sun. At the same time there are difficulties at the creating of International Standard for solar irradiance below 120 nm [Avakyan, 2005]. The monitoring does not exist due to technical and methodological difficulties in performing of measurements and calibration in the given spectral range. They are connected, first of all, with absence of ionizing radiation detectors, which must be true "blind" to high-power visible light of the Sun. But the SOI, using the long-term experience, has developed such stable, low-noise, highly effective SEM with the photocathode of beryllium oxide, which have the falling of sensitivity to 200 nm by ten orders [Avakyan et al., 1998]. The development and construction of the SSP instrumentation, which used the SEM detectors, occurred from 1996 to 2003 [Avakyan, 2005; Avakyan et al., 1998]. This experiment has been built for permanent absolute measurements of the ionizing (extreme ultraviolet (EUV) and soft X-ray) radiation from the full disk of the Sun. Every 72 seconds a spectrum from 0.14 nm to 198 nm will be recorded with a resolution fewer than 1.0 nm. The SSP instrumentation consists of two radiometers and two grating spectrometers (an EUV-Spectrometer of normal incidence and a X-ray/EUV-Spectrometer of grazing incidence) [Avakyan, 2005; Avakyan et al., 1998; Afanas'ev et al., 2005a]. The permanent monitoring will allow carrying out accurate spectroradiometric measurements of ionizing radiation from solar flares, determining absolute EUV and soft X-ray radiations and predicting all cooperation of solar events related with flares [Avakyan et al., 2003].

Space Solar Patrol instrumentation

The permanent SSP apparatus consists of following units:

1. The radiometer of ionizing radiation for 0.14-157 nm spectral range, which ensures measurements of the absolute radiation flux of the Sun in 20 spectral intervals, allocated by filters made from thin metal foils, thin films and also optical crystals [Avakyan et al., 1998; Avakyan et al., 2003]. The use of several filters (from different substances) on overlapped ranges of wavelengths allows us to execute mutual calibration of channels of the radiometer in flight. There is also the control of sensitivity stability of the radiometer by X-ray radiation of isotope ^{55}Fe.
2. X-ray/EUV-spectrometer of the space patrol (spectrometer of grazing incidence), which measures the spectrum of radiation of the Sun in the wide range (1.8–198 nm) owing to the use of the unique optical scheme without an input slit, with diffraction grating with the variable ruling step [Avakyan et al., 2002]. The entire spectral range is divided into four overlapping sections by four measuring channels: two main (1.8 – 23 nm and 22 – 63.1 nm) and two experimental (62 – 122.7 nm and 119 – 198.1 nm). The long-wave experimental channel contains a photoelectric multiplier with a MgF_2 window (FEU-142) to control the diffraction grating's efficiency in flight and to calibrate the spectrometer with UV lamps in laboratory conditions.
3. EUV-spectrometer (spectrometer of normal incidence), which is intended for measurement of radiation fluxes from full disk of the Sun in the region of extreme ultraviolet radiation (16-153 nm) with the spectral resolution better than 1 nm by six channels [Avakyan et al., 2001a; Afanas'ev et al., 2005b]. Thus, two channels for range 16-57 nm are experimental (for experimental determination of measuring ability of spectrometer) and there is the auxiliary channel for the 195-230 nm spectral range to align the spectrometer under the conditions of the normal atmospheric pressure.

Open SEM with the "solar - blind" photocathode from beryllium oxide and 16 trough-shaped beryllium bronze dynodes is the unique development of the SOI and is used as detectors of the ionizing solar radiation in all measuring channels of SSP apparatus. Using special technological processing of the dynodes, a quantum efficiency of about 10% can be obtained in the working wavelength range with an abrupt efficiency drop by no less than five orders of magnitude at wavelengths longer than 150 nm.

Now devices of SSP apparatus have passed laboratory calibration tests by UV and X-ray sources of radiation both in vacuum chambers of the SOI, and ESTEC (for radiometer) [Avakyan et al., 2001b, Avakyan et al., 1999].

Methodology of the Space Solar Patrol

The methodology of patrol measurements consists of simultaneous use both extreme ultraviolet (EUV) and X-ray/EUV spectrometers and two identical radiometers, and also in application of the special algorithm of detection of signals both radiation and charged particles from radiation belts. So, the spectrometers measure a detailed source function and its variations, whereas the radiometer

directed to the Sun give reference information to obtain absolute intensity of a solar radiation flux. The optical axis of the second radiometer lies at angle of 10-15^0 to that of the first radiometer, i.e. it does not track the Sun. It will allow to take into account the signals from the charged particle fluxes, which are detected by both radiometers at nearly the same pitch angles. So, the information about background of charge particles can be estimated, and as a result, the correct absolute measurements excluding the scattered light in the spectrometer can be obtained.

It should be noticed that all spectral ranges of channels in the SSP instrumentation (both the spectrometers and radiometers) are overlapped. So, the necessary methodological duplication of measurements is provided; thus, in spectrometers all spectral intervals of channels are overlapped in the most intensive and important lines of the solar spectrum.

Moreover, several channels of the SSP apparatus have been provided with monitoring of the stability of its absolute spectral sensitivity. Besides this, there is the plan (#2500 project of the International Science and Technology Center, executed together with the Budker Institute of Nuclear Physics, Novosibirsk, Russia [Nikolenko et al., 2004]) to carry out the absolute spectral calibration of the SSP instrumentation using a synchrotron radiation source just before the period of preparation of a spacecraft for its mission. In this case, two ^{55}Fe isotope radiation sources of different intensity will be used in the radiometer in the working spectral region around 0.2 nm. This allows to check the variation in the pre-flight calibration at this wavelength after launching. An additional possibility is to calibrate both the radiometer and the EUV spectrometer against the solar radiation with wavelengths longer than 150 nm appears in space. To this end, measuring the solar flux at wavelengths above 157 nm through a quartz crystal is provided in the radiometer, and the long-wavelength measuring channel in the EUV spectrometer is capable of detecting the spectrum up to 153 nm [Avakyan et al., 2003]. Finally, both of the spectrometers have auxiliary long-wave channels contained the FEU-142 photoelectric multiplier to measure radiation in the spectral region where the magnitude of variations in solar radiation fluxes does not exceed several percents during the eleven-year activity cycle and the 27-day period of rotation of the Sun. Therefore, these channels enable monitoring the stability of the diffraction grating's efficiency at the periods without solar flares. There were not found any effects of influence of space factors on working a FEU-142 photomultiplier at low orbits [Avakyan, 2005]. Lastly, with due account of the present success achieved in the patrol of the ionizing solar radiation at wavelengths shorter than 0.8 nm and longer than 120 nm, we provide a regular reference of our patrol data to these as well.

Conclusion

Till present there is no permanent monitoring of the short wavelength activity of the Sun in the most geoeffective spectral range (0.8 – 119 nm) due to methodological and technical difficulties with operation of detectors of windowless optics under space conditions. Due to use of the open secondary-electron multipliers we have overcome these difficulties and offer the Space Solar Patrol (SSP) instrumentation for monitoring of the extreme UV and X-ray radiation of the Sun. Now the SSP apparatus is completed and tested at the vacuum chambers of the S.I. Vavilov SOI and ESTEC (only radiometer). Within the frame new #2500 ISTC project the absolute calibration will be performed with high radiometric accuracy of all SSP instrumentation at the synchrotron radiation source. There are plans to launch of the SSP Mission at the Russian Module of the International Space Station for experimental operation (Radiometer and EUV-spectrometer) by the Rocket-Space Corporation "Energia" (Contract with Russian Space Agency). For permanent monitoring in the uninterrupted mode the SSP is also proposed to be installed on a satellite with solar synchronic orbit. So, the SSP mission for monitoring of the extreme UV and X-ray radiation of the Sun is a complete solution of the problem of the permanent patrol of ionizing radiation from the full disk of the Sun.

Acknowledgments This work has been supported by the grants of International Science and Technology Center (ISTC), Moscow, through the Projects #385, 385B, 1523 and 2500. The authors are grateful for the support of the foreign partners of these projects: A.D. Aylward (UK), J.-P. Delaboudiniere (France), A. Hilgers (Holland), N. Pailer, G. Schmidtke, and F. Scholze (Germany), Uk-Won Nam (Korea), and the heads and members of the Committee on Space Research (COSPAR), 1996; International Union of Radio Science (URSI), 1996; International Association of Geomagnetism and Aeronomy (IAGA), 1999; International Symposium on the Programme of the Thermospheric, Ionospheric and Geospheric Research (TIGER), 1999; Science and Technology Advisory Council under Russian Space Agency and Russian Academy of Science, 2000; International Standardization Organization (ISO), Working Group 4: Space Environment, 2004.

References

Afanas'ev I. M., Avakyan, S. V., Kuvaldin E. V., et al. Achievements in creation of the Space patrol apparatus of ionizing radiation of the Sun, *Nuclear Inst. and Methods in Phys. Res., Section A, 543,* 312-316, 2005.

Afanas'ev I. M., Voronin N. A., Suhanov V. L. et al. The organization of the channel of the "Solar patrol" instrumentation for correct orientation control to the Sun, *Opt. Zh. 72, No. 8,* 60-64, 2005. In press. [*J. Opt. Technol. 72 (8),* 2005, In press].

Avakyan, S. V., Space Solar Patrol: Absolute Measurements of Ionizing Solar Radiation, *Adv. in Space Res.*, 2005. In press.

Avakyan, S. V., Voronin, N. A., Yefremov, A. I., et al. Methodology and equipment for space-based monitoring of ionizing solar radiation, *Opt. Zh., 65, No.12,* 124-131, 1998. [*J. Opt. Technol., 65 (12),* 124-131, 1998].

Avakyan S. V., Andreev E. P., Kuvaldin E. V., et al. The laboratory testing of the space patrol apparatus for the solar ionizing radiation, *Proc. SPIE, 3870,* 451-461, Italy, 1999.

Avakyan S. V., Andreev E. P., Afanas'ev I. M., et al. Developing apparatus for permanent space patrol of the ionizing radiation of the sun, *Opt. Zh. 68, No. 6,* 54-62, 2001. [*J. Opt. Technol. 68 (6)*, 421-427, 2001].

Avakyan S. V., Andreev E. P., Afanas'ev I. M., et al. Laboratory studies of apparatus for monitoring ionizing solar radiation from space, *Opt. Zh. 68, No. 2,* 5-14, 2001. [*J. Opt. Technol. 68 (2),* 81-88, 2001].

Avakyan S. V., Andreev E. P., Afanas'ev I. M., et al. Development of an x-ray spectrometer for a Space Solar Patrol, *Opt. Zh. 69, No.11,* 36-40, 2002. [*J. Opt. Technol. 69 (11)*, 818-821, 2002].

Avakyan S. V., Andreev E. P., Afanas'ev I. M., et al. Creating of the permanent Space Patrol of ionizing solar radiation. *Proc. SPIE, 4853,* 600-611, USA, 2003.

Nikolenko A. D., Pindyurin V. F., Avakyan S. V., et al. Calibration of the apparatus of the Space solar patrol, *Digest Reports of the XV Int. Synchrotron Rad. Conf.,* 168, Russia, 2004.

Multi-channel ground-based and airborne infrared radiometers

Gérard Brogniez, Michel Legrand,
Laboratoire d'Optique Atmosphérique USTL 59655 Villeneuve d'Ascq cedex, France

Bahaiddin Damiri, Irina Behnert, Jean-Pierre Buis
CIMEL Électronique, 172 rue de Charonne 75011 Paris, France

Abstract. Infrared radiometers CLIMAT (Conveyable Low-noise Infrared radiometer for Measurements of Atmosphere and ground surface Targets) CE312 (Ground version), and CE332 (Airborne version) built by CIMEL Electronique, are conceived to measure, from the ground level, or from an aircraft, radiances coming from surfaces, clouds, or atmosphere. The radiometers achieve simultaneous measurements in three narrow spectral bands in the atmospheric window between 8 and 14 μm (700 and 1250 cm^{-1}).

Main characteristics and principles

- Digital radiometer with very good linearity.
- Very low noise, fast response, high stability over long term.
- Very weak change of sensitivity with the temperature, which permits its utilization in extreme thermal conditions, as at high altitudes.
- Only one sensitivity range whatever the incoming radiance.

The ground-based radiometer CE312 uses a thermopile situated into one cavity. A filter wheel allows the successive selection of the radiance incident into the thermopile in three narrow bands with FWHM = 1-μm, centered at 8.7 μm, 10.5 μm, and 12.0 μm. In addition, a broad-band (8-13 μm) measurement is also performed.

The airborne radiometer CE332 is composed of three cavities, i.e. one per channel, so that simultaneous measurement, particularly suitable for airborne measurements, can be performed. Each cavity has its own thermopile and optics.

Note that for each radiometer, the filters are interchangeable.

Both radiometers have Ge lenses with a non-reflective treatment. Dimensions and shapes of the objective (convex-plane lens), and of the condenser (meniscus lens), have been designed to minimize the geometrical aberrations. The condenser is located in the focal plane of the objective following the Köhler design. Then, the optical field of view is well delimited, with a value of 10° for CE312, and 3° for CE332, at half maximum.

The main advantages of thermopiles (thermal detectors) are the ambient temperature of operation, and a high level of detectivity, independent of the wavelength.

Detectors are equipped with a germanium window (between 8 and 14 μm). Above 15 μm, the radiation is blocked by a ZnSe window. Spectral transmittances of the objective $F_L(\nu)$, of the condenser $F_C(\nu)$, of the ZnSe filter $F_Z(\nu)$, of the detector window $F_D(\nu)$, and of the three narrow band-pass filters $F_i(\nu)$ have been measured. They are presented on the Figure 1 for the airborne instrument.

The global transmittance of the optics is given, for each channel i, by the transmittance product of each element:

$$F_G^i(\nu) = F^i(\nu) \times F_L(\nu) \times F_C(\nu) \times F_Z(\nu) \times F_D(\nu).$$

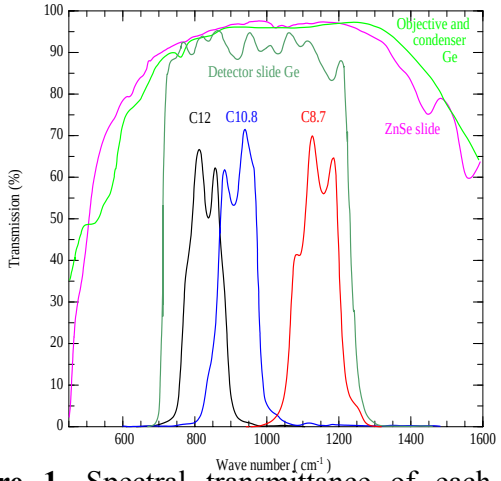

Figure 1. Spectral transmittance of each optic element of the radiometer CE332.

The cavities are not thermostatically controlled but accurately monitored by a platinum probe with a temperature sensor. Each cavity is used as a reference of radiance (Legrand et al., 2000). A gilded concealable mirror with a high reflection coefficient (99.74%) over the spectral domain 8-14 μm is located in front of the optical head. This mirror allows the radiance originating from the target (opened position) and from the thermopile cavity (closed position) to be compared. The airborne radiometer needs a pre-heating time of about 20 min (due to the thermal insulated cavities). The response time of the thermopile is 12 ms, and the acquisition frequency is 1s for the ground-based version, and 160 ms for the airborne

version. The noise N (expressed in term of standard deviation of brightness temperature for a cavity temperature T_C = 280 K) is about 0.05 K in each channel (Figure 2).

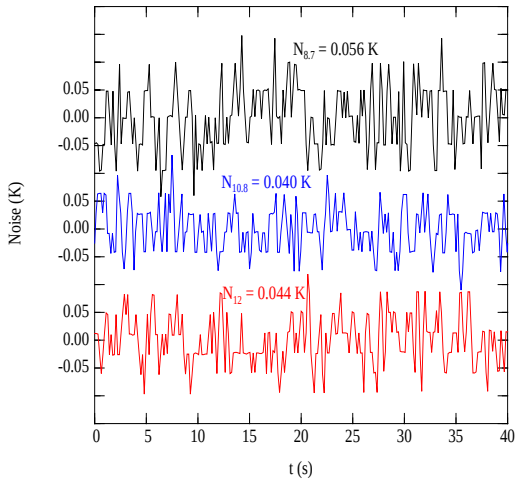

Figure 2. Noise of the radiometer in term of brightness temperature, on the three channels of the radiometer CE332.

The principle of the instrument is based on a differential method using the concealable mirror. The difference between the counts obtained with opened and closed positions of the mirror is linearly related with the corresponding radiances, as can be seen in Figure 3.

$C_s^i - C_m^i = \sigma^i \left(L_s^i - L_m^i \right)$, where σ^i is the sensitivity of the radiometer for channel i.

Stability $\frac{\Delta\sigma^i}{\sigma^i}$ of sensitivities is better than 1.5% per year, so that an internal blackbody is not useful.

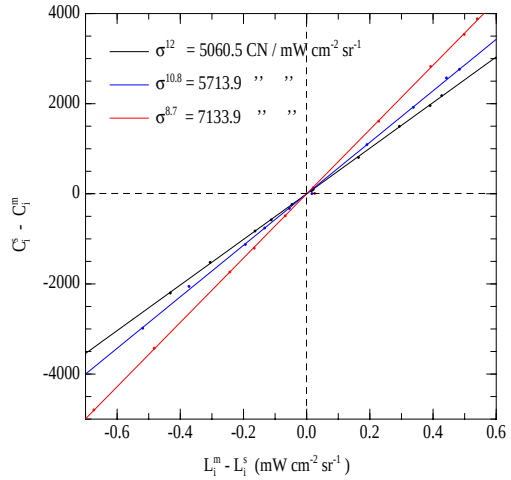

Figure 3. Sensitivities of the three channels of the radiometer.

Potential applications

The applications of these instruments are manifold. At the LOA they have been used for atmospheric research: cirrus cloud study – see French/Dirac airborne campaign (Brogniez et al, 2004), atmospheric dust (Pancrati, 2003). These instruments are also used in agronomy, geology, and for the determination of sea surface temperature using a split window method (Brogniez et al., 2003). They are also helpful for the determination of surface emissivities.

References

Legrand, M., C. Pietras, G. Brogniez, M. Haeffelin, N. Abuhassan, M. Sicard, A high-accuracy multiwavelengh radiometer for in situ measurements in the thermal infrared. Part1: Characterisation of the instrument. *J. Atmos. Ocean. Technol.*, *17*, 1203-1214, 2000.

Brogniez, G., C. Pietras, M. Legrand, P. Dubuisson, M. Haeffelin, A high-accuracy multiwavelength radiometer for in situ measurements in the thermal infrared. Part II: Behavior in field experiments. *J. Atmos. Oceanic Technol.*, *20*, 1023-1033, 2003.

Pancrati, O., Télédétection de l'aérosol désertique depuis le sol par radiométrie infrarouge thermique multibande. *Thèse de l'Université des Sciences et Technologies de Lille,* 203 pp, 2003.

Brogniez, G., F. Parol, L. Bécu, J. Pelon, O. Jourdan, J. F. Gayet, F. Auriol, C. Verwaerde, J. Y. Balois, B. Damiri, Determination of cirrus radiative parameters from combination between active and passive remote sensing measurements during FRENCH/DIRAC 2001. *Atmos. Res.*, *72*, 425-452, 2004.

Thermal Modelling and Digital Servo Algorithm for the next generation of Differential Absolute Radiometer

S. Mekaoui, and S. Dewitte
RMIB, Brussels, Belgium

Abstract. The Differential absolute radiometer developed at the Royal Meteorological Institute of Belgium operates on SOHO as part of the VIRGO experiment. DIARAD produces a 3 minutes sampled TSI time series since 1996 with 100 ppm repeatability after correction of the in-flight aging. This characteristic limits the detectability of the long term Total Solar Irradiance variability to 0.13 W/m². Any trend in the TSI signal below this level faces instrument's measurement limitations mainly due to the noise level of DIARAD's analogous servo system; if one assumes the stability of the reference voltages and the correct monitoring of the in-flight aging. In this paper we present a thermal model of the radiometric cavities using a finite difference approach and present the design of a new servo system. Adaptative servo system allows achieving noise levels as low as 20 ppm for DIARAD new generation, leading to a long term repeatability of about 0.03 W/m². We first recall the DIARAD's measurement principle and establish the radiometric equation. We then focus on the so-called thermal efficiency parameter defined as the fraction of the total heat dissipated in the cavity that flows through the heat flux sensor at the bottom of the cavity related to the incident radiation. We finally compare experimental results to a finite difference model and present the design of digital servo algorithm.

References

Crommelynck, D., V. Domingo, Solar Irradiance observation, *Science.,* 180-181, 1984.

Dewitte, S., D. Crommelynck, S. Mekaoui, A. Joukoff, Measurement and uncertainty of the long term total Solar Irradiance trend, *Sol. Phys 224*, 209-216, 2004.

Mekaoui, S., S. Dewitte, D. Crommelynck, A. Joukoff, Absolute accuracy and repeatability of RMIB radiometers for TSI measurements, *Sol. Phys 224*, 237-246, 2004.

Calibration of Filter Radiometers for Weathering and Photostability Tests

A. Schönlein
ATLAS MTT GmbH, Linsengericht, Germany

Abstract

The examination of the aging behavior of polymer materials and photostability examinations under the influence of sunlight or general weathering influences are also carried out in weathering devices.

With regard to the appearance of signs of aging, it is generally exposure to radiation which is seen as the primary cause of aging. In these cases, sunlight must be reproduced as realistically as possible by the equipment. The spectral distribution as well as the irradiance of sunlight on the earth's surface are dependent on the location as well as on the time of day and the time of year. The spectral distribution specified in CIE publication No. 85, Table 4, today serves as the reference spectrum for global radiation throughout the world. These requirements can be particularly well met by the spectral continuum provided by xenon radiation in conjunction with special filters in the UV range (photochemistry) and the IR range (thermal effect) for adjustment to various test conditions. A specific radiation function has been defined for global irradiation behind window glass, and this can also be reproduced very well through the employment of xenon radiation with corresponding filtration.

The level of irradiance at the exposure level has also been defined in test standards for the UV and visible ranges which are of such importance to photochemical processes.

In the test equipment itself, the irradiance within the wavelength range required for testing can be adjusted at the sample level within predefined tolerances.

Standardization requires the measurement of the irradiance primarily in the UV range which is important for photochemical processes.

Various filter radiometers have been developed to provide constant regulation as well as to test the irradiance at various wavelengths in the UV range as well as in the visible wavelength range at the sample level.

In the following, the filter radiometers employed in weathering equipment are introduced (relative spectral sensitivity, measuring range, stability, proper cosine evaluation). An extremely stable xenon lamp unit has been developed for the calibration of filter radiometers. The extensive calibration of these radiometers – starting from the national standard and going down to the radiometer's application in the weathering device – are also discussed.

Radiometric Calibration of a Coastal Ocean Hyperspectral Imager Using a Blue Enhanced Integrating Sphere

D. R. Korwan, J. H. Bowles, W. A. Snyder, M. R. Corson, C. O. Davis
Naval Research Laboratory, Washington, DC, USA

Abstract. The United States Naval Research Laboratory has been conducting hyperspectral remote sensing of the coastal ocean environment for nearly a decade and has recently extended the area under study into riverine estuaries. Data products include bathymetry, bottom and water classification, suspended sediments, CDOM, and phytoplankton. Surveys using the Portable Hyperspectral Imager for Low Light Spectroscopy (PHILLS) (Davis, et. al) have been performed at various locations including the Chesapeake Bay watershed region, Florida's east coast and Indian River areas, the Monterey coast, and the New Jersey coast at LEO XV.

Until now, radiometric calibrations have been performed using a Labsphere Unisource 4000, a 91cm integrating sphere with a 35.5cm exit port. It is illuminated by one to ten quartz halogen lamps internal to the sphere. The lamps are operated with a peak wavelength of about 1 micron or equivalently a black body temperature of about 3000K. Unfortunately the spectral shape of the lamps is not a good match to the spectral radiance measured in the field, as shown in figure 1. The net result is that the calibration of field data must be based on an extrapolation of a linear calibration curve since most of the spectral radiance levels from the sphere lie outside of the range of typical field radiances. This is shown in figure 1 for two measured field radiances. The first is of a cloud top and the other is for typical open ocean signal. The sensor is constructed so that it approaches full well capacity (yet not in the nonlinear region) when viewing clouds, and detects at the mid to lower end of the sensor's gain curve for water leaving radiances. As can be seen, at shorter wavelengths, the field radiances are larger than the sphere output at three lamps, and at the longer wavelengths the field radiances are smaller than the sphere output at just one lamp. Since calibrating the field data must rely on this extrapolation, small nonlinearities along the gain curve are hidden and can produce artifacts. One could argue that you could use lower intensity lamps, however this would only allow for a larger number of matched field/sphere radiances at longer wavelengths, but still no matches at the shorter wavelengths. Note that for most field modes (set by integration time, aperture, and lens), the sensor will saturate at longer wavelengths at three lamps. Since the sensor's CCD is read out in the spectral dimension, blooming creates unwanted signals at the shorter wavelengths. This sets an upper limit to the intensity of the lamps.

To combat these issues NRL, in conjunction with Labsphere, developed a "blue-enhanced" sphere using an external Xe arc lamp from Oriel in addition to an external halogen lamp. The sphere measures about 52cm in diameter and has a 23cm exit port. The resulting spectral output of the sphere is shown in figure 1, where it can be seen to more closely resemble typical field radiances over the full wavelength range of the instrument ,than does the Unisource 4000. During calibration, at-sensor radiance is controlled using apertures at the entrance ports of the sphere or by using well characterized, absorptive neutral density filters placed in front of PHILLS. In this paper, comparisons of calibrations using the two separate sources will be presented. Particular attention will be placed on possible calibration artifacts due to the spectral lines produced by the Xe lamp.

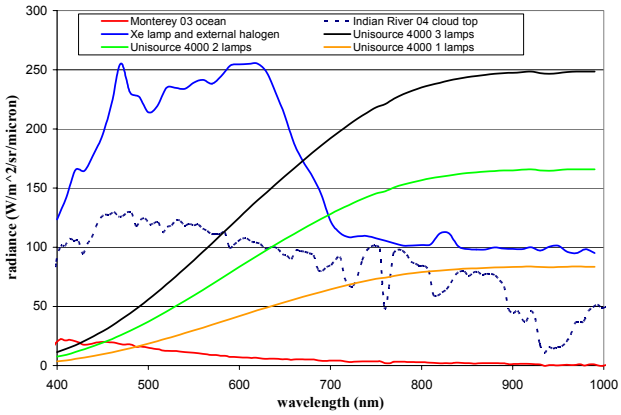

Figure 1. Comparison of the radiances of the Unisource 4000, the Blue-enhanced sphere, and typical field measurements (cloud top and open ocean)

Acknowledgments This work was funded by the Office of Naval Research.

References

C. O. Davis, J. Bowles, R. A. Leathers, D. Korwan, T. V. Downes, W. A. Snyder, W. J. Rhea, W. Chen, J. Fisher, W. P. Bissett, R. A. Reisse, "Ocean PHILLS hyperspectral imager: design, characterization, and calibration", Optics Express **10:4**, 210-221 (2002).

A Verification of the Ozone Monitoring Instrument Calibration

Using Antarctic Radiances

G. Jaross, J. Warner, R.P. Cebula, and A. Kashlinsky
Science Systems and Applications, Inc., Lanham, Maryland, USA

Abstract. A technique for evaluating the radiometric calibration of satellite-born radiometers has been developed utilizing the stable reflectance of the Antarctic land mass. Previously, the scene radiances measured over the Antarctic and Greenland land masses were used to monitor time evolution of sensor radiometric sensitivity and to compare instruments with similar spectral responses. Through the use of radiative transfer modeling, we can now evaluate the albedo calibration (Earth radiance sensitivity divided by solar irradiance sensitivity) of any nadir-viewing, polar orbiting sensor measuring in the 300-800 nm range. Our evaluation of the Ozone Monitoring Instrument on the NASA Aura spacecraft confirms a 2% calibration uncertainty.

The Ozone Monitoring Instrument

The Ozone Monitoring Instrument (OMI) launched aboard the Earth Observing System (EOS) Aura satellite on 15 July 2004 is intended as the successor to the Total Ozone Mapping Spectrometer (TOMS) operated by NASA over the past 25 years. With improved horizontal resolution and an expanded wavelength range (270-500 nm), the OMI capabilities extend well beyond those of TOMS. Traditional TOMS products (column ozone, surface reflectance, aerosol index, UV surface flux) depend upon knowledge of absolute albedo calibration and the relative albedo calibration between wavelengths. Establishing an accurate OMI calibration and maintaining calibration consistency with the TOMS instruments are of equal importance.

Furthermore, future data products will likely utilize OMI-measured radiances combined with radiances and products from other sensors, on Aura as well as on spacecraft in similar orbits. Given that no attempt was made to inter-calibrate OMI with other sensors prior to launch, a relative adjustment based upon in-flight data may be required to improve these products.

The ice radiance technique

Our approach to verifying a UV/VIS/NIR sensor's albedo calibration is to compare measured and computed radiances for Earth scenes with known backscatter properties. We have chosen the surface and atmosphere of Antarctica for their highly predictable behavior over a broad range of wavelengths and viewing conditions (Jaross et al.). The spatial extent of the continent provides good sample statistics for sensors with very large footprints, a characteristic that provides for verification of older data sets. The stable nature of the Antarctic radiances arises from the high surface reflectivity (> 90%), the regenerative nature of the pure snow coverage, and the relatively low aerosol concentrations.

The reflective properties of the Antarctic surface have been measured by numerous groups, most thoroughly and convincingly by Warren et al. They have published total hemispheric reflectance (Grenfell et al.) and a parameterization of reflectance anisotropy (Warren et al.) based on a variety of ground locations and viewing conditions. Their results compare well with model predictions for deep snow-covered surfaces. One important conclusion is that reflectance varies little between 300 nm and 650 nm, a range of primary interest for many Earth backscatter-measuring sensors.

Reflectance anisotropy is an important characteristic to include in radiative transfer models of snow surfaces. The top-of-the-atmosphere (TOA) radiance difference between a Lambertian and a forward scattering snow surface with the same reflectance grows from 2% at 350 nm to 7% at 600 nm. We have derived a mean bidirectional reflectance distribution function (BRDF) for the Antarctic surface using the Warren et al. anisotropy. We employed combinations of reciprocity and interpolation to generate a model covering 2π steradians in reflected angles and solar incidence angles down to 0°. Though the continent never receives direct illumination at less than 45° incidence, the radiative transfer model must account for diffuse scattered light that can arrive at any incident angle. Jaross et al. estimated that BRDF knowledge represents the largest error component in the TOA radiance predictions, approximately 2% at moderate solar zenith angles (SolZA).

In order to compare measured and calculated TOA radiances we created a look-up table of radiances using a Gauss-Seidel atmospheric modeling code (Herman et al.). This table has nodes covering all possible satellite viewing conditions, sensor wavelengths, surface pressures, and column ozone amounts. It does not include minor absorption species, aerosols, clouds, or a correction for rotational Raman scattering in the atmosphere. Monochromatic calculations were used to represent measurements with finite bandwidths, which are 0.4-0.7 nm in the case of OMI. A difference is computed between every valid Antarctic radiance measurement and a corresponding interpolated value from the table.

OMI results

In order to obtain the widest possible range of solar zenith angles, we chose OMI radiances measured during a 4 week period centered on December 21, 2004. The irradiance-normalized radiance differences at each wavelength were binned in solar and satellite zenith angles and the average computed for each bin.

Figure 1 contains the nadir-view results as a function of SolZA for several wavelengths. If OMI were perfectly calibrated and our model calculations were exact representations of the mean Antarctic surface and

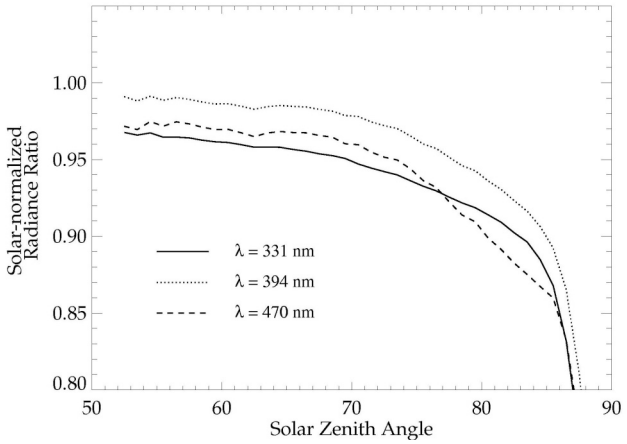

Figure 1. The ratio of solar-normalized radiances measured by OMI over Antarctica to those derived from a radiative transfer model. Shown for a selection of OMI wavelengths.

atmosphere, we would expect the result at each wavelength to be 1. The large radiance differences at high SolZA are primarily a result of poor surface characterization in our model. We have no reason to suspect a significant change in OMI sensitivity with angle. Large reflectance anisotropies, small measurement signals, and surface effects such as shadowing all contribute to model problems. The larger relative errors observed for long wavelengths are expected because of the greater contribution to TOA radiances from surface reflection compared to that from atmospheric Rayleigh scattering.

Results at low SolZA should be most accurate due to decreased sensitivity to modeling errors. Radiance ratios plotted in Figure 2 have been further averaged between 62° and 68° SolZA. These OMI results suggest a radiometric bias of 2.5% between 330 nm and 500 nm. The wavelength-independent albedo calibration uncertainty (1σ) for OMI in the nadir view is 2% (Dobber et al.). We anticipate substantially better relative calibration between wavelengths, something that is born out by these results. The residual structure observed between wavelengths is most likely the result of ignoring Raman scattering in our model, and the dip at 477 nm results from the O_2-O_2 collisional complex. The decrease at wavelengths less than 330 nm could be a result of ozone cross section errors caused by our monochromatic calculations.

MODIS comparisons

As a validation of our OMI results, we directly compared MODIS and OMI radiances. We chose MODIS data from the EOS Aqua spacecraft due the similarity of the Aura and Aqua orbits. Since we compared only nadir views, this restriction was not critical. The measured radiances for MODIS bands 3, 8, 9, and 10 were binned and aggregated in a manner identical to that described above for OMI. For the comparison, we averaged multiple OMI measurements over each MODIS spectral band width. The lack of any significant SolZA dependence in the radiance ratio confirms that the behavior seen in Figure 1 is caused by our model rather than instrumental effects.

After accounting for small differences in the solar flux measured by OMI compared to MODIS, we computed the albedo calibration difference of the two as a ratio of OMI to MODIS for each of the bands. These 5-6% differences are seen in Figure 2. We note that Band 10 data are available at only the highest solar angles over the continent, so we expect larger errors.

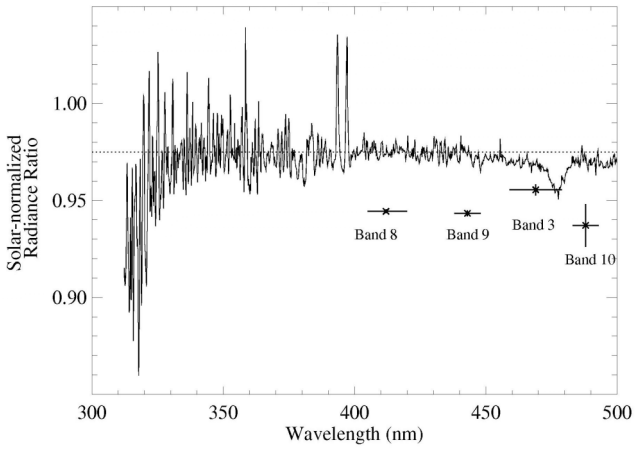

Figure 2. The ratio of measured and modeled Antarctic radiances are shown over part of the OMI spectral range. The ratio of OMI and MODIS /Aqua radiances are also shown for 4 of the MODIS reflective bands (1σ error bars shown).

Conclusions

The OMI solar-normalized radiances measured over the Antarctic continent compare well with our modeled radiances. Given the 2% radiometric calibration uncertainty of OMI and our 2% estimated fractional uncertainty for the ice radiance technique, we are pleased with the observed 2.5% difference. We believe there are good explanations for the spectral structure seen in the difference. Differences with MODIS are larger than can be explained by OMI calibration errors alone. The implication of Figure 2 is that MODIS differs from model results by approximately 3%. This is troubling because the published radiometric uncertainties for these MODIS bands are less than 2% (Esposito, et al.). It is our hope that a direct comparison between MODIS and our model will yield better agreement.

Acknowledgments The authors were supported under NASA contracts NAS5-00220, NAS5-01069, and NAS5-98016.

References

Dobber, M., Ozone Monitoring Instrument calibration, submitted to *IEEE Trans. on Geosci. and Rem. Sens.,* 2005.

Esposito, J., X. Xiong, A. Wu, J. Sun, W. Barnes, MODIS reflective solar bands uncertainty analysis, *Proc. SPIE Earth Observing Systems IX*, *5542*, 437-447, 2004

Grenfell, T., S. Warren, P. Mullen, Reflection of solar radiation by the Antarctic snow surface at ultraviolet, visible, and near-infrared wavelengths, *J. Geophys. Res.*, *99*, 18669-18684, 1994

Herman, B., T. Caudill, D. Flittner, K. Thome, A. Ben-David, A comparison of the Gauss-Seidel spherical polarized radiative transfer code with other radiative transfer codes, *Appl. Optics*, *34*, 4563-4572, 1995.

Jaross, G., A. Krueger, D. Flittner, Multispectral calibration of remote sensing instruments over Antarctica, *Metrologia*, *35*, 625-629, 1998.

Warren, S., R. Brandt, P. Hinton, Effect of surface roughness on bidirectional reflectance of Antarctic snow, *J. Geophys. Res.*, *103*, 25789-25807, 1998

Session 5

Photometry and Colorimetry

Review on new developments in Photometry

G. Sauter
PTB, Braunschweig, Germany

Abstract. Focused on light sources like LEDs or combinations of them, the specific needs for their characterization are mentioned and appropriate measurement devices are explained: Photometer bench - 40 m length with camera aided alignment tools and automated holders for sources and photometers - measures in one run luminous intensity and 6 related sensitivity coefficients to state value and associated measurement uncertainty. 2.5 m integrating sphere determines luminous flux values by substitution method with monitored throughput using an LED-cluster - instead of the auxiliary lamp - operated in modulated mode and measured by lock-in technique. Robot-goniophotometer scans the angular intensity distribution designed for a hemispherical mounting and optimized either for industrial needs (fast measurement with 8 heads measuring simultaneously at fixed 2.5 m radius) or for research and calibration capable to move heads on arbitrary traces with variable radius up to 3 m and speeds up to 1 m/s.

1. Introduction

This review on new developments in photometry is focused on LEDs and their combination to arrays or clusters including the needs of industrial measurements, which have to be traced back to national standards and noticed as equivalent to global key comparison reference values. The traditional separation between lamps and luminaires allowed to optimize their different properties individually to get the final combination for a certain illumination application. Simply spoken: lamps were designed for general purpose and characterized by the total luminous flux for a specified correlated color temperature and color rendering index, while luminaries gave the adaptation to the application under constraints like economics of installation and use, and ergonomic (quality of illumination) as well as stylistic factors (design of the luminaire). Besides the general demand for high efficiency, the spectral, angular and aerial distributions are main issues.

Such a separation no longer yields for light sources, which are assembled of a number of LEDs or OLEDs. If these are combined as an extended array for the back illumination of a diffuse transmitting window, the characterization has to use the quantities of luminaires (distance between LEDs is much larger than their maximum size, angular distribution of the LEDs is Lambertian or wider). If the combination forms a compact cluster, then the appropriate characterization has to follow the format known from reflector lamps (minimum distance between the LEDs, narrow or "beamed" angular intensity distribution). The luminous flux of an LED increases (nearly) linear with the forward current, and simultaneously the consumed electrical power increases as well as the temperature. For high power LEDs, with efficiencies comparable to known light sources, the temperature and cooling are main topics, specifically because a rise in temperature will change the luminous flux and will shift the relative spectral power distribution.

2. Photometer bench

The new photometer bench system at PTB is divided in 6 sections up to 17 m length, which allow a maximum distance between source and photometer of 40 m. On one side a 20 kW halogen-lamp operated at CIE illuminant A produces an illuminance up to 10 klx, while on the other side in 30 m distance a 12 kW metal halide lamp produces nearly 100 klx with a spectral power distribution close to daylight. A motor-driven carriage with one spectrometer and up to 6 photometers (reference and test) moves between the two lamps, which varies the two illuminance values by more than two orders of magnitude. The system is intended to characterize e.g. sensors for illumination management, which can be carried out software-controlled including the variation of distance and its measurement by absolute encoding, the change of photometers and sensors, any setting of shutters, amplifiers, and power supplies just as the data acquisition by the DVMs, with the spectrometer and for environmental quantities.

The bench system is also designed for the calibration of modern light sources, which are mounted and aligned (6 degrees of freedom) on two more carriages (similar to the photometer carriage) on a short bench. The short bench is located between the high power lamp and the end of the long photometer bench, with its optical axis rectangular to the axis of the long bench. Two telescopes for the lamp alignment at the ends of the short bench and a third telescope temporarily placed on the long bench are supported by three video cameras, which are connected to a computer. Their images are displayed on a screen and presented to the operator during the manual alignment procedure and finally stored for documentation.

Each carriage for a light source has two more motor-driven axes forming a spherical coordinate system: A vertical axis φ, rectangular to the optical axes of the two benches and a horizontal axis ϑ parallel to the optical axis of the short bench. The luminous intensity value assigned to the light source depends on these settings. The variation of the two rotations ϑ, φ, of the distance d to the photometer, of the dislocation Δx in direction of the short bench and finally of the lamp current J allow the determination of the related sensitivity coefficients for the measured luminous intensity $I = I(\vartheta, \varphi, d, \Delta x, J)$.

The variations are software-controlled as before and they are performed during one run for a typical lamp calibration procedure. This individual knowledge can reduce the measurement uncertainty associated to the luminous intensity value especially for LED-clusters with non-Lambertian angular distributions.

3. Integrating sphere

The determination of the total luminous flux Φ using integrating spheres is well known. Monitoring and correction of any changes of the sphere throughput between the measurements of the reference Φ_R and the device under test is explained. Instabilities can be corrected by the division of the measured indirect illuminances E, E_R (index "R" refers to reference) with the ratio of the two related photocurrents y_{AR}/y_A produced by the light of the auxiliary lamp (index "A" refers to auxiliary lamp) and it yields $\Phi = \Phi_R (E/E_R)(y_{AR}/y_A)$. Provided the auxiliary lamp is replaced by an LED cluster operated in modulated mode and the related photocurrents are measured using lock-in technique, then the two photocurrents for the ratio can be measured simultaneously with the sequentially determined indirect illuminances. This ratio of photocurrents corrects all changes of the throughput originated by self-absorption, temperature dependence of the coating etc.

In case of high power LEDs or clusters built from these LEDs, cooling with an extended heat sink is needed. Usually the light is emitted to one side of the LED in the related hemisphere, while the other side is connected to the heat sink, which would create very high self absorption, if the whole device would be placed inside the integrating sphere. Therefore, a geometry known as "external source" with the LED located outside the sphere, but close to a sphere port is preferred, and only a partial luminous flux is measured. This quantity is internationally discussed but not yet agreed.

Nevertheless, during industrial production of LEDs all devices are tested and have to be selected in several groups specified for colors and luminous intensity or luminous flux. The measurement of the total luminous flux would take too much time, therefore only a partial luminous flux is measured. The measurement method and the use of reference standards is discussed including effects of stray light and self absorption.

4. Robot-Goniophotometer

Goniophotometers are used for the measurement of the angular luminous intensity distribution of a light source, which is the basis for the fundamental determination of either the total luminous flux or of arbitrary parts of that, known as partial luminous fluxes. The conversion of the Cartesian coordinate system associated to the light source to the related spherical coordinate system $\{r, \vartheta, \varphi\}$ shows that any surface completely enclosing the light source in its center is achieved by only two rotations around the axes $\{\vartheta, \varphi\}$. These axes intersect rectangularly and several mechanical solutions are already known. But there are two disadvantages of these systems, first the long duration (>30 min) for a complete scan in all directions and second the constant radius of the enclosing sphere.

A new robot-goniophotometer of the compact type was developed, which offers several advantages. The fictitious enclosing sphere of the old systems is now divided in two hemispheres, each of which is mechanically realized by rotation of a head around two axes intersecting with an angle of only 45°. The lamp holder with the lamp operated in any burning position is placed in the plane just between the two hemispheres. This concept is already realized in two versions. One robot-goniophotometer is optimized for fast and flexible measurements in industrial environments with a constant radius of about 2.5 m and places for 4 different heads for each hemisphere measuring simultaneously. This allows the combination of a tristimulus head, a spectrometer, an UV-A-radiometer and one more spectral weighting depending on the type of light source.

The robot-goniophotometer realized at the PTB has three robots. One robot aligns the lamp in the center of the instrument and holds it in the defined burning position. The two other robots move the heads on arbitrary traces within that hemisphere with variable radius up to 3 m and maximum speed of 1 m/s in any direction. Within the working volume the mechanical properties (traces, locations) are verified by a laser tracker system taking up to 1000 readings per second for direction and distance with an expanded uncertainty ($k = 2$) of maximum 0.1 mm.

Each head combines tristimulus channels, an UV-A-radiometer and a spectrometer for the visible spectral range. The spectrally integrating channels have individual amplifiers with converters for data acquisition. The installation of the robot goniophotometer is nearly completed and first characteristics will be available at the time of the meeting.

5. Mobile Laboratories

The density of all traffic (automotive, aviation, ship) grows and the daily duration of high density traffic lengthens. This increases the demand for quality in e.g. road illumination, airport taxi-way marking and boat signaling and it reduces the time available for testing the proper functioning of these installations. Therefore, testing facilities denoted as "mobile laboratories", become popular. Often video cameras are mounted around a car, and driven with a speed up to 50 km/h. The recorded sequences are analyzed using digital image processing. Provided a traffic sign produces a specific light-pattern, then the image of the pattern of a standard can be taken as reference and compared relatively with those recorded earlier. If specified values of luminance have to be measured, then the camera system has to be calibrated with a homogeneous standard like the opening of an integrating sphere. These calibration techniques for cameras will be discussed briefly.

6. Conclusion

The facilities explained above are already declared as Major European Investments and by this offered to other National Metrological Institutes for cooperation either in projects for research or as tools for calibration and testing. Comparing the low relative standard uncertainty of the realized units (about 0.2%) with the much higher relative standard uncertainty (> 2%) at the industrial production control, then the reduction of this gap of about one order of magnitude is identified as an important aim, and more effort is spent to support applied photometry and colorimetry with appropriate reference standards and substitution methods.

Linking Fluorescence Measurements to Radiometric Units

C. Monte[1], U. Resch-Genger[1], D. Pfeifer[1], D.R. Taubert[2], J. Hollandt[2]

[1] Federal Institute for Materials Research and Testing (BAM), Richard-Willstätter-Straße 11, D-12489 Berlin, Germany
[2] Physikalisch-Technische Bundesanstalt (PTB), Abbestraße 2-12, D-10587 Berlin, Germany

Introduction

Fluorescence techniques are among the most widely used analytical tools and detection methods in material sciences, environmental analysis and the life sciences. However, comparability of fluorescence data across instruments, laboratories, and over time is only possible with large uncertainties due to the variety of fluorescence instruments and the many possible sources of error inherent to fluorescence spectroscopy. To improve this situation, there is an urgent need for simple, internationally accepted and ideally standardized procedures for the performance of fluorescence measurements and instrument characterization in combination with suitable physical and chemical transfer standards.

In the framework of the project "Development, Characterization and Dissemination of Fluorescence Standards for the Traceable Qualification of Fluorometers" by the Federal Ministry of Economics and Labour of Germany it was our goal to develop, provide, and promote suitable calibration tools and procedures to facilitate the traceability of fluorescence spectra to radiometric primary standards and to eventually link fluorescence measurements to radiometric units for a broad range of applications.

Two approaches to traceable fluorescence measurements

Due to different aims, it is necessary to address two target groups with different strategies and different types of standards.

For **metrological or reference laboratories** equipped with high accuracy fluorescence instruments, absolute measurements and minimization of calibration and measurement uncertainty are of primary interest. Accordingly, application of physical transfer standards for both spectral radiance (see references) and spectral responsivity with their small uncertainties is the method of choice for instrument characterization. The most critical point is here to develop a calibration method for the emission channel that ensures a similar spectral radiance at the sample position for instrument characterization as well as for typical fluorescence measurement tasks. We will present necessary procedures and currently achievable uncertainties. The uncertainties result from a state-of-the-art calibration of the current reference fluorometer at BAM, a modified commercial instrument. In addition, we will illustrate our attempts to further reduce these uncertainties with a new reference fluorometer designed and constructed by BAM and a calibration scheme relying only on trap detectors and a reflectance standard. This instrument (see references) is designed for measurement and dissemination of absolute fluorescence spectra and quantum yields with lowest possible uncertainties.

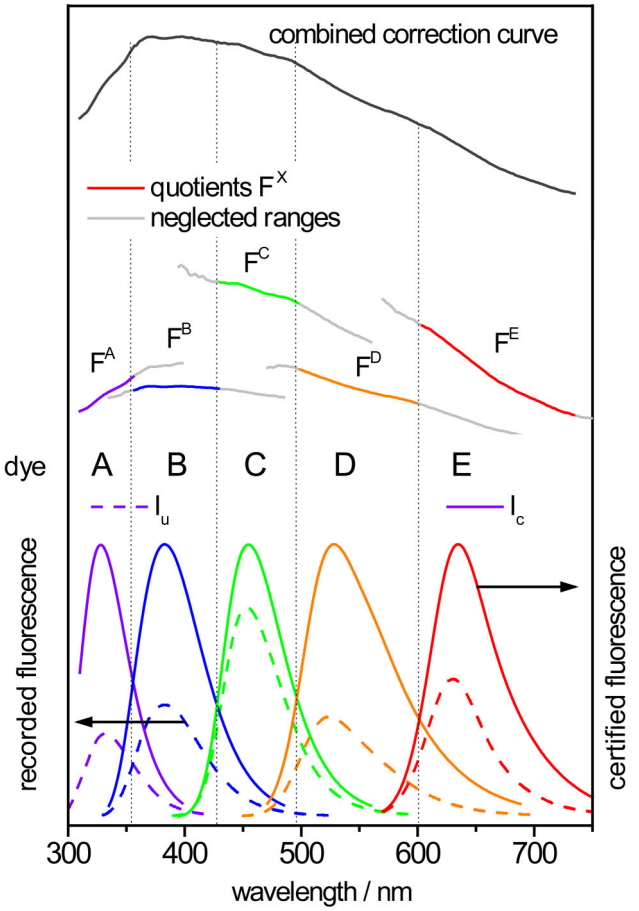

Figure 1. Determination of an emission correction curve with the liquid fluorescence standards dye A – E by division of recorded, i.e., uncorrected instrument-specific fluorescence emission spectra $I_U(\lambda_{em})$ and BAM-certified, i.e. corrected instrument-independent fluorescence emission spectra $I_C(\lambda_{em})$. A subsequent weighted combination of the individual quotients F^x results in an overall emission correction curve which equals the relative spectral responsivity of the instrument to be calibrated.

For the **broad community of users** of fluorescence techniques with instruments covering the range from spectrofluorometers over microplate readers to fluorescence microscopes, ease of use of standards has to be given priority. This is accomplished with a set of liquid spectral fluorescence standards developed by BAM and consisting of organic dyes. With these chemical standards and a simple procedure, determination of the spectral characteristics (Figure 1) and long-term performance of different types of fluorescence instruments is possible.

These standards match in an ideal way the optical and radiative properties of typical samples. Thus, many difficulties arising from the calibration with physical transfer standards can be elegantly avoided. The certified corrected fluorescence spectra of these standards are determined with the BAM reference fluorometer that was previously characterized with PTB-calibrated physical transfer standards. Accordingly, they are traceable to the primary standard of the spectral radiance realized in Germany by PTB.

Proficiency Test

The spectral fluorescence standards dye A – E (see references) and the according calibration procedure have been successfully employed for the characterization of the relative spectral responsivity of several commercial spectrofluorometers. Moreover, they have been successfully tested in a recently performed exploratory study on the state-of-the-art of the calibration of spectrofluorometers and colorimeters employing physical and chemical transfer standards. This study was organized by BAM and NIST with NPL, NRC, and PTB participating.

Acknowledgments This work has been funded as part of the project VI A2 -18 “Development, Characterization and Dissemination of Fluorescence Standards for the Traceable Qualification of Fluorometers” by the Federal Ministry of Economics and Labour of Germany.

References

Hollandt, J., Taubert, R.D., Seidel, J., Resch-Genger, U., Gugg-Helminger, A., Pfeifer, D., Monte, C., Pilz, W., Traceability in Fluorometry - Part I: Physical Standards, *Journal of Fluorescence*, *15*, 311, 2005

Resch-Genger, U., Pfeifer, D., Monte, C., Pilz, W., Hoffmann, A., Spieles, M., Rurack, K., Hollandt, J., Taubert, R.D., Schönenberger, B., Nording, P., Traceability in Fluorometry - Part II: Spectral Fluorescence Standards, *Journal of Fluorescence*, *15*, 325, 2005

Resch-Genger, U., Hoffmann, K., Nietfeld, W., Engel, A., Neukammer, J., Nitschke, R., Ebert, B., Macdonald, R., How to Improve Quality Assurance in Fluorometry: Fluorescence-Inherent Sources of Error and Siuted Fluorescence Standards, *Journal of Fluorescence*, *15*, 347, 2005

The design and the realization of the BAM reference fluorometer is the topic of an additional poster presentation at the conference

A new compact integrating sphere based spectral radiance standard with reduced radiance is also presented on an additional poster.

The fluorescence standards dye A – E are commercially available as BAM-F001 – BAM-F005.

Photoluminescence from White Reference Materials for Spectral Diffuse Reflectance upon Exposure to the Radiation Shorter than 400 nm

H. Shitomi, and I. Saito

National Metrology Institute of Japan, National Institute of Advanced Industrial Science and Technology (NMIJ/AIST), 1-1-1 Umezono, Tsukuba, Ibaraki, 305-8563, JAPAN

Abstract. Photoluminescent properties of white reference materials used as spectral diffuse reflectance standards were studied in the near UV to visible region. Spectroscopic analysis based on a two-monochromator method revealed that most of white reference materials produced the photoluminescence upon exposure not only to the near UV and UV radiation but also to the visible radiation shorter than 400 nm.

Introduction

Spectral diffuse reflectance measurements in the visible region are quite important for accurate reflectance colorimetry. At the National Metrology Institute of Japan (NMIJ), a national standard of spectral diffuse reflectance in the visible region have been successfully established with the combination of a new integrating sphere-based absolute reflectance measurement, modified Sharp-Little method[1], and a specially designed integrating sphere with uniform reflectance[2]. In addition, a new reference spectrophotometer has also been developed and new calibration services directly traceable to the national standard is now in operation[3].

General way to calibrate the spectral diffuse reflectance is substitution or comparison measurements. In principle, spectral diffuse reflectance of samples, in many cases white diffusing materials, can be calibrated by relative comparison to white reference materials of known reflectance. There are strict requirements for the white reference materials in terms of reflection properties, such as short-term and long-term stability, reflectance uniformity, lambertian approximation, non-photoluminescent property, spectral non-selectiveness and so on. At present, some kinds of white reference materials are commercially available, and their reflection properties have been thoroughly investigated and reviewed[4]. Photoluminescence is one of the most significant error factors related to the reflection properties of the white reference materials to be considered in diffuse reflectance measurements in the visible region, especially in the measurements using commercial instruments based on polychromators. It is well known that most materials produce photoluminescence upon exposure to intense UV radiation, which tends to be more noticeable in the shorter wavelength range. UV-cut filters are usually applied in commercial instruments to eliminate the UV radiation that would cause the photoluminescence from samples. As most white reference materials are considered not to produce photoluminescence upon exposure to the near UV and visible radiation, almost no attention has been paid so far to such kind of photoluminescence except for a few studies that referred to the existence of the photoluminescence on a kind of opal glasses[5] and ceramic tiles[6].

However, a series of our research revealed that some kinds of white reference materials produced the photoluminescence even on exposure to the shorter edge part of the visible radiation.

This paper describes the results on the evaluation of the photoluminescent properties for various kinds of white reference materials in the near UV to visible region. The effect of the photoluminescence in the general reflectance calibration is also discussed.

Samples and experimental setup

The photoluminescent properties were studied for these materials; 1) two kinds of pressed and sintered polytetrafluorethylene (PTFE) resins, 2) two types of matte ceramic tiles, 3) three kinds of matte opal glasses, and 4) three kinds of barium sulfates. These materials are well known for their excellent reflection properties and have been widely used as reflectance standards worldwide for many years.

Spectroscopic analyses in terms of photoluminescence spectra were applied to evaluate the photoluminescent properties of the samples. The photoluminescence spectra were measured with the NMIJ spectrofluorimeter based on the two-monochromator method over the wavelength range from 300nm to 700nm. The wavelength of the radiation for excitation was selected from 300 nm to 450 nm. A commercial spectrofluorimeter (Hitachi, F4500 ®) was also employed to check the reproducibility of the measurements.

The schematic diagram of the optical system of the NMIJ spectrofluorimeter is shown in Fig.1. It consists of two monochromators, a 150W Xe-arc lamp, a photo-multiplier tube (PMT) and some optical components. The first monochromator generates monochromatic radiation with the bandwidth of about 5nm, and the second one monochromatically detects the photoluminescence produced from samples. Relative spectral responsivity of each monochromator was calibrated using a spectral irradiance standard lamp and a Si photodiode with spectral responsivity scale. In this study, some UV-filters and sharp-cut filters were selected according to the excitation wavelength and put in front of the second monochromator to eliminate the reflected radiation.

Results and Discussion

Fig.2 shows a part of photoluminescence spectra of white reference materials; a PTFE resin, two matte ceramic

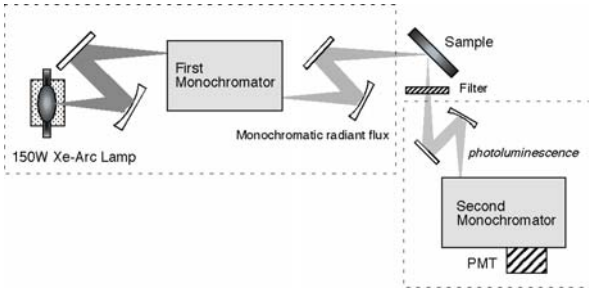

Figure 1. Schematic diagram of the optical system of the NMIJ spectrofluorimeter used in this study.

tiles, a matte opal glass and a sprayed barium sulfate plate, measured in this study. In Fig.2, the excitation wavelength is at 330 nm and 360 nm, respectively.

The matte ceramic tile (1) shows the greenish photoluminescence that has the spectrum with its peak around 530 nm. The matte ceramic tile (2) shows the unique red photoluminescence whose spectrum has relatively sharp structure around 670 nm. The matte opal glass shows the bright blue photoluminescence with the peak around 440 nm. The PTFE resin and the sprayed barium sulfate plate show the weak dark-purple or dark-blue photoluminescence with the peak around 405 nm and 420 nm, respectively. Roughly, the shorter the wavelength for the excitation becomes from 400 nm down to 300 nm, the larger the intensity of photoluminescence from each sample becomes.

From these measurements, it was found that most samples examined in this study showed the photoluminescence not only by the UV radiation but also by visible radiation. It is noticeable results that the photoluminescence was observed from most samples with excitation by the shorter edge part of visible radiation, which has not been considered in diffuse reflectance measurements. Among the five samples shown in Fig.2, the matte opal glass and matte ceramic tiles showed the relatively strong photoluminescence at both excitation wavelengths, whereas the other samples showed weak photoluminescence. The opal glass showed in Fig.2 is the same type of opal glass that the strong photoluminescence due to UV radiation was reported in the past[5]. By contrast,

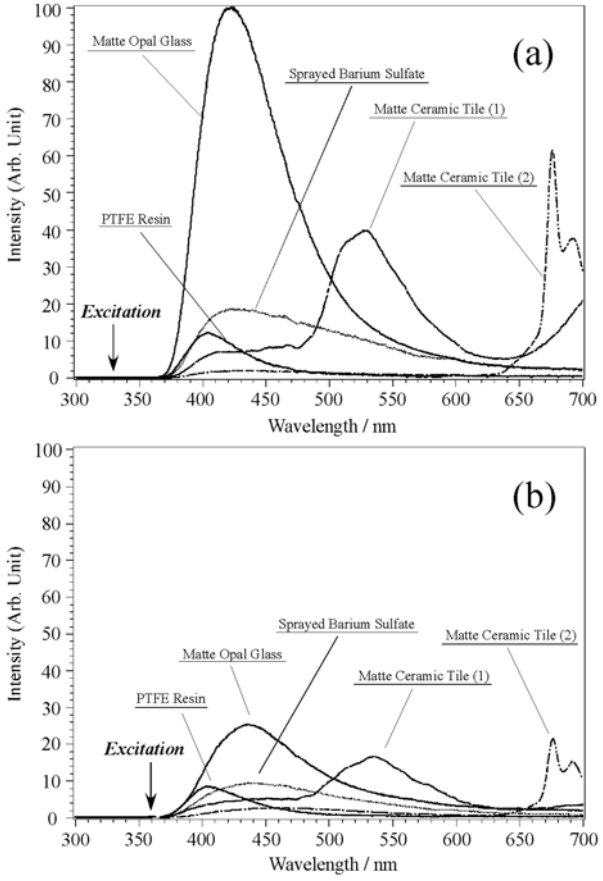

Figure 2. Photoluminescence spectra of white reference materials with excitation by the radiation at (a) 330 nm and (b) 360 nm, respectively. The vertical axis shows the relative photoluminescent intensity from each sample that was normalized using the strongest photoluminescent as unity.

another opal glasses examined in this study showed quite weak photoluminescence upon exposure to the visible radiation, although the spectra are not shown in this paper. Furthermore, photoluminescent properties of PTFE resins and barium sulfate plates showed strong dependence on the purchase date, brand of raw materials, frequency in use, forming procedures and store conditions. It is a tentative result but in this study, appropriately stored or fresh samples of these showed almost no photoluminescence upon exposure to both near-UV and visible radiation. More detailed investigation about the photoluminescent properties of white reference materials including the origin of the photoluminescence is now in progress.

Commercial instruments for spectral diffuse reflectance measurements basically are not equipped with structures to eliminate errors due to the photoluminescence upon exposure to the visible radiation. However, it would cause relatively large error in the spectral diffuse reflectance measurement, depending on the measurement condition such as the spectral responsivity of detectors, bandwidth, spectral distribution of incident radiation, measurement geometry and so on. More thorough attention to the photoluminescence from white reference materials is essential to ensure the accurate and reliable calibration for the spectral diffuse reflectance.

Conclusion

Most of white reference materials used as diffuse reflectance standards tend to produce the photoluminescence upon exposure not only by the UV radiation but also by visible radiation. Such photoluminescent effect was observed at the radiation shorter than 400 nm in this study. Although almost no attention has been paid to such photoluminescence, especially to that due to the visible radiation, it would cause relatively large error in the spectral diffuse reflectance measurement, depending on the various measurement conditions.

Acknowledgments We would like to thank Dr. A. Springsteen, Avian technologies LLC, for his useful comments and advices on the photoluminescent properties of white reference materials examined in this study.

References

1) Shitomi, H., and Saito, I., New realization of spectral diffuse reflectance standard at NMIJ, *Proceedings of 10th Congress of the International Colour Association (AIC Colour 05),* 523-526, 2005.
2) Shitomi, H., Mishima, Y. and Saito, I., Development of a new integrating sphere with uniform reflectance for absolute diffuse reflectance measurements, *Metrologia, 40,* S185-S188, 2003.
3) Shitomi, H., Mishima, Y. and Saito, I., Establishment of an absolute diffuse reflectance scale and calibration systems at NMIJ/AIST, *Proceedings of 25th Session of the CIE,* 78-81, 2003.
4) Springsteen, A., Standards for the measurement of diffuse reflectance - an overview of available materials and measurement laboratories, *Anal. Chim. Acta, 380,* 379-390, 1999.
5) Zwinkels, J. C., Gauthier, F., Investigation of photo-luminescent effect in opal glasses used as diffuse reflectance standards, *Proceedings of Fourth Oxford Conference on Spectroscopy, SPIE Vol.4826,* 70-78, 2003.
6) Pons, A., Campos, J., Spectrophotometric error in Colour Coordinates Introduced by Fluorescence of White Calibration tile, *Color. Res. Appl., 29,* 111-114, 2004.

A Simple Stray-light Correction Matrix for Array Spectrometers

Y. Zong, S. W. Brown, B. C. Johnson, K. R. Lykke, and Y. Ohno
National Institute of Standards and Technology, Gaithersburg, Maryland, USA.

Abstract. A stray-light correction matrix has been developed for array spectrometers. By using the correction matrix, measurement errors arising from stray light are corrected by a simple, fast matrix multiplication. Validation measurements demonstrate that stray-light errors are reduced by one to two orders of magnitude, to a level less than 10^{-5} of the measured signal of broad-band sources, equivalent to less than one count of the 15-bit-resolution instrument. By applying the stray-light correction, the error in a spectroradiometer calibration was significantly reduced in the UV region, and the error in a LED color measurement was reduced by ≈ 0.01 in chromaticity coordinates (x, y).

Introduction

Array spectrometers are used in a wide range of applications in the fields of spectroradiometry, spectrophotometry, colorimetry, photometry, and optical spectroscopy due to the benefits of measurement speed, sensitivity, portability, and affordability. Array spectrometers, however, are single grating instruments, and there are intrinsic limitations to their measurement accuracy. Among several sources of errors, stray light is often the dominant source of measurement error in these instruments. Because of stray light inside the instrument, significant errors can occur when measuring light sources having dissimilar spectra from the standard source. Stray light error is serious when measuring a very low level spectral component at some wavelength while there are high level components in other wavelength regions. Currently, reliable standard sources other than tungsten lamps (and deuterium lamps for UV) are not available and errors due to stray-light are inevitable.

Brown, *et al.*, developed an iterative algorithm previously that corrects stray-light errors in a spectroradiometer's spectral responsivity calibration and a test source's spectral distribution measurement in separate steps. In this paper, we describe a simpler and faster method using a matrix called the stray-light correction matrix. In this approach, the stray-light errors in measured signals are corrected by a simple matrix multiplication. The correction is applied to all measured raw output signals, and no distinction is made for the source being measured; i.e. whether the source is a calibration source or a test source.

The stray-light correction matrix

The array spectrometer is first characterized for the stray-light distribution function (SDF): the ratio of the stray-light signal to the total signal within the bandpass of a spectrometer when measuring a monochromatic spectral line source. By measuring a set of line sources covering the spectral range of the instrument, and interpolating between these line spectra, a SDF matrix is obtained. The SDF matrix is used to derive the stray-light correction matrix, and the instrument's response for stray light is corrected by

$$\boldsymbol{Y}_{\mathrm{IB}} = \boldsymbol{C} \cdot \boldsymbol{Y}_{\mathrm{meas}} \quad , \qquad (1)$$

where $\boldsymbol{C}$ is the stray-light correction matrix, $\boldsymbol{Y}_{\mathrm{meas}}$ is a column vector with the measured signals, and $\boldsymbol{Y}_{\mathrm{IB}}$ is a column vector with stray-light corrected signals. Note that development of matrix $\boldsymbol{C}$ is required only once, unless the imaging characteristics of the instrument change. Using Eq. 1, the stray-light correction becomes a single matrix multiplication operation, and the correction can be performed in real-time with minimal impact on acquisition speed.

The results of stray-light correction

The effectiveness and robustness of this stray-light correction matrix has been validated. Stray-light correction matrices have been developed for several different array spectrometers. Figure 1 shows an example validation measurement. This array spectrometer has a stray light of 10^{-4} for a narrow-band source measurement. The spectrometer was used to measure a green broad-band bandpass filter illuminated by a tungsten incandescent lamp. The transmittance of the filter below 420 nm is less than 10^{-9}. Figure 1 shows that the stray-light contribution to the measured raw signal is significant: $\approx 10^{-3}$ below 420 nm. After applying the stray-light correction, the signal below 420 nm is reduced by ≈ 2 orders of magnitude.

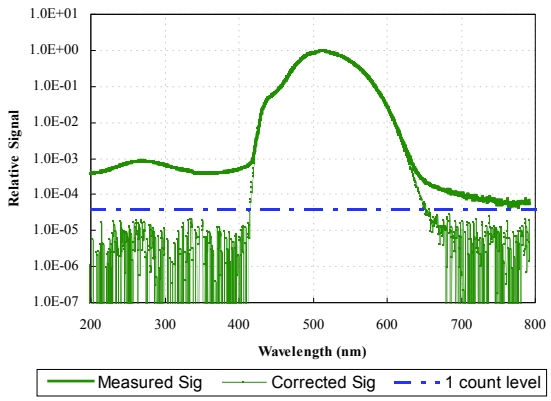

Figure 1. Validation result of the stray light correction for a broad-band source with a bandpass filter. Thick solid line: measured raw signals from the spectrograph; thin symbol line: stray-light corrected signals; horizontal dashed line: one-count level of the 15-bit spectrograph.

The stray-light correction matrix $\boldsymbol{C}$ can also be used to correct stray-light errors in narrow-band source measurements. Figure 2 shows an example of the stray-light correction for a laser source measurement. The stray-light errors are reduced by one to two orders of magnitude in this case as well.

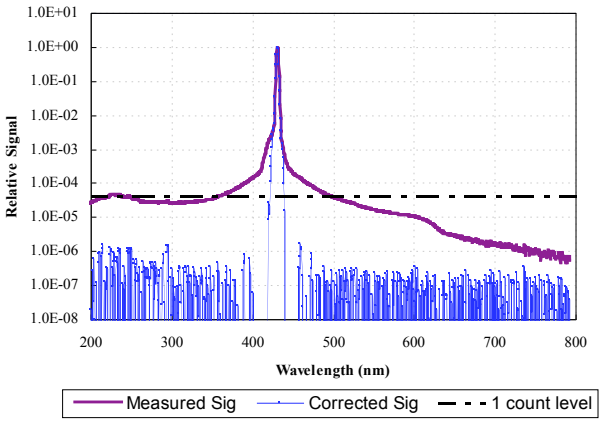

Figure 2. An example of the stray-light correction for a laser source measurement. Thick solid line: measured raw signals from the array spectrometer; thin symbol line: stray-light corrected signals; horizontal dashed line: one-count level of the 15-bit array spectroradiometer.

Improvement in measurement uncertainty

The stray-light correction can significantly reduce the errors in both the calibration of an array spectroradiometer and measurements of test sources. Figure 3 shows plots of the raw output signal, the stray-light corrected 'true' signal, and the percentage of the stray-light signal relative to the 'true' signal for a calibration of an array spectrometer system with stray light of 10^{-4}, using an incandescent standard lamp. The stray-light signals are significant compared to the 'true' signals below 400 nm. The error without correction reaches 30 % of the 'true' signal at 350 nm. By applying the stray-light correction, the spectroradiometer errors arising from stray light in the measurement of the standard lamp are reduced significantly below 400 nm.

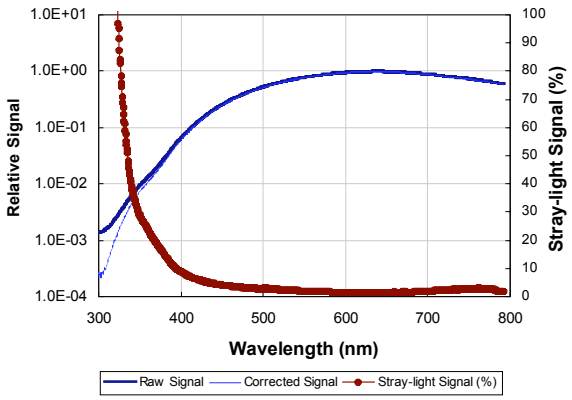

Figure 3. Stray-light correction for calibration of the spectral responsivity of an array spectrometer system. Thick solid line: raw output signal from the spectrograph; thin solid line: stray-light corrected 'true' signal; thick symbol line: percentage of stray-light signal relative to the 'true' signal.

Correction for stray light is critical when measuring test sources that have dissimilar spectra compared to that of the calibration source. As an example, an array spectroradiometer was used to measure the color of a blue LED, a green LED, and a red LED. The measurement results are shown in Figure 4. Errors arising from stray light are significant in the wings for measurements of all three LEDs. After the stray-light correction, the errors are reduced more than one order of magnitude, which corresponds to a reduction of measurement error in chromaticity coordinates (x, y) from 0.01 (original) to less than 0.001 (after correction) for the green LED.

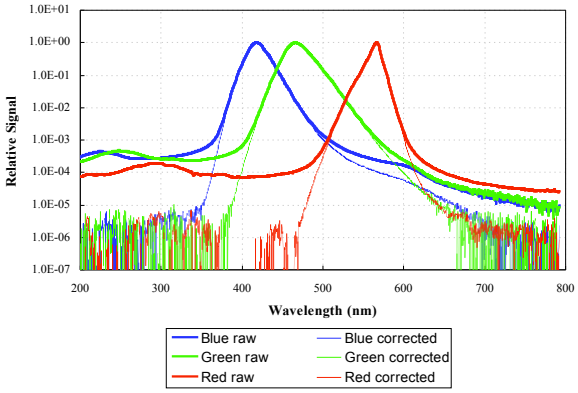

Figure 4. Stray-light corrections for measurements of a blue, a green, and a red LEDs. Thick solid line: measured raw signals from the spectrograph; thin symbol line: stray-light corrected signals.

Conclusion

A stray-light correction matrix has been developed for spectrometers to perform a simple, fast correction of stray-light errors in measured raw signals. This approach corrects stray-light errors using a simple matrix multiplication, which can be readily incorporated in an instrument's software for real-time stray-light correction. After the correction was applied, stray-light errors were reduced by one to two orders of magnitude, to a level less than 10^{-5} of the measured signal of broad-band sources, equivalent to less than one count of the 15-bit-resolution instrument. The principle of the stray-light correction can be used to correct other types of errors resulting from different mechanisms, for example, fluorescence of optical materials used in a spectrometer system. By correcting spectroradiometers for stray light, significant reductions in overall measurement uncertainties are expected in colorimetry (as shown in the LED example), radiometry, photometry, spectroscopy, and other areas where these instruments are commonly used.

The theory, the validation, and the example applications of the stray-light correction matrix approach will be presented.

References

Brown, S. W., Johnson, B. C., Feinholz, M. E., Yarbrough, M. A., Flora, S. J., Lykke, K. R., and Clark, D. K., Stray light correction algorithm for spectrographs, *Metrologia, 40*, S81-83, 2003.

New robot-based gonioreflectometer for measuring spectral diffuse reflection

D. Hünerhoff, U. Grusemann and A. Höpe

Physikalisch-Technische Bundesanstalt, Arbeitsgruppe 4.52 „Reflektometrie“, Bundesallee 100,
38116 Braunschweig, Germany

Abstract. At the Physikalisch-Technische Bundesanstalt (PTB) a new robot-based gonioreflectometer for measuring radiance factor and BRDF has been build up. The facility enables measurements of the directed reflection characteristics of materials with arbitrary angles of irradiation and detection relative to the surface normal.

Introduction

Measurements of directed diffuse reflection are an important quantity for a variety of applications in optical metrology. Measuring the BRDF allows one to describe the appearance of a material under user-defined lighting conditions. This includes calibrations for paper, textile and color industry, companies producing radiometric and photometric instruments, as well as measurements for radiometric on-ground calibration of remote sensing instruments for space-based applications on satellites.

Technical data of the gonioreflectometer

The facility uses broadband irradiation of the samples with spectrally selected detection of the reflected radiation. The unfiltered broadband irradiation is delivered by a special homemade sphere radiator with an internal 250 W quartz tungsten halogen lamp. This sphere radiator has a precision circular aperture of 4 cm and a homogeneity of the emitted radiance of ± 0.2 % within the whole opening. It is located on a large rotation stage with a diameter of 1.5 m and can be rotated 360° around the 5-axis-robot serving as the sample holder (see Fig. 1).

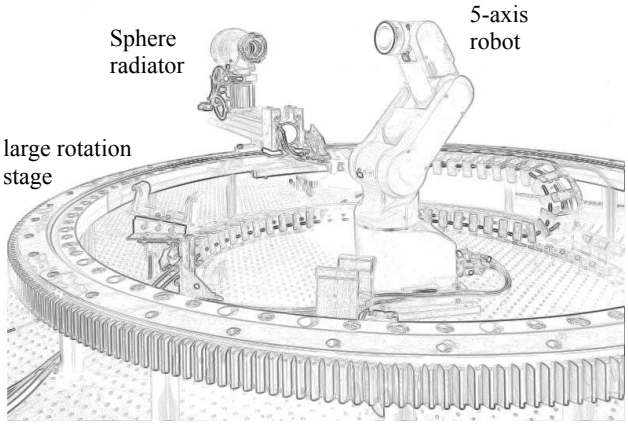

Figure 1. Schematic diagram of the gonioreflectometer facility

The direction of the detection path is fixed due to the fact that a triple grating half-meter monochromator for spectral selection of the reflected radiation is used. The sample holder is a small commercial industrial five-axis robot with an height of 550 mm, only (Fig. 1). It is able to carry and position samples with an outer diameter of up to 0.5 m and a weight of up to 2 kg. The position accuracy is 0.02 mm for arbitrary movements.

The combined adjustment of the rotation stage and the robot allows complete angular control of the directed beams of incident and reflected radiation within the full half space above the surface of the sample, allowing the measurement of out-of-plane reflection, too. The angular range of the directed radiation incident on and reflected from the sample is 0° to 85° for θ_i, θ_r and 5° to 355° for ϕ_i, ϕ_r (see Fig. 2). The apex angle of irradiation of the sample under measurement is 1.50° (solid angle $2.16 \cdot 10^{-3}$ sr), the apex angle of detection is 0.32° (solid angle $96.45 \cdot 10^{-6}$ sr), only.

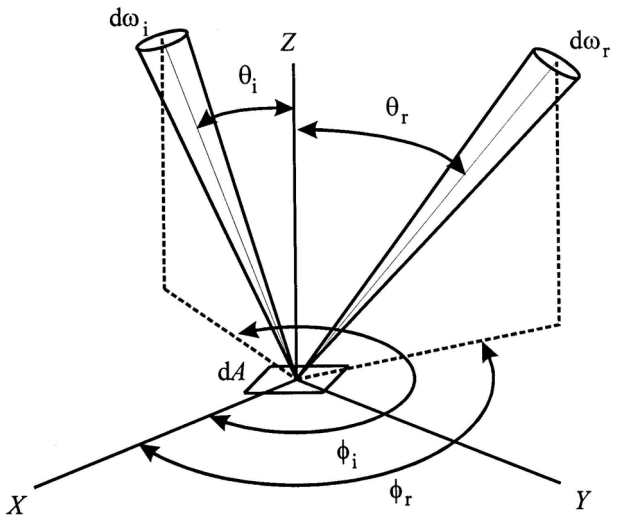

Figure 2. Geometry of incident and reflected beams at the gonioreflectometer

The current wavelength range for measurements of diffuse reflection is 250 nm to 1700 nm. It is planned to extend this range up to 2500 nm within the near future.

The facility uses a two-stage mirror-based 10:1 imaging optics to map a 20 mm circular area on the sample onto the 2 mm wide slit of the monochromator. This results in a 3 nm bandpass within the spectral range 250 nm to 900 nm and a 6 nm bandpass within the 900 nm to 1700 nm region, depending on the gratings used.

Four different detectors behind the monochromator are used for detecting the radiance signals of the incident and reflected beams: a solar blind channel PMT for the measurements between 250 nm and 350 nm, a yellow enhanced channel PMT between 300 nm and 450 nm, a silicon photodiode between 400 nm and 1100 nm, and a cooled InGaAs photodiode between 1000 nm and 1700 nm. All the signals were detected with a picoamperemeter and transferred to a computer for data storage and analysis.

The uncertainty budget for calibrations of the radiance factor and the BRDF ranges from 0.2 % in the visible spectral range to 0.5 % in the IR at 1700 nm and to 3.5 % in the UV at 250 nm.

Fig. 3 shows a typical measurement of the radiance factor of a diffuse reflecting material (Spectralon©) within the current spectral range of the facility.

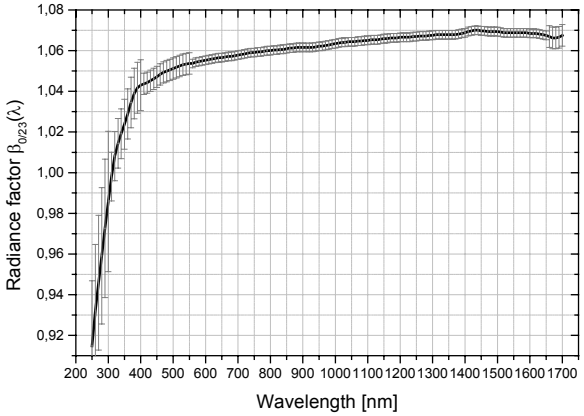

Figure 3. Radiance factor for a Spectralon© sample in 0/23 (in-plane) geometry in the spectral range 250 nm to 1700 nm

Acknowledgments The authors wants to thank B. Campe, K.O. Hauer and S. Teichert for construction and building several parts of the instrument.

References

W. Erb, Computer-controlled gonioreflectometer for the measurement of spectral reflection characteristics, *Appl. Opt., Vol. 19, No. 22*, 3789-3794, 1980

W. Erb, High-accuracy gonioreflectance at the PTB, in *Advances in Standards and Methodology in Spectrophotometry*, edited by C. Burgess and K. D. Mielenz, pp. 87-98, 1987

Rotational radiance invariance of diffuse reflection standards

A. Höpe

Physikalisch-Technische Bundesanstalt, Arbeitsgruppe 4.52 „Reflektometrie“, Bundesallee 100,
38116 Braunschweig, Germany

Abstract. Standards for diffuse reflection calibrations must not have any texture, i.e. their reflection behaviour should be independent of their rotational orientation. Explicit goniometric measurements on a selection of samples made of different materials show that is only half the truth. The absence of an obvious internal structure can nevertheless lead to variations in the reflected radiance of up to 1.2 % depending on the rotational orientation of the sample.

Results and discussion

Diffuse reflection materials are important calibration standards for a variety of applications in optical technology. They have applications in radiometric and photometric measurements, like radiance factor, BRDF and colorimetric quantities.

A selection of 16 different reflection standards were measured on PTB´s new gonioreflectometer. Their radiance was recorded while there were rotated 360° around an axis collinear with their surface normal. The radiance signal was taken from a circular area 2 cm in diameter. The apex angle of detection was 0.32° (solid angle $96.45 \cdot 10^{-6}$ sr), only. The samples were irradiated by a special homogeneous sphere radiator (solid angle $2.16 \cdot 10^{-3}$ sr) with an inhomogeneity of only 0.2 % across the whole beam profile emitted from the circular aperture of the lamp with a diameter of 4 cm. The measurements were taken at a wavelength of 950 nm with a high precision Si photodiode connected to a picoamperemeter. The reflection geometry was 45/0 in an in-plane configuration for all of the measurements.

Different kinds of reflection standards with varying materials and technologies were examined. Pressed $BaSO_4$ tablets, primed $BaSO_4$ standards (special kind of $BaSO_4$ standard fabricated by the PTB), opal glasses and sintered PTFE based reflection standards (like Spectralon© and identical materials).

The subsequent three diagrams show the influence of the rotation of the samples on their reflected radiance signals. Fig. 1 shows the rotational reflection behaviour of a Spectralon reflection standard. Shown as dashed lines are the mean value and the 0.5 % deviation line. Connected with the full 360° rotation is a variation of approximately 1.2 % in the radiance signal. Displayed in Fig. 2 is the measured signal of the matte side of an opal glass from the European Commission (a so called BCR 406A opal glass). The variation in the radiance signal for a full 360° rotation is about 0.4 %. Fig. 3 shows the same data for a pressed $BaSO_4$ tablet. The overall change in the radiance signal for a full 360° rotation is also about 0.4 %.

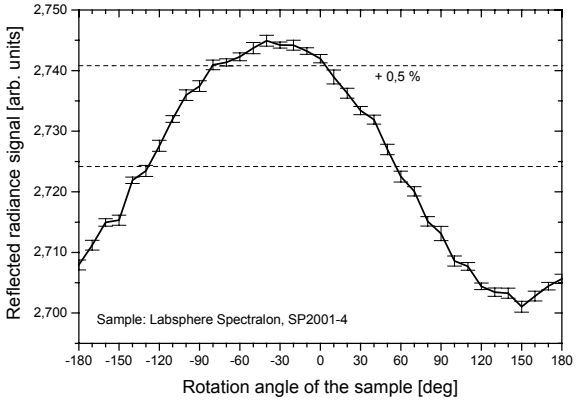

Figure 1. Orientation dependence of the reflected radiance of a Spectralon reflection standard for a full 360° rotation

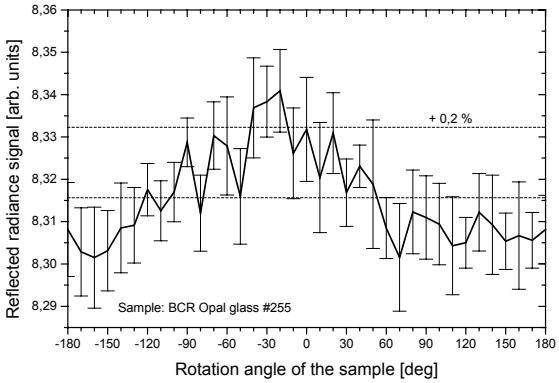

Figure 2. Orientation dependence of the reflected radiance of a BCR opal glass reflection standard for a full 360° rotation

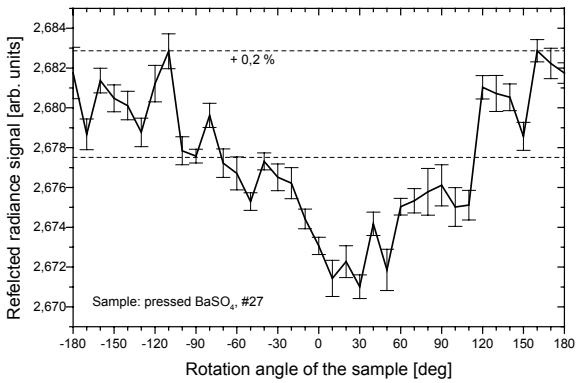

Figure 3. Orientation dependence of the reflected radiance of a reflection standard made of pressed $BaSO_4$ for a full 360° rotation

For all of the analysed reflection standards no obvious texture structure was visible, even when examined under a microscope. The influence of distance variations between the irradiating lamp and the sample during the rotation measurements were also tested. This distance change is 4/100 mm at maximum for a full 360° rotation of a sample mounted in the sample holder of the gonioreflectometer. Although this has a small affect on the irradiation E_i of the sample, the influence on the reflection signal is only 0.01 %.

Conclusion

Standard materials of diffuse reflection should be handled with caution when there are used in directional reflection geometries. The absolute reflection depends on the rotational orientation of the sample relative to the plane spanned by the beams of the incident and reflected radiation. Even small rotations about the surface normal can lead to deviations in the reflected radiance almost in the percent range similar to the measurement uncertainties of most of the goniometric calibration facilities. This underlines the necessity to indicate the orientation of samples during their calibration and also to reproduce this orientation when making adjacent measurements using the calibration data.

Acknowledgments The author wants to thank B. Campe and K.O. Hauer for the preparation of several samples.

References

W. Erb, Li Zai-Qing und P. Nikolaus, Super-Reflexion bei diffus reflektierenden Materialien, *Optik, 71, No. 2*, 80-88, 1985

Minimizing Uncertainty for Traceable Fluorescence Measurements –

The BAM Reference Fluorometer

C. Monte, W. Pilz, U. Resch-Genger

Federal Institute for Materials Research and Testing (BAM),
Working Group Optical Spectroscopy, I.3, Richard-Willstätter-Straße 11,
D-12489 Berlin, Germany

Introduction

Providing fluorescence emission spectra traceable to the units of spectral responsivity and spectral radiance with minimized uncertainties is currently limited by two factors: The uncertainty of the available transfer standards and the uncertainty of the measurement process itself.

A Reference Fluorometer

Here the requirements on a reference fluorometer enabling measurements with lowest possible uncertainty, its design, its simulation and its realization are presented. The fluorometer is designed with minimized chromatic and geometrical aberrations. To realize an efficient reduction of stray light and subtractive dispersion, a double monochromator design was necessary. The basic element is a so called U-type Czerny-Turner single monochromator featuring off-axis paraboloids and an entrance and exit slit virtually at the same place. Thereby spherical aberration, coma, and astigmatism are effectively reduced. The employed special double monochromator design further cancels out the remaining aberrations of the single monochromator. The design of the whole spectrometer was optimized and subsequently toleranced with a ray-tracing program.

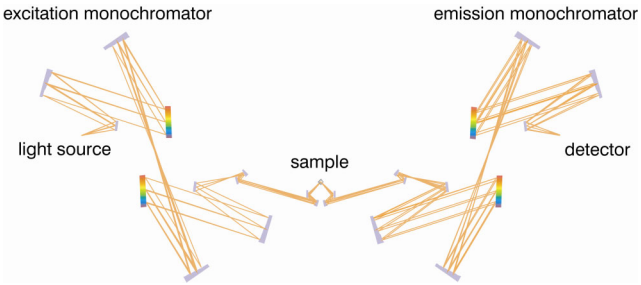

Figure 1. The optimized geometry of the reference fluorometer

Transfer Standards

To minimize calibration uncertainties due to the applied transfer standards, the reference fluorometer is exclusively traceable to the unit of spectral responsivity provided in Germany by a cryogenic radiometer at PTB. This is realized via trap detectors as radiometric transfer standards with the smallest possible uncertainty. Here trap detectors of common design are employed, but specially calibrated for a divergent light bundle according to their application.

Absolute Measurements

Based on this instrument with its achromatic design and precisely known numerical apertures the determination of absolute fluorescence spectra will be addressed.

Acknowledgments This work has been funded as part of the project VI A2 -18 “Development, Characterization and Dissemination of Fluorescence Standards for the Traceable Qualification of Fluorometers” by the Federal Ministry of Economics and Labour of Germany.

References

Hollandt, J., Taubert, R.D., Seidel, J., Resch-Genger, U., Gugg-Helminger, A., Pfeifer, D., Monte, C., Pilz, W., Traceability in Fluorometry - Part I: Physical Standards, *Journal of Fluorescence*, *15*, 311, 2005

Resch-Genger, U., Pfeifer, D., Monte, C., Pilz, W., Hoffmann, A., Spieles, M., Rurack, K., Hollandt, J., Taubert, R.D., Schönenberger, B., Nording, P., Traceability in Fluorometry - Part II: Spectral Fluorescence Standards, *Journal of Fluorescence*, *15*, 325, 2005

Chupp, V.L., Grantz, P.C., Coma Cancelling Monochromator with No Slit Mismatch, *Appl. Optics, 8*, 925, 1969

Fox, N.P., Trap Detectors and Their Properties, *Metrologia, 28*, 197, 1991

Development of a total luminous flux measurement facility for LEDs at the National Metrology Institute of Japan

K.Godo, T.Saito, H.Shitomi, T.Zama, and I.Saito
NMIJ/AIST 1-1-4, Umezono, Tsukuba, Ibaraki, JAPAN

Abstract. At the National Metrology Institute of Japan (NMIJ), the research of photometric standards for Light Emitting Diodes (LEDs) has been started. In this paper, we have developed the facility for the measurement of the LEDs total luminous flux based on the goniophotometric method and also have evaluated the uncertainty of the measurement of the LEDs total luminous flux.

Introduction

Light Emitting Diodes (LEDs) came into use in various fields and their importances are increasing. Accurate photometric techniques and standards for LEDs measurement are demanded. Therefore, the research on the LEDs measurements is done actively now at many National Metrology Institute (NMI) and Commission International de I'Eclariage (CIE). Also at the National Metrology Institute of Japan (NMIJ), the research of the photometric standards for LEDs has been begun in response to such situation in and outside the country.

In this study, we have developed the facility for the measurements of a LEDs total luminous flux and have evaluated its uncertainty with a calculation and experimental methods.

Goniophotometer for LEDs measurements

The measurement of LEDs total luminous flux at NMIJ is based on the goniophotometric method to cope with strong partially luminous intensity distribution of LEDs. The facility is composed of a rotation stage of LEDs, a photometer and an optical alignment stage. The schematic diagram of the facility is shown in Fig.1. The Photometer is installed on the automatic motion stage and the measurement in arbitrary distance up to 1.2m is possible. The illuminance responsivity (A/lx) and the relative spectral responsivity of the photometer are traceable to the NMIJ luminous intensity scale and the NMIJ spectral responsivity scale, respectively. Furthermore, when measuring the averaged LED intensity, the photometer with aperture area of 100mm^2 for the averaged LED intensity measurement is used instead of the photometer with high-illuminance responsivity for the LEDs total luminous flux measurement. The averaged LED intensity is measured by moving the photometer position to the CIE standard condition (condition A=316mm, condition B=100mm). By measuring the luminous flux measurement and the averaged LED intensity measurement in same geometric arrangement, we can evaluate both the uncertainty related to mechanical axis installation error and optical axis in the averaged LED intensity measurement. The laser beam from the optical alignment stage was designed to pass the azimuth axis (ϕ) and the polar axis (θ) of the rotation stage.

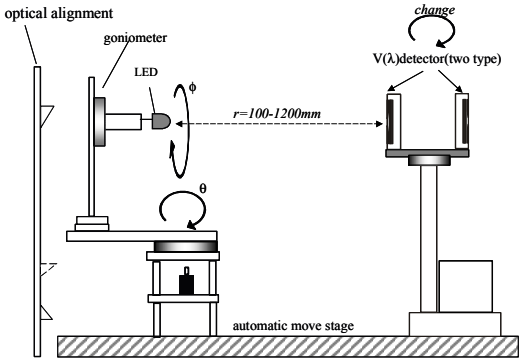

Fig 1. Schematic diagram of the LED goniophotometer

Evaluation of Uncertainty

The uncertainty of the LEDs total luminous flux measurement was evaluated about the twenty factors (for example, the temperature stability of LED, the uncertainty of the measurement distance etc). As a new trial of uncertainty evaluation of LED measurement, the uncertainty related to the geometric conditions between the photometer and a test LEDs was calculated using polar coordinates. Furthermore, the uncertainty of the color correction factor, which is derived from the uncertainty of spectral distribution of LEDs and spectral responsivity of photometer, was calculated using the Monte Carlo methods.

As a result, it turned out that the uncertainty of the illuminance responsivity of photometer (u=0.35%), the temperature stability of a LEDs (u=0.18%) and the installation error of a LEDs to rotations center (u=0.1%) are the largest uncertainty factors. Furthermore, the uncertainty of the measurement distance could almost be disregarded in the total luminous flux measurement that is measured at 1m. However, this uncertainty factor cannot be disregarded in the averaged LED intensity measurement, because of its short measurement distance. The uncertainty of a color correction factor of a white LED, a blue LED and a red LED was calculated to be u=0.02%, u=0.17%, and u=0.16% from the Monte Carlo method respectively. This calculation results clearly showed that there was a large uncertainty in the color correction factor of LED.

Conclusion

We developed the facility for the measurement of the LEDs total luminous flux based on the goniophotometric method and also have evaluated its uncertainty. The result of the uncertainty evaluation showed that the temperature stability of LEDs and the installation error of LEDs to rotations center were the largest uncertainty factors. Furthermore, the result of Monte Carlo calculation showed that the uncertainty of the color correction factor of LEDs couldn't be disregarded.

References

Commission International de I'Eclariage "Measurement of LEDs", CIE Publication 127, 1997.

Determination of the diffuser reference plane for accurate photometric and radiometric measurements

J. Hovila[1], P. Manninen[1], L. Seppälä[1], P. Kärhä[1], L. Ylianttila[2] and E. Ikonen[1,3]

[1]Metrology Research Institute, Helsinki University of Technology, P.O.Box 3000, FI-02015 TKK, Finland

[2]Radiation and Nuclear Safety Authority (STUK), P.O.Box 14, FI-00881 Helsinki, Finland

[3]Centre for Metrology and Accreditation (MIKES), P.O.Box 239, FI-00181 Helsinki, Finland

Abstract. A method for determination of the effective measurement plane of measuring heads with diffusers is presented. The method was tested with three commercial photometers and four spectroradiometer diffusers. The shifts of the diffuser reference planes were determined to be 5 – 9 mm and 0 – 7 mm, respectively. This effect causes measurement errors up to 3 % if the detectors are calibrated and used at different distances from the light source.

Introduction

Diffusers are often used to improve angular responsivities of photometers and spectroradiometers. This introduces additional uncertainty in distance measurements, as the reference plane for the inverse square law is not always obvious. In calibrations, distances are typically measured from the outermost surface of the diffuser. This produces systematic errors to measurements at any other distances, if the reference plane is located somewhere else, as it typically is with dome-shaped diffusers. For accurate illuminance responsivity and solar UV measurements, the reference plane positions of the detectors must be known precisely.[1]

We present a simple measurement method for this effect based on inverse square law and accurate distance measurements on an optical bench. The method is tested with three commercial photometers and four diffusers typically used with spectroradiometers.

Inverse-square law

The method is based on the measurement of illuminance/irradiance at various distances from the lamp. The measured values E obey the inverse-square law[2]

$$E = \frac{I}{\left(d + \Delta d_S + \Delta d_D\right)^2} \qquad (1)$$

where I is the luminous/radiant intensity of the point source, d is the distance between the reference planes of the source and the detector, Δd_S is the distance offset of the source and Δd_D is the distance offset of the detector.

The offset Δd_S of the lamp is first determined with a reference detector having a well-defined aperture plane by inserting measurement results to Equation (1) and applying a least-squares fitting. Intensity I and the distance offset Δd_S are used as free parameters (for the reference detector $\Delta d_D = 0$). After that, the measurements and the analysis are repeated with the studied detectors. The known offset Δd_S is used to obtain desired offset Δd_D for the reference plane of the detector.[3] The measurement distances are selected in such a way that the signal varies sufficiently and resolution of the detector is adequate.

Measurement set-up

Reference detector: In this work, we used a temperature-controlled standard photometer HUT-2 (of type PRC TH15) as a reference detector. It has a well-defined aperture plane with circular aperture of 8 mm. This plane was used as a reference plane for the distance measurements.

Studied photometers: The studied photometer heads were a dome diffuser of Minolta T-1 [Figure 1 (a)] a dome-shaped diffuser [Figure 1 (b)] and a cylindrical diffuser [Figure 1 (c)] of Hagner E2.

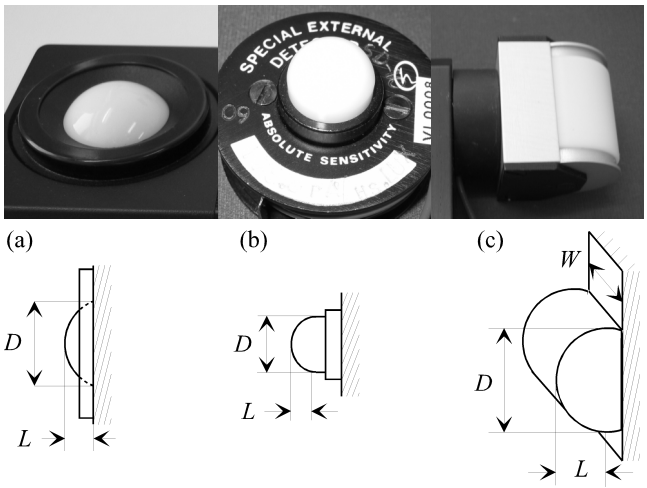

Figure 1. Images and schematic drawings of the studied photometer diffusers. Dimensions are given in Table 1.

Studied spectroradiometer diffusers: The tested measuring heads of the spectroradiometers were three mesa-shaped diffusers of Bentham and a dome-shaped type of Schreder diffuser. Images of the diffusers are presented in Figure 2. The Schreder diffuser has a removable quartz glass dome for weather protection. Distances d were measured from the outermost point of the diffusers for all studied measuring heads.

The incoming light from the measuring heads was guided with an optical fiber to a trap-detector from which the photocurrent was measured. Wavelength dependence of the reference planes was measured by using a filter between the fiber and the detector. Three filters were used: a UV-filter of type UG11, a $V(\lambda)$ filter, and a 700-nm interference filter. The Si-trap was replaced with a GaAsP trap when the wide-band UV filter was used.

A 180 W incandescent lamp was used with the photometers, and a 1 kW halogen lamp was used with the spectroradiometer heads. The front surface of the alignment mirror (incandescent lamp) and the front surface

of the lamp housing (halogen lamp) were used as reference planes of these lamps. Distances were measured on an optical rail using a magnetic length measuring device with 0.1 mm resolution and accuracy.

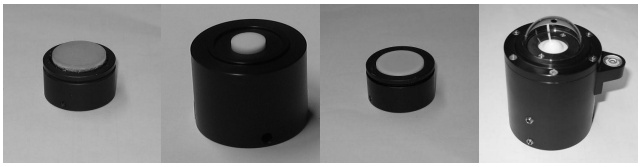

Figure 2. Images of the measured spectroradiometer diffusers (from left to right): Bentham D3 (∅ 25 mm), Bentham D7 (∅ 10 mm), Bentham D5 (∅23.5 mm), and the Schreder diffuser with the quartz glass dome.

Measurement results

Reference planes of the photometer diffusers: The reference planes of the tested photometer heads were determined by illuminance values measured at six distances between 500 mm and 1500 mm. The results for the photometer diffusers are presented in Table 1. All offsets of the reference planes were found out to be several millimeters behind the outermost surfaces of the diffusers.[3]

Table 1. Dimensions and offsets of the photometer diffusers. Uncertainties are deviations of the mean of four measurements.

Diffuser		(a)	(b)	(c)
Dimensions [mm]	D	24.3	16.0	30.0
	L	8.0	7.1	15.0
	W	-	-	26.1
Offset Δd_D [mm]		5.0·±·0.5	7.8·±·0.3	8.5·±·0.7

Reference planes of the spectroradiometer diffusers: Measurements with spectroradiometer heads were carried out at 10 distances between 300 mm and 2000 mm. This range includes typical calibration distances of 500 mm and 370 mm used. The results at each wavelength and for each diffuser are presented in Table 2.

Table 2. Measured reference plane offsets [mm] of the spectroradiometer diffusers.

Filter / Diffuser	Bentham D3	Bentham D7	Bentham D5	Schreder
UV	2.3	-0.3	0.4	6.4
$V(\lambda)$	2.6	0.1	1.2	7.1
700 nm	3.6	0.3	3.2	7.1

It can be seen that the mesa-shaped diffuser D3 has a significant offset, which is surprising for a planar diffuser. This is probably due to the poor material used to obtain a wide wavelength region. The other diffusers are made of Teflon, which results in increasing offset towards infrared wavelengths, where Teflon is not a very good diffuser material. The reference plane of the Schreder diffuser is surprisingly deep inside the measuring head. The effect is too large to be explained by the dome-shape only.

The influence of the quartz dome of the Schreder diffuser on the reference plane position was studied by repeating the measurement without the quartz glass dome. The measurement result, 5.0 mm in the UV region, indicates that the quartz dome increases the observed shift of the reference plane.

Conclusions

We have presented a method with which the location of the reference planes of photometers and radiometers with diffusers can be determined. Inverse square law works only, if distance measurements are made with respect to this reference plane.

The method has been demonstrated with various photometers and spectroradiometer diffusers. From the measurement results, we may discover that the distance reference plane is shifted with measuring heads having either thick mesa-shaped or dome-shaped diffusers. The material of the diffuser contributes to the shift. Large errors appear in the regions where the materials are transparent.

If these effects are not accounted for, systematic errors may occur in the calibrations of photometers and spectroradiometers. For the studied photometers, errors up to 3 % at a calibration distance of 500 mm would arise. There would also be inevitable distance dependence on the correction factors.

With the Schreder diffuser, the observed distance shift of 6.4 mm in the UV region may cause an error as large as 2 % in the calibration at a distance of 500 mm. This is a significant contribution in the uncertainty of spectral global UV irradiance measurements that is nowadays at the level of a few percent.

The uncertainty of the method may be estimated from the repeatability noted during the measurements that is of the order of 1 mm (k=2). It was checked that the wavelength dependence of the reference plane of the lamp is of the order of 0.4 mm.

References

1. Y. Ohno, *Photometric Calibrations, NIST Special Publication* **250-37**, U.S. Government Printing Office, Washington DC, 1997.

2. H. J. Kostkowski, *Reliable spectroradiometry*, La Plata, Md., Spectroradiometry Consulting, 1997.

3. J. Hovila, M. Mustonen, P. Kärhä, E. Ikonen, "Determination of the diffuser reference plane for accurate illuminance responsivity calibrations," *Appl. Opt.* (in press).

DEVELOPMENT OF A LUMINANCE STANDARD

Antonio Corróns and Joseluis Fontecha
Instituto de Física Aplicada. (IFA-CISC)
Serrano 144, Madrid 28006, SPAIN.

Abstract

In recent decades, a major aim of the Dept. of Metrology of the IFA (CSIC) has been the development of primary standards in optical Radiometry and Photometry. The realizations of the Absolute Spectroradiometric Scale, the Candela and the Lumen are all results of that work. This communication reports the development of a Luminance Standard.

From a visual point of view, luminance is of the most important photometric magnitude. The surfaces are visible because of their luminance.
Luminance meters need to be calibrated with respect to a reference scale, the quality of which has a direct impact on the uncertainty of any measurements made. This work describes the planning, construction and calibration of a Luminance Standard, basically a luminous, circular disc with a diameter of 70 mm, backlit with diffuse light whose spectral distribution corresponds to CIE Illuminant A.

On a smaller circle within this disc (diameter 50 mm), the uniform luminance perpendicular to the surface achieved was better than 1% (measured using a fibre optic system with Cartesian movement) (Fig. 1). The luminance at each point complied with Lambert's Law into an angular interval of ± 15º with respect to the normal to the surface.

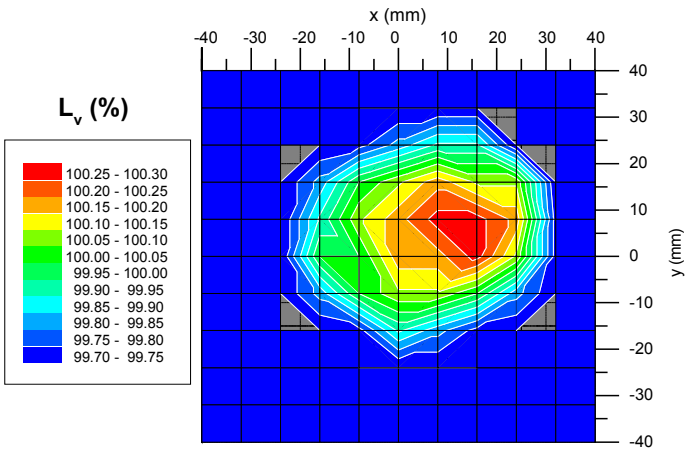

Fig. 1.- Relative luminance on the surface of Luminance Standard.

Figure 2 shows the temporal stability of the emitting surface.

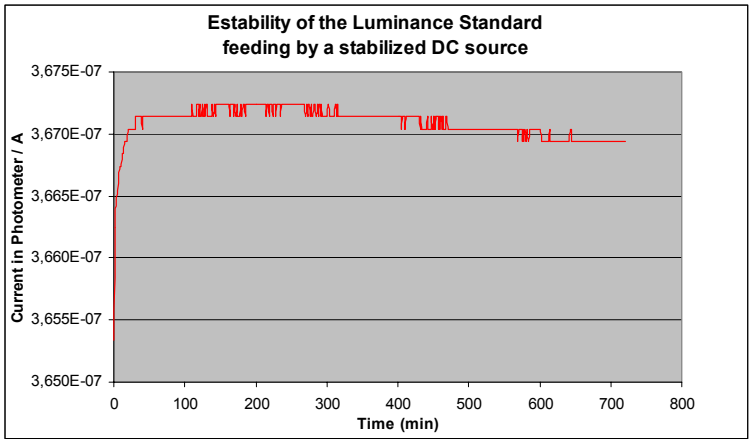

Fig. 2.- Time Stability of the Luminance Standard. Measured with the Photometer FOTI along 12 hours

The light emitted by the surface of the standard is not polarised.

A FOTI standard photometer was used in a photometric bank to calibrate the luminance of the surface of the standard in cd m^{-2}, measuring the illuminance on the photometer produced by the luminous surface at different distances. The FOTI photometer was previously calibrated against standard luminous intensity lamps.

The luminance of the luminous surface of the luminance standard was measured with a final expanded uncertainly (k=2) of ± 0.7%.

Measuring photon quantities in the International System of Units

M. L. Rastello
INRIM, Turin, Italy

Abstract. Advances in nanotechnology, biotechnology and quantum communication need access to even more accurate photon measurements traceable to the SI, from one hand, and open up the possibility of counting and controlling photons one by one, on the other, affecting photometry and present realizations at the National Metrology Institutes. This paper deals with this technological revolution.

Introduction

The optical domain provides great richness and potential given the latest engineering demonstrations and design of novel states of light either in their photon squeezing properties or at the single photon level. Photon metrology can complement and strengthen the results of quantum optical technology (QOT) research in two ways: increasing its practicability/application and therefore its social and industrial impact, and feeding it with new scientific stimula.

This paper deals with the development of metrological tools for promoting QOT, as well as establishing new photon standards to cover existing and future requirements in the wider realms of metrology. The fundamental scientific nature, the breadth of the approach, the wide variety of materials and techniques used, as well as the range of operating wavelengths of the resulting "single-photon devices", are key features to success.

The core of photon metrology is formed by the design and realization of efficient single-photon sources, and the integration and application of novel single-photon detectors. This paper will discuss these techniques offering improved uncertainties in photon counting regime. The detectors and sources considered in this paper may, in turn, prove to be suitable reference standards that can be used to calibrate detectors and sources in the industrial environment. Furthermore, they can result in a step towards the goal of a redefinition of the relevant SI unit, the candela. It is possible to scale such a realization from the photon-counting to the macroscopic level required for other applications and thus act as an independent verification of existing high level standards.

Photon quantities and units

This paper addresses firstly the question about what units are the more appropriate to photon metrology, as quantities related to counts, like the number of photons, will have an increasing importance as technology proceeds into counting photons one by one.

Light can be treated as a wave or a particle, depending on the application. The present definition of the photometric units links any photometric quantity to the corresponding radiometric quantity at one wavelength, under a wave scheme for radiation. It gives no indication as to how realize them, so that new techniques can be adopted without changing the definition of the base unit. Today, NMIs realize the candela by cryogenic radiometry with uncertainties around the 0.005 to 0.001 % level. The detector and source scales are established at discrete wavelengths in the 0.1 mW – 1 mW regime. In scaling down to the photon counting regime there is an unavoidable degradation in accuracy.

In principle, there might be no difficulty in counting the number of photons in a light beam. However, the number of photons per second in, say, a lumen of a monochromatic beam is extremely large and virtually uncountable using current techniques. It is sufficiently large that no essential information is lost in considering photon number to be a continuous quantity. Instead of counting the number of photons per second in a lumen, for the SI it can be compared with whatever the number of atoms is in 12 gram of carbon-12, i.e. the number called mole.

In that respect, please note that, in the 1979 definition of the candela, the value 683 was chosen to minimize the changes in the mean representations of the photometric units as maintained by NMIs. Its theoretical value based on T(Pt)= 2042 K was 682, whereas experimental values obtained by relating photometric and radiometric units by NMIs lie within the range 673 to 687. By changing 683 into 681, the candela could be nicely defined in both radiometric and photon terms, as spectral radiometric quantities can easily be described in terms of photons. In other words, any radiometric spectral quantity $X_{e,v}$ being described in terms of the corresponding photon quantity $X_{p,v}$ as $X_{e,v} = h\nu\, X_{p,v}$, one could have in radiometric terms that *the candela is the luminous intensity, in a given direction, of a source that emits monochromatic radiation of frequency 540 x 10^{12} hertz and that has a radiant intensity in that direction of 1/681 watt per steradian,* and, in terms of photons, that *the candela is the luminous intensity, in a given direction, of a source that emits photons of frequency 540 x 10^{12} hertz and that has a photon intensity in that direction of 681 10^{11} mole per second per steradian.*

The non trivial relationship between counting and measuring was already discussed by von Helmholtz, who came to the conclusion that, when counting identical objects, the counting unit is the object, not the number. In other words, when counting photons, the counting unit is one photon, not the number one. In metrology a unit of measurement is a particular quantity, defined and adopted by convention, with which other quantities of the same kind are compared in order to express their magnitudes relative to that quantity. On the contrary, a countable quantity is evaluated by counting its discrete and recognizable elements, e.g. photons, and differs from quantities that are treated as infinitely divisible in that its unit is indivisible. The question is whether it needs or not to be defined by reference to a standard or a physical experiment

Photon standards

In radiometry absolute standards are usually either sources or detectors. They both require using cumbersome metrological chains to reach the photon-counting level where QOT necessarily operates. QOT standards instead guarantee the better reliability and dynamic range for measurements in the quantum area of few-photon operation, i.e. the better accuracy when characterizing practical devices for quantum information processing and quantum communication.

As to detectors, the most important issue is the absolute measurement of the quantum efficiency of photon-counting detectors from the visible (VIS) to the IR region. This task is difficult to achieve due to a high level if intensity fluctuations in a weak light in general and, particularly, in the IR region where semiconductor detectors are typically extremely noisy. The major routes toward achieving this goal will be discussed thoroughly in this paper. Results on the absolute calibration of photo-detector quantum efficiency, using correlated photon sources generated via parametric down-conversion, have already been published. An inter-laboratory comparison demonstrated the inherent absoluteness of the photon correlation technique by showing its independence of the particular experimental setup used for down.conversion generation. The ultimate result of these investigations is the development of a robust measurement protocol that allows the uncertainties of individual measurements to be determined experimentally and verified operationally.

A new scheme proposed recently consists of producing polarization-entangled states. The measurement technique is based on a 90° rotation of the polarization of one photon member of a correlated pair produced by parametric down-conversion, conditioned on the detection of the other correlated photon after polarization selection. An interesting property of this technique is that measurement of the photons detected on the second detector allows a measurement of quantum efficiency of the first one, without needing, in principle, coincidence counts (at variance with the traditional bi-photon scheme).

As to standard sources, the major goal is the development of single-photon sources of known photon number over a wide spectral range. The truly efficient single-photon sources are presently still not available. The recent attempts using either single quantum dots, or single impurities, or single atoms as emitters bring hope and constitute a step forward in this direction. These devices provide 'on-demand' single photons in response to an optical or electrical pulse. A reasonable approximation of the physical single-photon source can be provided by the heralded SPDC with a multiplexed detection scheme and storage loop that has been proposed recently and the proof of principle has been demonstrated. In the short term the results from Parametric Down Conversion in a multiplexed configuration are expected to reach probabilities of single-photon generation of 70% per laser pump pulse (with a probability of multiple-photon emission suppression to better than 3%), given a theoretical expectation of 90% for an ideal quantum channel.

Conclusions

The major thrust of Photon Metrology is to make possible a scientifically supported performance analysis of different devices and procedures in real world applications of QOT. This paper shows that it provides a solid and accurate metrological basis governing the application and use of quantum resources, namely non-classical states of light and quantum entanglement, for characterizing detectors, sources and novel optical and photonics materials. Photon Metrology provides also intrinsically consistent, absolute, and self-testing methodology in terms of parameter evaluation, standards and procedures, and the necessary experimental background to move these methods out of the laboratory and into the hands of industry.

References

Migdall A., Castelletto S., Degiovanni I. P., Rastello M. L. Intercomparison of a correlated photon-based method to measure detector quantum efficiency. *Applied Optics* ***41***, 2914-2922, 2002

Castelletto S., Degiovanni I. P., Rastello M. L. Evaluation of statistical noise in measurements based on correlated photons. *J. Opt. Soc. Am. B* ***19***, 1247-1258, 2002.

Ghazi-Bellouati A., Razet A., Bastie J., Himbert M.E., Degiovanni I. P., Castelletto S., Rastello M.L. Radiometric reference for weak radiation: comparison of methods. *Metrologia* ***47***, 271-277, 2005.

G. Brida, M. Genovese, M.Gramegna, M. L. Rastello, M. Chekhova, L. Krivitsky: Single-photon detector calibration by means of conditional polarisation rotation. *J. Opt. Soc. Am. B 22*, 488-492, 2005.

G. Brida, M. Chekhova, M. Genovese, M. Gramegna, L. Krivitsky, M. L. Rastello: Absolute quantum efficiency measurements by means of conditioned polarization rotation. *IEEE Trans. IM 54,* 898-900, 2005

Castelletto S., I. P. Degiovanni, M. L. Rastello: Towards ultra-sensitive single photon measurements via two-photons entangled light. In "Recent Research Developments in Optics", Research Signpost Publ.,. 665-681, 2002.

Migdall A. L., D. Branning, S. Castelletto, M. Ware: A single photon on-demand source with decoupled single and multiphoton probabilities. *Proc. of The Sixth Intern. Conference on Quantum Communication, Measurement and Computing (QCMC'02)*, Eds. J. Shapiro and O. Hirota, Rinton Press, 528-531, 2002.

Migdall A. L., D. Branning, S. Castelletto, M. Ware: Single photon source with individualized single photon certifications. *SPIE Proc. of Free-Space Laser Communications and Laser Imaging II (AM104) 4821*, 455-465, 2002.

Migdall A. L., S. Castelletto, M. Ware: Status of multiplexed single photon on-demand source. *Proc. of SPIE Conf on Quantum Information and Computation 5105*, 294-302, 2003.

Session 6

Novel techniques

Characterization of germanium photodiodes and trap detector

A. Lamminpää[1], M. Noorma[1], T. Hyyppä[1], F. Manoocheri[1], P. Kärhä[1], and E. Ikonen[1,2]

[1] Metrology Research Institute, Helsinki University of Technology (TKK), P.O.Box 3000, FI-02015 TKK, Finland

[2] Centre for Metrology and Accreditation (MIKES), P.O.B. 239, FI-00181 Helsinki, Finland

Abstract. We have developed and characterized new detectors based on germanium (Ge) photodiodes. Our results for the spatial uniformities show improvements as compared with earlier studies. The spectral reflectances of a Ge photodiode and trap detector are studied, and the trap reflectance is found to be less than 10^{-4} in the near infrared wavelength region.

Introduction

The use of Ge photodiodes in the trap configuration [1, 2] has been reported earlier by Stock *et al.* in 2003 [3]. Also the spatial uniformities of Ge photodiodes have been reported in various publications, and they have been found to be a significant source of uncertainty at the level of ~1 % [4, 5].

On the contrary to the large area InGaAs photodiodes, Ge photodiodes with 10-mm diameter are available at moderate prices. The biggest drawback of the Ge photodiodes is low shunt resistance and in turn significant dark current. However, filter radiometers made of Ge photodiodes and the trap detector are suitable in applications, such as spectral irradiance measurements, due to the good spatial uniformity and low reflectance.

In order to extend the Finnish national scale of spectral irradiance [6] to the near infrared wavelength region, we have developed new detectors based on Ge photodiodes, which have sufficient responsivity between 900 and 1650 nm. In this work, we discuss the characterization of Ge photodiodes and a trap detector, consisting of three Ge photodiodes. Characterized quantities are spectral responsivity and spectral reflectance. The effects of spatial uniformity, temperature, polarization and low shunt resistance on the responsivity measurements are also studied. Finally, we analyze the anti-reflection (AR) coating of the photodiodes based on the spectral reflectance measurements at oblique angles of incidence.

Characterization of germanium detectors

The spectral responsivity measurements were carried out by using the monochromator-based spectrophotometer built at TKK [7]. All the studied photodiodes were manufactured by Judson Technologies LLC and their model number is J16-P1-R10M-SC. These photodiodes are large area diodes with circular active area of 10-mm and were ordered without any protecting windows.

The spectral responsivity results for a Ge photodiode and the Ge trap detector are illustrated in Fig. 1. In the responsivity measurements the spectral bandwidth was set to 2.9 nm. The spectral temperature coefficient of the Ge detectors was also studied and found to vary from -0.003/°C to 0.007/°C between the wavelength range of 850 nm and 1650 nm. The shape of the spectral temperature coefficient is comparable to earlier studies [3]. The temperature of the detectors was monitored during the responsivity measurements.

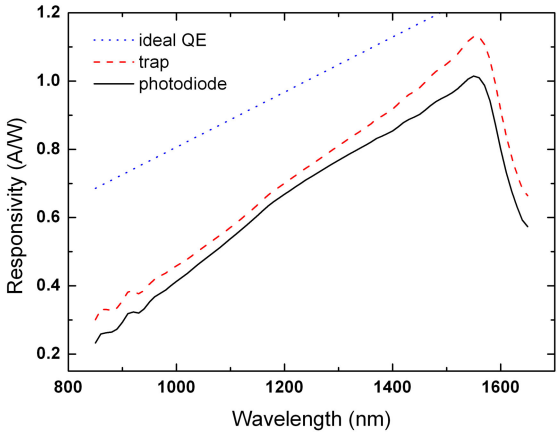

Figure 1. Spectral responsivity of the Ge photodiode and the Ge trap detector at 22.4 °C.

Spatial uniformity

The spatial uniformity was measured at 900 nm, 1308 nm, and 1550 nm wavelengths with three different laser sources. The measurement setup features a cube beam splitter to divide the beam to the monitor detector and the Ge detector under study. The results for a single photodiode at 1308 nm and 1550 nm are presented in Fig. 2. In these measurements the beam diameter was 1 mm and the step size was 0.5 mm.

With 3-mm beam diameter used at the circular central region of 5-mm, the spatial nonuniformity of all four Ge photodiodes is within 0.1 % at 1308 nm and 1550 nm wavelengths. At 900 nm, the spatial nonuniformity varies from 0.22 % to 0.55 % among the four studied diodes.

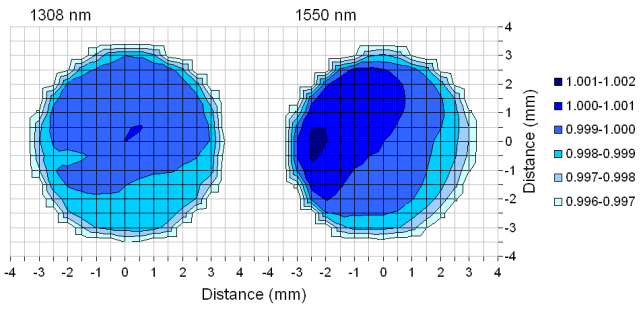

Figure 2. Spatial uniformity of a Ge photodiode at 1308 nm and 1550 nm. Legend lists relative differences compared to the center value of the photodiode.

In the trap configuration the light illuminates a larger area on the first two photodiodes, because they are at 45 degrees angle with respect to the incident light. As the spatial uniformity of a single diode is worse closer to edges and single photodiodes have reasonably low reflectances, the Ge trap detector does not improve the spatial uniformity.

Spectral reflectance

The reflectance measurements were performed for the photodiodes using the absolute gonioreflectometer programmed for specular reflectance measurements [8]. Comparison measurements were done with three different lasers at 1308 nm, 1523 nm, and between 1480 nm and 1600 nm. The results for a Ge photodiode are shown in Fig. 3.

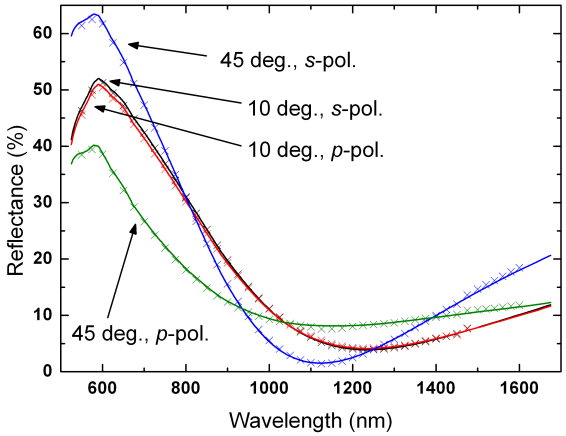

Figure 3. Spectral reflectance of the photodiode measured at 10 and 45 degrees with both *s*- and *p*-polarizations.

The reflectance of the Ge trap was calculated based on the reflectance measurements of the individual Ge photodiodes. This is needed, as the components of the filter radiometers are characterized separately. The result was verified with a laser measurement at 1523 nm. The spectral reflectance of the Ge trap is plotted in Figure 4.

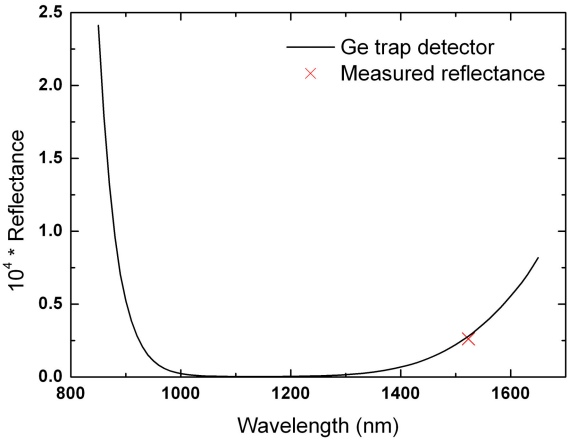

Figure 4. Calculated spectral reflectance of the Ge trap detector verified with a laser measurement at 1523 nm.

All the Ge diodes have AR coating, which explains the shape of the spectral reflectance. In the analysis of AR coating, we combine the spectral reflectance measurements at oblique angles of incidence with a mathematical model that considers a thin homogeneous layer of a dielectric material deposited on a macroscopically thick plane-parallel substrate [9]. For the substrate characteristics, we used tabulated values for bare Ge [10].

The analysis revealed that the thickness of AR coatings of the four Ge photodiodes varies between 175 nm and 182 nm. As the refractive index is found to be at the level of ~1.7, the optical thickness of the antireflection coating is approximately 300 nm, which makes it optimized for the wavelength region around 1200 nm. The analysis did not reveal any reasonable absorption in the AR coating.

Effects of shunt resistance on responsivity

When the gain setting of a current-to-voltage converter (CVC) is adjusted, the input impedance of the device can change. Therefore, reasonably low shunt resistances of the Ge photodiodes (~5 kΩ) and trap detector (~1.7 kΩ) need to be taken into account. Otherwise, a significant ratio of the photocurrent can leak through the shunt resistance instead of CVC. If the input impedance of the CVC increases from 1 Ω to 100 Ω, this can affect the apparent responsivity level of the Ge photodiodes or the trap detector by ~2 % or ~6 %, respectively. To overcome this, the detectors should be calibrated for the different gain settings or the shunt and input impedances should be measured.

Conclusions

The large area Ge photodiodes provide a cost-effective alternative for the InGaAs photodiodes of similar sizes. When the Ge detectors are used for high accuracy measurements, their shunt resistances, dark currents and temperature sensitivities need to be taken into account. The Ge photodiodes have nowadays good spatial uniformities, and the Ge trap detector offers a good alternative for the applications, where we want to avoid harmful interreflections. These properties make Ge detectors well suitable for e.g. the applications of spectral irradiance measurements.

References

1. E. Zalewski and R. Duda, Silicon photodiode device with 100 % external quantum external quantum efficiency, *Appl. Opt., 22*, 2867-2873, 1983.
2. N. P. Fox, Trap Detectors and their Properties, *Metrologia, 28*, 197-202, 1991.
3. K. D. Stock, R. Heine, and H. Hofer, Spectral characterization of Ge trap detectors and photodiodes used as transfer standards, *Metrologia, 40*, 163-166, 2003.
4. K. D. Stock, R. Heine, and H. Hofer, Influence of Inhomogeneity of NIR-Photodiodes on Calibrations at 1047 nm, *Metrologia, 28*, 207-210, 1991.
5. T. C. Larason and S. S. Bruce, Spatial uniformity of responsivity for silicon, gallium nitride, germanium, and indium arsenide photodiodes, *Metrologia, 35*, 491-496, 1998.
6. T. Kübarsepp, P. Kärhä, F. Manoocheri, S. Nevas, L. Ylianttila, and E. Ikonen, Spectral irradiance measurements of tungsten lamps with filter radiometers in the spectral range 290 nm to 900 nm, *Metrologia, 37*, 305-312, 2000.
7. F. Manoocheri, P. Kärhä, L. Palva, P. Toivanen, A. Haapalinna, and E. Ikonen, Characterization of optical detectors using high-accuracy instruments, *Anal. Chim. Acta, 380*, 327-337, 1999.
8. S. Nevas, F. Manoocheri, and E. Ikonen, Gonioreflectometer for measuring spectral diffuse reflectance, *Appl. Opt., 43*, 6391-6399, 2004.
9. A. Lamminpää, S. Nevas, F. Manoocheri, and E. Ikonen, Characterization of thin films based on reflectance and transmittance measurements at oblique angles of incidence, submitted to *Appl. Opt., Optical interference coatings feature issue*, 2005.
10. E. D. Palik, Germanium (Ge), in *Handbook of optical constants of solids*, pp. 465-478, Academic Press, 1985.

Determination of luminous intensity of light-emitting diodes with modified inverse-square law

P. Kärhä[1], P. Manninen[1], J. Hovila[1], L. Seppälä[1], and E. Ikonen[1,2]

[1]Metrology Research Institute, Helsinki University of Technology, P.O.B. 3000, FI-02015 TKK, Finland

[2]Centre for Metrology and Accreditation (MIKES), P.O.B. 239, FI-00181 Helsinki, Finland

Abstract. We present a method that can be used for accurate analysis of luminous intensity measurements of LEDs. The method is based on the modified inverse-square law where information on the LED behavior is included in three parameters; luminous intensity, radius of the image of the source, and location of the image of the source. The method was studied with 17 different LEDs. The standard deviation of the fitting was typically less than 1%.

Introduction

LEDs are finding more and more applications in e.g. traffic lights, LCD-displays, banners, maritime signal lights, general illumination and automotive headlights. This sets new needs for measurement standards.

As compared to traditional photometry, LEDs have narrow beams and spectral features, low power levels and troublesome geometries. LEDs are usually equipped with built-in lenses which enable desired angular distributions for the LEDs. These lenses produce problems in LED measurements as they transfer the image of the light source away from its physical place. Also the size of the image is different.[1]

To overcome the geometrical problems, CIE has recommended[2] that luminous intensities of LEDs should be measured at two defined geometrical conditions, CIE A and CIE B. We have built a setup for measuring these. An annoying feature in the measurements is that the two luminous intensities may vary quite a lot from each other which may cause difficulties when applying the measured LEDs in high-accuracy applications, e.g. as standard LEDs. We propose a new analysis based on the modified inverse square law that overcomes this limitation.

Studied methods

CIE 127 standard: The CIE 127 publication proposes to measure the luminous intensities of LEDs with a photometer having a circular aperture of 1 cm^2. Measurements are to be carried out at two distances, d_A = 316 mm and d_B = 100 mm. Measured illuminances are converted to luminous intensities using equation

$$I_{LED\ A/B} = E_v \cdot d_{A/B}^2 . \qquad (1)$$

The conditions A and B correspond to solid angles of 0.001 sr and 0.01 sr, respectively, and the measured quantity is called the averaged LED intensity. The distances $d_{A/B}$ should be measured from the aperture plane of the photometer to the front tip of the LED. The LEDs should be operated in constant-current mode and the temperature should be stabilized.

Modified inverse-square law: The proposed method is based on the measurements of illuminances at various distances from the LED. The measured illuminance values E_v obey the modified inverse-square law

$$E_v = \frac{I_v}{(d + \Delta d)^2 + r_1^2 + r_2^2} , \qquad (2)$$

where I_v is the luminous intensity of the LED, d is the distance between the reference planes of the LED and the photometer, Δd is the distance offset of the LED, r_1 is the radius of the emitting surface of the LED and r_2 is the radius of the aperture of the photometer. The modified inverse-square law takes into account the effects of transverse dimensions and distance offset of the LED light source and can be used to compensate for the effects of lenses.

Equation (2) is fitted to the measured illuminance values with the least-squares method by using parameters I_v, Δd and r_1 as free fitting parameters. The measurement distances are selected to cover the region where the measured LED is to be used. The signal should vary sufficiently and the resolution of the photometer must be adequate at each distance.[3]

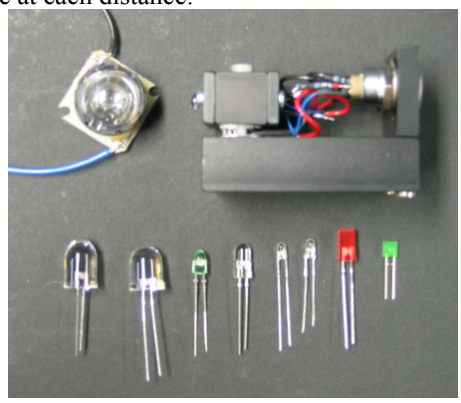

Figure 1. The studied LEDs. The high power LED and temperature-stabilized LED are shown on the top.

Measurement set-up

Photometer: In this work, we used a commercial LED standard photometer from LMT Lichtmesstechnik GmbH. This photometer is in accordance with the CIE 127. Behind the aperture there is a cosine-corrected diffuser, a temperature stabilized $V(\lambda)$-filter and a Si-photodiode.

Optical rail: The measurements were made mainly on a 1-m optical rail with accurate magnetic length scale. The photometer was mounted on a rail carrier. The studied LEDs were fixed to the other end of the optical rail. The studied LEDs and the photometer were aligned to the same optical axis by using a two-beam alignment laser. The

distances d were measured from the aperture plane of the photometer to the front tip of the LED.

Studied LEDs: Methods were tested with 17 different LEDs with varying geometries, colors and power levels. LED types are presented in Figure 1. Four of the studied LEDs had temperature stabilization at the temperature of 25°C. Constant-current of 20 mA was used for low power LEDs and 330 mA for the high power LEDs.

Measurement results

Illuminances were measured at various distances d between 100 mm and 1000 mm depending on the power level of the studied LED. The measurement distance selections also included the CIE recommended distances 316 mm and 100 mm for all LEDs.

Modified inverse-square law fitting for the green temperature-stabilized LED is presented in Figure 2 as an example of typical results.

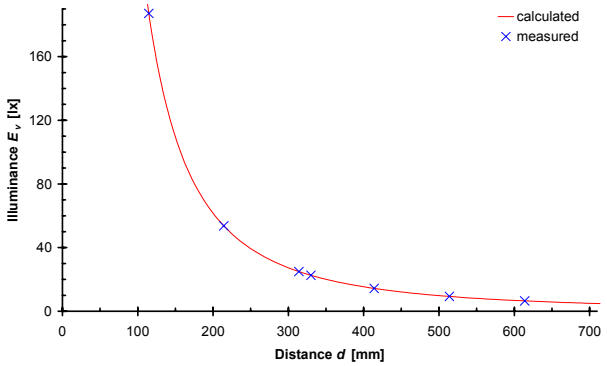

Figure 2. Inverse-square law for the green temperature stabilized LED.

The analysis was done at various fitting ranges due to different power levels. For the high power LEDs with and without a lens, illuminance values were fitted at the regions 100–3000 mm and 100–1600 mm, respectively. For the low power indicator LEDs, the distance measurements were done by steps of 50 mm between 100 mm and 316 mm. Other studied LEDs were analyzed using the region of 100–700 mm.

The results are presented in Table 1. It can be seen that most of the LEDs follow the modified inverse square law with standard deviation smaller than 1 %, biggest standard deviation being 2.1 %. Over more limited regions (e.g. excluding the 100-mm distance) agreement is typically better than 0.1 %. For most LEDs the size of the source can be assumed to be zero. For the LEDs containing powerful lenses this assumption can not be made, but an agreement can be found using r_1 as a free parameter. CIE luminous intensities typically vary quite a lot from each other for each of the studied LEDs.

It should be noted that the obtained values for Δd and r_1 are far from the physical dimensions. They should be considered merely as parameters in a two-aperture approximation of the optical system instead of true physical dimensions.

Table 1. Measurement results of the studied LEDs. The first column gives diameter and color of the LEDs. L is the length of the LED housing.

studied LED	Modified inverse-square law				$I_{LED\,A}$ / $I_{LED\,B}$	L [mm]
	I_v [cd]	Δd [mm]	r_1 [mm]	standard deviation		
3 mm w	3.6	0.2	0.0	0.85 %	0.989	6.0
3 mm r	1.4	4.8	0.0	0.60 %	1.081	4.6
3 mm g	3.6	5.2	0.0	0.11 %	1.071	4.8
5 mm w	1.9	7.2	0.0	1.23 %	1.089	8.6
5 mm b	0.8	9.5	36.7	0.23 %	1.247	8.7
5 mm g	2.5	13.7	14.4	0.03 %	1.206	8.7
5 mm r	3.4	12.0	0.0	0.48 %	1.179	8.7
5 mm g	1.9	6.2	0.0	0.96 %	1.094	7.0
5 mm g	15.7	7.8	102.7	1.03 %	1.907	9.8
5 mm b/g	6.9	-44.1	85.1	0.18 %	1.278	10.7
10 mm o	69	-23.4	215.8	0.62 %	3.958	15.1
10 mm r	6.5	1.6	65.6	1.28 %	1.378	13.5
1W w	285	-11.0	45.6	0.17 %	1.057	14.1
1W g	403	31.6	0.0	2.09 %	1.337	14.1
1W g	5.5	2.3	0.0	0.14 %	1.029	3.0
sideview g	0.004	5.7	0.0	0.21 %	0.700	5.7
square r	0.026	-0.4	0.0	0.89 %	0.250	5x5

Conclusions

Applicability of the modified inverse-square law for the luminous intensity measurements of the LEDs has been studied with seventeen LEDs. Many of the studied LEDs contain a lens which complicates the distance measurements. The analysis removes the effect of the lens by moving the image of the source and allowing its size to vary. The essential information of the LEDs can be included in three parameters, luminous intensity I_v, radius of the image of the source r_1, and location of the image of the source Δd.

Fitting made by the proposed method gives notably more consistent results than the CIE standard, and the solution includes the standardized parameters $I_{LED\,A}$ and $I_{LED\,B}$. The method is therefore useful in applications where more consistency is needed.

References

1. K. Muray, “Photometry of diode emitters: light emitting diodes and infrared emitting diodes,” *Appl. Opt.* **30**, 2178-2186 (1991).
2. CIE 127.2, *Measurement of LEDs*.
3. J. Hovila, M. Mustonen, P. Kärhä, E. Ikonen, “Determination of the diffuser reference plane for accurate illuminance responsivity calibrations,” *Appl. Opt.* (in press).

Single-photon source heralding efficiency and detection efficiency metrology at 1550 nm using periodically poled lithium niobate

*S. Castelletto, I.P. Degiovanni, V. Schettini, and A. Migdall**

Abstract. We explored the feasibility of using high-efficiency periodically-poled crystals configured to produce downconverted photons for photon counting detector calibration at 1550 nm, with obvious importance for metrology and quantum communication applications. Moreover key considerations for both applications is the coupling of the downconverted photons into single-mode fibers. This study ties together the results of our efforts to model the single-mode heralding efficiency of a two-photon parametric downconversion source and our work to improve the accuracy of photon-counting calibrations made with which such a source.

1. Introduction

Parametric down-conversion (PDC) consumes pump photons and produces light with a two-photon field description [1]. This two-photon light, which allows one photon to indicate or herald the existence of its twin, is key to applications such as quantum metrology [2] and quantum information [3, 4]. In particular, these PDC applications work by preparing one photon in a well defined state by measuring its twin, effectively creating a single-photon source. To realize such a single-photon source [5] for these applications, there are two key demands we address here. First, high efficiency photon pair production and collection is critical for the utility of the applications. Second, there is strong interest in having the heralded photon at a wavelength convenient for telecom (1550 nm) and collected in a single-mode fiber.

For high efficiency of pair production, the use of periodic poled crystals is becoming common [11], although they have not yet been used for metrology applications. While metrology applications would certainly benefit from the advantage of high pump conversion efficiency, it is not clear that other characteristics of the periodically poled crystals would be compatible with these applications. Specifically, the level of background fluorescence may limit the uncertainty that can be achieved.

As for the efficiency of collection of PDC light into a single mode fiber, there have been a number of such efforts recently. The goal of these efforts is to accurately understand and model the two-photon process whereby the detection of one photon of a PDC pair, in a well defined spatial and spectral mode, defines the correlated spatial and spectral mode which can then be efficiently collected. These efforts have included experiments and theoretical work in both continuous wave (CW) [6, 7] and pulse-pumped [8, 9, 10] PDC, generated in bulk crystals, and have highlighted the critical problem of coupling of the PDC photons into single-mode fibers (SMF) due to the difficulty of spatial and spectral matching of the photon pairs. The results show that optimization of the heralding efficiency is extremely sensitive to spectral and spatial mode selection.

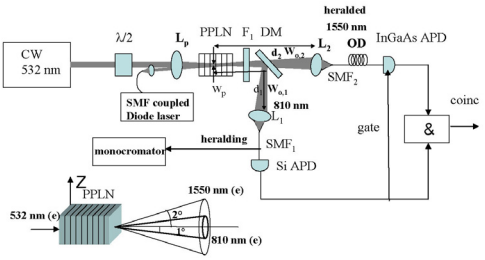

Figure 1. Setup to herald single-photons from CW PDC from a PPLN crystal.

We have set up (fig. 1) a 5 mm periodically poled lithium niobate (PPLN) crystal pumped by a CW laser at 532 nm to produce 810 nm and 1550 nm

S. Castelletto, I.P. Degiovanni, V. Schettini, and A. Migdall*: IEN G. Ferraris, Photometry Dept, Turin 10134, Italy, * NIST, Optical Technology Division, Gaithersburg, MD USA 20899-8441

photon pairs in a slightly noncollinear geometry. We use this source to measure the detection efficiency of an InGaAs APD at 1550 nm and in doing so also test our two-photon collection efficiency model. In our experiment, the crystal was operated in a quasi-phasematching configuration, with noncritical phase-matching (90° phase-matching angle) and a 7.36 μm period to produce PDC photons at 810 nm and 1550 nm at external angles of 1° and 2°. Fine tuning of this output was achieved by adjusting the crystal temperature to 149 °C. A lens, L_p was used in the pump beam to produce a gaussian beam waist of $w_p \simeq$100 μm at the crystal, a cutoff filter F_1 blocked the pump laser and a dichroic mirror (DM) separated the 810 nm (beam 1) and 1550 nm (beam 2) photons. A monochromator was inserted in the heralding path to align the 810 nm light, measure its spectral width, and as a filter. The heralding arm was routed to a SMF and then to a Si APD, while the heralded arm, also coupled to a SMF, was sent to a InGaAs APD, operating with gated bias. The heralded arm optical delay was adjusted with an appropriate length SMF to observe coincidences when the InGaAs detector was gated by the detection of a 810 nm photon in the heralding arm. The InGaAs detector, including the SMF and coupling lens optical losses, was calibrated against a conventional detector standard using a attenuated laser source, yielding a raw detection efficiency of $\eta_{det} = 9.8\%$.

The detector efficiency as measured by the PDC source is given by

$$\eta_{det} = (\chi_P \cdot \tau_{opt} \cdot \tau_{SMF-lens})^{-1} \times \frac{P_{coinc} - P_{uncorr}}{(1 - P_{uncorr})(1 - P_{backgnd}^{heralding})}, \quad (1)$$

where χ_P is the heralding efficiency (single-mode preparation efficiency)[7, 12], τ_{opt} is the overall heralded arm optical transmittance (including PPLN, F_1, DM), $\tau_{SMF-lens}$ is the optical transmittance of the L_2 and the SMF on the heralded arms, P_{coinc} is the probability of coincident counts per gate, P_{uncorr} is probability of uncorrelated or accidental coincidence counts per gate (determined by changing the heralding delay so the detection gate misses photons correlated to the herald photons), and $P_{backgnd}^{heralding}$ is the probability of gating counts produced by uncorrelated photons and dark counts on the heralding arm. The heralding efficiency χ_P [7] is the efficiency of preparing a photon in the heralded channel in a definite spectral and spatial mode, by specific mode selection of the heralding arm. This factor is in addition to the other optical transmittances in the *heralded* channel. It basically quantifies how well the collection system geometrically catches photons correlated to those seen by the trigger detector. To calibrate a SMF-coupled detector, the heralding efficiency must be optimized and estimated. It has been calculated in ref. [7] in the case of bulk crystal. For PPLN [12] it is

$$\chi_P = \frac{4\ w_p^2 w_1^2 w_2^2 (w_1^2 + w_p^2)}{(w_2^2 w_p^2 + w_1^2\ (w_2^2 + w_p^2))^2} \frac{\Delta_2}{(\Delta_1^2 + \Delta_2^2)^{\frac{1}{2}}} f(L), \quad (2)$$

where $\Delta_{1,2}$ =1 nm, 2.7 nm are the spectral bandwidths selected by the SMF in the two arms and $f(L)$ is a correction function depending on the crystal length. We used two lenses configuration to mode match the fields. With L_1 and L_2 both f=8 mm aspheric lenses, at d_1=270 mm and d_2=220 mm, and $w_1 = w_2$=100 μm, from Eq.(1), we obtained the experimental value of χ_p =64%, while from Eq. (2) we estimate χ_p=61%. With L_1 and L_2 both 20x microscope objectives at d_1=560 mm and d_2=190 mm, and $w_1 = 144\mu$m and w_2=76 μm, we obtained the experimental value of χ_p =77% and the theoretical χ_p=78 %. Those values are in good agreement considering the difficulty to measure the bandwidths and waists at the crystal. The measured values in Eq.(1)are P_{coinc}=2.2%, 2.9%, $P_{uncorr}^{heralded}$=0.2 %, 0.3 % and $P_{backgnd}^{heralding}$=41%, 29%. We measured the τ_{opt}=65 % and $\tau_{SMF-lens}$=83 %, 73%, for the lenses and objectives configuration, respectively. The heralding background, properly measured using the monochromator, is due to the fluorescence of the PPLN. This experiment, with the high level of 0.07 pairs/(mW gate) produced indicates that PPLN should be compatible with the detector efficiency application for direct calibration of single-mode coupled InGaAs photon-counting detectors at 1550 nm. In addition, the level of consistency (although very rough at this early stage of our work) between the two detector calibration methods reflects favorably on the validity of our mode-matching model. Because in this initial experiment the PDC source and optical collection system was not optimized for 1550 nm and losses were relatively high, we expect that there is significant room to improve the system to allow a high accuracy test to be performed.

References

1. D.N. Klyshko, *Photons and Nonlinear Optics*, (Gordon and Breach Science Publishers, 1988).
2. A.L. Migdall, et. al, Appl. Opt., **41**, 2914-2922(2002)
3. W. Tittel et al., **84**, 4737-40(2000)
4. E. Knill et al. Nature **409**, 46-52(2001).
5. S. Fasel et al., quant-ph/0408136, 7 pages.
6. C. Kurtsiefer et al. Phys. Rev. A, **64**, 023802(2001).
7. S. Castelletto et al., SPIE Proc. **5551**, 60-72(2004)
8. F.A. Bovino et al., Opt. Comm. **227**, 343-348(2003).
9. T.B. Pittmann et al. quant-ph/0408093, (2004)
10. S. Castelletto et al., submitted to Optics Express.
11. M. A. Albota et al., J. of Modern Physics, **51**, 1417-1432(2004)
12. S. Castelletto et al. , under preparation.

The Measurement of Surface and Volume Fluorescence at NPL

M. J. Shaw, T. A. Burnitt, C. J. Chunnilall
National Physical Laboratory, Tedddington, TW11 0LW, U.K.

Abstract. A spectrofluorimeter for quantifying the fluorescent emission from liquids and transmitting solids as well as opaque surfaces has been developed at the National Physical Laboratory (NPL). The system incorporates a goniometric detection system which allows the measurement of the fluorescent emission and scattered light at any angle to the incident radiation. This paper describes the optical design of the instrument and outlines methods used to calibrate the excitation and detection systems to allow determination of the normalized emission spectrum or total radiance factor and associated colorimetry of a fluorescent material. Uncertainty budgets for the measurements are also presented.

The NPL Reference Spectrofluorimeter

New measurement requirements, particularly in the biotechnology sector, have led NPL to extend its fluorescence measurement capability. To meet these needs a new reference spectrofluorimeter has been developed to allow analysis of fluorescent emission and scattering in multiple geometries over a range of wavelengths from the UV to NIR [1, 2].

The NPL Reference Spectrofluorimeter (RSF) (figure 1) has a high power xenon source, the output from which is focused onto the entrance slit of a double grating monochromator operated in additive mode. The beam exiting the monochromator is collimated by an off axis parabolic mirror and then steered by three plane mirrors onto a second off axis parabolic mirror which forms an image of the exit slit at a limiting aperture. The width of this limiting aperture sets the bandwidth of the light incident on the sample (usually 5 nm FWHM). A magnified image of the limiting aperture is produced at the sample plane by a lens. Using this optical arrangement the incident beam converges to a focus at the sample plane to form a rectangular patch. The polarization of the incident light, usually set at 45˚ to the vertical, is fixed by a Glan Taylor polarizing prism in a rotating mount. The last optical component before the sample is a silica window that acts as a beamsplitter, reflecting approximately 8% of the beam to a silicon photodiode trap detector [3] which is used to monitor the optical power incident on the sample.

The system has two different sample mounting stages, both incorporate a reflectance standard that can be measured along with the sample. Opaque reflecting samples are mounted on a linear stage which can be translated vertically to move either the sample or the reference standard into the excitation beam. When measuring volume fluorescence, cuvettes or similarly sized solids are mounted at one end of a rotating arm and the calibrated reflectance standard at the other. Rotating the arm by 180˚ switches between the sample and reference standard.

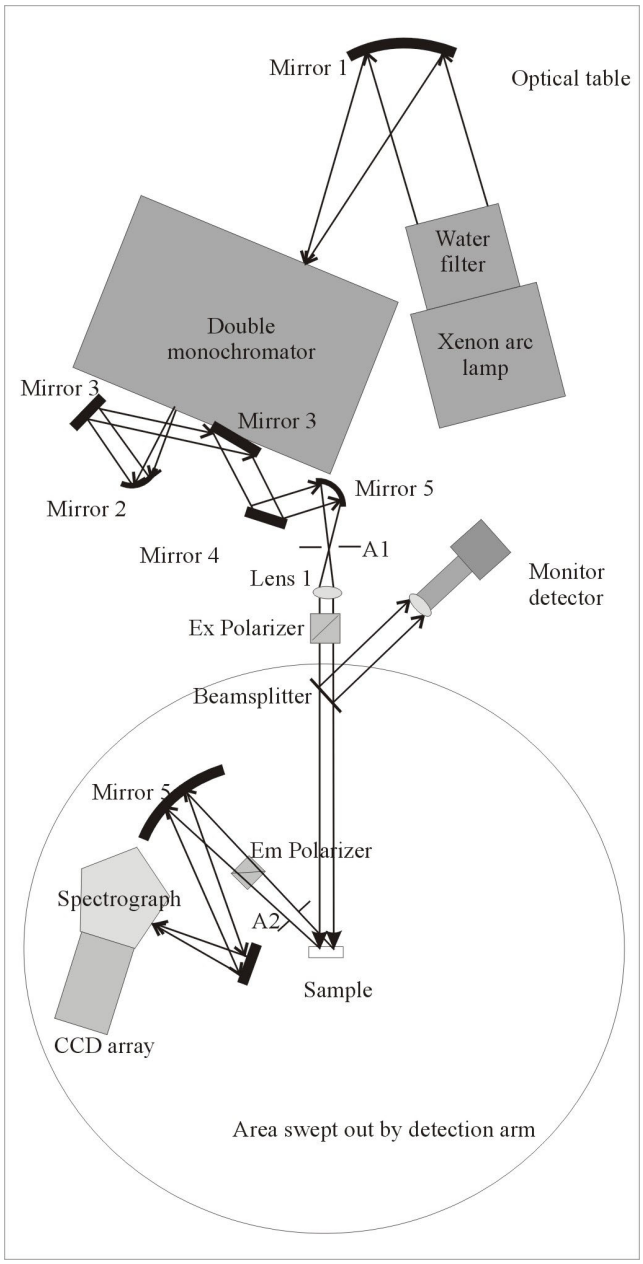

Figure 1. The NPL Reference Spectrofluorimeter configured for a 0°/45° measurement of surface fluorescence

The detection system is built around an arm that rotates about the point where the sample plane and the incident beam intersect. Light emitted by the sample into a fixed solid angle defined by an iris aperture is focused onto the entrance slit of a single grating spectrograph. The spectrograph entrance slit is imaged onto a Peltier cooled 1024 element CCD array which allows simultaneous measurement of the light spectrum across a 500 nm wavelength band. The range of wavelengths detected by the CCD array can be adjusted by rotating the grating; for

visible measurements this is usually set to be from 300 nm to 800 nm.

Calibration

In order to determine the normalised fluorescent emission from a sample it is necessary to determine both the relative spectral irradiance at the sample and the relative spectral responsivity of the detection system. Both of these properties are determined using physical transfer standards which have been calibrated at NPL.

The relative spectral irradiance at the sample is determined by calibration of the relative spectral responsivity of the monitor detector. A silicon photodiode of known spectral responsivity [5] is positioned in the sample plane such that it is underfilled by the incident beam. For each excitation wavelength the signal from the calibrated photodiode is compared to the signal from the monitor trap, this ratio is multiplied by the responsivity of the photodiode to give the responsivity of the monitor trap. The voltage from the monitor channel can then be used directly to determine the optical power incident on the sample at any time.

The light spectrum measured by the CCD array is the product of the spectral radiance of the sample under investigation and the spectral responsivity of the detection system (which is itself a product of the throughput of the collection optics, the efficiency of the diffraction grating and the responsivity of the array pixels). By illuminating the detection system with a source of known spectral radiance it is possible to calculate its spectral responsivity and hence normalize any measured sample spectrum. A non-fluorescent Spectralon plaque of measured spectral reflectance [4] is placed at the sample position and the wavelength of the excitation monochromator is scanned across the spectral band over which the detection system is to be calibrated. The detector responsivity is then determined by recording the monitor voltage and the signal at the CCD at each excitation wavelength

With both excitation and emission parts of the spectrofluorimeter calibrated it is possible to measure the normalized fluorescent emission and reflected scatter from a sample. Other properties can then be determined by calculation as required.

Volume Fluorescence

Fluorescence measurements are used extensively in biotechnology and pharmaceutical applications, such as drug discovery and biological imaging, diagnostics and research where the fluorescent species is often in solution or a bulk volume. In such cases the fluorescent emission is often measured in a 0˚/90˚ geometry as this configuration minimizes the amount of scatter at the exciting wavelength which reaches the detector.

The bispectral radiance factor of a sample is measured by scanning the excitation monochromator and recording the spectrum of the fluorescent emission at each wavelength. The fluorescent intensity from liquid samples tends to be considerably lower than that from surfaces (which are often designed to be highly fluorescent) and consequently longer detector exposure times are necessary. Such spectra often contain significant spurious signals due to cosmic rays striking the CCD array and methods have been developed to remove these features.

Surface Fluorescence

Measurements of surface fluorescence are important in a variety of industries including paper, high visibility clothing and signage. In most cases it is important to characterize the material in terms of how it is perceived by a human observer under different lighting conditions. The total radiance factor of a fluorescent surface is the sum of the reflected and luminescent radiance factors which are measured simultaneously. Measurements are usually made in 0˚/45˚ geometry with excitation and detection over the range 320 nm to 780 nm. Once a full bispectral scan has been carried out the total radiance factor and associated colorimetry can be calculated for any illuminant spectral power distribution.

Uncertainties

Full uncertainty budgets have been developed to cover the range of measurements made using the RSF. The total combined uncertainties depend upon the nature of the sample being measured and the spectral region of interest. In particular, uncertainties tend to increase in the short wavelength region of the UV. Typically normalized fluorescent emission spectra and total spectral radiance factor can be measured to an uncertainty of better than ± 3% (k = 2). There are several dominant components contributing to the overall uncertainty including the linearity of the CCD detector, stray light in the CCD spectrograph and calibration of the transfer standards. Work is ongoing to better understand and correct for these effects and reduce the total combined uncertainty.

Acknowledgments

The authors would like to thank all their colleagues at the National Physical Laboratory. This work was funded by the UK DTI National Measurement System Directorate's Programme on Optical Radiation Metrology.

References

[1] Williams, D. W., Fluorescent standards for surface colour, *NPL Report QU111*, August 1995

[2] Shaw, M. J., Clarke, P. J., Burnitt, T. A., The design of the new NPL Reference Spectrofluorimeter, *Proceedings of SPIE vol. 5192, pp 30 – 35,* November 2003.

[3] Fox, N. P., Trap detectors and their properties. *Metrologia*, 28, 197-202. 1991.

[4] Chunnilall C.J., Deadman A.J., Crane L., Usadi E., NPL Scales for Radiance Factor and total diffuse reflectance, *Metrologia*, 40, S192 – S195, 2003

[5] Fox N.P., Theocharous E., Ward T.H., Establishing a new ultraviolet and near-infrared spectral responsivity scale, *Metrologia*, 35, 535-541, 1998.

The evaluation of a pyroelectric detector with a carbon multi-walled nanotube coating in the infrared.

E. Theocharous
National Physical Laboratory, Teddington, U.K.

R. Deshpande, A.C. Dillon
National Renewable Energy Laboratory, USA

J. Lehman,
NIST, Boulder, USA

Abstract. The performance of a pyroelectric detector with a carbon multi-walled nanotube coating was evaluated in the 0.9 μm to 14 μm wavelength range. The relative spectral responsivity of this detector was shown to be flat over most of the wavelength range examined and the spectral flatness was shown to be comparable to the best infrared black coatings currently available. The performance of the detector (in terms of NEP and D*) was limited by the very thick (250 μm thick) $LiNbO_3$ pyroelectric crystal on which the coating was deposited. The responsivity of this detector was shown to be linear in the 0.06 mW to 2.8 mW radiant power range and its spatial uniformity was similar to other pyroelectric detectors utilising different types of black coatings. The carbon nanotube coatings were reported to be much more durable than other infrared black coatings commonly used to coat thermal detectors in the infrared, such as metal-blacks. This, in combination with its excellent spectral flatness demonstrated by this paper suggests that carbon nanotube coatings appears extremely promising for thermal detection applications in the infrared

Introduction

Coatings applied to thermal detectors must combine high absorptivity, to ensure that a large fraction of the incident radiation is absorbed, with low thermal mass to ensure that the resulting temperature increase is maximised for a certain level of incident radiant power [1]. These requirements are particularly important in the infrared where there is limited availability of black coatings whose characteristics match the conditions stated above. While the absorptivity of gold-black coatings in the infrared are very good [2, 3], their fibrous structure is very delicate leading to degradation in performance due to the collapse of this structure, particularly as a result of heating and physical contact. Lehman et. al. recognised that the characteristics of carbon nanotube coatings fulfill the main requirements of black coating for thermal detectors [4, 5]. The fabrication and evaluation of two pyroelectric detectors with two different types of carbon nanotube coatings was reported in the 600 nm to 1800 nm wavelength range [4, 5]. However, the main applications of thermal detectors are mainly in the infrared where the advantages of alternative (photon) detector technologies are not so overwhelming, allowing thermal detectors to compete for market share. The aim of this paper is to report the extension of the evaluation of a carbon Multi-Walled Nano Tube (MWNT) coated pyroelectric detector in the infrared. The carbon nanotube coating which was grown by Hot Wire Chemical Vapour Deposition (HWCVD) was deposited on a 250 mm thick $LiNO_3$ crystal [5]. The active area of the detector was 3 mm in diameter. Full details of this pyroelectric detector and the characteristics of the carbon nanotube coating can be found elsewhere [5].

The performance of the MWNT pyroelectric detector was characterised using the NPL infrared detector characterisation facilities [6]. Full details of the NPL infrared spectral responsivity measurement facility can be found elsewhere [7]. For further information on the NPL spatial uniformity of response measurement facility and the NPL linearity of response measurement facility the reader is referred to references 6 and 8 respectively. The maximum level of spectral irradiance at which linearity measurements were made was restricted by the maximum spectral radiance available from the 2 mm wide element of the tungsten strip lamp. During the linearity characterisation, the unfiltered output of a tungsten strip lamp with a silica window was used. This was deemed acceptable because of the spectral flatness of the spectral responsivity of the carbon nanotube pyroelectric detector.

For all the radiometric evaluations described in this paper, the MWNT pyroelectric detector was used in combination with a trans-impedance amplifier operated at a fixed gain of 10^8 V A^{-1}. All measurements presented in this paper were performed at a 70 Hz modulation frequency.

Results

Figure 1 shows the relative spectral responsivity of the carbon nanotube pyroelectric detector in the 0.9 μm to 14 μm wavelength range, normalised at 1.6 μm. The error bars shown in Figure 1 represent the 1σ uncertainty of the measurements. The plot shows that the relative spectral responsivity was approximately flat in the 1.6 μm to 14.0 μm wavelength range. This, in turn, means that the absorptivity of the MWNT coating was also flat because that is the main parameter governing the relative spectral responsivity of thermal detectors [1]. For wavelengths below 1.6 μm the response of the detector decreased monotonically with wavelength down to 0.9 μm, the shortest wavelength studied. This behaviour confirms data previously reported by Lehman et al [5]. A similar behaviour has also been observed in some other good-quality metal-black coatings such as silver-black and

some gold-black coatings. No measurements were attempted for wavelengths longer than 14 μm because the Signal-to-Noise Ratio (SNR) of the measurements was extremely poor due to the poor Noise Equivalent Power (NEP) of the detector and the low radiant power coming through the double grating monochromator.

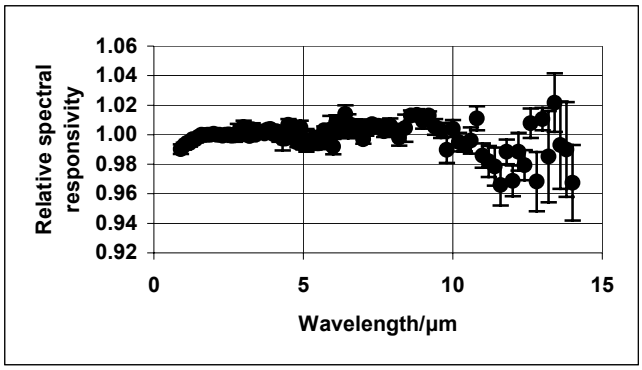

Figure 3: Relative spectral responsivity of the MWNT pyroelectric detector normalised at 1.6 μm. Error bars represent the 1σ uncertainty of the measurements.

The DC equivalent absolute spectral responsivity of the MWNT pyroelectric detector in combination with the trans-impedance amplifier with 10^8 V/A gain at 1.6 μm for a 70 Hz modulation frequency was measured by comparison with NPL standards to be 9.03 V W^{-1}. The Noise Power Spectral Density (NPSD) of the detector/amplifier combination at 70 Hz was measured to be 1.46 μV $Hz^{-1/2}$. Ignoring the noise contribution due to the transimpedance amplifier (the noise was dominated by the pyroelectric detector), the specific detectivity (D*) of the carbon nanotube pyroelectric detector at 1.6 μm at 70 Hz was estimated to be 1.82 x 10^6 cm $Hz^{1/2}$ W^{-1}. This is a relatively poor value compared to gold-black-coated $LiTO_3$ pyroelectric detectors which have typically two orders of magnitude higher D* values. The low D* value of the MWNT pyroelectric detector was not unexpected because this detector was based on a 250 μm thick $LiNbO_3$ crystal. The thicker crystal (typically a factor of 5 times thicker than $LiTO_3$ pyroelectric detectors studied previously) in combination with the poorer pyroelectric characteristics of the $LiNbO_3$ crystal can account for most of the observed difference. Furthermore, the coating deposition required the $LiNbO_3$ crystal to be heated to temperatures in excess of 300 ^oC [5], which may also have led to a deterioration of the its pyroelectric properties.

Theory predicts that the absorbance of MWNT coatings will depend on the fill factor and will exhibit some dependency on wavelength. The results of this study show that the relative spectral responsivity of the MWNT coated pyroelectric detector and therefore the absorbance of the MWNT coating does not exhibit any wavelength dependency in the 1.6 μm to 14 μm wavelength range. This observation can only be explained by the carbon nanotubes being long and crooked as well as being poorly aligned. This is supported by the shape of the nanotubes recorded by SEM and shown in Figure 2.

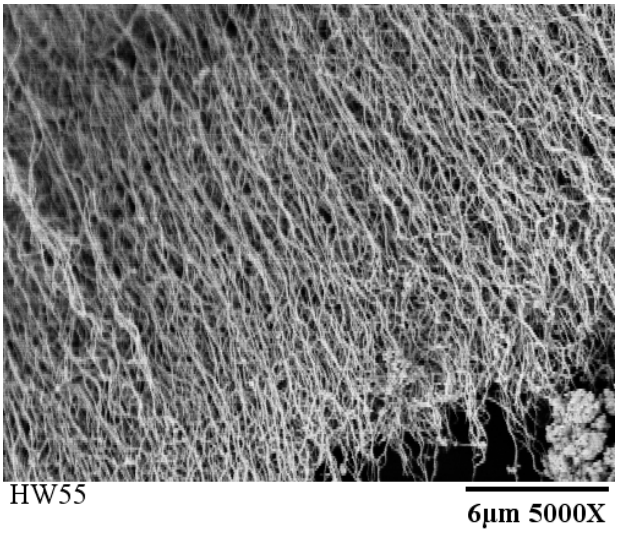

Figure 2. Scanning electron microscope image of the MWNT coating

Reference

1. W. R. Blevin and J Geist, "Influence of black coatings on pyroelectric detectors", Applied Optics, **13**, 1171-1178, 1974.
2. D. J. Advena, V. T. Bly and J. T. Cox, "Deposition and characterisation of far-infrared absorbing gold black films", Applied Optics, **32**, 1136-1144, 1993.
3. J. Lehman, E. Theocharous, G. Eppeldauer and C. Pannel, "Gold-black coatings for freestanding pyroelectric detectors" Measurement Science and Technology, **14**, 916-922, 2003.
4. J. H. Lehman, C. Engtrakul, T. Gennet and A. C. Dillon, "Single-wall carbon nanotube coating on a pyroelectric detector", Applied Optics, **44**, 483-488, 2005
5. J. H. Lehman R. Deshpande, P Rice and A. C. Dillon, "Carbon multi-walled nanotubes grown by HWCVD on a pyroelectric detector", To be published in Infrared Physics and Technology, 2005.
6. E. Theocharous, F. J. J. Clarke , L. J. Rodgers and N. P. Fox, "Latest techniques at NPL for the characterisation of infrared detectors and materials", Proc. SPIE Vol. **5209** "Materials for Infrared Detectors III", 228-239, 2003.
7. E. Theocharous, J. Ishii and N. P. Fox, "A comparison of the performance of a photovoltaic HgCdTe detector with that of a large area single pixel QWIP for infrared radiometric applications", Infrared Phusics and Technology, **46**, 309-322 2004.
8. Theocharous E., Ishii J. and Fox N. P., "Absolute linearity measurements on HgCdTe detectors in the infrared", Applied Optics, **43**, 4182-4188, 2004.

UV detector calibration based on an IR reference and frequency doubling

J. Hald and J. C. Petersen

Danish Fundamental Metrology, 307 Matematiktorvet, DK-2800 Kgs. Lyngby, Denmark

Abstract. We propose a new scheme for measuring the responsivity of an optical detector at the optical frequency 2ω based on a calibrated reference detector at frequency ω and a setup for cavity enhanced optical frequency doubling. We derive the theoretical uncertainty of the responsivity as a function of the cavity parameters. Furthermore, we demonstrate an experimental implementation of this scheme, which links detector responsivities in the IR and UV regions. This scheme may complement existing techniques for providing traceability in the UV region.

Introduction

Laser based detector calibrations are more difficult in the UV region than in the visible and near infrared regions of the spectrum as this wavelength range is not well covered with available laser sources. Less favorable light sources may be used instead, e.g. spectrally filtered lamps or synchrotron radiation. Calibrations in the UV range are usually not offered with the same uncertainties as for the visible and NIR range. Typical UV detector calibrations from national metrology institutes have standard uncertainties around 0.5%. The importance of UV detector calibrations is increasing because of the growing application of UV radiation in areas such as the semiconductor industry, environmental monitoring, medical treatment and biotechnology. Thus, development of new techniques for UV detector calibrations is highly desirable. Cavity enhanced frequency doubling is a widely used technique for efficient generation of continuous wave (cw) light at wavelengths that are otherwise not easily available. This technique has previously been used in radiometry as a way to generate UV light at wavelengths of interest (Talvitie *et al*). The conversion process obeys the law of energy conservation. Hence it is possible to derive the generated UV power without a direct measurement at the UV wavelength if the loss of optical power at the fundamental wavelength can be measured with high accuracy. Knowledge of the UV power level allows for UV detector calibration.

Theory

Figure 1 shows a typical setup for optical frequency doubling in a ring resonator. The fundamental field at frequency ω is coupled into the cavity via the input coupler (M_1) and the generated second harmonic field escapes the cavity through mirror M_4. The optical power can be measured at four different positions: The injected fundamental power P_ω^{in}, the fundamental power circulating in the resonant cavity P_ω^c, the generated second harmonic power $P_{2\omega}$, and the fundamental power reflected off the cavity P_ω^r. In practice, P_ω^c is inferred from the small leakage through mirror M_2, and $P_{2\omega}$ is inferred from the second harmonic power escaping through mirror M_2. The relevant parameter from the cavity reflection is the ratio R between the reflected power when the cavity is on resonance and off resonance. In the following we ignore the uncertainty from transmissivity of the cavity mirrors M_2 at frequency ω and M_4 at frequency 2ω as well as possible interference filters used for separating different wavelengths; these are relative measurements that does not require an absolute calibration. We assume that the detectors used at the fundamental frequency have been calibrated with negligible uncertainty. The responsivity α of the detector for the second harmonic measurements is assumed to be unknown, and we write $V_{2\omega}=\alpha P_{2\omega}$, where $V_{2\omega}$ is the measured signal (e.g. voltage) from the detector.

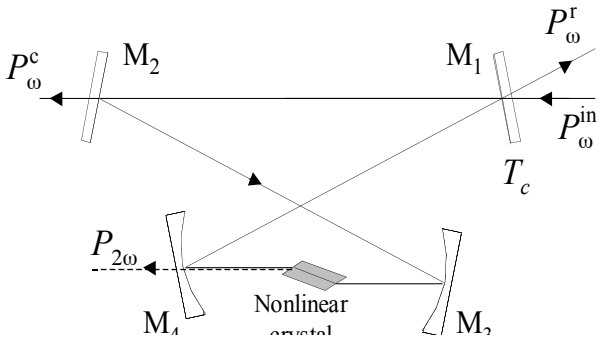

Figure 1. Frequency doubling setup. M_1: Partially reflecting mirror (input coupler) with transmissivity T_c. M_2, M_3 and M_4: Highly reflecting mirrors at the fundamental frequency ω. M_4 has high transmissivity at the second harmonic frequency 2ω.

According to the theory of cavity enhanced optical frequency doubling, the four power parameters P_ω^{in}, P_ω^c, $V_{2\omega}$, and R fulfill the following relations (Ruseva *et al*):

$$\begin{aligned} V_{2\omega}/\alpha &= E_{\mathrm{NL}}\left(P_\omega^c\right)^2 \\ mm\,P_\omega^{in} &= P_\omega^c\left(1-\kappa\right)^2/T_c \\ R &= 1-mm+mm\left(\frac{\left(1-T_c-\kappa\right)\left(1-\kappa\right)}{\left(1-T_c+\kappa\right)\left(1+\kappa\right)}\right)^2 \end{aligned} \qquad (1)$$

The round trip field attenuation factor κ is given by $\kappa=[(1-T_c)(1-E_{\mathrm{NL}}P_\omega^c)(1-L)]^{1/2}$. E_{NL} is the single pass nonlinearity of the crystal, L the passive roundtrip losses in the cavity due to imperfect optics, and mm the mode matching efficiency that describes the overlap between the spatial mode of the cavity and the injected field. If the four power parameters are measured simultaneously at n different input power levels, they must fulfill Eq. 1 at each power level. Thus, we can determine the unknown parameters, and in particular the calibration parameter α by a general least squares fit of the $4n$ power parameters and 4 unknown parameters (α, E_{NL}, L, and mm) to the $3n$ equations (Nielsen).

The uncertainty in the determination of α can be calculated numerically for given values of E_{NL}, L, mm, n, the maxi-

mum available input power $P_{\omega}^{in,\max}$, and the uncertainty in the 4n power measurements. For simplicity, we limit our calculations to the situation where the n power measurements have P_{ω}^{in} evenly spaced between zero and $P_{\omega}^{in,\max}$. Furthermore, we assume that all of the 4n power measurements have identical statistical uncertainty. The calculation is based on a least squares algorithm. T_c is adjusted within the calculation to the value that minimizes $u(\alpha)/\alpha$. The result is approximated by the following expression:

$$\frac{u(\alpha)}{\alpha} = V(x)\sqrt{\frac{22.5}{n-2.5}}\frac{u(P)}{P} \qquad (2)$$
$$x \equiv P_{\omega}^{in,\max} E_{\mathrm{NL}} / L^2$$

The dependence on the cavity parameters and available optical power is described by the empirical function V, which is plotted in Fig. 2. $u(P)/P$ is the relative statistical uncertainty in each of the 4n power measurements.

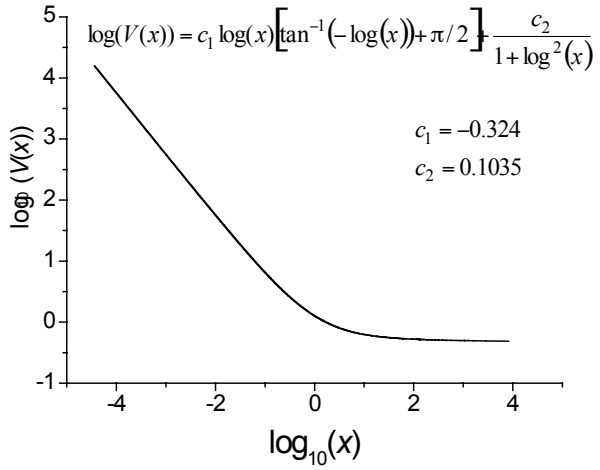

Figure 2. The empirical function $V(x)$, which is used in the approximate result in Eq. 2.

The relative discrepancy between the full numerical calculations and the empirical expression in Eq. 2 is found from Monte Carlo simulations to be within ±10% in the parameter range $0.001<u(P)/P<0.02$, $0.02\mathrm{W}< P_{\omega}^{in,\max} <2\mathrm{W}$, $10^{-6}/\mathrm{W}<E_{\mathrm{NL}}<10^{-2}/\mathrm{W}$, $0.001<L<0.05$, mm=0.90 and $12<n<50$. This parameter range covers most practical values for the cavity parameters in optical frequency doubling. In particular, when $P_{\omega}^{in,\max} E_{\mathrm{NL}} / L^2 >1.7$ and $n>24$, the relative uncertainty in α is smaller than $u(P)/P$. However, uncertainty in mirror and filter transmissions, uncertainty in the calibration of the reference detector at frequency ω as well as undesirable effects in the crystal (e.g. thermal lensing) will add to this uncertainty.

Experiment

Experimental data on frequency doubling from 768 nm to 384 nm in BIBO (BiB_3O_6) and LBO (LiB_3O_5) have previously been published (Ruseva *et al*). Here we reanalyze these data for testing the proposed scheme for responsivity measurements. The experiment use about 900 mW of light from a Ti:Sapphire laser at 768 nm, and the frequency conversion takes place in a cavity as in Fig. 1 with either BIBO or LBO as the nonlinear crystal. An internal conversion efficiency of 70% is reached with BIBO, whereas LBO achieves 40% due to smaller nonlinearity. The key parameters for the experiment are: $u(P)/P$=0.01, mm=0.93, L=0.004, $E_{\mathrm{NL,BIBO}}=2.3\cdot10^{-4}$/W, and $E_{\mathrm{NL,LBO}}=2.6\cdot10^{-5}$/W. The derived detector responsivity is shown in Fig. 3. The major contributions to the uncertainties come from inaccurate measurements of mirror and filter transmissions as well as the IR detector calibration. If these contributions are ignored, the remaining uncertainty compares well with the result from Eq. 2. In Fig. 3 we also show an independent calibration of the UV detector directly against a thermopile detector. This result is consistent with the results from the frequency doubling scheme.

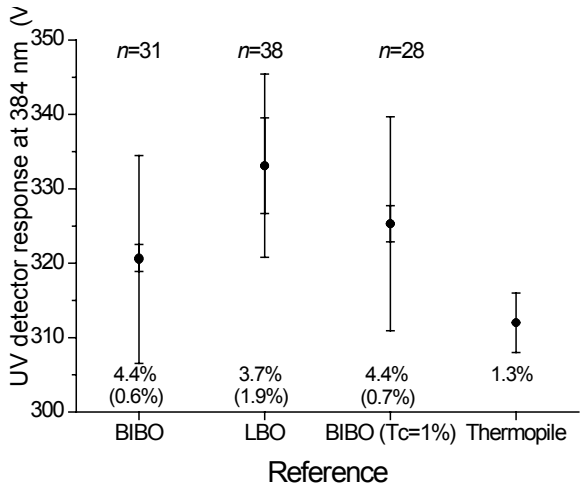

Figure 3. The responsivity of a UV detector at 384 nm is derived from the proposed scheme based on cavity enhanced frequency doubling in LBO (T_c=0.65%) and BIBO (T_c=0.65% and T_c=1.0%). Calibration against a thermopile is shown for comparison. The numbers below error bars are the relative standard uncertainties. The numbers in brackets are the uncertainties when contributions from mirror/filter transmissions and IR detector calibration are ignored.

References

Talvitie, H., A. Seppänen, A. Äijälä, and E. Ikonen, Continuous-wave light source at 317 nm based on frequency doubling of a diode laser, *Appl. Phys. B, 66*, 397-400 (1998).

Nielsen, L., Least-squares estimation using Lagrange multipliers, *Metrologia, 35*, 115-118, 1998. Erratum, *Metrologia, 37*, 183 (2000).

Ruseva, V., J. Hald, Generation of UV light by frequency doubling in BIBO, *Opt. Commun.*, *236*, 219-223, 2004.

NEWRAD 2005:

Non selective thermal detector for low power measurements

F. Durantel, D. Robbes,
ENSICAEN, GREYC – UMR 6072, 6 boulevard du Maréchal Juin, 14000 Caen, France

B. Guillet *, J. Bastie
LNE-INM / CNAM, 292 rue Saint Martin, 75003 Paris, France
* Previously : ENSICAEN, GREYC – UMR 6072, 6 boulevard du Maréchal Juin, 14000 Caen, France

Abstract. This paper describes a non selective thermal detector intended for measuring the relative spectral responsivity of selective detectors at the exit slit of a monochromator. It is based on thin film technology. It uses a bolometer for measuring the temperature and an electrical substitution method for running the measurement under computer control operation. The expected characteristics are a spectral range from 200 nm to 2500 nm, a dynamic range from 1 µW to 100 µW, a signal to noise ratio of about 1000 at 1µW level and a time constant in the range of 1 second. The preliminary theoretical and practical studies have given the necessary information for starting the realization of the device.

Introduction

In the French National Metrology and Test Laboratory (LNE) the spectral responsivity measurement of detectors is carried out using a two steps method. In a first step the relative spectral responsivity is measured by comparison to a non selective thermal detector when both detectors are irradiated by the same flux coming out from a monochromator. In a second step the absolute spectral responsivity is determined at some laser wavelengths by direct or indirect comparison to a cryogenic radiometer. At present time the major limitations in the accuracy of the measurements come from the low responsivity of the thermal detector used and the low level of flux available at the exit slit of the monochromator. To overcome these difficulties, the development of a new thermal detector has been undertaken by the GREYC laboratory in the framework of a collaboration project with the LNE. The main characteristics of this detector should be : a spectral range from 200 nm to at least 2500 nm, an active area between 0.5 cm^2 and 1 cm^2, a dynamic range from 1 µW to 100 µW, a time constant of about 1 second and a signal to noise ratio of 1000 at the 1 µW level.

Description of the detector

The principle of the detector is described in figure 1. The sensor uses a thin film of Mylar coated with aluminium on both side, tight on a metallic support. The support, in copper, works as a heatsink at constant temperature and can be, if necessary, cool and temperature controlled. On the membrane, electrical resistors are etched using optical photolithography. Some of these resistors are used as thermometers and some others as heaters for applying the electrical substitution method. The upper part of the detector is coated with a black paint in order to absorb the radiation in the useful spectral range. An electronic device can control the temperature of the sensor and determine the radiant flux received by the sensor. [1, 2]

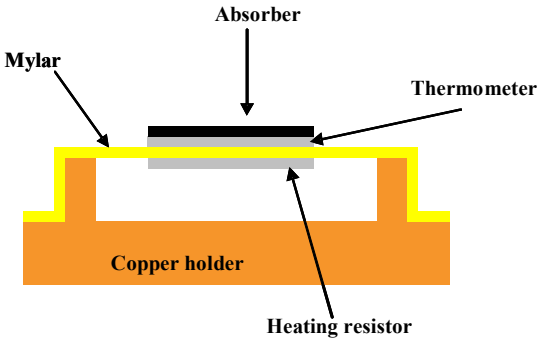

Figure 1. Schematic drawing of the detector (thickness of the various layers are not scaled).

Theoretical studies

In order to determine if a such device could be able to fulfil the requirement, a theoretical study has been carried out using computer simulations. Two cases have been considered, the first when the active part of the detector is in air and the second when it is in the vacuum. The results of these studies have shown that the responsivity of the detector is 10^{-3} K/µW when the detector is in air. When it is in the vacuum the responsivity is increased by a factor greater than 10 but nevertheless it is still a little below the requirement indicated at the beginning of this work. In order to increase the responsivity it has been decided to add a spherical mirror over the detector in order to reflect back the incident radiation reflected by the black coating and the radiation emitted by the detector itself (figure 2). With this mirror the device could be in the range of the requested responsivity.

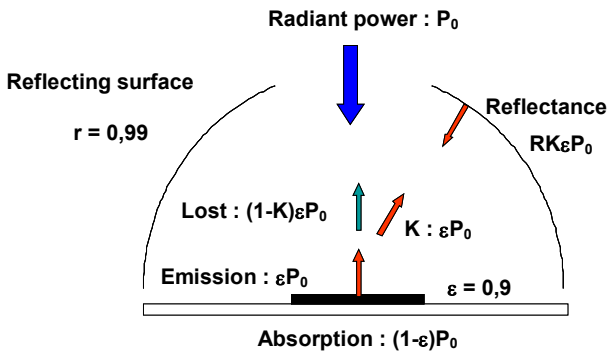

Figure 2. Power transfer between the detector and the mirror

The time constant of the detector has been also calculated and found in the range of approximately 1 to 2 seconds when the detector is in the vacuum. This value is perfectly acceptable.
The thermal behaviour of the support when it is temperature controlled by a Peltier element put at its bottom has also been studied using the Quickfield software. The results have been found in agreement with the expected characteristics of the detector.

Practical studies

In order to realise the heaters and the thermometers the electrical parameters of the thin aluminium coating on the Mylar have been checked. The variation of the electrical resistance of the aluminium film with temperature has been studied and the measured temperature coefficient was 0.00190 K^{-1} at 300 K.
In order to realise thermometers and heaters, the thin aluminium layers on both side of the Mylar film are etched using optical photolithography. On one side of the membrane 3 thermometers are realised and on the other side 2 heaters are etched. The determination of the shape of the figures for realising these resistors have been done according to the following requirements : the pattern must be not too small in order to have an easy realisation, the resistance must be in the range of some ten to some hundred of ohms in order to keep the Johnson noise at a reasonable level. For the heaters the heating must be as homogenous as possible. The figure 3 gives the patterns used for the thermometers and the heaters on each side of the membrane. For the thermometer the width of the strips are 200 µm and space between strips is also 200 µm. For the heater the width of the strips is 100 µm and the space between strips is 200 µm. The diameter of the active part is 5 mm.

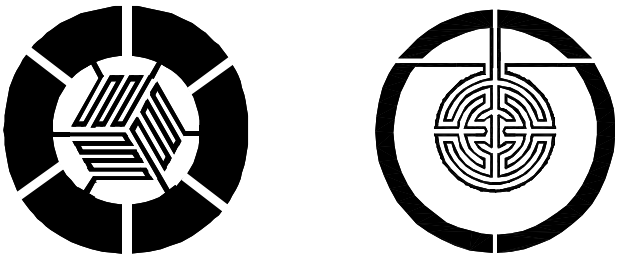

Figure 3. Left, Three resistors for temperature measurements, right, two resistors for heating the detector (two sides of the membrane).

The procedure for realizing these resistors has been studied and implemented. Several samples have been fabricated and checked. The mean values of the resistors are typically 195 ohms for the thermometers and 1040 ohms for the heaters.
For absorbing the radiation a black paint is used. It is a special paint developed for space applications by the Map-Coating society. A method for realizing a homogeneous thin layer has also been implemented and good layers with a thickness of 35 µm have been realized. This thickness could be adjusted to optimize the absorption and the time constant. Measurement of reflectance and transmittance of the layers has been done on the spectral range from 2 µm to 15 µm. With the checked samples the transmittance is always lower than 3.10^{-4} and the reflectance is less than $5\ 10^{-3}$ and increases very slowly with wavelength.
After these theoretical and practical studies the final design of the detector has been finalized. It is shown schematically in the figure 4.

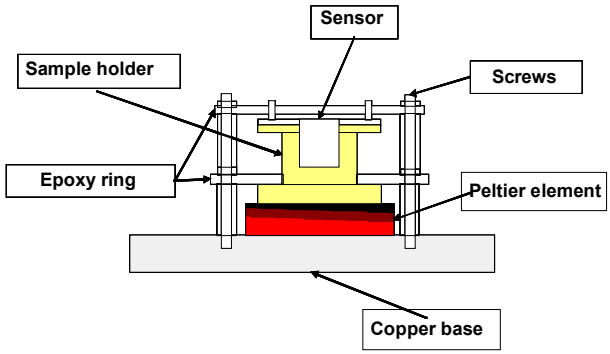

Figure 4. Schematic final design of the detector.

Conclusion

The thermal simulations carried out on various types have shown that it is possible to fulfil the requirements only if the detector is put in vacuum and a reflector is place in front of it. The determination and the method to realize the resistors used as thermometers and heaters have been implemented and the results are in agreement with what it is expected. The preliminary tests on the paint used to coat the detector for absorbing the radiation are also very encouraging. The next step will be the realization of a first prototype of the detector in order to check it in practical condition of use.

Acknowledgments : This work is supported by the contract N° 04 3006 from the French National Metrological and Test Laboratory (LNE).

References

Guillet B., Robbes D., Méchin L, Low noise temperature control application to an active cavity radiometer, *Rev.Sci.Instrum., 74(1)* 2003

Guillet B., Lecture et contrôle faible bruit de température à très haute résolution : application à la mesure du bruit excédentaire, à la bolométrie résistive et à la radiométrie à substitution électrique., Thèse de doctorat de l'université de Caen, 2000.

NEWRAD 2005

Calibration of Current-to-voltage Converters for Radiometric Applications at Picoampere Level

P. Sipilä[1], R. Rajala[2], P. Kärhä[1], A. Manninen[2], E. Ikonen[1,2]

[1] Metrology Research Institute, Helsinki University of Technology (TKK), P.O.Box 3000, FI-02015 TKK, Finland

[2] Centre for Metrology and Accreditation (MIKES), P.O.B. 239, FI-00181 Helsinki, Finland

Abstract. A constant-voltage method for accurate calibration of current-to-voltage converters has been studied and implemented down to 1-pA level with expanded uncertainty (k=2) of 3800 ppm. The same method is implemented for the characterisation of standard resistors, which is crucial for the calibration itself. The goal of this work is to achieve accurate and traceable measurements for radiometric and photometric applications producing photocurrents at picoampere level.

Introduction

Filter radiometers are increasing their popularity in modern photometry and radiometry. At the Helsinki University of Technology (TKK) they have been successfully used in spectral irradiance, illuminance and radiation temperature measurements. One major limitation of extending the use of filter radiometers is the measurement of the photocurrent. Measuring spectral irradiance in the ultraviolet region or measuring relatively low temperatures results in photocurrents that are in the picoampere range. Current-to-voltage converters needed for the measurements rarely have a traceable calibration for currents smaller than 10 nA.

To reduce the uncertainties of ultraviolet and temperature measurements, TKK and MIKES (Centre for Metrology and Accreditation) have developed a calibration method for the picoampere range. At present we report progress on 0.1 fA resolution that allows us to measure photocurrents down to 1 pA with an uncertainty of 3800 ppm (k=2).

Constant-voltage method for current calibration

In the constant-voltage method for current calibrations a precise voltage, U, is applied over a precise resistor, R, and the current, I, determined by the classical Ohm's law, is measured. The schematic of the setup is presented in Figure 1. The accuracy of the method is determined in practice by the accuracy of the resistor and the stability of the current-to-voltage converter as accurate voltage generators are easy to obtain.

Active guarding is not needed, because the leakage current from the high voltage source is conducted to the ground lead and thus not measured by the current meter. In most cases, the input impedance of the current-to-voltage converter, the internal resistance of the voltage source and the lead resistances can be assumed to be small enough not to have a measurable effect on the results. On the other hand, the offset voltage of the current-to-voltage converter can be assumed to be small enough and the insulation resistance of the high quality cables large enough that no leakage current occurs from the low potential of the resistor.

The main advantage of this method is its simplicity. However, with this method a trade-off for the accuracy has to be made as compared to methods based on capacitive components [1,2]. Also, there are difficulties with the use of resistive components, such as their long term stability and voltage dependence.

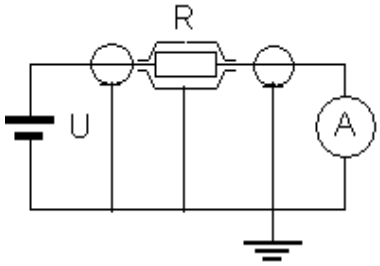

Figure 1. Schematic diagram of the current calibration setup based on the constant-voltage method. The applied voltage U over the resistor R generates a current which is measured with the current-to-voltage converter, A.

Characterisation of standard resistors

The importance of the characterisation of the standard resistor rises from the fact that the accuracy of these resistors dominates the uncertainty of the current calibration (if noise is not considered). The poor long term stability of the high ohmic resistors forces a frequent characterisation of the standard resistors to be part of the current calibration process itself.

The voltage dependence characterisation of the standard resistors was done with the same constant-voltage method as the current calibration itself. The current was measured with Keithley 6157 electrometer, the supply voltage source was Fluke 5440B/AF (max. output 1000 V) and the standard resistors were hermetically sealed five-part 9331S-series resistors from Measurement International Ltd. (from 10 GΩ to 100 TΩ). With this setup one could achieve precise currents between 1 pA and 100 nA.

The characterisation procedure for resistors from 10 GΩ to 100 TΩ was done in a ladder type sequence. In the characterisation process, first the electrometer's range used for characterising the 10 GΩ standard resistor was calibrated with a known calibrated standard resistor of 1 GΩ. The precise value of the 1 GΩ resistor was traceable to the reference value from the quantum Hall-effect. The main principle is that the current measured with the electrometer should be the same when 100 V over a 1 GΩ resistor and 1000 V over a 10 GΩ resistor is applied. Thus, the

correction factor for the current value, obtained from the known 1 GΩ resistor, is transferred to measurements of 10 GΩ resistor. Only one value for the correction factor of the current meter is rarely sufficient, because the current meter suffers from non-linearity and other non-idealities, and the correction factor for the current value does not remain the same throughout the range. Thus the correction factor is measured in multiple points from 20 V to 100 V with 1 GΩ resistor, which is transferred to measurements with 10 GΩ (corresponding to currents generated with voltages from 200 V to 1000 V, respectively). Both polarities should be measured and the results averaged to eliminate the effect of offsets. Without this a systematic error of 500 fA is measured in the worst case.

The biggest difficulty in the calibration is to distinguish which part of the deviation is due to the resistor and which is due to the current meter. This was solved so that first a model for the correction factor of the electrometer was extended down to the currents corresponding to 20 V applied voltage. Then respective currents were measured. A model for the voltage dependence of the resistor was formed from the measured values between 20 V to 1000 V with the correction factor. The modelling was based on the observation that the resistance was linearly dependent on the applied voltage. It is crucial that the electrometer's range-setting does not change during this procedure. One should repeat the resistance measurements from voltages 20 V to 100 V with range setting a decade lower and form a correction factor for this range (the range for characterising the next resistor). The procedure is then repeated with resistors up to 100 TΩ.

With the lowest calibrated current values the 1/f-noise becomes the limiting factor for the accuracy of the characterisation. The temperature drift component of 1/f-noise is minimised by using a temperature stabilised environment (23 ºC ± 0.025 ºC) for the resistor and the meter. A 1/f noise value of 2 fA has been measured at current levels of 1 pA and 10 pA.

Calibration of current-to-voltage converters

For TKK's radiometric applications the two highest sensitivity ranges of Vinculum SP042-series current-to-voltage converter were calibrated with the constant-voltage method. The calibrated current range was from 1 pA to 100 pA. The largest possible voltage values were used to minimise the effect of the offset voltage. A method for eliminating the offset voltage by applying both voltage polarities and then averaging the results is not applicable as it also eliminates the offset current, which should exist in the calibration. The error effects of the input resistance of the current-to-voltage converter were neglected as the lowest standard resistor value used was 1 TΩ. The output of the current-to-voltage converter and its offset were measured with HP3458A multimeter with time span long enough for the current to settle and to minimise noise (except the 1/f-noise).

The reported 3800 ppm uncertainty of the current calibration at 1 pA consists in practice of the 1/f noise and the resistor value (Table 1). The resistor uncertainty at the two lowest current levels also consists mostly of the 1/f noise. The source of the 1/f-noise is in practice the current-to-voltage converter and, thus, its quality determines the noise level and the accuracy of the calibration. The reported 1300 ppm 1/f-noise was measured with the Keithley 6517 electrometer, but with the Vinculum SP042 the value was a decade higher leading to expanded uncertainty (k=2) of 1.5 %.

Other uncertainty components are close to insignificant as compared to these. One should also note the poor long term stability of the high-value resistor elements. A maximum of 1 % variation for the resistor element within 3000 hours in unstable temperature and non-hermetic conditions (5 - 35 ºC and 45 - 85 % relative humidity) have been reported by the manufacturer (Japan Hydrazine Inc.). Thus the current calibration itself must be made within a month of the characterisation measurements of the resistors.

Table 1. Uncertainty budget of the current-to-voltage converter calibrations for the 100 pA, 10 pA and 1 pA -levels.

Uncertainty component	1 pA [ppm]	10 pA [ppm]	100 pA [ppm]
Voltage measurement	50	10	10
Resistor value	1350	190	70
1/f-noise	1300	130	13
Source voltage	10	10	10
Combined standard uncertainty	1900	230	75
Expanded uncertainty (k=2)	3800	460	150

Conclusions

A traceable calibration setup for currents was implemented based on the constant-voltage method. With this method one can achieve expanded uncertainty (k=2) of 3800 ppm at 1 pA-level, 480 ppm at 10 pA-level and 150 ppm at 100 pA-level (if high-quality current meter is used). Alternative methods should be sought if smaller currents than 1 pA need to be calibrated. The 1/f-noise and the uncertainty of the resistor value used in the calibration are the limiting factors for the accuracy. Due to the instability of the standard resistors, the characterisation of these is an inseparable part of the current calibration process itself.

References

1 Böhm, J., A Measuring and Calibration System for Currents Down to 10^{-17} A, *ATKE, 27*, 139-143 1976.

2 van den Brom, H.E., de la Court, P., Rietveld. G., Accurate subpicoampere Current Source Based on a Differentiating Capacitor With Software-Controlled Nonlinearity Compensation, *IEEE Trans. Instrum. Meas.* ***54,*** 554-558 (2005).

Simplified diffraction effects for laboratory and celestial thermal sources

Eric L. Shirley
National Institute of Standards and Technology, Gaithersburg, MD 20899-8441, USA

Abstract. We discuss how evaluating the diffraction effects on total power in blackbody calibrations and total-solar-irradiance measurements can be done more efficiently. The methodology that is outlined has been applied to the VIRGO and SOVIM PMO6 radiometers, the DIARAD radiometer, and the SORCE TIM radiometer.

Introduction

Diffraction affects the flow of electromagnetic radiation through optical systems, because light is a wave phenomenon. More or less radiation emitted by a source reaches a detector than the amount expected from geometrical optics. Detailed analysis of this effect is necessary in the most careful studies of optical systems, especially at longer wavelengths. People have devoted much attention to this and established a significant impact on practical radiometry. Rayleigh and Lommel analyzed diffraction effects on the intensity distribution in the detector plane for Fraunhofer and Fresnel diffraction. Wolf derived an expression for the encircled spectral power by integrating Lommel's distribution over a circular area of the detector plane for a point source, and Focke analyzed the asymptotic properties of Wolf's result. Blevin extended diffraction analysis to thermal sources and promoted the concept of the effective wavelength λ_e. At this wavelength, diffraction effects on spectral power typify diffraction effects on total power for the complex radiation of interest. Steel *et al.* considered effects of having an extended source, and Boivin studied that and diffraction effects in the form of gains in the total flux reaching an overfilled detector in the case of a non-limiting aperture. Shirley (1998) and Edwards and McCall also considered extended sources, showing how calculating diffraction effects for a point source is easily generalized to the case of an extended source.

The above work mainly considered monochromatic radiation, even if within the effective-wavelength approximation. In at least two important applications, monitoring total solar irradiance and blackbody total-power measurements, one wants to know how diffraction affects propagation of (complex) Planck radiation and total power reaching the detector. In two earlier works, Shirley (2001) and Shirley (2004), the author generalized Wolf's result to Planck radiation for Fraunhofer diffraction losses and Fresnel diffraction losses and gains, respectively. The latter work presents a means to analyze diffraction effects for a point source in terms of a double numerical integral at low source temperature and an infinite sum of divergent asymptotic expansions at high source temperature. Either analysis can be used at intermediate temperatures, but both analyses have key disadvantages, in the form of extensive computation at low temperature and the need to evaluate a complicated double sum at high temperature.

This work addresses both of the above difficulties. The numerical integration is greatly simplified except at very high source temperatures, and the lowest-order asymptotic terms have been regrouped to eliminate one summation. The simplifications have been demonstrated in the treatment of diffraction effects for the VIRGO and SOVIM PMO6 radiometers and the DIARAD radiometer, all of which are affected by diffraction at a non-limiting, view-limiting aperture, as well as the SORCE TIM radiometer, which has a limiting aperture.

Discussion

Diffraction effects depend on wavelength λ and must be treated accordingly when considering effects on spectral or total power reaching the detector in a given optical system. Spectral power $\Phi_\lambda(\lambda)$ at the detector is related to source spectral radiance $L_\lambda(\lambda)$ by $\Phi_\lambda(\lambda) = F(\lambda)GL_\lambda(\lambda)$, where G is the geometrical throughput of an optical system. The factor $F(\lambda)$ accounts for diffraction effects and is taken as unity in geometrical optics. A Planck source has

$$L_\lambda(\lambda) = \varepsilon c_1 / (\pi\lambda^5 \{\exp[c_2/(\lambda T)] - 1\}),$$

where ε, c_1 and c_2 are the source emissivity and radiation constants and T is the source temperature. For the total flux this gives

$$\Phi_0 = 6G\zeta(4)\varepsilon c_1 T^4/(\pi c_2^4) = \varepsilon G\sigma_M T^4/\pi,$$

according to the Stefan-Boltzmann Law, where σ_M is the Stefan-Boltzmann constant.

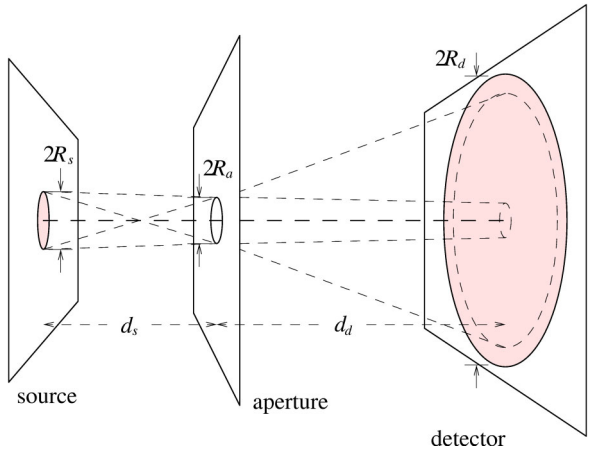

Figure 1. Generic geometry for considering diffraction effects for an extended source. It is specified by the five parameters shown and aperture focal length *f*. If the detector perimeter lies outside the larger dashed circle (as shown), the aperture is limiting. If the detector perimeter lay within the smaller dashed circle, the aperture would not be limiting.

The source radiance and power reaching the detector may be related in many systems as follows. Consider the optical system illustrated in Fig. 1, which is specified by source, aperture and detector radii, R_s, R_a and R_d, distances d_s and d_d, and aperture focal length (if it is a powered optic) *f*. As examples, these may correspond to blackbody or solar dimensions for the source, and to defining (or view-limiting) aperture and detector entrance dimensions for the optical instrumentation, with distances chosen accordingly. With $k = 2\pi/\lambda$, one may introduce the parameters

$$v_s = kR_sR_a/d_s$$
$$v_d = kR_dR_a/d_d$$
$$u = kR_a^2\,|1/d_s + 1/d_d - 1/f\,|$$
$$v_0 = \max(v_s, v_d)$$
$$\sigma = \min(v_s, v_d)/v_0$$
$$D = 4\pi^3 R_a^4 R_s^2 R_d^2/(d_s d_d \lambda v_0)^2$$

and the function

$$g(x) = \{(1-x^2)[(2+\sigma x)^2 - \sigma^2]\}^{1/2}/(1+\sigma x).$$

In paraxial systems, the spectral power reaching the detector and source spectral radiance are then related by

$$\Phi_\lambda(\lambda) = D\int_{-1}^{1} \mathrm{d}x\, g(x) L(u,v) L_\lambda(\lambda).$$

Here we abbreviate $v = v_0(1+\sigma x)$, and $L(u,v)$ is Wolf's result for a point source. This integral allows one to deduce diffraction effects in the case of an extended source from Wolf's result. Note that many quantities, such as σ, D, $g(x)$, or u/v, as well as conditions such as $u < v$, do not depend on λ.

Extension to thermal sources

For a given value of x, and a given value of λ, one can introduce $\alpha = \lambda v$, $w = \min(u,v)/\max(u,v)$, and $q = \varepsilon c_1/(\pi\alpha^4)$, which also do not depend on λ. Similarly, for a given value of x, and a given value of T, one can introduce $A = c_2/(\alpha T)$. Suppose that one defines

$$Q(T) = q^{-1}\int_0^\infty \mathrm{d}\lambda L(u,v) L_\lambda(\lambda),$$

and the constant $Q_0 = 6\zeta(4)/A^4$. This integral allows one to deduce diffraction effects on total power reaching the detector for a small thermal source from Wolf's result. Then for $u < v$ one has

$$Q(T) = Q_0 - F_B(A,w),$$

and for $u > v$ one has

$$Q(T) = w^2[Q_0 + F_B(A,w)] - F_X(A,w).$$

The functions $F_B(A,w)$ and $F_X(A,w)$ are defined in Shirley (2004) and are closely related to various contributions to Wolf's function, $L(u,v)$. Omitting these functions in the above expressions suppresses diffraction effects. Correspondingly, the fractional change of $Q(T)$ because of their inclusion yields diffraction effects on the total power reaching the detector. Once $Q(T)$ is known, it may be integrated over x in the case of an extended thermal source to obtain the expected total power reaching the detector, with diffraction effects taken into account:

$$\Phi(T) = Dq\int_{-1}^{1} \mathrm{d}x\, g(x) Q(T).$$

Here the dependence of $Q(T)$ on x is implicit.

The chief difficulties arise when calculating $F_B(A,w)$. Its asymptotic expansion in ascending powers of A and $\log_e A$ has two disadvantages. First, because it is asymptotic, it can diverge if enough terms are included and must therefore be used with care. Second, each term involves an infinite summation over powers of w. We have found a modification of Barnes' integral representation of generalized hypergeometric functions that allows a simple, exact evaluation of $F_B(A,w)$, with very few integration points. In the case of very small A, we have also found that one can analytically sum the terms involving the lowest powers of A over all powers of w, obtaining a useful analytical expression.

We have used these innovations to analyze diffraction effects on blackbody calibrations and performance of the radiometers already mentioned. A detailed report of the innovations and application to studying the radiometers is in preparation and will be presented at the conference.

References

Blevin, W. R., Diffraction losses in radiometry and photometry, *Metrologia 6*, 39-44, 1970.

Boivin, L. P., Diffraction corrections in radiometry: comparison of two different methods of calculation, *Appl. Opt. 14*, 2002-2009, 1975.

Boivin, L. P., Diffraction corrections in the radiometry of extended sources, *Appl. Opt. 15*, 1204-1209, 1976.

Edwards, P., McCall, M., Diffraction loss in radiometry, *Appl. Opt. 42*, 5024-5032, 2003.

Focke, J., Total illumination in an aberration-free diffraction image, *Optica Acta (Paris) 3*, 161-163 (1956).

Lommel, E., Die Beugungseirscheinungen einer kreisrunden Oeffnung und eines kreisrunden Schirmschens theoretisch und experimentell bearbeitet, *Abh. Bayer. Akad. 15*, 233-328, 1885.

Rayleigh, Lord, On images formed without reflection or refraction, *Phil. Mag. 11*, 214-218, 1881.

Shirley, E.L., Revised formulas for diffraction effects with point and extended sources, *Appl. Opt. 37*, 6581-6590, 1998.

Shirley, E.L., Fraunhofer diffraction effects on total power for a Planckian Source, *J. Res. Nat. Inst. Stand. Technol. 106*, 775-779, 2001.

Shirley, E. L., Diffraction corrections in radiometry: Spectral and total power, and asymptotic properties, *J. Opt. Soc. Am. A 21*, 1895-1906, 2004.

Steel, W. H., De, M., Bell, J. A., Diffraction corrections in radiometry, *J. Opt. Soc. Am. 62*, 1099-1103, 1972.

Wolf, E., Light distribution near focus in an aberration-free diffraction image, *Proc. Roy. Soc. A 204*, 533-548, 1951.

Widely Tunable Twin-Beam Light Source based on Quasi-Phase-Matched Optical Parametric Generator as a Spectral Responsivity Comparator between InGaAs and Si Photodiodes

Dong-Hoon Lee, Seung-Nam Park, Seung Kwan Kim, Jae-Yong Lee, Sang-Kyung Choi, Hee-Su Park, and Chang-Yong Park

Division of Optical Metrology, Korea Research Institute of Standards and Science (KRISS), Daejeon, Korea

Abstract. We present a twin-beam light source based on quasi-phase-matched (QPM) continuous-wave (CW) optical parametric generator (OPG). The source emits collinearly the signal and the idler beams at a power level of 1 nW in wavelength ranges from 790 nm to 920 nm and from 1260 nm to 1620 nm, respectively, with a bandwidth of less than 2 nm. The quantum correlation in the OPG process can be used to directly compare the spectral responsivity of an InGaAs photodiode with that of a Si photodiode, offering a new calibration method for InGaAs photodiodes.

1. Introduction

A twin-beam light source simultaneously emits two beams that are strongly correlated but distinguishable. Most such sources are based on parametric wavelength conversion in an optically nonlinear medium, which convert the incident pump laser beam into two lower-energy beams called the signal and the idler. Of particular interest for photometry and radiometry is the device based on spontaneous parametric down-conversion (SPDC) with its potential application for absolute calibration of detector quantum efficiency by single-photon coincidence counting [1-3]. With SPDC, however, only photon-counting detectors such as photomultipliers or avalanche photodiodes can be calibrated at a low power level, and the wavelength tunability is limited.

At power levels above several microwatts, a CW optical parametric oscillator (OPO) is a useful coherent twin-beam source. Tunability in a wide wavelength range can be achieved by applying the quasi-phase-matching (QPM) technique [4]. The quantum correlation between the signal and idler beams from an OPO is influenced by the cavity and can be characterized, e.g., by measuring the noise spectrum of the photocurrent difference [5]. Twin-beam based radiometric metrology using tunable OPOs is one of our on-going research topics at KRISS.

In this paper, we report on an optical parametric generator (OPG) as a wavelength-tunable twin-beam light source, which offers an interesting application for IR photodiode calibration. An OPG consisting of a pump laser and a nonlinear crystal is in essence a building block for an OPO that has an optical cavity added to an OPG. We distinguish, however, an OPG from SPDC in the aspect that the optical modes of the OPG output beams are defined by the pump laser mode propagating collinearly in a long crystal (usually longer than 1 cm). The spectral power density of OPG is therefore much larger than that of SPDC. We have developed an OPG emitting the signal beam in a wavelength range detectable with a Si photodiode, and the idler beam detectable with an InGaAs photodiode. Based on the quantum correlation between the numbers of generated signal and idler photons, the spectral responsivity of two detectors at different wavelengths can be directly compared by measuring the photocurrent ratio. We present first the experimental setup and characteristics of the OPG twin-beam source, and then introduce the principle of spectral responsivity comparison. Finally, the major systematic error source of IR photodiode calibration using the OPG is stated.

2. The OPG Twin-Beam Source

Figure 1 shows the schematic setup of the OPG source. As the pump laser, we use a frequency-doubled CW Nd:YAG laser providing a 1-W single-mode beam at 532 nm. After passing through a concave lens (f = 150 mm), a Faraday isolator, and a half-wave plate (HWP), the pump beam is collimated to a diameter of approximately 1 mm, which is then focused using a lens (f = 100 mm) to the center of the nonlinear crystal.

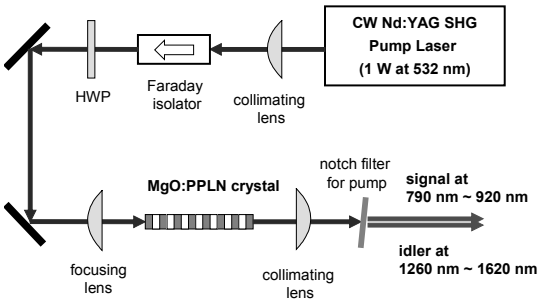

Figure 1. Schematic setup of the tunable twin-beam source based on quasi-phase-matched CW OPG.

For the nonlinear crystal, we use a MgO-doped periodically poled lithium niobate (MgO:PPLN) that is 40 mm long, 13 mm wide, and 0.5 mm thick. The crystal has six poling periods of from 7.1 μm to 7.6 μm for QPM, and is mounted in a temperature-controlled oven with stability better than ± 0.05 ˚C. The generated signal and idler beams from the crystal are collimated using a lens (f = 100 mm), and the pump beam at 532 nm is blocked out with a holographic notch filter. The collinearly propagating signal and idler beams can be separated using a dichroic beam-splitter.

The wavelength and spectral shape of the signal and the idler beams are measured with a double-grating optical spectrum analyzer (Agilent 8614B). Figure 2 shows the measured peak wavelength as a function of poling period (Λ) and crystal temperature. The signal and the idler

wavelengths can be tuned from 790 nm to 920 nm and from 1260 nm to 1620 nm, respectively. The spectral bandwidth remains within 1 nm and 2 nm (FWHM) over the whole tuning range. The radiation power of the OPG output beams is on the order of 1 nW, which is sufficient for photocurrent detection with conventional photodiodes and low-noise pre-amplifiers.

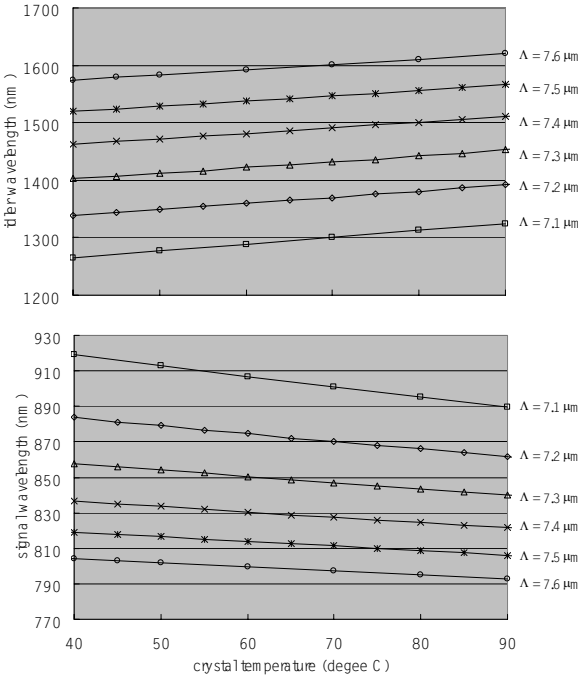

Figure 2. Measured signal and idler wavelengths of the QPM OPG as a function of poling period and crystal temperature.

3. Spectral Responsivity Comparison

The optical parametric conversion process creates one signal photon and one idler photon in pair by annihilating one high-energy pump photon, so that the flux rate N (in number of photons per second) of the signal and idler photons from the OPG is the same:

$$N_S = N_I \tag{1}$$

This quantum correlation is at the heart of the absolute calibration method of photon counting detector efficiency using SPDC [1-3]. Our approach using OPG is for relative calibration of detector quantum efficiency, but the method can be applied generally to photodiodes producing photocurrents proportional to the incident radiation power.

In our OPG twin-beam source, the signal beam can be optimally detected with a Si photodiode (designated with index 1), while the idler beam with an InGaAs photodiode (designated with index 2). The ratio of the measured photocurrents I_1/I_2 is then given as

$$\frac{I_1}{I_2} = \frac{R_1 P_S}{R_2 P_I} \tag{2}$$

with the power responsivities R_1 and R_2 of the Si photodiode and the InGaAs photodiode, respectively, and the signal and idler powers P_S and P_I, respectively, incident on the detector active area. Note that the photocurrent ratio in Eq. (2) is the same as the ratio of the quantum efficiencies of the two photodiodes at the given wavelengths. Using Eq. (1), the power ratio P_S/P_I in Eq. (2) can be written as

$$\frac{P_S}{P_I} = \frac{N_S}{\lambda_S} \cdot \frac{\lambda_I}{N_I} \cdot \frac{T_S}{T_I} = \frac{\lambda_I T_S}{\lambda_S T_I}. \tag{3}$$

Here, T_S and T_I are the transmissions from the OPG crystal to the detector at the signal and the idler wavelengths λ_S and λ_I, respectively. The ratio of the spectral power responsivities finally follows from Eqs (2) and (3):

$$\frac{R_2}{R_1} = \frac{I_2 \lambda_I T_S}{I_1 \lambda_S T_I}. \tag{4}$$

From Eq. (4) we see that, using the OPG twin-beam source, two photodiodes of different types, i.e., a Si and an InGaAs photodiode, can be directly compared in their spectral power responsivity by measuring the photocurrent ratio at different signal and idler wavelengths. The transmission ratio is a property of the experimental setup, which needs to be characterized once.

As the spectral responsivity standard usually is disseminated by Si photodiodes, Eq. (4) can be used to calibrate InGaAs photodiodes, which are the most widely used IR detectors, with respect to the Si-based responsivity standard. The potential advantage of this new calibration method for InGaAs photodiodes is the absence of a thermal detector as a transfer standard between different wavelengths, thereby overcoming the present limits on sensitivity and accuracy of IR detector calibration. However, the new method requires still more study on possible systematic errors and uncertainty factors, which are presently under investigation.

Preliminary experimental results show that a discrimination of the OPG modes from those of spontaneous parametric fluorescence is of particular importance for accurate calibration. Because the crystal has a considerable length of 40 mm, the spontaneous parametric fluorescence from each length element of the crystal can be collected in the detector accumulating a comparable amount with that of the OPG modes. We experimentally found out that the detection of spontaneous fluorescence significantly violates the correlation of Eq. (1) due to the large difference between the signal and idler wavelength values. Discrimination of the OPG modes is successfully achieved by using a pinhole-based spatial filter, resulting in a correct calibration of InGaAs photodiode responsivity compared with that of the conventional method using a thermal detector. We will present the results of our investigation regarding this effect and other factors affecting the accuracy of the proposed calibration method.

Acknowledgments The research is partly supported by "Measurement Science Research on Emerging Future Technologies" program of KRISS.

References

1. Rarity, J. D. et al., Absolute measurement of detector quantum efficiency using parametric downconversion, *Applied Optics, 26,* 4616-4619, 1987.
2. Brida, G. et al., Measurement of the quantum efficiency of photodetectors by parametric fluorescence, *Metrologia, 35,* 397-401, 1998.
3. Czitrovszky, A. et al., Measurement of quantum efficiency using correlated photon pairs and a single-detector technique, *Metrologia, 37,* 617-620, 2000.
4. Sutherland, R. L., *Handbook of nonlinear optics*, 2nd edition, 217-226, Marcel Dekker, New York, 2003.
5. Bachor, H.-A., Ralph, T. C., *A guide to experiments in quantum optics,* 2nd edition, 173-303, Wiley-VCH, Weinheim, 2004.

Measurement of quantum efficiency using the correlated photon technique

J. Y. Cheung, P. J. Thomas, C. J. Chunnilall, J. R. Mountford and N. P. Fox
National Physical Laboratory, Tedddington, TW11 0LW, U.K.

Abstract. Correlated photons offer a direct means of calibrating detector quantum efficiency in the photon counting regime. This paper describes the facility being developed at the National Physical Laboratory for calibrating such detectors using this technique. An uncertainty budget for the measurements currently achievable with the technique is presented, and the related effects of after-pulsing and spatial uniformity are also discussed. Progress on an intercomparison of the correlated photon technique with that traceable to cryogenic radiometry is also reported. The facility currently operates in the visible part of the spectrum, and plans to cover the key telecommunication wavelengths in the infrared will be discussed.

Low light measurements

Detectors operating in the photon counting regime are being developed for a wide variety of applications, such as quantum information processing, astronomy and biotechnology. The main challenge of low light level measurement is in the development of detector technology to meet the requirements of the user. Detector properties such as quantum efficiency (q.e.), spatial uniformity, dead time, jitter, after pulsing, photon number resolving capabilities, room temperature operation and robustness in harsh conditions need to be improved. In addition, high accuracy metrology techniques are required to quantify these properties. Correlated photon metrology is currently being developed to meet the metrology challenges.

Correlated photon metrology

Spontaneously produced correlated photons can be used to measure the absolute quantum efficiency of photon counting detectors while those produced via stimulated downconversion can be used to measure source radiance. The technique is direct, requiring no calibration chain, and absolute [1]. The technique relies on the process of optical parametric downconversion. A high-energy photon (pump) entering a non-linear crystal will spontaneously decay [2] into two lower energy photons (signal, idler) which are fundamentally related by the laws of conservation and momentum. Detection of an idler photon indicates that its twin signal photon must exist. Moreover the emission time, direction, wavelength and polarisation of the signal and idler photons are correlated, i.e. given the values for the idler, those of the signal can be inferred.

Figure 1 is a schematic of the correlated photon setup, used to measure the q.e. of a detector at 702 nm. When the trigger (TRIG) registers a photon it heralds the arrival of its twin at the device under test (DUT). Photons lost due to optical elements in the trigger channel are of no concern, what is crucial is whether the DUT captures every twin of every photon detected by the trigger. Rearranging the equations in figure 1 shows that the q.e. of the DUT channel can be expressed as $\eta_{DUT} = N_c / N_{TRIG}$ and is the q.e. from the point of downconversion in the crystal.

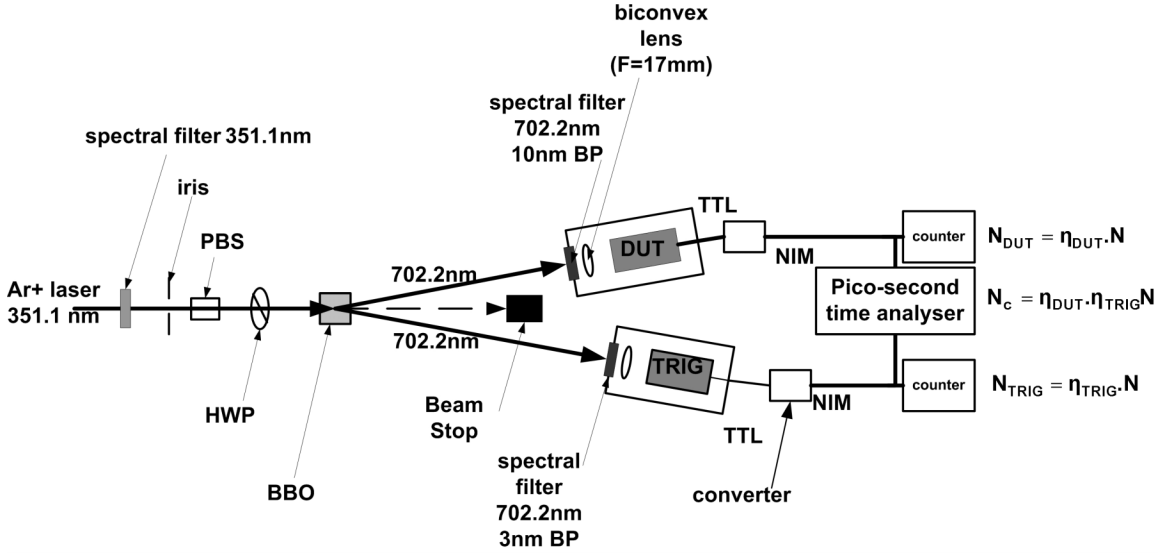

Figure 1. Schematic of q.e. measurement using the correlated photon technique, N_{DUT} and N_{TRIG} = the number of photons counted on each detector, N = the number of photons pairs emitted by the crystal, N_c = number of coincident photons measured by time-analyser, BBO = barium beta borate downconversion crystal, HWP = half-wave plate, PBS = polarising beamsplitter. When a photon is detected the detectors output a TTL pulse which is converted into a NIM pulse to be compatible with the counting electronics. In this diagram, degenerate downconversion, i.e. signal and idler photons having same wavelength, is being used.

The following represents a calculation of the quantum efficiency of the detector:

$$\eta_{DUT} = \frac{N_C - A_C}{T_{DUT}\left(N_{TRIGGER} - D_{TRIGGER}\right)} \qquad (1)$$

N_c is the number of coincidences, A_c the number of accidental coincidences, T_{DUT} the transmittance losses in DUT channel, $N_{TRIGGER}$ the number of photons detected by the trigger, $D_{TRIGGER}$ the number of false triggers.

The transmittance T_{DUT} includes the transmittance of the downconversion medium, focussing optics, filter, and losses due to misalignment or aperturing, as well as losses in the electronic chain [3-10]. All of these components can be measured with high accuracy using existing facilities at NPL [6,7,11].

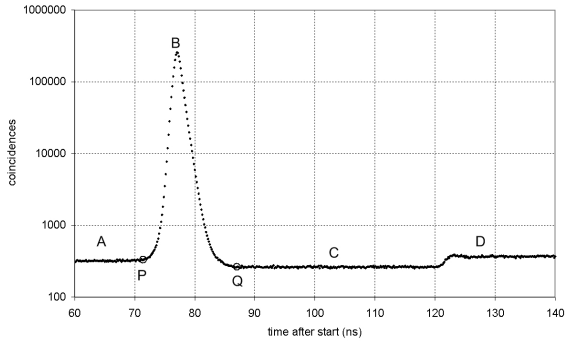

Figure 2. Histogram of coincidence counts versus time interval between trigger and DUT pulses. The DUT pulses are artificially delayed by 74 ns to compensate for the timer deadtime.

Figure 2 shows a typical histogram of coincidences. The evaluation of the true number of coincidences as given by the numerator of equation (1) requires a detailed analysis of this curve, and involves effects such as detector after-pulsing, and detector and timer deadtime [7].

Taking into account the optical and electronic uncertainties, at the time of writing the technique has an overall uncertainty of 0.36% with the dominant uncertainty being that due to the non-uniformity of the transmittance losses of the crystal. An overall uncertainty of 0.06% should be achievable with current capabilities if a downconversion medium with better uniformity could be used, and work is in progress to investigate this.

Current and future work

Work for an in-house comparison against measurements traceable to the NPL cryogenic radiometer is currently underway and progress will be reported at the meeting. The spatial uniformity of any detector used in such a comparison is a critical component. Figure 3 shows the uniformity in one example of a Perkin-Elmer SPCM detector. The variation of around 0.5% in the central region may limit the level at which a comparison can currently be carried out, even if the techniques are expected to have a higher accuracy.

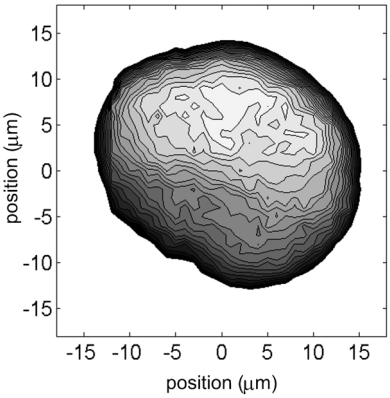

Figure 3. Contour plot of response of a photon-counting detector over the central region where the normalized response varies between 0.95 and 1.0. Each contour corresponds to 0.0025 units.

Acknowledgments This work was funded by the UK DTI National Measurement Systems Directorate's Programmes on Optical Radiation Metrology and Quantum Metrology.

References

1. Migdall, A. L., Correlated-photon metrology without absolute standards., *Physics Today 52*, 41-46, 1999.
2. Louisell, W. H., Yariv, A. & Siegman, A. E., Quantum fluctuations and noise in parametric process. I. *Phys. Rev. A 24*, 1646-1654, 1961.
3. Castelletto, S., Degiovanni, I. P. & Rastello, M. L., Theoretical aspects of photon number measurement. *Metrologia 37*, 613-616, 2000.
4. Castelletto, S., Degiovanni, I. P. & Rastello, M. L., Evaluation of statistical noise in measurements based on correlated photons, *J. Opt. Soc. Am. B 19*, 1247-1258, 2002.
5. Castelletto, S., Godone, A., Novero, C. & Rastello, M. L., Biphoton fields for quantum efficiency measurements, *Metrologia 32,* 501-504*,* 1995/96.
6. Cheung, J. Y., Chunnilall, C. J. & Wang, J., Radiometric applications of correlated photon metrology, *Proc. SPIE 5551*, 220-230, 2004.
7. Cheung, J. Y., Vaughan, M. P., Mountford, J. R. M. & Chunnilall, C. J., Correlated photon metrology of detectors and sources, *Proc. SPIE 5161*, 365 - 376, 2004.
8. Migdall, A. L., Absolute quantum efficiency measurements using correlated photons: toward a measurement protocol, *IEEE Trans. on Instr. and Meas. 50*, 478-481, 2001.
9. Migdall, A. L., Datla, R. U., Sergienko, A., Orszak, J. S. & Shih, Y. H., Absolute quantum efficiency measurements using correlated photons, *Metrologia 32,* 479-483, 1995/96.
10. Ware, M. & Migdall, A., Single photon detector characterization using correlated photons: the march from feasibility to metrology, *J. Mod. Opt. 51*, 1549-1557, 2004.
11. Hartree, W. S., Theocharous, E. & Fox, N. P., A wavelength tunable, quasi-cw laser source for high accuracy spectrometric measurement in the 200 nm to 500 nm region. *Proc. SPIE 4826*, 104-112, 2003.

Session 7

International Comparisons

The CCPR K1-a Key Comparison of Spectral Irradiance 250 – 2500 nm: Measurements, Analysis and Results

Emma R. Woolliams, Nigel P. Fox, Maurice G. Cox, Peter M. Harris, Neil J. Harrison
National Physical Laboratory, Hampton Road, Teddington, TW11 0LW, UK

Abstract. The CCPR K1-a Key Comparison of Spectral Irradiance (250 – 2500 nm) was carried out to meet the requirements of the Mutual Recognition Arrangement (MRA) by 13 participating National Measurement Institutes (NMIs). The comparison artefacts were tungsten halogen lamps and because of the fragile nature of these lamps the comparison was arranged as a star comparison. The National Physical Laboratory (NPL) acted as pilot for the comparison and, by measuring all lamps, provided the link between measurements made by different participants. The comparison was analysed using a model-based method, which was able to ensure that all participants, including the pilot, were treated equitably. This paper presents the comparison philosophy, methodology, analysis and the results.

Comparison philosophy

The Mutual Recognition Arrangement (MRA) was signed in 1999 with the objectives of establishing the degree of equivalence of national measurement standards and providing for the mutual recognition of calibration and measurement certificates issued by National Metrology Institutes (NMIs). Under the MRA the equivalence of national measurement standards maintained by the NMIs is determined by a set of key comparisons chosen and organised by the Consultative Committees of the International Committee for Weights and Measures (CIPM), working closely with the Regional Metrology Organisations (RMOs). The Consultative Committee of Photometry and Radiometry (CCPR) identified several key comparisons at its meeting in March 1997. One of these was the CCPR Key Comparison K1-a for Spectral Irradiance in the spectral region 250 to 2500 nm.

The National Physical Laboratory (NPL), the NMI of the United Kingdom, was asked to be the pilot laboratory for the CCPR K1-a Key Comparison and had the responsibility for organising the key comparison and writing the Technical Protocol in discussion with a working group comprising representatives of NPL, NIST (USA) and PTB (Germany). NPL was responsible for purchasing and distributing the technical artefacts, for collating the measurement reports from all participants, and for analysing the results and preparing the Draft Reports [1].

In addition to NPL, 12 other NMIs participated in the CCPR K1-a Key Comparison. These were BNM-INM (France), CENAM (Mexico), CSIRO (Australia), HUT (Finland), IFA-CSIC (Spain), MSL-IRL (New Zealand), NIM (China), NIST (United States of America), NMIJ (Japan), NRC (Canada), PTB (Germany) and VNIIOFI (Russian Federation).

Because of the fragile nature of lamps, the comparison was organised as a star comparison. Each individual lamp was measured by the pilot and by one participant NMI only. Lamps were sent in batches of three to each participant. The pilot was required to measure each lamp on at least two occasions and the participant was asked to make measurements also on two occasions. Some participants were only able to measure a lamp once.

The key comparison was designed to include redundant measurements so that it would be expected that at least one lamp for each NMI would have a successful "Pilot – NMI – Pilot" or "NMI – Pilot – NMI" measurement sequence. In other words, it would be expected that at least one lamp for each participant would survive two successive transportations without significant drift. In the more general case where all four measurements of a lamp could be used and/or multiple lamps were transported without degradation, it would be expected that averaging multiple measurements would reduce the uncertainties associated with the comparison itself.

Comparison artefacts

The comparison artefacts for the CCPR K1-a Key Comparison were tungsten lamps. NMIs were required to use a minimum of three (with the option of up to four) tungsten halogen lamps designated "Type I" and given the option to use in addition tungsten lamps of "Type II". The Type I lamps were mounted 1000 W FEL type lamps and were bought pre-selected, pre-aged and mounted from the manufacturer, Gigahertz Optik GmBH. These lamps consist of a double-coiled tungsten filament, supported at the top and bottom of the filament, and operated in a bromine-filled quartz envelope. Two NMIs also used the Type II lamps, which were manufactured by the Polaron group. These lamps were pre-aged at NPL.

Both types of lamp were operated at a constant direct current. The voltage drop across the lamp was monitored as an indicator of the stability of the lamp.

Measurements

Measurements were made between the years 2000 and 2004. All lamp measurements by the pilot were measured directly against NPL's primary spectral irradiance scale using the high temperature blackbody as a reference source [2,3]. In addition, reference lamps were measured at NPL in order to determine and ensure stability of the reference scale. The comparison scale was maintained on a set of FELs regularly calibrated during the comparison.

All other participants calibrated their lamps with respect to their primary spectral irradiance scales. The methods used to realise the primary scale varied considerably between participants. Many participants base their primary scale on high temperature blackbodies, using radiometric or ITS-90 methods for determining the temperature; others measure the spectral irradiance of lamps using filter radiometers. NRC base part of their scale on the World Mean as represented by the 1975 comparison and MSL-IRL obtained traceability directly from NIST. Otherwise all the different realisations can be considered independent.

Discussion process

The participants supplied a full description of their measurement process and a detailed uncertainty statement. These uncertainty statements were discussed by all participants, and in some cases changed, prior to the final analysis and the publication of any results in the comparison Draft A report. This process, which lasted several months following completion of the measurements, ensured that the final data set was as reliable as reasonably possible.

Analysis

The fundamental outcomes of a key comparison are the degrees of equivalence (DoEs). These include a unilateral DoE for each NMI, concerning the deviation of a measurement made by the NMI from a key comparison reference value (KCRV), and bilateral DoEs for each pair of NMIs, concerning deviations between measurements made by the NMIs. In this case the DoEs correspond to a measurement (at each wavelength) by each participating NMI of a single typical lamp. The determination of the KCRV for this comparison was made according to the guidelines of the CCPR and is based on the weighted mean with "cut-off" of each NMI's unilateral DoE. The philosophy of this analysis has been to provide such a KCRV and the corresponding DoEs in a way that ensures that each NMI is treated equitably and that the results do not depend on the number of lamps measured by any NMI.

The measurements at each wavelength were treated as an entirely independent comparison for the purposes of the analysis, as dictated by the protocol.

The analysis was based on a model that assumes that each lamp has a stable spectral irradiance and that the measurements made by an NMI are systematically influenced by a factor that applies to all that NMI's measurements. The measurement by an NMI is an estimate, (hopefully) consistent with the declared uncertainty associated with the NMI's random effects, of the lamp irradiance multiplied by the systematic factor. The aim of the analysis was to determine an estimate of the systematic factor for each NMI. This aim was met by solving, by least squares adjustment, a set of linked equations that relate the NMI measurements to the lamp irradiances and systematic factors under a constraint that ensures that these systematic factors have a weighted geometric mean (with cut-off) of unity.

The unilateral DoE for an NMI is the difference from unity of the typical ratio of a measurement according to that NMI's scale and the spectral irradiance of a lamp. The best estimate of the value of this unilateral DoE for an NMI is the difference between the estimated systematic factor for that NMI and unity. The unilateral DoE uncertainty (which is quoted at a 95% level of confidence) can also be evaluated from the model. Since the comparison consists of many separate artefacts, the KCRV is itself unrelated to a physical artefact. The choice of KCRV is mathematically arbitrary, but to meet the metrological requirements of the CCPR KCWG, it is assigned here as the value unity, corresponding to the weighted geometric mean (with cut-off) of these estimated systematic factors. Bilateral DoEs are calculated from the unilateral DoEs.

The model has been described elsewhere [4] and is a development of a method suggested by White [5].

Lamp behaviour

Before the analysis was completed, the pilot discussed with each participant individually which of the pilot's and participant's lamp measurements should be included as representative of the comparison between the pilot and that participant. For this process, the difference between first and second measurements made by the pilot and first and second measurements made by the participant were compared with the uncertainties associated with random effects associated with the pilot's or participant's measurements, respectively. As a consequence of this comparison approximately one third of the lamps had at least one measurement rejected because of changes due to transportation.

The comparison thus highlighted the difficulty facing the user community with respect to dissemination and the availability of suitable transfer standards for spectral irradiance. Whilst the use of multiple lamps allowed sufficient redundancy to ensure that all participants had a satisfactory representation, it is noticeable that overall it is the lamps' stability that has limited the uncertainty with which this comparison was carried out.

Results

At the time of submission of this abstract the results are still confidential to the participants but it is anticipated that they will be approved and available in time to be fully reported at NEWRAD.

Acknowledgements The measurements for this comparison at NPL took three years and involved a large team. David Pollard, Leon Rogers, Boris Khlevnoy, Ruth Montgomery, Heather Pegrum and Andy Sibley in particular made significant contributions. The analysis procedure was discussed with all the participants and the comments from these participants were valuable in improving the technique and its description. This work was supported by the National Measurement System Policy Unit of the UK Department of Trade and Industry.

References

[1] E. R. Woolliams, M. G. Cox, N. P. Fox and P. M. Harris. 'Final Report of the CCPR K1-a Key Comparison of Spectral Irradiance 250 nm to 2500 nm'. 2005.

[2] E. R. Woolliams, N. J. Harrison, B. B. Khlevnoy, L. J. Rogers and N. P. Fox, 'Realisation and dissemination of spectral irradiance at NPL'. *UV News*, 2002. **7**, pp. 39-42.

[3] E. R. Woolliams. 'Development and evaluation of a high temperature blackbody source for the realisation of NPL's primary spectral irradiance scale'. Thesis. 2003. *University of Manchester*.

[4] M. G. Cox, P. M. Harris and E. R. Woolliams. 'Data evaluation of key comparisons involving linked bilateral measurements and multiple artefacts.' in *2005 NCSL International Workshop and Symposium*. 2005. Washington DC. pp.

[5] D. R. White, 'On the analysis of measurement comparisons'. *Metrologia*, 2004. **41**, pp. 121-131.

Comparison of Measurements of Spectral Irradiance (UV/VIS) by an International Round Robin Test

J. Hussong, A. Schönlein
ATLAS MTT GmbH, Linsengericht, Germany

Ch. Schroeder
opto.cal gmbH, Movelier, Switzerland

K. Scott
ATLAS MTT LLC, Chicago, USA

R. Dreiskemper
Heraeus Noblelight GmbH, Hanau, Germany

W. Ketola
3M, St. Paul, USA

J. Maybee
ATLAS DSET Laboratories Inc., Phoenix, USA

A. Geburtig
Bundesamt für Materialforschung und -prüfung BAM, Berlin, Germany

M. Köhl
Fraunhofer Institut für Solare Energiesysteme, Freiburg, Germany

St. Brunold
Institut für Solartechnik, Hochschule für Technik, Rapperswil, Switzerland

F. Christiaens
L'Oréal, Clichy, France

Abstract

In metrology it is often difficult to estimate the uncertainty of measurement. In highly sophisticated and complex technical measurements the uncertainty budget is based on elaborate but mostly pure theoretical work or on poor statistical data. A well established method to substantiate theoretical considerations is to arrange an interlaboratory comparison or a Round Robin test.

A round robin of spectral irradiance measurements was coordinated by a laboratory for photometric and radiometric measurements (ATLAS, Germany) in which ten well established laboratories (some accredited) commercial companies and non-profit institutes took part.

The ISO/IEC guide 43 deals with the organization and evaluation of such kinds of comparison. But due to the small number of participating laboratories the test was done without abiding by all rules and guidelines. However, the procedures were harmonized with all the participants.

The comparisons consisted of measurements of absolute spectral irradiance between 250 nm and 800 nm with the focus on the UV range. It was decided to measure two different kinds of light sources. One was a 1000 W halogen lamp (GE Q1000CL/4CL) as an example for an "easy" DC device (temperature radiator), often used as a source for calibration. This device had to be replaced during the test by an Ushio lamp (also 1000 W) due to accidental breakage. The second source was a 1500 W Xenon arc lamp (Heraeus NXe1500A driven in a Suntest CPS weathering device), as an example of an AC source with spectral emission lines and other measurement challenges. Both lamp types were measured first without any spectral filter in the light path and then with a WG280 and a WG335 as well. The Suntest device was operated with a line frequency of 50 Hz or 60 Hz depending on the location/country of the lab, because it is driven unregulated thus the lamp power depends on the line frequency by the inductive reactance of the ballast. If possible both frequencies were to be measured.

It should be mentioned that the participants not measured their individual lamps but received the same one after the other. In addition to the lamps most of the auxiliary equipment (optical benches, diaphragms, ampere and voltmeters, photometer, filters etc.) was also included in the measurement package. Thus all labs worked with the same kit. The only devices which had to be supplied by each participating lab were a voltage stabilizer and a spectrometer.

The measured spectra are kept anonymous for publication. A comparison was performed for all spectra and all different lamps and/or measuring conditions. All results were discussed concerning the aspect of the budget of the uncertainty of measurement with concentration on UV range.

The results will give an overview of the deviation of absolute spectral irradiance measurements in professional labs which are not part of national or international institutes of metrology (such as PTB, NIST, NPL, etc).

Remarks

The comparison was not completed by the deadline of this (abstract) publication. Thus the final list of participants could not be provided. The full set will be given at the conference.

Acknowledgement

We want to thank all the members of the labs who could not be mentioned in the list of authors.

APMP PR-S1 comparison on irradiance responsivity of UVA detectors

Gan Xu, Xuebo Huang, Yuanjie Liu

National Metrology Centre, Standards, Productivity and Innovation Board (SPRING Singapore)

Abstract. The APMP PR-S1 comparison on irradiance responsivity of UVA detectors has been carried out in seven national metrology institutes since 2002. Two quantities, the narrow band UV (365±5nm) irradiance responsivity and the broad band UVA (315-400nm) irradiance responsivity of the traveling detectors, have been compared. The results from most participating labs lie within ±5% against the weighted mean.

Introduction

Broadband UVA radiometers are widely used in a variety of industrial, medical, environmental and other applications. There are so far no internationally agreed standard procedures for the calibration of such radiometers and this has caused unacceptable discrepancies in measurement results.

The aim of this comparison is to assess the equivalence of the standards and techniques used for calibration and measurement of UVA irradiance responsivity of photo-detectors among the participating laboratories.

Seven national metrology laboratories (SPRING Singapore, NMIA of Australia, NMIJ of Japan, CSIR of South Africa, ITRI of Chinese Taipei, KRISS of South Korea and NIM of China) have participated in this comparison. SPRING Singapore is the pilot laboratory.

Method, Measurands and Conditions

The comparison was carried out through the calibration of a group of two traveling UVA detectors (Combination of a UV enhanced silicon photodiode, a UVA filter and a quartz wide eye diffuser manufactured by International Light) under irradiation of a UV source provided (a medium pressure mercury lamp with a liquid light guide manufactured by EFOS). The comparison took the form of a star comparison through six phases. Each phase consists of one participating lab plus the pilot lab. The artifacts were first measured by the pilot lab then sent to one lab for measurements then returned to the pilot lab for repeat measurements to check the drift.

There are two measurands in the comparison, the narrow band UV (365±5nm) irradiance responsivity (s_{365}) and the broad band UVA (315-400nm) irradiance responsivity (s_{UVA}) of the traveling detectors with respect to the provided UV source according to their definitions as shown in equations (1) and (2) respectively.

$$s_{365} = \frac{i}{E_{365}} = \frac{i}{\int_0^\infty E(\lambda)T(\lambda)d\lambda} \qquad (AW^{-1}cm^2) \qquad (1)$$

where i is the photocurrent of a detector under the narrow band (centre wavelength: 365nm, bandwidth: ±5nm FWHM) UV irradiance (E_{365}) produced by the UV source through a 365nm interference filter. $E(\lambda)$ is the spectral irradiance of the UV source and $T(\lambda)$ is the spectral transmittance of the filter.

$$s_{UVA} = \frac{i}{E_{UVA}} = \frac{i}{\int_{315}^{400} E(\lambda)d\lambda} \qquad (AW^{-1}cm^2) \qquad (2)$$

where i is the photocurrent of a detector under the broad band radiation from the UV source and E_{UVA} is the UVA irradiance produced by the UV source at the detector surface .

The measurement was made under specified conditions using the setup shown in Fig.1. The traveling detectors were overfilled and irradiated normally by the UV beam of divergence smaller than 5^o at irradiance levels of ≤0.5 mW/cm^2 for narrow band UV (365nm) radiation and ≤2.0 mW/cm^2 for broad band UVA radiation on the plane of measurement respectively.

Preliminary Measurements

Preliminary measurements were carried out by the pilot lab for characterizing the artifacts (UVA traveling detector, UV source and 365nm filter), before the comparison. These included the spectral responsivity (see Fig.2), spatial uniformity, linearity and temperature effect of the traveling detectors, the spectral transmittance and spatial uniformity of the 365nm filter, and the spectral power distribution, (see

Fig. 2), spatial uniformity of the UV beam as well as short term stability of the UV source.

Correction and Transfer Uncertainty

Corrections were made for the measurement results under different measurement conditions (room temperature, irradiance level) in different laboratories. The experiments showed that the temperature effect and non-linearity effect in the comparison are less than 0.1%.

The measurement uncertainty of each lab and the transfer uncertainty in each phase were combined together as the combined uncertainty of the results of the lab. The transfer uncertainty includes the drift of irradiance responsivity of the traveling detectors before sent to the lab and that after returned to pilot lab, and the spatial non-uniformity of a UV beam.

The drifts of irradiance responsivity are different in different phases (0.01-1.1%). The transfer uncertainty caused by the spatial non-uniformity of a UV beam is less than 0.4% according to the experiment with different aperture radius from 3mm to 10mm in SPRING Singapore.

Results and Conclusion

The preliminary analysis of the comparison results show most of the results lie within ±5% against the weighted mean with a few exceptions.

The degree of agreement of such comparison depends not only on the base scales of spectral responsivity and spectral irradiance of a laboratory, but also equally important on the method used for such measurement. A number of major uncertainty sources have been identified for discrepancies observed in the comparison (e.g. the uncertainty caused by stray light in the measurement of spectral irradiance or spectral power distribution of the UV source). Detailed results and discussions will be reported in the paper.

This comparison also allowed some labs to improve their experimental method and arrangement so as to eliminate previously undetected errors.

Acknowledgements

The pilot lab wishes to thank all the participants for their cooperation which allowed the comparison to be completed in time.

References

G Xu and X Huang, Characterization and calibration of broadband ultraviolet radiometers, Metrologia 2000, 37, 235-242

G Xu, Methods of characterization and calibration of broadband UV radiometers, First draft, CIE TC2-47 document, 2001

G Xu and X Huang, Calibration of broadband UV radiometers - methodology and uncertainty evaluation, Metrologia, 40, (2003), S21- S24

X Huang, G Xu and Y Liu, Comparison of two calibration methods for UVA broadband detector, Proceedings on CIE Midterm Meeting and International Lighting Congress, LEON 05

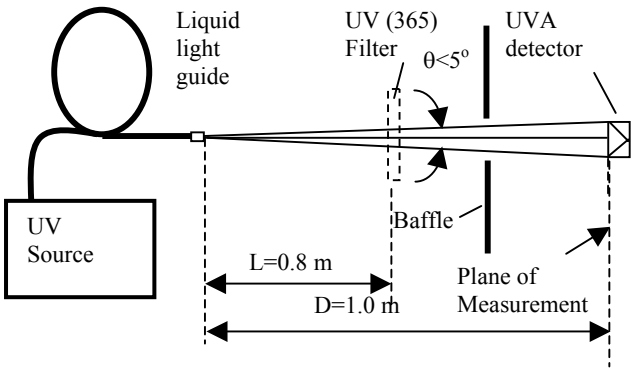

Figure 1. Block diagram of measurement setup and measurement conditions

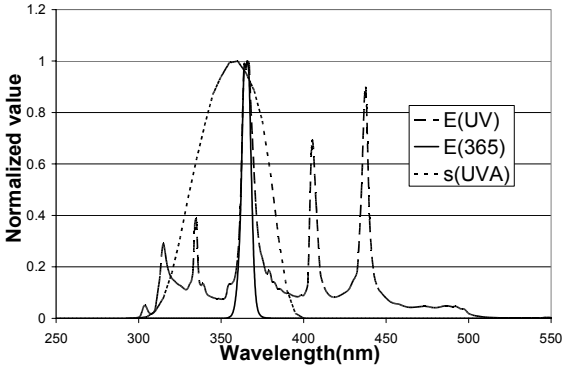

Figure 2. Spectral power distributions of UV source with and without 365 filter, E(365) & E(UV) and spectral responsivity of UVA detector, s(UVA)

Comparison Measurements of Spectral Diffuse Reflectance

Saulius Nevas[1], Silja Holopainen[1], Farshid Manoocheri[1], Erkki Ikonen[1,2], Yuanjie Liu[3], Tan Hwee Lang[3] and Gan Xu[3]

[1] Metrology Research Institute, Helsinki University of Technology (TKK), P.O.Box 3000, FI-02015 TKK, Finland
[2] Centre for Metrology and Accreditation (MIKES), P.O.B. 239, FI-00181 Helsinki, Finland
[3] National Metrology Centre, SPRING Singapore, 1 Science Park Drive, Singapore 118221

Abstract A comparison of the scales of spectral diffuse reflectance of the Helsinki University of Technology (TKK) and the Singapore National Metrology Centre (SPRING) was made. A PTFE-type reflectance standard with a nominal reflectance of 98% was measured for the 8/d reflectance factors over the wavelength range from 360 to 780 nm. A good agreement was found between the results of TKK and SPRING. Most of the measured values of spectral diffuse reflectance agreed within 0.36 %, the relative standard uncertainty of the comparison (1σ level).

Introduction

The diffuse reflectance characteristics of a sample under test are normally expressed in terms of reflectance factors that compare the reflectance of the test sample to that of the perfect reflecting diffuser under standardized geometric conditions. The reflectance factor is traceable to its definition and as such there are no fundamental standards physically available for the diffuse reflectance measurements. Therefore diffuse reflectance measurements are usually performed relative to a reference standard traceable to an absolute scale maintained by a national standards laboratory [1, 2, 3, 4, 5].

The reliability of the diffuse reflectance measurements by a national standards laboratory is normally verified via international comparisons [6, 7]. In this report we present results of the bilateral comparison measurements between the diffuse reflectance scales maintained by TKK and SPRING. The realization of the absolute scale of spectral diffuse reflectance at TKK is based on the gonioreflectometric method [5]. The diffuse reflectance scale at SPRING is also traceable to an absolute scale based on the gonioreflectometric method [4].

Instruments and methods

The important features and settings of the instruments used in this comparison are given in Table I. At TKK, the comparison measurements were carried out by using a gonioreflectometer [5]. The instrument consists of a light source and a goniometric detection systems controlled by a PC. The setup is mounted on a vibration-isolated optical table in a light-tight enclosure. The wavelength selection is accomplished with a double monochromator operating in subtractive-dispersion mode.

The hemispherical reflectance factor of a test sample at a selected wavelength is determined through the following procedure. First, the sample is moved out of the beam and the photodetector measures the intensity of the incident beam. Next, the photodetector is turned to the starting position of the angle-resolved measurements bounded to the horizontal plane of the detector movement. In the case of 0° incidence of the beam, the measurements are made over 10° to 85° polar angles with a 5° angle increment. They are also repeated for -10° to -85° angles and the average of the two results is used in the further calculations. The 0/*d* reflectance factor is calculated from the measurement results by spatial integration of the measured solid angles over the whole hemisphere excluding the specular component,

$$R = \frac{\int_{5^o}^{90^o} \frac{I(\theta)}{I_i} \frac{4L^2}{D^2 \cos(\theta)} \sin(2\theta) d\theta}{\int_{5^o}^{90^o} \sin(2\theta) d\theta}, \quad (1)$$

where $I(\theta)$ denotes the signal reading for the intensity that is reflected from the sample and collected by the detector aperture at a polar angle θ, I_i denotes the signal reading for the full-intensity of the incident beam, L is the distance between the detector aperture stop and the sample surface, and D is the diameter of the aperture. For the interpolation/extrapolation of the measured flux distribution at other than the measurement angles, we employed piecewise cubic hermite interpolating polynomial [8].

The comparison measurements at SPRING were carried out using a double-beam, double-monochromator spectrometer fitted with a 150 mm diameter integrating sphere. The 8/d spectral reflectance factors of the sample were measured with the specular components excluded. The measurements were carried out by substitute method using a reference standard traceable to National Physical Laboratory, UK.

Comparison sample and measurements

A commercially available Gigahertz-Optik's reflectance standard made from PTFE-based material (marketing name OP.DI.MA) with nominal reflectance of

Table I. Settings and features of the instruments at TKK and SPRING.

Laboratory	Geometry	Method	Bandpass (nm)	Beam size (mm)	Beam f/#	Beam polarization	Wavelength range and increment
TKK 2004	0/d	Absolute, gonioreflectometer	5.4	17	f/∞	Linear(s- and p-pol)	360-820, 20 nm
TKK 2005	0/d, 8/d	Absolute, gonioreflectometer	5.4	10	f/80	Linear(s- and p-pol)	360-820, 20 nm
SPRING	8/d	Double-beam spectrophotometer with 150mm integrating sphere	5.0	8x16	f/8	Non polarized	360-780, 5 nm

98% was used for the measurements in the comparison. The sample had a flat reflecting surface with the dimensions of 50x50 mm.

The first set of the comparison measurements was completed at TKK in January 2004. The 0/d reflectance of the sample was measured over 360-820 nm wavelength range with a 20 nm step. In October 2004, SPRING measured the 8/d reflectance of the sample over 360-780 nm wavelengths with a 5 nm step. After half a year, in April 2005 the sample was measured again at TKK for both 0/d and 8/d reflectance.

Results

The results of the comparison measurements are provided in Table II. In the table, only the overlapping spectral values of the measurements at TKK and SPRING are listed. The TKK results shown in the second column were obtained by calculating the average of the 0/d values in 2004 and 2005 and applying a correction factor for the difference between the 0/d and 8/d geometries. The correction is provided by the 8/d and 0/d reflectance factor values measured in April 2005 and is below 0.1 % for most of the spectral range. The third column lists the results of the measurements at SPRING. The next columns denoted by u_{TKK}, u_{SPRING} and u_c represent the combined uncertainties of the measurements at TKK, SPRING and those of the comparison at 1σ level, respectively.

The combined uncertainty of the comparison u_c was calculated by adding in quadrature u_{TKK} and u_{SPRING}. The last column of the table shows the relative percent-difference between the 8/d reflectance measurement results at SPRING and at TKK.

All spectral values of 8/d diffuse reflectance factor determined by TKK and SPRING are shown in Figure 1. The relative differences between the measurements at SPRING and those at TKK with the associated uncertainty of the comparison are plotted in Figure 2.

Table II. Results of the comparison measurements. The values presented are in percent units.

λ	TKK (av)	SPRING	u_{TKK}	u_{SPRING}	u_c	δR
nm	8/d	8/d	(σ=1)	(σ=1)	(σ=1)	[%]
360	98.41	98.51	0.30	0.30	0.42	0.11
380	98.66	98.86	0.25	0.30	0.39	0.19
400	98.58	98.82	0.25	0.30	0.39	0.25
420	98.72	99.01	0.22	0.30	0.37	0.29
440	98.82	99.12	0.22	0.30	0.37	0.31
460	98.87	98.86	0.22	0.30	0.37	-
480	98.81	98.77	0.20	0.30	0.36	-
500	98.88	98.91	0.20	0.30	0.36	0.03
520	98.91	98.88	0.20	0.30	0.36	-
540	98.94	98.94	0.20	0.30	0.36	0.00
560	98.92	98.91	0.20	0.30	0.36	-
580	98.96	98.90	0.20	0.30	0.36	-
600	98.94	98.89	0.20	0.30	0.36	-
620	98.94	98.95	0.20	0.30	0.36	0.01
640	98.95	98.83	0.20	0.30	0.36	-
660	98.99	99.00	0.20	0.30	0.36	0.01
680	99.01	98.86	0.20	0.30	0.36	-
700	99.02	98.58	0.20	0.30	0.36	-
720	99.02	98.66	0.20	0.30	0.36	-
740	99.02	98.77	0.20	0.30	0.36	-
760	99.03	98.23	0.20	0.30	0.36	-
780	99.03	98.86	0.20	0.30	0.36	-

Conclusions

The comparison verifies a good agreement between the diffuse reflectance scales of TKK and SPRING. The deviations are well within the combined standard uncertainty of the comparison, except for a few values at the edges of the spectral range over which the measurements were made.

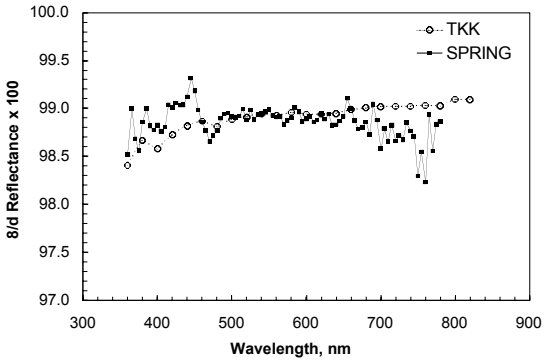

Figure 1. Results for 8/d reflectance factor values of the sample used in the comparison.

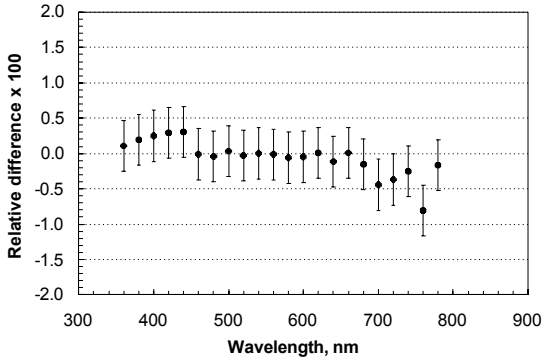

Figure 2. Relative difference in the measurement results between SPRING and TKK. The error bars indicate the relative values of the combined standard uncertainty of the comparison (1σ level).

References

1. W. Budde, and C. X. Dodd, "Absolute reflectance measurements in the d/0° geometry," *Die Farbe* **19**, 94-102 (1970).
2. W. Erb, "Requirements for reflection standards and the measurements of their reflection values," *Applied Optics* **14**, 493-499 (1975).
3. W. H. Venable, J. J. Hsia, and V. R. Weidner, "Establishing a scale of directional-hemispherical reflectance factor: The Van den Akker method," *J. Res. NBS* **82**, 29-55 (1977).
4. C. J. Chunnilall, A. J. Deadman, L. Crane and E. Usadi, "NPL scales for radiance factor and total diffuse reflectance," *Metrologia* **40**, S192-S195 (2003).
5. S. Nevas, F. Manoocheri, and E. Ikonen, "Gonioreflectometer for measuring spectral diffuse reflectance," *Applied Optics* **43**, 6391-6399 (2004).
6. W. Budde, W. Erb, and J. J. Hsia, "International intercomparison of absolute reflectance scales," *Col. Res. Appl.* **7**, 24–27 (1982).
7. J. C. Zwinkels and W. Erb, "Comparison of absolute d/0 diffuse reflectance factor scales of the NRC and the PTB," *Metrologia* **34**, 357-363 (1997).
8. F. N. Fritsch, and R. E. Carlson, "Monotone piecewise cubic interpolation," *SIAM J. Numerical Analysis* **17**, 238-246 (1980).

Comparison of mid-infrared absorptance scales at NMIJ and NIST

J. Ishii
National Metrology Institute of Japan (NMIJ) / AIST, Tsukuba, Japan

L. M. Hanssen
National Institute of Standards and Technology (NIST), Gaithersburg, USA

Abstract. National Institute of Standards and Technology (NIST) realizes scales for infrared absolute absorptance using the integrating-sphere method. National Metrology Institute of Japan (NMIJ) realizes an independent scale for infrared spectral emissivity equivalent to absorptance traceable to the ITS-90. Comparisons of these scales in the mid-infrared part of the spectrum have been performed successfully for the first time and the results are reported here. The results of the comparison show agreement is lying within uncertainty levels for the majority of values measured for opaque materials, and the level of equivalence of the NMIJ and NIST scales.

Introduction

Infrared optical properties such as absorptance are essential in the fields of both radiometry and radiation thermometry. Under the Mutual Recognition Agreement, the metrological equivalence of national measurement standards based on comparisons between the national metrological institutes has increased over time. Recently, the CCT (Consultative Committee for Thermometry) – Working Group 9 is organizing international comparisons of thermophysical properties including emissivity (emittance) of solids. Under such circumstances in this study, a comparison of spectral absorptance scales near room temperature in the mid-infrared portion of the spectrum from 5 μm to 12 μm at NIST and NMIJ based on fundamentally different methods has been performed for the first time. The normal spectral emissivity scale of NMIJ is realized by a direct comparison method between a sample and the reference blackbody cavities traceable to the ITS-90 [1, 2]. On the other hand, NIST realizes the same scale by an integrating sphere based absolute measurements of directional-hemispherical reflectance and transmittance[3].

Measurement techniques and apparatus

Both facilities at NIST and NMIJ employ Fourier transform infrared spectrometers (FTS), however, major differences exist between the techniques used to realize these scales. NMIJ applies the conventional direct technique that consists in measuring the ratio of the spectral radiance of the sample to that of a blackbody radiator at the same temperature and at the same wavelength to derive emissivity values. On the other hand, NIST uses a direct absolute technique with an improved integrating sphere method for measuring spectral reflectance and transmittance of materials. Absolute absorptance is indirectly obtained when the sum of the absolute reflectance and transmittance is subtracted from unity based on Kirchoff's law, which is written in the form for an opaque surfaces which is of primary concern in this study

$$\alpha(\lambda;\theta,\phi) = 1 - \rho(\lambda;\theta,\phi;2\pi) = \varepsilon(\lambda;\theta,\phi), \qquad (1)$$

where α is spectral-directional absorptance, ρ is the spectral-directional-hemispherical reflectance, and ε is spectral-directional emissivity, at wavelength λ, incident angle of radiation θ, ϕ, respectively.

Detailed descriptions of the apparatus of both NMIJ and NIST are found in references[1-3]. Here only brief introductions are presented here.

NMIJ: The spectrometer is a custom designed Michelson interferometer. For calibration of the response of the FTS, two reference blackbody cavities are installed. One is a liquid nitrogen cooled cavity and the other is a variable temperature one operated at 100 °C. The solid sample attached to the holder is heated from the backside by direct contact with the circulating thermostatic fluid. The temperature of the heating fluid is measured with a calibrated PRT sensor placed close to the backside surface of the sample. For minimal uncertainty the samples were measured at 100 °C. To reduce the effects of absorption by air and convective heat exchange, all of the components are assembled and operated in vacuum. The combined standard relative uncertainty for samples with good thermal conductivity is typically around 1 % for high emissivity values and less than 5 % for low emissivity values.

NIST: The spectrometer is a bench-top FTS with external beam output that is interfaced to a custom diffuse gold-coated integrating sphere with an MCT detector. Measurements of absolute reflectance and transmittance are performed at semi-normal incidence (8°) using custom developed methods described in References [3] and [4]. The samples were measured at an ambient temperature of 24 °C, determined by a Pt thermometer. The expanded uncertainty (k=2) for reflectance and transmittance measurements is 3 % of the values for samples of unknown scattering nature, and 0.3 % for specular samples.

We prepared several kinds of solids and coated surfaces as the transfer samples of the comparison. The samples

were 45 mm diameter discs of approximately 1 mm thickness. The samples were measured first at NMIJ and then sent to NIST for measurement.

Results and discussions

Figures 1 to 3 summarize the results measured by NMIJ and NIST for the solids and the coated samples in which transmittance can be disregarded. Figure 1 shows the results for a silicon dioxide sample having a roughened surface. The values measured by the two methods agree to within the combined uncertainty over the entire wavelength range. The discrepancy is at most 0.02 for an absorptance value of 0.6 around 9 μm, which is comparable to the NMIJ uncertainty level of emissivity. Figure 2 illustrates the results obtained for the silicon nitride sample, which is a standard reference material provided by the JFCC (Japan Fine Ceramics Center). It is also seen that the difference between NMIJ and NIST gradually increases as the absorptance values decreases. The discrepancy is about 0.03 when the absorptance value is at its minimum of 0.2 around 10.5 μm. This trend is consistent with an increase in the uncertainty of the radiance measurement for low emissivity materials near room temperatures. Figure 3 shows the results for a black paint, a Heat-resistant black manufactured by Asahi-paint, coated on a copper substrate. It is found that the paint maintains an absorptance value higher than 0.9 and the values observed by NMIJ and NIST are in good agreement over the entire wavelength range. The maximum discrepancy is less than 0.01 and within the combined uncertainty.

Summary

In this study a comparison of spectral absorptance (emissivity) scales in the middle-infrared wavelength region near room temperatures at NIST and NMIJ has been performed for the first time. NIST and NMIJ have established independent scales based on basically different approaches. NIST employs absolute reflectance and transmittance measurement using an improved IR integrating sphere. NMIJ applies a radiance comparison method with reference blackbody radiators traceable to the ITS-90. The results observed by the different approaches almost agree for opaque solid materials within their combined uncertainty levels. The results observed for other materials and details of uncertainty analysis will be also given in the presentation.

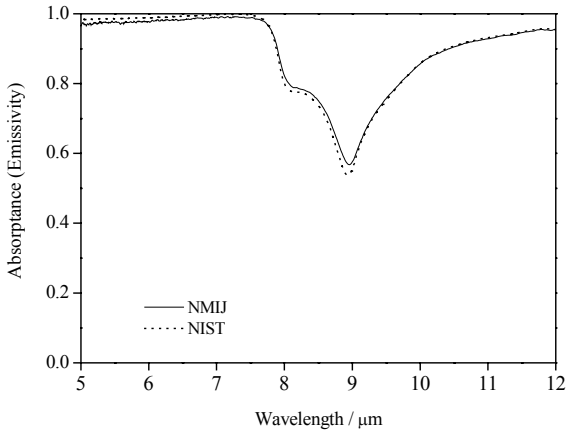

Figure 1. (Semi-) normal spectral absorptance (emissivites) of Silicon dioxide observed by NMIJ and NIST

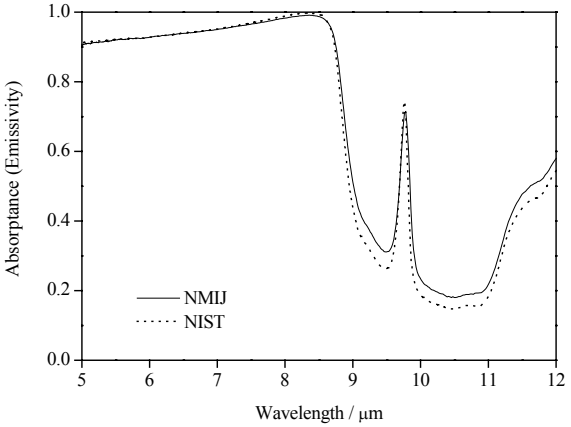

Figure 2. (Semi-) normal spectral absorptance (emissivites) of silicon nitride observed by NMIJ and NIST

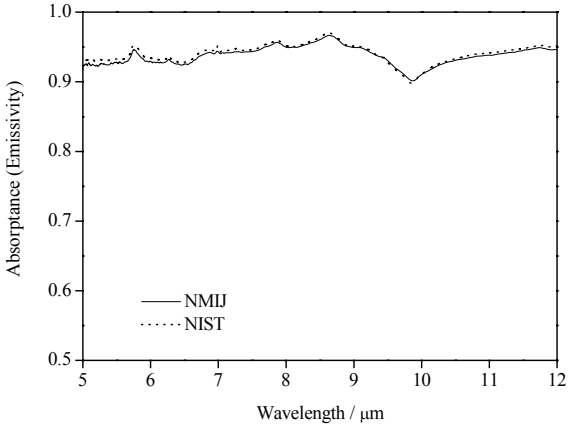

Figure 3. (Semi-) normal spectral absorptance (emissivites) of the black paint (Heat-resistant black, Asahi-paint) on copper substrate observed by NMIJ and NIST

References

1. Ishii J., Ono A., Uncertainty estimation for emissivity measurements near room temperature with a Fourier transform spectrometer, Meas. Sci. Technol. 12, 2103-2112 (2001).
2. Ishii J., Ono A., A Fourier-Transform Spectrometer for Accurate Thermometric Applications at Low Temperatures, Temperature: Its Measurement and Control in Science and Industry, Ripple D. C. (Ed), vol. 7, 705-710, AIP (2003)
3. Hanssen L. M, Integrating-sphere system and method for absolute measurement of transmittance, reflectance and absorptance of specular samples, Applied Optics, 40, 3196-3204 (2001).
4. Hanssen L. M., Snail K. A., Integrating Spheres for Mid- and Near Infrared Reflection Spectroscopy, in *Handbook of Vibrational Spectroscopy*, Chalmers J. M. and Griffiths P. R. (Eds), John Wiley & Sons, Ltd, vol. 2, 1175 - 1192 (2002).

Comparison of photometer calibrations at six different facilities of PTB and NIST

S. Winter, D. Lindner, A. Sperling and G. Sauter
PTB, Braunschweig, Germany

S. Brown, T. Larason, Y. Zong and Y. Ohno
NIST, Gaithersburg, USA

Abstract. Two photometers were calibrated at six different facilities of the PTB and the NIST. At each institute a secondary calibration against other reference photometers at an optical bench, a primary calibration against reference photodiodes at monochromator facilities and a primary calibration with tunable lasers were performed. All measurements are traceable to the respective cryogenic radiometers used as primary and national standards. Most of the measurements have been completed; the remaining measurements will be done this summer before NEWRAD. The deviations of the already performed measurements are within ± 0.6%.

Facilities

The six facilities are described briefly below.

a) Optical bench of the PTB

At the optical bench of the PTB the calibration is performed using a network of different standard lamps at different distribution temperatures as sources and different photometers as detectors [1]. The photometric responsivity related to standard illuminant A (T_A = 2856 K) is obtained as a result of a fit. This fit also gives an index for a simplified spectral mismatch correction.

b) Optical bench of the NIST

At the optical bench of NIST the calibration is performed using a standard lamp with a distribution temperature of T_A = 2856 K against a group of reference photometers that maintain the NIST illuminance unit [2].

c) Monochromator facility of the PTB (DSR)

The calibration of the absolute spectral irradiance responsivity of a photometer is done by a monitor-based substitution method at the DSR facility (Differential Spectral Responsivity) [3]. The photometer and a calibrated reference photodiode are illuminated (overfilled) by the monochromatic beam, far enough away from the monochromator. In front of the reference photodiode is a calibrated aperture. As the area of the photometer is larger than the area of the aperture, the area of the photometer is mapped by the photodiode at every wavelength. These measurements are repeated within the very homogeneous field of a mercury lamp (at a long distance without imaging optics) at a wavelength of 546.1 nm. This method and the next three methods measure the spectral irradiance responsivity $s(\lambda)$ and allow to calculate the photometric responsivity s_v with the formula

$$s_v = \frac{\int_0^\infty P(\lambda,T_A)\cdot s(\lambda)\,d\lambda}{K_m \cdot \int_0^\infty P(\lambda,T_A)\cdot V(\lambda)\,d\lambda} \quad \text{with } T_A = 2856\ \text{K}.$$

where $P(\lambda,T_A)$ is the Planck function at 2856 K.

d) Monochromator facility of the NIST (SCF)

The monochromator-based facility for detector spectral responsivity at NIST is the "Spectral Comparator Facility", SCF [4]. As the beam underfills the reference photodiode and the photometer, a mapping procedure is used for irradiance responsivity calibration.

e) Tunable laser-based facility of the PTB (TULIP)

The TULIP facility (TUnable Laser In Photometry) of the PTB is based on different tunable cw lasers, covering the visible range and a sphere to create a uniform monochromatic radiation field at a high power level [5]. In this uniform radiation field, the photometer is substituted by a reference photodiode or a trap detector.

f) Tunable laser-based facility of the NIST (SIRCUS)

The SIRCUS facility (Spectral Irradiance and Radiance Responsivity Calibrations with Uniform Sources) was the first tunable laser-based facility covering the complete radiometric range from UV to IR [6] and, in principal, is similar to TULIP.

Results of comparison

In the presentation the results of illuminance responsivities, measured at the different facilities a) – f) are presented.

These results are analyzed and discussed, comparing also with the results of 1997 CCPR Key Comparisons of photometric units. The results of spectral irradiance responsivities are also analyzed and discussed.

References

[1] W. Erb and G. Sauter, PTB network for realization and maintenance of the candela, Metrologia, 34, 115-124 (1997).

[2] Y. Ohno, NIST Measurement Services: Photometric Calibrations, NIST Spec. Publ. 250-37 (1997).

[3] S. Winter, T. Wittchen, J. Metzdorf: Primary Reference Cell Calibration at the PTB Based on an Improved DSR Facility; in "Proc. 16th European Photovoltaic Solar Energy Conf.", ed. by H. Scherr, B. Mc/Velis, E. Palz, H. A. Ossenbrink, E. Dunlop, P.

Helm (Glasgow 2000) James & James (Science Publ., London), ISBN 1 902916 19 0
[4] T. C. Larason, S. S. Bruce and A.C Parr, NIST Special Publication 250-41: Spectroradiometric Detector Measurements (1998).
[5] A. Sperling, O. Larionov, U. Grusemann, and S. Winter: Stray-light correction of array spectroradiometers using tunable pulsed and cw lasers; in Proc. of NEWRAD Conference 2005, Davos, Sept. 2005, to be published.
[6] Steven W. Brown, George P. Eppeldauer, Joseph P. Rice, Jun Zhang, Keith R. Lykke, Spectral Irradiance and Radiance responsivity Calibrations using Uniform Sources (SIRCUS) facility at NIST, Proceedings of the SPIE 49th Annual Meeting, Denver, CO, August 2004

A Comparison of Re-C, Pt-C, and Co-C fixed-point cells between NIST and NMIJ

N. Sasajima*, F. Sakuma, Y. Yamada
NMIJ/AIST, Tsukuba, Japan (* guest researcher at NIST)

H. W. Yoon, C. E. Gibson, V. Khromchenko,
NIST, Gaithersburg, USA

Abstract. A comparison of Re-C, Pt-C, and Co-C eutectic fixed-point cells was conducted between NIST and NMIJ at NIST. In the comparison, two high temperature furnaces, two radiation thermometers and one gold-point blackbody were used. Nagano furnace and an LP-3 radiation thermometer were transferred from NMIJ and were used in conjunction with a Thermogauge furnace and an AP-1 radiation thermometer of NIST to check the differences in measurement equipment. Agreement of Re-C and Co-C between NMIJ and NIST cells was better than 100 mK. The melting temperature of NIST Pt-C cell was 270 mK lower than that of NMIJ cell due to the poor purity of Pt powder.

Introduction

Above the freezing temperature of silver (1234.93 K), the International Temperature Scale of 1990 (ITS-90) is defined using Planck's law of blackbody radiation. The temperature is determined by ratio of its emitted radiance against the radiance from Ag, Au, or Cu freezing-point blackbody. Because the temperatures above these fixed points are extrapolated from these lower temperature blackbodies, the uncertainties increase dramatically with increasing temperatures. Recently, metal (carbide)-carbon (M(C)-C) eutectic blackbodies have been developed in several national laboratories to reduce the uncertainties of high temperature region of the ITS-90. Even if eutectic cells could be made and these cells showed good repeatability, their performance can only be confirmed by international comparison by use of high temperature furnaces with good temperature uniformity and stable radiation thermometers [1].

NIST has also started development of M(C)-C eutectic high-temperature fixed points. At NIST, absolute radiometry has already been used to determine the thermodynamic temperature of the freezing-temperatures of gold and silver. The NIST-determined values of the eutectic fixed-point temperatures would contribute for the discussion of the next ITS.

The NIST has constructed three eutectic cells for the first time: Re-C, Pt-C, and Co-C. To confirm the performance of these cells, a comparison was conducted between NIST and NMIJ at NIST. Nagano M furnace (VR10-A23) and an LP-3 radiation thermometer were transferred from NMIJ and were used in conjunction with a Thermogauge (TG) furnace and an AP-1 radiation thermometer of NIST to check the differences in measurement equipment. Gold-point blackbody of NIST was also used to check the short term and long term stability of radiation thermometers during the comparison. A Cu-point cell that can be placed into Nagano furnace was also measured by LP-3 to check the stability during comparison and before and after transportation from NMIJ.

This paper presents the preparation method of eutectic cells including information of metal sources and crucible materials, comparison results of three eutectic cells constructed by NIST and NMIJ, and stability of radiation thermometers.

Filling of eutectic cells

NIST: The crucibles containing M-C eutectics are same in size: outer diameter of 24 mm and a length of approximately 50 mm. The internal dimensions of the blackbody cavity are: aperture diameter: 4 mm; length: 33 mm; bottom shape: conical with an apex angle of 120°. Wall thickness of the cavity: 2 mm. The crucible with nominal purity of 99.9995% was machined and purified by Carbone of America.

The NIST M-C cells were filled as follows: rhenium or cobalt powder and graphite powder were mixed at approximately 1% hypo-eutectic composition. For the Pt-C cell, graphite powder was not added. Purities and suppliers of metals and graphite powder are summarized in Table 1. The crucible was filled with the mixture and placed in the BB3200cc furnace for vertical operation. It was then heated under argon atmosphere to just above the eutectic temperature. For a complete filling the filling process was repeated approximately 10 to 15 times.

Several Co-C cells were broken during filling at NIST. The possible origin is difference in density between liquid and solid of eutectic alloy and temperature nonuniformity of the furnace. To avoid freezing of the molten alloy from the surface of the crucible, which result in the cracking of crucible due to the expansion of the alloy during freezing, the furnace temperature was decreased quickly until the end of freezing. During the measurement of the Co-C, however, the NIST cell was again broken. The main reason might be the crucible material.

NMIJ: The dimensions of crucibles containing M-C eutectics were the same in size: outer diameter of 24 mm and a length of 45 mm. The internal dimensions of the blackbody cavity are: aperture diameter: 3 mm; length: 34 mm; bottom shape: conical with an apex angle of 120°. Wall thickness of the cavity: 2 mm. For Co-C and Pt-C, crucible with a nominal purity of 99.9995% was supplied by Toyo Tanso KK. For Re-C, the crucible was supplied by SGL carbon in order to prevent cracking of crucible due to difference of thermal expansion between metal and

crucible material.

Nominal purities of powders and suppliers are described in Table 1. The filling procedures were almost the same as those of NIST procedures except for the furnace and filling atmosphere: The crucible was filled with the mixture and placed in the Nagano VR20-A10 vertical furnace. It was then heated under argon atmosphere for Re-C and under vacuum atmosphere for Co-C and Pt-C cells.

Table 1: Nominal purity of materials and their suppliers

	Graphite	Co	Pt	Re
NIST	99.9999 % Alfa Aesar	99.998 % Alfa Aesar	99.999 % Alfa Aesar	99.995 % Alfa Aesar
NMIJ	99.9999 % Alfa Aesar	99.999 % Nikko Materials	99.999 % Tanaka Kikinzoku	99.999 % Alfa Aesar

Apparatus

NIST TG furnace and NMIJ Nagano furnace were used for the comparison. The TG furnace has graphite furnace tube of 25.4 mm inner diameter. To improve the temperature uniformity, radiation shields, whose design was almost the same as those used in the Nagano furnace, were placed on front and back of the cell. The fixed-point cells were wrapped with graphite sheet to fit into the center of the furnace.

Nagano furnace has CC composite heater elements around a 27 mm inner-diameter furnace tube, made of the same material. The M-C cells were wrapped with graphite felt and put in the furnace. Radiation shields were used on front and back of the cells. Detailed description is in [2].

Two radiation thermometers of different design were used in the comparison to check the stability or other radiation-thermometers related effects: an AP-1 supplied by NIST and an LP-3 from NMIJ. The operating wavelength of both thermometers was 650 nm.

A daily measurement was done as follows: 1) melting plateau of Au-point blackbody was measured by AP-1 and its freezing plateau was measured by LP-3. 2) Melting and freezing plateau of M-C eutectic cell in TG furnace was measured by AP-1, and M-C cell in Nagano furnace was measured by LP-3 simultaneously. 3) The M-C cell in Nagano furnace was measured by AP-1. 4) M-C cell in TG furnace was measured by LP-3. 5) Au-point blackbody was measured by use of both radiation thermometers with the same procedure described in 1).

Results and discussion

Fig. 1 and 2 show typical melting curves of Pt-C and Re-C realized in Nagano furnace. Agreement of Re-C and Co-C between NMIJ and NIST cells was better than 100 mK. The melting temperature of NIST Pt-C cell was approximately 270 mK lower than that of NMIJ cell.

The melting temperature of Pt-C cell constructed by NPL using nominal purity of 99.999 % powder provided by Alfa Aesar has also showed 330 mK lower than NMIJ cell [3]. Even though nominal purity is the same, the real purity of Pt might worse than Pt provided by Tanaka Kikinzoku.

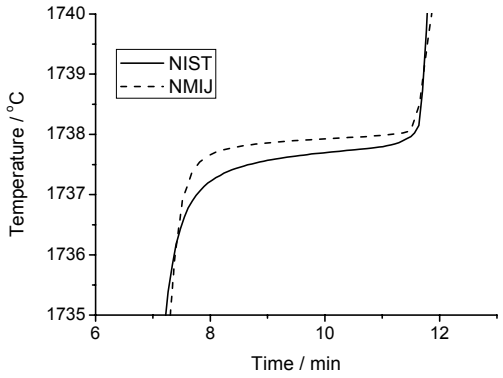

Figure 1. Typical melting curves of NIST and NMIJ Pt-C cells in Nagano furnace measured by LP-3. Time scale was adjusted to become the same plateau duration.

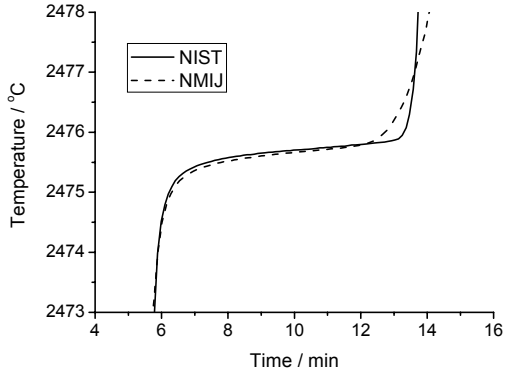

Figure 2. Typical melting curves of NIST and NMIJ Re-C cells in Nagano furnace measured by LP-3. Time scale was adjusted to become the same plateau duration.

Stability of thermometers during 2 weeks comparison by use of Au point was within +/- 50 mK: The freezing temperature of Au-point blackbody measured by LP-3 after eutectic cell measurement was always higher than the temperature before measurement in the same day. There is no apparent drift for both radiation thermometers.

These results show that high temperature M-C eutectic cell like Re-C cell can be used as stable radiance source; it is possible to make these cells at independent laboratories with exchange of information of material sources, filling procedures, crucible materials and so on.

Acknowledgments Tanaka Kikinzoku Kogyo is acknowledged for lending the high purity metal powder for the NMIJ Pt-C cell.

References

[1] Machin, G., et al., "A comparison of high temperature fixed points of Pt-C and Re-C constructed by BIPM, NMIJ and NPL", Proc. of Tempmeko 2004.

[2] Yamada, Y., et al., "High temperature furnace systems for realizing metal-carbon eutectic fixed points", Proc. of Temperature, Vol. 7, AIP Conf. Proc., 2003, pp. 985-990.

[3] Lowe, D., Yamada, Y., "Reproducible metal-carbon eutectic fixed points", to be presented Newrad 2005

Session 8

Radiometric and Photometric Sources

Application of Metal (Carbide)-Carbon Eutectic Fixed Points in Radiometry

Y. Yamada, Y. Wang
National Metrology Institute of Japan (NMIJ)/AIST, Tsukuba, Japan.

T. Wang
National Institute Metrology (NIM), Beijing, China.
Guest scientist at the NMIJ.

B. Khlevnoy
All Russian Research Institute for Optical and Physical Measurements (VNIIOFI), Moscow, Russia.
Guest scientist at the NMIJ.

Abstract. Application of metal (carbide)-carbon eutectic fixed points to radiometry has its own specific requirements: temperature preferably exceeding 3000 K, large aperture, robustness, and long plateau duration. The large aperture BB3500YY furnace, newly introduced at the NMIJ, has been optimally tuned for fixed point realization. Together with a novel cell structure that utilizes an inner insulation by carbon composite sheet material, the requirements are close to becoming reality.

Introduction

Radiometry and radiation thermometry have large technical similarities. The emergence of the high-temperature metal-carbon (M-C) and metal carbide-carbon (MC-C) eutectic fixed points in radiation thermometry will inevitably have a major impact on radiometry [1]. In this paper, possible application of the fixed points to radiometry will be outlined, and requirements specific to these applications will be spelled out. At the NMIJ, efforts to meet these requirements have been initiated and, although still preliminary, promising and highly important improvements are already achieved. This paper attempts to capture and report these most recent developments.

The impact on radiometry

The Metal (Carbide)-Carbon eutectic fixed points can potentially be utilized in many aspects of radiometry. For instance, simply taking advantage of its repeatability and long-term stability, one can monitor the stability of filter radiometers easily and accurately over an extended period of time.

The fixed points, with the knowledge of its thermodynamic temperature, can serve to reduce two major sources of uncertainty in the realization of the primary spectral irradiance scale: the blackbody source temperature and the effective emissivity of its cavity (due to temperature gradient along the cavity wall). Either by transferring the fixed-point temperature of a given eutectic to a large-aperture blackbody by means of a radiation thermometer, or by directly calibrating FEL lamps against a large-aperture fixed-point blackbody source, the first of the two is achieved. The large aperture fixed-point irradiance source inherently achieves cavity temperature uniformity and thus overcomes the second.

The use of the fixed points enables spectral radiance and irradiance calibration obviating the need for a full detector-based calibration facility and as frequently as necessary. The TiC-C point is very promising in this respect since the colour temperature is almost the same as that of the FEL 1 kW lamps. The high-temperature sources exceeding 3000 K have the potential of a highly reproducible UV source. For instance, UV networks that observe the change in ozone layer thickness by linking UV solar monitors worldwide can benefit from a direct calibration of the instruments against these sources in the UV B range.

Requirements specific to radiometry

The radiometric applications impose requirements to the fixed points that are not always met in their applications to thermometry.

1) The temperature needs to be high, so the fixed points of interest are those beyond the Re-C point (2747 K), especially the MC-C points (δ(Mo carbide)-C: 2856 K, TiC-C: 3034 K, ZrC-C: 3156 K, HfC-C: 3458 K). The MC-C fixed points, although there is no indication of inferior performance, have not yet been fully investigated. Thus far, the MC-C points have only been constructed and tested at the NMIJ and the VNIIOFI. A comparison for the TiC-C point has been made between these institutes, and an agreement of 0.24 K, or 0.06 % in terms of the spectral radiance at 650 nm, has been observed [2]. The high temperature entails two complications: the limitation in the operating temperature of the furnaces commonly available, and the breakage of cells due to the large temperature change they experience.

2) To be an irradiance source the cell needs to have an aperture larger than 8 mm in diameter and possibly larger than 10 mm.

3) To use the cells for spectral calibrations, the plateau duration should cope with the time needed for the monochromator to scan the wavelength over the required wavelength range.

Recent developments at the NMIJ

In view of the above requirements imposed by the radiometric applications, two major developments have been pursued recently at the NMIJ.

1) The introduction of a large aperture BB3500 furnace

A new BB3500YY furnace (manufacturer: VEGA International) with a large furnace-tube inner diameter of 47 mm has been designed at the VNIIOFI and installed at the NMIJ, which can reach 3500 K. Work has been performed to push the furnace to its maximum capability. Temperature distribution measurements have been performed and the temperature uniformity has been optimised. The furnace, which uses a stack of pyrolitic graphite rings as the heater / furnace tube, has the feature that the axial temperature distribution can be optimized by selecting the optimum order of the ring elements in the furnace after having measured the electrical resistance of each of them before at room temperature. The furnace-temperature uniformity after optimisation, measured with a radiation thermometer, was within 2 K over 40 mm, roughly corresponding to the length of the fixed point cell (45 mm). Details are presented in another presentation at this conference [3].

2) Inner insulated fixed-point cell

The other improvement is the use of purified carbon cloth material (C/C sheet TCC-019, manufacturer: Toyo Tanso Co. Ltd., impurity content: less than 10 ppm) inside the graphite crucible. The CC composite sheet has thickness of 0.5 mm, and up to 4 layers were inserted between the metal and the graphite crucible wall. This cell structure has several advantages:

(1) The C/C sheet acts as a physical buffer layer that keeps the outer wall of the crucible free from any stress, thus preventing breakage. This method has been successfully applied to Re-C point cells and no breakage has occurred since.

(2) The cell becomes relatively immune to temperature nonuniformity of the furnace. The sheet acts as a thermal insulator in the direction perpendicular to the sheet. The sheet is strongly anisotropic and good thermal conductance is achieved in the lateral direction along the surface, thus enhancing temperature uniformity in the ingot.

(3) The plateau duration is extended, due to the thermal insulation of the sheet.

(4) The amount of the metal required to fill the cell is reduced, while still maintaining the same plateau duration and shape.

(5) The time required for filling a cell is drastically reduced. The filling process is basically an iterative process, and thus usually the final "topping off" with metal powder takes time. However, since the cell no longer needs to be filled completely, and the remaining gap can be filled by C/C sheet layers, it can be filled in approximately half of the time needed thusfar. The last two points are quite effective in reducing the price of these fixed-point cells.

Applicability of this technique to MC-C eutectics is currently under investigation. The technique also paves the way for realizing large aperture cells required for irradiance sources. The solution to the breakage problem enables accommodation of the large-aperture cavity in a cell with the same outer diameter by reducing the outer-wall thickness. The extended length of the cell is expected not to be a problem because of the enhanced immunity to furnace-temperature nonuniformity. Preliminary results will be presented.

The inner insulated cell relaxes the requirement on the furnace temperature uniformity. However, if the cell is combined with a furnace with good temperature uniformity, the plateau quality is further improved. An example is shown in Fig. 1, where a Re-C cell with 3 mm cavity aperture and with a single layer of C/C sheet inserted between the 74 g of the eutectic metal and the outer crucible wall was placed in the BB3500YY furnace. A plateau extending well over 30 minutes was obtained, which is three times longer than what is usually observed with a cell with the same outer dimension.

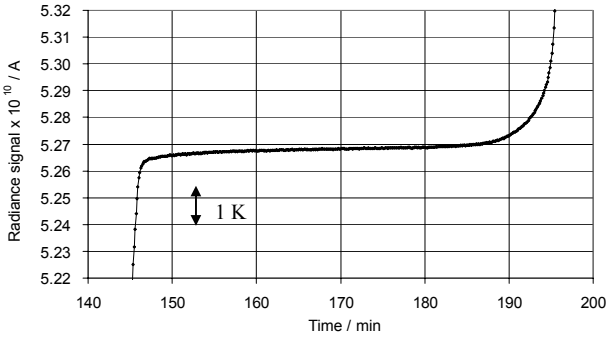

Figure 1. Melting plateau of a Re-C fixed point cell with a single layer of C/C sheet. Furnace: BB3500YY.

Conclusion

The eutectic fixed points hold promise for becoming indispensable tools for radiometry in the near future. Major obstacles for their successful applications are now being cleared away. Involvement of radiometrists in the development of M(C)-C eutectics is strongly encouraged, allowing thermometrists to profit from their expertise. From the thermometric point of view the fixed-point temperatures need to be determined with the smallest uncertainty possible, and thus thermodynamic temperature measurements based upon radiometric methods are deemed to be essential.

References

[1] Yamada Y., Advances in High-temperature Standards above 1000°C, *MAPAN - Journal of Metrology Society of India*, v.20, No 2, 2005, pp.183-191.

[2] Sasajima N., Sakharov M. K., Khlevnoy B. B., Yamada Y., Samoylov M. L., Ogarev S. A., Bloembergen P., and Sapritsky V. I., A comparison of Re-C and TiC-C eutectic fixed-point cells among VNIIOFI, NMIJ and BIPM, in *9th International Symposium on Temperature and Thermal Measurements in Industry and Science (TEMPMEKO)*. 2004. Dubrovnik, to be published

[3] Khlevnoy, B., Sakharov, M., Ogarev, S., Sapritsky, V., Yamada, Y., Anhalt, K., Furnace for High-Temperature Metal (Carbide)-Carbon Eutectic Fixed-Point, *to be presented in this conference*

On Estimation of Distribution Temperature

P. Rosenkranz and M. Matus

Bundesamt für Eich- und Vermessungswesen (BEV), Vienna, Austria

M. L. Rastello

Istituto Elettrotecnico Nazionale (IEN), Turin, Italy

Abstract. Different least square estimation methods for determination of distribution temperature are compared. Their applicability is discussed in regard to uncertainties of spectral irradiance data of incandescent lamps. Experimental results are analyzed to support theoretical conclusions.

Introduction

Radiation from an incandescent lamp, especially a tungsten filament lamp, has a relative spectral power distribution which is reasonably close to that of a blackbody radiator. Therefore, it is often convenient to describe incandescent radiation in terms of the temperature of an equivalent Planckian radiator. Corresponding to CIE recommendations [1] the distribution temperature T_D of a source in a given wavelength range (λ_1 to λ_2) is obtained by minimizing the following sum with regard to the parameters a, T:

$$\sum_{\lambda_i=\lambda_1}^{\lambda_2}\left[1-E(\lambda_i)/aP(\lambda_i,T)\right]^2 \qquad (1)$$

$E(\lambda_i)$ relative spectral irradiance of the source at wavelength λ_i

$P(\lambda_i,T)$ relative spectral irradiance of a blackbody radiator at temperature T and wavelength λ_i

$$P(\lambda_i,T)=\lambda_i^{-5}\left[\exp(c_2/\lambda_i T)-1\right]^{-1} \qquad (2)$$

$c_2 = 1.4388\cdot10^{-2}$ mK (second radiant constant)

a scaling factor

Summation over wavelengths with equidistant intervals of maximum (λ_{i+1}-λ_i) = 10 nm are recommended in photometry in the spectral range from λ_1 = 400 nm to λ_2 = 750 nm [1].

Least Squares Estimation

The concept of least squares estimation is generally based on the following model:

$$E(\lambda_i)+\varepsilon(\lambda_i)=aP(\lambda_i,T) \qquad (3)$$

$\varepsilon(\lambda_i)$ random error with:

expectation value zero	$E[\varepsilon(\lambda_i)] = 0, \forall\lambda_i$,
no correlation	$E[\varepsilon(\lambda_i)\varepsilon(\lambda_k)] = 0, \forall\lambda_i \neq \lambda_k$,
constant variance	$E[\varepsilon^2(\lambda_i)] = \sigma^2, \forall\lambda_i$.

For spectral irradiance data sets $\varepsilon(\lambda_i)$ is usually in proportion to the value of spectral irradiance $E(\lambda_i)$:

$$\varepsilon(\lambda_i)=E(\lambda_i)\eta(\lambda_i) \qquad (4)$$

Thus the variance of ε is not constant for all λ_i, but the variance of η may be considered as constant over a limited wavelength region. This leads to:

$$E(\lambda_i)\left(1+\eta(\lambda_i)\right)=aP(\lambda_i,T) \qquad (5)$$

To apply least squares techniques on this model, equation (5) is logarithmised and simplified (Taylor series):

$$\ln\left(E(\lambda_i)\right)+\eta(\lambda_i)\approx\ln\left(aP(\lambda_i,T)\right) \qquad (6)$$

Thus, for estimation of a and T the following sum is minimized:

$$\sum_{\lambda_i=\lambda_1}^{\lambda_2}\left[\ln\left(E(\lambda_i)/aP(\lambda_i,T)\right)\right]^2 \qquad (7)$$

Since the values of the argument of the logarithm will tend to 1 due to the minimization process, (7) can be simplified to (Taylor series):

$$\sum_{\lambda_i=\lambda_1}^{\lambda_2}\left[1-E(\lambda_i)/aP(\lambda_i,T)\right]^2 \qquad (8)$$

This resembles formula (1). Therefore, the estimation method recommended by CIE is designed for errors, which are in proportion to the corresponding value of spectral irradiance. A numerical solution of the minimization problem (8) is provided in [2].

If the condition of homoscedasticity for least squares estimation (i. e. the variance of ε is constant for all λ_i) is not fulfilled, usually the method of weighted least squares is applied:

$$\sum_{\lambda_i=\lambda_1}^{\lambda_2}\left[E(\lambda_i)-aP(\lambda_i,T)\right]^2/u^2\left(E(\lambda_i)\right) \qquad (9)$$

It seems, that this estimation method is already well in use to determine T_D [3]. A numerical solution for the minimization problem (9) is also given in [3]. If the uncertainties are in proportion to $E(\lambda_i)$ (i. e. $u(E(\lambda_i)) = u_{rel}\cdot E(\lambda_i)$) and the relative uncertainty u_{rel} is constant over the wavelength range from λ_1 to λ_2, the CIE estimation method (8) and weighted least squares (9) should provide similar results for T_D. Based on the results in [4] a Monte Carlo simulation was developed to generate realistic spectra of an incandescent lamp at 2856 K (CIE A). The wavelengths range from λ_1 = 400 nm to λ_2 = 750 nm with wavelength intervals of 5 nm. u_{rel} was chosen in the range of 0.5% to 1.5%. Differences between the two estimators for T_D obtained by minimizing (8) and (9), respectively, did not exceed 0.8 K and are therefore negligible. In addition, the spectrum of the BEV detector-based FEL-lamp (irradiance standard) was generated employing natural cubic splines based on calibration data provided by PTB (Physikalisch-Technische Bundesanstalt). The relative uncertainties of spectral irradiance data in the wavelength range from 400 nm to 750 nm were 0.8%. The wavelength interval was again 5 nm. The results of the two estimation methods (8),

(9) were identical (T_D = 3112.7 K). This confirms, that the estimation method recommended by CIE and weighted least squares with constant u_{rel} provide statistically equal results. Further simulations will be presented.
The use of the CIE method weighted with u_{rel} to determine T_D is suggested in [5]:

$$\sum_{\lambda_i=\lambda_1}^{\lambda_2}\left[1-E(\lambda_i)/aP(\lambda_i,T)\right]^2/u_{rel}^2\left(E(\lambda_i)\right) \qquad (10)$$

(10) can be written as:

$$\sum_{\lambda_i=\lambda_1}^{\lambda_2}\left(\frac{E(\lambda_i)}{aP(\lambda_i,T)}\right)^2\left[E(\lambda_i)-aP(\lambda_i,T)\right]^2/u^2\left(E(\lambda_i)\right) \qquad (11)$$

Since the values of the fraction in the first factor in (11) will tend to 1 due to the minimization process, (10) will provide results similar to weighted least squares (9).

Experimental Results

A spectrometer calibrated at the above mentioned detector-based FEL-lamp was employed to obtain the spectrum of an incandescent lamp (Wi41/G). The distribution temperature of the lamp should be close to 2856 K (CIE A). The wavelength interval was about 5 nm. The responsivity of the spectrometer was rather low in the blue region of the wavelength range from 400 nm to 750 nm. This led to increasing relative uncertainties of spectral irradiance in the region from 500 nm down to 400 nm (Fig. 1):

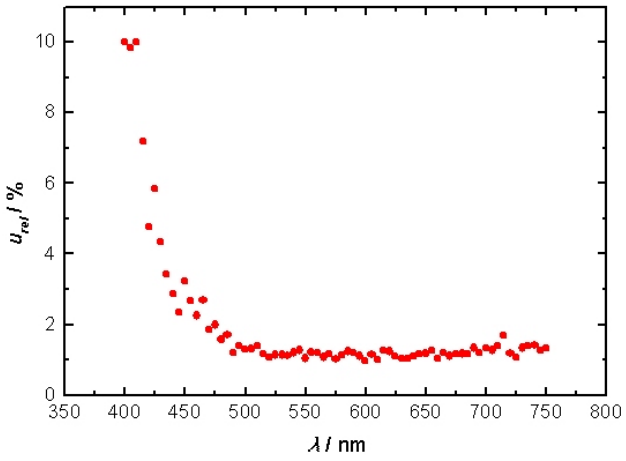

Figure 1. Relative uncertainties of the obtained spectral irradiance values of a Wi41/G incandescent lamp at approximately 2856 K (CIE A).

Since the deviations of the measured values from the curve fit obtained by CIE estimation method (8) did not exceed 5%, the concept of distribution temperature is applicable according to [1]. But the crucial condition of constant u_{rel} and constant variance of η, respectively, is obviously not fulfilled. The estimated value of T_D by minimizing (8) is unreasonable low ($T_{D,CIE}$ = 2837.6 K), while the estimator obtained by weighted least squares (9) seems plausible ($T_{D,LS}$ = 2855.0 K). T_D obtained with the weighted CIE method (10) is 2855.5 K.
In spectral regions with relative low values of spectral irradiance (blue) the CIE estimation method (8) tends to reduce the deviations from the fit curve more than in regions with high values (red). This is due to the design of this estimation method, but only desirable, if u_{rel} of spectral irradiance remains constant or approximately constant over the considered wavelength region. However, in most spectroradiometric systems, u_{rel} is greater at low wavelength (400 nm to 450 nm) than it is in most of the visible spectrum [5]. In these cases weighted least squares (9) or the weighted CIE estimation method (10) will provide more reasonable results for T_D than the estimation method currently recommended by CIE (8). Further experimental results will be presented and discussed.

Conclusions

The irradiance spectrum shape of an incandescent lamp always shows deviations to the corresponding blackbody spectrum. This is mainly due to the fact, that a tungsten filament is no genuine blackbody radiator and also due to the transmittance of the glass bulb envelope surrounding the filament [3, 6]. Thus, it seems inappropriate to denote any of the discussed estimators as “best estimator”.
From a statistical point of view all available information should be used for parameter estimation. Therefore, weighted least squares seem more feasible to determine distribution temperature, provided that the statistical information about the uncertainties of spectral irradiance data is valid.
A fundamental principle of metrology is that a measurand should be defined in such a way that its value does not depend on the method of measurement [5]. The use of weighted least squares as definition of distribution temperature would contradict this principle.
A possible solution for this problem might be to leave the CIE definition at its present form. But it should be explicitly pointed out, that this estimation method will lead to feasible results only, if the relative uncertainties of spectral irradiance data over the chosen wavelength region can be presumed constant. Otherwise weighted least squares, or the CIE estimation method weighted with u_{rel} of spectral irradiance data are to be used. The later seems more convenient and will provide similar results as weighted least squares. This would improve the comparability of distribution temperature data regarding for instance comparisons or traceability.

References

1. Distribution Temperature and Ratio Temperature, *CIE 114-1994, 114/4*, 24-28, 1994.
2. Robertson A. R., Computation of Correlated Color Temperature and Distribution Temperature, *J. Opt. Soc. Am., 58*, 1528-1535, 1986.
3. Cox M. G. , P. M. Harris, P. D. Kenward, Spectral characteristic modelling, *NPL Report CMSC 27/03*, 2003.
4. Erb W., G. Sauter, PTB network for realization and maintenance of the candela, *Metrologia, 34*, 115-124, 1997.
5. Robertson A., R., R2-35 Uncertainties in Distribution Temperature Determination, *CIE R2-35*, 2005
6. Kärhä P., P. Toivanen, F. Manoochehri, E. Ikonen, Development of a detector-based absolute spectral irradiance scale in the 280-900 nm region, *Applied Optics, 36*, 8909-8918, 1997.

Hyperspectral Image Projectors for Radiometric Applications

J. P. Rice, S. W. Brown, and B. C. Johnson
NIST Optical Technology Division, Gaithersburg, MD, USA

Abstract. We describe a new type of Calibrated Hyperspectral Image Projector (CHIP) intended for radiometric testing of instruments ranging from complex hyperspectral or multispectral imagers to simple filter radiometers. The CHIP, based on the same digital mirror arrays used in commercial digital light projector* (DLP) displays, is capable of projecting any combination of as many as approximately one hundred different arbitrarily programmable basis spectra into each pixel of the instrument under test (IUT). The resulting spectral and spatial content of the image entering the IUT can simulate, at typical video frame rates and integration times, realistic scenes to which the IUT will be exposed during use, and its spectral radiance can be calibrated with a spectroradiometer. Use of such generated scenes in a controlled laboratory setting would alleviate expensive field testing, allow better separation of environmental effects from instrument effects, and enable system-level performance testing and validation of space-flight instruments prior to launch. Example applications are testing the performance of simple fighter-fighter infrared cameras under simulated adverse conditions, and system level testing of complex hyperspectral imaging instruments and algorithms with realistic scenes. We have built and tested a successful prototype of the spectral light engine, a primary component of the CHIP, that generates arbitrary, programmable spectra in the 1000 nm to 2500 nm spectral range. We present an overview of this technology and its applications, and discuss experimental performance results of our prototype spectral light engine.

Introduction

A general problem in radiometric characterization and calibration is that the instrument under test is not easily tested with realistic spatial and spectral scenes to which it will be exposed during its use. For example, a typical Earth-observing space flight instrument is calibrated pre-flight with a spatially uniform source such as a lamp-illuminated integrating sphere or a blackbody. The spectral radiance of such sources is often quite different than that of the Earth scenes that the instrument measures on orbit, but effects arising from this difference are not often discovered until after launch. While proper incorporation of the relative spectral responsivity of the IUT into the calibration can, in principle, be used to correct for spectral radiance differences, in practice effects such as out-of-band leakage from the calibration source used during calibration that does not match the Earth scene still plague many instruments. As multispectral and hyperspectral instruments become more common, so will this problem.

A related problem occurs when testing sensors used in other application areas such as chemical plume detection or fire-fighter thermal imaging. In the latter case, for instance, performance testing of the IUT under realistic conditions often requires starting fires in order to generate the required spectral radiance images, and testing operation under conditions of smoke, snow, and fog in the path is even more challenging.

Below we describe a new image projection technology that has the potential to solve these problems by generating realistic spectral radiance images that can be projected into the IUT in a controlled laboratory setting. The basic concept is to use a mirror array such as those used in DLP projectors to project a simulated image. However, in place of the red-green-blue (RGB) color wheel, we use a spectral light engine described below that is also based on another, separate mirror array. The resulting spectral and spatial content of the image entering the IUT can simulate, at typical video frame rates and integration times, realistic scenes to which the IUT will be exposed during use. Also, the spectral radiance of the CHIP can be measured with an absolute spectroradiometer, providing calibration.

Spectral Light Engine

For the prototype spectral light engine we used a commercially-available computer-interfaced mirror array having 1024 columns × 768 rows illuminated with broadband spatially uniform light as shown in Fig. 1. The tiny mirrors that make up the mirror array are on a 13.6 micrometer pitch. When powered, each aluminum mirror can be set to be either "on," reflecting light to the projection optics, or "off," reflecting light to a beam dump (Hornbeck). Switching times are such that binary images can be updated at a frequency on the order of 5000 Hz.

A spectrally dispersive prism (or diffraction grating) maps each column of the mirror array to the exit slit, in a reverse spectrograph configuration, such that each column corresponds to a particular wavelength (Nelson et al.). That is, the entrance slit of the traditional spectrograph is replaced by an image of the mirror array, and each column of the mirror array corresponds to a virtual entrance slit that has a one-to-one correspondence with wavelength. At any instant in time, the number of rows turned on in a given column determines the relative spectral radiance at the wavelength corresponding to that column. Thus, the spectrum can be programmed simply by writing a binary image to the mirror array. Higher fidelity (than 1/768) is conceivable by using pulse-width modulation on the mirror array to form a grey scale. However, depending on how it is implemented, that may begin to use up the degree of freedom afforded by the time domain that is needed for the full CHIP described in the next section. The resulting spectral radiance is alternately projected into the instrument under test and a reference radiometer, enabling the calibration of the instrument under test to be tested with controlled arbitrary spectra. In our prototype, we used a mirror array with a protective window antireflection coated in the 1000 nm to 2500 nm range, a grating, all-reflective aluminum and gold imaging optics, and a Fourier-Transform Infrared (FTIR) spectroradiometer with an InGaAs detector to measure the spectra. By writing different binary images to the mirror array, we were able to produce different spectra, as expected.

Calibrated Hyperspectral Image Projector

The concept for the complete CHIP is shown in Fig. 2.

It uses two mirror arrays, optically in series. Mirror Array #1 is used in the spectral light engine to generate arbitrary programmable basis spectra. Mirror Array #2 is illuminated by the spatially uniform light from the spectral light engine, and the spatial image programmed into Mirror Array #2 is projected into the instrument under test. Alternatively, it is projected into the reference radiometer for spectral radiance calibration. For an IUT frame rate of 50 Hz, the 5000 Hz binary update frequency of the spectral light engine means that it can cycle through up to about one hundred basis spectra within the single-frame integration time of the IUT. The duty cycle that a given mirror (image pixel) of Mirror Array #2 spends in the "on" state during the "on" time of a particular basis spectrum determines, during that frame, the fractional component of that basis spectrum projected from that image pixel. Thus, arbitrary programmable spectra can be projected into each spatial pixel of the instrument under test.

A key difference from the commercial DLP projectors is that, whereas those are limited to the three RGB basis functions defined by human perception of color, the CHIP can have up to about one hundred basis functions limited only by the spectral range and resolution of the broadband source, mirror arrays, and optics. Thus realistic hyperspectral images can be projected into the instrument under test. In addition, after each IUT frame cycle the hyperspectral image can be changed, enabling dynamic testing capability.

Acknowledgments The prototype was built and tested with support from the NIST Advanced Technology Program. We thank Jerry Fraser, Anthony Hamins, and Francine Amon of NIST for useful discussions of hyperspectral and fire-fighter applications.

*Any reference made to commercially-available products in this abstract does not imply recommendation or endorsement by NIST; nor does it imply that the products are the best for the purpose stated.

References

Hornbeck, L. J., "Digital light processing for high-brightness, high-resolution applications," *Proc. SPIE* **3013**, 27-40 (1997).

Nelson, N. R., Bryant, P., and Sundberg, R., "Development of a hyperspectral scene generator," *Proc. SPIE* **5151**, 480-484 (2003).

Figure 1. Schematic of the spectral light engine.

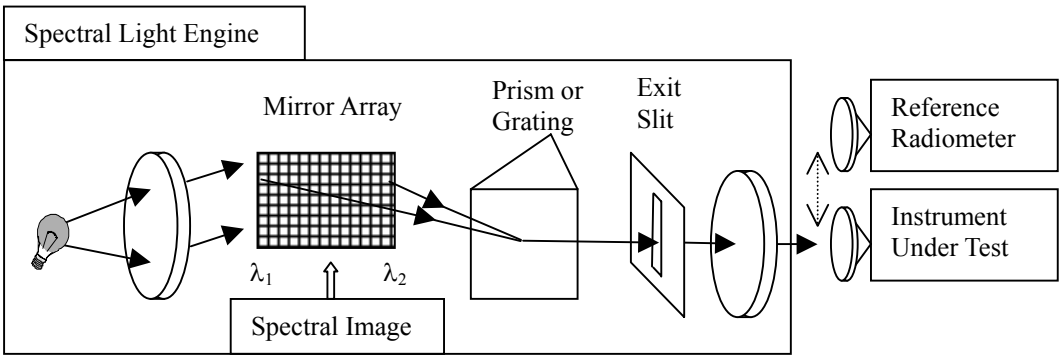

Figure 2. Schematic of the CHIP.

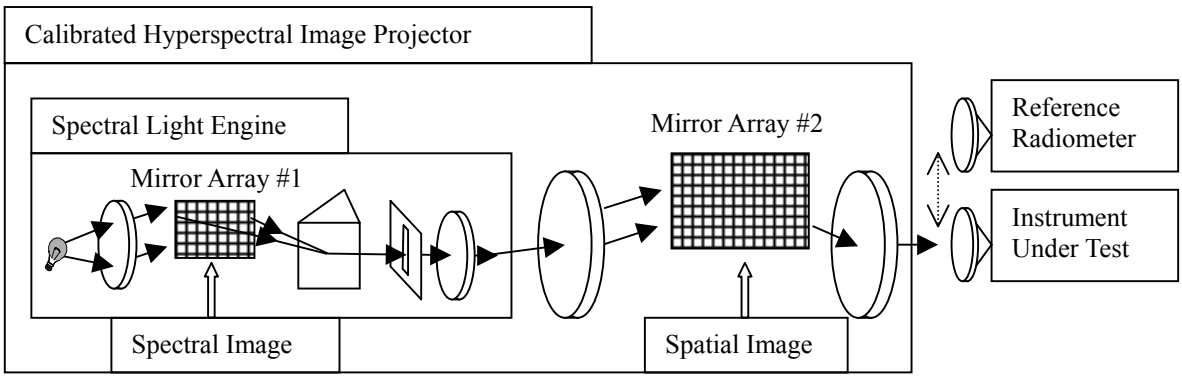

Reproducible Metal-Carbon Eutectic Fixed-Points

D. Lowe
National Physical Laboratory, Teddington, UK

Y. Yamada
National Metrology Institute of Japan, AIST, Tsukuba, Japan

Abstract. The potential reproducibility of high-temperature metal-carbon fixed-points has been investigated. Crucibles and metals from NPL were used to construct fixed-points using NMIJ facilities. Agreement at 2700 K was better than the 80 mK uncertainty. Appropriate construction should permit this level of reproducibility between cells made at different National Measurement Institutes.

Introduction

High-temperature fixed-points would provide reference standards for radiance and temperature scales. The needs for radiance are primarily highest temperature to provide stable UV output; while temperature metrology would benefit from additional fixed-points from the freezing temperature of gold (1337 K) upward. Fixed-points based on metal-carbon (or metal-carbide carbon) eutectic alloys have been shown to give a range of repeatable transition temperatures from about 1426 K to above 3300 K.

A key requirement for reference use is demonstrated good reproducibility, i.e. agreement between sources constructed at different institutes. So far there has been limited success in achieving the suggested 100 mK at 2300 K [1] between clearly independent sources.

In 2004 a comparison was carried out at PTB of fixed-points constructed by BNM-INM, NMIJ and NPL [2]. While the results were approaching the required reproducibility there were clear differences between the sources from different institutes. In particular the cells of NMIJ had longer melts, better defined plateaus, and were more repeatable. They also consistently gave the highest radiance temperature for the melt temperature, as defined by the point of inflexion in the melt curve.

There are scenarios in which specific impurities raise the melt temperature or modify grain structure in a way that would explain the differences. However it is unlikely this would show a consistent trend. It is more likely that the NMIJ cells were better than those of NPL. This could be due to impurities or poor ingot formation. It was suspected that the NPL cells were being contaminated during construction.

To check for this NPL took crucibles and metals to NMIJ to construct fixed-points. This would show the level of agreement that should be possible given suitable filling facilities when using different design crucibles and materials from different suppliers. Differences to the results given in [2] would show effects due to the method of fixed-point manufacture.

Filling of Fixed-Points

NPL uses the same furnace (blackbody) to make and evaluate fixed-points and to perform radiation thermometer calibrations. It works horizontally which complicates cell construction and hinders visual monitoring of the ingot quality. Before making a fixed-point the furnace is heated to about 100 °C above the temperature of use as the empty crucible is baked for 15-30 minutes in argon. Other than this no purification steps are taken. Furnace tubes as supplied are purified (<5 ppm ash content) but are replaced as they wear out rather than between different fixed-point materials. The NPL crucibles are made at the NPL graphite workshop. To reduce risk of contamination where possible ceramic tools are used.

The NMIJ facilities include a furnace solely for filling fixed-points. The crucibles are post-purified after manufacture. Cells are filled vertically which simplifies the operation. The furnace itself is first baked, then used to bake the empty crucible and then used to make the fixed point. The furnace can be evacuated while baking to improve purification.

Filling of fixed-points is carried out separately from any other operations, and care is taken to avoid cross-contamination between different materials. Disposable items are used where possible and all items are cleaned with ethanol. Plastic wrap is used to avoid contact with any surface.

To make the cells metal and graphite powders are weighed out and mixed at approximately half eutectic composition. Material is added to the crucible in an argon filled glove-bag, and each filling melt is carried out under argon, after pumping and backfilling the furnace two times. Once the crucible is considered sufficiently full the crucible end cap is screwed into place and the fixed-point is complete.

For this study NPL supplied materials were used to make cells of; rhenium (99.999 % nominal purity) in an NPL Ringsdorff graphite crucible (R1), cobalt (99.998 %) in an NMIJ Toyo Tanso crucible (C1), cobalt in an NPL Poco crucible (C2), cobalt in an NPL Ringsdorff crucible (C3) and platinum (99.999 %) in an NMIJ Toyo Tanso crucible (P1).

These fixed-points were then compared to NMIJ cells previously prepared with the same facilities, and used in the comparison at PTB [2].

Realisation of Fixed-Points

Measurements were made in two furnaces. The larger Nagano M (VR10-A23) able to reach 2500 °C and smaller Nagano S (VR10-A20) limited to 2000 °C have

very similar temperature distribution [2]. The radiance temperature of a melt was determined using an IKE LP3 radiation thermometer with a wavelength of about 650 nm.

NPL and NMIJ Re cells were measured in the M furnace alternating daily. Co and Pt cells were measured side-by-side in the M and S furnace, then exchanged. The following uncertainty contributions were considered; the stability of the LP3 during one days measurements and over the course of the comparison, the repeatability of the interval measurements, the repeatability of the fixed-point measurements.

The size-of-source correction was assumed to be the same for both fixed-points. No account was taken of differences due to the different lengths of the cells. Any difference in emissivity was assumed to be negligible.

Results

Figure 1 shows typical melt curves for the two Re cells. The difference between the NMIJ and NPL cells was found to be 25 mK with uncertainty 80 mK (k=2).

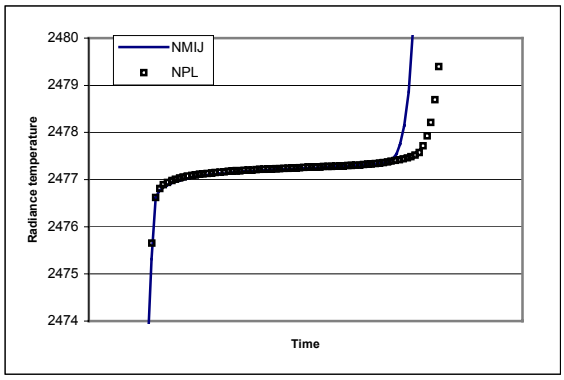

Fig 1. Typical melt curves for NMIJ and NPL Re fixed-points.

Three of the four cobalt cells agreed within ±15 mK of each other. The cell made from Poco graphite (C2) was found to be significantly lower than the others, over 100mK. There was no indication in the plateau shape or duration to suggest any impurities.

The melt temperature of the NPL Pt cell was 330 mK lower than the NMIJ cell. The NPL melt duration was only about half that of the NMIJ cell although in an identical crucible.

Discussion

The results show that with suitable filling equipment fixed-points can be made with the reproducibility between sources needed to establish M-C fixed-points as reference standards. The fixed-points made at NMIJ are generally much improved over previous NPL cells, better in some cases than the NMIJ standards. If rhenium cells continue to have this level of agreement using readily available material and crucibles of different design and graphite then at least one high-temperature fixed-point will have been established. Even rhenium-carbon on its own could significantly improve temperature scale realisation, and is high enough in temperature to satisfy the need for a stable UV reference source of radiance.

The cobalt measurements emphasize the need for comparison to verify the performance of high temperature fixed-points; there is nothing in the performance of C2 that indicates a problem. It is possible the crucible was contaminated either as the graphite supplied or during manufacture. The platinum result was especially disappointing. It was noted during filling that the ingot had an unusual, mottled appearance not seen before. Subsequent analysis suggested the platinum was not the claimed 99.999 % purity

Of the routes of contamination listed above (poor metal purity, contaminated graphite for crucibles and cross-contamination during filling) there is evidence that NPL has suffered from all three of them. The metal purity issue is not simple. Purity analysis rarely provides the definite answers needed. Graphite on the other hand is readily purified to ash contents of a few ppm. Any machining work to make crucibles should be followed by purification to this level. Cross-contamination is an area where measures can be taken. All items that come in contact with the cell should be considered as potential contaminants. Simple baking of furnace components that have been used to make fixed-points is not enough. Graphite furnace components should be properly purified between uses, or separate parts kept for different materials (or both).

The use of a vertical furnace makes it much easier to check the ingot quality during filling. It also simplifies handling and cell filling, which makes it less likely that contamination will happen.

Conclusions

There has been a lot of published work on M-C fixed-points, but little convincing evidence of reproducibility. This is at least partly due to the difficulties of measurement at the high temperatures involved. This work suggests that adequate filling arrangements should permit agreement between sources that satisfy the 100 mK at 2300 K requirement of CCT/CCPR. Knowing that sources agree would in turn help in the improvements to furnaces and instrumentation needed to get the full benefit from high temperature reference sources.

References

[1] CCT/96 Recommendation T2, see also T. J. Quinn, “News from the BIPM”, Metrologia, Vol.34, pp.187-194, 1997

[2] Anhalt K., Hartmann J., Lowe D., Sadli M., Yamada Y., “A comparison of Co-C, Pd-C, Pt-C, Ru-C and Re-C eutectic fixed-points independently manufactured by 3 different institutes”, to be presented at Newrad 2005

Thermodynamic temperature determinations of Co-C, Pd-C, Pt-C and Ru-C eutectic fixed points cells

K. Anhalt, J. Hartmann
Physikalisch- Technische Bundesanstalt Braunschweig und Berlin, Germany

D. Lowe, G. Machin
National Physical Laboratory, Teddington, UK

M. Sadli
CNAM- INM, Paris, France

Y. Yamada
National Metrology Institute of Japan, AIST, Tsukuba, Japan

Abstract. Thermodynamic temperatures of Co-C, Pd-C, Pt-C, and Ru-C metal-carbon fixed-point cells manufactured by CNAM-INM, NMIJ and NPL were determined by absolutely calibrated PTB filter radiometers and a radiance comparison method using an IKE LP3 radiation thermometer.

Introduction

In order to implement metal-carbon (M-C) eutectic fixed-points in thermometry and radiometry it is essential that their thermodynamic melting temperature is determined by means of absolute radiometric methods. At PTB the use of precision apertures in conjunction with absolutely calibrated filter radiometers is a well established approach for the measurement of thermodynamic temperature in the irradiance mode [1]. However an irradiance measurement involving fixed-point cells and precision apertures requires radiating cavities with a minimum aperture diameter of 8 mm, necessitating rather voluminous fixed-point cells [2]. For the determination of the fixed-point melting temperature the temperature homogeneity across the cell is critically important [3]. In the furnace systems available up to now the best temperature homogeneity is such that only cells at most 50 mm in length can be used. To keep good emissivity the apertures of the radiating cavity in the eutectic fixed point cells investigated here are 3 mm in diameter only. Since such cells can only be measured in radiance mode a radiance comparison method was developed to determine the thermodynamic temperature of the eutectic fixed-point cells.

Measurement principle

Two high-temperature furnace systems are used: one which holds the eutectic fixed-point cells and a second as a reference source of thermal radiation. The thermodynamic temperature of the reference source is determined by an irradiance measurement with filter radiometers. The thermodynamic temperature of the eutectic fixed point can be derived via a radiance comparison by means of a radiation thermometer on the basis of Planck's law of blackbody radiation.

Experimental setup

An overview of the experimental setup is given in Figure 1.

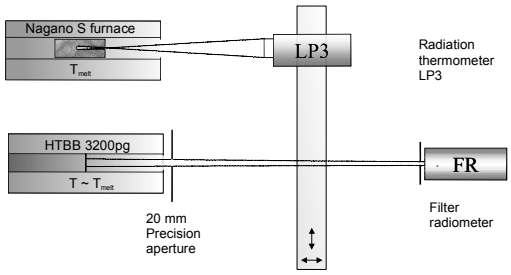

Figure 1: Experimental setup for the thermodynamic temperature measurements of M-C fixed point cells

Furnace systems PTBs high-temperature blackbody HTBB3200pg was used as the reference source of thermal radiation. The eutectic cells were placed in the NMIJ Nagano S furnace VR10-A20, a smaller variant of the Nagano M VR10-A23 described in [4].

Irradiance measurement The high- temperature furnace HTBB3200pg was operated at a temperature close to the melting temperature of the fixed points in question. A 20 mm precision aperture in front of the HTBB defines the radiating area for measurements with a filter radiometer positioned at about 1110 mm from this aperture. Two narrow- bandwidth interference- filter radiometers with center wavelengths around 676 nm and 800 nm have been used to determine the thermodynamic temperature of the HTBB. The spectral irradiance responsivity of the filter radiometers has been calibrated traceable to the cryogenic radiometer of the PTB [5].

Radiance comparison An LP3 radiation thermometer was positioned for a radiance measurement 700 mm in front of the HTBB and focused onto its entrance such that both LP3 and filter radiometer see an equivalent area at the bottom of the HTBBs cavity. For the radiance measurement at the metal-carbon eutectic melting temperature the LP3 was repositioned in front of the Nagano S furnace at a distance of 700 mm from the aperture of the fixed- point cell, and

aligned to the center of this aperture. Four melts and freezes were initiated with temperature steps of +-30, +-20, +-10, +-30.

Stability measurements The radiance and irradiance measurements of the HTBB were repeated with both filter radiometer and radiation thermometer after the M-C cell measurement to check the stability of the LP3.

SSE For assessing the size-of-source corrections horizontal scans of the spectral radiance across the aperture of the HTBB and the fixed-point cell in the Nagano S-furnace were taken. This procedure was applied during 12 days for Co-C, Pd-C, Pt-C and Ru-C eutectic fixed-point cells produced by NPL, CNAM-INM, and NMIJ [6].

Uncertainties Uncertainty components in the assignment of the thermodynamic melting temperatures are the uncertainties in the thermodynamic temperature of the HTBB and in the radiance comparison via the radiation thermometer LP3. Uncertainties in emissivities are included.

Results

In each case the average of four measurements was corrected for SSE and drift. The resulting thermodynamic melting temperatures for Co-C, Pd-C, Pt-C and Ru-C are presented in Table 1.

		T / K	U / K, k=2
Ru-C	**NMIJ**	2227.44	0.40
Ru-C	**NPL**	2227.22	0.39
Ru-C	**BNM**	2226.96	0.37
Pt-C	**NMIJ**	2011.88	0.33
Pt-C	**NPL**	2011.74	0.32
Pt-C	**BNM**	2011.74	0.30
Pd-C	**NMIJ**	1765.19	0.26
Pd-C	**NPL**	1765.07	0.27
Pd-C	**BNM**	1765.00	0.26
Co-C	**NMIJ**	1597.30	0.23
Co-C	**NPL**	1597.16	0.22
Co-C	**BNM**	1597.23	0.21

Table 1: Thermodynamic melting temperatures of Co-C, Pd-C, Pt-C and Ru-C eutectic fixed-point cells manufactured by NPL, BNM-INM and NMJ

Discussion

The results of the thermodynamic-temperature measurements of the 12 eutectic fixed-point cells can be compared with results of a previous study on the differences in radiance temperature of the melting points of all cells and with results of a comparison of local thermodynamic temperature scales for a subset of the fixed point cells.

Temperature differences The same eutectic fixed point cells were investigated in a previous study with regard to differences in radiance melting temperature [6]. The results are confirmed by this work: The largest temperature differences between cells are seen for Pd-C and Ru-C; the cells produced by the NMIJ always showed the highest melting temperatures. Keeping in mind the complexity of the thermodynamic temperature determination this is a remarkable result, which shows the general applicability of the presented technique as well as the long- and mid-term stability of the setup.

Thermodynamic temperature scale 9 months prior to the PTB measurements described here the NPL fixed-points thermodynamic melting temperatures were determined at NIST using a Thermo Gage furnace and an absolutely calibrated radiation thermometer [7]. The agreement between these data and the measurement presented here is better than 500 mK over the whole temperature range and just within the combined extended uncertainty (k=2).

Conclusion

Thermodynamic temperatures during the melt of Co-C, Pd-C, Pt-C, and Ru-C eutectic fixed points were determined with uncertainties below 400 mK at temperatures up to 2250 K. The excellent agreement with previous measurements shows the applicability of the described technique. Furthermore it demonstrates the potential of eutectic metal-carbon systems in metrology. A thermodynamic-temperature scale comparison involving detectors would be far more time consuming and more delicate, since it involves sending and handling sensitive optical equipment.

Acknowledgement This work was part supported by the European Commission "GROWTH" Programme Research Project "Novel high temperature metal-carbon eutectic fixed-points for Radiation Thermometry, Radiometry and Thermocouples" (HIMERT), contract number: G6RD-CT-2000-00610. Tanaka Kikinzoku Kogyo is acknowledged for lending the high purity metal powder for the NMIJ Pt-C cell. The authors would like to thank Stephan Schiller for technical assistance during the measurements.

References

[1] Hartmann, J., Taubert D., Fischer, J., "Measurements of T-T90 down to Zinc point temperatures with absolute filter radiometry", Proc. of Tempmeko 2001, B. Fellmuth, J. Seidel, G. Scholze (eds.) VDI Verlag, Berlin, (2002) 377-382

[2] Hartmann et al., Proc. of Tempmeko 2004, Dubrovnik

[3] Machin et al., "A comparison of high temperature fixed-points of Pt-C and Re-C constructed by BIPM, NMIJ and NPL", Proc. of Tempmeko 2004, Dubrovnik

[4] Yamada, Y., Sasajima, N., Gomi, H., Sugai, T., Proc. of Temperature, Vol. 7, ed. by Ripple D., AIP Conference Proceedings, Chicago, 2003, pp. 985-990.

[5] Taubert, D.R. , Friedrich, R., Hartmann, J. and Hollandt, J., Metrologia, 40 (2003), p35–p38

[6] Anhalt, K. et al. To be presented at Newrad 2005

[7] Machin et al., "A comparison of ITS-90 and detector-based scales between NPL and NIST using metal-carbon eutectics", Proceedings of Tempmeko 2004, Dubrovnik

Spatial Light Modulator-based Advanced Radiometric Sources

S. W. Brown, J. P. Rice, B. C. Johnson, D. W. Allen, G. T. Fraser, and Y. Ohno
National Institute of Standards and Technology, Gaithersburg, MD, USA

I. Fryc
Bialystok University of Technology, Bialystok, Poland

Abstract. We describe the development of spectrally programmable light sources that can generate complex spectral distributions for radiometric, photometric and colorimetric applications. One of the underlying goals of this work is to establish application-specific metrics to quantify the performance of radiometric systems. For example, systems may be quantified in terms of the accuracy of measurements of standardized, spectrally complex, sets of source distributions. In essence, the programmable spectral source will be a radiometric platform for advanced instrument characterization and calibration that can also serve as a platform for algorithm testing and instrument comparison.

Introduction

Current radiometric standards disseminated by National Metrology Institutes (NMIs) such as the National Institute of Standards and Technology (NIST) in the U. S. are spatially uniform and have spectral properties that vary smoothly with wavelength. The spectral and spatial characteristics of radiometric sources based around traditional technologies, *e.g.*, tungsten filament lamps and blackbodies; reflectance plaques and integrating spheres, are important for general calibration applications, but tend to have limited utility for advanced characterization and calibration measurements. The absence of relevant, application-specific, radiometric artifacts to evaluate the performance of instruments limits the ability of end users to verify the measurement results, sometimes with adverse consequences. Consequently, the need exists for advanced calibration artifacts to improve measurement accuracies in a wide variety of applications, ranging from basic colorimetric characterization to remote sensing radiometry.

Advanced calibration artifacts include spatially as well as spectrally complex sources. Spatial scene generators have been developed for infrared calibrators [Nelson], and spectrally programmable light engines are under development for use in medical endoscopes [MacKinnon], to generate standard source distributions [Fryc, Wall] and for general use in radiometric, colorimetric, and photometric research [Fryc]. In a fully integrated hyperspectral scene generator, spatially complex scenes with high spectral fidelity would be generated. There is a leadership role for NMIs, responsible for the development and dissemination of radiometric calibration standards, in the development of advanced radiometric artifacts, in particular in multidisciplinary fields where no other government agency or standards organization has a mandate. In this work, we describe the development of an Advanced Radiometric Source (ARS) and give several example radiometric characterization and calibration applications of the technology.

Advanced Radiometric Sources

A variety of different approaches to the development of spectrally tunable sources have recently been described, including the use of spatial light modulators [Serati] or light-emitting diodes (LEDs) [Fryc, Gamma Scientific, Ries]. In this work, we describe an ARS based around a dispersing element and a spatial light modulator (SLM). The system is basically a spectrograph, with a spatial light modulator replacing the multi-element detector at the focal plane of the spectrograph. In this case, the dispersed light falls on the SLM, creating a relationship between the spatial location on the modulator and the wavelength of the light. By varying the transmittance or reflectance of the elements comprising the SLM, spectrally diverse distributions can be created. High fidelity spectral matches to a specific target distribution can be readily achieved, with the resolution defined by the properties of the imaging system. The system can be operated in either dc or ac mode, creating either constant or pulsed spectral distributions.

While a variety of SLMs can be used, the ARS described in this work uses a Digital Micromirror Device (DMD) as a spatial light modulator. DMDs are selectively and dynamically controllable, micro-mirror arrays; they are commonly found in projector displays and wide format televisions. DMDs use aluminum mirrors, and spectrally tunable sources can be created from the ultraviolet to the short-wave infrared, limited only details of the imaging system. Replacing the window, spatial light modulators can be created in the infrared as well.

An arbitrarily shaped spectrum, representing a target spectral radiance, is generated by turning on different numbers of elements of a micro-mirror column corresponding to the required wavelengths. The fundamental radiometric distribution of the source depends on the spectral output of the primary source and details of the imaging properties of the spectrograph. Consequently, the source intensity can be modulated by changing the number of mirror elements ‘on’ while maintaining a constant spectral distribution.

Example Applications

Colorimeters are calibrated against Illuminant A and their uncertainties when measuring sources with spectral distributions similar to Illuminant A are commonly provided. However, those data provide little information about the performance of colorimeters when measuring sources with different spectral distributions. Using the ARS, a variety of spectral distributions can be readily generated to provide a more useful or accurate metric for the evaluation of the general performance of colorimeters. Example distributions, for example distributions similar to those used to generate a Color Rendering Index for sources, will be presented and discussed.

The ARS can produce spectral distributions tailored to a particular application. In a specific application to be

presented, the ARS generates the spectral distributions of ocean color with varying chlorophyll concentrations. Instruments that measure ocean color can measure the same spectral distributions in the laboratory, thereby establishing or verifying their radiometric accuracy.

Summary

With the trend toward performance-based metrology requirements, NMIs well-defined role in measuring and verifying the performance of radiometric systems is becoming more critical. The development of spectrally tunable sources enables NMI measurement and calibration services to respond to new radiometric requirements by providing necessary, relevant technology that tests the end performance of radiometric systems used in critical applications.

Acknowledgments We would like to acknowledge and thank Jacqualine Jackson from the Brigham Young University for her assistance with this work.

References

Fryc, I., S. W. Brown, G. P. Eppeldauer, and Y. Ohno, LED-based spectrally tunable source for radiometric, photometric, and colorimetric applications, *Opt. Eng*., accepted for publication.

Gamma Scientific, Inc., San Diego, CA, USA; www. gamma-sci.com; RS-5M light source.

MacKinnon, N. et al., Spectrall programmable light engine for *in vitro* or *in vivo* molecular imaging and spectroscopy, *Appl. Opt.* 44, 2033-2040, 2005.

Nelson, N. R., P. Bryant, and R. Sundberg, Development of a hyperspectral scene generator, *Proc. SPIE* 5151, 480-484, 2003.

Ries, H., I. Leike, and J. Muschaweck, Optimized additive mixing of colored light-emitting diode sources, *Opt. Eng*. 43, 1531-1536, 2004.

Serati, S., T. Ewing, and J. Stockley, "New developments in high-resolution liquid-crystal spatial light modulators for wavefront control, *Proc. SPIE* 4825, 46-55, 2002.

Wall, C., et al., Construction of a programmable light source for use as a display calibration artifact, *Proc. SPIE* 4295, 259-266, 2001.

Novel subtractive band-pass filters based on coloured glasses.

E. Theocharous
National Physical Laboratory, Teddington, U.K.

Abstract. A novel type of band-pass filter is proposed and demonstrated. The filter is based on replacing the mechanical shutter used in radiometric measurements with a long-pass coloured glass filter. The performance of the new filter was evaluated and is compared to the performance of band-pass filters based on multi-layer dielectric (interference) filters. The new filter is simple, robust, should exhibit little ageing in comparison with dielectric filters, has a very smooth transmission profile and can be designed to have very broad bandwidths with a near "top hat" transmission profile. It has excellent out-of-band rejection for wavelengths shorter than the peak, while out-of band rejection for wavelengths longer than the peak is likely to be inferior compared to interference filters. However the performance of subtractive band-pass filters should be sufficiently good to allow their adoption in a number of applications.

Introduction

Long-pass coloured glass filters are widely available throughout the UV, visible and NIR. These filters are characterised by very sharp cut-off regions and are used extensively in a number of applications, including the suppression of the out-of-band transmission of dielectric filters and as "order sorting" filters in grating monochromators. If short-pass filters were available, then the combination of a short-pass and a long-pass filter will result in a band-pass filter offering a number of advantages over multi-layer dielectric band-pass filters. However, short-pass coloured glass filters do not exist. To overcome this problem, the author proposed and experimentally demonstrated [1] a novel type of subtractive band-pass filter. This filter relies on using one long-pass coloured glass filter and replacing of the mechanical shutter used in radiometric measurements with a second long-pass coloured glass filter whose cut-off wavelength is shifted from that of the cut-off of the first coloured-glass filter. The effective transmission of this subtractive band-pass filter at a wavelength λ is the difference of the transmissions of the two coloured glass filters at the same wavelength. This means that the transmission of the subtractive band-pass filter at long wavelengths (where the transmission of the two component coloured glass filters is high) is going to be zero provided the transmission of the two coloured glasses are equal. This condition is satisfied by the GG, OG and RG-series of long pass coloured glasses which have internal transmission well in excess of 99.9% for wavelengths longer than their transmission edges.

Results

Consider the case when a detector is monitoring the output from a broadband visible source through, say, an RG630 Schott glass filter [2]. The internal transmission of a 6 mm thick sample of RG630 glass calculated from reference 2 is shown in figure 1. Assume that the amplified detector signal with the RG630 filter in the beam as being V_{RG630}. Now instead of closing the shutter for the dark signal the author proposes replacing the RG630 filter with another filter say an RG645. The internal transmission of a 6 mm thick sample of RG645 glass is also shown in figure 1. The amplified detector output will now give a different signal, V_{RG645}. Consider the properties of the difference between the two readings, V_{RG610}-V_{RG645}. Simple calculations show that the difference is equivalent to the zero-corrected reading when a filter is inserted in the beam which has a transmission profile equivalent to the difference in the spectral transmission between the RG630 filter and the RG645 filter. This transmission profile is shown by the green trace in figure 1. It is obvious from figure 1 that the technique results in a band-pass filter whose short wavelength edge is governed by the transmission characteristics of the RG630 glass while the long wavelength edge is determined by the characteristics of the RG645 coloured glass. In this particular case the resulting "subtractive" band-pass filter has a Full Width Half Maximum (FWHM) bandwidth of approximately 25 nm. Furthermore, because the transmission characteristics of the two coloured glasses are smooth, the transmission of the resulting band-pass filter also has a smooth profile, unlike the case for interference filters of similar transmission characteristics. It is important to remember that this process does NOT require a "dark signal" measurement since the stray light and drifts in the detector amplification system are common to the measurements made with the RG630 and RG645 filters and therefore the subtraction process eliminates their effects.

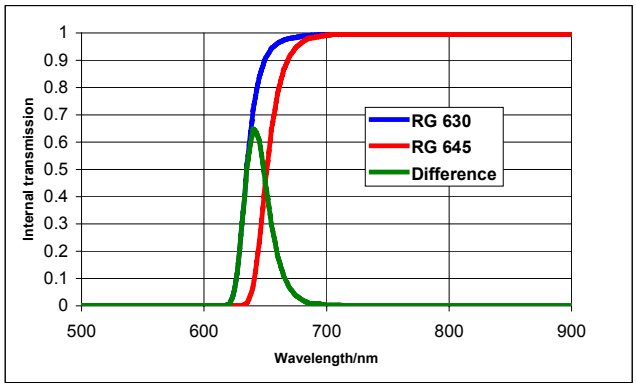

Figure 1. Transmission characteristics of a 6 mm thick RG630 glass (blue line), a 6 mm thick RG645 glass (red line) as well as the effective transmission characteristics of the subtractive band-pass filter resulting from this combination (green line).

Figure 2 shows (on a logarithmic scale) the experimentally measured (external) transmission characteristics of a 6 mm thick RG665 coloured glass filter, as well as the measured transmission of a 6 mm thick RG715 nm glass. Also shown in figure 2 is the transmission of the resulting subtractive band-pass filter. This filter peaks at 685 nm, has a FWHM bandwidth of approximately 35 nm, peak external transmission of 90% and a very smooth profile. Data shown in Figure 2 were plotted on a logarithmic scale in order to illustrate the out-of-band transmission of the subtractive band-pass filter. The subtractive filter has excellent blocking for all short wavelengths whereas the transmission for wavelengths longer than 800 nm appears to be lower than 0.1%. However, the effective transmission is lower than that 0.1% and this is confirmed by the broken line. The line is broken because the values of the measured transmission were negative at some wavelengths and negative values cannot be plotted on a logarithmic plot.

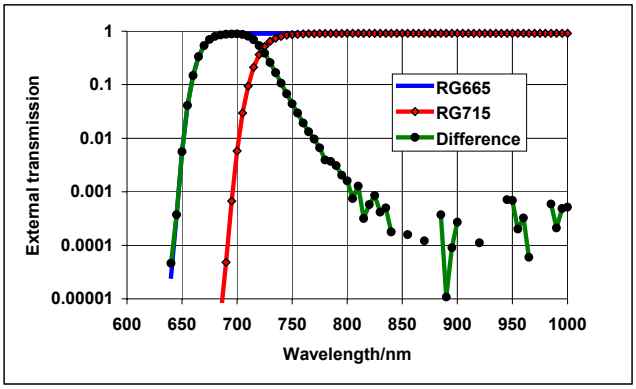

Figure 5: Experimentally measured external transmission characteristics of a 6 mm thick RG665 coloured glass filter, a 6 mm thick RG715 filter as well as the measured transmission of the resulting subtractive band-pass filter (note logarithmic scale).

The performance of the new subtractive band-pass filter was evaluated and was compared to the performance of band-pass filters based on multi-layer dielectric (interference) filters. The new band-pass filter is simple, robust, should exhibit little ageing compared to multi-layer dielectric filters, has a very smooth transmission profile and can be designed to have very broad bandwidths with near "top hat" transmission profiles. It has excellent out-of-band rejection for wavelengths shorter than the peak, while out-of band rejection for wavelengths longer than the peak is expected to be inferior compared to some multi-layer dielectric filters. However the performance of subtractive band-pass filters should be sufficiently good to allow their adoption in a number of applications. The experimental investigation of subtractive bandpass filters will be described and a number of potential applications of the subtractive band-pass of filters will be discussed.

Reference

1. E. Theocharous "Novel band-pass filters based on coloured glasses", *NPL report* No. COAM N3, March 2004.
2. Filter'99 Version 1.1US program available from Schott Glass Technologies Inc., Duryea, PA 18642, USA

Analysis of the Uncertainty Propagation through Fitting Spectral Irradiance Data

S. Nevas[1], A. Lamminpää[1], P. Kärhä[1], and E. Ikonen[1,2]

[1] Metrology Research Institute, Helsinki University of Technology (TKK), P.O.Box 3000, FI-02015 TKK, Finland

[2] Centre for Metrology and Accreditation (MIKES), P.O.B. 239, FI-00181 Helsinki, Finland

Abstract. Uncertainties and correlations are propagated in absolute spectral irradiance scale, where a modified Planck's radiation law is fitted to filter radiometer (FR) data. The lack-of-fit error component is included in the uncertainty analysis with the purpose of finding an optimal degree for the polynomial describing the effective emissivity of quartz-tungsten halogen lamps.

Introduction

Absolute scales of spectral irradiance are widely established using detector-based facilities [1, 2, 3, 4, 5, 6]. In general, such scales are realized at discrete wavelengths while the irradiance over the entire spectral range is obtained by interpolation or fitting, as suggested for example in [7]. It has been shown recently that rigorous uncertainty analysis for the derived spectral irradiance values requires correlations through fitting and those in the FR data to be determined and included in the propagation of uncertainties and covariances [8, 9, 10]. This is also required by the internationally agreed rules for expressing uncertainties in measurements [11].

In our earlier report we presented analysis of the propagation of the uncertainties and covariances in the spectral irradiance scale where the lamps are measured directly, without the use of a black body radiator [10]. The study estimated the effect of the correlations in the FR data on the fitted irradiance values. The other useful finding of the uncertainty analysis including correlations between the fitted parameters was that it could be useful for selecting the FR wavelengths.

In this contribution, we expand the study to include the lack-of-fit component in the uncertainty of the fitted values. The lack-of-fit error and the propagated uncertainty are both depended on the description of the effective emissivity of the lamp. The purpose of the analysis is to find an optimal degree for the emissivity polynomial such that the observed overshoots in the output uncertainty between the FR wavelengths are reduced while keeping the lack-of-fit error reasonably small.

Propagation of Uncertainties in FR Data

With the purpose of studying the propagation of uncertainties and correlations through the spectral irradiance scale, where a modified Planck's radiation law is fitted to a full range of FR data points, we applied the matrix formalism by Woeger [10, 12]. In the modified Planck's formula being fitted, an N^{th}-degree polynomial was employed for the description of the effective emissivity of quartz-tungsten halogen lamps [5, 10]. The coefficients of the polynomial were determined during the fitting.

Results of the Analysis

The uncertainties of the spectral irradiance propagated from those in the FR measurements (input uncertainty) of a 1-kW FEL-type lamp (same as the one analyzed in [10]) through the fitting are plotted in Figure 1. Here, for demonstrational purposes the FR data point at 850 nm was excluded from the analysis. From the figure it would appear that the uncertainties in the fitted spectral irradiance values could be reduced by decreasing the order of the emissivity polynomial. However, as can be seen from Figure 2 the decrease in the order of the polynomial has an opposite effect on the lack-of-fit error. The increase in the lack-of-fit error is especially pronounced at the lower wavelengths where the effective emissivity of tungsten lamps has a complex structure [5]. It can be also noticed from Figure 1 and Figure 2 that the use of higher-order emissivity polynomial although reduces the lack-of-fit error, but at the same time it may cause overshoots in the uncertainty between the FR wavelengths. It has to be noted, however, that the presence of strong correlations in FR data would lead to a lower level of oscillations in the propagated uncertainty [9, 10]. Having correlation coefficients of 0.5 between all wavelengths reduces the amplitude of the uncertainty oscillations at longer wavelengths as shown in Figure 1 by almost one third.

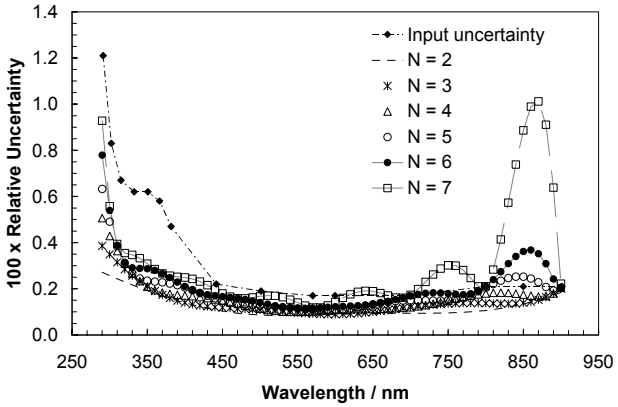

Figure 1. Uncertainty propagation through fitting the Planck's radiation law modified by N^{th}-degree emissivity polynomial to the FR data. The input uncertainty is the uncertainty in the FR measurements at discrete wavelengths. The output uncertainties denoted as N = 2,…, N = 7 were calculated for 290 to 900 nm wavelengths with a 10 nm step and no correlations between the FR-measured values.

In Figure 3, the uncertainty component due to the lack-of-fit error is shown together with the uncertainty propagated from the FR measurements when the lack-of-fit uncertainty is and is not included. The lack-of-fit

uncertainty component was estimated as a standard deviation of the differences between the fitted and measured spectral irradiance values at the FR wavelengths. The combined uncertainty was calculated by quadratically adding the propagated uncertainty and that due to the lack-of-fit error. The uncertainties depicted in Figure 3 represent average of the values calculated every 10 nm within 290 to 900 nm spectral range. As can be seen from the figure, if average uncertainties over the whole spectral range are considered the selected 6th-degree polynomial is an optimal choice for the description of the effective emissivity of the tungsten lamp. However, this may not necessarily be true if individual wavelengths are considered, such as those within 800 to 900 nm range where an overshoot in the propagated uncertainty is caused by the high order of the polynomial. It can be also noticed from the figure that the 6th-degree polynomial remains still an optimal choice even if moderate correlations in the FR data are considered.

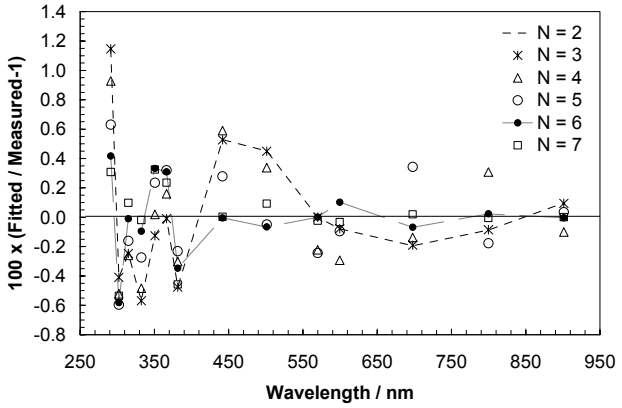

Figure 2. Relative difference between the measured and fitted spectral irradiance values when the effective emissivity is modeled by Nth degree polynomial.

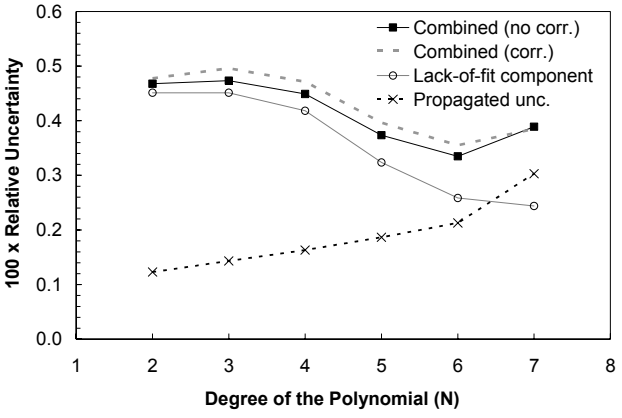

Figure 3. The lack-of-fit uncertainty component (open circles), the uncertainty propagated from the FR-measurements without correlations at the input values (crosses), and their quadratic sum (filled squares). The uncertainty denoted as combined correlated (dashed line) is the result with a correlation coefficient of 0.5 in the FR data. The uncertainties are plotted as a function of the degree of the emissivity polynomial. The shown values are averages of all the values calculated over 290 to 900 nm wavelengths with a 10 nm step.

Conclusions

We propagated the uncertainties and correlations in the primary spectral irradiance scale where the irradiance of a lamp is obtained from direct measurements with filter radiometers (FRs). The lack-of-fit component was also included in the uncertainty calculations. The effect of the degree of the polynomial describing the effective emissivity of the lamp on the lack-of-fit error and on the propagated uncertainty values was studied with the purpose of finding an optimal value. The mathematically optimal degree of the emissivity polynomial was found to remain the same even in the case of moderate correlations in the FR data.

References

1. Boivin L.P., Gaertner A.A., Analysis of the uncertainties involved in the realization of a spectral irradiance scale in the infrared at the NRC, *Metrologia*, *28*, 129-134, 1991.
2. Anderson V.E., Fox N.P., A new detector-based spectral emission scale, *Metrologia, 28*, 135-139, 1991.
3. Johnson B.C., Cromer C.L., Saunders R.D., Eppeldauer G., Fowler J., Sapritsky V.I., Dezsi G.A, A method of realizing spectral irradiance based on an absolute cryogenic radiometer, *Metrologia, 30*, 309-315, 1993.
4. Sperfeld P., Raatz K.-H., Nawo B., Möller W., Metzdorf J., Spectral-irradiance scale based on radiometric black-body temperature measurements, *Metrologia, 32*, 435-439, 1995.
5. Kübarsepp T., Kärhä P., Manoocheri F., Nevas S., Ylianttila L., Ikonen E., Spectral irradiance measurements of tungsten lamps with filter radiometers in the spectral range 290 nm to 900 nm, *Metrologia, 37*, 305-312, 2000.
6. Yoon H. W., Gibson C. E., Barnes P. Y., Realization of the National Institute of Standards and Technology detector-based spectral irradiance scale, *Appl. Opt., 41*, 5879-5890, 2002.
7. Walker J. H., Saunders R. D., Jackson J. K., McSparron D. A., NBS measurement services: spectral irradiance calibrations, *Natl. Bur. Stand. Spec. Publ., 250-20*, 1987.
8. Gardner J. L., Correlations in primary spectral standards, *Metrologia, 40*, S167-S171, 2003.
9. Gardner J. L., Uncertainty propagation for NIST visible spectral standards, *J. Res. NIST, 109*, 306-318, 2004.
10. Nevas S., Ikonen E., Kärhä P., and Kübarsepp T., Effect of correlations in fitting spectral irradiance data, *Metrologia, 41*, 246-250, 2004.
11. Guide to the Expression of Uncertainty in Measurement, 101 p., *International Organization for Standardization,* Geneva, 1993.
12. Woeger W., Uncertainties in models with more than one output quantity, in *CIE Proceedings of the CIE Expert Symposium 2001*, pp. 12-17, CIE, Vienna, 2001.

Absolute linearity measurements on a PbS detector in the infrared

E. Theocharous
National Physical Laboratory, Teddington, U.K.

Abstract. The non-linearity characteristics of a commercially available thin-film photoconductive PbS detector were experimentally investigated in the infrared using the NPL detector linearity characterization facility. The deviation from linearity of this detector was shown to be significant even for relatively low values of radiant power incident on the active area of the detector. For example, the linearity factor was approximately 0.8 when 0.6 μW of radiant power at a wavelength of 2.2 μm was illuminating a spot of 1 mm in diameter on the active area of the PbS detector. These figures demonstrate the very poor linearity characteristics of this detector and provide a warning to other users of PbS detection systems. The deviation from linearity was shown to be a function of the size of the spot being illuminated on the detector active area, as well as the wavelength of the incident radiation. The plot of the linearity factor as a function of irradiance was shown to be independent of the wavelength of radiation illuminating the detector as well as the area of the spot being illuminated, thus confirming that the non-linearity is a function of the incident spectral irradiance.

Introduction

PbS detectors are widely used in radiometry for the detection of infrared radiation in the 1 μm to 3.2 μm wavelength region as well as in instruments such as gas analysers. This is because PbS detectors offer relatively high D* values in this wavelength region at relatively high operating temperatures, which can be attained by thermoelectric coolers [1, 2]. Photoconductive (PC) PbS detectors are operated with a constant DC bias current to sense the photo-generated change in the detector electrical conductance, which should be proportional to the radiant power incident on the detector. While the change in the conductance at low incident radiant power levels is expected to be proportional to the change of the incident radiant power, at higher radiant power levels the dependence is expected to be non-linear.

The purpose of this paper is to report the results of an experimental investigation carried out at NPL into the characterization of the linearity of a commercially available thin-film PC PbS detector. Special care was paid to the identification of the true dependence of the deviation from linearity of this detector on parameters such as the area of the detector being illuminated by the incident radiation as well as the wavelength of the incident radiation.

The PbS detector whose linearity characteristics are reported in this paper was manufactured by Hamamatsu [2], Model No. P2682-01. The detector had a 4mmx5mm active area and was mounted in a hermetically sealed TO-8 package so it could be cooled using a two-stage thermoelectric cooler. A Hamamatsu C1103-series temperature controller was used to maintain the PbS detector at –20 ^{o}C throughout the work described in this paper. The detector was biased with a 10 V bias voltage and had a 560 kΩ load resistor, as recommended by the detector manufacturer [2]. A modulation frequency of 70 Hz was used throughout the characterisation of this detector.

Results

The NPL detector linearity measurement facility was used to evaluate the linearity characteristics of the PbS detector. A full description of this facility, which is based on the double-aperture linearity measurement method, can be found elsewhere [3]. The linearity of the PbS detection system was investigated at 1.3 μm and 2.2 μm in order to identify the dependence of the non-linearity on the wavelength of the incident radiation. A tungsten strip lamp with a 2 mm wide element and a silica window was used as a source for all measurements performed. The double-aperture linearity characterization method was adopted for these measurements because it is an absolute linearity measurement method. The adoption of a relative linearity measurement method would have required the availability of an infrared detection system whose linearity characteristics are known. Field stops of diameters 1.8 mm, 1.0 mm and 0.76 mm were used in order to identify the dependence of the linearity factor on irradiance. The magnification of the optics used to image the field stop on the active area of the PbS detector was unity (two identical off-axis parabolic mirrors were used) so the diameter of the spot formed on the active area of the test detector was equal to the diameter of the field stop. Knowledge of the diameter of the illuminated patch allowed the irradiance (radiant areance) to be calculated.

The absolute spectral responsivity of the PbS detector was measured on the NPL infrared responsivity measurement facility [4] so the output voltage could be converted to radiant power incident incident on the detector.

Figure 1 shows the linearity factor of the PbS detector as a function of radiant power incident on the detector when the radiant power is imaged into spots of 0.76 mm, 1 mm and 1.8 mm diameter, for radiation of wavelength 1.3 μm and 2.2 μm. Figure 1 confirms that the linearity factor is strongly dependent on spot diameter. Data in Figure 1 are plotted on a linear scale to demonstrate that for low incident radiant powers the linearity factor decreases linearly with increasing radiant power.

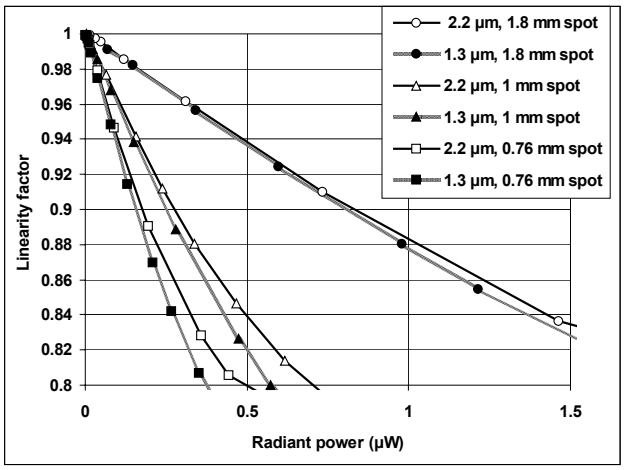

Figure 1. Linearity factor of the PbS detector as a function of incident radiant power at 1.3 µm and 2.2 µm for 0.76 mm, 1 mm and 1.8 mm diameter spots illuminating the active area of the detector.

Figure 2 shows the linearity factor of the PbS detector as a function of irradiance (radiant areance) incident on the detector when the radiant power is imaged into spots of 0.76 mm, 1 mm and 1.8 mm diameter, for radiation of wavelength peaking at 1.3 µm and 2.2 µm. Figure 2 shows that the linearity factor plotted as a function of irradiance is largely independent on the diameter of the illuminating spot and the wavelength of the incident radiation. It is therefore safe to conclude that the plot of the linearity factor as a function of irradiance is independent of the illumination conditions and the wavelength of incident radiation. It is therefore this parameter which should be used in correcting for the non-linear behaviour of PbS detectors [5]. This is only valid for irradiance values below 1 µW mm^{-2}, whereas for higher irradiance values at the 2.2 µm wavelength, the dependence of the linearity factor on irradiance ceases to be linear and "oscillations" are observed on the linearity factor versus irradiance plots (see Figure 2).

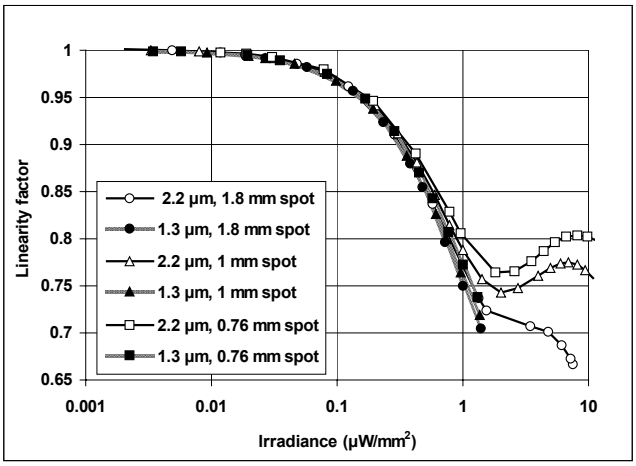

Figure 2: Linearity factor of the PbS detector as a function of incident irradiance at 1.3 µm and 2.2 µm for 0.76 mm, 1 mm and 1.8 mm diameter spots illuminating the active area of the detector.

The dependence of the linearity factor on irradiance suggests that the heating effect due to the incident radiation and the subsequent rise in the local temperature of the detector could be the source of the non-linearity. The temperature coefficient of response of the PbS detector was investigated and was shown to be independent of the bias voltage in the 5 V to 10 V bias voltage range. The values of the temperature coefficient of response of the PbS detector were measured to be -3.44 % $^{o}C^{-1}$ and -3.08 % $^{o}C^{-1}$ at 2.2 µm and 1.6 µm respectively for a detector temperature of -10 ^{o}C. The corresponding values of the temperature coefficient of response of the PbS detector were -3.10 % $^{o}C^{-1}$ and -2.77 % $^{o}C^{-1}$ at 2.2 µm and 1.6 µm respectively for a detector temperature of -16 ^{o}C. The corresponding values increase to -4.04 % C^{-1} and -3.86 % $^{o}C^{-1}$ at 2.2 µm and 1.6 µm respectively for a detector temperature of 0 ^{o}C. The negative sign indicates that the response of the detector decreases as the temperature increases. These figures indicate that it is unlikely that the observed non-linearity is due to the local increase in the detector temperature, as this would require local temperature increases above 10 ^{o}C.

Reference

1. http://www.calsensors.com
2. http://usa.hamamatsu.com/assets/applications/ssd/characteristics_and_use_of_infrared_detectors.pdf
3. E. Theocharous, J. Ishii and N. P. Fox, "Absolute linearity measurements on HgCdTe detectors in the infrared", *Applied Optics*, **43**, 4182-4188, 2004.
4. E. Theocharous, F. J. J. Clarke, L. J. Rogers, N. P. Fox, "Latest measurement techniques at NPL for the characterization of infrared detectors and materials", *Proc. of SPIE* Vol. **5209**, 228-239, 2003.
5. C. L. Sanders, "Accurate Measurements of and Corrections for Nonlinearities in Radiometers", *J. Res. Nat. Bur. Stand*, **76A**, 437-453, 1972.

Comparison of two methods for spectral irradiance scale transfer

K. M. Nield, J. D. Hamlin and A. Bittar
Measurement Standards Laboratory of New Zealand (MSL), IRL, Lower Hutt, New Zealand.

Abstract.
In the past at MSL transfer of spectral irradiance scales have been made via a commercial spectroradiometer. This resulted in large uncertainties in the ultraviolet region due to temporal instability of the spectroradiometer and low S/N ratios. More recently, and to meet the requirements of users in New Zealand measuring small changes in atmospheric solar ultraviolet irradiance levels, the calibrations have been transferred to a dedicated, double monochromator based system. This move warranted a closer examination of two options for input optics to the monochromator that have been used extensively at several NMIs to achieve smaller transfer uncertainties (Wilkinson, 1998, Walker et al, 1987), especially in the ultraviolet wavelength range.

This paper will outline these two options, being an integrating sphere and a flat diffusing plate, and the transfer methodologies that enable direct comparison of spectral irradiance sources via a common monochromator (Kostkowski, 1997). The main sources of possible error and uncertainty considered for each of these are: S/N, geometrical effects and source uniformity. These will be described and compared and the achievable uncertainties in transferring a scale of spectral irradiance in the ultraviolet wavelength region with each methodology compared. The usefulness and applicability of each method is then highlighted.

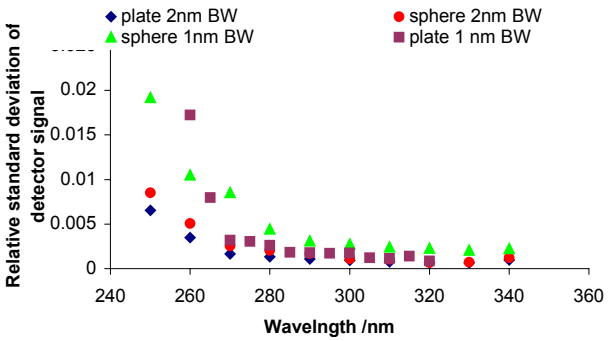

Figure 1. Relative standard deviation of the output current from the photomultiplier tube (PMT), mounted at the exit slits of the monochromator, detecting the irradiance source. The 2 nm bandwidth measurements for both the plate and the sphere methods used an Oriel 57860 solar blind filter for stray light reduction and a PMT voltage of 1000 V. In the case of the 1 nm bandwidth measurements the sphere method used the previously mentioned stray light filter however, the plate method measurements used a UG11 stray light filter which had much lower transmittance than the Oriel filter below 270 nm; the PMT voltage was 1100 V for the sphere method and 800 V for the plate method.

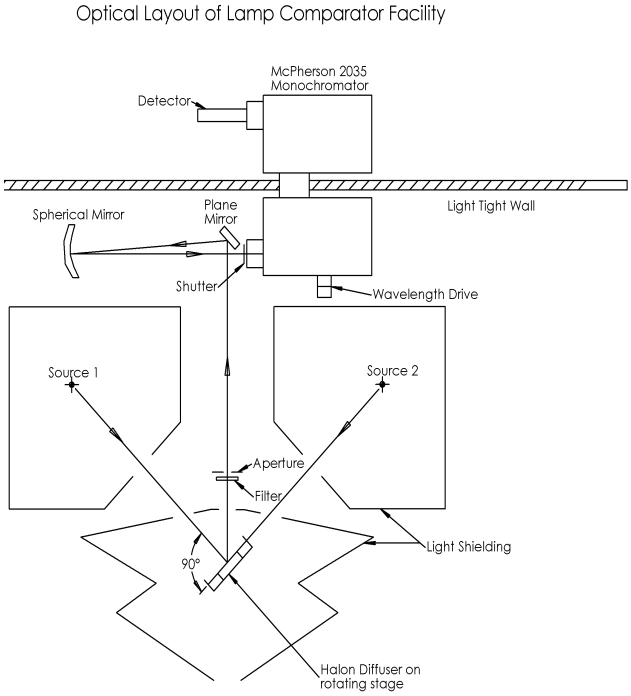

Figure 2. Arrangement for the flat plate diffuser comparator. Each source is mounted normal to the diffuser with the diffuser at 45 ° to the entrance optics of the monochromator. For a given calibration a repeat measurement is made with the lamps alternated between positions Source 1 and 2.
In the case of the integrating sphere method the sphere replaces the diffuser with its exit port normal to the entrance optics of the monochromator. The entrance port of the sphere is at 90 ° to exit port; the sphere rotates 180 ° about the entrance optics axis. The Source 1 and 2 positions are located either side of the sphere normal to the entrance port.

Acknowledgements
The authors would like to acknowledge Mr. Malcolm White, formerly MSL, for establishing the monochromator system and suite of software upon which this facility is based.
This work was funded by the New Zealand Government as part of a contract for the provision of national measurement standards.

References

Wilkinson. F., NMIA, Australia (formerly NML, CSIRO), personal communication describing the spectral irradiance facility at that laboratory, April 1998.
Kostkowski, H. J., Reliable spectroradiometry, Spectroradiometry Consulting, 1997.
Walker. J. H. Saunders. R. D. Jackson. J. K. McSparron. D. A., Spectral irradiance calibration, National Bureau of Standards, NBS/SP-250/20, September 1987

Precision Extended-Area Low Temperature Blackbody BB100-V1 for IR Calibrations in Medium Background Environment

S. Ogarev, M. Samoylov, V. Sapritsky, A. Panfilov
All Russian Research Institute for Optical and Physical Measurements (VNIIOFI), Moscow, Russia.

Suzuki Koichi, Takahiro Kawashima
NEC Toshiba Space Systems, Ltd., Tokyo, Japan

Abstract. Paper reviews a new large-area high-precision blackbody BB100-V1, designed at the All-Russian Research Institute for Opto-Physical Measurements (VNIIOFI, Russia) as a source within 240 to 350 K temperature range for preflight calibration of space-borne radiometric instruments at such research organizations as NEC TOSHIBA Space Systems and JAXA (Japan), Keldysh Space Center (Russia). The temperature non-uniformity and long-term stability account for less than 0.1K and 0.1% for 1.5 μm to 15 μm wavelength region under cryo-vacuum conditions of medium background environment.

Introduction

The 10-year implementation plan for the GEOSS ("The Global Earth Observation System of Systems") program by representatives of more than 50 countries and more than 30 international organizations, besides the other tasks, assumes development of optical instruments that can measure radiance, reflective properties, and radiant temperature of objects of observation [1]. Calibration of IR sensors, thermal imagers, instrumentation for remote earth sensing, signature recognition, and low background spaceborne radiometers requires development of low- and near-ambient-temperature reference standard sources capable of operating in vacuum at low or medium background conditions. The required accuracy and long-term stability of measurement account correspondingly for 0.1% and 0.02% per decade within the 0.2 to 3 μm spectral region; and 0.1K and 0.01K per decade for 3 to 15 μm region. The most stringent requirements for radiometric measurements come from climatology, which requires decades-long high-quality time series. The uniformity of those measurements should be based upon uniform scales for the radiometric quantities to be measured – spectral radiance and spectral irradiance. The requirements can only be met if the ground calibration is executed at a very high level of accuracy. As an additional requirement, many applications require a compact standard planckian source – blackbody (BB) for near ambient temperatures operating both in vacuum and in air with optional window and having high accuracy in temperature setting.

In order to provide complete metrological support and such precise pre-flight calibration of spaceborne instruments, the development of precision BB sources of radiation operating within VIS-IR wavelength ranges, like BB100-V1, is of a great importance.

Blackbody BB100-V1 specifications

The blackbody BB100-V1 under consideration is basically an extended area blackbody for low temperatures (250 K up to 350 K), which operates under cryo-vacuum conditions. The BB100-V1 was designed and manufactured designed at the All-Russian Research Institute for Opto-Physical Measurements (VNIIOFI, Russia) for calibration of space-borne radiometric instruments at NEC TOSHIBA Space Systems; JAXA (Japan), and Keldysh Space Center (Russia). BB100-V1 specifications (obtained in tests) are presented in Table 1.

Table 1. BB100-V1 specifications

Parameter	Value
Operating temperature range	240 K - 350 K
Spectral range	1.5 μm – 15 μm
Cavity effective emissivity	0.997 ± 0.001
Opening (non-precision aperture)	Ø100 mm
System Field-of-View (FOV)	12 mrad (0.688º)
Environment operation conditions	Vacuum chamber (10^{-6} Torr, below 100 K)
	Air environment (clean room at 23 ± 3ºC)
Temperature non-uniformity across opening	0.1 K
Temperature set point resolution	0.01 K
Maximum temperature instability under thermostabilization	0.05 K
Limitation on the blackbody warning-up time (approx.)	2 hrs.
Total Wattage (approx.)	3500 W (with usage of thermostat LAUDA Proline PR1845)
Input Voltage	100 V AC or 200 V AC
Blackbody temperature set up and control	External controller with RS-232 interface to (optional) PC computer
Temperature sensors for control system	Pt RTD, 5 pieces (by MINCO Products, Inc.)
Calibration traceability of Pt RTD to NIST	Yes, assumed for one Pt RTD only
Operating Environment Pressure	10^{-6} Torr
Orientation of the blackbody	Facing down (±30º leaned)
Cable (tubing) length	5 m inside and outside vacuum chamber

BB100-V1 prototypes and realization

In order to meet the requirements to accuracy and long-term stability of measurements, the design of BB100-V1 was based on the prototypes of high-precision unique BBs developed within the last decade at VNIIOFI [2,3]. Among them there are variable-temperature and fixed-point models BB100, BB300, BB900, BB1000,

VTBB, BB29Ga, and BB156In with 100 K to 1000K working temperature range, designed for calibration of spaceborne IR sensors and high-precision radiometry at such research organizations as German Aerospace Center (DLR) and Physikalisch-Technische Bundesanstalt (Germany), National Physical Laboratory (UK), Space Dynamics Lab (USA), NIM and IAO (China).

Cavity-type BB100-V1 as a source of thermal radiation features a series of advantages over any other thermal sources – such as high reproducibility, low sensitivity of its effective emissivity to variations and degradation of optical properties of its cavity inner surface.

Low-temperature and cryogenic BB100-V1 is build up on the principles of the usage of external liquid-based thermostat LAUDA Proline PR1845-LCK1891 with circulating coolant KRYO-51 in a closed loop.

As a material of radiating cavity for low-temperature and cryogenic BB one can use copper and aluminum alloys. The necessary value of emissivity was obtained with the usage of black cover paints, e.g. Chemglaze Z-302 for BB29gl blackbody or Nextel Velvet 811-21 for BB100 / BB100-V1 radiation sources. While identifying appropriate coating for BB-100V1 bottom possessing emissivity better 0.9 in the spectral range of interest (see Fig. 1), the Nextel Velvet Coating 811-21 was chosen by ourselves after comparative analysis of several comprehensive reviews [e.g., 4] on application and optical properties of black paints and various coatings to stray light suppressing, solar energy absorbing, for thermal detectors of optical radiation, radiation losses control, etc.

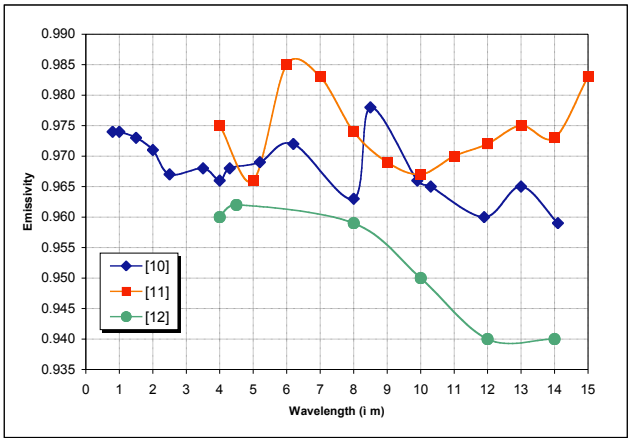

Figure 1.
Spectral emissivity of Nextel Velvet Coating 811-21

It is enough to assume that the spectral hemispherical emissivity of Nextel 811-21 is within 0.935…0.990 interval for wavelength range from 1.5 to 15 μm. The measurements of reflectance performed for the predecessor of Nextel 811-21, the 3M Velvet Black, show the presence of a small specular component, less than 10% from overall hemispherical reflectance; the diffuse component of reflectance has the near-Lambertian BRDF.

The drawing of BB100-V1 design performed with the account of above-mentioned studies is depicted in Fig. 2.

The computations of the normal effective emissivities of an isothermal cavity depicted in Fig.2 using STEEP3 [5] software. We have used the limiting values of wall emissivity (0.935 and 0.990) and 4 values of wall diffusity. The results of computations are presented in Table 2.

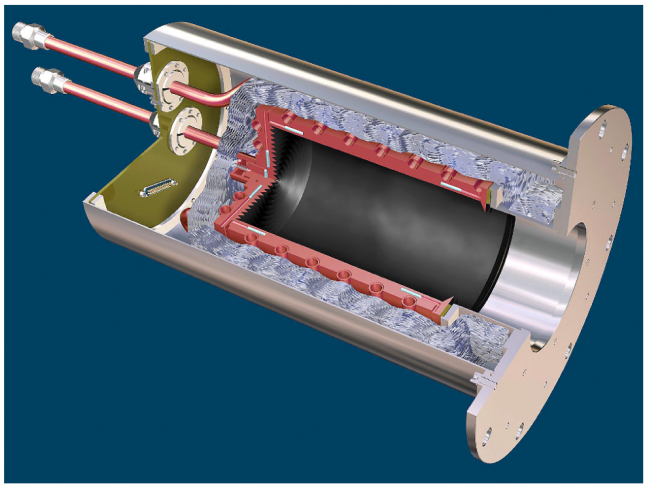

Figure 2. BB100-V1 cross-section.
Cavity dimensions: 200 mm length x 120 mm diameter.

Table 2.
Normal Effective Emissivity of BB100-V1 Isothermal Cavity

Cavity Wall Emissivity	Cavity Wall Diffusity			
	0.7	0.8	0.9	1.0
0.935	0.9972	0.9976	0.9980	0.9983
0.990	0.9996	0.9996	0.9997	0.9997

The BB100-V1 is currently under testing in cryo-vacuum chamber. The uncertainty of thermodynamic temperature reproducibility of BB100-V1 within working temperature ranges did not exceed 0,5K (1σ). The temperature non-uniformity and long-term stability account for less than 0.1K and 0.1% for 1.5 μm to 15 μm wavelength region under cryo-vacuum conditions of medium background environment. The results of these measurements will be presented in the paper.

References

[1] V.I.Sapritsky, S.P.Morozova, B.E.Lisiansky, S.A.Ogarev, M.K.Sakharov, M.L.Samoylov, A.S.Panfilov, B.B.Khlevnoy, V.E.Privalsky "The Global Earth Observation System of Systems (GEOSS) and problems of measuring the radiant properties of objects of observations" . Proceedings of NEWRAD'2005 (in print).

[2] V.I.Sapritsky, S.A.Ogarev, B.B. Khlevnoy, M.L.Samoylov, V.B.Khromchenko "Blackbody sources for the range 100 K to 3500K for precision measurements in radiometry and thermometry" – in Proceedings of the 8th Symposium on temperature: its measurement and control in science and industry. Chicago, IL, U.S.A. October 21-24, 2002.

[3] V.I.Sapritsky, V.B.Khromchenko, S.N.Mekhontsev, M.L.Samoilov, A.V.Prokhorov, S.A.Ogarev, A.Shumway "Medium Background Blackbody BB1000". Conference CD of CALCON'2000. SDL, Utah, USA, 2000.

[4] Hameury J, Hay B, Filtz J R 2003 Measurement of Infrared Spectral Directional Hemispherical Reflectance and Emissivity at BNM-LNE – Paper presented at the Fifteen Symposium on Thermopysical Properties, June 22-27, 2003, Boulder, CO, USA

[5] STEEP3, version 1.3. User's Guide. Virial, Inc., NY, 2000

Flash Measurement System for the 250 – 2100 nm Wavelength Range

J. Blanke and G. Mathe
Instrument Systems GmbH, Munich, Germany

Modern flash lamp systems are extensively used by manufacturers of solar panels for quality assurance as well as research and development issues. Demands on the state-of-the-art solar panels for terrestrial and space applications are very high. Therefore a reliable characterization and calibration of the test equipment on a regular basis is essential. The measurement of the spectral irradiance of flash lamp systems has evolved to an important application.

A solar-like spectral distribution (AM1.0, AM1.5) with total irradiance levels of one or multiple solar constants (1 SC = 1371 W/m^2) and perfect homogeneity over areas of several square meters is required to test large panels. A realization with steady-state solar simulators is difficult. Therefore solar simulators equipped with flash tubes are used to irradiate the solar panels.

The spectrum varies during the rising and falling flanks of the flash signal. A fast and reliable shutter controlled by electronic timers is needed to limit the "effective" flash measurement time to the stable plateau only.

Figure 1 shows a time resolved flash measurement as an example: A steep rising of the irradiance followed by a stabilization period within the first roughly 500 µs. The stable plateau typically lasts from one to ten milliseconds.

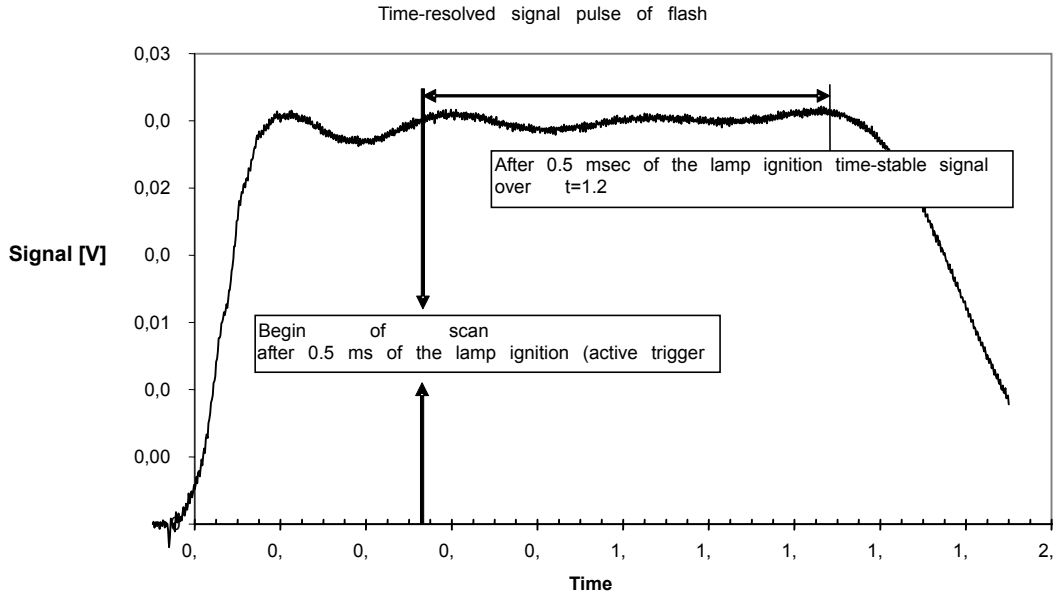

Figure 1. Flash measurement of a solar simulator. A stable plateau is reached about 0.5 ms after the lamp ignition.

Array spectroradiometers are ideal for measuring these types of light sources.

In contrast to scanning spectrometers a broad spectral range can be captured simultaneously and within a few milliseconds. However, a single array spectrometer is not able to measure the whole solar spectrum with a sufficient spectral resolution. Therefore a setup with three different array spectrometers that are connected to a single optical probe via a trifurcated fiber bundle has been developed by Instrument Systems Germany.

Figure 2 describes the setup schematically. The UV/VIS spectrometer covers a wavelength range between 200 nm and 850 nm, the IR1 model is equipped with an InGaAs array and can be used from 800 nm to 1650 nm. The IR2 model makes use of an extended InGaAs array offering a spectral range from 1400 nm to 2150 nm.

The flash measurement system is able to measure the spectral irradiance of a minimum 1ms flash plateau from 200nm up to 2150nm and the sensitivity ranges from ~ 1–20 solar constants (1.4 - 28 kW/m^2). The software controls high speed triggering and prepares the data for evaluation.

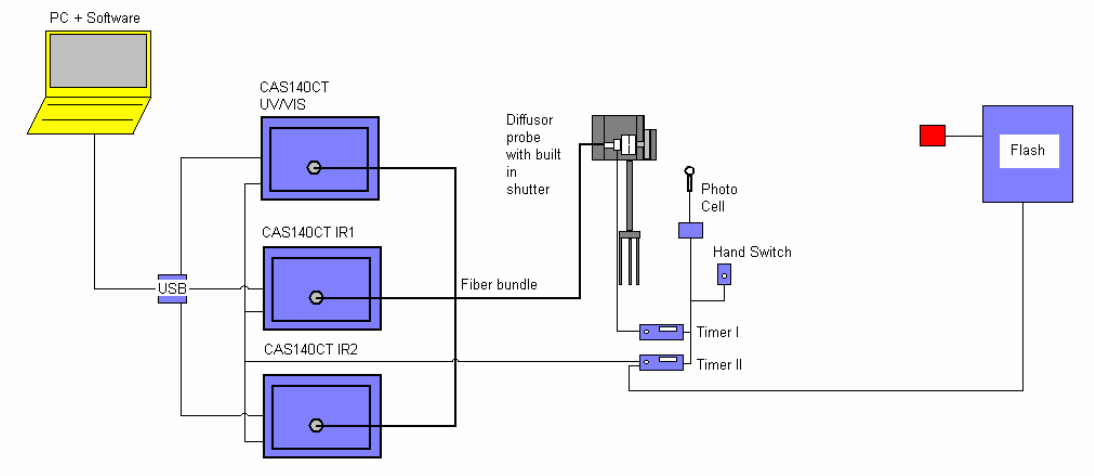

Figure 2. Layout of the measurement setup. The system can be triggered either by actively triggering the flash or by the signal of a photocell.

References

Espinar, B., Blanke, J., Ramírez, L., Bolós, M., Rodríguez, J.A., Blanco, M., Measurement of the spectral distribution of globar solar radiation and its components by the SPECTRO 320D Scanning Spectrometer, *Measurement and modeling of Solar Radiation & Day-light Conference*, Edinburgh, September 2003.

A normal broadband irradiance (Heat Flux) calibration facility

M. Ballico and E. Atkinson
National Measurement Institute of Australia, Lindfield Australia

Abstract. The existing heat flux scale in Australia is based on a set of thermopile and Gardon type sensors, calibrated against a room temperature ESR using an 800°C blackbody filtered by crown glass. NMIA has recently set up a new calibration system based on heat-pipe blackbodies with temperatures measured on the ITS-90, calibrated apertures and careful control of the ambient infra-red radiances. As measurements are made in air, corrections based on LOWTRAN data are made to the data, and the accuracy of this correction has been assessed using inert purging of part of the optical path. The facility is used to allow confirmation of the spectral flatness of heat-flux sensors into the thermal IR.

Introduction

Heat flux sensors are often calibrated under total hemispherical irradiance conditions by inserting the sensor fully into the mouth of a large blackbody source at a known temperature and using Planck's law to calculate the irradiance [1]. This technique places significant thermal load on the detector, requiring water cooling, but avoids problems of atmospheric absorption, since the gas in the blackbody is at essentially the same temperature as the radiation field.

The present standard used in Australia [2] calibrates heat flux sensors using an 800°C blackbody filtered by crown glass (and reported as such). Whilst giving reproducible calibration results, these sensors are usually used to measure surface irradiance due to thermal sources as low 600°C. In such cases, a substantial fraction of the radiation is above the 1-2 μm radiation source against which they were calibrated, and spectral blackness of detector is essential for the calibration to be meaningful.

Accordingly, NMIA has developed a facility to measure the total normal irradiance responsivity to a range of blackbody source spectra.

Experimental apparatus

The facility is based on the blackbody sources and pyrometers from the NMIA radiation thermometry calibration facility [3]. For 400-1100°C Cs and Na heatpipes are used whilst for 1000-2900°C, a Thermogage blackbody is used. Temperature gradients have been measured and emissivities both measured and calculated [3,4,5], and are included as uncertainties. Temperature measurements are made using NMIA's 850 nm and 650 nm pyrometers (MTSP and HTSP) calibrated on the ITS-90 give uncertainties from 0.2°C over 400°C-1100°C rising to 0.5°C at 1700°C.

The measurement is essentially trivial: the blackbody temperature is measured, and an aperture of known area in front of the blackbody provides a calculable irradiance in the measurement plane. However, at low source temperatures the irradiance from the surroundings is comparable to that from the aperture. Retro-reflection from the thermopile and its surrounds, ambient reflection and thermal emission from the plane containing the aperture must be controlled.

The aperture is mounted in a 300 mm square ribbed anodized panel (Figure 1). Its IR reflectance, is measured [4] at below 0.5%. The aperture itself is covered by a light trap consisting of anodized concentric sharpened annuli, with a reflectance estimated below 0.2%. Over 100 W flux from the blackbody illuminates the aperture assembly, but its temperature rise (and consequent re-radiation to the thermopile) is kept below 0.1°C by water cooling. Either side of the aperture is clear of an F/1 viewing cone to minimize the risk of stray reflections.

The pyrometers, aperture assembly and thermopile are on a translating stage in front of a range of blackbody sources, and a typical measurement sequence consists of measuring the blackbody temperature, then measuring the thermopile signal with the aperture assembly opposite either the blackbody or a light trap at ambient temperature.

Atmospheric absorption corrections

The commercial computer package LOWTRAN has been used to compute the transmission through a range of atmospheres and paths (Figure 2) It is interesting to note that the integrated absorption predicted by LOWTRAN increases nearly as the square root of the distance (naively, one may expect something like Beer's law). This results from the strong overlapping of numerous absorption lines. One consequence of this is that the absorption initially decreases very quickly (with distance) however, after 600 mm the rate falls to 5%/m for an 800°C source. At higher source temperatures, less of the spectrum falls in the major CO_2 and H_2O bands and the total absorption is lower.

The total path length between the aperture of the blackbody and sensor is about 600 mm however the air column in the mouth of the blackbody is not at ambient temperature. Air near the blackbody temperature will radiate equal to its absorption, and may be considered part of the blackbody, but air at temperatures intermediate between the blackbody and ambient will have lower density and hence shorter effective optical thickness, but will also have thermally broadened absorption bands. We have not yet fully studied this effect, and as the insulation in the front of the blackbody is 100 mm in length, it is simply included as a 70 mm uncertainty in the effective atmospheric path. This results in an uncertainty in transmission varying from 0.3% at 600°C to 0.2% at 1500°C.

Experimental measurements of atmospheric absorption

As the correction for atmospheric absorption is so significant, and it was not clear if the accuracy of the LOWTRAN calculations was sufficient for metrology purposes, experiments were conducted to confirm its predictions. Ideally one would compare the total detected flux a distance from a blackbody source through normal atmospheric and inert atmospheres. However, two difficulties with purging the total path were anticipated: firstly, the heavy oxide coating on the Inconel heatpipe is not stable in a neutral atmosphere, and secondly, the thermopile sensitivity may be slightly different under different atmospheres. We arranged to be able replace a part of 830 mm atmospheric path by a dry nitrogen atmosphere, leaving the heatpipe and thermopile in air. A 450 mm purge tube between the blackbody and thermopile with 15 mm apertures at either end could be flushed with dry nitrogen, whilst at either end small fans were used to ensure nitrogen escaping through the apertures was blown out of the optical path. Automatic cycling with a 5 minute period between dry N_2 and air in to tube modulated the detected thermopile signal allowing a clear measure of the absorption. Figure 3 shows a comparison of the measured and calculated absorption. The error band on the calculated data is due to uncertainties in the knowledge of the length of the effective air path, due to the hot air region in the heatpipe mouth and the ends of the purged tube (10 mm at each end). The measured and computed values agree within the measurement uncertainties.

Uncertainty analysis

The dominant uncertainty sources are the blackbody temperature measurement and uniformity, the temperature rise of the aperture plane and the uncertainty in effective atmospheric path length. Diffraction corrections are negligible, 0.04% at 20 μm (assuming a 20 mm aperture 200 mm from a 50 mm blackbody). Together these give a 2σ uncertainty of 0.3% over 500-1700°C. Experiments using aperture-thermopile spacings of 300-600 mm, and with 10, 15 and 20 mm apertures give results agreeing well within these bounds.

Conclusions

A new facility for characterizing the response of heat-flux sensors to blackbody irradiance at a range of source temperatures has been established, with uncertainties as low as 0.3%. The new facility will be used to examine IR spectral sensitivity effects in heat-flux sensors.

Acknowledgments The author would like to acknowledge Mr Chris Freund, who designed the experimental apparatus, and Mr Mark Darlow, who performed to precision machining and construction.

References

[1] Grosshandler, W.L., Heat Flux Transducer Calibration: Summary of the 2nd Workshop, NISTIR 6424, NIST Washington, 1999

[2] CSIRO report RS22350, KB33/NML-1/13, 1992

[3] Ballico, M.J.,The CSIRO-NML Radiation thermometer Calibration Facility, *in proc*, Tempmeko 2004, Dubrovnik

[4] M.Ballico, A simple technique for measuring the infrared emissivity of blackbody radiators, Metrologia, 2000, 37, 295-300

[5] M.Ballico,Modelling the effective emissivity of a graphite tube blackbody, Metrologia 1995/6,32, 259-265

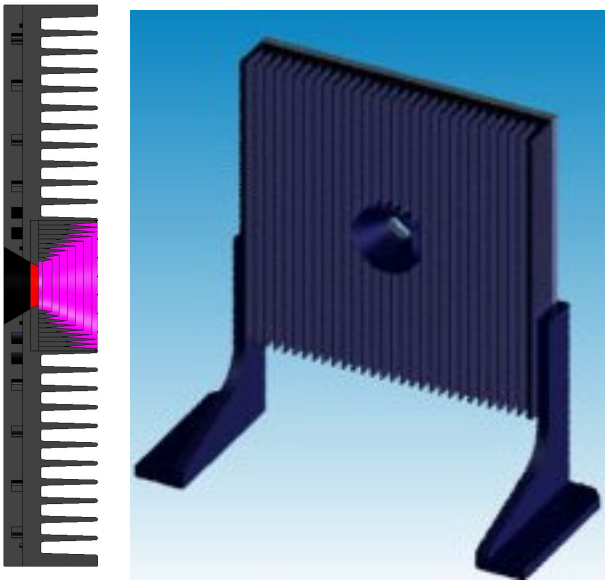

Figure 1. Cross section and image of the water cooled low reflectance plate for stray IR control and holding the precision aperture and annular light trap.

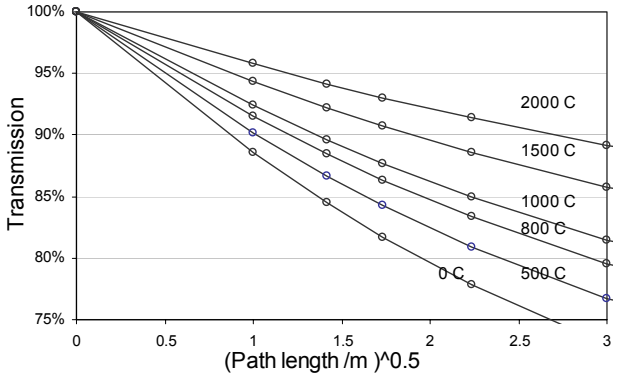

Figure 2. Calculated integrated absorption as a function of distance for 50%RH at 21°C and a range of source radiance temperatures.

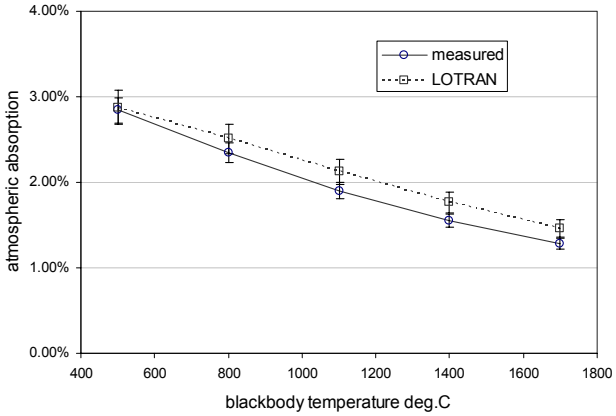

Figure 3. Comparison of measured and calculated absorption between over 450 mm of a total 830 mm air path (50% RH, 21°C)

A laser-based radiance source for calibration of radiation thermometers

M. Ballico and P. B. Lukins
National Measurement Institute of Australia, Lindfield Australia

Abstract. An optical radiometric system based on a laser-diode-illuminated integrating sphere, a pair of calibrated apertures and calibrated silicon detectors is described. The radiance of the source has been determined to better than 0.04% (1σ), is stable in wavelength to <1 pm and radiance to 0.005%. The system is designed to replace the gold freezing point as a reference radiance source for radiation thermometry. Although its performance as a radiance reference is excellent, preliminary results are presently limited by coherent inter-reflection within the pyrometer optics.

Introduction

The present temperature scale above 1000°C is based on the use of narrow-band filter radiance meters (pyrometers) which use Planck's law and a knowledge of their spectral bandpass to determine the temperature of a blackbody source. Under the ITS-90, pyrometers require a single point calibration against a blackbody at a known temperature. This is usually achieved by slowly freezing a crucible containing a few 100 grams of a pure metal (Ag, Au or Cu) surrounding a high emissivity blackbody cavity. Emissivities over 99.97% and temperature reproducibility of typically 10 mK (0.012% in 650 nm radiance) are routinely achieved [5]. Although the temperature of these reference points is defined (zero uncertainty) on the ITS-90, the thermodynamic temperature of these points is currently thought to be as much as 60 mK from the ITS-90 assigned value. Further, it is now accepted that some impurities (eg. those that are solid-soluble) can lead to a depression of the freezing temperature of thermometric fixed points without significantly affecting the flatness of the freezing curve. Consequently, the fixed points are not "self-checking" realizations, and will require calibration against either a batch of cells or another "higher-level" method. The comparison uncertainties available through the existing thermometry international key comparisons CCT-KC5 and APMP-T.KC05 are at the 0.1 to 0.2°C level and so are only marginally adequate for this purpose.

At NMIA, we are developing a traceability system based on replacement of the thermometric fixed point blackbodies by a diffuse-lambertian radiance source, which can be traced to SI electrical and length units. A side benefit will be the possibility of a thermodynamically based temperature scale to replace the use of the ITS-90 above 1000°C.

Several approaches to thermodynamic temperature measurement using filter radiometry are presently in use. One approach [1] uses a narrow-band pyrometer calibrated against an integrating sphere illuminated by tunable lasers to fully characterize its spectral responsivity, whilst another [2] uses a single wavelength laser diode illuminated sphere to characterize the response of a monochromator configured as a pyrometer. A third [3,4] uses a filter radiometer with power responsivity calibrated against a cryogenic radiometer using lasers.

The approach taken here is similar to Briaudeau et. al. [2]. We characterize the reference pyrometer in the same way as for ITS-90, but to simply replace the gold point blackbody. This should allow us to either provide ITS-90 or thermodynamic temperature using the same equipment.

Laser Sphere Source

The source comprises an integrating sphere (Fig. 1) with a 10 mm coating of powdered PFTE of selected particles sizes and with a resulting ID of approximately 200 mm. A 5 mW direct-coupled 650 nm single-mode diode laser directly illuminates the sphere from above. It is temperature stabilized by a Peltier cooler to a few mK, leading to wavelength stability of ~0.6 pm and stable single-mode operation. A monitor photodiode integral to the laser diode is used to feedback stabilize the output power. One port in the horizontal plane is used to mount a precision aperture, whilst a second port contains photodiode monitor of the actual sphere radiance, to account for changes in the sphere gain. The diode laser was calibrated in-situ using a Coherent-Wavemaster wavemeter which itself was calibrated against several known fixed laser lines in the red region. An overall 5 pm wavelength uncertainty was estimated.

Measurements over a period of days show the sphere radiance and wavelength stable to better than 0.005% and 1 pm respectively.

Radiance measurements

The radiance of the sphere was determined using 2 apertures and a calibrated detector. One aperture was attached to the sphere and the other, a distance 300 to 800 mm away, was held either (i) in front of a 4 element Si transmission trap detector (3 mm precision aperture) or (ii) almost against a large area un-windowed Hamamatsu S-6337 18 mm Si photodiode (10 mm precision aperture). The aperture diameters were measured by the NMIA length group's modified Lietz PMM866 coordinate measuring machine, with an effective diameter uncertainty of ±0.15 μm. Photocurrents were measured directly on a Keithley 486 pA meter with a calibration uncertainty of 0.01%. The beveled edges of the apertures faced the sphere and detector, and distances were measured using a stick micrometer. The distance uncertainty was limited by the parallelism of the apertures to ±0.05mm. The trap had been calibrated against a cryogenic radiometer to ±0.02%, whilst the large area photodiode had been calibrated against several calibrated traps using a monochromator system to ±0.03%. Spatial scans of the large area detector showed uniformity of ±0.03% over the area of the aperture used. The sphere radiance, as measured by the two techniques, agreed to within the diode calibration uncertainties.
Although the trap detector measurements could in

principle achieve better accuracy, the large area photodiode approach is very easy to align using the front surface reflection of the diode and may offer a more practical link from radiometry to thermometry.

Measurements were taken with sphere apertures from 10 to 20 mm, and aperture separations from 300 to 800 mm. This tested both the radiance uniformity of the rear wall of the sphere and that inter-reflections were sufficiently low. All results agreed within ±0.04%. The sphere was also scanned horizontally by the pyrometer, and also indicated a uniformity of better than ±0.04% (limited by the measurement noise of the pyrometer). As the aperture can be easily changed to ensure that the diode and the pyrometer both view the same area of the wall, the effect of radiance non-uniformity is expected to be <0.02%.

Pyrometer spectral responsivity measurements

The pyrometer used to test the approach was the HTSP, which operates at 650 nm with a 10 nm bandpass achieved by two interference filters and a windowed Hamamatsu S1337 detector. Simple 1:1 imaging F/10 optics with a 50 mm objective lens and 0.8 mm aperture, followed by a collimating lens is used. Its spectral response (Fig. 2) was assessed [5] using a 1 m McPherson monochromator with a holographic grating, illuminated by a 150 W QTH lamp and a 0.1 nm bandwidth. The pyrometer imaged the monochromator exit slit, and its objective lens was fully filled by the monochromator's F/8 beam. A 3-element reflection trap was used as the reference detector. Coloured glass filters were used to reduce stray light when measuring the 700-1100 nm region, and allowed confirmation that the out of band transmission was well below 10^{-6}. The monochromator was calibrated against 9 Ne lines from 630-670 nm, allowing a wavelength uncertainty of ±20 pm, repeatable to ±2 pm. The measurement noise was typically 0.001% near the transmission peak. The calculated Plank-spectrum-weighted-effective-wavelength, is reproducible to better than ±4 pm.

Thermodynamic Gold Point determination

The pyrometer signal obtained when viewing a gold point blackbody is compared with that calculated from Plank's law, spectral response measured by the monochromator, and scaled by the response to the integrating sphere radiance. The pyrometer signals viewing the sphere and gold point were of similar magnitude. The laser diode was temperature tuned to be within 1 nm of the peak of the pyrometer spectral response, so that the sensitivity to wavelength is below a few % per nm. The repeatability of the measurements was better than 0.05% for a given laser diode setting. However, the results for different diode temperature (wavelength) settings led to differences in computed gold point signal of a few % (around the measured Au point signal)! The source of this unfortunate effect is thought to be coherent reflections between the Si photodiode and other nearby optical surfaces (like an optical etalon). For example, a 4 mm gap will lead to fringes with a spacing of 50 pm, which would not be visible in the monochromator measurements. Unfortunately, although perfectly usable for usual pyrometry applications, the reference pyrometer HTSP is unsuitable for use with coherent sources.

Conclusions

The laser-diode sphere source can provide a reproducible reference radiance at the 0.04% (1σ) level. Although the spectral response of the pyrometer has been characterized to achieve a total uncertainty of 0.1% at the gold point, unexpected coherent interreflections within the pyrometer lead to up to ±2% variations in signal. A pyrometer design avoiding inter-reflections, or possibly temperature tuning the laser over the fringes, is required in future.

Acknowledgments The authors wish to acknowledge the assistance of Mr Chris Freund and Mr Mark Darlow for their invaluable assistance in design and construction.

References

1. H. W. Yoon, Temperature Determination of the Ag and Au freezing points using a detector based radiation thermometer, Tempmeko conf., Dubrovnik, 2004
2. S. Briaudeau et. al., Thermodynamic Temperature Determination in high temperature range at BNM-INM, in proc. Tempmeko conf. , Dubrovnik, 2004
3. R. Goebel et.al., Thermodynamic Temperature Measurements of metal-carbon eutectics fixed points, in proc. Tempmeko conf., Dubrovnik, 2004
4. J. Hartmann,et. al., Thermodynamic Temperature measurements of the melting curves of Re-C, TiC-C and Zr-C-C eutectics, in proc. Tempmeko conf., Dubrovnik, 2004
5. M. Ballico, Independent Australian Realization of the International Temperature Scale of 1990 using the recommissioned APEP2 pyrometer, Internal CSIRO Australia, report TIPP-48, Nov 1997

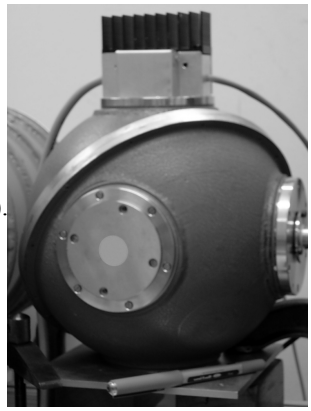

Figure 1: Picture of the radiance source with aperture(front) laser diode (top) and monitor photodiode (right).

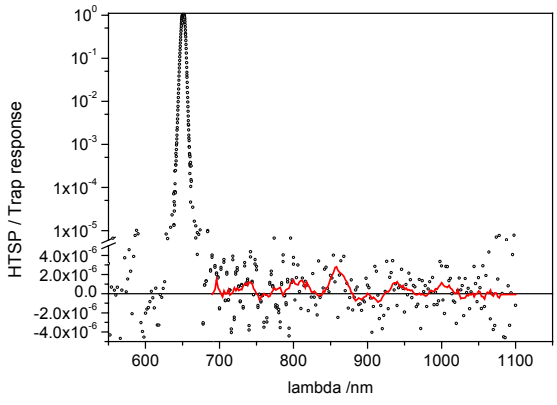

Figure 2: Spectral response of the HTSP, relative to a Si trap detector. The solid line shows smoothed data.

Furnace for High-Temperature Metal (Carbide)-Carbon Eutectic Fixed-Point

B. Khlevnoy*, M. Sakharov, S. Ogarev, V. Sapritsky

All Russian Research Institute for Optical and Physical Measurements (VNIIOFI), Moscow, Russia.
*A guest-scientist at the NMIJ at the time of investigation.

Y. Yamada

National Metrology Institute of Japan, AIST, Tsukuba, Japan.

K. Anhalt*

PTB, Berlin, Germany. *A guest-scientist at the NMIJ at the time of investigation.

Abstract. A new large-area furnace with maximum temperature of 3500 K was designed at the VNIIOFI as a furnace for high-temperature M(C)-C fixed points, and then investigated at the NMIJ. Temperature uniformity was investigated as to its dependence on various heater and cell holder arrangements. One Re-C and one TiC-C cells were made using BB3500YY and then compared with a Re-C cell made in a NAGANO furnace at the NMIJ and with a VNIIOFI-made TiC-C cell.

Introduction

High-temperature metal-carbon (M-C) and metal carbide-carbon (MC-C) fixed points have been attracting attention of many researchers and hold promise to take an important role in radiometry and photometry in the nearest future [1]. Three type of furnaces are conventionally used for the highest temperature M(C)-C fixed-points: Thermogage, Nagano and VNIIOFI-made BB3200pg/ BB3500 [2]. It was shown [3, 4] that the temperature uniformity of furnaces is very critical for reproducibility and plateau quality of the fixed points. To get the better uniformity a new, BB3500YY, furnace was designed at the VNIIOFI and then investigated at the NMIJ.

Furnace design

The BB3500YY furnace has a design similar to the pyrographite (PG) blackbody BB3200pg [5]. The cross-section of the BB3500YY is shown on Fig.1. It has a cylindrical heater consisting of a set of PG rings, compressed by a spring between front fixed copper and rear movable graphite electrodes, and surrounded by carbon cloth thermoshield.

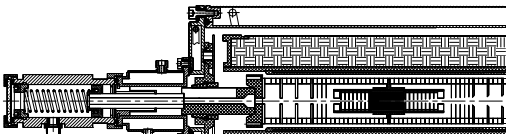

Figure 1. Cross-section of the BB3500YY furnace

In comparison with previous PG furnaces the BB3500YY has longer thermoshield and set of PG rings: 455 mm and 355 mm respectively instead 370 and 290 mm. This makes the central part of the furnace more uniform. The length of the rings set can be increased to 400 mm if necessary. The inner diameter of the rings is 47 mm instead 37mm, which also improves the uniformity because of better conditions for radiation heat flux exchange. The larger space between the cell, which is placed in the center of the furnace tube, and the rings allows placement of an additional screen for further improvement of uniformity.

Advantages of the rings set design: numerous baffles and a cell holder can be easily placed at any position between the rings; different resistance ring order can be chosen to change the temperature gradient.

BB3500YY has a rear radiation channel that can be used for a monitor/control pyrometer or thermocouple.

Temperature uniformity at 1500 °C

Because of difficulties of temperature distribution measurement at high temperatures the uniformity was investigated first at 1500 °C using two type R thermocouples. One of them was fixed in the rear channel and used for furnace control and the second one was moved through the front opening to make a scan along the furnace axes.

At the first step the arrangement of the furnace was as follows: a graphite cell holder of 80 mm length and 30 mm in outer diameter designed to hold a cell of 45 mm length and 24 mm in diameter. The holder was wrapped in 3-mm graphite felt. Inside the holder there were eight thin-sheet PG baffles: four in front of and four behind the cell. The cell itself was not in place during the measurements. In front of the holder and behind it there were sets of outer baffles from the same thin-sheet PG material placed between the heater rings. Fig.2 shows a family of distributions measured. Curve 1 was measured when all baffles and the felt were at their places as described above. Then outer baffles were removed and curve 2 was measured. Then outer baffles were put back, inner ones removed and curve 3 was measured. Curve 4 was measured with all baffles but without the felt. Curve 5 represents the distribution measured for just the same heater except four rings around the rear end of the graphite holder replaced by those with about two times higher resistance according to resistance measured at room temperature. One can see that neither baffles (inner or outer) nor felt hardly changes the distribution. What significantly changes it is resistance of the rings.

Comparing curves 5 and 6 shows that the graphite holder does not improve the uniformity.

Another holder we used was a 3 mm thick CC tube of 150 mm length rapped with 4 layers of graphite cloth. Such a holder, in distinction from the graphite one, improves the uniformity, which is shown on Fig.3.

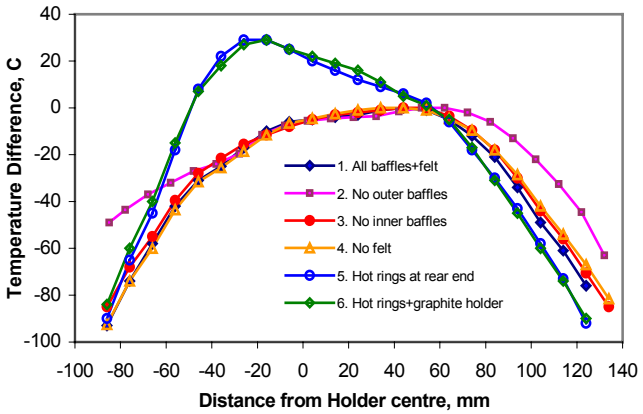

Figure 2. Temperature distributions measured by thermocouple at T=1500 °C for BB3500YY with a graphite holder

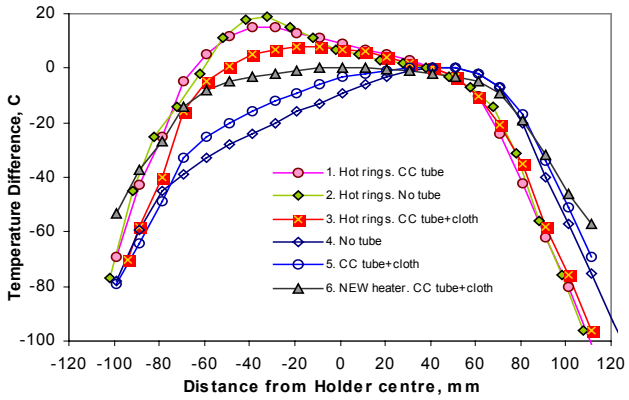

Figure 3. Temperature distributions measured by thermocouple at T=1500 °C for BB3500YY with a CC-tube holder

Distribution measured first for the arrangement with some high resistance rings at the rear end of the cell position but without any holder (curve 2), then for the same arrangement but with the CC-tube (curve 1), and then with the tube wrapped in the cloth (curve 3). Comparison of the curves shows that the cloth has more significant effect than the tube itself. Curves 4 and 5 represent distributions measured without and with the tube wrapped with cloth respectively but for arrangement with low resistance rings around the rear end of the cell position. Finally a new set of rings was arranged, which showed (in combination with CC holder) the uniformity (curve 6) within 5 degrees along the distance of 110 mm.

Temperature uniformity at 2500°C

Two radiation thermometers were used for temperature distribution measurement at higher temperatures. One of them, narrow-beam fiber radiation thermometer looked through the rear channel of the furnace to a blind baffle placed at the rear end of the CC-tube holder and used for furnace temperature control. The second thermometer looked through the front opening to a movable target inside the holder. The target was a 10 mm length graphite tube with soot-blackened bottom at one end and 5 mm aperture at another one.

At the beginning the target was placed inside the CC tube near its front end, the furnace was brought to the desired temperature of 2500 °C, and the temperature of the target was measured by means of the second radiation thermometer. Then the furnace was brought to the temperature of 1500 °C, the target was pushed by an alumina rod to be moved by one step of 10 to 20 mm, the furnace was brought back to the temperature of 2500 °C and the second point of the temperature distribution measurement was taken. This was repeated to cover the length of the CC tube.

As a test of the validity of this method, the temperature distribution was measured at 1500 °C and was compared with measurement with the thermocouple with the same furnace arrangement. Both methods agreed within one degree. Then the method was applied to measure the temperature distribution at 2500 °C. The measurements showed that the hottest point was just in the center of the CC tube and temperature gradually decreased towards its ends. The central 40 mm and 80 mm parts of the tube were uniform within 2 and 5 degrees respectively.

Work with eutectics cell

The NMIJ Re-C cell of 45 mm length, 24 mm outer diameter and 3 mm aperture cavity was heated in BB3500YY furnace to observe melting and freezing plateaus. The same cell was then used for observing the plateaus in VR10-A23 furnace [6], which has operation temperature limited to 2500 °C. The former showed better melting plateau shapes.

BB3500YY was used for filling one Re-C and one TiC-C cells. The Re-C cell was compared with a similar one but filled in VR10-A10 furnace (vertical variant of VR10-A23). The TiC-C cell was compared with a cell manufactured by VNIIOFI. The results of these comparisons will be presented in the paper.

References

[1] Yamada Y., Advances in High-temperature Standards above 1000°C, *MAPAN - Journal of Metrology Society of India*, v.20, No 2, 2005, pp.183-191.

[2] Sapritsky, V., Ogarev, S., Khlevnoy, B., Samoylov, M., and Khromchenko, V., *Metrologia* **40** (2003), S128-S131. 2003

[3] N. Sasajima, M. K. Sakharov, B. B. Khlevnoy, Y. Yamada, M. L. Samoylov, S. A. Ogarev, P. Bloembergen and V. I. Sapritsky. 'A comparison of Re-C and TiC-C eutectic fixed-point cells among VNIIOFI, NMIJ and BIPM'. in *9th International Symposium on Temperature and Thermal Measurements in Industry and Science (TEMPMEKO)*. 2004. Dubrovnik.

[4] Woolliams E., Khlevnoy B., Sakharov M., Samoylov M., Sapritsky V., Investigation of TiC-C and ZrC-C eutectic fixed-point blackbodies., *Submitted to Metrologia*.

[5] Sapritsky V. and others, *Applied Optics,* 36, 5403-5408, 1997.

[6] Y. Yamada, N. Sasajima, H. Gomi, and T. Sugai, *in Temperature: Its Measurement and Control in Science and Industry, 7 (Ripple et al ed.), AIP Conference Proceedings*, Melville, New York (2003) 965-990.

Investigations of Impurities in TiC-C Eutectic System as a Fixed Point

A. Bourdakin, M. Sakharov, B. Khlevnoy, S. Ogarev, V. Sapritsky[1]
A. Elyutin[2]

[1]All-Russian Research Institute for Optical and Physical Measurements (VNIIOFI), Moscow, Russia

[2]Academician of Russian Academy of Science

Abstract. Data on elimination of impurities from TiC-C are presented and discussed. The idea of less sensitivity of eutectics as the fixed points to impurity, than that in case of pure materials, is suggested. It is concluded that criteria of both initial metals purity and metal-carbon eutectics purity are not as tough as for fixed points on pure metals.

Statement of the problem

In paper [1] there were presented results conducted at VNIIOFI investigations of melting/freezing phase transition in eutectic system TiC-C as a prospective fixed point for radiometry, photometry and radiation thermometry. The biggest requirement for a fixed point is its temperature reproducibility. Further investigations are to be directed at lowering the non-reproducibility and discovering its fundamental roots.

Deviations from equilibrium transition temperature could be classified in the following way. 1) Caused by physico-chemical properties of the real materials. 2) Caused by thermal non-equilibrium in the sample volume in conditions of real experiment. The present work focuses on deviations originated from intrinsic material properties.

It is commonly accepted that the main factor of non-equilibrium of phase transition in mono-component (uniform) metals and eutectic alloys is impurity [2-4].

In uniform metal short-range order of atoms disposition remains in molten state and thus melting involves just minimal rearrangement of atoms [5]. Melting mechanism keeps identical in the whole sample volume if structural defects are neglected. In case of high-purity metal melting kinetic factor of impurity distribution between solid and liquid phases does not essentially change the mechanism.

On the contrary, even in totally pure eutectic system mechanism of melting is not identical in the sample volume. Structural factor can not be neglected now. Melting transition of eutectic alloy, occurring in accordance with equilibrium phase diagram, can be preceded by premelting on interphase surfaces and grain boundaries [5].

Kinetics of eutectic transformation leads to additional deviation from equilibrium, because melting of extremely non-uniform eutectic system requires mass transfer of eutectic components through liquid phase. Atoms of eutectic alloy are transferred for distances comparable to structural parameters of solid eutectic. That is many times as much as for melting transition in pure metal where only minimal displacements of atoms from crystal lattice nodes are required.

Influence of structural factor on melting point and melting plateau shape was discussed by example of eutectic Fe-C [6]. Slight decrease of melting temperature, which was preceded by "fast" solidification from melt, the authors explained by two main grounds. 1) After "fast" solidification eutectic comes to metastable state. Having more refined phase structure than eutectic in stable equilibrium state it possesses enhanced interphase surface Gibbs energy. 2) Premelting on more developed grain boundaries provides for more substantial contribution to entire melting process than in stable state.

The problem is that eutectic alloys intrinsically are systems with highly refined phase structure and developed interphase surfaces. It is unclear so far what eutectic structure should be attributed to stable state, and what structure – to metastable. Consequently, it remains unclear what degree of fine-dyspersation of eutectic phases forces us to take into account excessive surface energy.

We suppose that there is a certain "threshold purity level" for different substances above which other causes of non-equilibrium become more important than content of impurities. In our opinion, for eutectic systems this level should be lower than that of relatively simple uniform metals, for the reason of complexity of the mechanism and kinetics of eutectic transformation.

While reaching "the threshold purity level" structural and kinetic factors should play the key role in deviation from equilibrium temperature of eutectic melting/freezing. Proceeding from this assumption we set the task to evaluate the level of impurities content in metal-carbon eutectics, above which further purification brings no result in terms of melting plateau quality and reproducibility.

Experimental

At the first stage we investigated influence of initial titanium purity on final composition of eutectic TiC-C. Earlier Yamada et al. observed elimination of impurities in initial rhenium after smelting Re and C.

Two samples of initial titanium and four eutectic alloys TiC-C were analyzed by SSMS method with susceptibility at 0.001 ppm. For very low impurity content uncertainty can exceed 100%, mostly due to strong non-uniformity of impurity distribution and extreme locality of this method. As will be seen later, it is quite sufficient for targeted goal.

The first and the second samples TiC-C were prepared out of titanium hydride 0.9999 purity (Ti#1) and 0.999995 extra purity carbon powder by smelting in argon flux and under vacuum correspondingly. The third and the fourth TiC-C samples were prepared in the same way, but out of titanium powder 0.9985 purity (Ti#2). Ti#2 was preliminary eliminated of hydrogen.

Whatever initial titanium had been taken, the final purity of solid ingots was 0.99995 after smelting in argon and 0.99997 after smelting under vacuum. Results obtained

for smelting under vacuum are presented in Table 1 for Ti#1 and in Table 2 for Ti#2.

Table 1. Impurity content in Ti#1 and TiC-C, ppm

Impurity	Al	Cr	Fe	Cu	Ni
Ti#1	40	10	9	5	2
TiC-C	0.04	0.8	0.5	0.1	0.08

Table 2. Impurity content in Ti#2 and TiC-C, ppm

Impurity	Al	K	Si	Ca	Fe	Cr	Cu	Mn
Ti#2	700	300	100	100	60	30	30	20
TiC-C	0.04	0.05	0.04	0.06	0.08	0.7	0.1	0.05

Discussion

In case evaporation of atoms from molten alloy goes in "molecular" mode (e.g. under vacuum or in inert gas flux), velocity of evaporation obeys Langmuir-Knudsen law $U_i \sim p_i^0 \sqrt{T}$ (1), where U_i - velocity of evaporation of i-element (including T_i and C), p_i^0 – equilibrium pressure of saturated vapour. Vapour pressure of carbon is so low that it can be neglected. For most metallic impurities dissolved in titanium inequality $p_i^0 > p_{Ti}^0$ (2) is correct. Thus purification of initial titanium is thermodynamically favorable even in absence of carbon. Kinetics also can be in no way the limiting factor at melting temperature of titanium. Nevertheless, metallic impurities do not leave molten titanium because they chemically interact with Ti atoms forming strong inter-metallic compounds [7]. In molten state, inter-metallic compounds undergo some structural changes but remain chemical bounds strong enough. Purification of titanium from Fe, Si, Al atoms goes especially hard. According to thermodynamics of perfect solutions Fe atoms should have been evaporated from molten solution with titanium. But experiments showed that TiFe compound melts keeping strict stoichiometry.

It is carbon whose presence is of critical importance for purification of TiC-C. Having strong affinity to titanium carbon bounds all the existing Ti atoms and blocks formation of inter-metallic compounds. Staying in form of free atoms metallic impurities evaporate from molten eutectic TiC-C according to (1), (2) more intensively than Ti and C, and purification occurs. Compound TiAl may react with carbon forming aluminium carbide, which is fugitive and also evaporates from molten TiC-C.

On the other hand, the possibility of dissolving some amount of impurities in adjoining layer of graphite crucible must be verified. It is related to Fe atoms first of all. Depending on distribution coefficient in complex system "eutectic alloy-graphite crucible" impurity atoms, dissolved in inner crucible walls, may appear in eutectic on melting plateau.

At room temperature titanium (especially titanium powder) willingly absorbs H, O, N atoms not determined by mass-spectroscopy method. Hydrogen is totally removed from Ti at temperatures over 700^0 C [7]. So there is no hydrogen in titanium-carbon mixture at carbide synthesizing temperatures. That is why we see no problem in using both titanium hydride and titanium powder for preparing TiC-C eutectics. Quality of melting plateau usually was better if we used titanium hydride. This empirical fact has no explanation in terms of eutectic purity.

At heating Ti and O atoms interact forming a number of oxides Ti_3O, TiO, Ti_2O_3, TiO_2. Atoms of Ti and N form high-melting compound δ-TiN with variable stoichiometry which solidus line extends up to 3290^0 C [7]. Carbon reduces Ti from titanium oxides, e.g. for mono-oxide of titanium the following reaction goes:

$$TiO + 2C = TiC + CO\uparrow \text{ (gas)} \quad (3)$$

Direct reaction (3) becomes thermodynamically favorable at about 1600^0 C when there can be no kinetic limitations. Therefore, oxygen is removed from TiC-C system in form of CO gas prior to eutectic melting. It concerns both melting under vacuum and in argon flux; in the former case CO is removed due to pumping-out, in the latter - carried away by argon flux.

Similar reaction goes with participation of TiN compound:

$$2TiN + 2C = 2TiC + N_2\uparrow \text{ (gas)} \quad (4)$$

Direct reaction (4) becomes thermodynamically favorable at about 1800^0 C. So despite the fact, that TiN has higher melting temperature than TiC-C, nitrogen evaporates prior to eutectic melting.

We see that presence of carbon again is of critical importance for elimination of O, N from eutectic TiC-C.

Conclusion

It is at the stage of metal-carbon eutectics preparation, that most impurities contained in initial metal are eliminated. Therefore demands to initial purity of metal for preparing eutectics are not as tough as for pure substances. For the reason of complexity of melting mechanism we suggest that eutectic systems should be less sensitive to impurity than uniform metals. If this is the case, demands to final purity of eutectics can be not so tough as well. Above certain purity level structural and kinetic factors can become more significant in terms of deviation from equilibrium phase transition in M-C and MC-C eutectics.

References

[1] M.K. Sakharov, B.B. Khlevnoy, V.I. Sapritsky, M.L. Samoylov, S.A. Ogarev, "Development and investigation of high-temperature fixed point based on TiC-C eutectic", TEMPMEKO 2004, in progress

[2] J. Ancsin, "Equilibrium melting curves of relatively pure and doped silver samples", Metrologia, 38, 2001, pp. 229-235

[3] J. Ancsin, "Impurity dependence of Cu-Ag eutectic melting temperatures", TEMPMEKO 2004, in progress

[4] P. Bloembergen, Y. Yamada, N. Sasajima, S. Torizuka, N. Yoshida, N. Yamamoto, "On the effect of impurities on the melting curve of the eutectic system Fe-C", 7, AIP Conference proceeding, 2003, pp. 261-266

[5] A.R. Ubbelohde "The Molten State of Matter", J. Wiley, London, 1978

[6] N. Sasajima, Y. Yamada, P. Bloembergen, Y. Ono, "Dependence of iron-carbon eutectic melting on pre-freezing rate and annealing conditions", TEMPMEKO 2004, in progress

[7] N.P. Liakishev, "Phase-equilibrium Diagrams of Binary Systems", Moscow, 1999

Determining the temperature of a blackbody based on a spectral comparison with a fixed temperature blackbody

T. Zama and I. Saito

National Metrology Institute of Japan, National Institute of Advanced Industrial Science and Technology (NMIJ/AIST). AIST Tsukuba Central 3, 1-1, Umezono 1-Chome, Tsukuba-shi, Ibaraki-ken 305-8563 Japan

Abstract. The temperature of a blackbody has been determined from a spectral radiance comparison between the blackbody and a fixed temperature blackbody (whose temperature is copper freezing point). A multichannel spectroradiometer was used for the comparison. The spectral resolution and bandpass property of the spectroradiometer was evaluated and the signal to noise ratio of the spectroradiometer was measured. The uncertainty of the spectral radiance comparison was evaluated from the signal to noise ratio, the bandpass property and the spectral distribution difference between two blackbodies. The result of spectral radiance comparison was fitted to Planck's low and the temperature of the blackbody was determined. The fitting curve agreed well with the measurement result in longer wavelength region, but did not agreed with that in shorter wavelength region. The bandwidth and the signal noise of the multichannel spectroradiometer caused the disagreement.

Introduction

Blackbody is widely used for establishing scales, for example spectral irradiance or radiance. For using a blackbody as primary standard light source, evaluating the blackbody's temperature is required. The temperature is evaluated by (a) radiant flux comparison between the blackbody and other blackbody whose absolute temperature is well known or (b) absolute spectral radiance measurement by an absolute detector. For the comparison of (a), a fixed temperature blackbody is required. For the measurement of (b), absolute filter radiometer is required.

In this paper, we introduce a method for determining blackbody's temperature according to (a) comparison. A spectral comparison has been conducted from 600 nm to 780 nm by using a multichannel spectroradiometer. We compared a blackbody whose operative temperature is variable from 1300 K to 3300 K (HTBB) with a copper-freezing-point blackbody (CUBB). The CUBB was used as the blackbody whose absolute temperature is well known.

Equipment for Measurement

The multichannel spectroradiometer consists of a polychromator and a silicon photodiode array detector and offers a spectral measurement from 380 nm to 780 nm with increment of 2 nm. The image of an object is focused onto the entrance slit of the polychromator. The signal from each pixel of the array is converted to 16-bit digital value and recorded by a computer. A filter, which has low transmittance, has been used for avoiding saturation of a signal on measuring HTBB.

The temperature change of the HTBB is monitored by a radiation thermometer. The temperature of the HTBB is kept constant by a feedback from the signal of the radiation thermometer.

We have used the CUBB, which is operated copper freezing point, for temperature standard.

Principle of Temperature Determination

The HTBB and CUBB have been measured by the multichannel spectroradiometer. The spectral radiant flux of each blackbody was converted into a spectral data. The spectral data is shown as follows.

$$L_M(\lambda_0, T) = \int L(\lambda, T) S(\lambda_0, \lambda) d\lambda \qquad (1)$$

Where $L_M(\lambda_0, T)$ is spectral data of the multichannel spectroradiometer at λ_0 nm (that is dimensionless, because the output data of the spectroradiometer is simply numerical data), $L(\lambda, T)$ is spectral irradiance of blackbody whose temperature is T at λ nm (whose unit is W m^{-2} sr^{-1} nm^{-1}) and the function $L(\lambda, T)$ is given by Planck's law and $S(\lambda_0, \lambda)$ is spectral radiance responsivity of the multichannel spectroradiometer (whose unit is sr m^2 W^{-1}). The $S(\lambda_0, \lambda)$ represents bandpass property of the multichannel spectroradiometer.

The HTBB temperature T is determined from the CUBB temperature T_0. Expressing the ratio of HTBB spectral radiance to CUBB spectral radiance as C_λ, the following equation is derived.

$$C_\lambda = \frac{L(\lambda, T)}{L(\lambda, T_0)} = \frac{e^{hc/\lambda k T_0} - 1}{e^{hc/\lambda k T} - 1}$$

$$T = \frac{hc}{\lambda k} \frac{1}{\ln\left(\frac{e^{hc/\lambda k T_0} - 1}{C_\lambda} + 1\right)} \qquad (2)$$

As mentioned above, the spectral data we can measure by the multichannel spectroradiometer is shown as (1), and hence the measurable ratio is not C_λ but C_{M,λ_0} that is expressed as follows.

$$C_{M,\lambda_0} = \frac{L_M(\lambda_0, T)}{L_M(\lambda_0, T_0)} = \frac{\int L(\lambda, T) S(\lambda_0, \lambda) d\lambda}{\int L(\lambda, T_0) S(\lambda_0, \lambda) d\lambda} \qquad (3)$$

Where $L_M(\lambda_0, T)$ and $L_M(\lambda_0, T_0)$ are the measured spectral data of HTBB and CUBB respectively.

If spectral radiance of HTBB $L(\lambda, T)$ and CUBB $L(\lambda, T_0)$ has a similar shape, the influence of the bandpass property of the multichannel spectroradiometer will be small and C_{M,λ_0} is almost equal to C_{λ_0}. However, the spectral shape of $L(\lambda, T)$ and $L(\lambda, T_0)$ is considerably different in shorter wavelength (while the CUBB is operated copper freezing point 1357.77 K, we operate the HTBB at about 3000 K); and there is no assurance that the influence of the bandpass property is negligible.

In order to clarify the relation between C_{M,λ_0} and C_λ, expanding $L(\lambda, T)$ near λ_0 and introducing new valuable $\Lambda = \lambda - \lambda_0$, the following equation is derived.

$$L(\lambda,T)=L(\lambda_0,T)+\left.\frac{\partial L}{\partial\lambda}\right|_{\lambda=\lambda_0}\Lambda+\frac{1}{2}\left.\frac{\partial L}{\partial\lambda}\right|_{\lambda=\lambda_0}(\Lambda)^2\Lambda$$

$$L_M(\lambda_0,T)=(1+\delta(\lambda_0,T))L(\lambda_0,T)\int S(\lambda_0,\lambda_0+\Lambda)d\Lambda \qquad (4)$$

The $\delta(\lambda_0, T)$ in above equation is expressed as follows.

$$\delta(\lambda_0,T)=\frac{\int\left(\left.\frac{\partial L}{\partial\lambda}\right|_{\lambda=\lambda_0}\Lambda+\frac{1}{2}\left.\frac{\partial L}{\partial\lambda}\right|_{\lambda=\lambda_0}(\Lambda)^2\Lambda\right)S(\lambda_0,\lambda_0+\Lambda)d\Lambda}{L(\lambda_0,T)\int S(\lambda_0,\lambda_0+\Lambda)d\Lambda} \qquad (5)$$

From the equations (3) and (4), the following equation

$$C_{M,\lambda_0}=\frac{(1+\delta(\lambda_0,T))L(\lambda_0,T)\int S(\lambda_0,\lambda_0+\Lambda)d\Lambda}{(1+\delta(\lambda_0,T_0))L(\lambda_0,T_0)\int S(\lambda_0,\lambda_0+\Lambda)d\Lambda}$$

$$=C_{\lambda_0}\frac{(1+\delta(\lambda_0,T))}{(1+\delta(\lambda_0,T_0))}$$

$$C_{\lambda_0}\cong C_{M,\lambda_0}(1+\delta(\lambda_0,T_0)-\delta(\lambda_0,T)) \qquad (6)$$

is derived.

The equation (5) shows that $C_{\lambda 0}$ is expressed by $C_{M,\lambda 0}$ and two modification factors, which are $\delta(\lambda_0, T)$ and $\delta(\lambda_0, T_0)$.

Determination of HTBB Temperature

At first, we have determined the temperature of the HTBB, substituting the $C_{M,\lambda}$ for the C_λ. The temperature of the HTBB was determined from the equation (2) at each wavelength in which the multichannel spectroradiometer offers the spectral data. Figure 1 shows a result of temperature determination.

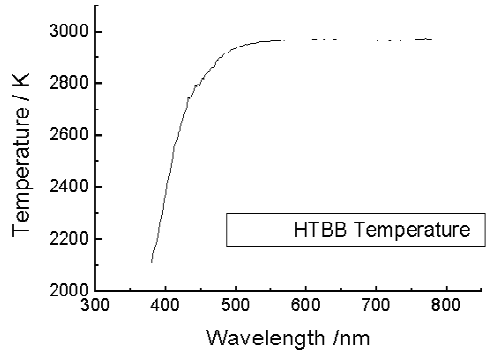

Figure 1. The temperature of the HTBB determined from spectral data of the multichannel spectroradiometer.

The determined temperature is almost constant in longer wavelength region but depends on wavelength in shorter wavelength region. The modification factors mentioned above are one of the causes of this dependence.

The following equation (7) is derived from differentiating equation (2) and shows the other causes of the dependence.

$$\frac{dT}{T}=\left(\left(\frac{T}{T_0}\right)\frac{e^{(hc/\lambda_0kT_0-hc/\lambda_0kT)}}{C_{\lambda_0}}-1\right)\frac{d\lambda_0}{\lambda_0}+\left(\frac{T}{T_0}\right)\frac{e^{(hc/\lambda_0kT_0-hc/\lambda_0kT)}}{C_{\lambda_0}}\frac{dT_0}{T_0}$$

$$+\left(\frac{hc}{\lambda_0kT}\right)\frac{e^{(hc/\lambda_0kT_0-hc/\lambda_0kT)}}{C_{\lambda_0}}\frac{dC_{\lambda_0}}{C_{\lambda_0}} \qquad (7)$$

The $d\lambda_0$, dT_0 and $dC_{\lambda 0}$ show the accuracy of reading wavelength λ_0 of the multichannel spectroradiometer, the uncertainty of the CUBB temperature T_0 and the uncertainty of the ratio $C_{\lambda 0}$, respectivily. The $dC_{\lambda 0}$ has been derived from the modification factors mentioned above, and signal noise (due to stray light and the measurement repeatability) of the multichannel spectroradiometer.

The evaluation of the three terms in the equation (7) showed the third term was much larger than the first and second terms in shorter wavelength region; and the first and second terms had weak dependence on wavelength compared to the third term.

Figure 2 shows the third term in the equation (7). The modification factors due to the bandpass property and the signal noise of the multichannel spectroradiometer is shown in this figure.

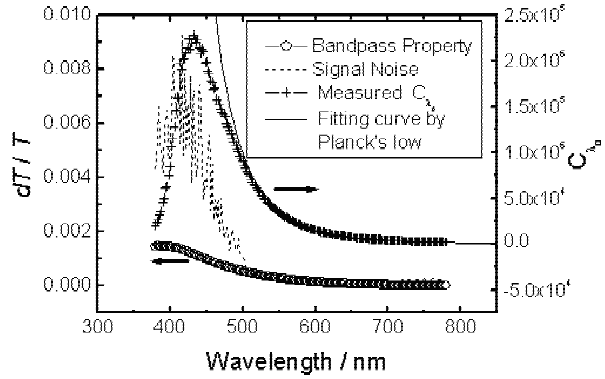

Figure 2. The relation between dT and $dC_{\lambda 0}$, and a measured $C_{\lambda 0}$ and a fitting curve by Planck's low. The $dC_{\lambda 0}$ has been evaluated from the bandpass property and the signal noise of the multichannel spectroradiometer.

To evaluate the modification factors, we have measured some spectral lines by the multichannel spectroradiometer and estimated the spectral radiance responsivity $S(\lambda_0, \lambda)$. In this estimation, we assumed the $S(\lambda_0, \lambda)$ was close to a symmetric function with respect to λ_0 and we neglected the term that has Λ^m whose m is odd number in the equation (5).

Figure 2 shows that the uncertainty of the ratio $C_{\lambda 0}$ increases at a wavelength below 600 nm, and hence we have determined HTBB temperature from the measured $C_{\lambda 0}$, whose wavelength is above 600 nm.

Figure 2 also shows a measured ratio $C_{\lambda 0}$ and a fitting curve by Planck's low. The $C_{\lambda 0}$ data, whose wavelength is from 600 nm to 780 nm, is used for this fitting. The fitting curve agreed well with the measured $C_{\lambda 0}$. The HTBB temperature has determined from this fitting is 2965.7 K and the uncertainty of this fitting is under 0.1 K.

Conclusions

We have determined the temperature of a blackbody based on a spectral comparison with a copper-freezing-point blackbody. A multichannel spectroradiometer was used for this comparison. From the evaluation of the signal noise and the bandpass property of the multichannel spectroradiometer, we determined an appropriate wavelength range for the spectral comparison. The results of the spectral comparison agreed well with Planck's low.

References

van der Ham, E. W. M., Bos, H. C. D., Schrama, C. A., Primary realization of a spectral irradiance scale employing monochromator-based cryogenic radiometry between 200nm and 20μm, *metrologia*, *40*, S177-S180, 2003.

High-temperature fixed-point radiators: The effect of the heat exchange between cavity and furnace tube on the effective emissivity of the radiator

P. Bloembergen, Y. Yamada
National Metrology Institute of Japan, AIST, Tsukuba, Japan

B. B. Khlevnoy
All Russian Research Institute for Optical and Physical Measurements (VNIIOFI), Moscow, Russia

P. Jimeno Largo
University of Valladolid, Valladolid, Spain

Abstract. At high temperatures the heat exchange between cavity and front end of the associated furnace markedly influence the effective emissivity of the radiator, precluding treating the cavity as a separate unit. This will be demonstrated for the eutectic fixed point Re-C, radiating at a temperature of 2474 °C.

Introduction

Effective emissivities, $\varepsilon(tot)$ and $\varepsilon(\lambda)$ - over the range 250 to 2500 nm - have been calculated by means of STEEP-3, a software package created by A. Prokhorov [1], assuming diffusely reflecting grey surfaces with emissivity 0.85. The calculations have been done (a) for the actual cavity-furnace combination constituting the radiator, taking into account the estimated temperature profile $T(x)$ of the furnace tube, where x is the distance from the cavity aperture, (b) for a uniform furnace-temperature distribution $T(x) = T_{cav}$ and (c) for the cavity only, formally implying $T(x) = 0$ K. The cavity itself is assumed to be uniform in temperature, i.e. $T_{cav} = 2474$ ° C.

Experimental context

The results presented below have been calculated for the cylindro-conical cavity in the Re-C eutectic cell 3S2, mounted in furnace VR10 –A19 [2]. Cavity dimensions: L= 45 mm, diameter = 8 mm, angle of the conical bottom 120 °, without and with an aperture, 3 mm in diameter.

The furnace-temperature profile (full line, *low*) given in Figure 1 has been directly measured by means of the radiation thermometer (RT), LP-3 8040, by scanning along the radiation shields placed within the furnace tube in front of the Re-C fixed point (3S2) in study. The actual profile $T(x)$, to be associated with the effective emissivity of the radiator is supposed to be situated in-between the *low* and *high* profiles.

Results

In Figure 2 we present the differences 1- ε(650) and 1 - ε(950) as a function D^2, where D defines the diameter of the cavity aperture, for the profiles *low* and *high*, embedded between those obtained for the profiles $T(x) = 0$ K, cavity only, and $T(x) = T_{cav}$, isothermal overall temperature

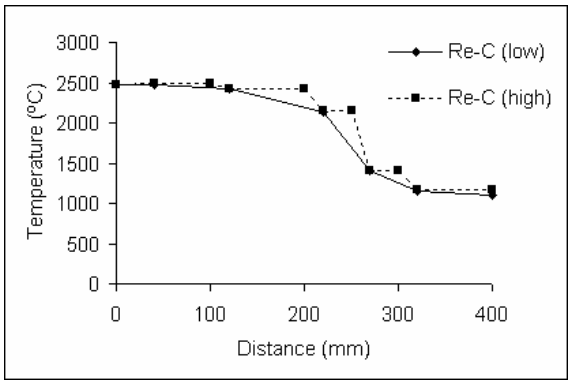

Figure 1: Furnace-temperature profiles $T(x)$, *low* and *high*, used for calculating the effective emissivities shown in Figures 2 to 4.

profile. Figure 3 shows 1– $\varepsilon(tot)$ in the same representation. Finally in Figure 4 we show 1- $\varepsilon(\lambda)$ as a function of λ, calculated within the range λ = 250 nm to λ = 2500 nm for the *high* and *low* temperature profiles, and aperture diameters D of 3 and 8 mm.

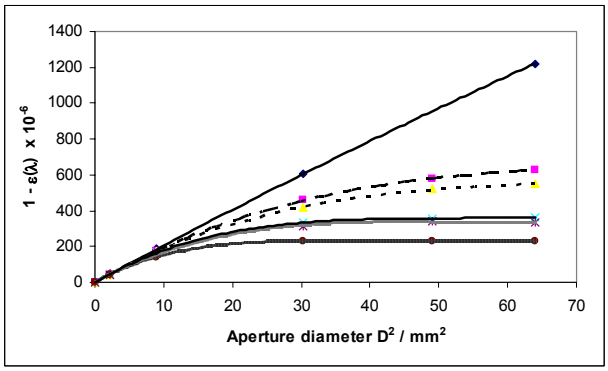

Figure 2: 1-$\varepsilon(\lambda)$ versus D^2. Diamonds: $T(x) = 0$ K, squares: 650 nm-*low*, triangles: 950 nm-*low*, crosses: 650 nm-*high*, asterisks: 950 nm-*high*, circles: *isothermal* $T(x) = T_{cav}$

The variation in apparent cavity temperature ΔT_{cav}(h,l,650) associated with the variation of ε(650) with $T(x)$ between the *high* and *low* profile (Figure 2) is shown in column 2 of the upper half of Table 1 for apertures of 3 mm and 8 mm. Column 3, upper half, shows ΔT_{cav}(av, 0 K, 650) associated with the variation of ε(650) with $T(x)$ between the average of the *high* and *low* profiles $T(x, av)$ and the profile $T(x) = 0$ K, cavity only.

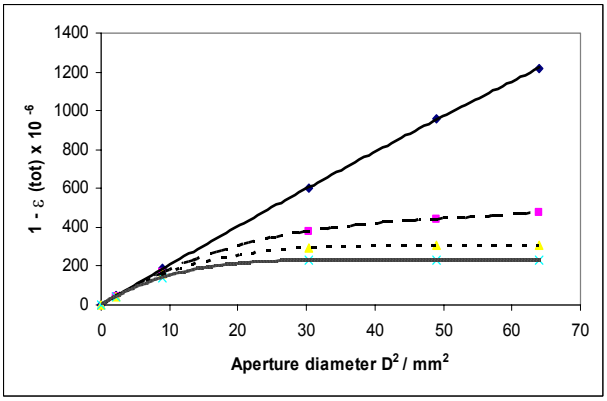

Figure 3: 1-ε(tot) versus D^2. Diamonds: $T(x)$ =0 K, squares: *low*, triangles: *high*, crosses: *isothermal* $T(x) = T_{cav}$

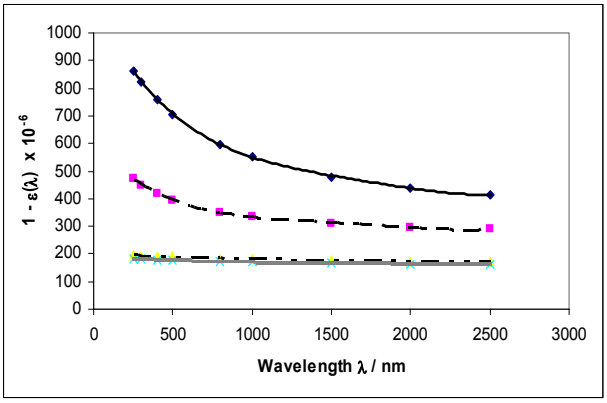

Figure 4: 1-$\varepsilon(\lambda)$ versus λ. Diamonds: 8 mm-*low*, squares: 8 mm-*high*, triangles: 3 mm-*low*, crosses: 3 mm-*high*

D mm	ΔT_{cav}(h,l,650) mK	ΔT_{cav}(av,0,650) mK
3	3.5	6.1
8	91	248
λ nm	ΔT_{cav} (h,l,3) mK	ΔT_{cav}(h,l,8) mK
250	1.5	51
1000	6.3	114
2500	9.3	125

Table 1: Variation ΔT_{cav} in apparent cavity temperature T_{cav} with $T(x)$ for different cavity diameters D and wavelengths λ. Details are given in the text.

Finally in the lower half of Table 1 we show ΔT_{cav}(h,l,3) and ΔT_{cav}(h,l,8) , for D = 3 mm and D = 8 mm, respectively, associated with the variation of $\varepsilon(\lambda)$ with $T(x)$ between the *high* and *low* profile , shown in Figure 4, for wavelengths between 250 nm and 2500 nm. All of the results compiled in Table 1 are based upon the Wien approximation.

Discussion

Figures 2 to 4 clearly show the influence of the furnace-temperature profile $T(x)$ on the calculated emissivities. The upper curve in Figures 2 and 3 is representative for the 'cavity only', $T(x)$ = 0 K; the effect of the furnace is bending this curve downwards, and the more the 'higher' the profile. Below about D = 3 mm the differences 1-ε (λ) and 1 - $\varepsilon(tot)$ are only slightly dependent on $T(x)$ but beyond 3 mm we see a marked variation of the curves with $T(x)$ and -for 1-$\varepsilon(\lambda)$- to a lesser extent with wavelength λ. These observations are reflected by the results shown in Table 1. The variation in apparent cavity temperature T_{cav} with $T(x)$ for D = 8 mm is considerably larger than that for D = 3 mm.

This is all in all a strong argument for keeping the cavity emissivity ε_{cav} as close as possible to unity which -at least in the *present* cavity-furnace configuration- would imply keeping the diameter D of the cavity aperture below about 3 mm. The last column, upper half, of Table 1, showing the variation ΔT_{cav}(av, 0, 650) for D = 3 mm and D = 8 mm is noteworthy, since thus far cavity emissivities have been associated with the profile $T(x)$ = 0 K, cavity only. The effect of the cavity aperture D -at a given cavity-furnace configuration- on the temperature distribution within the cavity will be discussed elsewhere.

It should be stressed that the prime parameter governing the contribution of the furnace to the overall emissivity is the cavity emissivity ε_{cav} rather than D^2. Volume and shape of the cavity for a given D could be further optimized -within the restrictions set by the furnace- so as to increase $\varepsilon_{cav}(D)$ and thereby reducing the contribution of the furnace. This would open opportunities for utilizing fixed-point radiators with relatively large cavity apertures, when fitted into the proper furnace.

Conclusions

From the above it can be concluded that heat exchange between cavity and furnace precludes treating the cavity as a separate unit. It has to be taken as an integral part of the furnace-cavity combination making up the radiator.

Acknowledgements

We are indebted to Dr. Alexander Prokhorov for consulting us on the use of the software package STEEP-3. We wish to thank Dr. Naohiko Sasajima of NMIJ for the information on the furnace and its temperature distribution.

References

[1] Prokhorov, A.V., 'Monte Carlo method in optical radiometry', *Metrologia,* **35,** 1998, pp. 465-471.

[2] Yamada Y., Sasajima N., Gomi H., Sugai T., 'High-temperature furnace systems for realizing metal-carbon eutectic fixed points' *TMCSI,* **7,** 2003, pp. 965-990.

Long-term experience in using deuterium lamp systems as secondary standards of UV spectral irradiance

P. Sperfeld, J. Metzdorf, S. Pape

Physikalisch-Technische Bundesanstalt, Braunschweig, Germany
Email: Peter.Sperfeld@ptb.de

Abstract. During the CCPR-K1.b key comparison "Spectral irradiance in the wavelength range 200 nm to 350 nm", a set of 6 newly developed deuterium lamp systems (DLS) have been used as transfer standards. The long-term experiences during this intercomparison demonstrated the quality of the system and confirmed the intention to provide the DLS for the use as a transfer standard of spectral irradiance in the UV spectral range.

The deuterium Lamp system DLS

The DLS consisting of up to four lamps each, a power supply and a monitor-detector have been developed by the Physikalisch-Technische-Bundesanstalt (PTB). They are the result of a thorough investigation of a variety of deuterium lamps and operating conditions in order to test and optimize their capability (stability, reproducibility, sensitivity to misalignment) for the use as traveling standard [1].

Figure 1. Deuterium lamp system (DLS)
Lamp housing with lamp exchangeably and reproducibly mounted inside and monitor detector that can reproducibly be aligned on the optical axis in front of the housing.

A Cathodeon J64 30W deuterium lamp is the central part of the DLS. The lamp is mounted within a housing in order to protect the lamp and to achieve sufficiently stable and reproducible operating conditions. It is pre-aligned so that the mechanical axis of the housing is in coincidence to the optical axis of the lamp defined by the direction of the maximum output. The exit port of the housing is designed to either hold an alignment target (jig) or a monitor detector as shown in Fig. 1. The reflecting jig with a reticle in its centre defines both the optical and mechanical axis and the reference plane of the lamp system.

A built-in resistor as well as several electronic circuits are used to permanently monitor electrical voltage, current and heating voltage of the lamp during operation.

A group of these housed lamps are reproducibly operated within one DLS which also comprises an external power supply assigned to the DLS. A typical spectrum of a DLS lamp is shown in Fig. 2.

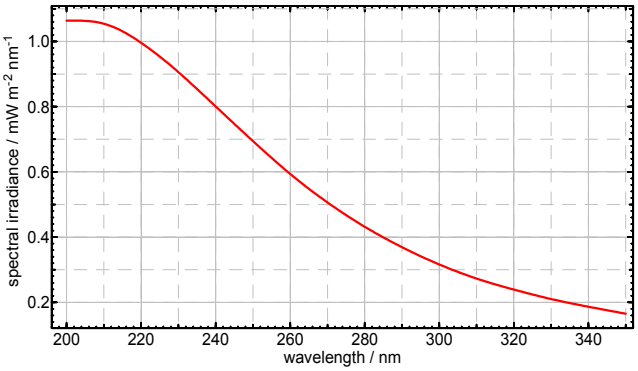

Figure 2. Typical irradiance spectrum of a DLS lamp

Lamp stability during the intercomparison

During the CCPR key comparison K1.b the lamp systems have been treated in different ways: Two systems remained at the PTB, two systems have been hand-carried to and from the participants and two systems were shipped by courier. In combination with the ageing of the lamps during their operation time of up to 45 hrs and the associated realignment and re-ignition processes, the stability and reproducibility of the DLS could be investigated. Earlier investigations of the lamp system showed that under laboratory conditions the long-term drift is less than $-3 \cdot 10^{-4}$ h^{-1} and the re-ignition reproducibility is better than ± 0.1 % [1].

The analysis of the intercomparison which is still in progress showed that during the intercomparison the majority of the lamps changed by less than 2 % in the whole spectral region from 200 nm to 350 nm during up to 45 hrs of burning time. At the PTB which acted as a pilot laboratory for the intercomparison, the mean drift of all

20 lamps was below -2 %. Compared to precedent experiences with UV working standards [2] and compared to the results of the lamp characterizations, this drift is acceptable low.

Implementation of monitor detectors

In conjunction with these promising results, the ability of external SiC photodiodes to monitor the stability of the DLS could be demonstrated. The monitor detector is an optional part of each DLS. It consists of a hybrid SiC photodiode with built-in operational amplifier. The monitor detector can easily and reproducibly be flanged to the lamp housing and is used before and after spectral measurements of the lamp to monitor the drift of the lamp irradiance at about 280 nm during and between miscellaneous measurements.

Using this technique, sudden changes of the lamps as well as the long-term drift can be identified and documented. Thus, it is then possible to at least correct the calibration data by a constant factor which represents the drift. If the spectral drift of a lamp has been measured during the lamp characterization, it is also possible to carry out a spectral correction.

In Fig. 3 three typical examples of lamp changes (low, medium and high drift) and the corresponding variation of the monitor detector signals are shown. This demonstrates the applicability of monitor detectors.

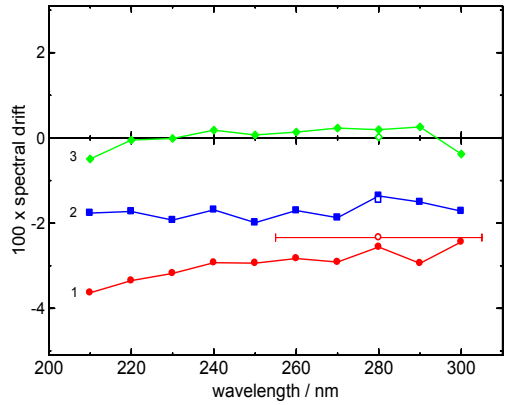

Figure 3. Spectral changes of three different lamps between the first and second calibration sequence at the PTB (the lamp with the highest drift (1), typical example of lamp with medium (2) and low drift (3), respectively). The open symbols at 280 nm refer to the corresponding changes of the monitor detector signals, where the FWHM of the SiC photodiode is indicated.

Conclusion and outlook.

It could be verified that the new deuterium lamp system (DLS) can be used as transfer standard of spectral irradiance in the spectral region from 200 nm to 350 nm. The use of monitor detectors allow to document the long-term changes of the lamps and gives the possibility to correct calibration data for lamp changes.

This gives the possibility to extend the recalibration periods of such transfer standards. The DLS which has been developed by the PTB will be the recommended working standard for the UV spectral range. It will soon be commercially available by the Austrian company Schreder CMS [3].

References

[1] Sperfeld P., Stock K. D., Raatz K.-H., Nawo B., Metzdorf J., Metrologia, 2003, 40, S111 S114.

[2] Hollandt J., Becker U., Paustian W., Richter M., Ulm G., Metrologia, 2000, 37, 563-566.

[3] Schreder J., http://www.schreder-cms.com, Austria, 2005

High-temperature fixed-point radiators: The effect of the heat exchange within the cavity and between cavity and furnace tube on the temperature drop across the back wall of the cavity

P. Bloembergen, Y. Yamada
National Metrology Institute of Japan, AIST, Tsukuba, Japan

P. Jimeno Largo
University of Valladolid, Valladolid, Spain

B.B. Khlevnoy
All Russian Research Institute for Optical and Physical Measurements (VNIIOFI), Moscow, Russia

Abstract. At high temperatures the heat exchange within a cavity radiator and between cavity and front end of the associated furnace are considerably enhanced and by this the temperature drop across the back wall of the cavity within the cavity-furnace combination is markedly influenced. This will be demonstrated, theoretically and experimentally, for the eutectic fixed point Re-C, radiating at a temperature of 2474 °C.

Introduction

For the freezing points of silver and gold the following equation has been used earlier to estimate the temperature drop ΔT across the back-wall of the cavity [1]:

$$\Delta T = \cos\theta \cdot \varepsilon \cdot \sigma \cdot T^4 \cdot \frac{d}{K} \cdot \left(\frac{r}{L}\right)^2 \qquad (1)$$

where θ is the tilt angle of the conical bottom, ε the emissivity of graphite, σ the Stefan-Boltzmann constant, T the temperature in Kelvin, d the thickness of the cavity bottom, K the thermal conductivity of graphite, r the aperture radius and L the cavity length. As shown below this estimate can be considered only as an upper bound to ΔT since in its derivation heat exchange within the cavity (radiative and conductive) and between cavity and furnace front-end (radiative) has been neglected.

Simulations based upon the finite-element method

Simulations are presented for the cylindro-conical cavity in the Re-C eutectic cell 3S2, mounted in furnace VR10 –A19 [2] with following cavity dimensions: L= 45 mm, diameter = 8 mm, θ = 30 °, d = 3 mm, without and with an aperture, 3 mm in diameter. For graphite we assumed : ε = 0.86, K(at 2500 °C) = 36.4 $Wm^{-1} K^{-1}$.

Columns 2 and 3 of Table 1 show the temperature drop $\Delta T(3)$ for a cavity aperture of 3 mm and the difference $T(3)$-$T(8)$ between cavity-bottom temperatures for apertures of 3 mm and 8 mm, calculated for the furnace-temperature profiles $T(x)$, denoted as *low* and *high*, shown in Figure 1. In the table these results are compared with calculations (a) for the cell only, formally implying $T(x)$ = 0 K, (b) by means of Eq. (1), and (c) with experimental results, obtained at wavelengths of 650 and 950 nm, shown in columns 4 and 5, and discussed below. As demonstrated in Table 1, column 2, Eq. (1) indeed constitutes an upper bound to $\Delta T(3)$; the result for the 'cell only' relative to that for Eq. (1) shows the influence of the heat exchange within the cavity.

Profile	$\Delta T(3)$ mK	$T(3)$-$T(8)$ mK		$T(3)$-$T(8)$ 650 nm mK	$T(3)$-$T(8)$ 950nm mK
High	79	130		140 ±80	130 ±30
Low	88	201			
Cell	136	684			
Eq. (1)	219	1340			

Table 1: Temperature drop $\Delta T(3)$ calculated for a cavity aperture of 3 mm and differences $T(3)$-$T(8)$ between cavity-bottom temperatures calculated and measured for apertures of 3 mm and 8 mm. Details are given in the text.

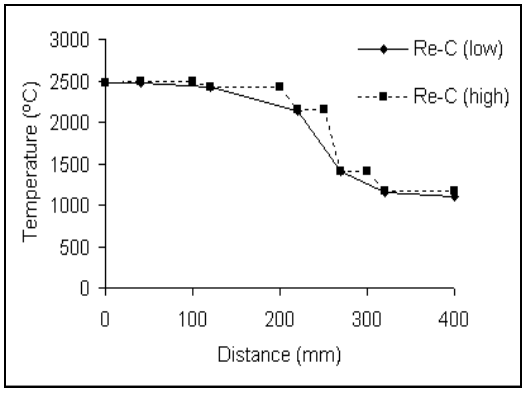

Figure 1: Furnace-temperature profiles $T(x)$, *low* and *high*, used for calculating the temperature drop $\Delta T(3)$ and the differences $T(3)$-$T(8)$; x defines the distance to the cavity aperture.

All of the calculated results presented here are based upon simulations of the temperature drop ΔT at the end of the melting plateau in which-ideally-the liquid-solid interface coincides with the outer wall of the cavity tube. The simulations have been performed using ANSYS, a finite-element software package; details are given in [3].

Experiments

The profile (full line, *low*) given in Figure 1 has been directly measured by means of the radiation thermometer (RT), LP-3 8040, by scanning along the radiation shields placed within the furnace tube in front of the Re-C fixed point (3S2) in study. The dashed profile (*high*) has been constructed so as to represent an upper boundary to the profile as seen by the cavity.

The experimental results given in the last two columns of Table 1 show the temperature difference *T(3)-T(8)* measured with LP-3 8040 for the cavity bottom of the cell 3S2 (a) without aperture (8 mm) and (b) with a 3 mm aperture placed in front of the cavity tube, for filter wavelengths of 650 nm and 950 nm. The measurements were performed on two consecutive days. Drift of the RT has been corrected for by simultaneously measuring the radiance of a second Re-C fixed point (1S1) on both days, realized in parallel in Nagano VR10-A20, a smaller variant of VR10-A23 [2]. The quoted standard uncertainties are based upon the repeatability of the melting temperatures, associated with the inflection points of the melting curves.

Model versus experiment

As may be appreciated from an inspection of Table 1 experimental and calculated results, shown for *T(3)-T(8)* in rows 2 and 3, agree within the combined uncertainties, when roughly associating the uncertainties in the calculated results with the difference between the results obtained for the *high* and *low* furnace profiles. Both experimental and simulated results for *T(3)-T(8)*, rows 2 and 3, are significantly smaller than (a) the results calculated on the basis of the 'cell only' and (b) those calculated by means of Eq. (1), rows 4 and 5, respectively.

Correlation of ΔT with the effective total emissivity

Effective emissivities, $\varepsilon(tot)$ and $\varepsilon(\lambda)$ -for 650 and 950 nm- have been calculated by means of STEEP-3, a software package created by Prokhorov [4], assuming diffusely reflecting grey surfaces with emissivity 0.85. The calculations have been done for the actual cavity-furnace combination constituting the radiator, taking into account the temperature profile *T(x)* of the furnace tube. The cavity itself is assumed to be uniform in temperature.

More details are given in an accompanying paper [5]. Here we confine ourselves to showing (Figure 2) that ΔT and $1-\varepsilon(tot)$ in their variation with cavity aperture are clearly correlated. The three pairs of data points correspond - at increasing values of their coordinates- with cavity apertures of 3 mm, 5.5 mm (interpolated) and 8 mm, respectively ; similar correlations are observed between ΔT and $1-\varepsilon(\lambda)$. A noticeable dispersion of these correlations with $T(x)$ is showing up for values of $1-\varepsilon(tot)$ above about $160 \cdot 10^{-6}$ i.e., within the present cavity-furnace configuration,for apertures above 3 mm, as demonstrated in Figure 2.

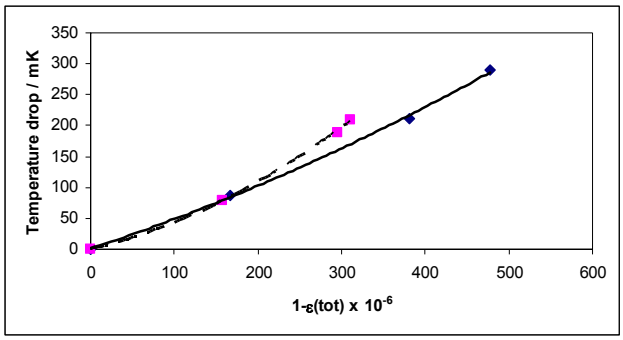

Figure 2: Temperature drop ΔT vs. $1-\varepsilon(tot)$ for the *high* (squares) and *low* (diamonds) profiles *T(x)*

Whether correlations such as shown in Figure 2 can be modeled for a given cavity-furnace geometry and by this allowing to deduce ΔT from direct measurement of *T(x)* via the associated total emissivity $\varepsilon(tot)$, or at least correcting ΔT to that corresponding with a reference distribution *T(x,ref),* remains to be seen.

Conclusion

From the above it can be concluded that at high temperatures heat exchange between cavity and furnace precludes treating the cavity as a separate unit. It has to be taken as an integral part of the cavity-furnace combination making up the radiator in question.

Acknowledgements

We wish to thank Dr. Naohiko Sasajima of NMIJ for the information on the furnace and its temperature distribution. This study was partly supported via the European Commission Project HIMERT, contract number: G6RD-CT-2000-00610.

References

[1] Fischer J. and Jung H. J., 'Determination of the thermodynamic temperatures of the freezing points of silver and gold by near-infrared pyrometry', *Metrologia*, **26**, 1989, pp. 245-252.

[2] Yamada Y., Sasajima N., Gomi H., Sugai T., 'High-temperature furnace systems for realizing metal-carbon eutectic fixed points ' *TMCSI,* **7,** 2003, pp. 965-990.

[3] Jimeno-Largo P., Yamada Y., Bloembergen P., Villamanan, M.A., Machin G., 'Numerical analysis of the temperature drop across the cavity bottom of high-temperature fixed points for radiation thermometry' *Proceedings of Tempmeko 2004,* to be published.

[4] Prokhorov, A.V., 'Monte Carlo method in optical radiometry' , *Metrologia,* **35,** 1998, pp. 465-471

[5] Bloembergen P., Khlevnoy B.B., Yamada Y., Jimeno Largo P., 'High-temperature fixed-point radiators: The effect of the heat exchange between cavity and furnace tube on the effective emissivity of the radiator'. This conference.

A comparison of Co-C, Pd-C, Pt-C, Ru-C and Re-C eutectic fixed points independently manufactured by three different institutes

K. Anhalt, J. Hartmann
Physikalisch- Technische Bundesanstalt Braunschweig und Berlin, Germany

D. Lowe, G. Machin
National Physical Laboratory, Teddington, UK

M. Sadli
CNAM- INM, Paris, France

Y. Yamada, P. Bloembergen
National Metrology Institute of Japan, AIST, Tsukuba, Japan

Abstract. In order to assess the performance and capability as well as the reproducibility of cell production five different Metal-carbon (M-C) eutectic cells from three institutes were measured by radiation thermometry at PTB. The reproducibility of the melting temperature approached the requirements set by CCT/CCPR but significant differences were seen between different manufactures.

Introduction

Metal- Carbon (M-C) eutectics are possible candidates for thermometric and radiometric fixed-points above the Au point temperature of 1337.33 K. They are being manufactured and investigated at a wide number of institutes. To become recommended temperature fixed points the repeatability and reproducibility of these systems have to be carefully investigated so as to guarantee a high level of world wide equivalence. For this reason a comparison was carried out at PTB in May 2004 of five different M-C cells manufactured by CNAM-INM, NPL and NMIJ within the EU project HIMERT [1].

Outline and experimental setup

In order to assess the performance of the cells with low uncertainty the relative differences in radiance temperature of the melting of the M-C cells were determined by installing them in furnace systems with virtually identical temperature homogeneity. Measurements were done with two radiation thermometers.

M-C eutectic cells with Co-C, Pd-C, Pt-C, Ru-C and Re-C as fixed point material and melting temperatures between 1300 K and 2800 K were manufactured by CNAM-INM, NPL and NMIJ and brought to PTB. Their outer dimensions were similar: approx. 25 mm in diameter, 40-50 mm in length, and a cavity aperture of 3 mm.

Furnace systems As in former comparisons effects of the furnace on the melting process could not be excluded [2], two similar Nagano furnaces were supplied by the NMIJ: Nagano S (VR10-A20) and Nagano M (VR10-A23) [3]. Their equivalence has been investigated prior to the comparison, showing similar temperature homogeneity for temperatures up to 2300 K resulting in an equivalent performance of both M-C cells to be compared.

Radiation thermometers For the radiance measurements two LP3 radiation thermometers with low size-of source-effect were used, the LP3 80-46, brought to Berlin by the BNM-INM, and the LP3 80-05, provided by the PTB, both with an improved interference filter setup for measurements at high temperatures characterized by an effective wavelength of about 650 nm [4].

Experimental procedures During 14 days measurements in both furnaces were performed. For each cell in each furnace four melting and freezing plateaus with defined temperature steps were monitored with both radiation thermometers resulting in a total of 16 melts and freezes per day.

For the measurements of the Co-C, Pd-C, Pt-C eutectics both furnaces were equipped with a cell of the same material allowing a 'parallel scheme' to be established during one day. The temperatures sensed by the radiation thermometers never exceeded the melting temperature of the cell material under investigation by more than 30 K. For furnace temperatures higher than 2500 K the temperature homogeneities of the two furnaces are no longer identical; then the Nagano M furnace provides the best available conditions. Therefore, the Re-C cells were compared consecutively in the Nagano M furnace, while on these days the Nagano S furnace was used to investigate the Ru-C cells.

Uncertainties

Uncertainty components considered are: cell repeatability, size-of-source-effect, uncertainty of the inflection point determination, and the radiation thermometers stability.

Size-of-source-effect The nearly identical temperature profiles of both furnaces, equipped with an identical set of radiation shields results in a small size-of-source-effect (SSE) difference between the cells (maximum 15 mK for Re-C). Therefore, the signal is not corrected for the SSE and instead the effect is included in the uncertainty budget.

Radiation thermometer stability In order to detect a drift of the radiation thermometers certain cell-furnace combinations remained unchanged on consecutive days or were reinstalled during the time of the comparison. From the difference between such two measurements the stability of the radiation thermometers can be derived. During the measurements of Co-C, Pd-C, Pt-C the drift was less than 40 mK for both radiation thermometers. At 2300 K (Ru-C) and 2750 K (Re-C) larger and significant drifts of up to 100 mK were observed, resulting in higher uncertainties for

these materials.

Repeatability of a single cell For each cell an average melting temperature was determined from the four melt/freezes obtained. The standard deviation of this average temperature was taken as a measure for the cell repeatability. The repeatability for all cells from all manufacturers was better than 80 mK, and when omitting the Pd-C cells of NPL and INM better than 40 mK.

Results

The differences from the average melting temperature for each material are summarized as measured by both radiation thermometers in Table 1 and Figure 2.

	T / K	T / K	T / K	u / K, (k=1)	
Co-C	-0.00 0.01	0.04 0.06	-0.04 -0.06	0.04 0.04	LP3 (PTB) LP3 (INM)
Pd-C	-0.07 -0.07	0.21 0.20	-0.14 -0.13	0.06 0.05	LP3 (PTB) LP3 (INM)
Pt-C	-0.06 -0.07	0.03 0.04	0.02 0.03	0.05 0.04	LP3 (PTB) LP3 (INM)
Ru-C	-0.03 -0.01	0.23 0.16	-0.20 -0.15	0.12 0.10	LP3 (PTB) LP3 (INM)
Re-C	-0.06 -0.02	0.08 0.09	-0.02 -0.07	0.12 0.10	LP3 (PTB) LP3 (INM)
	NPL	NMIJ	INM		

Table 1: Differences of cells melting point temperature with respect to the materials average melting point temperature, shown for both radiation thermometers

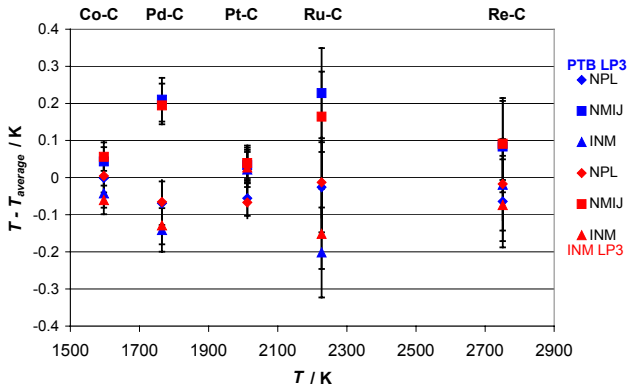

Figure 2: Differences of cells melting point temperature with respect to the materials average inflection point temperature. PTB LP3 in blue, and INM LP3 in red.

Discussion

Differences between materials From the results presented above the cells can be split up into two groups, one which shows an internal agreement to within ~ 200 mK (Co-C, Pt-C and Re-C), the other showing an agreement to within ~ 450 mK (Pd-C and Ru-C). This result reflects the purity level of the used metals. Pd (99.99%, only NMIJ 99.999 %) and Ru (99.95 %) were not available at the same purity level as Co (99.998 %), Pt (99.999 %) and Re (99.999 %).

Differences in manufacture Systematic differences in manufacture can be inferred from the distribution of melting temperatures and from a comparison of plateau shapes. The data do not scatter randomly around the averaged values used in creating Table 1 and Fig 2. For all materials the cells which showed the highest melting temperatures, smallest melting ranges and longest plateaus were produced by the NMIJ. Melting point depression and reduction in melting range are properties usually understood to be related to less pure material components. For most of the metals the nominal purity levels, as specified, were the same for all institutes, and if reliable, the experimental results obtained suggest that contamination has occurred during the manufacturing processes. This conclusion was further investigated by studies on the effect of different methods used for cell manufacture [5].

Conclusion

Co-C, Pd-C, Pt-C, Ru-C, and Re-C eutectic fixed-point cells manufactured by CNAM-INM, NPL and NMIJ were investigated by directly comparing their melting temperatures. In order to achieve lowest uncertainties it proved essential to use two virtually identical furnaces in a parallel scheme, as the largest source of uncertainty was the radiation thermometer instability. The already achievable high level of agreement found for Co-C, Pt-C and Re-C proves the applicability of these systems as fixed points in thermometry. Systematic differences found in the manufacture of the cells are indicative for further improvements in cell construction. In future, direct comparisons similar to the one described above will be necessary to assess such improvements.

Acknowledgement This work was part supported by the European Commission "GROWTH" Programme Research Project "Novel high temperature metal-carbon eutectic fixed- points for Radiation Thermometry, Radiometry and Thermo- couples" (HIMERT), contract number: G6RD-CT-2000-00610. Tanaka Kikinzoku Kogyo is acknowledged for lending the high purity metal powder for the NMIJ Pt-C cell. The authors would like to thank S. Schiller for technical assistance.

References

[1] Machin, G., Beynon, G., Edler, F., Fourrez, S., Hartmann, J., Lowe, D., Morice, R., Sadli, M., Villananan, M., "HIMERT: a pan-European project for the development of metal carbon eutectics at temperature standards", Proc. of Temperature:, Vol. 7, ed. Ripple, D., AIP Conf. Proc., Chicago, 2003, pp. 285-290

[2] Machin et al., A comparison of high temperature fixed-points of Pt-C and Re-C constructed by BIPM, NMIJ and NPL, Proceedings of Tempmeko 2004, Dubrovnik

[3] Yamada, Y., Sasajima, N., Gomi, H., Sugai, T., "High temperature furnace systems for realising metal-carbon eutectic fixed points", Proc. of Temperature: Its Measurement and Control in Science and Industry, Vol. 7, ed. Ripple D., AIP Conf. Proc., Chicago, 2003, pp. 985-990.

[4] Hartmann, J., Anhalt, K., Hollandt, J., Schreiber, E., Yamada, Y., "Improved thermal stability of the linear pyrometer LP3 for high temperature measurements within the EU-project Himert" Temperatur 2003, VDI-Bericht 1784, Berlin, 2003.

[5] Lowe, D., Yamada, Y., "Comparison Of Metal-Carbon Eutectic Fixed-Point Construction Methods", to be presented at Newrad2005

Irradiance measurements of Re-C, TiC-C and ZrC-C fixed point blackbodies

K. Anhalt, P. Sperfeld, J. Hartmann
Physikalisch- Technische Bundesanstalt Braunschweig und Berlin, Germany

M. Sakharov, B. Khlevnoy, S. Ogarev, V. Sapritsky
All-Russian Research Institute for Optical and Physical Measurements (VNIIOFI), Moscow, Russia

Abstract. Specially designed Re-C, TiC-C and ZrC-C fixed-point cells for irradiance measurements have been produced by VNIIOFI. In several investigations at VNIIOFI and PTB the usability of the design for irradiance measurements has been demonstrated. Current developments of furnace uniformity demonstrate further improvements to the systems.

Introduction

High-temperature fixed-points using Metal carbon (MC) and metal carbide carbon (MC-C) systems provide innovative reference standards for radiometry and thermometry [1]. While temperature metrology would benefit from any additional fixed-point higher than the freezing temperature of gold (1337.33 K) [2], the needs for radiometry are primarily highest temperature to provide sufficient and stable radiance and irradiance even in the UV spectral range with a considerable large cavity aperture [3].

Fixed-point design

VNIIOFI introduced a special design of MC and MC-C fixed-point cells for the use in the VNIIOFI/VEGA BB3200/BB3500 furnaces [4]. These furnaces are in use worldwide in research institutes and NMIs. The cells have a length of approx. 95 mm and a diameter of 30 mm, as can be seen in Fig. 1.

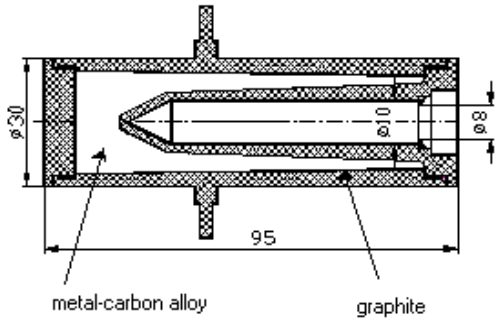

Figure 1: Schematics of the large aperture eutectic fixed-point cells manufactured by the VNIIOFI

Due to their special design a diameter of the radiating cavity of 10 mm is realized, which is more than a factor of three larger than the 3 mm diameter usually obtained with the smaller cells [3]. This large radiating area offers the possibility to perform irradiance measurements using absolutely calibrated filter radiometers. If the spectral irradiance is measured in absolute units under a well-defined geometry and the emissivity of the cavity is known, it is possible to determine the thermodynamic transition temperature of the eutectic material via Planck's law of thermal radiation. With such a calibration a fixed-point cell can serve as an absolute standard for radiance and irradiance in radiometry and photometry.

Experimental setup

The large cavity diameter allows a precision aperture to be positioned in front of the cavity outside the furnace, defining the radiating area. A schematic of the experimental set-up is given in Fig. 2.

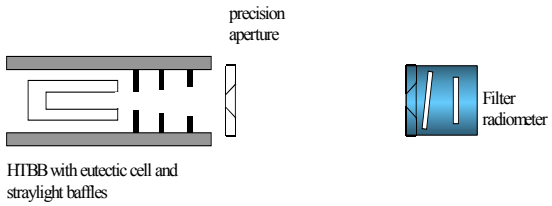

Figure 2: Scheme of the experimental set-up used for measuring the thermodynamic temperature of the cells

In the experiments at VNIIOFI and PTB the precision aperture in front of the HTBB has a diameter of 3 mm, while the apertures of the filter radiometers are approx. 5 mm in diameter, the distance between the two apertures was about 1110 mm.

Detectors

Two different types of filter radiometers were used: Three narrow-band interference filter radiometers with centre wavelengths around 676 nm, 800 nm, and 900 nm, and one broad-band glass filter radiometer, having a centre wavelength around 550 nm [5]. The spectral irradiance responsivity of the filter radiometers has been calibrated traceable to the cryogenic radiometer of the PTB [6].

Experiments at VNIIOFI and PTB

The HTBB furnace was stabilized at a temperature approx. 25 K below the melting temperature of the eutectic material. The melting process was initiated by a step-like current increase of approx. 40 A after which the furnace was stabilized at a temperature of about 25 K above the melting temperature. For initiating the freezing of the eutectic alloy the temperature in the furnace was suddenly reduced and stabilized at a temperature of about 25 K below the freezing temperature.

From the measured temperature profiles the point of inflection during the melt was taken as the transition

temperature of the cell. The obtained temperatures were additionally corrected for diffraction loss, occurring at each of the two precision apertures.

Results

	Re-C		
	# melts	**average ± *u***	**Std. dev.**
FD 17	2	2745.55 ± 0.31	0.45
FR 676	6	2746.15 ± 0.38	0.33
FR 800	10	2745.81 ±0.45	0.33
FR 900	3	2745.48 ± 0.51	0.25

	TiC-C		
	# melts	**average ± *u***	**Std. dev.**
FD 17	5	3031.22± 0.36	0.16
FR 676	11	3031.13± 0.44	0.22
FR 800	6	3031.00± 0.53	0.14
FR 900	1	3030.53±0.59	-
FD 17 @VNIIOFI		3031.6 ± 0.35	-

	ZrC-C		
	# melts	**average ± *u***	**Std. dev.**
FR 676	3	3153.86 ± 0.44	0.16
FR 800	6	3153.78 ± 0.53	0.47
FD 17 @VNIIOFI		3154.28 ± 0.40	-

Table 1: Temperatures in Kelvin for the measurements at PTB and VNIIOFI.

The results presented in Table 1 are the first thermodynamic temperature measurements of eutectic fixed-point cells by absolute radiometry using filter radiometers in the irradiance mode. The results obtained at the VNIIOFI and the PTB all agree within their combined uncertainty, indicating that the reproducibility of the large irradiance cells in different furnaces measured with different detectors is very good.

However, all three fixed-point cells showed poor plateaus compared to fixed-point cells with smaller dimensions and a 3 mm aperture [7]. This is probably due to the larger dimensions of the large VNIIOFI cells, which require a uniform furnace temperature over a larger distance than smaller cells. Additionally a regular ingot formation is more difficult to achieve for with increasing cell dimensions. The measurements can therefore not be taken representative for the materials thermodynamic melting temperature.

Improvements to plateau shape and furnace systems

In a recent study improvements of the melting and freezing plateau of the VNIIOFI large area eutectic fixed-point cells have been shown by enhancing the uniformity of the furnace [8].

A good agreement in the melting temperature of small and large eutectic fixed-point cells for an optimized furnace setup has been shown [3]. Systematic methods to improve the uniformity of a BB3200/BB3500 furnace have recently been presented [9].

It was shown that the cavity is up to 10 times more uniform during melt and freeze [8]. Such cavity uniformity is important for applications in radiometry as it allows more accurate spectral irradiance measurements in the ultraviolet.

Additionally, for irradiance measurements the uncertainty due to diffraction at the apertures can be reduced with the upcoming of the BB3500 furnaces by the use of larger precision apertures of up to 6mm in diameter. The BB3500 furnaces have larger inner diameters of up to 50 mm, and therefore can hold fixed point cells with a cell aperture of up to 15 mm.

Conclusions

The thermodynamic temperature of Re-C, TiC-C, and ZrC-C has for the first time be measured using absolute filter radiometers in the irradiance mode. Such kind calibrated fixed-points with large radiating area can serve as absolute standards for radiance and irradiance in radiometry and photometry. Due to the huge dimensions the performance of the investigated cells was not ideal, but is presently under further improvements using an ameliorated furnace design.

Acknowldgement The authors would wish to thank Emma Wooliams from the NPL for supplying the 3mm precision aperture.

References

[1] Yamada, Y., "Advances in High-Temperature Standards above 1000 °C", MAPAN, J. of Metrol. Soc. Of India, Vol.20, No.2, 2005, pp.183-191

[2] Quinn T.J., *International Report: News from the BIPM*, Metrologia **34**, 1997, pp. 187-194

[3] Khlevnoy, B.B., Sapritsky, V.I., Ogarev, S.A., Sakharov, M.K., Samoylov, M.L., Pikalev, Yu.A., Development of fixed-points above 2700 K based on M-C and MC-C eutectics at VNIIOFI radiation thermometry and radiometry, *Tempmeko 2004,* to be published

[4] Sapritsky V. et al. , *Applied Optics,* 36, 5403-5408, 1997.

[5] Hartmann, J., Anhalt, K., Sperfeld, P., Hollandt, J., Sakharov, M., Khlevnoy, B., Pikalev, Y., Ogarev, S., Sapritsky, V., "Thermodynamic temperature measurements of the melting curves of Re-C, TiC-C and ZrC-C eutectics irradiance mode fixed-point cells, *Tempmeko* 2004, to be published.

[6] Friedrich, R., Fischer, J., Stock, M., *Metrologia*, **32**, 1995/96, pp. 509-513

[7] Machin G., Beynon G., Edler F., Fourrez S., Hartmann J., Lowe D., Morice R., Sadli M., and Villamanan M., *AIP Conference Proceedings* **684,** 2003, 285-290

[8] Woolliams E., Khlevnoy B., Sakharov M., Samoylov M., Sapritsky V., Investigation of TiC-C and ZrC-C eutectic fixed-point blackbodies., *Submitted to Metrologia*.

[9] B. Khlevnoy, M. Sakharov, S. Ogarev, V. Sapritsky, Y. Yamada, K. Anhalt., A New Furnace for High-Temperature Metal (Carbide)-Carbon Eutectic Fixed-Points., NEWRAD2005, *in these proceedings.*

Evaluation and improvement of the performance of a commercially available detector stabilized radiance sphere source

E. F. Zalewski and S. F. Biggar
University of Arizona, College of Optical Sciences, Tucson, Arizona, USA

Abstract. Many national standards laboratories have recently introduced new and more accurate radiometric calibrations (White et al. 1996; Sperfeld et al. 1996; Yoon et al. 2002). In order to improve measurements in the field these new calibrations must be reliably transferred to the user's laboratory. Incandescent lamps are typically used as calibration transfer devices but are of questionable stability. Improvements in calibration transfer devices have been made using silicon photodiodes to monitor and correct for lamp instabilities (Fox et al. 1998; Windsor et al. 2000). Recently sphere sources of spectral radiance have become available commercially that are based on an incandescent lamp and that incorporate a silicon photodiode to control radiance within the sphere. The incandescent lamp is located outside the sphere and its output is attenuated by a variable slit at the entrance to the sphere. The signal from the silicon photodiode is used in a feedback circuit to control the slit width in order to correct for lamp fluctuations. In addition, by changing the slit width the radiance level can be varied continuously over a very large dynamic range; presumably without changing the spectrum of the incandescent light source.

We have purchased and examined one of these commercial sphere sources and found it to be repeatable within the manufacturer's specifications at one radiance level (within +/-0.5% after the recommended warm-up interval). However, we have found that upon changing the slit width the spectral output of the sphere source varied outside the limits of the specifications. In order to correct for these spectral changes we have introduced additional spectrally filtered detectors to measure the sphere spectral radiance. Other changes we have incorporated include thermal stabilization of the manufacturer's control detector and flushing the sphere with dry nitrogen to improve repeatability in the short-wave ir where absorption by water vapor would cause non-repeatability.

These modifications were tested as a prototype before final incorporation into the sphere source system. Repeatability of the absolute spectral radiance was measured by comparisons with our highly stable VNIR (Biggar, 1998) and SWIR (Spyak et al., 2002) transfer radiometers.

Our prototype modifications have improved the repeatability of the sphere source by a factor of five not only at a single radiance level but also over a wide dynamic range of radiance output. We will present details of the design of our improvements to the sphere source and the results of our repeatability tests.

References

Biggar, S. F., Calibration of a visible and near infrared portable transfer radiometer, *Metrologia*, 35, 701-706, 1998.

Fox, N. P., C. J. Chunnilall, M. G. White, Detector based transfer standards for improved accuracy in spectral irradiance and radiance measurements *Metrologia*, 35, 555-561, 1998.

Sperfeld, P., K.-H. Raatz, B. Nawo, W. Moeller, J. Metzdorf, Spectral irradiance scale based on radiometric black-body temperature measurements, Remote sensing aids in sea-ice analysis, *Metrologia*, 32, 435-439, 1996.

Spyak, P. R., D. S. Smith, J Thiry, C. Burkhart, Short-wave infrared transfer radiometer for the calibration of the Moderate-Resolution Imaging Spectrometer and the Advanced Spaceborne Thermal Emission and Reflection Radiometer, *Applied Optics*, 39, 5694-5706, 2000.

White, M. G., N. P. Fox, V. E. Ralph, The characterization of a high temperature blackbody as the basis for the NPL spectral irradiance scale, *Metrologia*, 32, 431-434, 1996.

Windsor, S. A., N. J. Harrison, N. P. Fox, The NPL detector stabilized irradiance source, *Metrologia*, 37, 473-476, 2000.

Yoon, H. W., C. E. Gibson, P. Y. Barnes, The realization of the National Institute of Standards and Technology detector-based spectral irradiance scale, *Applied Optics*, 41, 5879-5890, 2002.

The Spectrally Tunable LED light Source – Design and Development Issue

I. Fryc[1], S. W. Brown and Y. Ohno
National Institute of Standards and Technology, Gaithersburg, MD 20899, USA
[1]Guest Scientist from the Bialystok University of Technology, Bialystok, Poland

Abstract. A spectrally tunable light source using a large number of LEDs and an integrating sphere has been developed at the National Institute of Standards and Technology (NIST). The source is designed to have a capability of producing any spectral distribution, mimicking various light sources in the visible region by feedback control of the radiant power emitted by individual LEDs. The spectral irradiance or radiance of the source is measured by a standard reference instrument; the source will be used as a transfer standard for colorimetric, photometric and radiometric applications. Source distributions have been realized for a number of target distributions.

Introduction

Photometric and colorimetric quantities of a light source can be measured with a spectroradiometer (calculated from its spectral power distribution) or with a photometer or a colorimeter that have a relative spectral responsivity approximated to the spectral luminous efficiency function, $V(\lambda)$, or the color matching functions defined by the CIE[1, 2]. The spectral correction filter is an essential component of a photometer or colorimeter. Tristimulus colorimeters typically use three or four channels of detectors with filters to mimic the CIE color matching functions. No photometer or colorimeter exactly matches their spectral responsivities to $V(\lambda)$ or the color matching functions. Due to this imperfect matching of the spectral responsivities, measurement errors are inevitable. These measurement errors can increase dramatically when the relative spectral power distribution (SPD) of a test source is dissimilar from that of the calibration source. Such spectral mismatch errors will be minimized by calibrating the photometer or colorimeter with standard sources having similar spectra as the source to be measured. Spectroradiometers also have various sources of error including stray light, and these errors can be minimized by calibrating the instrument with a standard source having similar spectra as the source being measured.

A spectrally tunable source, capable of matching the Spectral Power Distribution (SPD) of a variety of light sources, would enable accurate and rapid calibration of colorimeters or photometers used to measure various types of sources. Such a spectrally tunable source using multiple LEDs has been designed and constructed at the National Institute of Standards and Technology (NIST). Utilizing LEDs with different peak wavelengths and spectral power distributions, it is possible to make a spectrally tunable light source[3] (STS) capable of providing a high fidelity spectral match to given "target" SPDs[4]. The STS is able to approximate the distributions of a wide variety of light sources, including daylight illuminants, with high spectral fidelity. In this paper, we present the construction and performance of the LED-based STS that has been developed.

1. Construction of the STS

The STS (Fig. 1) is an integrating sphere source illuminated by a large number of LEDs having different spectral peaks and distributions. The sphere (30 cm diameter) has an opening of 10 cm maximum diameter. The LEDs can be driven and controlled individually with a 256 channel, computer-controlled power supply. The large number of spectral channels helps facilitate accurate matching of fine structure in target source SPDs.

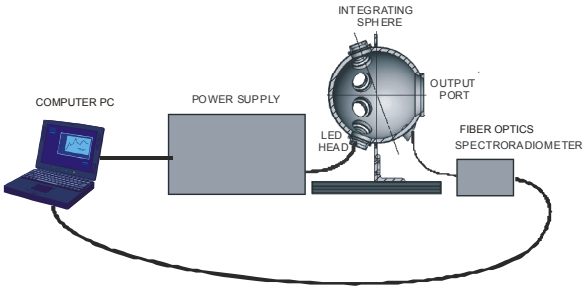

Fig. 1. Configuration of the NIST STS.

A diode array spectroradiometer and a photometer are used as monitor devices to determine the real-time radiometric and photometric output of the STS, respectively. A computer logs the output of the spectroradiometer and individually controls the drive currents of the LEDs to obtain the required target source distribution. The LEDs are mounted in 8 to 10 heads equipped with a temperature-controlled mounting plate to cool the LEDs and stabilize their temperature.

2. Spectral matching algorithm

An algorithm was developed to achieve the best matching of the output spectrum of the source to any input target spectrum. In the optimization, the values of power coefficients k_i, $i = 1...n$ for the n different LEDs are determined. The power coefficient k is strongly related to the current applied to, or radiant flux from, the LED belonging to that variable. The resulting spectrum is the sum of all LED SPDs, weighted by the k 's calculated according to the optimization algorithm.

The optimization consists of the following steps:

1) Select the initial values of power coefficients $k_i^{(0)}$, $i = 1...n$ of i-th LED; they can be any positive number.

2) Calculate the j-th value of k_i from the *(j-1)*-th value, based on the partial derivative with respect to k_i of the square of the difference between the target spectrum and the STS spectrum built up from the LED spectra weighted by the variables k:

$$k_i^{(j)} = k_i^{(j-1)} - a \frac{\partial \sum_{380}^{780} \left(\sum_{i=1}^{n} k_i^{(j-1)} S_{\mathrm{LED}_i}(\lambda) - S_{\mathrm{TARGET}}(\lambda) \right)^2}{\partial k_i^{(j-1)}},$$

where a should be between 0 and 1. To achieve an optimal calculation time while still ensuring convergence of the solution, a parameter was set to 0.001.

3) Continue the iterations until the solution converges, i.e. when

$$\sum_{380}^{780} \left| \sum_{i=1}^{n} k_i^{(j)} S_{\mathrm{LED}_i}(\lambda) - S_{\mathrm{TARGET}}(\lambda) \right| = \sum_{380}^{780} \left| \sum_{i=1}^{n} k_i^{(j-1)} S_{\mathrm{LED}_i}(\lambda) - S_{\mathrm{TARGET}}(\lambda) \right|$$

The equality is obtained from a large number of iterations where the individual LED currents (power coefficients k) are increased or decreased in small increments. It can be interpreted that the algorithm stops when the values k_i reach a steady-state solution. The individual LED currents are obtained from the optimization. The integral-sum of the differences at each wavelength is an indication of the quality of the realized spectral match.

3. Realized STS spectral distributions

Figs. 2 to 4 shows examples of the output spectra of the STS source matched to the given spectra. The deviations from the given spectra are mainly caused by limitations in the availability of LEDs with the appropriate peak wavelengths, their finite spectral widths (SPD curves), as well as drifts due to temperature dependence, instability, and aging of the LEDs. The matching will be improved by changing the selection of LEDs used. The average luminance of the STS, which depends on the specific spectral distribution desired, is between several hundred and one thousand [$\mathrm{cd \cdot m^{-2}}$]. Further results of characterizaion of the STS source developed will be presented in the full paper.

4. Conclusions

A spectrally tunable LED source (STS) has been developed. The source can approximate various CIE illuminants (D65, etc.) as well as common source spectral distributions for other photometric and colorimetric applications, and may be useful for visual experiments on colorimetry as well.

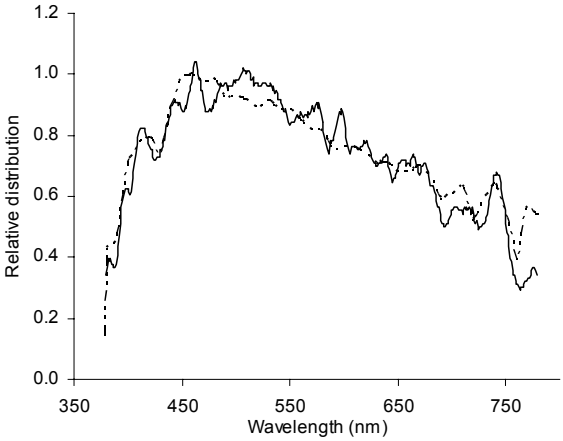

Fig. 2. SPD of CIE illuminant D65 (dashed line) and the STS output measured by spectroradiometer (solid line).

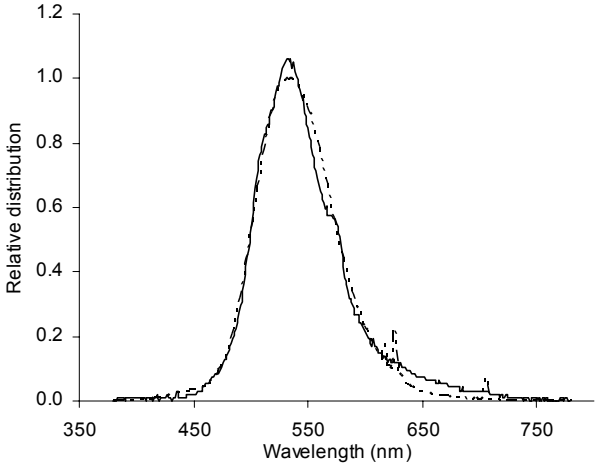

Fig. 3. SPD of a CRT green (dashed line) and the STS output measured by spectroradiometer (solid line).

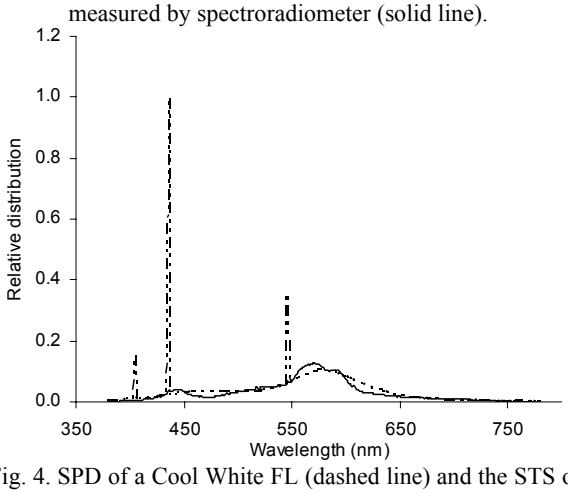

Fig. 4. SPD of a Cool White FL (dashed line) and the STS output measured by spectroradiometer (solid line).

References

[1] ISO/CIE 10527-1991, CIE standard colorimetric observers, 1991.

[2] ISO/CIE 10526-1991, CIE standard colorimetric illuminants, 1991.

[3] S. W. Brown, C. Santana, and G. P. Eppeldauer, Development of a tunable LED-based colorimetric source, J. Res. Nat'l. Inst. Stands. Technol. 107, 363-371, 2002.

[4] I. Fryc, S. W. Brown, G. P. Eppeldauer, Y. Ohno, A spectrally tunable solid-state source for radiometric, photometric, and colorimetric applications, Proceedings of SPIE, 5530, 150 – 159, 2004.

Session 9

Realisation of scales

The Realization and the Dissemination of Thermodynamic Temperature Scales

H. W. Yoon
NIST, Gaithersburg, MD, USA

Abstract. Since the establishment of the International Temperature Scale of 1990 (ITS-90), much progress has been made in the development of radiometers and blackbody sources. Cryogenic electrical-substitution radiometry is widely used in detector and radiometer calibrations, and stable, high-temperature metal-carbon eutectic blackbodies are under development. Radiation thermometers can be calibrated for absolute radiance responsivity, and blackbody temperatures determined from the amount of optical power without the use of any fixed points. These temperatures can be measured with lower final uncertainties than the ITS-90 derived temperatures. Just as the definition the photometric base unit, the candela, has been changed to one of optical power, the thermodynamic temperatures can be directly realized from optical power and length units. Because of these developments, any future international temperature scale should be revised so that a thermodynamic temperature scale can be directly disseminated with transfer standard sources or radiation thermometers.

Introduction

In the ITS-90, temperatures above the freezing temperature of silver are determined with radiation thermometers calibrated using spectral radiance ratios to one of the Ag-, Au- or Cu-freezing temperature blackbodies and the Planck radiance law. However, due to the use of spectral radiance ratios, the temperature uncertainties of the ITS-90 increase as the square of the temperature ratios, and recent acoustic-thermometry measurements have also shown that the temperatures used in the radiance ratios in determining the Ag- and Au-fixed point temperatures could be in error. Furthermore, as radiation thermometry is improved, the ITS-90 scale may be non-unique due to the choice of any one of the three fixed points as the basis for the scale.

Another strong impetus for the development of direct thermodynamic temperature measurements traceable to optical power has been the development of metal-carbon eutectic blackbodies. A temperature scale could be generated from the use of these eutectics as interpolation points to be used by the radiation thermometer. Such a scheme would simplify radiation thermometer calibrations especially transfer to the secondary laboratories. Thus far, one of the most pressing issues has been the lack of a sufficient number of thermodynamic temperature determinations of the metal-carbon eutectic transition temperatures at the different NMIs.

This talk will review the different techniques for realizing thermodynamic temperature and why detector-based radiance temperature has proven to be so useful. Some of the smaller NMIs are beginning to develop the capabilities for such measurements. The techniques used at NIST for the realization of thermodynamic temperatures will be reviewed. The development of stable radiation thermometers with low size-of-source effect will be discussed. Possible detector-based replacements for the fixed-points using light-emitting diodes will be discussed.

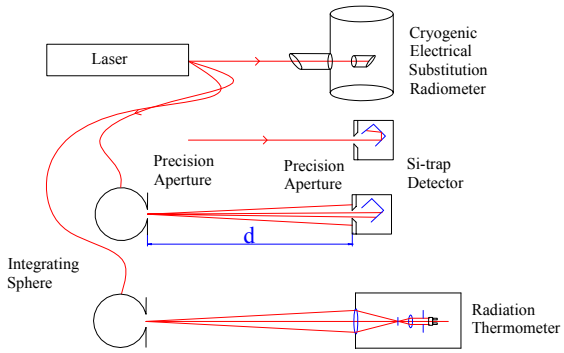

Experimental Setup

The basis of the calibration of the radiation thermometer at NIST is the measurement of optical power using the cryogenic electrical substitution radiometer and the steps of the calibrations are shown in Fig. 1.

Figure 1. The sequence of calibrations to realize thermodynamic temperatures at NIST.

The traceability to the length unit is necessary for the measurements of distances and the aperture areas in the second and the third steps in the realization.

One of the barriers to thermodynamic temperature dissemination is the need for radiometric characterizations of radiation thermometers. Radiation thermometers have been constructed at NIST to achieve the desired imaging, low size-of-source effect, and long-term stability. Figure 2 shows the schematic of one of the NIST radiation thermometer designs.

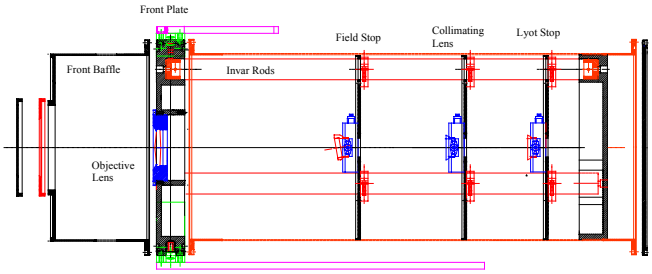

Figure 2. NIST Absolute Pyrometer 2 (AP2) design utilizing Invar rods for structural stability.

The AP2 utilizes temperature-stabilized filters and detectors for long-term stability. The AP2 also utilizes a low-scatter objective lens with a Lyot stop to reduce the size-of-source effect (SSE). A comparison of the radiation thermometer with and without the Lyot stop is shown in Fig. 3.

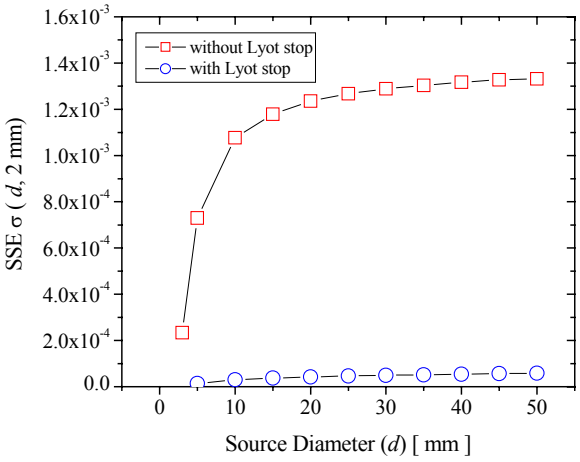

Figure 3. The SSE measured with and without the Lyot stop.

Irradiance Mode Radiation Thermometers

Since the procedure for the detector-based candela realization can be also used for the characterization of irradiance mode filter radiometers, these filter radiometers can also be used to measure thermodynamic temperatures. Some of the NMIs use a monochromator-based facility since laser-based spectral irradiance or radiance responsivity calibration facilities can be prohibitively expensive.

The difficulties in utilizing monochromator-based calibrations will be discussed. The non-imaging filter radiometer also suffers from a "size-of-source" effect arising from the uncertainties in the diffraction corrections from the source aperture when used with fixed-point cavities with small openings.

Detector-based Validation Sources

One of the major difficulties in disseminating the low uncertainties achievable with modern cryogenic radiometers is that filter radiometers and radiation thermometers change due to environmental and aging effects primarily due to the change in the filter transmittance. Hermetically sealed silicon diodes have demonstrated long-term stability of < 0.02 % from 450 nm to 900 nm over a ten-year period and it might be possible to use these detectors in conjunction with light-emitting diodes (LED) to develop spectral sources with similar long-term stability. Such sources have the potential to replace the metal fixed-points which have been thus far used to measure the stability of the radiation thermometers. Signal-to-noise comparisons of the LED sources with the Au freezing-temperature blackbody will be discussed.

Discussion

The needs for developing detector-based thermodynamic temperatures are driven by the desire to reduce the uncertainties in the disseminated temperatures and for the measurements of new metal-carbon eutectics. In recognition of such a need, the Consultative Committee on Temperature passed a recommendation, T-2 (2005), "that national laboratories initiate and continue experiments to determine values of thermodynamic temperatures…".

The establishment of the NPL infrared relative spectral responsivity scale using cavity pyroelectric detectors.

E. Theocharous
National Physical Laboratory, Teddington, U.K.

Abstract. The establishment of a relative spectral responsivity scale requires the availability of a detection system with a known relative spectral responsivity. NPL has addressed this requirement by designing a new detector with a measurable relative spectral response profile in the 800 nm to 25 μm wavelength range. The new detector is based on a large area pyroelectric detector which is prepared for NPL by John Lehman of NIST Boulder. The large area pyroelectric detector is enclosed in a removable gold-coated hemispherical reflector. The novel feature of the new cavity pyroelectric detector is that the hemispherical reflector is removable. This makes the relative spectral responsivity of the new detector self-calibrating. A number of these cavity pyroelectric detectors were fabricated. Three have been selected and are currently being used as the primary standards for the establishment of the NPL relative spectral responsivity scale in the infrared. The presentation will summarize the design and performance characteristics of the new NPL cavity pyroelectric detectors and will demonstrate how they are being used to establish the NPL relative spectral responsivity scales in the infrared.

Introduction

A number of authors reported the assembly of cavity pyroelectric detectors based on a reflective hemispherical reflector mounted above a large pyroelectric detector [1, 2]. Some of these devices were designed to be used with lasers and their design if far from ideal when used with non-collimated radiation over a wide spectral region from sources such as monochromators. For example the design of the cavity pyroelectric detector reported by Day et al. [1] assumes that the coating of the pyroelectric detectors has a dominant specular reflection. This design was copied in the cavity pyroelectric detectors reported by Nettleton et al [2]. The aim of both these designs was to reduce the variation in the relative spectral responsivity of the pyroelectric detector by the addition of the reflective hemisphere so as to make it insignificant over the range of wavelengths of interest. Boivin reported an electrical substitution radiometer incorporating a hemispherical reflector [3]. The aim of his work was to reduce the uncertainty associated with the measurement of the absorbance of the black coating deposited on his thermal-detector-based radiometer. However, his work still required the measurement of the spectral absorbance of a witness sample.

The purpose of this paper is to report the construction of new design of Cavity Pyroelectric Detector (CPD) which is modular and allows the "self-calibration" of the relative spectral responsivity of this detector. Over thirty of these detectors have been assembled by John Lehman of NIST Boulder on behalf of NPL. The aim of this paper is to discuss the performance of these detectors, as well as the way they are being used to establish the NPL relative spectral responsivity scale in the 0.8 μm to 25 μm wavelength range.

Results

The design of the new NPL cavity pyroelectric detectors was completed in 1996. They are being referred to as the new detectors to distinguish them from a previous design [2] which was essentially a copy of the design reported by Day et al [1]. The new NPL CPDs have a modular design, as can be seen from figure 1. The modular design allows components to be easily interchanged and provides the means to determine the relative spectral responsivity of these detectors without the need to characterise witness samples. Each CPD incorporates a pyroelectric detector module designed and assembled on behalf of NPL by John Lehman of NIST Boulder. The pyroelectric detector incorporated in the NIST pyroelectric detector module has an 8 mm diameter active area and is based on a 10 mm diameter $LiTO_3$ crystal which is approximately 50 μm thick. Metal electrodes are deposited on both the surfaces of the $LiTO_3$ crystal and one side is coated with a gold-black coating [4]. This pyroelectric detector module is housed in a larger cylindrical housing made of anodized Aluminium so that the plane of the detector is at an angle of 20^o to the axis of the CPD cylindrical housing, as shown in Figure 1. Furthermore the centre of the pyroelectric crystal lies on the axis of the CPD cylinder (see Figure 1). Finally a reflective hemisphere with a 20 mm diameter is mounted on top of the pyroelectric detector so that the centre of the pyroelectric detector coincides with the centre of the reflective hemisphere. The reflective hemisphere has a 3 mm diameter aperture which is located so that the centre of this aperture coincides with the axis of the cylindrical body. All gold-coated reflective hemispheres used during the course of this work were nominally identical.

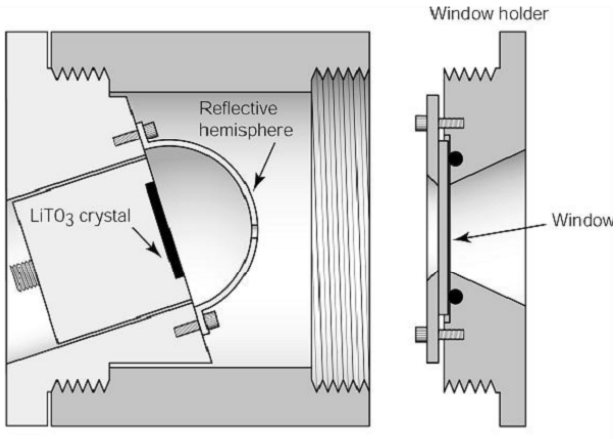

Figure 1. Then new NPL cavity pyroelectric detector.

A total of 35 CPDs have been assembled and studied over the period from 1998 to 2003. The gain G(λ) [5] as a function of wavelength was measured for the majority of these CPDs. Figure 2 shows the spectral responsivity of a 3 mm by 3 mm Pt-black-coated pyroelectric detector measured in the 0.8 µm to 25 µm wavelength range relative to both the CPD75 and pyroelectric detector 75 i.e. against the same pyroelectric detector, with and without a gold-coated reflective hemisphere. These plots are typical for the pyroelectric detectors with the very best quality gold-black coatings. Division of the two traces shown in Figure 2 gives the relative spectral responsivity of CPD75 relative to pyroelectric detector 75. This ratio is also the gain G(λ) resulting from the addition of the reflective hemisphere onto the pyroelectric detector. The values of G(λ) as a function of wavelength for CPD75 are shown in Figure 3. Figure 3 shows that the gain is greater than unity for all wavelengths. This confirms that the gold-black coating deposited on pyroelectric detector 75 is not perfect and that the addition of the hemisphere redirects some of the radiation reflected by the gold-black coating back to the gold-black coating thus enhancing its effective absorbance and therefore its response. Moreover Figure 3 shows that G(λ) increases monotonically with increasing wavelength. This indicates that the reflectance of the gold black coating gradually increases with wavelength (assuming the effective reflectance of the reflecting hemisphere is not a function of wavelength). This observation is in agreement with measurements of the reflectance of all good quality gold-black coatings [6].

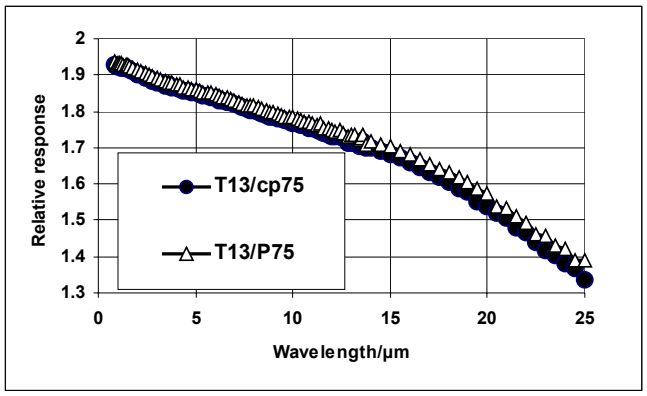

Figure 2: Spectral response of a 3 mm by 3 mm Pt-black-coated pyroelectric detector measured in the 0.8 µm to 25 µm wavelength range relative to both CPD75 and pyroelectric detector 75

All parameters of the cavity pyroelectric detectors were fully evaluated and will be presented at the meeting. These include their relative and absolute spectral responsivities, spatial uniformity of response, linearity of response, temperature coefficient of response, temporal response, long term stability and noise characteristics.

The presentation will also describe how the relative spectral responsivity of a cavity pyroelectric detector is estimated from the knowledge of its gain G(λ) as a function of wavelength. It will also deal with the uncertainty budget developed to estimate the uncertainty of the NPL infrared relative spectral responsivity scale.

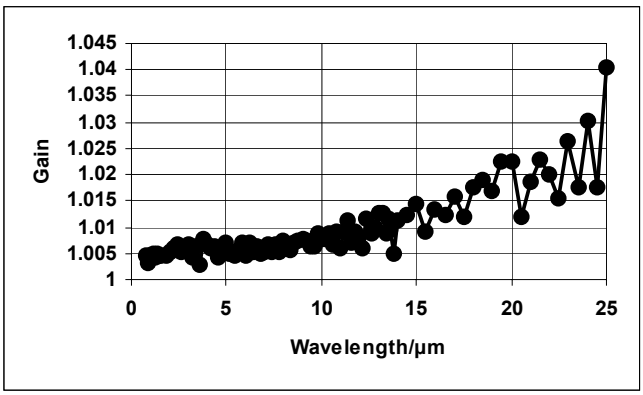

Figure 3: Gain in the 0.8 µm to 25 µm wavelength range measured when a reflective hemisphere was added to pyroelectric detector 75.

Acknowledgements Special thanks must go to John Lehman of NIST Boulder for assembling all the pyroelectric detector modules used in the new NPL CPDs and for many useful discussions. The author also wishes to thank Nick Nelms of the Space Research Centre of the University of Leicester, UK and Mark Proulx of Laser Probe Inc.

Reference

1. G. W. Day, C. A. Hamilton and K. W. Pyatt, *Applied Optics*, **15**, 1865-1868, 1976.
2. D. H. Nettleton, T. R. Prior and T. H. Ward, " Improved spectral responsivity scales at NPL, 400 nm to 20 µm", *Metrologia*, **30**, 425-432, 1993.
3. L. P. Boivin, "Current work at NRC of Canada on absolute radiometer based calibrations in the infrared", in New developments and *Applications in optical Radiometry*, N. P. Fox and D. H. Nettleton (eds), 1989, 81-88.
4. J. Lehman, E. Theocharous, G. Eppeldauer, and C. Pannel, "Gold-black coatings for freestanding pyroelectric detectors" *Measurement Science and Technology*, **14**, 916-922, 2003.
5. E. Theocharous, "The establishment of the NPL infrared relative spectral responsivity scale using cavity pyroelectric detectors", to be published.
6. N. Nelms and J. Dawson, "Goldblack coating for thermal infrared detectors" Accepted for publication in *Sensors and Actuators*, January 2005.

The PTB High-Accuracy Spectral Responsivity Scale in the VUV and X-Ray Range

A. Gottwald, U. Kroth, M. Krumrey, M. Richter, F. Scholze, G. Ulm
Physikalisch-Technische Bundesanstalt, Berlin, Germany

Abstract. At the electron storage ring BESSY II, the Physikalisch-Technische Bundesanstalt operates ten experimental stations at six synchrotron radiation beamlines for photon metrology in the spectral range from ultraviolet radiation to X-rays. At five beamlines, detector calibration is realized based on cryogenic radiometers as primary detector standards. The current status of instrumentation and measurement capabilities is described. Best measurement capabilities for the calibration of photodiodes vary between 0.4 % and 2.3 %.

Instrumentation

The spectral responsivity scale of semiconductor photodiodes realized with dispersed synchrotron radiation by the Physikalisch-Technische Bundesanstalt (PTB) at the electron storage ring BESSY II covers the wavelength range from 400 nm down to 0.02 nm, i.e. the photon energy range from 3 eV to 60 keV (Fig. 1). For this purpose, three beamlines for bending magnet synchrotron radiation (NIM, SX700, FCM) are operated within the PTB laboratory at BESSY II (*Klein et al.* 2002). In addition, a wavelength shifter (WLS) beamline for hard X-rays is used outside the laboratory. Measurements are routinely performed under ultra-high vacuum conditions with average radiant power values from 10 nW to 50 µW. The measurement capabilities can be extended also into the regime of single photon counting. Moreover, the use of an excimer laser allows measurements with radiation pulse energies up to 1.5 mJ at the wavelenghts of 157 nm and 193 nm.

For absolute measurement of average radiant power, two cryogenic radiometers, SYRES I and SYRES II, are used as primary detector standards, SYRES II being an upgraded version of SYRES I (*Rabus et al.* 1997). Both systems are optimized for the specific requirements of using spectrally dispersed synchrotron radiation in the µW regime with a monotonic radiant power decrease of 1 % within a few minutes. For photon energies above 20 keV, a standard ionization chamber is used for detector calibration and dosimetry.

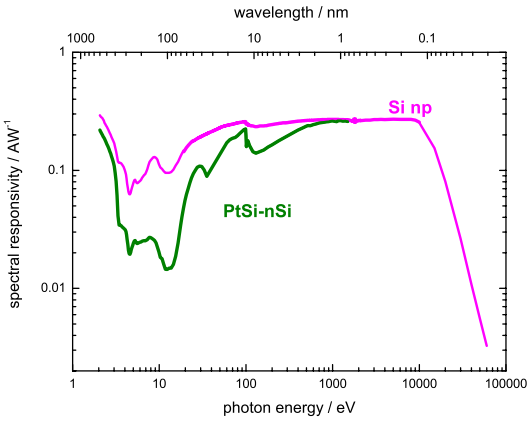

Figure 1. PTB's spectral responsivity scale of semiconductor photodiodes realized with dispersed synchrotron radiation at BESSY II.

Calibration of Transfer Detector Standards

Different types of semiconductor photodiodes are routinely used as transfer detector standards within the framework of customer calibrations. They are critically selected under aspects of stability, homogeneity, and linearity of their spectral responsivity in order to reduce the calibration uncertainties. Important contributions to the uncertainty budgets also arise from spectral impurities of the monochromatized synchrotron radiation. The best measurement capabilities, i.e. the extended (k=2) relative uncertainties, for the calibration of semiconductor photodiodes with synchrotron radiation are shown in Fig. 2. The lowest values are achieved within spectral regimes of highest radiant power. Uncertainties for the calibration of, e.g., photocathodes or photon counting devices are generally higher, depending on the individual detector performance. Calibrations performed with excimer laser radiation are, in addition, influenced by the laser instabilities.

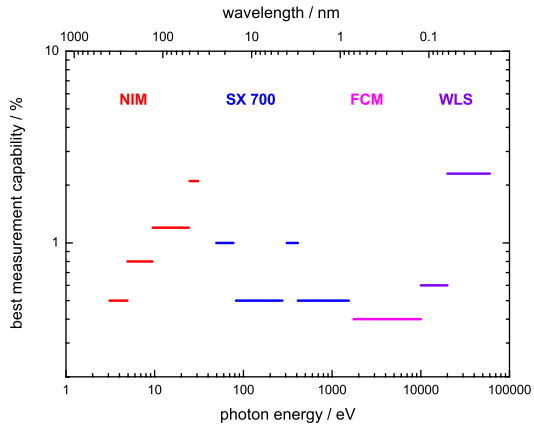

Figure 2. PTB's best measurement capabilities for the calibration of semiconductor photodiodes with synchrotron radiation.

References

Klein, R., Krumrey, M., Richter, M., Scholze, F., Thornagel, R., Ulm, G., *Synchrotron Radiation News*, 15, No. 1, 23-29, 2002.
Rabus, H., Persch, V., Ulm, G., *Appl. Opt.*, 36, 5421-5440, 1997.

New method for the primary realization of the spectral irradiance scale from 400 to 900 nm

R. Monshouwer, H.C.D. Bos, E.W.M. van der Ham

Abstract. A method is presented to measure the absolute spectral irradiance of light sources in the wavelength range from 400 nm to 900 nm. Use is made of a double monochromator based spectrometer which is calibrated with direct traceability to the detector spectral responsivity scale maintained at the NMi-VSL. For the implementation at the NMi, at present, the uncertainty is about 0.8 % (k=2) within the wavelength range studied. A preliminary comparison with an externally calibrated irradiance standard shows agreement well within the combined uncertainty of the two calibrations.

1. Introduction

At present, the most accurate photometric and radiometric measurements are achieved for detector responsivity in the visible part of the optical spectrum. In the visible spectrum uncertainties better than a few times 10^{-4} have been reported based on absolute cryogenic radiometers. In contrast to the high accuracy achieved for responsivity, irradiance measurements have a considerably higher uncertainty of about 1%. In this paper first results of a new method will be described where the absolute irradiance responsivity of a continuously scannable spectrometer is disseminated from the responsivity of a silicon trap detector [1]. This spectrometer can subsequently be used to calibrate the spectral irradiance of photometric and radiometric sources. The direct tracability is convenient for the monochromator based facilities at the NMi-VSL, and can lead to a more convenient and accurate means of realizing the irradiance scale.

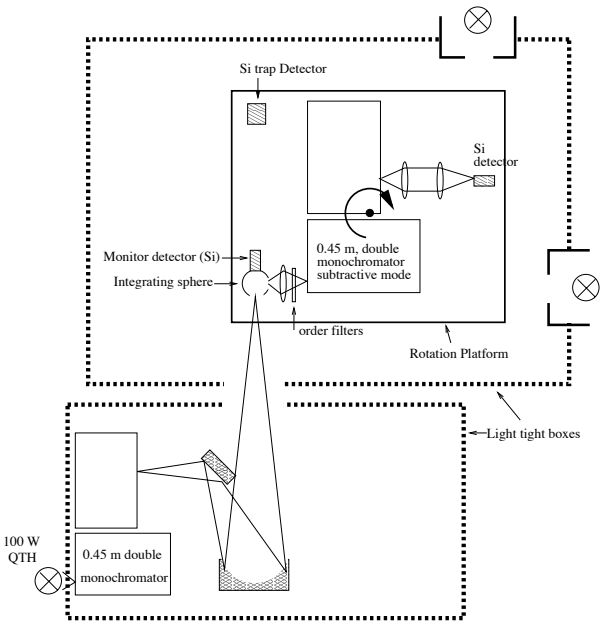

Figure 1. Layout of the ACR/SIR-facility.

2. Measurement Method

The calibration setup is schematically drawn in figure 1. The first part of the setup is a tunable lightsource consisting of a double monochromator combined with a 100 W quartz tungsten halogen lamp. The output of the source monochromator is directed to the Spectral IRradiance Facility (SIRF) setup using a mirror system. The output is focussed either to the input port of the spectrometer integrating sphere or to a silicon trap detector by rotating the rotation platform on which both are mounted to the appropriate angle. The response of the spectrometer at a specific wavelength is derived from a spectral integration of the response curve of the spectrometer, when scanning the source monochromator. The response of the SIRF spectrometer can be derived to be:

$$R_s(\lambda_0) \equiv \int R(\lambda, \lambda_0) d\lambda = \int \frac{i(\lambda_p)}{i_t(\lambda_p)} R_t(\lambda_p) d\lambda_p \quad (1)$$

Where $R_s(\lambda_0)$ is the responsivity of the spectrometer, $i(\lambda_p)$ the wavelength dependent current of the output

R. Monshouwer, H.C.D. Bos, E.W.M. van der Ham: Nederlands Meetinstituut Van Swinden Laboratorium B.V., Thijsseweg 11, 2629 JA Delft, the Netherlands

detector of the spectrometer and $i_t(\lambda_p)$ and $R_t(\lambda_p)$ the current and responsivity of the trap detector respectively. The irradiance responsivity is calculated by using a separately determined value for the aperture area. For sources that have a slowly varying irradiance level around λ_0, $R_s(\lambda_0)$ can directly be used to calculate the irradiance at λ_0 from the measured spectrometer current.

3. Measurement Results

3.1. Spectral irradiance responsivity calibration

In figure 2 a graph is shown of $R_s(\lambda)$ for the range from 400 to 900 nm with wavelength steps of 10 nm. The shape of the wavelength dependent responsivity

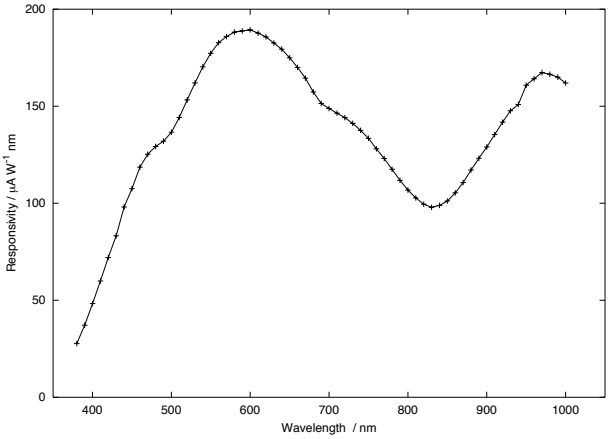

Figure 2. Responsivity of the spectrometer for different wavelength settings.

is dependent on the transmission and reflection of all the optical components and the responsivity of the silicon detector at the output port of the monochromator. A complete calibraton from 400 nm to 900 nm with 10 nm interval takes about 13 hours and is typically performed at night. The aperture area of the integrating sphere input port was determined using the "scanning spot" method as described in reference [2].

3.2. Calibration of a FEL lamp

Measurements were done on 1 kW FEL type lamps to test the calibration method. For reference the lamp was sent to the Optical Technology division at NIST for calibration. In figure 3 a measurement of the irradiance of this FEL lamp is shown. Also shown in the figure is the difference between the NIST calibration results and the calibration at the NMi-VSL. The difference is well within the combined uncertainty of

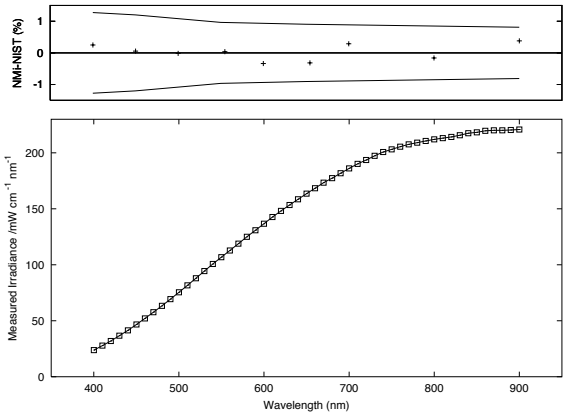

Figure 3. Irradiance measurement of FEL lamp with the calibrated spectrometer. The solid line in the lower panel shows the measured irradiance with 10 nm intervals. The upper panel shows the difference between the measured values and the NIST calibration values. The solid lines in the upper panel represent the combined uncertainty of both calibrations

the NIST calibration and the uncertainty budget of the calibration at the NMi-VSL.

4. Conclusion

Results of a new method of disseminating a continuous irradiance scale in the visible part of the spectrum have been presented. The method described directly disseminates the irradiance scale from the detector scale. Preliminary comparisons with an externally calibrated irradiance source shows that the measurements agree well within the combined uncertainty of the measurements. At the moment the estimated uncertainty is about 0.8% (k=2) around 400 nm, decreasing to about 0.6% above 500 nm. Further improvement of the uncertainty and extension of the method to the IR and the UV is presently pursued at the NMi-VSL

References

1. Ham, E.W.M., Bos, H.C.D., Schrama, C.A., *Metrologia*, 2003, **40**, S177-S180.
2. Schrama C.A., Reijn H., *Metrologia*, 1999, **36**, 179-182.

An integrated sphere radiometer as a solution for high power laser calibrations in fibre optics

Pedro Corredera Guillén[(1)], Félix Rodríguez-Barrios[(1)], Ana Carrasco-Sanz[(1)], Sonia Martín-López[(1)], Miguel González-Herráez[(1,2)] y María Luisa Hernanz Sanjuan[(1)].

[(1)] Dep. de Metrologia, Instituto de Física Aplicada (IFA) CSIC, Serrano 144, 28006 Madrid. Spain

[(2)] Dep. de Electrónica, Escuela Politécnica Superior, Universidad de Alcalá, Campus Universitario, 28871, Alcalá de Henares, Madrid

Abstract. This paper describes the design, characterization and calibration of a high power transfer standard for optical power measurements in optical fibres based on an integrating sphere radiometer. This radiometer, based on two detectors (Si and InGaAs), measure power between 10 µW to 10 W and, and it is useful in the wavelength range of 400 to 1700 nm. The radiometer has been calibrated along the total spectral range of use against an electrically calibrated pyroelectric radiometer and different fibre laser diodes and ion lasers. The total uncertainty obtained is lower than ±1.5% for these wavelength and power ranges.

Introduction

The proliferation of high power fibre lasers used to pump Raman amplifiers having output powers of several watts, drives the need to improve the calibration capabilities for absolute power measurements in optical fibres at levels from 0.5 W to 10 W. Integrating sphere radiometers (ISR) have been demonstrated as a realizable system to develop fibre-optic power meter scales [1, 2, 3], and NIR spectral responsivity scales using cryogenic radiometers [4, 5].

This paper presents the design, characterization and calibration of an ISR useful in the 400-1700 nm wavelength range.

Integrated sphere radiometer design

Figures 1 shows the sphere radiometer design. It is composed of a Spectralon® integrating sphere and two detectors. The sphere has an internal diameter of 2-inches with 0.5-inch thick walls. Three ports have been opened in the sphere with 90° orientation between one another. The input port has a 3 mm -diameter aperture and a FC fibre connector. The other two ports are used to place the two detectors, a 5 mm diameter Si detector and a 3 mm diameter InGaAs detector. Several adapters have been designed in order to ensure, by changing the distance fibre/sphere, that the maximum irradiance on the sphere wall does not overcome 1.7 W/cm^2.

Integrated sphere radiometer characterization

A complete radiometer characterization has been carried out. The temperature coefficient, the spatial uniformity of response, the relative spectral responsivity, the linearity, the effect of fiber connectors and numerical aperture and the absolute spectral responsivity has been measured. The most relevant results are described in the next paragraphs.

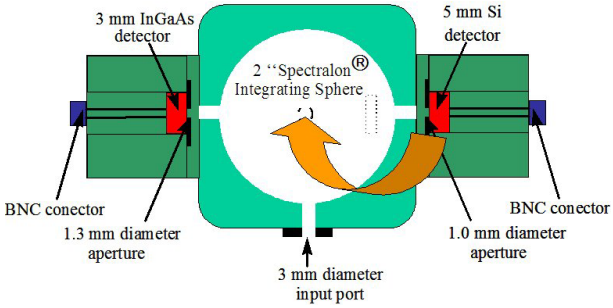

Figure 1: Integrating sphere radiometer (scheme).

Linearity

Si and InGaAs detectors are highly lineal when are illuminated within their active area [6]. In order to assure the overfilled illumination in the detector surface, two apertures of 1.0 and 1.3 mm of diameter have been placed just in front of the Si and InGaAs detector respectively.

Figures 2 and 3 show the non-linearity and its uncertainties (k=2) for both Si and InGaAs detectors, before being attached to the sphere radiometer. In the upper axis of these figures we represent the equivalent power level in the ISR calculated with their responsivities at 632.8 and 1550 nm respectively. The maximum non-linearity found in the range between 10 µW and 10 W was +0.21%, with an uncertainty of 0.50% (k=2) in the ISR-Si, and +0.41%, with an uncertainty of 0.36% (k=2) for the ISR-InGaAs.

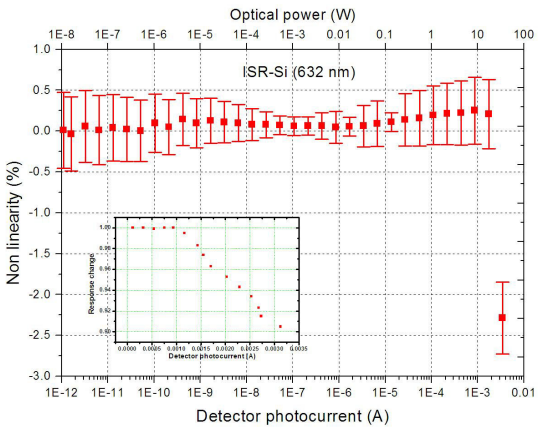

Figure 2: Linearity of the ISR-Si. The inserted figure shows the behavior near the saturation point.

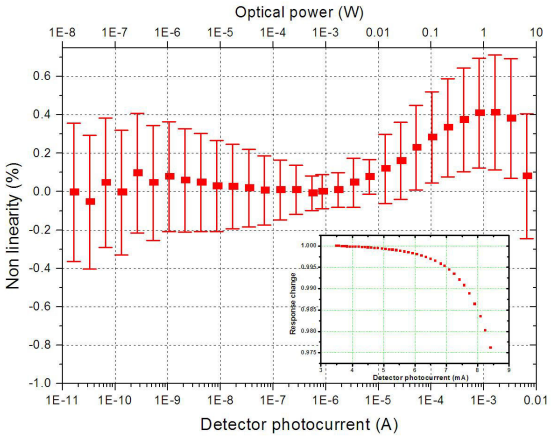

Figure 3: Linearity of the ISR-InGaAs. The inserted figure shows the behaviour near the saturation point

Absolute spectral responsivity measurement.

The absolute spectral responsivity of the ISR has been performed by direct comparison with an Electrically Calibrated Pyroelectric Radiometer (ECPR) model RsP 590 with RS5900 display, manufactured by Laser Probe Corp., USA [7]. This ECPR radiometer is traceable to our cryogenic absolute radiometer [5]. Four tunable laser diodes covering the range between 1250-1650 nm was used in a calibration setup similar to the used by reference [5]. At 850 nm a multimode laser diode has been used. For the visible range we used the emission lines of an Ar and He-Ne laser.

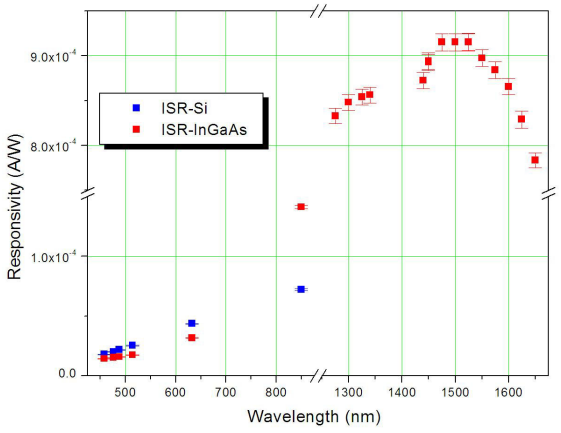

Figure 4: Spectral relative responsivity of the radiometer in the water vapour absorption region.

Uncertainty budget for the sphere radiometer calibration.

The contributions of the different sources of error to the final calibration uncertainty of the radiometer are summarized in Table 1. The results obtained show a total expanded uncertainty lower than ±1.5 % (k=2) in all the useful wavelength range and for power levels from 10 µW to 10W.

Table 1: Uncertainties in the calibration of the integrating sphere radiometer with the ECPR.

Source of error	ISR-Si	ISR-InGaAs
	Valour (%)	Valour (%)
ECPR calibration constant	0.200	0.200
ECPR power measurement	0.100	0.100
ECPR resolution	0.020	0.020
ECPR wavelength response	0.165	0.165
ECPR spatial uniformity)	0.100	0.100
ISR current measurement	0.200	0.200
ISR resolution)	0.030	0.030
Picoammeter calibration	0.025	0.025
Picoammeter drift	0.020	0.020
ISR spatial uniformity	0.033	0.029
ISR temperature coefficient	0.240	0.080
Connector effect (ISR)	0.260	0.260
ISR linearity (10 µW to 10 W)	0.495	0.360
Uncertainty (k=2)	1.416	1.156

Conclusions.

The design, construction and characterization of a sphere radiometer useful for laser and optical fibre power meter calibrations has been described. The radiometer uses two detectors: Si and InGaAs and covers the wavelength range between 400 to 1700 nm. Their calibration was done by direct comparison with an electrically calibrated piroelectric radiometer. Using the linearity factors of the detectors, we extend the radiometer calibration up to 10 W, with an estimated uncertainty lower than ±1.5 % (k=2) in this spectral range.

Acknowledgments Our acknowledge to the financial support from the Ministerio de Educación y Ciencia (project TIC2003-01869 and the grant associate FPI), and the support of the Social European Fund (grant I3P program of the CSIC)

References

[1] Nettleton D.H., "Application of absolute radiometry to the measurement of optical power in fibre optic systems", *New developments and applications in optical radiometry*. (Techno House, Bristol, UK, 1989), pp. 93-97.

[2] Corredera P., Campos J., Hernanz M.L., Fontecha J.L., Pons A. and Corróns A., "Calibration of near-infrared transfer standards at optical fibre communication wavelengths by direct comparison with a cryogenic radiometer". Metrologia **35**, 273-277 (1998).

[3] Envall J., Kärhä P. and Ikonen E., "Measurements of fibre optic power using photodiodes with and without an integrating sphere ". Metrologia **41**, 353–358 (2004).

[4] Boivin P., "Properties of sphere radiometers suitable for high-accuracy cryogenic-radiometer-based calibrations in the near-infrared". Metrologia, **37**, 273-278 (2000).

[5] Corredera P., Hernanz M.L., Campos J., Corróns A., Pons A. and Fontecha J.L., "Absolute power measurements at wavelengths of 1300 nm and 1550 nm with a cryogenic radiometer and a tuneable laser diode". Metrologia **37**, 513-516 (2000).

[6] Corredera P., Hernanz M.L., González-Herráez M. and Campos J.. "Anomalous non-linear behaviour of InGaAs photodiodes with overfilled illumination". Metrologia, **40**, 150-153 (2003)

[7] Doyle W.M., McIntosh B.C. and Geist J.. "Implementation of a system of optical calibration based on pyroelectric radiometer". Optical Engineering **15**, 541-548 (1976

From X-rays to T-rays: Synchrotron Source-based Calibrations at SURF III

Uwe Arp, Alex Farrell, Eliott Fein, Mitch Furst, Edward Hagley, and Ping-Shine Shaw

Synchrotron Ultraviolet Radiation Facility, National Institute of Standards and Technology, 100 Bureau Dr, Gaithersburg, MD 20899-8410, United States of America

The calculability of synchrotron radiation (SR) makes electron storage rings wonderful light sources for radiometry. The broadband nature of SR allows coverage of the whole spectral region from the x-ray to the far-infrared. Compact low-energy storage rings like the Synchrotron Ultraviolet Radiation Facility SURF III are perfect sources for radiometric applications, because the output spectrum can be custom-tailored to the user's needs: Low current operations can help simulate the solar spectrum, changes to the electron energy can help to deal with higher-order contributions of spectrometers and monochromators, and manipulation of the source size can increase the lifetime or change the radiation density, if necessary. At large scale multi-user facilities these special operational conditions are generally not possible, since many users have to be satisfied simultaneously. Compact storage rings for radiometric applications are so advantageous that the Physikalische-Technische Bundesanstalt (PTB) in Berlin, Germany, decided to build one to improve its radiometry capabilities.

At SURF currently two beamlines make use its well-established calculability. Beamline 2 (BL-2), the spectrometer calibration beamline, provides absolute irradiance calibrations of spectrometers and other radiometric instrumentation. This beamline is partly funded by the National Aeronautics and Space Administration (NASA), because most of its customers work within NASA-funded programs, like, *e.g.*, the "Living with a Star" or "Sun Earth Connection" programs. Beamline 3 (BL-3), the ultraviolet source-calibration beamline, became recently the U.S. primary standard for deuterium lamp irradiance calibrations. Its usefulness was first proven during the Consultative Committee for Photometry and Radiometry (CCPR) key comparison CCPR-K1.b "Spectral irradiance" in the wavelengths range from 200 nm to 350 nm with deuterium lamps.

Recently the University of Alaska Fairbanks performed a calibration using BL-2 at a wavelength of 0.2 nm (roughly 6200 eV photon energy). This calibration was only possible by increasing the energy of the electrons stored to the absolute maximum the magnet allows. The increase from the standard operating energy of 380 MeV to this maximum energy of 408 MeV pushed down the critical wavelength λ_c, which is a measure of the short wavelength cut-off of the emitted synchrotron radiation, from 8.5 nm to 6.9 nm.

During the key CCPR-K1.b comparison "Spectral irradiance", NIST was the only laboratory to use synchrotron radiation in the calibrations process, leading to the smallest uncertainties among the participating laboratories. The uncertainty achieved at SURF was 0.5 % (coverage factor $k = 1$) for the entire spectral range. Since then this new calibration capability has been used extensively and several deuterium lamps have been calibrated directly against SURF.

SURF maintains one of the best synchrotron radiation based calibrations programs in the world, which has now proven to reach into the soft x-ray range. Standard lamp calibrations, detector calibrations, and measurements of optical properties are routinely performed at SURF with great reliability and accuracy.

Infrared Radiometry at LNE: characterization of a pyroelectric detector used for relative spectral responsivity measurement

J. Dubard, J.R. Filtz , T. Valin, and M. Lièvre
LNE, Trappes, France

Abstract. Measurement facilities for detector calibration in the Infrared on the spectral range 1µm-14µm are currently setting-up. Four techniques are developed: Monochromator, Laser, Fourier Transform spectrometer and Blackbody. Characteristics of the measurement set-ups are presented. The traceability to SI units is showed. Result of the characterization of a pyroelectric detector as well as the preliminary results of the comparison between the different techniques on near IR detector are presented too.

Introduction

LNE, Laboratoire National de Métrologie et d'Essais, as the French National Metrology and Testing Laboratory is developing a new platform for Infrared and Laser radiometry. Laser facility has been built and offers calibration services over a wide range of power and wavelengths in CW or pulse mode. UV, visible and near Infrared (NIR) radiometry calibration services are also available. The laboratory is now in the process of extending the spectral range to Mid IR and Far IR up to 14µm to address the industrial needs in domains such as temperature measurement using thermal camera. Calibration techniques used, traceability to SI units and the main result concerning the characterization of a flat response detector are described in this paper.

Measurement techniques

Measurement set-ups based on four different techniques have been recently developed [1-2]. The aim is to compare detector calibration results in order to achieve a good agreement between these complementary techniques. They are:

- **Monochromator based techniques:** the set-up uses a 460mm focal length single monochromator equipped with a set of interchangeable gratings and filters order. The source is either a Tungsten-Halogen lamp or a 900°C Blackbody cavity. The output from the monochromator is focused onto the reference detector or the detector under calibration using gold plated mirrors. Detector signals are measured with lock-in amplifier.
- **Laser based technique**: the laboratory is equipped with a set of CW IR lasers (NdYag, HeNe and CO2) with wavelength ranging from 1.06µm to 10.6µm. The output power is measured using a power meter that we have developed [3].
- **Fourier Transform spectrometer based technique**: a Brucker® type 55 spectrometer is used as a reference instrument with the step-scan analysis technique. Sources include a Tungsten-Halogen lamp and a globar lamp. The spectral range is 1µm-20µm.
- **Blackbody based technique**: the output of a Blackbody cavity of a known temperature is used as a reference source. Combination of the output spectral power distribution and the transmission of a well characterized interference filter gives access to a known monochromatic beam irradiance.

Traceability

Calibration performed using the monochromator based technique is traceable to the cryogenic radiometer of LNE-INM through a silicon photodiode. The Hamamatsu® type 1337 is calibrated on the spectral range 400nm-1100nm. This detector is used to calibrate a NIR detector such as Ge or InGaAs on the spectral range 800-1700nm using this procedure:

- The relative spectral sensitivity of the NIR detector is measured using a reference pyroelectric detector
- Then absolute sensitivity of the InGaAs detector is determined using the Si detector at wavelengths corresponding to the overlapping wavelength range of the two detector types.

The two measurements are combined to get the spectral sensitivity of the InGaAs over the entire spectral range.
Mid IR and Far IR detectors are calibrated using the same procedure in a cascade traceability scheme.
This traceability scheme applies also to the Fourier Transform spectrometer based technique.

Laser based technique calibration is traceable to the electrical units. The power meter used as a reference is a thermal cavity. Temperature increase due to laser beam absorption is related to the same temperature increase due to the electrical power dissipated by a resistor wrapped around the cavity.

Blackbody based technique is traceable to the temperature scale and to radiometry through the measurement of the transmission of the interference filters.

The traceability scheme is summarized in table 1.

Technique	Traceability
Monochromator	Cryogenic radiometer Cascade calibration scheme starting with a Si detector
Laser	Electrical power
Fourier Transform spectrometer	Cryogenic radiometer Cascade calibration scheme starting with a Si detector
Blackbody	Temperature and radiometry

Table 1: Traceability scheme

Results

IR radiometry calibration capability of the laboratory

relies on the use of a pyroelectric detector chosen for the wavelength non-selectivity . The schematic of the detector is shown on figure 1. The detector consists in a 60° cone shape pyroelectric sensor put in a laboratory-made housing with a 12mm diameter input aperture which can be fitted with interchangeable windows and vacuum pumped.

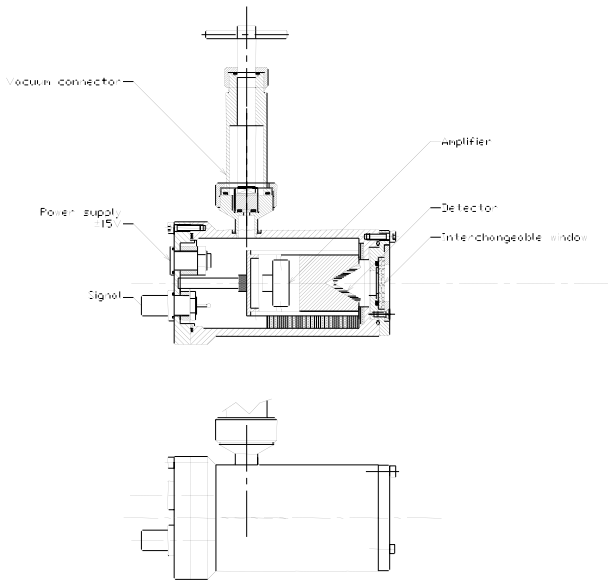

Figure 1: Schematic of the pyroelectric detector

The detector is characterized for two parameters: spatial sensitivity [4] and spectral response flatness. Reflectance measurement of the sensitive area is performed to evaluate the spectral response flatness. This is done by measuring the total reflected power with an integrating sphere. The result is shown on figure 2 on the spectral range 2µm-12µm.

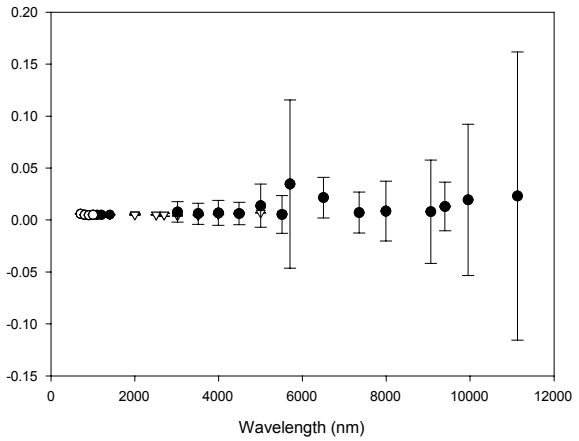

Figure 2: Spectral reflectance of the pyroelectric detector

It has been found that spectral sensitivity of this pyroelectric detector is nearly wavelength independent. Increase of the reflectance around 6µm is due to fluctuation in ambient air characteristics. Additional measurements will smooth-up this feature.

In order to validate the results obtained with the different techniques, we have performed measurement on Si and InGaAs detectors using the monochromator and the laser based techniques. Agreement between the two techniques are found to be better than 1% which is below the uncertainty level for monochromator radiometry (1.5%) and for laser radiometry (2%).

Conclusion

Infrared or Laser techniques used to characterize a new pyroelectric detector has been described and the scheme of validation processes outlined.

Works are currently still under way to extend the spectral range for the monochromator and laser based techniques comparison and for monochromator and FT spectrometer based techniques comparison

Therefore future work will concentrate on the optimization of the techniques applied, and on the investigation of the measurement protocols differences.

References

[1] Dubard J, Filtz JR, Valin T, R&D Annual Report BNM 2004, Technical report, March 2005
[2] Grum F, Becherer R.J, Radiometry. Optical Radiation Measurements, Vol 1, Academic press, 1979.
[3] Lièvre M, CORM 98 conference (Council for Optical Radiation Measurements)
[4] Filtz JR, Valin T, Lièvre M, , R&D Annual Report BNM 2000, Technical report, April 2001

Transfer standard pyrometers for radiance temperature measurements below the freezing temperature of silver at NIST

M. Noorma[1,2], S. Mekhontsev[1], V. Khromchenko[1], A. Gura[1], M. Litorja[1], B. Tsai[1], and L. Hanssen[1]

[1]National Institute of Standards and Technology (NIST), Gaithersburg MD, USA

[2]Metrology Research Institute, Helsinki University of Technology (TKK), Espoo, Finland

Abstract. New transfer standard pyrometers operating at 900 nm and 1.55 μm have been designed, characterized, and calibrated with defined fixed points of ITS-90. The pyrometers are optimized for radiance temperature measurements in the range between the freezing temperatures of Sn (231.928 ºC) and Ag (961.78 ºC). The calibrations at different fixed points demonstrate good agreement. The size of source correction for a source with 40 mm diameter has been measured to be as low as 0.01 %. These instruments feature a compact and ruggedized design. The pyrometers may be used to interpolate, maintain and disseminate radiance temperature scales as well as for inter-laboratory comparisons.

Introduction

According to the ITS-90, the temperature scale between the triple point of equilibrium hydrogen and the freezing point of silver is defined by means of a platinum resistance thermometer (PRT) calibrated at a specified set of fixed points, and use of specified functions for interpolation at intervening temperatures[1]. Thus blackbodies (BB) with known emissivity equipped with a calibrated PRT can be used as reference standards for radiometric temperature measurements.

Another approach for radiometric temperature measurements, which is used by several national metrology laboratories including NIST, is based on fixed-point BB sources with their temperature assigned according to ITS-90, but relies on accurate pyrometers for interpolation to other temperatures. This eliminates errors due potential temperature differences between the PRT and radiating cavity.

In both cases, high-accuracy transfer standard radiometers are needed for interpolation of the radiance temperatures scale and its transfer from the reference sources to customer BBs.

Pyrometers

Two first generation pyrometers, "RT900," were built at NIST in 2003. They are based on a highly linear silicon photodiode and a bandpass filter and can be used above 500 ºC. After substantial modification of both the optical unit and control software, in 2005 we built two second generation pyrometers, "RT1550," (shown in Fig. 1) with an InGaAs detector and a bandpass filter at 1.55 μm, and which can be used down to 200 ºC. The relative spectral responsivities of the pyrometers are shown in Fig. 2.

Both radiometers have a 3 mm spot size at 500 mm from the front plane, and an AR-coated GRIN lens with a 47 mm optical diameter. The size of source effect (SSE) has been studied with a special source with a central obscuration[2] with results shown in Fig. 3.

Other features include a built-in laser diode for backward tracing of the axial beam, a field stop made of polished Ni-plated Invar, non-hygroscopic refractory oxide

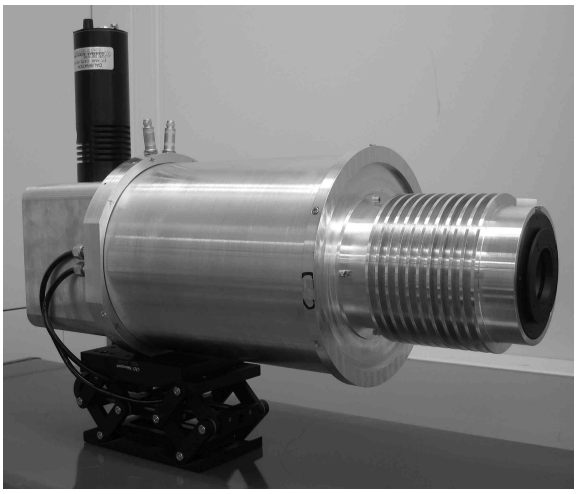

Figure 1. Transfer standard pyrometer RT1550

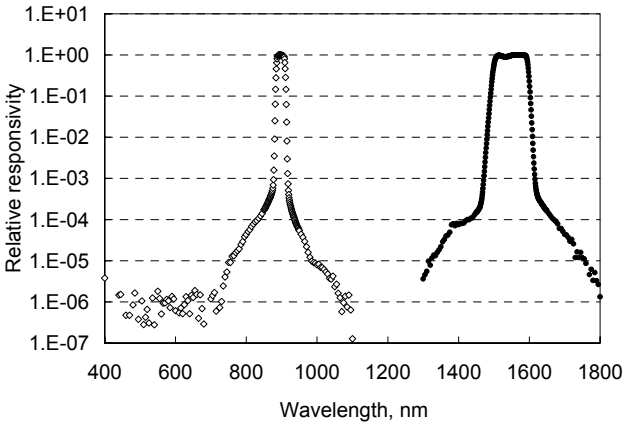

Figure 2. Relative spectral responsivities of an RT900 and an RT1550

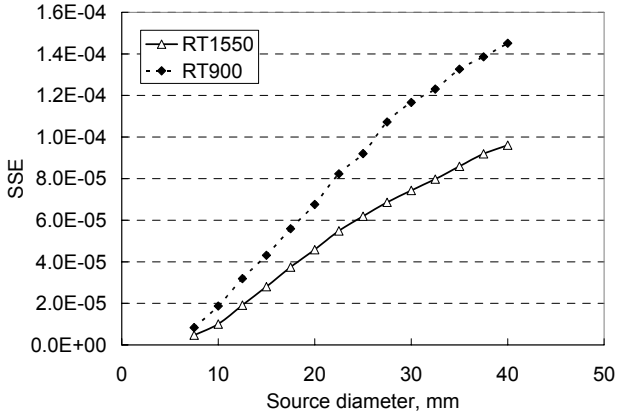

Figure 3. SSE of an RT900 and an RT1550 as a function of source diameter.

filters with $4 \cdot 10^{-6}$ nm/K thermal drift, and a light weight carbon fiber frame with a very low coefficient of axial expansion. The RT1550 is also equipped with a water-cooled lens mount for additional temperature stabilization. The total length of each pyrometer is 550 mm, and they have an integrated electronic module with a single USB connection to a laptop computer that contains the control software.

Calibration of pyrometers

Fixed-point BBs at the freezing temperatures of Sn, Zn, Al, and Ag have been used as reference standard sources of spectral radiance. In addition, a Au fixed point has been used to verify the calibration of an RT900. As an example, the freezing plateau of the Zn is shown in Fig. 4.

The defining equation of ITS-90, which is based on Planck's radiation law, has been used with a RT900 pyrometer to compare the calibrations with Al, Ag, and Au fixed points. The deviations, shown in Table 1 for an RT900, are calculated relative to the calibration at the Ag fixed point.

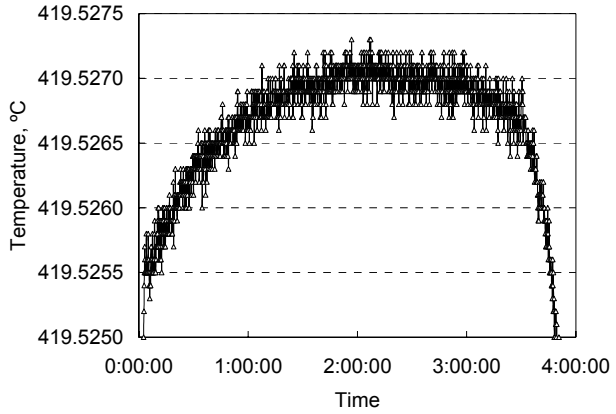

Figure 4. Freezing plateau of Zn measured with an RT1550.

An RT1550 has been calibrated with Sn, Zn, Al, and Ag fixed points. Next, the Sakuma-Hattori interpolation equation[3] has been fitted with the measurement results using a nonlinear fitting software[4]. The deviations, shown in Table 1 for the RT1550, demonstrate the difference between the defined fixed-point temperatures and the temperatures achieved with the Sakuma-Hattori interpolation equation.

Table 1. Evaluation Results of Pyrometers

Fixed point	ITS-90 freezing temperature, ℃	Deviation from ITS-90, mK	
		RT900	RT1550
Sn	231.928	n/a	3
Zn	419.527	n/a	23
Al	660.323	-18	-13
Ag	961.780	0	44
Au	1064.18	25	n/a

We do not have sufficient history to fully account for long term stability, but after round-trip transportation to a customer in California and one year of use, the RT1500 and RT900 agreed to within 0.1 ºC.

Discussion

Pyrometer development was performed in the framework of a project to build a customer facility for IR spectral emissivity calibration[5]. Currently both pyrometer models are being incorporated into a new NIST facility that will be dedicated to the spectral radiance characterization of IR radiation sources as well as to the maintenance and dissemination of the radiance temperature scale below the silver point.

This new facility will employ two different fixed-point BB designs with different crucible geometry and furnace designs: a traditional NIST design[6] as well as more a recent one[7]. We have performed a first round of comparisons of these two different BBs, which indicates the existence of a small but statistically significant difference in radiance temperatures. A consistent offset is found even in the case of using the same furnace with different crucibles.

One possible cause of such a systematic offset in measurement with two different furnaces is the out-of-field-scatter (SSE) that is very dependent on the furnace design. However, the SSE correction cannot be easily applied because of the partially obscured observation conditions of many features of the radiation field. Because of this, we have decided to take an approach originally suggested by Jones and Tapping[8] and demonstrated in Fig. 5 below. A fixed-point blackbody is used in a regular configuration. The only difference is that in place of the metal filled crucible we use an empty one that has had the rear half of the cavity removed. In this case the ideal field of view of the pyrometer is totally filled with a highly absorbing cone attached to BB rear flange.

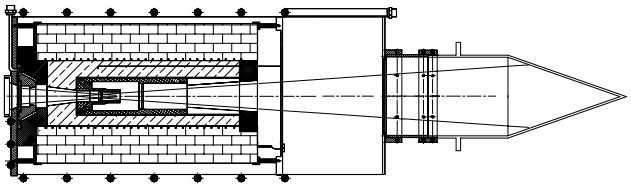

Figure 5. Out-of-field scatter experiment schematic

The results of the crucible comparison and out-of-field scatter contribution for both furnaces should be available by the time of the conference.

Acknowledgments The authors would like to thank Peter Saunders (MSL, New Zeeland) for providing the nonlinear fitting software used for the calculation of Sakuma-Hattori parameters, and Howard Yoon (NIST) for his advice on lens selection.

References

1. Preston-Thomas, H., The ITS-90," *Metrologia 27*, 3-10, 1990.
2. Ohtsuka M., Bedford R.E., Measurement of size-of-source effects in an optical pyrometer, *Measurement 7*, 2-6, 1988.
3. Sakuma, F. and Kobayashi, M., Interpolation Equations of scales of radiation thermometers, in *Proc. TEMPMEKO 1997*, 305-310, 1997.
4. Saunders, P., White, D. R., Physical basis of interpolation equations for radiation thermometry, *Metrologia*, *40*, 195–203, 2003.
5. Hanssen, L.M., Mekhontsev, S.N., and Khromchenko, V.B., Infrared spectral emissivity characterization facility at NIST, *Proc. SPIE 5405*, 1-12, 2004.
6. Mielenz, K.D., Saunders, R.D., and Shumaker, J., Spectro-radiometric Determination of Freezing Temperature of Gold*, J. Res. Natl. Inst. Stand. Techn. 95*, 49-67, 1990.
7. Hanssen, L. M., Mekhontsev, S. N., Khromchenko, V. B., Prokhorov, A. V. and Zeng, J., Study of infrared emissivity of a fixed-point blackbody cavity, *Proc. NEWRAD 2005.*
8. Jones T.P., and Tapping, J., Precision Photoelectric Pyrometer for the Realization of the IPTS-68 above 1064.43 ° C, *Metrologia 18*, 23-31, 1982.

Preliminary Realization of a Spectral Radiance Scale in the Range of 2.5 μm to 20 μm

S. Mekhontsev[1], M. Noorma[1,2], and L. Hanssen[1]

[1]National Institute of Standards and Technology (NIST), Gaithersburg MD, USA
[2]Metrology Research Institute, Helsinki University of Technology (TKK), Espoo, Finland

Abstract. We summarize recent progress in our infrared (IR) spectral radiance metrology effort. A preliminary scale realization has been undertaken in the temperature range of 232 °C to 962 °C and spectral range of 2.5 μm to 20 μm. We discuss the spectral radiance scale realization process that includes the use of Sn, Zn, Al and Ag fixed-point blackbodies (BB), as well as the transfer of the spectral radiance scale to transfer standard BBs based on water, Cs and Na heat pipes. As an example of customer source calibration we present results of the spectral radiance and emissivity measurements of two secondary standard BB sources. For one of the BBs, a substantial deviation of emissivity values from the manufacturer specifications was found. Further plans include expansion of the adopted methodology for temperatures down to 15 °C and building a dedicated facility for spectral characterization of IR radiation sources.

Introduction

NIST has well established measurements of spectral radiance in the spectral range below 2.5 μm.[1] But many applications critically depend on spectral radiance of calibration sources in the 3 to 5 μm and 8 to 14 μm ranges. Several recent papers have demonstrated that Fourier Transform (FT) spectrometers can perform BB radiation measurements with high accuracy[2]. A facility for direct measurements of spectral directional emissivity of materials,[3] developed in our group, has certain capabilities for spectral characterization of BB sources. This paper covers results of a realization of the IR spectral radiance scale at temperatures above the tin point, as well as the status of building a dedicated facility for spectral calibration of IR standard sources.

Realization Approach and Tasks

Our approach, illustrated in Fig. 1 below, is common for spectral radiance realization for higher temperatures and the associated visible and near-IR spectral range. The spectral radiance scale is derived from a set of fixed-point BBs, the design and characterization of which was our first task. Secondly, we developed transfer standard pyrometers to maintain and interpolate the temperature scale at particular wavelengths. The third task was the construction of a spectral comparator consisting of a spectrometer and fore-optics for spectral scale transfer. Finally, we built a set of variable temperature blackbodies to maintain the scale and interpolate over the temperature range.

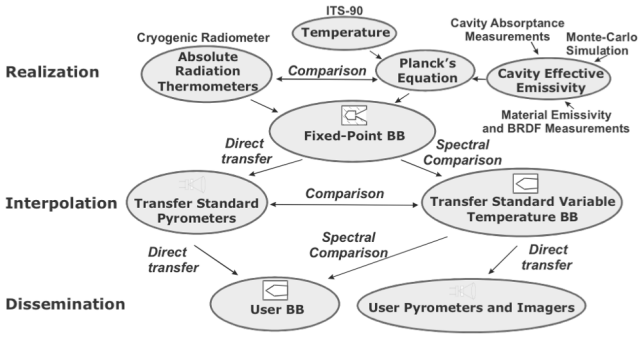

Figure 1. Approach for the spectral radiance scale realization.

Experimental Setup

As it was already mentioned, for this project we used facility which is a part of the Fourier Transform (FT) Infrared Spectrophotometry Laboratory, which is dedicated to characterization of the optical properties of solid materials. Relevant part of the setup is shown in Fig. 2.

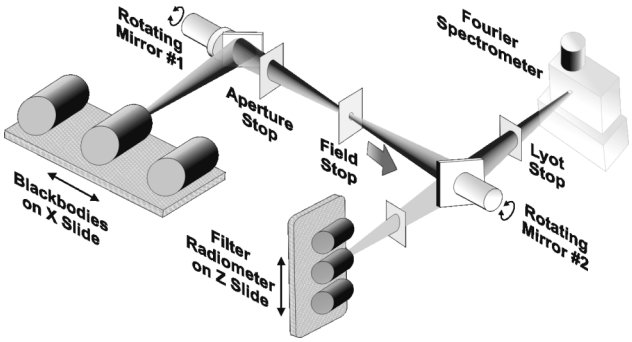

Figure 2. Schematic of the experimental setup

A set of fixed-point BBs, which we have designed, built and characterized, serves as a basis for the spectral radiance scale realization at discrete temperatures. The BBs have 7 mm diameter exit apertures and are designed to have high IR emissivity and plateaus of several hours to allow long measurement times. Further details of the BB design, results of emissivity modeling and additional evaluations are described in another paper at this conference[4,5]. Temperatures are derived from ITS-90, although radiometrically based scale derivation will be attempted in the nearest future.

Two transfer standard pyrometers, designated *RT900* and *RT1550*, with spectral responsivity centered at 900 and 1550 nm, respectively, are used to interpolate the temperature scale between fixed point temperatures, as well as to measure radiance temperature of the customer blackbody. Pyrometers design and evaluation details can be found in another paper presented in this conference[6].

The spectral comparator contains fore-optics and a spectrometer. The fore-optics, a schematic of which is shown in Fig. 3, contains two off-axis aspherical mirrors and has a low level of out-of-field scatter in the visible and IR. Details of the optical train design and characterization can be found elsewhere[7]. Our medium resolution FT

spectrometer BOMEM DA3 is not necessarily optimal to the task of blackbody characterization. Nevertheless, we have been able to demonstrate the concept and obtain useful results . For data processing we have employed an algorithm[2], which involves the spectral comparison of an unknown source with two known sources.

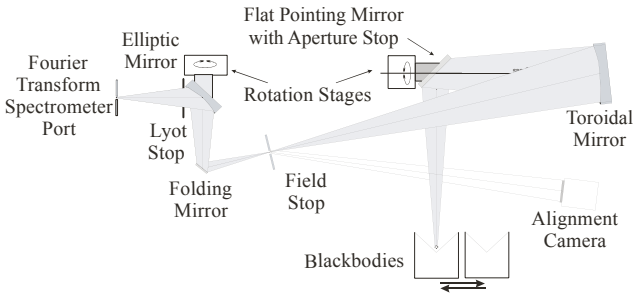

Figure 3. Schematic of the optical interface

Experimental Results

Measurements were performed according to the diagram shown in Fig. 4. In the first stage of the experiment, we performed spectral comparisons of heat pipe BBs with a

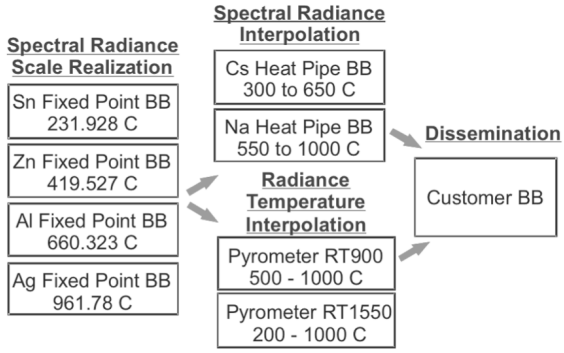

Figure 4. Sequence of measurements

number of fixed-point BBs. As an example we show the result of calibration of the Cs BB with the Al fixed-point BB (Fig. 5). For ease of data analysis we show the effective emissivity, which was always calculated using the radiance temperature at 1550 nm as the true (reference) temperature. The spectral radiance and the radiance temperature data are also generated during data processing.

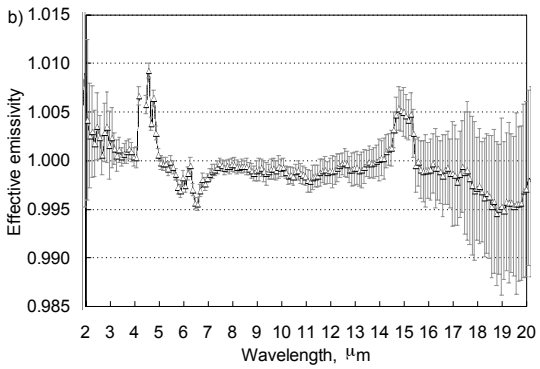

Figure 5. Effective emissivity of the Cs heat pipe BB

After calibration of the Cs and Na heat pipe blackbodies, they were used to calibrate customer blackbodies at temperatures from 300 to 1000 ° C in 100 ° C steps. The emissivity of one of these had a distinctive pattern evident at all temperatures (600 ° C in Fig. 6)

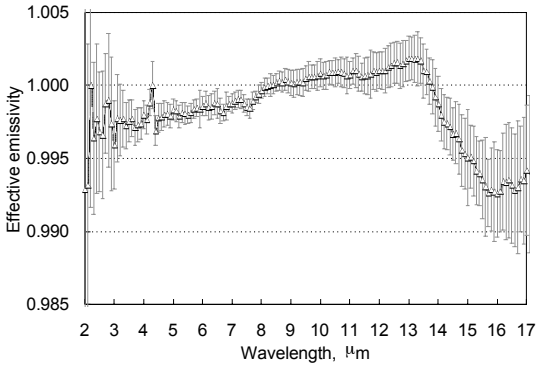

Figure 6. Customer BB calibration result with a distinctive spectral pattern

Discussion

A systematic realization of an IR spectral radiance scale has been performed. In the spectral band of 8 to 14 μm, the standard deviation of the mean for spectral radiance was typically at the level of 0.1%. In the spectral band from 3 μm to 5 μm, scatter of the results for most temperatures is substantially larger, possibly relating to use of a wide band pyroelectric detector, and needs further attention. The results show no systematic spectral features for the transfer standard blackbodies but reveal some systematic features for one of the customer BBs. The results will be used to optimize the design of the dedicated facility for spectral characterization of IR sources under construction at NIST.

References

1. Walker J. H., Saunders R. D., and Hattenburg A. T., Spectral Radiance Calibrations, *NBS Spec. Publ. 250-1*, 1987.
2. Reesink A. L., Rowell N. L., and Steele A. G., Using Fourier-Transform Blackbody Spectra to Determine Thermodynamic Temperature in the 600 ° C to 1000 ° C Range, in *Temperature: Its Measurement and Control in Science and Industry, Volume 7, ed. D.C. Ripple, AIP*, 19-24, 2003.
3. Hanssen L.M., Mekhontsev S.N., Khromchenko V. B., Infrared spectral emissivity characterization facility at NIST, *Proc. SPIE 5405*, 1-12, 2004.
4. Mekhontsev, S., Khromchenko, V., Prokhorov, A., Hanssen, L., Emissivity evaluation of fixed-point blackbodies, *Proc. TEMPMEKO 2004* (in print).
5. Hanssen, L. M., Mekhontsev, S. N., Khromchenko, V. B., Prokhorov, A. V. and Zeng, J., Study of infrared emissivity of a fixed-point blackbody cavity, *Proc. NEWRAD 2005.*
6. Noorma M., Mekhontsev S. N, Khromchenko V. B., Gura A. V., Litorja M., Tsai B. K., Hanssen L. M., Transfer standard pyrometers for radiance temperature measurements below the freezing temperature of silver at NIST, *NEWRAD 2005*
7. Mekhontsev S.N. and Hanssen L.M., Low scatter optical system for emittance and temperature measurements, in *Temperature: Its Measurement and Control in Science and Industry, Volume 7, ed. D.C. Ripple, AIP*, 693-698, 2003.
8. Revercomb, H. E., Buijs, H., Howell, H. B., LaPorte, D. D., Smith, W. L., and Sromovsky, L. A., Radiometric calibration of IR Fourier transform spectrometers: Solution to a problem with the High-Resolution Interferometer Sounder. *Applied Optics 27 (15)*, 3210-3218, 1988.

New photometric standards development at NIM-Romania

M. Simionescu, A. Seucan
NIM-Romania

J. Bastie, A. Stepnik
LNE-INM, France

Abstract. Traditionally the National Institute of Metrology of Romania (NIM-Ro) used to maintain the luminous intensity and the luminous flux units on groups of specially designed lamps periodically calibrated by the Photometry Laboratory of the BIPM. Following the closure of the calibration service of this laboratory, it was decided to proceed to independent realization of the candela and subsequent goniophotometric derivation of the lumen. Accordingly, during 2002-2003, the candela was realized on the basis of a trap radiometer traceable to the LNE-INM (France) primary reference. To validate the new realization several internal and bilateral comparisons were organized, with good results. Following, a group of three similar absolute photometers were developed at NIM-Ro in order to be used as the new national (group) reference. To validate both the new standards and the corresponding transfer capabilities, bilateral comparisons were organized with LNE-INM, within the **EUROMET 823** project. Theoretical basis, design solutions and so far obtained results are reported. **Key words:** luminous intensity, luminous sensitivity.

1 Theory

The luminous intensity (I_v) of a point source, placed at a distance ***d*** from a photometer, is **[1, 2]:**

$$I_v = K_m \cdot \frac{d^2}{A} \cdot \frac{F}{s_m} \cdot Y_{ph} \qquad (1)$$

where:
Y_{ph} = the photocurrent generated by the photometer;
K_m = the maximum luminous efficacy of the CIE standard observer (**683 lm / W**);
d = the lamp-photometer distance **(m)**;
s_m = the peak absolute, spectral responsivity of the photometer **(A/W);**
A = the effective area of the photometer aperture **(m^2)**;
The spectral matching factor ***F*** employed in **(1)** is **:**

$$F = \frac{\int S(\lambda) \cdot V(\lambda) \cdot d\lambda}{\int S(\lambda) \cdot s_r(\lambda) d\lambda} \qquad (2)$$

where $S(\lambda)$ is the relative spectral power density of emitted flux and $V(\lambda)$ is the relative luminous efficacy function of the **CIE** standard observer **[3]** and $s_r(\lambda)$ is the relative spectral responsivity of the photometer defined with:

$$s_r(\lambda) = s(\lambda) / s_m \qquad (3)$$

Such a photometer is intrinsically characterized by it`s luminous sensitivity:

$$s_v = \frac{A \cdot s_m}{K_m \cdot F} \qquad (4)$$

Using such an absolute photometer the luminous flux unit may be derived and transferred to secondary standard lamps using the NIM designed goniophotometer. Basically, the total flux is given by :

$$\Phi_v = \int_{-\pi/2}^{\pi/2} \int_{0}^{2\pi} I_v(\alpha,\theta) \cdot \sin\theta \cdot d\theta \cdot d\alpha = K_m \frac{d^2 \cdot F}{A \cdot s_m} \int_{-\pi/2}^{\pi/2} \int_{0}^{2\pi} Y_{ph} \cdot \sin\theta \cdot d\theta \cdot d\alpha$$

where α and θ are, respectively, the azimuth and the polar, angles.

2 Practical realization of the candela

A filtered trap detector using three Hamamatsu S 1337 1010 BQ windowless photodiodes was used. The basic design of the photometer's transducer and general set up are shown in **Fig. 1.**

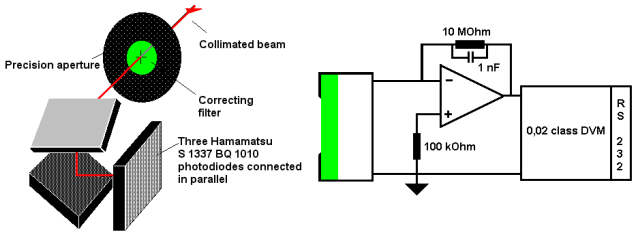

Figure 1. Candela realization at NIM; Experimental set up

3 Characterization and first comparison

Work was conducted within a bilateral cooperation project **[4].** The absolute and relative spectral responsivity of the new photometer was measured against the NIM-Ro reference radiometer, traceable to the LNE-INM primary standard.
Detailed characterization of the photometer led to the following values: $s_{v,NIM\text{-}Ro}$ = 9,5678 nA/lx; u_c = 0,45%.
To check these figures, a bilateral comparison was organised with LNE-INM **[5].**
The results are synthesized in **Tab. 1.**

s_{vFA02} NIM-Ro	s_{vFA02} LNE-INM	Δs_{vFA02}	Comp. combined u_c

(nA/lx)	(nA/lx)	(%)	(%)
9,568	**9,590**	**- 0,23**	**0,67**

Table 1. INM-Ro – LNE-INM comparison results

4 Development of new national references and preliminary results

Following, during 2004, three similar photometers were developed by NIM. They were characterised in a similar manner. To check the candela realization and the transfer capability of NIM-Ro, an internal comparison with the lamps previously calibrated by BIPM was realised. All three photometers were used to measure the luminous intensity of the existing standards. The mean values obtained with the three photometers was compared to the BIPM certified values. First a check of the group stability was performed. Except for a lamp that proved to be out of order (much higher luminous intensity for the certified electrical parameters) all the other lamps were found to be in good condition. After elimination of the faulty lamp, the group configuration fitted the initial one well within the BIPM calibration uncertainty.

The comparison with the newly developed photometers (Fsr 01…Fsr 03) showed quite good agreement (within +/-0,5%, see Figure 2).

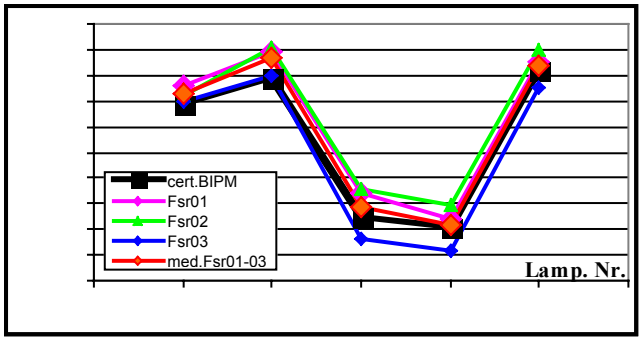

Figure 2. Comparison of the newly developed standards with the lamps calibrated by BIPM.
Lamps serials-graph correspondence: #195/473 = 1;
#196/474 = 2; #197/475 = 3; # 91/1 = 4; #91/3 = 5

5 Preliminary conclusions

New, primary references for luminous intensity and luminous flux units were developed by NIM. Validation comparisons for the realization and transfer capability of NIM-Romania are in progress within a bilateral comparison project **[6]** and are sought to be completed by October 2005.

Acknowledgments. The authors thankfully acknowledge for the theoretical and practical support from Prof. I.M.Popescu, of the Polytechnica University in Bucharest.

References

1. Campos, J. A. et.al, *Metrologia, Vol. 32, nr.6,* 675-679, 96.
2. Bastie, J., Coutin, J. M., *Proceedings of the LNE-INM International Conference, Vol. 1,* 99-104, 2001
3. CIE Communication 15, 81-82, 1970
4. EUROMET Project nr. 741
5. Bastie, J., Simionescu, M., Final report on the bilateral comparison for luminous intensity, 2004.
6. EUROMET project nr. 832

Distribution temperature scale realization at NIM-Romania

Author's name, M. Simionescu and A. Seucan
Affiliation, NIM-Romania

B. Rougie,
LNE-INM, France

Abstract. The closure of the photometric calibration service of BIPM stirred more national laboratories to find new SI traceability routes for luminous intensity and luminous flux calibrations. Therefore, as reported elsewhere **[1]**, NIM-Romania developed it`s own, radiometer based, references for luminous intensity and flux units. To allow units transfer to secondary standards, a temperature distribution scale was realized using a multi filtered irradiance meter traceable to the INM/CNAM-France primary standard for radiant flux. Theory, design information and so far obtained results are reported. Key words: spectral irradiance, distribution temperature.

1 Theory

Secondary standards most frequently used in photometry are incandescent lamps of special design that exhibit a quasi Gray Body behaviour in the VIS and near IR ranges. This also apply to halide lamps operated in the 2700 K...3300 K range. Assuming a filtered irradiance meter with two spectral bands, $\lambda_1...\lambda_2$ and $\lambda_3...\lambda_4$, for the range $\lambda_1...\lambda_4$, the distribution temperature ($T_{1,4}$) should be the solution of eq.:

$$\frac{Y_{1,2}}{Y_{3,4}} = \frac{\int_{\lambda 1}^{\lambda 2} s_{1,2}(\lambda)\cdot L_0(\lambda, T_{1,4})\cdot d\lambda}{\int_{\lambda 3}^{\lambda 4} s_{3,4}(\lambda)\cdot L_0(\lambda, T_{1,4})\cdot d\lambda} \qquad (1)$$

where : $Y_{1,2}$ and $Y_{3,4}$ are the photocurrents generated by the radiometer in the two different spectral bands; $s(\lambda)$ is the (absolute) spectral responsivity of the filtered radiometer and $L_0(\lambda_{1,4})$ is the spectral radiance of a Black Body at temperature $T_{1,4}$.

2 Practical realization

A multichanell irradiance meter was developped at NIM-Romania, covering the wavelength range of (400…800) nm (**Fig. 1).**

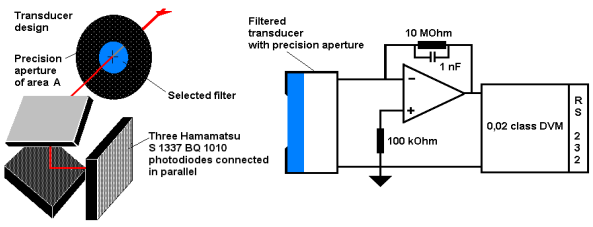

Figure 1. Filtered irradiance meter basic design

The definying characteristic of the filtered irradiance meter is it`s spectral responsivity:

$$R_e(\lambda) = \frac{Y(\lambda)}{E(\lambda)} = A\cdot s(\lambda) \qquad (2)$$

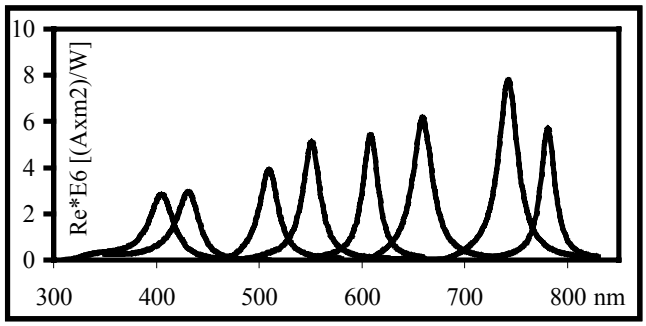

Figure 2. Spectral responsivity of the irradiance meter in different spectral bands

3 Characterization

Related to eq. **(1)**, the signals ratios $Y_{1,2} / Y_{3,4}$ have an estimated combined uncertainty of 0,15 %. The spectral responsivity on different measurement channels (as defined by the different filters) was measured against the NIM-Romania reference, traceable to the LNE-INM, France primary standard. The obtained values were characterised by an estimated standard uncertainty of 0,50 %.
From **eq. (1)** it becomes apparent that the estimated distribution temperature is a function of many parameters:

$$T_{1,4} = f\left[Y_{1,2}/Y_{3,4}, s_{1,2}(\lambda), s_{3,4}(\lambda), c_1, c_2\right]$$

so numerical calculation was used troughout for sensitivity estimations. This approach led to the uncertainty budget tabulated below :

Quantity	Associated standard uncertainty (%)	Sensitivity coefficient (K / %)	Contribution to the combined std. uncertainty (K)
$Y_{1,2} / Y_{3-4}$	0,15 %	$\delta T_{1,4} / \delta(Y_{1,2}/Y_{3,4}) \approx$ 50 K / %	≈ 7,5 K
$s_{1,2}(\lambda)$	0,50 %	$\delta T_{1,4} / \delta s_{1,2}(\lambda)$ ≈ 30 K / %	≈ 15 K
$s_{3,4}(\lambda)$	0,50 %	$\delta T_{1,4} / \delta s_{3,4}(\lambda)$ ≈ 30 K / %	≈ 15 K
$T_{1,4}$			**≈ 23 K**

Table 1. Temperature distribution measurement uncertainty budget

4 Unit transfer

As a typical application, a halide lamp of 40 W was calibrated in terms of distribution temperature. The distribution temperature values obtained for different spectral sub-intervals are tabulated below :

Nr.	Wavelength range	$T_{i, i+1}$
1	400 nm…500 nm	2920 K
2	440 nm…550 nm	2929 K
3	500 nm…600 nm	2934 K
4	550 nm…670 nm	2938 K
5	600 nm…750 nm	2955 K
6	670 nm…800 nm	2983 K

Table 2. Temperature distribution of a calibrated lamp

5 Conclusions and further steps

A multifiltered radiometer was developped and characterised at NIM-Romania. It allows both temperature distribution and spectral irradiance measurements. To validate the method employed and the estimated mesurement uncertainty a bilateral comparison with LNE-INM, France is in progress.

References

1. J.Bastie, M.Simionescu, A.Seucan, Candela realization at NIM-Romania, *Proceedings of CNRI International Conference, Light and Lighting 2002*, 205-210

Gloss standard calibration by spectrophotometer reflectance measurement-suggested method

Anne Andersson
SP Swedish National Testing and Research Institute, Borås, Sweden

Abstract. By definition, the ultimate reference or primary standard for gloss measurements is a glass surface having a refractive index of 1,567 for the wavelength 589.26 nm for all angles, (Budde, ISO2813, Andor). This paper suggests a method to calibrate gloss by near normal reflection measurements in a spectrophotometer. The near normal reflectance of a high gloss standard is measured at 589.3 nm in a spectrophotometer with reference to a standard Aluminium mirror with traceability. From the reflection value the refractive index is calculated using Fresnel equations. The monochromatic gloss value, G, can be obtained for all different angles. Correction factors between the monochromatic definition and the polychromatic luminous use in the gloss meter is added as suggested by Budde, 1980. The total uncertainty of gloss reference standard value G_{lum} is calculated for all angles 20º, 60º and 85º to be < 1 gloss unit.

Introduction

Specular gloss is widely used in the paint, paper, plastic and textile industries for the characterisation of mirror-like appearance of a surface by specific reflectance measurements. The measurement geometry and conditions are well defined in international and national standards, f ex ISO 2813. By definition [1,2], the primary standard for gloss measurements is a piece of highly plane black glass having a refractive index of 1.567 at the wavelength of the sodium line D (589.3nm). For all angles of incidence this surface by definition has an assigned gloss value of 100 GLU (Gloss Units). For calculation of the corresponding specular reflectance, r(angleº, n=1,567), values the Fresnel equations are applied, giving:

r (20º, n=1.567) = 0.049078
r (60º, n=1.567) = 0.100056 (1)
r (85º, n=1.567) = 0.619148

Primary standards of different refractive index than n = 1.567 results in different, G(angleº, n), gloss values in GLU (gloss units). From the reflection, r(angleº,n) values the G(angleº, n) can be calculated for all angles with formula (2):

G(angleº, n) = 100* r(angleº,n)/ r (angleº, n=1.567) (2)

The r(angleº,n) values are in this work calculated from the refractive index assuming an ideal surface having the property of all light that are not reflected are absorbed. However the gloss meter specified with the standard uses a daylight source (CIE C) and a photometer with a CIE V(lambda) spectral response function covering a rather broad spectral range. The inconsistency between the monochromatic specification of the reference and the polychromatic instrument leads to ambiguities in the calibration of the used reference standards and may cause differences in the practical gloss measurements of up to 0,5 %, according to Budde. Correction factors between the monochromatic definition and the polychromatic use in the gloss meter is recalculated, from values presented by Budde. The ratios of luminous data to spectral data, at the wavelength 589,26 nm, are presented in Table 1.

Table 1: Conversion from reflection at 589,26 nm to luminous gloss values G_{lum} for angles 20º, 60º, and 85º,according to Budde 1980.

Angles	20º	60º	80º
r(lum)/r(589,26)	1.005	1.003	1.000

Method

The reference gloss value are obtained by calculating the refractive index from the near normal spectrophotometer measurement and deduction of the G for each angle followed by multiplication of the conversion factor to get the luminous G_{lum} values that the instruments are working with.

1. measure the reflectance r at near normal incidence (8º)
2. calculate the refractive index from the Fresnel equations (in this work assuming equal polarisation of p and s components)
3. reflection at other angles was calculated with the same assumption as in 2.
4. the monochromatic gloss value G was calculated for angles 20º, 60º and 85º from (2)
5. apply conversion to luminous G_{lum} for all angles

Reference and sample preparation The quality and long time stability of the reference standard is of crucial importance. Cleaning of the surface of the gloss standard used in this work is done with alcohol with a developed technique until the gloss meter presents same values as calibrated values within ± 0.3 GLU for all angles. If any G(angle) deviates more it is an implication of having scattering effects and the surface is not cleaned properly.

Results

The gloss standard used in this example is a Byk Gardner black glass standard of the size 15cm × 15cm. Investigation of this standard over 8 year shows variation of about ± 0.5 GLU. If the values have changed polishing restores the original values within these values. Changes over the surface also varies about the same amount.

First the gloss standard was measured in a Lambda 900 Perkin Elmer spectrophotometer at 8º near normal incidence. The beam size was about 1cm × 1cm. An aluminium mirror with reflectance value 0.8787 ± 0.0035(k=2) at 590 nm and at 8º was used as reference for the reflectance measurement. Reflectance r = 0.044492 of the gloss standard was obtained from 12 measurements at the centre part of the surface with a standard deviation, of 0.000017. From the reflectance measurement the average refractive index was calculated to be n = 1.5346 ± 0.0010. The resulting monochromatic reflection r(angleº,n) values for angles 20º, 60º and 85º were calculated with Fresnel formula assuming equal size of the s and p components on the incident light. Results from calculated G, gloss values for angles 20º, 60º and 85º according to (2), including G_{lum} with luminous correction(Table 1) and deviation from earlier calibration are presented in Table 2. The earlier calibration was done in a goniphotometer setup with a laser at 633 nm. Correction from wavelength to the definition and to the luminous G values was done. The standard deviation of this earlier measurements were in the order of % and hence the uncertainties are much improved with measurements in a spectrophotometer.

Table 2: This table presents results of gloss values, G, at 589.26 nm, luminous gloss, G_{lum}, uncertainty and deviation from earlier calibration, all presented in gloss units (GLU).

Results	GLU/20	GLU/60	GLU/85
$G_{589.26}$	91.2	94.8	99.5
G_{lum}	91.7	95.1	99.6
U (k=1)	0.45	0.41	0.48
U (k=2)	0.90	0.81	0.96
Earlier cal.	92.2	95.4	99.6

Uncertainty calculation

The uncertainty calculation can be studied in Table 3. The long time stability of about 0.5 GLU was not used in the uncertainty calculation. The reflection, r, is the measurement of the standard reference at 8º . The gloss, G, is calculated from the r (8º) via the refractive index and r (angle). In measurements diffuse scattering and polarisation effects (Budde , 1979) are estimated to play an increasing role the larger the angle although the calculation of r to get G and the luminous correction factor are estimated to have a minor importance the smaller the angle.

Table3: In this table the uncertainties are estimated in % of the measurment value. The uncertainty values in % are used to calculate the uncertainties in GLU presented in Table 2.

Uncertainty,U		**r (%)**	**G (%)**	**G (%)**	**G (%)**
angle		8	20	60	85
Stddev of measurement		0,0017			
Al mirror reference uncertainty		0,2			
Diffuse scattering of standard		0,05	0,1	0,2	0,3
Polarisation dependant uncertainty		0,1	0,1	0,2	0,3
Calculation of r to get G assuming n:+/-0,001			0,3	0,15	0,02
Estimation of luminous correction			0,3	0,2	0,1
U	k=1	0,224	0,490	0,427	0,480
U	k=2	0,447	0,980	0,854	0,960

Summary and conclusion

This paper suggests a method of calibration of high gloss reference standards. The method is based upon a standard reflectance measurement in a spectrophotometer, the definition of gloss at n = 1.567 at 589.26 nm wavelengths to be 100 GLU and from luminous correction factors deduced by Budde. The uncertainty obtained is in the order of ± 1 GLU and the obtained gloss values deviated at the most ± 0.5 GLU from earlier calibration values. These are the results from first measurements and further improvements and analysis of the method have to be done. The the gloss standard long time stability of about ± 0.5 GLU was not used in the uncertainty calculation.

References

Budde, W., Polarization effects in gloss measurements, A*pplied Optics 18*, 2252, 1979.

Budde, W., The calibration of Gloss Reference standards, *Metrologia 16*, 89-93, 1980.

International Standard ISO 2813: Paint and varnishes-Measurement of specular gloss on non-metallic paint films at 20°, 60° and 85°. 3rd ed.,1994.

Andor, G., Gonireflectometer-based gloss standard calibration, *Metrologia 40*, 97-100, 2003.

Absolute cryogenic radiometry in the extreme ultraviolet at NIST

R. E. Vest, S. Grantham, and C. Tarrio
National Institute of Standards and Technology, Gaithersburg, MD, USA

Abstract. The absolute cryogenic radiometer (ACR) is an optical power detector with inherently lower uncertainty. At the National Institute of Standards and Technology (NIST) in Gaithersburg, MD, USA, we have recently implemented an ACR on a synchrotron beamline to establish a new radiometric scale in the wavelength range from 11 nm to 35 nm. The new scale is in good agreement, within the combined uncertainty of the measurements, with the extant scale based on an ionization chamber. Here we describe the high-throughput beamline at NIST's Synchrotron Ultraviolet Radiation Facility (SURF III) and the measurement system for calibration of Si photodiodes against the ACR, we present the calibration results for an uncoated Si photodiode and a photodiode with a Si/Zr coating deposited directly onto the active area, and we compare the ACR-based calibrations with calibrations traceable to an ionization chamber on a different synchrotron beamline.

Detailed Comparison of Illuminance Scale Realizations of KRISS and TKK

Seung-Nam Park, Dong-Hoon Lee, Yong-Wan Kim, In-Won Lee,

*Erkki Ikonen, *Mart Noorma and *Farshid Manoocheri

Division of Optical Metrology, Korea Research Institute of Standards and Science (KRISS) PO Box 102, Yuseong, Daejeon 305-600, Korea

*Metrology Research Institute, Helsinki University of Technology (TKK) and Centre for Metrology and Accreditation (MIKES) P.O. Box 3000, FI-02015 TKK, Finland

Abstract. A detailed comparison of the illuminance realizations of KRISS and TKK is performed. The relative difference of spectral responsivity at 555 nm is (-0.3±0.8) %, while the difference of the color correction factor for the illuminant A is (0.28±0.38) %, and the expanded uncertainties are given for coverage factor k=2. The area measurement for the radiometric aperture agrees within (-0.04±0.06) %. Accordingly the difference of the illuminance responsivity is (-0.6±0.8) %. A direct comparison of the illuminance responsivity scales which are realized and maintained by the procedure of each institute shows an agreement of (-0.1±0.9) %.

I. Introduction

Since the candela as well as the related quantities are generally derived from illuminance, accurate realization of the illuminance is critical in photometry and radiometry. However, as realizing the illuminance scale requires a series of measurements, such as responsivity, spectral characteristics and aperture area of a photometer, a set of comparisons for only illuminance responsivity between NMIs as in the case of the CCPR-K3.b [1] may be insufficient for an appropriate guide to improve the uncertainty.

In this paper, the measurement processes for the illuminance realization, such as the spectral responsivity at 555 nm, color correction factor for the illuminant A and the aperture area of the artifact photometer are in parallel compared between KRISS and TKK. Finally, the illuminance scales realized and maintained by both institutes are also compared to give material for a discussion on the comparison of the measurement processes.

II. Detailed Comparison of Illuminance Scale Realizations

The illuminance responsivity of a photometer is obtained by the equation

$$R_{\mathrm{vi}} = \frac{A \cdot S_{555}}{683\ \mathrm{lm/W} \cdot f(e)} \qquad (1),$$

where A is the aperture area, S_{555} the absolute spectral responsivity at 555 nm, and $f(e)$ the color correction factor (ccf). The ccf is defined as

$$f(e) = \frac{\int_{\lambda} e(\lambda)\, V(\lambda)\, \mathrm{d}\lambda}{\int_{\lambda} e(\lambda)\, s(\lambda)\, \mathrm{d}\lambda} \qquad (2),$$

where $e(\lambda)$ is relative spectral power distribution of the source and $s(\lambda)$ the normalized spectral responsivity of the photometer.

The artifact photometer for the comparison consists of a temperature-stabilized photometer head supplied by LMT and an external aperture of 7 mm diameter. The edges of the aperture were trimmed by a diamond-turning machine. The artifact was transferred to TKK after measurement at KRISS and then returned to KRISS for the drift check.

At KRISS, the illuminance scale is realized by calibrating spectral responsivity of the photometers using a spectral responsivity comparator traceable to the absolute cryogenic radiometer. Relative spectral responsivity is measured against the single element silicon reference detector, while the absolute responsivity at 555 nm is compared to the silicon trap detector. The aperture area of the photometer is measured by two independent methods, Gaussian beam superposition (GBS)[2] and optical edge detection (OED). The OED method can be easily implemented by inserting a microscope and focusing the beam on the aperture plane in the GBS.

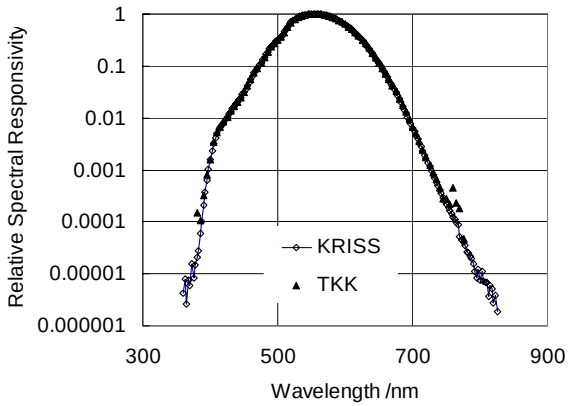

Figure 1. Relative spectral responsivity comparison of the artifact photometer.

As far as the spectral characteristics measurement of the photometer for the illuminance realization is concerned, TKK has the procedure different from KRISS.[3]. However, TKK measured the spectral characteristics of the artifact by comparison to the spectral responsivity reference. For the comparison, TKK used the spectral responsivity facility [4] and the reference trap detector which is traceable to the cryogenic radiometer.

Figure 1 shows a comparison of the relative spectral responsivity. The spectral bandwidths of the measurements at TKK and KRISS are 1 nm and 4 nm, respectively. Even

if the measurement range of KRISS is wider than that of TKK, the data measured beyond the measurement range of TKK affect the ccf within a part in 10^6. The difference of the ccf for the illuminant A is 0.28 %, which exceeds the standard uncertainty denoted in the parenthesis in Table 1.

The difference of the absolute responsivity at 555 nm is -0.3 %. Considering the degree of equivalence of the spectral responsivity between both institutes, -0.12 % at 550 nm [5], we can see that an additional difference, -0.18 %, though much smaller than its standard uncertainty of 0.40 %, has appeared in the responsivity comparison.

The aperture area measurements are compared using four apertures with diameters of 5 mm, 7 mm and 8 mm. For all apertures, the relative area difference of KRISS and TKK is between -0.005 % and -0.048 %. The area measured by TKK and its difference with KRISS shown in Table 1 is estimated from the area comparison result for the aperture which has the same diameter as the aperture attached in the artifact photometer.

The final difference of the illuminance responsivity of the artifact is -0.6 %, which mainly comes from contributions of difference of the responsivity at 555 nm and of the ccf for the illuminant A. The aperture area difference is somewhat larger than the standard uncertainty, but its contribution to the illuminance responsivity difference is almost negligible.

Table 1. Comparison of quantities obtained during realization of the illuminance responsivity for the artifact. The numbers in the parentheses correspond to the standard uncertainty.

Quantities	KRISS	TKK	KRISS-TKK
Responsivity at 555 nm (A/W)	0.1974(6)	0.1980(4)	-0.3(4) %
Aperture area (cm^2)	0.38492(6)	0.38507(10)	-0.04(3) %
ccf for illuminant A	0.9958(14)	0.9930(12)	0.28(19) %
Illuminance responsivity (nA/lx)	11.17(4)	11.24(3)	-0.6(4) %

III. Comparison of illuminance responsivity

At TKK, the illuminance scale is not realized by using the above procedure, but by using trap-detector based photometers, for which the $V(\lambda)$ filter is separately measured in terms of spectral transmittance.[3] The spectral responsivity of the trap detector is also calibrated traceable to the cryogenic radiometer. The radiometric aperture area is measured by GBS.[2]

The TKK reference photometer was compared with the artifact photometer at TKK. The artifact drift during the comparison period and transportation was checked after return to KRISS and revealed to be insignificant. The difference in the illuminance scales was -0.1 %, with an expanded uncertainty of 0.9 %, which is much smaller than the difference of -0.6 % shown in Table 1. However, the differences are within combined standard uncertainties of the comparisons. In another illuminance responsivity comparison the difference between KRISS and TKK was -0.2 % with an expanded uncertainty of 0.6 % [6]. Considering these facts, the deviation of -0.6 % of Table 1 is acceptable. However, both institutes seem to be somewhat too optimistic with the uncertainty estimates.

IV. Conclusions

The illuminance scales realized and maintained at KRISS and TKK have been compared to show a good agreement between 0.1 and 0.2 %. TKK was asked to yield the illuminance responsivity of the artifact photometer supplied by KRISS according to the KRISS procedure. The illuminance responsivity given by TKK using the KRISS procedure is 0.6 % higher than that given by KRISS. Considering the uncertainties of the measurements, the difference is acceptable. However, since both institutes seem to be somewhat too optimistic with the uncertainties of the ccf and the aperture area, the uncertainties may need to be addressed to cover these deviations.

References

[1] Köhler R., Stock M. and Garreau C., Final Report on the International Comparison of Luminous Responsivity CCPR-K3.b, Metrologia **41**, Tech. Suppl., 02001, 2004.

[2] Ikonen E., Toivanen P. and Lassila A., A new optical method for high-accuracy determination of aperture area, Metrologia **35**, 369, 1998.

[3] Kärhä P., Haapalinna A., Toivanen P., Manoochehri F. and Ikonen E., Filter radiometry based on direct utilization of trap detectors, Metrologia **35**, 255, 1998.

[4] Manoochehri F., Kärhä P., Palva L., Toivanen P., Haapalinna A., and Ikonen E., Characterization of Optical Detectors Using High-Accuracy Instruments, Anal. Chim. Acta **380**, 327 (1999).

[5] Goebel R. and Stock M., Report on the comparison CCPR-K2.b of spectral responsivity measurements in the range 300 nm to 1000 nm, Metrologi, **41**, Tech. Suppl.,02004, 2004.

[6] Ikonen E. and Hovila J., Final Report of CCPR-K3.b.2-2004: Bilateral Comparison of Illuminance Responsivity Scales between the KRISS (Korea) and the HUT (Finland), Metrologia **41**, Tech. Suppl. 02003, 2004.

Radiometric Temperature Comparisons of Three NIST Gold Freezing-point Blackbodies

N. Sasajima,
NMIJ, Tsukuba, Japan

C. E. Gibson, V. Khromchenko, R. D. Saunders, H. W. Yoon
NIST, Gaithersburg, MD, USA

Abstract.

We describe the radiometric temperature comparisons of three NIST gold freezing-temperature blackbodies. The respective blackbodies are used in different facilities for the radiance temperature and spectral radiance scales and the comparisons are needed to determine the equivalence of the gold-point based realizations. The temperatures of each gold-point blackbody are compared against each other using a detector-based radiation thermometer which is calibrated using the cryogenic electrical substitution radiometer. These measurements were performed over a month period in 2004 and compared to the previous measurements of two of the same blackbodies in 1991. The freezing temperatures of all three blackbodies are found to be in agreement to < 10 mK (k=2) and the differences are within the comparison uncertainties. These differences are in agreement, within the combined uncertainties, with the < 16 mK (k=1) differences found in 1991.

Introduction

In the International Temperature Scale of 1990 (ITS-90), the temperatures above the freezing temperature of Ag can be derived from the use of Ag, Au, or Cu freezing-temperature blackbodies and radiances from Planck's radiation law. Although in ideal situations, the freezing temperatures of the respective metals are presumed to be equivalent, the transition temperatures will be depend upon many factors such as the material purity, cavity design, furnace design and operational parameters. The long-term use might also be compromised by the possible contaminations of the pure metal during use. Thus, to determine whether there are intrinsic differences in the temperature scales at the different national measurement institutes (NMI) related to the ITS-90 realizations, the fixed-points should be directly compared.

Direct fixed-point blackbody comparisons are difficult due to the need to transport the furnaces and the power supplies between the institutes. Furthermore, the cost of the quantity of the pure metal required can be a barrier to constructing the number of fixed-points needed for comparisons, and due to the expense of acquiring the quantity of pure Au, many NMIs utilize fixed-points made from either Ag or Cu.

We compared three Au fixed-point blackbodies with three different furnaces utilizing Na-heatpipe liners. Two of the blackbodies are constructed with same physical dimensions and the other blackbody was slightly smaller. The blackbodies were operated in two furnaces with different physical dimensions but with a similar design. Measurements of radiance temperatures were performed with and without a graphite aperture to determine the change in the cavity emissivity. The emissivity was also modeled, and the results compared with the experimental change in the radiance temperatures.

Experimental Setup

The furnace and the fixed-point cell are shown in Fig. 1. The purified Au (99.9999 %) metal is placed in a purified graphite crucible. The long alumina or fused silica tube is placed at the center of a cylindrical, Na-heatpipe liner, and the furnace is electrically heated from the outside of the liner with two, semi-cylindrical heaters which enclose the heatpipe liner. The crucible is physically separated from the heating elements by the alumina or the silica tube, and argon is flowed through from the rear of the furnace to be vented at the front opening. The use of the heatpipe liner

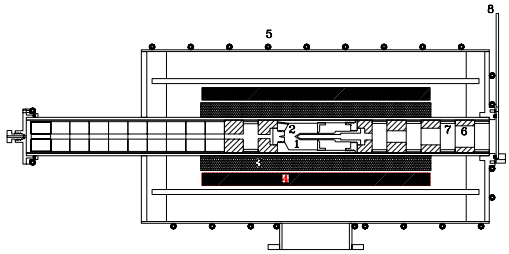

Figure 1. The schematic of the gold-point furnace.

enables simple two-level control of the electrical heaters for melting or freezing of the metal.

The radiance temperature measurements were performed using the NIST Absolute Pyrometer 1 (AP1). The design of the AP1 has been described in previous publications. The AP1 has been measured for absolute spectral radiance responsivity in the NIST Spectral Irradiance and Radiance Responsivity Calibrations using Uniform Sources (SIRCUS) facility. Since these measurements are radiance temperature comparisons of blackbodies at almost equal temperatures, the spectral responsivity and other sources of uncertainties such linearity, size-of-source effect are do not contribute to these comparisons.

Blackbody Design and Emissivity Calculation

The design of the graphite crucible is shown in Fig. 2. The blackbody is designed so that limiting apertures could be placed into the 6 mm diameter opening to increase the emissivity if desired. The large crucible contains about 1.3 kg of high-purity Au to achieve a uniform temperature distribution during the freeze and to achieve long-time duration of the freeze plateau.

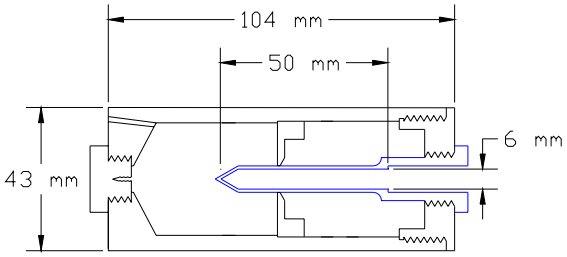

Figure 2. The design of two of the Au-freezing temperature crucibles. The conical cavity has an apex angle of 57 °.

During the experiments, the cavity was fitted with a 2 mm diameter aperture to validate the predicted increase in the emissivity as well as to verify the emissivity prediction of the 6 mm diameter cavity with no apertures. The calculated emissivities are listed in Table 1. The calculations are performed using a Monte Carlo program

Table 1. Calculated emissivity of the graphite blackbody cavity with 50 mm depth and 57 ° conical bottom.

Aperture diameter [mm]	Emissivity with graphite emissivity, ε = 0.86	Emissivity with graphite emissivity, ε = 0.80
6.0	0.99964	0.99943
2.0	0.99996	0.99993
1.5	0.99998	0.99996
1.0	0.99999	0.99998

Discussion

These results demonstrate the long-term stability of the Au points constructed at NIST and the equivalence between the three blackbodies. All three of the blackbodies are still in service after almost 20 years of intermittent usage after being stored in laboratory environment without any special care. All three of the NIST Au-points showed the same shape of the freezing plateau without noticeable slopes indicating that the material purity and the temperature uniformity of the furnaces are equivalent. These results will be compared against similar measurements using the Ag- and Cu-point blackbodies at other NMIs to realize the ITS-90.

Characterization of Thermopile for Laser Power Measurements

A. K. Türkoğlu
Ulusal Metroloji Enstitüsü, Kocaeli, Turkey

Abstract. Due to their high wavelength and power range, thermal detectors were employed in our measurement set-up for optical power measurements. A link between optical power calibrations at medium power levels and our primary standard cryogenic radiometer was established by means of transfer standards. Analysis of the set-up and characterization of our working standard thermal detectors to yield uncertainty budget is presented in this study.

Detector Based Measurements

As the needs and applications of optical measurements increase, we frequently face with new radiation detectors and lasers with different structure, speed, range or beam properties. However in the calibration and measurements, commercially, there is no single suitable working standard detector available to cover all the power and optical wavelength range of interest.

In our laboratory, treaceability from our Cryogenic Radiometer (Oxford Instr., Radiox) is provided by using a set of home-built 3-element reflection type trap detectors as the transfer standards. Due to the type of silicon detectors used, those trap detectors can be used safely in 300 to 1100 nm wavelength range but only up to 3 mW incident power due to their linearity limits. The measurements at wider wavelength ranges have become possible by employing our Electrically Calibrated Pyroelectric Radiometer. But for higher power ranges, it was found out that it is not feasible to use filtered photodetectors due to the heating effects, nonhomogeneity of the filter surface and strong depen- dence of the alignment and on incident angle. Therefore, we have chosen and employed thermopiles in our laser power measurement and detector calibration set-up.

Laser Sources

Our monochromatic line source facility contains an 11 mW HeNe of 632.8 nm and a 20 mW Tunable Argon lasing at 488 and 514 nm. For medium power ranges, we added an intensity stabilized 2W Nd-YAG laser to our set-up, which has a main beam at 1064 nm wavelength and an additional green line at 532 nm.

Detectors

For internal checks and dissemination, we have used filtered UV and Ge detectors which are capable up to optical powers of 30 mW. We have added three thermopiles with 3, 30 and 250 W maximum optical power thresholds to our measurement facility. Circular active areas of the thermopiles were defined with the diameters of 12, 18 and 50 mm respectively. Selected detectors had response times of 0.8 to 2.5 s. These detectors were chosen especially for their good repeatibility, spatial uniformity and rather flat responsivity over a wide range which was stated as 0.2 to 20 μm.

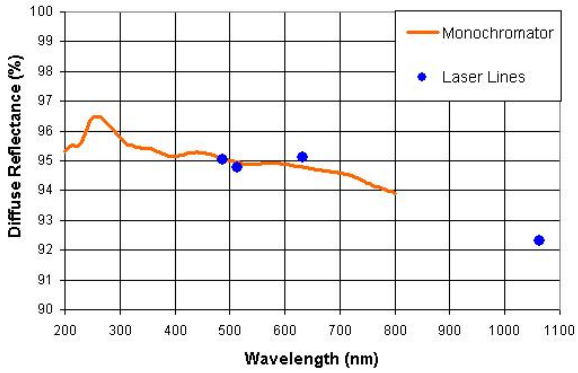

Figure 1. Reflectance Curve of Thermopile Coating

Characterization

For the flatness of the spectral responsivity, the diffuse reflectance of the thermopile was measured by mono- chromator and found to be as 95,2 ± 1,2 % between 200 and 800 nm. Reflectances at single laser lines were also measured seperately as shown in Fig.1.

Nonlinearity behaviour was studied by means of detector sensitivity measurements taken at eight different levels and found to be increasing up to 0.4 % level as optical power goes to 1.6 W. Homogeneity of sensitivity was analyzed 7 mm around the center and detected as below 0.25 % except for the largest area detector. The stray light and divergence effects was also measured to be very low, around 0.05 % for nominal 60 cm measurement distance on the set-up. Over 100 mW level, random power fluctuations by the source were seen to be more effective than the any other factor, and therefore were tried to be minimized by employing a monitor detector.

Results

A thermopile based laser power measurement set-up working at medium power levels from visible to near infrared range has been established. Responsivity, linearity and uniformity focused analysis resulted that measurements at an uncertainty level (k=2) of 1.4 % for the visible range (up to 20 mW) and of 1.9 % in the infrared (for 1.6 W at 1064 nm), have become possible by this power and wavelength range extension study.

References

Li, X., T. R. Scott, C. L. Cromer, D. Keenan, F. Brandt, K.Möstl, Power Measurement Standards for High-Power Lasers: Comparison between the NIST and the PTB, *Metrologia, 37*, pp.445-447, 2000.

Li, X., T. Scott, S. Yang, C. Cromer, M. Dowell, Nonlinearity Measurements of High-Power Laser detectors at NIST, *Journal of Research of the NIST, 109*, No.4, pp429-434, 2004.

Möstl, K., Laser Power and Energy Radiometry, *Institute of Physics, Conference Series*, No.92, pp.11-18, London, 1988.

Turkoglu, K., F. Samadov, M. Durak, U. Kucuk, Construction of a Reference Photometer Head for the Realization of Candela, *Proceedings of CIE Congress*, Volume II, pp. 379-386,

Istanbul, 2001.

Detector Based Traceability Chain Established at the UME

F.Sametoglu*, O.Bazkir, O.Celikel

TUBITAK-Ulusal Metroloji Enstitusu (UME),
Gebze, 41470, Kocaeli, Turkey

Abstract. In UME, detector based traceability chain for radiometry and photometry was established in 2003, which is presented.

1. Introduction

The concept of traceability to a national laboratory is fundamental to a unified system of metrology. Metrology institutions establish their own traceability chains and cross-linkings in measurements depending on primary and secondary standards. In optical metrology this type of chain can be established either with source or detectors based standards. We developed detector-based radiometric and photometric scales and established traceability chain in measurements, which is given in Figure 1.

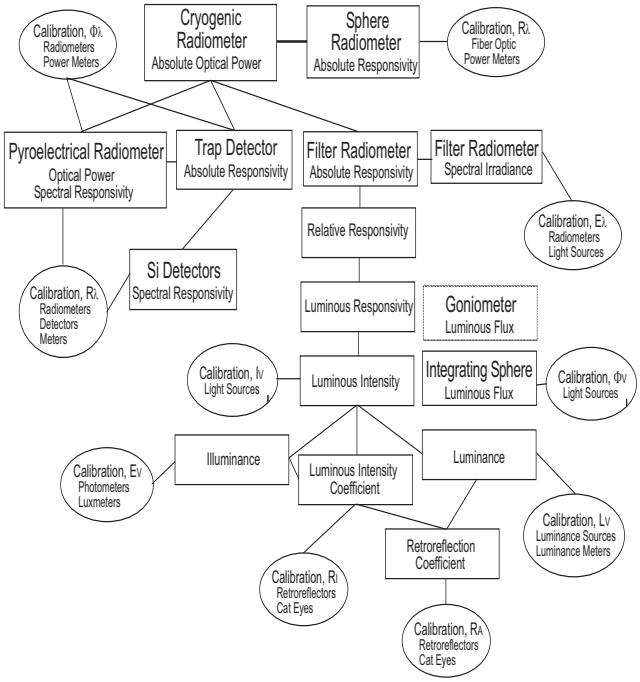

Figure 1. Traceability chain for radiometry and photometry established at the UME.

2. Absolute Optical power Scale

Top of chain constitutes the absolute measurement of optical power (W) measured by using a helium-cooled electrical-substitution cryogenic radiometer (ESCR). Intensity stabilized and vertically polarized lasers (He-Ne, Ar^+ and Nd:YAG) are used for the realization. The measurement of optical power at each laser wavelength was performed using static substitution method by which optical temperature induced by optical heating is sandwiched between two electrical temperatures, which are slightly above and blow the optical temperature, obtained by electrical heating. Then optical power was obtained by equating it to the electrical power calculated by interpolation of an optical and two electrical temperatures and two electrical powers. Effects of all the parameters like scattering, window transmittance and imperfect cavity absorbance on the optical power were examined and the optical power scale was realized with an expanded uncertainty of a few parts of 10^4.

3. Responsivity Scale

Absolute responsivity scale is based on calibration of homemade reflection type trap detectors, which consist of three Hamamatsu S1337-11 windowless silicon photodiodes, against ESCR. The absolute spectral responsivity scales for optically characterized each trap detectors were obtained at two steps. In the first step, the absolute spectral responsivities at the mentioned discrete laser wavelengths were measured. Then in the second step, developing the interpolation and extrapolation models for the internal quantum efficiency and reflectance of detectors the scale was expanded to 350 - 850 nm wavelength range with an expanded uncertainty of 0.05 %.

The relative optical power and spectral responsivity scales from 250 nm to 350 and 850 nm to 2500 nm wavelength ranges were realized by calibrating the detectors against another transfer standard called as electrically calibrated pyroelectric radiometer (ECPR). The ECPR has flat response pyroelectric detector made from lithium tantalite crystal, which has permanent dipole moment. The pyroelectric detector was calibrated against ESCR and the responsivity scale was realized between 250 and 2500 nm wavelength range with an expanded uncertainty of 1.74 % by using the spectral reflectance of coating of pyroelectric detector.

3. Spectral Irradiance Scale

Temperature-controlled home-made filter radiometers were used in order to realize spectral irradiance scale between 286 nm and 901 nm wavelength range. Filter radiometer consists of three element silicon trap detector, band-pass filters and precision aperture. The temperature of each radiometer housing including, aperture and filter can be adjusted from 18 °C to 35 °C range with stability of better than 0.05 °C using circular thermo-electric Peltier element. The irradiance scale was realized using the measurements of aperture area, transmittance of filters and

* Corresponding author. Phone: +902626795000; Fax: +902626795001
E-mail address: ferhat.sametoglu@ume.tubitak.gov.tr

responsivity of trap detector with expanded uncertainties between 2.3 % and 1.5 % in UV region and 0.6 % above 400 nm wavelengths.

4. Photometric Scale

The traceability chain in photometry was established by realization of SI based unit of candela according to its last definition with an expanded uncertainty of 0.29 % by using home-made temperature-controlled filter radiometers consisting of reflection type trap detector, V(λ)-filter and precision aperture. Luminous responsivity of each radiometer was calculated by measuring the relative spectral responsivity of radiometer, spectral transmittance of filter and effective area of aperture. In order to calculate correlated color-correction factor, spectral power distribution of Osram Wi41/G lamp was measured by using characterized interference filters inside the filter radiometer.

Characterized filter radiometers and integrating sphere were also used for realization of the photometric unit of luminance with an expanded uncertainty of 0.38 %. Sphere output geometry was defined by using a circular aperture. Integrating sphere was characterized by measuring its aperture area and sphere output non-uniformity. Optical scanning technique was developed for defining of effective are of the aperture with a relative standard uncertainty of 2.3×10^{-4} (k=1). The similar technique was used for the light uniformity analysis of the sphere output.

In order to measure luminous intensity and retroreflection coefficients of retroreflectors a fully automated retroreflection measurement system was established. The system is composed of a lighting projector, a goniometer and filter radiometers. A calibrated filter radiometer was placed to the goniometer center so as to measure illuminance level on the retroreflector surface and to determine correlated color temperature of a lighting projector. The luminous intensity and retroreflection coefficients of a retroreflector at 1°30` and 20` observation angles were measured using two calibrated and identical filter radiometers.

The luminous flux unit of lumen was realized by using a characterized and $BaSO_4$ coated integrating sphere with diameter of 2 m. During the measurements lamp current was kept stable at about 5×10^{-5}A with expanded standard uncertainty of 0.028 % (k=2) by using developed control system. Substitution principle was used to obtain lumen from 5 lm to 5000 lm with an expanded uncertainty of 1.14 %. For absolute realization of the unit in UME a spherical goniophotometer is planned to be constructed in the future.

5. Fiber Optic Power Scale

The calibration of fiber optic power meters used in optical communication is an important side of the optical fiber metrology. A spectralon coated sphere radiometer, which has an InGaAs detector, was characterized and calibrated against the cryogenic radiometer. Intensity stabilized DFB laser sources (1310 nm and 1550 nm) were used in the absolute power and responsivity measurements. The responsivities of sphere radiometer at 1310 nm and 1550 nm were calculated as 2.576×10^{-4} (A/W) and 2.488×10^{-4} (A/W) with expanded uncertainties of 0.283 % and 0.315 %, respectively.

References

Bazkir, O., Ugur, S., Samedov, F., and Esendemir, A., High-accuracy optical power measurements by using electrical - substitution cryogenic radiometer, *Optical Engineering, 44*, 1-6, 2005.

Bazkir, O., Samedov, F., Electrical substitution cryogenic radiometer based spectral responsivity scale between 250–2500 nm wavelengths, *Opt. Appl., 34*, 427-438, 2004.

Bazkir, O., Samedov, F., Characterization of silicon photodiode-based trap detectors and establishment of spectral responsivity scale, *Optics and Lasers in Engineering, 43*, 131-141, 2005.

Durak, M., Samedov, F., Realization of a filter radiometer based irradiance scale with high accuracy in the region from 286 nm to 901 nm, *Metrologia, 41*, 401-406, 2004.

Samedov, F., Bazkir, O., Realization of photometric base unit of Candela traceable to cryogenic radiometer at UME, *Journal of European Applied Physics*, *30(3)*, 205-213, 2005.

Samedov, F., Durak, M., Bazkir, O., Filter-radiometer based realization of Candela and establishment of photometric scale at UME, *Optics and Lasers in Engineering*, *43(11)*, 1252-1256, 2005.

Samedov, F., Durak, M., Realization of luminous flux unit of Lumen at UME, *Opt. Appl., 34*, 265-274 2004.

Samedov, F., Celikel, O., Bazkır, O., Establishment of a computer controlled retroreflection measurement system in UME, *Review of Scientific Instruments*, *76(9)*, 2005 (in press).

Celikel, O., Bazkır, O., Kucukoglu, M., Samedov, F., Absolute spectral responsivity calibration of integrating sphere radiometer to be used at optical fiber communication wavelengths as a transfer standard, traceable to the cryogenic radiometer, *Optical and Quantum Electronics*, *37(6)*, 529 - 543, 2005.

Comparison of the PTB Radiometric Scales for UV Source Calibration

R. Friedrich, J. Hollandt, W. Paustian, M. Richter, P. Sperfeld, R. Thornagel
Physikalisch-Technische Bundesanstalt, Braunschweig and Berlin, Germany

Abstract. The radiometric scales of the Physikalisch-Technische Bundesanstalt for the calibration of radiation sources in the ultraviolet have been compared. The work refers to the measurement of spectral radiant intensity, spectral irradiance, and spectral radiance of deuterium and tungsten lamps in the wavelength range from 120 nm to 400 nm. The scales are based on calculable temperature radiation of black body radiators as primary source standards as well as calculable synchrotron radiation of the electron storage rings BESSY I and BESSY II. As a result, the agreement is within a few percent, i.e. well within the combined measurement uncertainties.

Introduction

The Physikalisch-Technische Bundesanstalt (PTB) has realized different radiometric scales for source calibration by spectrally dispersed measurements. Within the framework of applied radiometry, spectral irradiance calibrations are performed in the ultraviolet (UV), visible (VIS), and infrared (IR) based on calculable high-temperature black body radiation (*Sperfeld et al.* 1998). Black body radiators are used as primary source standards also within the framework of high-temperature physics to measure, e.g., spectral radiance of UV, VIS, and IR sources (*Friedrich et al.* 2000). Photon metrology at shorter wavelengths, i.e. in the spectral range of UV, vacuum-UV (VUV) radiation, and X-rays, is performed using calculable synchrotron radiation in the PTB laboratory at the electron storage ring BESSY II. Within the framework of UV and VUV radiometry, deuterium (D2) lamps are calibrated in the wavelength range from 120 nm to 400 nm with respect to spectral radiant intensity and spectral radiance using BESSY II as a primary source standard (*Richter et al.* 2003). In the UV, the different scales overlap allowing a radiometric comparison. The present work also includes measurements performed at the former storage ring BESSY I which was shut down in 1999.

Results

Fig. 1 summarizes the results. The red lines represent the ratio of spectral radiant intensity of D2 lamps as measured at BESSY I with respect to BESSY II. The results were obtained by the calibration of two different lamps in the wavelength range from 120 nm to 165 nm and from 165 nm to 400 nm, respectively, with different spectral resolution. Within the regime of continuous emission of a D2 lamp above 180 nm, the agreement is perfect, i.e. better than 1 %. The increasing variations of the measured ratio towards shorter wavelengths are due to the D2 lamp emission consisting more and more of a discrete distribution of numerous spectral lines. This makes the measurements more sensitive to the reproducibility of the wavelength scale of the spectrometer used and increases the measurement uncertainties. The relative standard uncertainties (k=1) for the BESSY II calibrations with respect to spectral radiant intensity are indicated by the dashed lines in Fig. 1.

The green data points in Fig. 1 represent the ratio of spectral irradiance of a standard D2 lamp as measured within the framework of applied radiometry, traceable to black body radiation, with respect to measurements performed at BESSY II. For this comparison, the BESSY II spectral radiant intensity data were divided by the square of the distance for the black body irradiance measurements and, by that, transformed also into spectral irradiance values. The excellent agreement indicates the latter transformation to be valid for the standard D2 lamp used which may be regarded as a point source for the measurement geometries applied.

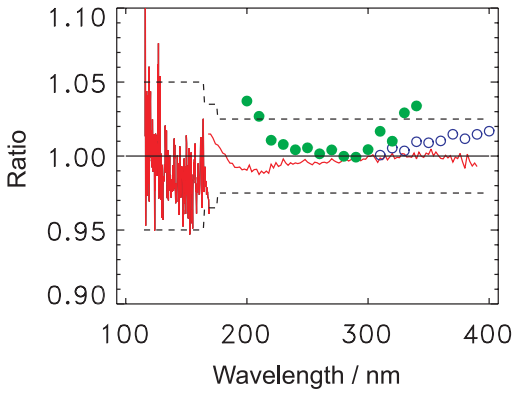

Figure 1. Comparison of radiometric scales and primary source standards of PTB in the UV and VUV: BESSY I vs. BESSY II via spectral radiant intensity of deuterium lamps (red), high-temperature black body radiator vs. BESSY II via spectral irradiance of a deuterium lamp (green), high-temperature black body radiator vs. BESSY II via spectral radiance of a tungsten ribbon lamp (blue). The dashed lines represent the standard uncertainty range (k=1) of the BESSY II calibrations.

The blue data points in Fig. 1, finally, represent the ratio of spectral radiance of a standard tungsten ribbon lamp as measured within the framework of high-temperature physics, traceable to black body radiation, with respect to corresponding measurements performed at BESSY II. The agreement is better than 2 % which is in the order of magnitude of non-uniformities in the emission along the tungsten band.

References

Sperfeld P., Metzdorf J., Galal Yousef S., Stock K.D., Möller W., Metrologia, 35, 267, 1998.
Friedrich, R., Fischer, J., Metrologia, 37, 539, 2000.
Richter, M., Hollandt, J., Kroth, U., Paustian, W., Rabus, H.,

Thornagel, R., Ulm, G., Metrologia, 40, S107, 2003.

Spectral Responsivity Scale between 1 μm and 19 μm at the NIST

G. P. Eppeldauer, J. Zeng, and L. M. Hanssen
National Institute of Standards and Technology
Gaithersburg, Maryland 20899, USA

Abstract. Most of the present spectral responsivity measurements at the National Institute of Standards and Technology (NIST) are based on the responsivity scale realized on the recently developed facility for Spectral Irradiance and Radiance Responsivity Calibrations using Uniform Sources (SIRCUS). The SIRCUS facility and the NIST reference responsivity scale are being extended. In this work, the scale extension from the silicon to the infrared (IR) wavelength range, using both NIST designed pyrometers and commercial pyroelectric detectors, is discussed.

Pyroelectric radiometers

New radiometers, based on $LiTaO_3$ pyroelectric detectors, have been developed at the National Institute of Standards and Technology (NIST) to realize and maintain the extended spectral power responsivity scale. The gold-black coated pyroelectric detectors are temperature controlled using a thermoelectric cooler/heater and a thermistor sensor. A gold coated reflecting dome is mounted above the tilted detector to decrease the IR reflectance loss and increase signal absorption. The result was improved spatial non-uniformity of responsivity at long wavelengths. The dome has a 4 mm diameter opening in the optical axis. Figure 1 shows the picture of the pyroelectric radiometer.

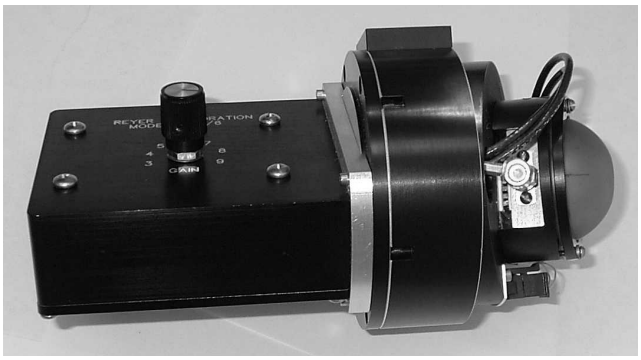

Fig. 1. Pyroelectric radiometer (top cover is removed)

The current measuring preamplifier is attached with a connector to the bottom of the detector (front) unit. Two identical radiometers were made to utilize the advantage of group policy.

Two commercial pyroelectric detectors have also been added to the group of the pyroelectric radiometer standards. These two detectors are temperature monitored and black paint coatings are applied on the detectors to convert optical power change into temperature change.

Calibration facilities

The facility for Spectral Irradiance and Radiance Responsivity Calibrations using Uniform Sources (SIRCUS) made it possible to improve the uncertainty of monochromator-based spectral radiant power responsivity measurements and to extend the calibrations from power mode to irradiance [1] and radiance measurement modes. The high beam power and stability of the tunable IR lasers of the SIRCUS facility makes it possible to calibrate a wide range of IR detectors and radiometers for spectral power, irradiance, and radiance responsivity.

In addition to the SIRCUS facility, the Ambient Infrared Detector Characterization Facility was used to measure frequency- and temperature-dependent responsivity, signal-gain stability, and noise performance. The IR-Laser Scatter and Detector Characterization Facility was used to measure the spatial non-uniformity of responsivity, linearity, angular responsivity, absolute responsivity, stability, and repeatability. The Fourier Transform IR Spectrophotometry Facility was used to measure the spectral reflectance of the coated detectors to determine the relative spectral responsivity.

Spectral responsivity calibrations

The relative spectral responsivity of all four pyroelectric detectors has been determined from spectral reflectance measurements. The spectral responsivity of the commercial pyroelectric detectors is significantly structured because of the black paint coating on the detectors. The absolute responsivity tie points for the four radiometers have been derived from trap and single element Si and Ge photodiodes traceable to the NIST reference responsivity scale [2]. More tie points have been derived from an earlier developed $LiNbO_3$ pyroelectric radiometer standard [3] and also from a single element $LiTaO_3$ pyroelectric transfer detector (PD2) calibrated against the primary standard cryogenic radiometer at 10.6 μm [4]. From these measurements, the spectral power responsivity in the 1 μm to 19 μm range was determined. Figure 2 shows the spectral power responsivity curves of the two commercial pyroelectric detectors. The relative expanded uncertainty of the spectral power responsivity calibrations of the pyroelectric working standard radiometers is 2.7 % within the 1 μm to 19 μm wavelength range.

Radiometer characterizations

All four pyroelectric devices have been fully characterized to operate them under application conditions so that the measurement uncertainty in use will not be significantly higher than when calibrated. The characterizations help the users to determine the optimum spot size of the incident beam, chopping frequency, and temperature dependent responsivity corrections for different applications.

The commercial radiometers were selected for extended frequency response at the highest, 10^{10} V/A signal, gain. The electronic and thermal time constants were determined from frequency dependent signal gain measurements. Figure 3 shows that the responsivity roll-on originating from the differentiating time constant m_4 can cancel the responsivity roll-off produced by the integrating time constant m_2, resulting in a m_3 = 109 Hz upper roll-off frequency (produced by the remaining integrating time constant).

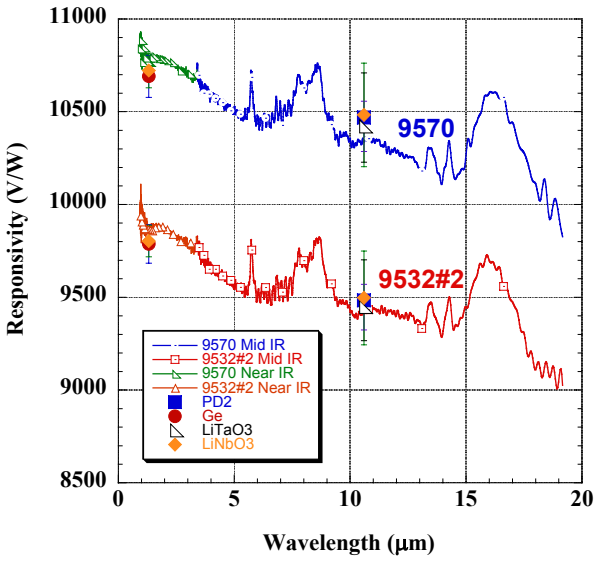

Fig. 2. Spectral power responsivity of two pyroelectric detectors. The individual points with error bars are values obtained with laser sources at 1.32 µm and 10.6 µm.

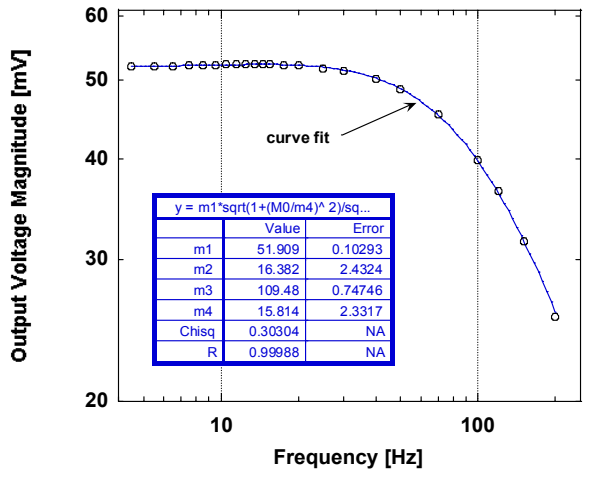

Fig. 3. Frequency dependent responsivity of a pyroelectric detector at a signal (current) gain of 10^{10} V/A.

The spatial non-uniformity of responsivity was measured at 10.6 µm. The results in Figure 4 show that the commercial device has a roughly 1 % spatial variation of responsivity in the center area which makes it possible use of this detector in radiant power measurement mode with low uncertainty. A temperature coefficient of responsivity of 0.19 %/degree C was measured for the commercial pyroelectric detectors with a relative expanded measurement uncertainty of 20 % (k=2).

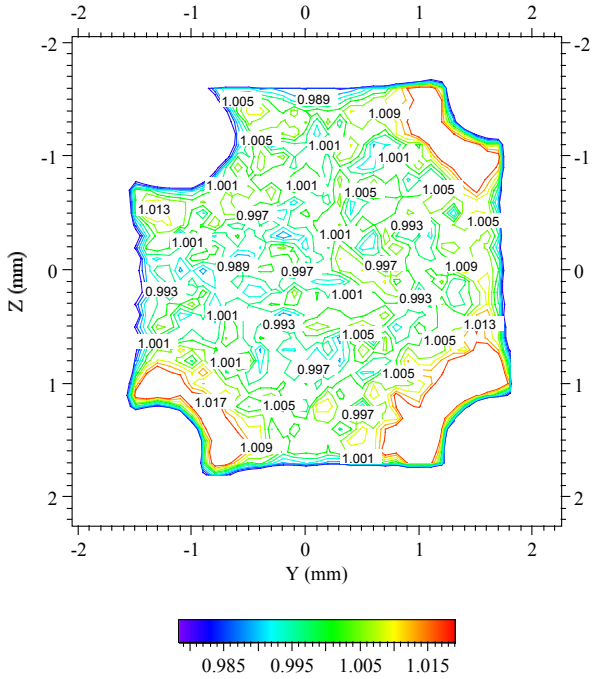

Fig. 4. Spatial non-uniformity of responsivity of one of the paint coated pyroelectric detectors at 10.6 µm.

References

[1] Eppeldauer G. P., Rice J. P., Zhang J., and Lykke K. R., Spectral irradiance responsivity measurements between 1 µm and 5 µm, SPIE Proc. Vol. 5543, pp. 248-257, 2004.

[2] Larason T. C., Bruce S. S., and Parr A. C., Spectroradiometric Detector Measurements, Part II – Visible to Near-Infrared Detectors, NIST Special Publication 250-41, February, 1998, U.S. Government Printing Office, Washington, DC.

[3] Lehman J., Eppeldauer G., Aust J. A., and Racz M., Domain-engineered pyroelectric radiometer, Applied Optics, Vol. 38, No. 34, p. 7047-7055, 1999.

[4] Gentile T. R., Houston J. M., Eppeldauer G., Migdall A. L., and Cromer C. L., Calibration of a pyroelectric detector at 10.6 µm with the NIST High-Accuracy Cryogenic Radiometer, Applied Optics, **36**, p. 3614-3621, 1997.

Realization of the NIST Total Spectral Radiant Flux Scale

Y. Ohno and Y. Zong
National Institute of Standards and Technology, Gaithersburg, Maryland USA

Abstract. The total spectral radiant flux scale has been realized at National Institute of Standards and Technology using a goniospectroradiometer for the 360 nm to 800 nm region. The construction of the goniospectroradiometer and results of the scale realization as well as the uncertainty budget are presented.

Introduction. There are increasing needs for total spectral radiant flux standards, which are required to calibrate integrating sphere systems employing a spectroradiometer. Such integrating sphere systems are increasingly used for measurement of color and total luminous flux of light sources such as discharge lamps and light-emitting diodes (LEDs) as well as for measurement of total radiant flux of ultraviolet (UV) sources.

A realization of total spectral radiant flux in the visible region using a gonio-colorimeter was reported (Goodman, 1991), which was based on measurement of the correlated color temperature of a test lamp in many directions, and the average spectral distribution of the lamp was derived based on Planck's equation. No further developments have been reported. Since then, new methods and technologies have become available to realize the scale more directly, possibly with lower uncertainties.

To address the strong needs for total spectral flux standards in the U.S. (CORM, 2001), a project has started at National Institute of Standards and Technology (NIST) to realize the total spectral radiant flux scale from the UV to visible region. Two independent methods are employed to realize the scale, allowing cross-check of the realized scales. The first method uses a goniospectroradiometer designed and built at NIST. The second method uses the NIST 2.5 m integrating sphere, applying the principles of the Absolute Integrating Sphere (AIS) method, which is successfully used for the realization of the lumen since 1995 at NIST (Ohno, 1996).

For the first phase of the project, NIST total spectral radiant flux scale has been realized in the 360 nm to 800 nm region using the goniospectroradiometer. This paper presents the principles of the methods of realization, the construction of the goniospectroradiometer, and the results of the realization of the scale as well as its uncertainty budget.

Methods for Scale Realization

Goniospectroradiometric method

The spectral radiant intensity of a light source is measured in many directions (θ, ϕ) over 4π steradian using a goniospectroradiometer. The total spectral radiant flux $\Phi_\lambda(\lambda)$ of the light source is given by

$$\Phi_\lambda(\lambda) = \int_{\phi=0}^{2\pi} \int_{\theta=0}^{\pi} I_\lambda(\lambda,\theta,\phi)\, \sin\theta \, \mathrm{d}\theta \, \mathrm{d}\phi, \qquad (1)$$

where $I_\lambda(\lambda,\theta,\phi)$ is the spectral radiant intensity distribution of the source on spherical coordinates (θ, ϕ). If the goniospectroradiometer measures spectral irradiance, the total spectral radiant flux $\Phi_\lambda(\lambda)$ of the light source is given by

$$\Phi_\lambda(\lambda) = r^2 \int_{\phi=0}^{2\pi} \int_{\theta=0}^{\pi} E_\lambda(\lambda,\theta,\phi)\, \sin\theta \, \mathrm{d}\theta \, \mathrm{d}\phi, \qquad (2)$$

where $E_\lambda(\lambda,\theta,\phi)$ is the spectral irradiance distribution on the spherical surface with radius r around the light source being measured.

The realization of the scale can be done more easily if the absolute scale is brought from the luminous flux unit. Then the spectral irradiance measurements can be done relatively. In such a method, the total spectral radiant flux of a lamp is given by

$$\Phi_\lambda(\lambda) = k_{\mathrm{scale}} \int_{\phi=0}^{2\pi} \int_{\theta=0}^{\pi} S(\lambda,\theta,\phi)\, \sin\theta \, \mathrm{d}\theta \, \mathrm{d}\phi, \qquad (3)$$

and

$$k_{\mathrm{scale}} = \frac{\Phi_{\mathrm{v}}}{K_{\mathrm{m}} \int_{\lambda=0}^{\infty} V(\lambda) \int_{\phi=0}^{2\pi} \int_{\theta=0}^{\pi} S(\lambda,\theta,\phi)\, \sin\theta \, \mathrm{d}\theta \, \mathrm{d}\phi \, \mathrm{d}\lambda} \qquad (4)$$

where $S(\lambda,\theta,\phi)$ is the relative spectral and spatial distribution of the lamp as given by

$$S(\lambda,\theta,\phi) = k \cdot E_\lambda(\lambda,\theta,\phi) \quad (k : \text{an arbitrary constant}), \qquad (5)$$

and Φ_{v} is the total luminous flux (lumen) of the lamp, determined using other methods. With this relative method, errors in the rotation radius r of the goniospectroradiometer, the positioning of lamp and detector, stray light from surrounding walls, and the absolute scale calibration of the spectroradiometer are mostly not relevant.

Absolute Integrating Sphere Method

The AIS method is applied spectrally. Figure 1 shows the arrangement of an integrating sphere system for this application. The flux from the spectral irradiance standard lamp is introduced through a calibrated aperture placed in front of the opening. The internal source, a lamp to be calibrated, is mounted in the center of the sphere. The external source and the internal source are operated alternately. The flux $\Phi_{\lambda,\mathrm{ref}}(\lambda)$ introduced from the external source is given by,

$$\Phi_{\lambda,\mathrm{ref}}(\lambda) = A \cdot E_\lambda(\lambda), \qquad (6)$$

where $E_\lambda(\lambda)$ is the average spectral irradiance from the external source over the limiting aperture of known area A. The total spectral radiant flux $\Phi_{\lambda,\mathrm{test}}(\lambda)$ of the test lamp is obtained by comparison to the external radiant flux:

$$\Phi_{\lambda,\mathrm{test}}(\lambda) = \frac{y_{\mathrm{test}}(\lambda)}{y_{\mathrm{ref}}(\lambda)} \cdot k_{\mathrm{cor}}(\lambda) \cdot \Phi_{\lambda,\mathrm{ref}}(\lambda), \qquad (7)$$

where $y_{\text{test}}(\lambda)$ is the detector signal of the spectroradiometer for the test lamp at wavelength λ, and $y_{\text{ref}}(\lambda)$ is that for the introduced flux at wavelength λ. $k_{\text{cor}}(\lambda)$ is a correction factor for spatial nonuniformity of the integrating sphere system and the ratio of diffuse reflectance of the sphere coating at 0° and 45° incidence. Similar to the case with the goniospectroradiometric method, the measurement can be done for relative total spectral radiant flux, with the absolute scale determined by the luminous flux unit.

Instrumentation

The mechanical design of the goniospectroradiometer developed at NIST is shown in Fig. 1. The detector arm and lamp holder are rotated by servo motors, and the actual angles are measured by rotary encoders. Measurements are taken, typically at 5° or 10° intervals, and the motor stops during measurement. The arm holding the lamp holder can also be rotated to change the burning position of the lamp.

The spectral irradiance of the test lamp is measured with an array spectroradiometer employing a fiber optic input. The fiber bundle is connected to the spectroradiometer through a rotation coupler, which allows free rotation of the arm without twisting the fiber. The constancy of the spectral transmittance of the coupler was tested with a white LED mounted on the irradiance head. The variations in measured spectra depending on the arm angle was found to be less than 2 %, and is corrected in actual measurements. From the rotation coupler to the irradiance measuring head, a fiber bundle of 8 mm diameter is used. The fiber bundle on the spectroradiometer side is 5 mm diameter.

The array spectroradiometer covering the UV and visible region is calibrated by a spectral irradiance standard lamp (1000 W FEL type quartz halogen lamp) traceable to the NIST spectral irradiance scale [7]. The stray light of the array spectrometer has been corrected (Zong, 2005). For the consistency with the total luminous flux unit, the total spectral radiant flux scale has been realized using Eqs.

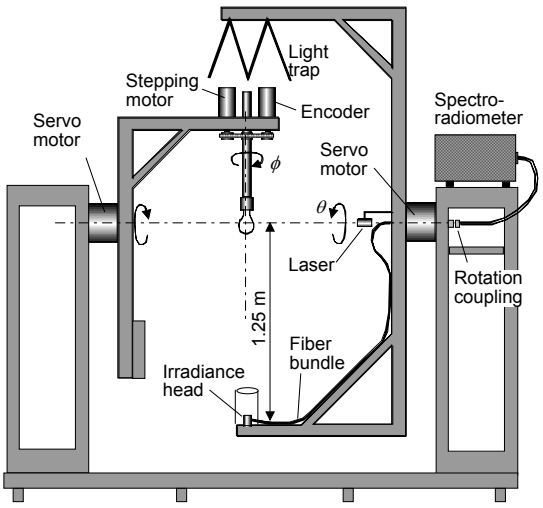

Figure 1. *Construction of the NIST goniospectroradiometer.*

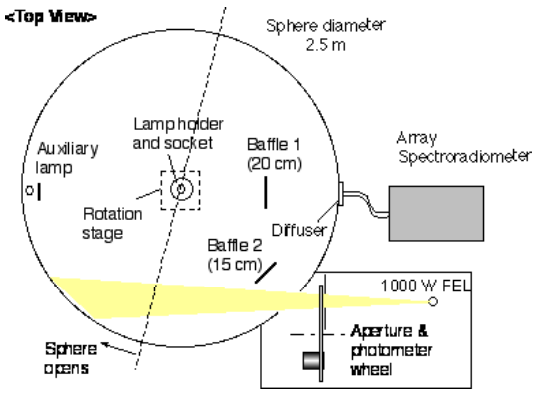

Figure 2. *NIST 2.5 m integrating sphere configured for the total spectral radiant flux measurement.*

(3)-(5). The uncertainty budget is to be reported at presentation and the full paper.

Figure 2 shows the arrangement of the NIST 2.5 m sphere configured for total spectral radiant flux measurement. The sphere is equipped with a high-sensitivity spectroradiometer employing a back-lit CCD array. The external source is a 1000 W FEL type quartz halogen lamp calibrated for spectral irradiance. The aperture is 50 mm in diameter. The spectroradiometer is an array spectroradiometer, which is corrected for stray light (Zong, 2005). Linearity of the spectroradiometer has also been determined and corrected. The integrating sphere response has been mapped spectrally by rotating a beam scanner. Angular correction factor for the coating has also been measured spectrally. An experimental realization of total spectral radiant flux scale in the near UV region (360 nm – 450 nm) has been successfully made at NIST using the 2.5 m integrating sphere to calibrate the total radiant flux of deep blue and UV LEDs (Zong, 2004). Work is underway to realize the scale in the full visible region.

Conclusion

The total spectral radiant flux scale has been established at NIST using a goniospectroradiometer for the 360 nm to 800 nm region. The AIS method, now under development, will enable realization of the scale with much simpler instrumentation and fast measurements.

References

Goodman T. M., et al, The Establishment of a New National Scale of Spectral Total Flux, Proc., 22nd Session of CIE, Melbourne 1991, Vol. 1, Part 1, 50-53 (1991).

CORM 7th Report 2001–Pressing Problems and Projected National Needs in Optical Radiation Measurements, December 2001.

Ohno Y., Realization of NIST 1995 Luminous Flux Scale using Integrating Sphere Method, *J. IES*, **25**-1, 13-22 (1996).

Zong, Y., et al, A Simple Stray-light Correction Matrix for Array Spectrometers, to be presented at NEWRAD 2005

Zong, Y., Miller, C.C., Lykke, K., Ohno, Y., Measurement of Total Radiant Flux of UV LEDs, Proceeding of the CIE Expert Symposium on LED Light Sources, June 2004, Tokyo, 107-110 (2004)

Goniometric Realisation of Reflectance Scales in the Ultra Violet to Near Infrared

M. J. Shaw & C. J. Chunnilall
National Physical Laboratory, Tedddington, TW11 0LW, U.K.

Abstract. The National Physical Laboratory (NPL) realizes UK diffuse reflectance scales from 350 nm to 1 μm using a gonioreflectometer and from 2.5 μm to 56 μm using a hemispherical technique. This paper presents work carried out to extend the spectral range of goniometric measurements made using the National Reference Reflectometer (NRR) to realize scales for radiance factor and hemispherical reflectance in the near infrared from 1 μm to 2.5 μm. The NRR is also used to realize a scale for multi-angle regular reflectance from 300 nm to 2.5 μm. Detailed uncertainty analyses covering the various capabilities over the full spectral range will be presented.

The National Reference Reflectometer (NRR)

The NRR is built around a pair of concentric rotary turntables, one which rotates the sample to set the angle of incidence and the other which moves the detector to set the receiver angle. Using these two turntables the light reflected off the sample can be measured at any position within the plane of incidence. The light source is a tungsten ribbon lamp the output from which is collimated and then passed through a rotatable linear polariser. The wavelength of the incident radiation is set using various bandpass interference filters with a bandwidth of approximately 15 nm [1, 2]. For measurement of regular reflectance the interference filters are removed and the light from the tungsten source is coupled into a double grating monochromator used in subtractive mode for high spectral resolution.

For earlier scale realization measurements in the visible the incident beam was brought to a focus at the sample by a pair of silica lenses. To reduce aberrations when using the NRR in the near infrared, this lens pair has been replaced by a new system of reflective optics. The collimated light beam is deflected away from the optical axis onto a spherical mirror that steers the light off a plane mirror and brings it to a focus at the sample plane (figure 1).

Light reflected from the sample is viewed through a precision circular aperture mounted in front of the detector. For measurements from the UV to 1 μm a silicon photodiode detector is used and from 0.9 μm to 1.6 μm an InGaAs detector is used. For near infrared measurements from 1.5 μm to 2.5 μm the incident light is chopped and the reflected flux measured using a cooled InSb detector and lock in amplifier for phase sensitive detection.

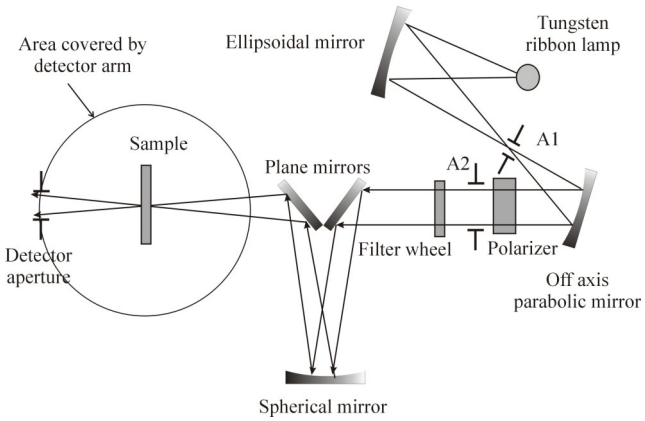

Figure 1. Optical design of the NPL Reference Reflectometer with reflective launch optics.

Diffuse Reflectance

For several years NPL has independently realized UK diffuse reflectance scales from 350 nm to 1000 nm using the NRR. The 0º/45º scale is realized directly by measurement of the directional radiance factor and the hemispherical scale is determined by spatial integration of goniometric values [1, 2]. From 2.5 μm to 56 μm, an absolute hemispherical technique [3, 4] is used to establish a scale for hemispherical reflectance. In the near infrared from 1 μm to 2.5 μm NPL has until recently relied on published values of barium sulphate [5] modified by measurements made at 2.5 μm using the hemispherical technique.

Using the infrared detectors and reflective optics, the NRR has now been used to independently realize diffuse reflectance scales in the range 1 to 2.5 μm. Measurements at either end of this range show good agreement with existing near and mid infrared scales completing a single continuous scale from the UV to the far infrared.

Measurement of glossy samples

The NRR is also used to measure the reflectance of glossy reference standards. In order to determine the reflectance of such materials under 8˚/t (specular included) and 8˚/d (specular excluded) geometries a series of measurements are made with an increased angular resolution around the specular peak. The specular and diffuse components of reflection are then separated mathematically allowing the hemispherical reflectance to be determined under different measuring conditions.

Regular Reflectance

The source optics of the NRR may be reconfigured to

incorporate a monochromator to allow full spectral measurements of multi-angle regular reflectance. Measurements have shown good agreement with existing near and mid infrared reflectance scales. This complements the existing V-W measurements at 7° in the 200 nm to 2500 nm region, and V-only and multiangle reflectance capabilities in the mid infrared [6]

Uncertainties

The uncertainty budget covering diffuse reflectance measurements in the ultra violet to visible [2] has been refined and extended to cover diffuse and regular reflectance measurements up to 2.5 μm. The total combined uncertainty varies depending upon the scattering properties of the sample and the spectral region of interest. In the UV signal to noise and reproducibility are dominant, whilst in the visible these are less significant and geometry becomes important. The non-uniformity of the detector becomes a considerable source of uncertainty in the near infrared. For 0°/45° radiance factor and total hemispherical reflectance of a white Spectralon target, the total combined uncertainty is better than ± 0.25% (k = 2) in the visible.

Acknowledgments

This work was funded by the UK DTI National Measurement Systems Directorate ' s Programme on Optical Radiation Metrology**.**

References

[1] Williams, D. C., Establishment of absolute diffuse reflectance scales using the NPL Reference Reflecteometer, *Analytica Chimica Acta*, *380, 165-172*, Elsevier 1999
[2] Chunnilall, C. J., NPL Scales for Radiance Factor and Total Diffuse Reflectance, *Metrologia*, 40, no. 1, S192 – S195, 2003
[3] Clarke, F. J. J. & Larkin, J. A. Measurement of total reflectance, transmittance and emissivity over the thermal IR spectrum. *Infrared Physics* **25**, 359-367 (1985).
[4] Chunnilall C. J., Clarke F. J. J. & Shaw M. J., Diffuse reflectance scales at NPL, *Proc. SPIE 4826,* 12-20, (2003).
[5] Morren, L., A study of the reflection factor of usual
photometric standards in the near infra-red, *Lighting Research and Technology **4***, pp. 243-249, 1972.
[6] Clarke, F. J. J., Birch, J. R., Chunnilall, C. J. & Smart, M. P. FTIR measurements, standards and accuracy. *Vibrational Spectroscopy* **30**, 25-29 (2002).